AGARD-CP-214

AD A047370

AGARD-CP-214

AGARD

ADVISORY GROUP FOR AEROSPACE RESEARCH & DEVELOPMENT

7 RUE ANCELLE 92200 NEUILLY SUR SEINE FRANCE

AGARD CONFERENCE PROCEEDINGS No. 214

Secondary Flows in Turbomachines

DDC
RECEIVED
DEC 8 1977
F

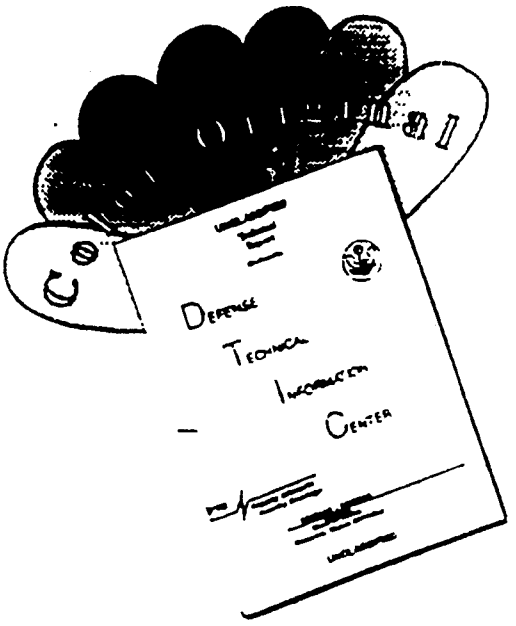
NORTH ATLANTIC TREATY ORGANIZATION

AD NO.
DDC FILE COPY

DISTRIBUTION AND AVAILABILITY
ON BACK COVER

DISTRIBUTION STATEMENT A
Approved for public release;
Distribution Unlimited

DISCLAIMER NOTICE



THIS DOCUMENT IS BEST QUALITY AVAILABLE. THE COPY FURNISHED TO DTIC CONTAINED A SIGNIFICANT NUMBER OF COLOR PAGES WHICH DO NOT REPRODUCE LEGIBLY ON BLACK AND WHITE MICROFICHE.

NORTH ATLANTIC TREATY ORGANIZATION

ADVISORY GROUP FOR AEROSPACE RESEARCH AND DEVELOPMENT

(ORGANISATION DU TRAITE DE L'ATLANTIQUE NORD)

DDC
RECEIVED
DEC 8 1977
F

(9) AGARD Conference Proceedings No. 214

(6) **SECONDARY FLOWS IN TURBOMACHINES**

(11) Sep 77 (12) 347p.

(14) AGARD-CP-214

Papers presented at the 49th Meeting of the AGARD Propulsion and Energetics Panel held at the Koninklijk Instituut van Ingenieurs, Prinsessegracht, 23, The Hague, The Netherlands, from 28 to 30 March 1977.

400 043 LB

THE MISSION OF AGARD

The mission of AGARD is to bring together the leading personalities of the NATO nations in the fields of science and technology relating to aerospace for the following purposes:

- Exchanging of scientific and technical information;
- Continuously stimulating advances in the aerospace sciences relevant to strengthening the common defence posture;
- Improving the co-operation among member nations in aerospace research and development;
- Providing scientific and technical advice and assistance to the North Atlantic Military Committee in the field of aerospace research and development;
- Rendering scientific and technical assistance, as requested, to other NATO bodies and to member nations in connection with research and development problems in the aerospace field;
- Providing assistance to member nations for the purpose of increasing their scientific and technical potential;
- Recommending effective ways for the member nations to use their research and development capabilities for the common benefit of the NATO community.

The highest authority within AGARD is the National Delegates Board consisting of officially appointed senior representatives from each member nation. The mission of AGARD is carried out through the Panels which are composed of experts appointed by the National Delegates, the Consultant and Exchange Program and the Aerospace Applications Studies Program. The results of AGARD work are reported to the member nations and the NATO Authorities through the AGARD series of publications of which this is one.

Participation in AGARD activities is by invitation only and is normally limited to citizens of the NATO nations.

The content of this publication has been reproduced
directly from material supplied by AGARD or the authors

Published September 1977

Copyright © AGARD 1977
All Rights Reserved

ISBN 92-835-0199-3

Printed by Technical Editing and Reproduction Ltd
Harford House, 7–9 Charlotte St, London, W1P 1HD

PROPULSION AND ENERGETICS PANEL

Chairman: Dr Ing. Gert Winterfeld, DFVLR, Institut für Luftstrahlantriebe, Köln, Germany
Deputy Chairman: Dr J. Dunham, NGTE, Pyestock, Farnborough, Hants, UK

PROGRAM COMMITTEE

Mr Jean Fabri (Chairman), ONERA, Châtillon-sous-Bagneux, France
Mr John Acurio, Lewis Directorate US Army Air Mobility R and D Lab, Cleveland, Ohio, USA
Professor Guiseppe Bussi, Politecnico di Torino, Italy
Professor Jacques Chauvin, VKI, Rhode-St-Genèse, Belgium
Dr John Dunham, NGTE, Pyestock, Farnborough, Hants, UK
Professor Friedrich Wazelt, TH Darmstadt, Lehrstuhl für Flugantriebe, Darmstadt, Germany

HOST COORDINATOR

Mr R.A.Jager, Kluyverweg 1, Delft, Netherlands

PANEL EXECUTIVE

Dipl. Ing. Joachim H.Krengel, D.I.C.

ACKNOWLEDGEMENT

The Propulsion and Energetics Panel wishes to express its thanks to the hosts, the Dutch National Delegates to AGARD, for the invitation to hold its 49th Meeting at the Koninklijk Instituut van Ingenieurs in The Hague, The Netherlands, and for the provision of the necessary facilities and personnel to make this meeting possible.



CONTENTS

	Page
PROPULSION AND ENERGETICS PANEL	iii
TECHNICAL EVALUATION REPORT by K. Papailiou	vii
	Reference
SESSION I – INTRODUCTION	
RECENT DEVELOPMENTS IN SECONDARY FLOW by J.H.Horlock	1
SESSION II – FUNDAMENTAL RESEARCH ON SECONDARY FLOWS IN COMPRESSORS	
CALCULATIONS CONCERNING THE SECONDARY FLOWS IN COMPRESSOR BLADINGS by F.Leboeuf, A.Comte, and K.Papailiou	2
EXPERIMENTAL STUDY OF THE BEHAVIOR OF SECONDARY FLOWS IN A TRANSONIC COMPRESSOR by G.Bois, F.Leboeuf, A.Comte and K.Papailiou	3
SECONDARY FLOWS AND ANNULUS WALL BOUNDARY LAYERS IN AXIAL-FLOW COMPRESSOR AND TURBINE STAGES by H.E.Gallus and W.Kümmel	4
SECONDARY FLOWS IN AXIAL FLOW COMPRESSORS WITH TREATED BLADES by M.P.Boyce	5
INFLUENCE DE DISTORSIONS INITIALES SUR LES ECOULEMENTS SECONDAIRES DANS UNE GRILLE D'AUBES ANNULAIRE FIXE par J.Huard	6
HOT-WIRE MEASUREMENTS IN AN AXIAL COMPRESSOR AND CONFRONTATION WITH THEORETICAL PREDICTIONS OF SECONDARY FLOWS by J. de Ruyck, Ch.Hirsch and P.Kool	7
DUAL BEAM LASER ANEMOMETRY STUDY OF THE FLOW FIELD IN A TRANSONIC COMPRESSOR by H.B.Weyer and R.Dunker	8
SESSION III – SECONDARY FLOWS IN LINEAR CASCADES	
SECONDARY FLOW AND LOSSES IN TURBINE CASCADES WITH INLET SKEW by H.B.Carrick	9
EFFETS DES ECOULEMENTS SECONDAIRES DANS LES GRILLES D'AUBES RECTILIGNES par G.Meauzé	10
SECONDARY FLOWS WITHIN TURBOMACHINERY BLADINGS by Ph.Marchal and C.H.Sieverding	11
INFLUENCE OF SECONDARY FLOW EFFECTS ON BLADE SURFACE PRESSURE MEASUREMENTS IN 2-D TRANSONIC TURBINE CASCADES by H.-J.Heinemann	12
SECONDARY FLOW IN CASCADES by D.Glynn, A.Spurr and H.Marsh	13

Reference

SESSION IV – SECONDARY FLOWS IN TURBINES

UNDERSTANDING TURBINE SECONDARY FLOW
by W.A.Tall 14

EFFECT OF ENDWALL COOLING ON SECONDARY FLOWS IN TURBINE STATOR VANES
by L.J.Goldman and K.L.McLallin 15

SESSION V – SHORT INFORMAL ADDITIONAL PRESENTATIONS

A NUMERICAL TIME-DEPENDENT APPROACH FOR DESCRIBING COMPRESSIBLE INVISCID NON-ISENTROPIC ROTATIONAL FLOWS IN CURVED DUCTS
by G.Bussi and M.Pandolfi 16

Presentation by B.Barry. No written version available. 17

SECONDARY FLOW STUDIES IN HIGH-SPEED CENTRIFUGAL COMPRESSOR IMPELLERS
by D.Eckardt and H.Krain 18

SOME OBSERVATIONS FROM LOW-SPEED CASCADE TESTS CONCERNING SIDE WALL BOUNDARY LAYER SUCTION
by B-A.Gustafson 19

THREE-DIMENSIONAL FLOW IN HIGHLY LOADED ANNULAR CASCADES WITH ZERO SECONDARY VORTICITY
by H.H.Fruehauf 20

CORNER BOUNDARY LAYER AND SECONDARY FLOW WITHIN A STRAIGHT COMPRESSOR CASCADE
by J.H.Renken 21

NOTE ON RELATIVE VORTICITY
by J.W.Railly 22

SESSION VI – ROUND TABLE DISCUSSION

ROUND TABLE DISCUSSION RTD 1
J.H.Horlock, UK, Moderator
R.Bouillet, SNECMA, FR: Viewpoint of engine manufacturers
J.Chauvin, VKI, BE: Theoretical research
D.Eckardt, DFVLR, GE: Experimental research
P.Runstadler, Creare, US: Visualisation and hot wires
J.H.Horlock, UK, Concluding remarks

Preceding Page Blank FILMED

TECHNICAL EVALUATION REPORT

by

K.D.Papailiou

1. INTRODUCTION

Improvement of the theoretical calculation of the inviscid core of the high performance turbomachines makes more and more necessary the better understanding of the secondary flows, i.e. the part of the flow field that is close to the inner or the outer walls and is therefore subjected to high viscous stresses as well as to the effect of the vortices induced by the blade-casing junction.

Such problems have been frequently discussed during various technical meetings but the Specialists Meeting held during the 49th AGARD Propulsion and Energetics Panel Meeting at The Hague, Netherlands, 28-30 March 1977, is the first international congress entirely devoted to this subject.

The meeting was divided into four sessions – a total of fifteen invited papers and seven short presentations – followed by a round table discussion.

2. CONTENT OF THE MEETING

A review paper by J.Horlock (Salford University, U.K.) summarized the earlier work on secondary flows in turbomachines. The secondary flow effects in compressors and turbines are very different:

- Compressor bladings give small deflections, and the relative motion between the blading and the wall is such that the secondary vorticity can be calculated by means of simplified methods and the estimation of boundary layer effects can be based on integral methods;
- Turbine blades induce large deflections and the relative motion is such that the three-dimensional effects are predominant. Complete flow calculations are required;
- Correct loss prediction methods useful for engine manufacturers do not exist for either compressor or turbine.

From the presentations made during the Specialists Meeting several tendencies for the development of theoretical research can be distinguished:

- As shown by J.Horlock, the followers of W.R.Hawthorne investigate the detail of the structure of the secondary flow field. Renewed interest in this field of research is manifested in the so-called Beltrami flows in which total pressure is constant and vorticity components exist parallel to the local velocity;
- A slightly different method was presented by H.Marsh (University of Durham, U.K.) who emphasizes the role of the time lag between pressure side and suction side flows to approximate estimation of the different components of the secondary vorticity;
- An alternate way was followed by the research team of the Ecole Centrale de Lyon, F., G.Bois, F.Leboeuf, A.Comte, K.Papailiou. By means of generalizing the classical boundary layer methods, they estimate the overall effect of the secondary flows. Apparently such an approach is very satisfactory even in the transonic range. The junction between the inviscid or at least the low loss flow region and the secondary flow region is made on the basis of static pressure compatibility. An experimental paper given by the same team showed the validity of this approach that may be considered as a first step towards the estimation of losses and blockage factors due to the development of wall boundary layers amplified by the secondary effects.

For higher Mach numbers, namely in the case of supersonic compressors all these approaches become irrelevant and Fruehauf, University of Stuttgart, Ge., gave some preliminary results of flow calculations.in compressors using the characteristics method.

Outside of these theoretical papers, most of the presentations described experimental results. The techniques included probe surveys, laser velocimetry, and several forms of flow visualization.

Results obtained by advanced methods were presented:

- hot wire anemometry in a subsonic compressor (Ch. Hirsch, Free University of Brussels, B.),
- detailed boundary layer measurements near the casing wall of another subsonic compressor (W.Kümmel, Technisch Hochschule, Aachen, Ge.),
- laser anemometry in a transonic compressor (H.Weyer, DFVLR, Köln Wahn, Ge.),
- turbine flow analysis using advanced theoretical methods (W.Tall, Wright-Patterson AFB, in the United States) and multistage turbine experiments (B.Barry, Rolls Royce 1971 Ltd. in the United Kingdom).

Due to the difficulties encountered in measurement in actual turbomachines, some presentations were restricted to laboratory tests. The study of the flow distortion in an annular blade cascade by J.Huard, ONERA, F., showed all the complexity of distorted flows in a three-dimensional test facility: the streamlines undergo inwards or outwards radial shifts according to their total pressure.

Using a moving belt at one wall of his linear blade cascade, H.B.Carrick, I.C.I., U.K., analyzed the effect on the secondary phenomena in the cascade of a skewed boundary layer in which the velocity is not parallel to the main flow velocity. This test set-up simulates in a laboratory the test conditions at the entrance of an actual compressor.

In a similar way, L.Goldman, NASA, Lewis Research Center, U.S., simulates the effect of endwall cooling air injection on the performance of an annular cascade of turbine blades, and Ph.Marchal and C.Sieverding, Von Kármán Institute, B., analyzed the structure and the loss repartition in the endwall zone of a linear low speed turbine blade cascade.

No new loss correlations were extracted from all these measurements, although it was understood that secondary flows lead to high losses and a good understanding of them is necessary to improve turbomachine performances. In order to decrease these losses some devices were proposed.

Wall boundary layer suction was proposed by both B.A.Gustafson (Chalmers University, Sweden) who uses porous walls and G.Meauze, ONERA, F., who eliminates the blade cascade end wall boundary layer through slots positioned near the blade channel minimum section. In both cases improvement of the flow field and reduction of the secondary losses were obtained. No overall balance taking into account the work necessary for boundary layer suction has been presented in either case.

A new blade surface treatment was proposed by M.P.Boyce, Texas A. & M. University, U.S. Axial grooves on the blade suction surface were reported to delay the stall phenomenon.

A proposal by J.Renken (DFVLR, Ge) to smooth out the blade-casing wall junction in order to diminish the secondary losses was disapproved, since some compressor tests reported by J.Horlock showed no efficiency improvements.

3. ROUND TABLE ON THE NEEDS OF ENGINE MANUFACTURERS OF SECONDARY FLOW KNOWLEDGE AND THE CONTRIBUTION OF THE PRESENT AGARD MEETING TO THIS KNOWLEDGE

A better knowledge of the flow field in the wall region and a correct estimation of secondary losses are of paramount interest to engine manufacturers, according to R.Bouillet, SNECMA, F. A better knowledge of secondary effects is required for the following reasons:

- secondary flows affect the engine efficiency: in some cases such as high pressure turbine stages, the secondary losses account for half of the stage losses,
- secondary flows modify the main stream both through the channel blockage and the pressure equilibrium condition,
- a better knowledge of the blockage factor and the inviscid flow calculation leads to a better blade setting.

A typical example of the effect of secondary flows on compressor design is the case of a seven stage axial compressor that has large secondary losses due to high pressure gradients and an eight stage compressor designed for the same performances that has higher efficiencies.

Reduction of secondary losses by complex methods such as casing boundary layer suction, grooves or any other casing treatment, reduction of peripheral gaps using abradable materials is not a final solution, The stall margin may be extended but the efficiency is generally decreased.

The use of correct secondary flow models and correct loss predictions at the engine design stage is the preferred way to minimize the effect of secondary flows.

By summarizing earlier work and presenting recent analytical researches the present AGARD meeting gives already part of the answers to these questions. That is how J.Chauvin, Von Kármán Institute, B., evaluates the contribution of this meeting to the progress in secondary flow research. For compressors almost all the necessary tools are in the hands of engine designers. For turbines, the development of fully three-dimensional calculations still seems necessary.

The simple loss and blockage factor correlations the engine manufacturers use now lack generality and it will be necessary for them to learn to use the new theoretical models proposed by research people. On the other hand, if the theoreticians wish to improve their models, they have to take advantage of all the advanced experimental data presently available. The empirical factors that still exist in the best formulas can be estimated more correctly in that way.

This approach could refine the theoretical methods that are already available and seem to fit correctly the compressor data. For turbine flows the complete three-dimensional theory has to be developed. But in an ultimate stage these three-dimensional calculations may replace costly experimentations.

For D.Eckardt, DFVLR, Köln-Wahn, Ge., the lack of experimental results on secondary flow in actual turbomachines is one of the difficulties in building three-dimensional models. The hot wire anemometer that has been widely used in low speed compressors should be more and more replaced by laser anemometry. Measurements closer to the wall become possible with the use of the fluorescent technique.

P.Runstadler, CREARE Corp., U.S., agreed on this point. He emphasized the role of correctly planned flow visualization that may be a great help for theoreticians to build a model. The main difficulty in flow visualization comes from the unsteady effects. The most promising techniques are;

- sheet of light
- laser holography
- wall trace

From the general discussion that followed these comments made by the round table leaders, this summary can be given:

Everyone agreed that the engine manufacturers were reluctant to use the present day theories (with some exceptions), feeling that they were not developed enough to provide useful information. It was observed, however, that not enough cases had been treated in order to decide whether or not these theories could be of some use.

As far as the state of the art is concerned, it was generally agreed that boundary layer type methods helped by the simplified inviscid flow theories (as developed by Hawthorne, Horlock, Lakshminarayana and Marsh) could provide a sound basis for annulus wall viscous layer prediction for compressors at design and off design conditions. There is a lack of information, however, as far as the last stages of multistage compressors are concerned and as far as tip clearance effects are concerned.

The turbine secondary flow physics are quite different because of the effect of secondary vorticity on the boundary layer and so fully three-dimensional calculation methods ought to be used.

These could seem quite expensive and difficult, but recent advances in computers make them more accessible.

All agreed that progress in experimental techniques helped the understanding of flow phenomena and that they ought to be used regardless of the costs.

J.Horlock pleaded for carefully planned experiments. He seemed to imply that it was not yet possible to use the full equations and that the simplified models used should come from the experimental results.

Figure 1 summarizes the content of the meeting.

4. CONCLUSION AND EVALUATION OF THE MEETING

The massive participation – over 120 attendees for a meeting on such a specialized subject as "Secondary flows in turbomachines" – shows the importance and timely nature of the subject chosen by the AGARD Propulsion and Energetics Panel for its 49th meeting.

Most of the fifteen invited papers and the seven short presentations made during the meeting came from research organizations with only a few papers presented by industry. It is unfortunate that a more complete representation of industry could not be obtained, but most of the main engine manufacturers were represented.

The discussion periods were generally very lively. The representatives from industry made clear:

- why up to now they were not able to use the theoretical approaches available in the literature,
- the need for a theoretical estimation of the blockage factor to help them to calculate more correctly the low-loss core of the flow,
- the need for correct loss estimation formulas.

The response from research workers suggested:

- simplified secondary vorticity considerations and pseudo-boundary layer approaches seem to be promising for multistage compressor analysis if backed by experimental results,
- this analysis seems to be inadequate for turbines and fully three-dimensional calculation methods must be used. These are still time consuming but are certainly less expensive than experiments,

- new experimental techniques must be used, in spite of cost and effort, to provide the necessary flow models. However, experiments must be carefully planned,
- lack of understanding and experimental information exists in the following areas:
  (i) multistage environment
  (ii) tip clearance effects
  (iii) radial machines

The attendees were unanimous in recommending that the same subject be considered for a future AGARD Specialists Meeting when new theoretical and experimental results are again available.

	No.	AUTHORS	THEORETICAL	EXPERIMENTAL	COMPRESSOR	TURBINE	SINGLE STAGE	MULTISTAGE	CASCADE (Plane of annular)	AXIAL	RADIAL	OPTIMIZATION	HIGH SPEED	LOW SPEED
PRESENTATION	(x)													
	2	LEBOEUF – COMTE – PAPAILIOU	*		*			*		*			*	
	3	BOIS – LEBOEUF – COMTE – PAPAILIOU		*	*		*			*			*	
	4	GALLUS – KUMMEL	*	*	*	*	*			*		*	*	
	5	BOYCE		*	*		*			*		*		*
	6	HUARD		*	*				*	*			*	
	7	DE RUYCK – HIRSCH – KOOL		*	*		*			*				*
	8	WEYER – DUNKER		*	*					*			*	
	9	CARRICK	*	*		*			*	*				*
	10	MEAUZE		*	*				*	*		*	*	
	11	MARCHAL – SIEVERDING		*		*			*	*				*
	12	HEINEMANN		*		*			*	*			*	
	13	GLYNN – SPURR – MARSH	*			*			*	*				*
	14	TALL	*	*		*	*			*		*	*	
	15	GOLDMAN – McLALLIN		*		*			*	*		*		
SHORT TALKS	16	BUSSI – PANDOLFI	*						*					*
	17	BARRY		*		*		*		*			*	
	18	ECKARDT – KRAIN		*	*		*				*		*	
	19	GUSTAVSON		*	*				*	*		*		*
	20	FRUEHAUF	*		*		*			*			*	
	21	RENKEN	*	*	*				*	*				*
	22	RAILLY	*											

Figure 1

(x) Paper 1, the introductory lecture by Professor Horlock is not considered in this list.

RECENT DEVELOPMENTS IN SECONDARY FLOW

by
Professor J H Horlock FRS
Vice-Chancellor
University of Salford
SALFORD
M5 4WT
United Kingdom

The "state-of-the-art" in secondary flow work is reviewed:

(a) for the period up to the early 1970's when a similar review was made for the Annual Review of Fluid Mechanics (1973), and

(b) for the past few years.

Major recent developments include:

(i) clarification of earlier work on the inviscid analysis of secondary flows,

(ii) a new emphasis on Beltrami flows (flows with uniform stagnation pressure but streamwise vorticity),

(iii) integration of boundary layer calculations with inviscid secondary flow analyses,

(iv) full three dimensional flow calculations, both inviscid and viscid, and

(v) improvements in correlations of secondary losses.

Notation

s, n, b	natural co-ordinates
x, y, z	rectilinear co-ordinates
c	velocity
ω	vorticity
p	pressure
ρ	density
T	temperature
R	principal radius of curvature of streamlines
p_0	stagnation pressure
ρ_0	stagnation density
T_0	stagnation temperature
c_p	specific heat at constant pressure
γ	angle betwen ∇h and $\underline{b}$
ψ_S	secondary stream function
s	blade spacing
$s' = s\cos\alpha$	staggered blade spacing
α	flow angle
$\delta\alpha$	flow deflection
β	blade angle
ξ, η, ζ	vorticity components in x, y, z directions
t	time
Δt	difference in transit time over aerofoil
Γ	circulation
C_∞	mainstream velocity
δ	boundary layer thickness
δ^*, θ	displacement thickness, momentum thickness
ϵ	flow deviation in boundary layer
τ	shear stress
D	deficit terms defined in text
P, Q	quantities defined in text
f	blade force in boundary layer
F	blade force in main stream
λ, ϕ	parameters defined in text
k	turbulent kinetic energy
μ_t	turbulent viscosity
l_t	turbulent length scale
ϵ_d	volumetric rate of dissipation
L	blade height (or length)
l	blade chord
C_L	lift coefficient
U	blade speed

Subscripts

0	stagnation
s, n, b	in s, n, b directions
x, y, z	in x, y, z directions
p	primary
1	inlet to cascade
2	exit from cascade
p	pressure surface
s	suction surface
TF	trailing filament
TS	trailing shed
m	mean through cascades
δ	edge of boundary layer

Superscripts

$\bar{}$	mean over pitch
$'$	perturbation from mean
I, II	solutions from two similar equations

1. Introduction

For the purposes of this review lecture we shall define secondary flow as that flow associated with the development of streamwise vorticity. This definition itself is open to some discussion; it is essentially the definition used by Professor Sir William Hawthorne in his secondary flow work - that secondary flows are associated with all components of streamwise vorticity. However, we may note that in parallel pioneering work on this subject, Dr L H Smith of the General Electric Company (USA) chose to define secondary flow in terms of the velocities arising from excess streamwise vorticity - that streamwise vorticity in the real flow in excess of the streamwise vorticity associated with an axisymmetric rotational flow through closely spaced blades. We shall come back to this point of definition later.

The author has been concerned (with Professor B. Lakshminarayana) in reviewing this subject on three previous occasions (References 1, 2 & 3). The first review (1963) was directed at giving guidance to turbomachinery designers; the second (1973) was a more general review of theoretical and experimental work in secondary flows up to the late 1960's-early 1970's; and the third (1973) was an attempt to bring together analytical work on the development of streamwise vorticity into a unified presentation.

Rather than go over the work of the earlier reviews in full detail, the author has chosen to take the second of those reviews as read and to concentrate on developments since that date. However, by way of introduction the situation as described in that paper (in the Annual Review of Fluid Mechanics (ARFM 1973)) will be summarized briefly. Recent attempts to synthesise the work in this field into logical presentations and new developments in secondary flow work over the last five or six years are also described.

2. The Situation in the Early 1970's

The chapter by Horlock and Lakshminarayana in the Annual Review of Fluid Mechanics (ARFM 1973) attempted to summarize the position on secondary flows up to the early 1970's. The review was divided into two main parts: theoretical work on secondary flows and experimental work. We summarize these two areas below (Sections 2.1 and 2.2 respectively).

2.1 Theoretical Work

In the theoretical work five particular lines of analysis could be identified.

2.11 In the first general equations have been obtained for the development of streamwise vorticity in inviscid flow (Squire and Winter (4), Hawthorne (5) and Marris (6). A subsequent attempt by Lakshminarayana and Horlock to bring together these various approaches was published in the Journal of Fluid Mechanics (3) and the most general equation given there for the development of the streamwise vorticity (ω_s) along the streamline s in inviscid but compressible flow, is

$$\frac{\partial}{\partial s}\left(\frac{\omega_s}{\rho c}\right) = \frac{2\omega_n}{\rho c R} - \frac{1}{\rho^2 c^2}\left[\frac{\partial p}{\partial n}\frac{\partial \rho}{\partial b} - \frac{\partial p}{\partial b}\frac{\partial \rho}{\partial n}\right] \qquad (1)$$

The notation is indicated in Fig. 1, which shows the direction of the principal normal $\bar{n}$, defined from $\bar{n}/R = (\bar{s}\cdot\nabla)\bar{s} = \partial\bar{s}/\partial s$, where R is the principal radius of curvature. $\bar{b}$ is the binormal vector $\bar{b} = \bar{s}\times\bar{n}$ so that ($\bar{s}$, $\bar{n}$, $\bar{b}$) form a right handed set of normal vectors. p and ρ are pressure and density respectively, and ω_n is the vorticity component in the n direction.

In inviscid flow, it may be shown that $\frac{\partial p}{\partial b} = 0$ and $\frac{\partial p}{\partial n} = -\frac{\rho c^2}{R}$ so that Eq.(1) becomes

$$\frac{\partial}{\partial s}\left(\frac{\omega_s}{\rho c}\right) = \frac{2\omega_n}{\rho c R} + \frac{1}{\rho^2 R}\frac{\partial \rho}{\partial b} \qquad (2)$$

Additional assumptions about the fluid may be made and simpler equations for the growth of ω_s can be obtained. For example:

Incompressible fluid (ρ = constant)

$$\frac{\partial}{\partial s}\left(\frac{\omega_s}{c}\right) = \frac{2\omega_n}{cR} = \frac{2}{cR}\frac{\partial c}{\partial b} = \frac{\nabla p_o \cos\gamma}{\rho c^2 R} \qquad (3)$$

Barotropic fluid

$$\frac{\partial}{\partial s}\left(\frac{\omega_s}{\rho c}\right) = \frac{2\omega_n}{\rho c R} \qquad (4)$$

Perfect gas $(p/\rho T)$ = constant, specific heat (c_p) constant)

$$\frac{\partial}{\partial s}\left(\frac{\omega_s}{\rho c}\right) = \frac{2}{\rho_o c^2 R}\frac{\partial p_o}{\partial b} \qquad (5)$$

In these expressions p_o is the total pressure, γ is the angle between the direction of ∇p_o and $\underline{b}$, and ρ_o is the stagnation density.

Further details of the various analyses for the growth of both streamwise and normal vorticity, including the effects of viscosity are given in ARFM (1973), with references to the original work by numerous authors.

2.12 The second theme of analytical work, developed by Hawthorne (7) and Smith (8) involves determination of the secondary velocities from the secondary vorticity. Solutions of the Poisson equation for secondary stream function (ψ) may be obtained within a bounded plane normal to the mainstream. For example, at the exit from a cascade (Fig. 2) solutions to the equation

$$\nabla^2\psi = \frac{\partial^2\psi}{\partial n^2} + \frac{\partial^2\psi}{\partial z^2} = -\omega_s \qquad (6)$$

have been given by both authors who assumed that the Bernoulli surfaces did not rotate in the incompressible flow through the cascade. (Note that the s, n, b natural co-ordinates are now replaced by s and n along and normal to the mainstream outside the boundary layer and z normal to the wall.

Essentially this is the small shear/large disturbance approach in Hawthorne's classification of secondary flow analysis (9). Variations on these solutions have been attempted by several authors (e.g. Ehrich and Detra (10), Armstrong (11), Lakshminarayana and Horlock (12)) in which the streamwise vorticity is traced to new locations within the duct and the stream function equations solved for those new locations, rather than assuming that the vortex filaments are carried by the primary (undisturbed) flow. One of the major limitations in this work is that the effect of separation in the corners of the duct (and the resulting displacement of the streamlines) cannot be predicted accurately.

2.13 The third theme that can be identified in the analytical work is the study of the vorticity that arises in the wakes downstream of blades in cascades or turbomachinery blade rows. This led to the definition of the vorticity components in the wakes of the blades. Two such components were identified by Hawthorne (13) - the trailing filaments being bent round the blades and embedded in the wake, and the trailing shed vorticity arising within the wake from vorticity shed from the blade bound vorticity. These components are illustrated in Fig. 3, together with the channel vorticity which has a streamwise (secondary) component.

Both Hawthorne and Smith have derived expressions for the trailing vorticity, and these are given in the ARFM (1973) review, together with the original references. Recently, Marsh (14) has presented another method for determining the strength of the vorticity components developed in a cascade flow, and we refer to this approach below.

2.14 Fourthly, we note the development of aerofoil theory by several authors (essentially large shear/small disturbance analyses). The work of Namba (15) in which dipoles are placed on the blades and induced velocities associated with those dipoles estimated and matched to the kinematic boundary conditions on the blades is described in ARFM 1973, where again references to the original work of several authors is made. This approach is elegant but mathematically complex and it has not yet been applied very widely.

2.15 Finally, in ARFM (1973) some attempts to integrate three-dimensional boundary layer analysis (developed mainly for aircraft aerodynamics) with secondary flow analysis were reported. In particular reference was made to the work of Johnston (16) who studied the cross-flows developed in three dimensional boundary layers as they approached an obstacle or as they were deflected by a cascade. Fig. 4 shows typical streamwise and cross-flow velocity distributions with notation. (Capital letters are now used for mainstream and the angle ϵ denotes flow deviation from the mainstream direction). It can be shown that the cross-flow associated with the outer part of the boundary layer may be described by simple secondary flow analysis whereas the inner flow required a detailed boundary layer study. Developments from this work are given below.

2.2 Experimental Work

Much of the experimental work described in ARFM (1973) was directed towards verification of the analyses described above. Broadly, in the absence of severe viscous effects, it has been shown that secondary flow analysis is reliable, but when viscous effects are present inviscid flow analysis, not surprisingly, is found wanting.

A second stream of experimental work has been aimed at practical measurements of loss data. The early work of Howell (17) - for compressors - and Vavra (18) and Ainley and Mathieson (19) - for turbines - is well known and various attempts have been made to bring this data up-to-date. Particular reference was made in ARFM (1973) to the work of Dunham (20) in comparing previous loss correlations and providing a new, more reliable one.

Finally, a few detailed measurements of wall boundary layers in compressors and turbines had begun by the early seventies.

3. Theoretical Developments since 1970

The theoretical developments since 1970 are mainly associated with the following areas:

(1) Clarification of earlier ideas (the definition of secondary flow; the secondary flow through a rotor; extension of general vorticity analysis to more complex flows such as stratified flows and flows with temperature gradients; and alternative approaches to the estimation of trailing and filament vorticity).

(2) A new interest in "Beltrami" flows. It is now appreciated that many secondary flows in turbomachines are dominated by the fact that the inlet flow is of nearly uniform stagnation pressure but is skewed (i.e. the vorticity is parallel to the vorticity vector). The theoretical work has involved analysis of general Beltrami flows past objects such as spheres, or through specific cascades; actuator disc analysis of Beltrami flow through closely spaced cascades; and aerofoil type analyses of the Beltrami flow problem in cascades.

(3) A substantial amount of work directed at integrating some inviscid secondary flow analyses into the boundary layer methods of calculation developed for the study of annulus wall boundary layers in compressors and turbines.

(4) Detailed numerical analysis and calculation of three-dimensional duct flows.

We deal with these theoretical developments in more detail below.

3.1 Definitions of Secondary Flow; Rotor Secondary Flow; Vorticity Tracing

A general discussion of the differences between the Hawthorne and Smith definitions of secondary flow is given by Horlock in reference (21) - NASA SP 304 (Fluid Mechanics, Acoustics and Design of Turbomachinery). In that discussion of the paper by Dixon (page 196) it was argued that there was no inconsistency between the two definitions.

Consider, for example, the shear flow through a cascade. Hawthorne (13) treats this as a small shear, large deflection flow in which a "primary" uniform flow transports the vortex filaments from entry (Station 1) to exit (Station 2). He derives the secondary circulation per unit height in the channel as

$$\omega_s S \cos\alpha_2 = \frac{dc_1}{dz}\left[c_1 \oint_{BLADE} \frac{ds}{c} + \frac{S}{2}\left(\frac{\sin 2\alpha_2 - \sin 2\alpha_1}{2\cos\alpha_1}\right)\right] \qquad (7)$$

where α is the flow angle, $\omega_{s_1} = 0$, $\omega_{m_1} = \frac{dc_1}{dz}$ and S is the blade spacing.

Smith's "primary" flow on the other hand is one in which the shear flow passes through a closely spaced cascade and is in radial equilibrium upstream and downstream of the cascade. Downstream the axial, tangential and spanwise components of vorticity are $\xi_2 = \cos\alpha_2 (dc_2/dz)$, $\eta_2 = \sin\alpha_2 (dc_2/dz)$, $\zeta_2 = 0$. ξ_2 and η_2 are thus components of a vorticity vector ($\omega_{m_2} = dc_2/dz$) lying perpendicular to the downstream primary flow direction, so there is no streamwise vorticity in this primary flow, $\omega_{s_{p_2}} = 0$. (The subscript p indicates "primary"). We should therefore expect Smith's equation for the secondary circulation (the "excess" vorticity over a (zero) primary streamwise vorticity),

$$(\omega_s - \omega_{s_p})_2 S \cos\alpha_2 = -\left[c_1 \frac{dc_1}{dz} \frac{\Gamma_{VA}}{c_{a_1}^2} + \frac{d\Gamma_p}{dz} \right] \qquad (8)$$

to be identical to that given by Hawthorne. (Γ_{VA} is the actual (primary plus secondary) vane circulation and Γ_p is the primary circulation). It is shown in Reference (21) that this is indeed the case. An example of flow through a cascade in which Smith's primary flow does have streamwise vorticity is also given there; it is shown that while the Smith

and Hawthorne definitions of what comprises the secondary flow differ for this type of flow, there is no difference in the final description of the acutal (complete) flow.

Some confusion existed in the late 60's about the development of the secondary vorticity in the flow through a rotating blade row and an attempt was made to clarify this situation in ARFM (1973). In that paper expressions were derived for

(i) the absolute secondary vorticity that is developed in the flow through a rotor, and

(ii) the relative secondary vorticity, the vorticity relative to the rotating blades.

It was shown in the paper that the two derivations were consistent. It was also made clear there and at the Pennsylvania State University Conference in 1970 (Reference (21), see Dixon, and discussion by Hawthorne and Horlock) that the vorticity which should be used in calculating the relative secondary velocity in a rotating blade row is the absolute vorticity resolved in the relative direction. There is the same difficulty in defining the secondary flow as in the stationary cascade and we refer to the discussion at the Penn State Conference on this point; once again, the critical point is whether the secondary flow is defined as a perturbation from a primary potential flow (Hawthorne), or from a primary axisymmetric flow which is rotational (Smith).

To summarize the position, for rotors and stators, it would appear that there is no problem in calculating the inviscid secondary flow if the secondary velocities are clearly defined. If the definition is on Hawthorne's basis (perturbation from potential flow) then all components of secondary streamwise vorticity should be included in the calculation of induced velocities. However, if the Smith definition is used (the extra velocities over and above those produced by closely spaced blade rows) only the excess secondary vorticity should be used in calculating those "extra" velocities. It should be emphasised that in both approaches approximations are implied for both involve models of the real flow. The Hawthorne model requires the assumption of vortex filaments being carried by the primary uniform flow; the Smith model requires the representation of the real flow as the addition of a flow through a closely spaced blade row and the "extra" velocities associated with finite spacing.

Further theoretical work on basic inviscid secondary flow has been carried out by Hawthorne (22) who has described the development of streamwise vorticity in stratified fluids in rotating systems. Here the fluid is incompressible but of non-uniform density; each particle retains its initial density throughout the flow. Greitzer (23) has discussed why deflection of a stratified flow with constant stagnation pressure, but with velocity and density gradients, produces no secondary vorticity. Essentially this is because ρc^2 is constant, $\partial p/\partial n$ is constant at all z and there is no tendency for secondary motions to take place.

Marsh (14) has provided a new approach to the calculation of secondary vorticity (channel, trailing filament and trailing shed vorticity - see Fig. 3). He has used some earlier work on the averaged flow between blade rows to calculate the downstream of two initially adjacent particles on a vortex line (A and B) which are split by a bladed cascade. He obtains the time difference for these particles in their transit across the surfaces of the blade, and hence their separation, from an averaged flow equation developed by Horlock and Marsh (24).

This equation gives the difference between the axial velocity (c_x) on the two surfaces of a thin blade in cascade

$$c_{xq} - c_{xp} = S \cos^2\beta \frac{d\bar{c}_y}{dx} \tag{9}$$

(see Fig. 4; the bar superscript indicates a pitchwise mean, e.g. $\bar{c}_y = \frac{1}{S}\int_0^S c_y \, dy$). The difference in transit time from leading to trailing edge for particles on the pressure (p) and suction (q) surfaces is

$$\begin{aligned} \Delta t &= \int_{le}^{te} \frac{ds}{c_p} - \int_{le}^{te} \frac{ds}{c_q} \\ &= \int_{le}^{te} \left(\frac{c_{xq} - c_{xp}}{c_{xp} c_{xq}} \right) dx \\ &= \int_{le}^{te} \frac{S \cos^2\beta}{c_{xp} c_{xq}} \frac{d\bar{c}_y}{dx} \, dx \end{aligned} \tag{10}$$

With $(c_{xp} c_{xq})^{\frac{1}{2}} \approx \bar{c}_x$, the mean velocity, and with $\frac{d\bar{c}_y}{dx}$ from continuity, it follows that the separation of initially adjacent particles at the trailing edge is $\bar{c}_x \Delta t / \cos\alpha_2 = S(\alpha_2 - \alpha_1)\cos\alpha_2$. With this separation determined, Marsh is able to calculate the streamwise component of vorticity and the vorticity components left in the wake. He has also extended these ideas to give the effect of compressibility on the development of the three components on vorticity (25).

3.2 Beltrami Flows

A major effort has recently been made by Hawthorne and his colleagues at Cambridge to improve the understanding of Beltrami flows. A Beltrami flow is one in which the stagnation pressure is constant but a vorticity component can exist along the streamlines. If

the stagnation pressure is constant then the general equation (3) shows that the vorticity along the streamline is proportional to the local streamwise vorticity i.e.

$$\omega_{s_2}/c_2 = \omega_{s_1}/c_1$$

$$\omega_s/c = \text{constant} \tag{11}$$

and the (streamwise) vorticity is proportional to the velocity everywhere. Some elegant work on the general Beltrami flows past obstacles (e.g. spheres and special cascades) has been undertaken by Hawthorne and Kingcombe and is included in Kingcombe's doctoral thesis (26). However, the work has not yet been generally published and it is not therefore reviewed here. Kingcombe has also completed a simple actuator disc analysis of a flow in which the flow on either side of the disc is of constant stagnation pressure but variable skew. This work is directly analagous to the earlier work by Hawthorne and Armstrong (27) and Hawthorne and Horlock (28) for the shear flow through cascades of high solidity, in which the component of the vorticity is perpendicular to the stream. Again this work is not discussed in detail here as it has yet not appeared in published form.

Perhaps the most important part of Kingcombe's work is an aerofoil analysis of Beltrami flows through cascades (see also (29)). This analysis involves an assumption from the work of Hawthorne and McCune (30) in which it is shown that accurate estimates of induced velocity may be obtained if it is assumed that the shed and trailing vortex filament lines lie along the undisturbed flow paths downstream of the cascade. Kingcombe first solves for the cross-flow velocity c_{n_2}', due to the distributed vorticity in the channel

$$c_{n_2}' = -\int_z^\infty \omega_{s_2}\, dz \tag{12}$$

He then considers additional secondary velocities c_n'', c_z'' due to the trailing filament (TF) and shed vorticity (TS) solving a Poisson type equation

$$\nabla^2\psi'' = -\left[\omega_{TF} + \omega_{TS}\right] \sum_{m=-\infty}^{m=+\infty} \delta(n - mS) \tag{13}$$

where $\omega_{TF} = S\cos\alpha_2 \frac{d\alpha_1}{dz} \oint \frac{dz}{c}$, $\omega_{TS} = \frac{d\Gamma}{dz}$ and δ is the Dirac delta function. He then relates the circulation distribution along the span, $\Gamma(z)$, to the velocities induced at the blade lifting line by the total streamwise vorticity. The solution of the simultaneous equations for ψ'' and Γ is complex but is an important step forward in the analysis of secondary flows, including Beltrami effects.

3.3 Boundary Layer Calculations

We next review recent attempts to integrate some results from secondary flow analysis into the boundary layer work undertaken by Mellor and Wood (31) and Horlock and Perkins (32) respectively.

The solution of the secondary velocities induced by the streamwise vorticity is a complex process (see Section 2.12 above). Horlock (33) attempted to obtain approximate solutions to the cross-flow in the secondary flow in cascades, basing the solution on a modification of the cross-flow c_n observed in three-dimensional boundary layers by Johnson (16). This latter is expressed in the form

$$c_n = 2\delta\alpha\left(C_s - c_s\right) \tag{14}$$

is illustrated in Fig. 6, and may be derived simply from equation (3). If the entry vorticity is dc_s/dz, and for wide blade spacing the exit vorticity is $-dc_n/dz$, then since $R\,d\alpha = ds$, Eq.(3) yields

$$\frac{d\omega_n}{dz} = -2\delta\alpha\,\frac{dc_s}{dz} \tag{15}$$

which integrates to Eq.(14), since $c_n = 0$ at $y = \delta$, where $c_s = C_s$. Horlock's modification of the cross-flow velocity due to finite blade spacing is

$$c_{n_2} = \left[2\delta\alpha\left(C_s - c_s\right) - C_s k\,\delta^*\exp\left(-kz\right)\right] \tag{16}$$

where $k = \sqrt{12}/S'$, δ^* is the streamwise displacement thickness and $S' = S\cos\alpha$ is the "staggered" blade spacing. This describes the cross-flow distribution at exit from a cascade (Fig. 2), perpendicular to the mainstream outside the boundary layer; the last term arises from finite blade spacing. An initial assumption is made in the analysis for the form of the secondary velocities within the channel (a parabolic variation for the cross-flow velocities and a linear variation for the spanwise velocities, both across the pitch).

The basis of the integral equation methods for calculating turbomachinery wall boundary layers is the simultaneous solution of two integral equations in the s and n directions. Derivations of such equations are given by Mellor and Wood (31), by Horlock and Marsh (34) and by Horlock and Perkins (32); in the last paper they are rewritten in terms of streamwise and cross-flow thicknesses (θ_{ss}, θ_{sn}, θ_{nn}, H_1, H_4) as dependent variables

of x (the independent variable):

$$\frac{d\theta_{ss}}{dx} - \tan\alpha_s\left[\frac{d\theta_{ns}}{dx} + (\theta_{ss} - \theta_{nn})\frac{d\alpha_s}{dx}\right] + P(2\theta_{ss} + \delta_s^*) - Q(2\theta_{sn} + \delta_n^*) = \frac{\tau_w}{\rho C_x^2}\cos\epsilon_w\cos\alpha_s + \frac{D_y}{2C_x^2}\sin 2\alpha_s + \frac{D_x}{C_x^2}\cos^2\alpha_s \quad (17)$$

$$\frac{d\theta_{ns}}{dx} - \tan\alpha_s\left[\frac{d\theta_{nn}}{dx} + 2\theta_{ns}\frac{d\alpha_s}{dx}\right] + P\left[2\theta_{ns} - \tan\alpha_s(\theta_{ss} + \theta_{nn} + \delta_s^*)\right] + Q(\theta_{ss} + \delta_s^* - \theta_{nn}) = \frac{\tau_w}{\rho C_x^2}\sin\epsilon_w\cos\alpha_s + \frac{D_y\cos^2\alpha_s}{C_x^2} - \frac{D_x\sin 2\alpha_s}{C_x^2} \quad (18)$$

where τ_w is wall shear stress, ϵ_w is the wall shear stress angle as shown in Fig. 4 and

$$P = \frac{1}{C_x}\frac{dC_x}{dx} + C_x\tan\alpha_s\frac{d\alpha_s}{dx}, \quad Q = \frac{1}{C_x}\frac{d}{dx}(C_x\tan\alpha_s)$$

$$\delta_s^* = \int_0^\delta\left(1 - \frac{c_s}{C_s}\right)dz \qquad \delta_n^* = \int_0^\delta\frac{c_n}{C_s}dz \qquad \theta_{ss} = \int_0^\delta\frac{c_s}{C_s}\left(1 - \frac{c_s}{C_s}\right)dz$$

$$\theta_{nn} = \int_0^\delta\left(\frac{c_n}{C_s}\right)^2 dz \qquad \theta_{sn} = \int_0^\delta\left(1 - \frac{c_s}{C_s}\right)\frac{c_n}{C_s}dz \qquad \theta_{ns} = \int_0^\delta\left(\frac{c_s c_n}{C_s}\right)dz$$

These are averaged equations across the pitch of the blades and there are extra terms which do not arise in normal boundary layer equations. These are the so-called deficit terms D_x and D_y which are defined as follows:

$$D_x = D_{x_1} + D_{x_2} + D_{x_3} \quad (19)$$

$$D_{x_1} = \int_0^\delta\frac{(F_y - f_y)}{\rho}\tan\alpha_s dz \quad (20)$$

$$D_{x_2} = \int_0^\delta\frac{\partial}{\partial x}\left(C_x'^2 - c_x'^2\right)dz \quad (21)$$

$$D_{x_3} = \frac{1}{\rho}\int_0^\delta\left[\left(\frac{d\bar{p}}{dx}\right)_\delta - \left(\frac{\partial\bar{p}}{\partial x}\right)\right]dz \quad (22)$$

$$D_y = D_{y_1} + D_{y_2} \quad (23)$$

$$D_{y_1} = \int_0^\delta(F_y - f_y)\,dz \quad (24)$$

$$D_{y_2} = \int_0^\delta\frac{\partial}{\partial x}\left(C_x'C_y' - c_x'c_y'\right)dz \quad (25)$$

The terms D_{x_1} and D_{y_1} arise from a variation in the tangential component of the blade force through the boundary layer, from (f_y) to (F_y). The terms D_{x_2} and D_{y_2} arise from variations in the perturbation in axial and tangential velocity (c_x', c_y') from the pitchwise mean values ($\bar{C}_x$, $\bar{C}_y$), through the boundary layer. The term D_{x_3} arises from variation of the mean pressure gradient ($\frac{\partial\bar{p}}{\partial x}$) through the boundary layer.

It is shown from inviscid secondary flow analysis by Horlock and Perkins that the summation term D_x is zero. This follows from consideration of the mean axial momentum equation and the averaged continuity equation, both within a Bernoulli surface, which for the small shear/large deflection assumption does not rotate in passage through a cascade. The combination of axial momentum and continuity equation gives

$$-\frac{1}{\rho}\frac{\partial\bar{p}}{\partial x} - \frac{f_y\tan\alpha_s}{\rho} - \frac{\partial}{\partial x}(c_x'^2) = 0 \quad (26)$$

which, when integrated through the boundary layer, gives the result $D_x = 0$.

It is also shown by Horlock and Perkins, following work by Lindsay (35), that an estimate may be made of the term D_{y_1} from the cross-flow expressions (15) and (16) given by Johnston and Horlock.

For wide spacing it may be shown that the Johnston cross-flow velocity distribution leads to $D_{y_1} = 0$. For finite spacing, the Horlock cross-flow velocity distribution (Eq.(16)) may be used to obtain D_{y_1}. Assuming a one/seventh power boundary layer and taking the integral to $z = 2\delta$ Lindsay (35) obtains

$$D_{y_1} = C_x^2(2\delta - \delta_s^*)\frac{4\sqrt{3}}{S}\delta_s^*\sec^3\alpha\frac{d\alpha}{dx} \quad (27)$$

Some results from Lindsay's method of calculation (using $D_x = 0$ and $D_y = D_{y_1}$) are illustrated in Fig. (7) for the flow through a row of inlet guide vanes. The axial velocity profiles are shown at entry and exit, together with the flow angle variations through the wall boundary layer.

A more comprehensive experimental investigation of this approach is given by Papailiou, Flot and Mathieu in reference (36). They have compared their measurements of the defect forces D_{x_1}, D_{y_1} in cascade flows with the analysis outlined above. Agreement between theory and experiment appears to be good for turbines (Fig. 8), less good for compressors, although it is not clear that the correct analytical term has been used for D_{y_1}. Prediction of boundary layer thickness appears to be surprisingly good for turbine cascades and surprisingly poor for compressor cascades.

These authors have also looked at the detailed assumptions of Mellor's analysis, in particular the assumption that the spanwise direction of the blade force in the cascade is constant through the boundary layer. They found that this was quite a good assumption for the flow through a cascade in which the entry flow was collateral (i.e. no Beltrami effect was present).

It is clear from this recent work that the integral boundary layer method for the calculation of wall boundary layer thickness is quite well developed, although it does not always give exactly the right answers. The effects of tip clearance are critical and Horlock found it necessary to make somewhat sweeping assumptions for the form of the deficit when clearance was present. Nevertheless, good estimates of axial and momentum thickness growth can be made for actual compressors (see (32)).

[illegible] has reservations about whether this work can be taken much further. The computer programs are readily available and can be used to obtain quite good estimates of blockage within compressors, if not the full detail of boundary layer development including cross-flows. However, it is clear that in the turbine, where the boundary layer is swept off the wall and a new boundary layer is created, these integral momentum methods are unlikely to prove adequate.

3.4 Detailed Calculations of Three-Dimensional Flow

The alternative to these "pitch-averaged" methods must be the three-dimensional calculation of the full details of the fluid flow within each blade row. Here there have been two major developments recently; the work of Stuart and Hetherington (21) and the work of Patankar, Pratap and Spalding (37, 38). The work of Stuart and Hetherington is briefly described as follows.

The equations of motion are written in curvilinear co-ordinates, and calculations performed on a fixed grid based on streamlines computed outside the boundary layer. The velocity in the (mainstream) streamwise direction is written as c_3 and the other two velocity components are written as $\lambda_1 c_3, \lambda_2 c_3$. The basic equations (one continuity and three momentum) are rewritten in the form (one continuity, two momentum (across the stream) and one Bernoulli). The two momentum equations are solved for c_3^{I}, c_3^{II} from a previous iteration which gave λ_1, λ_2 and the pressure. The difference between the solutions c_3^{I} and c_3^{II} is inserted as a source/sink term ($\rho(c_3^{I} - c_3^{II})$) into two continuity equations, which are solved for λ_1, λ_2.

Pressure is obtained by tracing back, using the Bernoulli equation, and is substituted into the momentum equation on the next iteration. Computation continues until the source term goes to zero.

Carrick (39) has extended this approach by allowing for stagnation pressure loss along the streamlines. At present this extension involves a somewhat crude assumption that the turbulent kinetic energy (k) along the streamline remains constant and that the local shear stress (proportional to k) remains unchanged. The associated loss in stagnation pressure is calculated and put into the Stuart and Hetherington method through modification of the Bernoulli equation. Surprisingly small differences result from the addition of the viscous terms to the calculation of flow in cascades. Comparison of the calculation of stagnation pressure contours in a turbine cascade with and without viscous dissipation are given by Carrick in reference (39) and later in this conference.

The methods of Patankar, Pratap and Spalding (37) and Pratap and Spalding (38) are based on different methods, in which viscous effects are included from the start. A brief description of these methods is as follows.

Spalding and his co-workers transform the equations of motion (three momentum equations and one continuity equation) into finite difference equations by volume integration of the local equations over a small control volume. Similarly they employ two finite difference equations for the turbulence. The turbulence parameters that are used are the turbulent kinetic energy k; a turbulent length scale l_t; and the volumetric rate of dissipation is ϵ_d which is proportional to $k^{3/2}/l_t$. The turbulent viscosity is

$$\mu_t = C_\mu' \rho k^{\frac{1}{2}} l_t \qquad (28)$$

OR

$$\mu_t = C_\mu \rho k^2/\epsilon_d \qquad (29)$$

There are two governing equations for k and ϵ_α; with these solved locally the shear stress may be derived from (29) and substituted into the main equations of motion.

The key to the first method of solution (Patankar/Pratap/Spalding - PPS - the parabolic method) is that an average pressure $\bar{p}$ used in the mainstream direction is decoupled from the "cross-stream" distribution of pressure ($p(r,\theta)$ say). The pressure distribution $\bar{p}(s)$ is first guessed, together with the pressure distribution $p(r,\theta)$ at the downstream station. The finite difference momentum equations are then solved for a first approximation to the downstream velocity distribution (c_s, c_r, c_θ say). The mean pressure and the through flow velocity (c_s) are then corrected from the continuity and longitudinal momentum equations to ensure continuity of mass flow. The cross-stream velocities do not then satisfy the continuity equation locally so these are then corrected from linearized cross-stream momentum equations together with the pressure field. Finally, the kinetic energy and dissipation equations are solved to provide the new values of k and ϵ_α at the downstream station; the shear stress is thus determined and the forward step to the next station may then be taken. However, if large steps are taken in the through flow direction, then the velocity changes are under relaxed and the first operations are repeated at the same section, the new values of pressure, kinetic energy and dissipation being used in the current step before movement to the next station.

In the second method (Pratap and Spalding - PS - the partially parabolic method) the pressure $\bar{p}$ is not used, the actual pressure being stored in a three-dimensional array. All other variables (velocity components, turbulence parameters, which are stored in two-dimensional arrays) are evaluated over the cross-stream planes, by marching in the mainstream direction. The pressure field is then updated (in similar fashion to the PPS method) by removing errors in continuity and momentum.

Clearly this second (PS) method should be used in flows with sharp curvature, in which pressure effects are transmitted far upstream. Spalding and his colleagues have had remarkable success in the prediction of the total pressure contours in a closed duct (a curved pipe flow). They have still to tackle the problem of a three-dimensional flow through a cascade, with its associated problem of the definition of the trailing edge conditions where streamwise vorticity will be shed.

However, we may conclude that these two groups of workers have made considerable strides in the calculation of the detailed three-dimensional flow. It appears probable that this type of analysis is the only one that can be used for the flow through turbine cascades, where the variations across the pitch are very large due to strong secondary vorticity, and local flow separations may take place. This is illustrated below in discussion of some recent experimental work.

4. Experimental Work

4.1 Cascade Experiments

Apart from the work of Papailiou et al referred to already, the main experimental work carried out recently has been on compressor and turbine cascades. We refer here to the work of Salvage (40) on compressor cascades, and Langston (41) and Carrick (39) on turbine cascades.

Salvage (40) has described some detailed measurements of secondary flow in compressor cascades. He had some success in predicting angle variations using the analysis of reference (33), confirmed that a critical parameter was not aspect ratio (height (L)/Chord (l)) but δ_1^*/L (inlet boundary layer thickness (δ_1^*)/height (L)), and showed that away from the region with concentrated passage vorticity, boundary layer development could be quite well described.

Langston (41) has traced in detail the development of the boundary layer flow through a turbine cascade, amplifying earlier similar work by Armstrong (42). The important new experimental information is the discovery of a saddle point, the intersection of attachment and separation lines near the leading edge of a blade.

Parallel work by Carrick has been directed at the analysis of skewed flows in turbine blade rows. Carrick describes the flow coming into a rotating blade row from a turbine nozzle, as is illustrated in Fig. 9. The relative flow into the rotating blade is strongly skewed, with high streamwise (Beltrami) vorticity. Carrick therefore set up a cascade experiment with a moving wall in front of the cascade by which he could create such a skewed flow. He confirmed the basic flow with a saddle point observed by Langston (41) and he then showed that the secondary vorticity was more intense when the moving wall was introduced; all the effects observed by Langston became exaggerated with entry skew. Fig. 10 shows the saddle points observed by Carrick (i) with zero entry skew, and (ii) high entry skew, and the flow directions at the surface.

Carrick compared his observations with three methods of calculation:

1. a pitch-averaged boundary layer analysis,

2. the Stuart and Hetherington analysis (including dissipation),

3. a three-dimensional boundary layer analysis based on developments of work by Dring (43) and Smith (44).

The full details of Carrick's work are given in a later paper. For the purposes of this review we simply conclude that the integral type analysis is valid only for about the first 30% of the cascade - it cannot describe the major disruption of the flow that occurs subsequently. The three-dimensional boundary layer analysis gives a fair description of the flow (it is integrated with secondary flow analysis which give the velocities at the edge of the boundary layer). Finally, the detailed calculations of Stuart and Hetherington give a surprisingly good description of the flow, even without allowance for viscosity.

We conclude from this work on turbines that it is unlikely that we should be able to develop an integral boundary layer analysis which will be adequate to describe the flow through turbines row by row. There thus appears to be some chance of calculating the detailed flow within a turbine blade passage (using either the Stuart and Hetherington method or the work of Spalding et al). However, the prospects of dealing with the trailing edge problems at each blade row, of switching co-ordinates from stationary to rotating blade rows and vice versa and hence of undertaking a full detailed calculation, row by row through a turbomachine, appear extremely remote.

The compressor problem appears to be less intractable. As the secondary rotations are always small in compressors, where the secondary vorticity grows then decreases in rotors and stators (see Horlock (45)), the boundary layer remains a valid description of the end wall region.

4.2 Loss Correlations

Finally, on the experimental work we must note the up-dating of Dunham's loss expressions by Morris, who gives the expression for total pressure loss coefficient as

$$Y_S = \frac{p_{01} - p_{02}}{p_{02} - p_2} = \frac{\ell}{L} \frac{\cos\alpha_2}{\cos\beta_1} \left(\frac{C_L}{S/\ell}\right)^2 \frac{\cos^2\alpha_2}{\cos^3\alpha_m} \left(0.011 + 0.294 \frac{\delta_1^*}{\ell}\right) \qquad (30)$$

where ℓ is now chord, C_L is lift coefficient and α_m denotes mean angle. (see (46)).

5. Conclusions

The paper has reviewed recent theoretical and experimental work on secondary flows. For small flow deflections, inviscid secondary flow theory, integrated with boundary layer analysis, can give good descriptions of end-wall flows in turbomachines. However, if the secondary rotations become excessive, as they appear to do in turbine rows (where the inlet Beltrami vorticity adds to the conventional mechanism of growth of secondary vorticity), then resort to numerical analysis must be made. In compressors the Beltrami flow opposes the conventional mechanism of growth of secondary vorticity, secondary rotations are small, and the pitch-averaged boundary layer analysis is a powerful tool for the designer.

Bibliography

1. Lakshminarayana, B. Horlock, J. H. — Review - Secondary flows and losses in cascades and axial flow turbomachines. Int. J. Mech. Sci., Vol.5, 1963, p.287.

2. Horlock, J. H. Lakshminarayana, B. — Secondary flows: theory, experiment and application in turbomachinery aerodynamics. Ann. Rev. Fluid Mech., Vol.5, 1973, p.247.

3. Lakshminarayana, B. Horlock, J. H. — Generalized expressions for secondary vorticity using intrinsic co-ordinates. J. Fluid Mech., Vol.59(1), 1973, p.97.

4. Squire, H. B. Winter, K. G. — The secondary flow in a cascade of aerofoils in a non-uniform stream. J. Aero. Sci., Vol.18, 1951, p.271.

5. Hawthorne, W. R. — Secondary circulation in fluid flow. Proc. Roy. Soc. A. Vol.206, 1951, p.374.

6. Marris, A. W. — Generation of secondary vorticity in a stratified fluid. J. Fluid Mech., Vol.20, 1964, p.177.

7. Hawthorne, W. R. — Some formulae for the calculation of secondary flow in cascades. 1955, Aero. Res. Council Rep.17,519.

8. Smith, L. H. — Secondary flow in axial flow turbomachinery. Trans. ASME, Vol.77, 1955, p.1065.

9. Hawthorne, W. R. — Fluid mechanics of internal flow. (ed. G. Sovran), Amsterdam: Elsevier, 1967, p.268.

10. Ehrich, F. F. Detra, R. W. — Transport of the boundary layer in secondary flow. J. Aero. Sci., Vol.21, 1954, p.136.

11. Armstrong, W. D. — The non-uniform flow of air through cascades of turbine blades. Ph.D Thesis, Cambridge University, 1954.

12. Lakshminarayana, B. Horlock, J. H. — Effect of shear flows on the outlet angle in axial compressor cascades - methods of prediction and correlation with experiments. J. Basic. Eng., Trans. ASME D, Vol.89, 1967, p.191.

13. Hawthorne, W. R. — Rotational flow through cascades (Part I). Quart. J. Mech. Appl. Math., Vol.8, 1955, p.266.

14. Marsh, H. & Came, P. — Secondary flow in cascades. J. Mech. Eng. Sci., Vol.16, 1974, p.402.

15. Namba, M. — Lifting-surface theory for cascade of blades in subsonic shear flow. J. Fluid. Mech., Vol.36, 1969, p.735.

16. Johnston, J. P. — On the three-dimensional turbulent boundary layer generated by secondary flow. J. Basic. Eng., Trans. ASME D, Vol.82, 1960, p.233.

17. Howell, A. R. — The present basis of axial flow compressor design. 1942, Aero. Res. Council R & M 2095.

18. Vavra, M. H. — Aero-thermodynamics and fluid flow in turbomachines. New York: John Wiley, 1960.

19. Ainley, D. G. Mathieson, G. C. R. — An examination of the flow and pressure losses in blade rows of axial turbines. 1951, Aero. Res. Council R & M 2891.

20. Dunham, J. — A review of cascade data and secondary losses in turbines. J. Mech. Eng. Sci., Vol.12, 1970, p.49.

21. Lakshminarayana, B. Britsch, W. R. Gearhart, W. S. — The fluid mechanics, acoustics and design of turbomachines (Part I). NASA. SP 304, 1974.

22. Hawthorne, W. R. — Secondary vorticity in stratified compressible fluids in rotating systems. 1974, Cambridge University TR 63.

23. Greitzer, E. M. — A note on the non-existence of secondary flows. 1976, Cambridge University TR 76.

24. Horlock, J. H. Marsh, H. — Flow models for turbomachines. J. Mech. Eng. Sci., Vol.13 (5) 1971, p.358.

25. Marsh, H. — Secondary flow in cascades - the effect of compressibility. 1976, Aero. Res. Council R & M 3778.

26. Kingcombe, R. C. — Beltrami flows in cascades. Ph.D Thesis, Cambridge University, 1976.

27. Hawthorne, W. R. Armstrong, W. D. — Shear flow through a cascade. Aero. Quart., Vol.VII, 1956, p.247.

28. Hawthorne, W. R. Horlock, J. H. — Actuator disc theory applied to wall boundary layers in cascades. 1952, Aero. Res. Council Rep. 15490.

29. Kingcombe, R. C. — A lifting line approach to secondary flows. 1974, Cambridge University TR 61.

30. McCune, J. E. Hawthorne, W. R. — The effects of trailing vorticity on the flow through highly loaded cascades. J. Fluid Mech., Vol.74(4), 1976, p.721.

31. Mellor, G. L. Wood, G. M. — An axial compressor end-wall boundary layer theory. J. Basic Eng. Trans. ASME D, Vol.93, 1971, p.300.

32. Horlock, J. H. Perkins, H. J. — Annulus wall boundary layers in turbomachines. 1974, AGARDograph AG-185.

33. Horlock, J. H. — Cross-flows in bounded three-dimensional turbulent boundary layers. J. Mech. Eng. Sci., Vol.15(4), 1973, p.274.

34. Marsh, H. Horlock, J. H. — Wall boundary layers in turbomachines. J. Mech. Eng. Sci., Vol.14(6), 1972, p.411.

35. Lindsay, W. L. — Tip clearance effects in the growth of annulus wall boundary layers in turbomachines. Ph.D Thesis, Cambridge University, 1974.

36. Papailiou, K, Flot, R. Mathieu, J. — Secondary flows in compressor bladings. 1976, Trans. ASME. Paper 76-GT-57.

37. Patankar, S. V. Pratap, V. S. Spalding, D. B. J. — Prediction of turbulent flow in curved pipes. J. Fluid Mech., Vol.67(3), 1975, p.583.

38. Pratap, V. S. Spalding, D. B. — Numerical computations of the flow in curved ducts. Aero. Quart., Vol.XXVl, 1975, p.219.

39. Carrick, H. B. — Secondary flow and losses in turbine cascades with inlet skew. Ph.D Thesis, Cambridge University, 1976.

40. Salvage, J. — Investigation of secondary flow behaviour and end-wall boundary layer development through compressor cascades. Doctoral Thesis, University of Brussels, 1974.

41. Langston, L. S. Nice, M. L. Hooper, R. M. — Three-dimensional flow within a turbine cascade passage. 1976. Trans. ASME. Paper 76-GT-50.

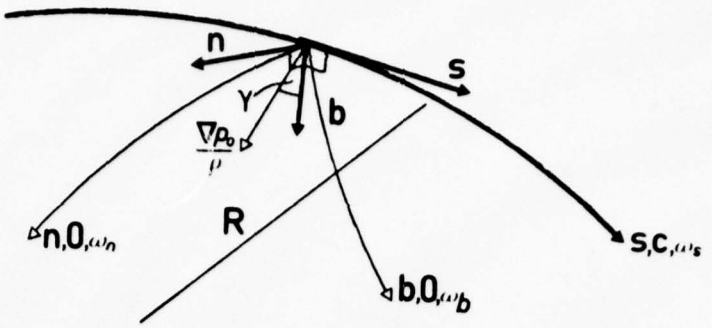
42. Armstrong, W. D. — Secondary flow in a cascade of turbine blades. 1957, Aero. Res. Council R & M 2979.

43. Dring, R. P. — Momentum integral analysis of three-dimensional turbine end-wall boundary layers. J. Eng. for Power, Trans. ASME. Vol.93, 1971, p.386.

44. Smith, P. D. — An integral prediction method for three-dimensional compressible turbulent boundary layers. 1974, Aero. Res. Council R & M 3739.

45. Horlock, J. H. — Annulus wall boundary layers in axial compressor stages. Trans. ASME D, Vol.85, 1963, p.55.

46. Morris, A. W. H. Hoare, R. G. — Secondary loss measurements in a cascade of turbine blades with meridional wall profiling. 1975, Trans. ASME Paper 75-WA/GT.



s,n,b coordinates

p_0 total pressure

ρ density

c velocity

ω vorticity

γ angle between b direction and gradient of total pressure

R principle radius of curvature of streamline

Fig.1 Notation used for natural coordinate system

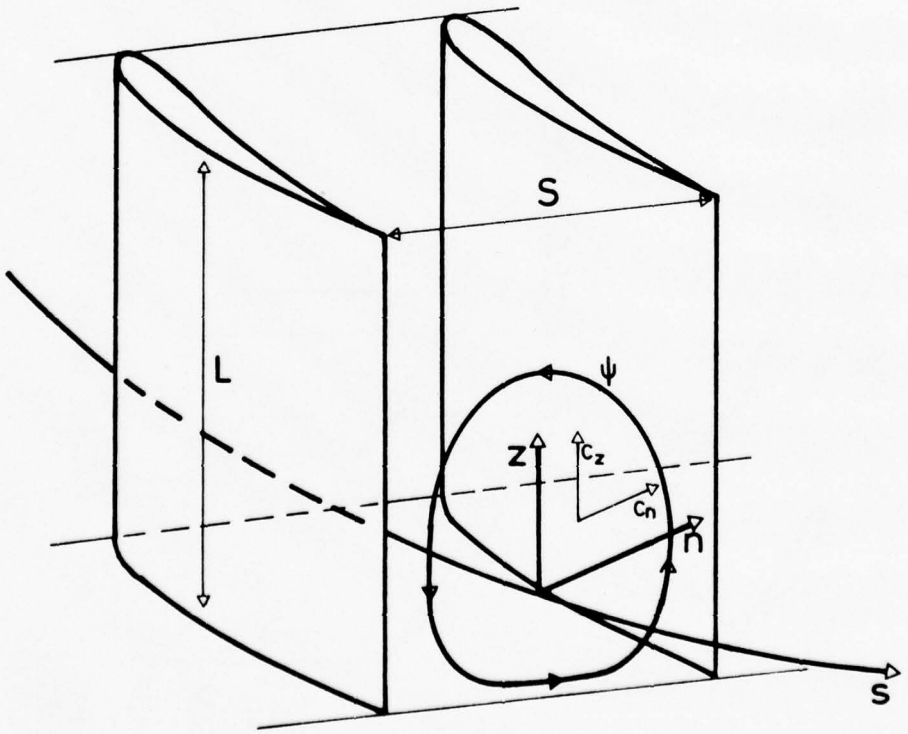


Fig.2 Secondary flow in a cascade

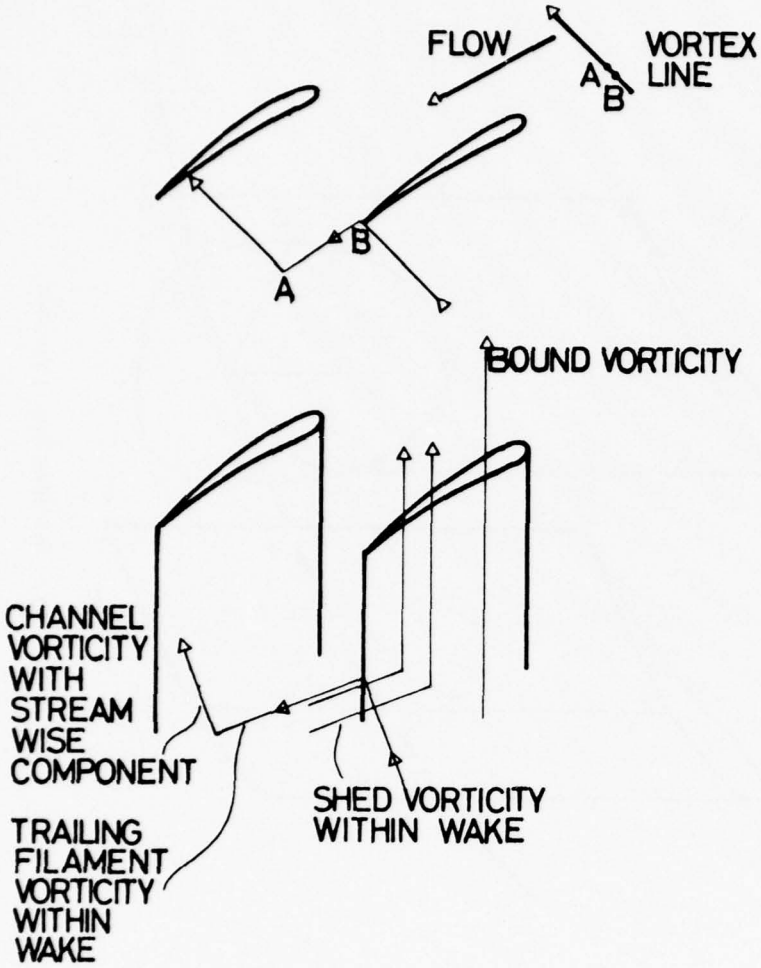


Fig.3 Vortex geometry

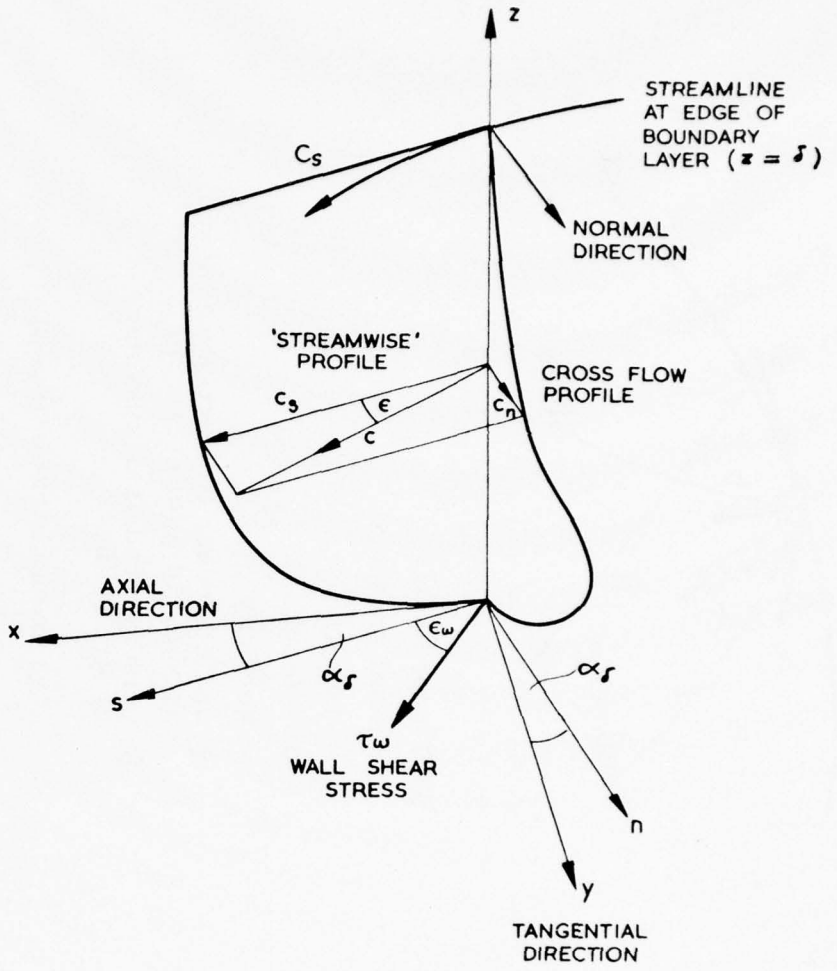


Fig.4 Boundary layer velocity distribution

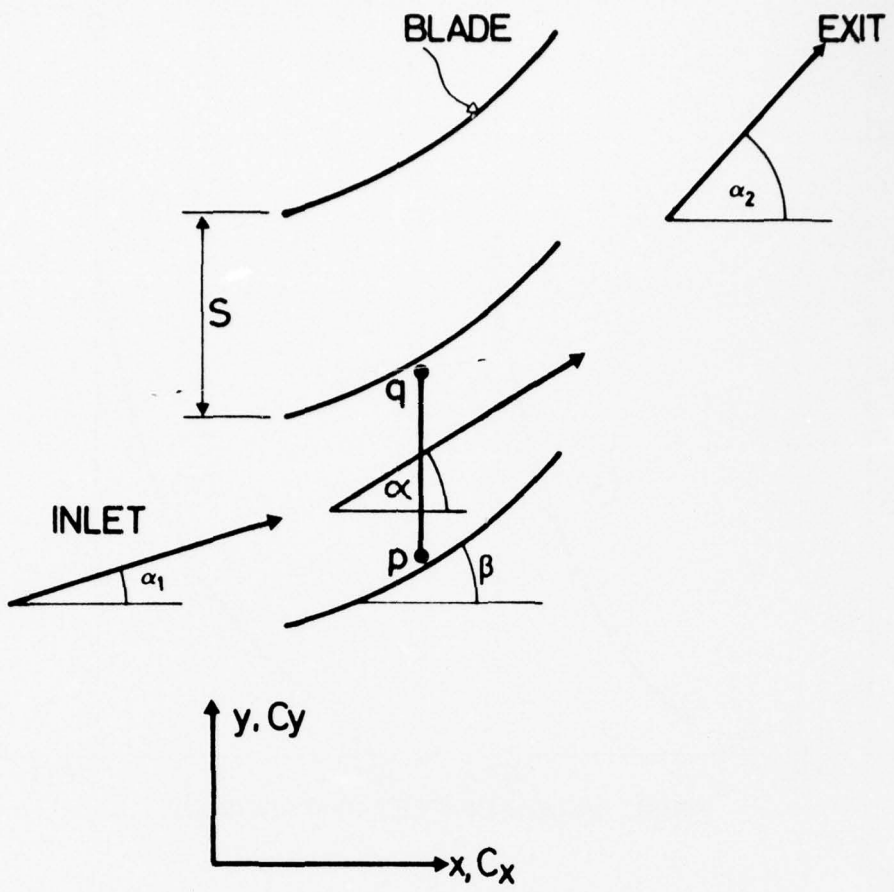


Fig.5 Pitch-averaged flow in a cascade of thin blades

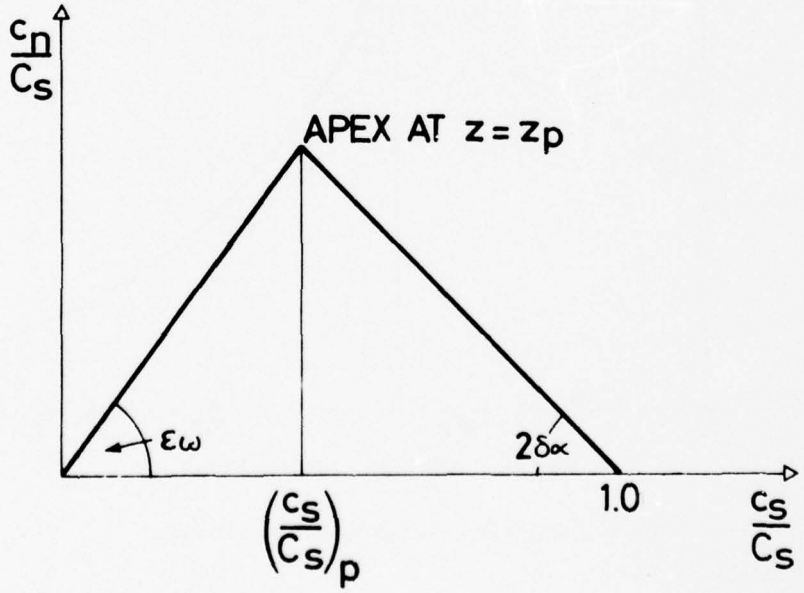


Fig.6 The Johnston cross flow profile

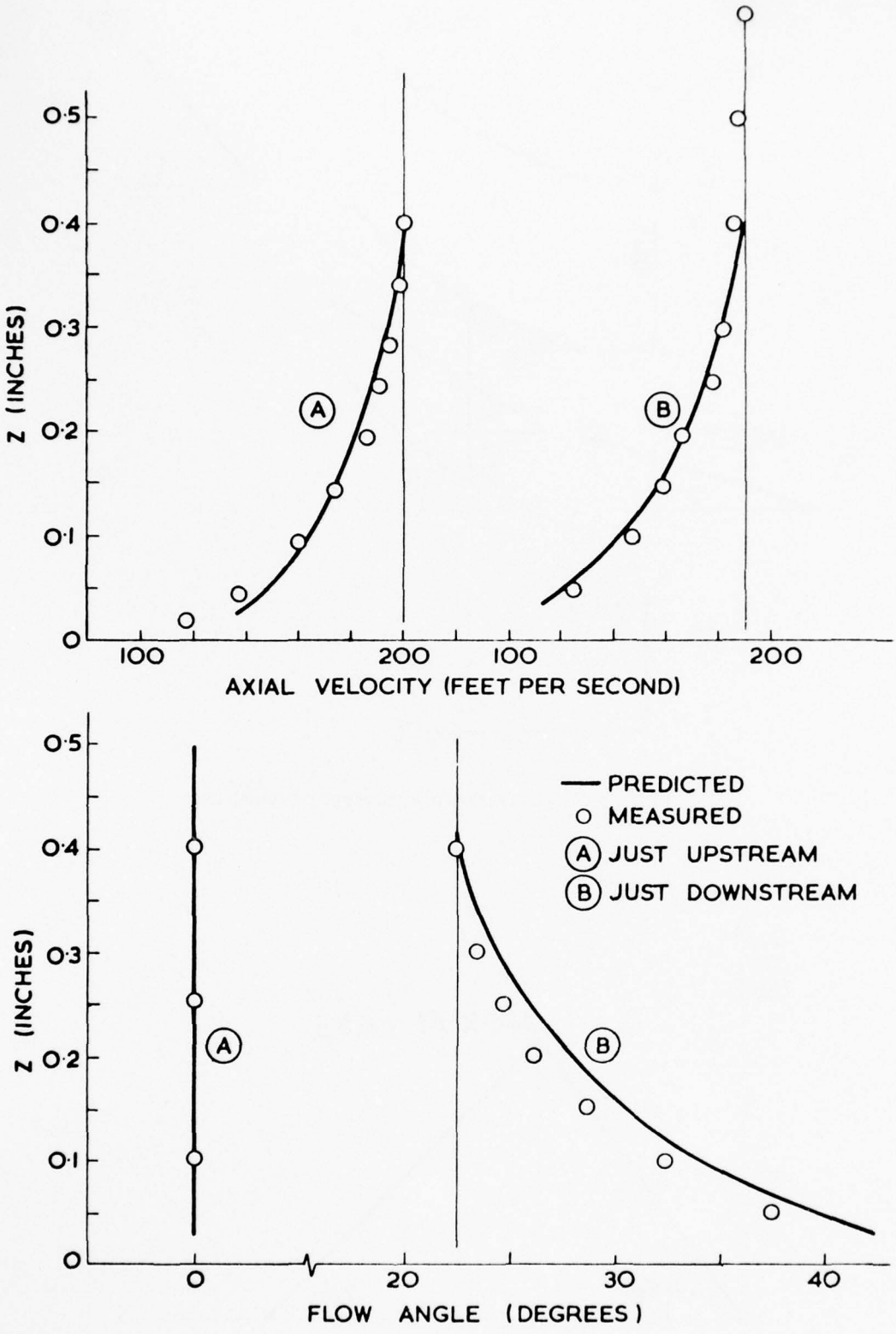


Fig.7 Detailed flow through Horlock's guide vanes

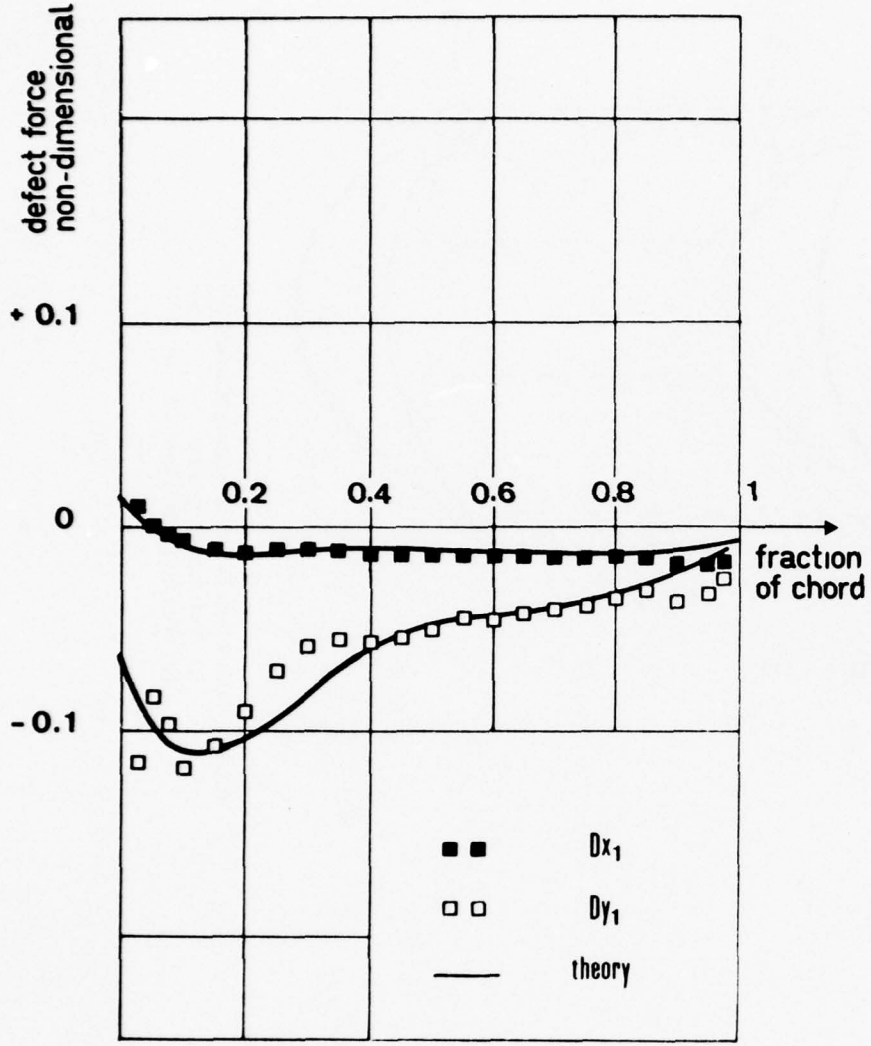


Fig.8 Distribution of the blade defect force inside the passage of a turbine cascade (after Papailiou et al.)

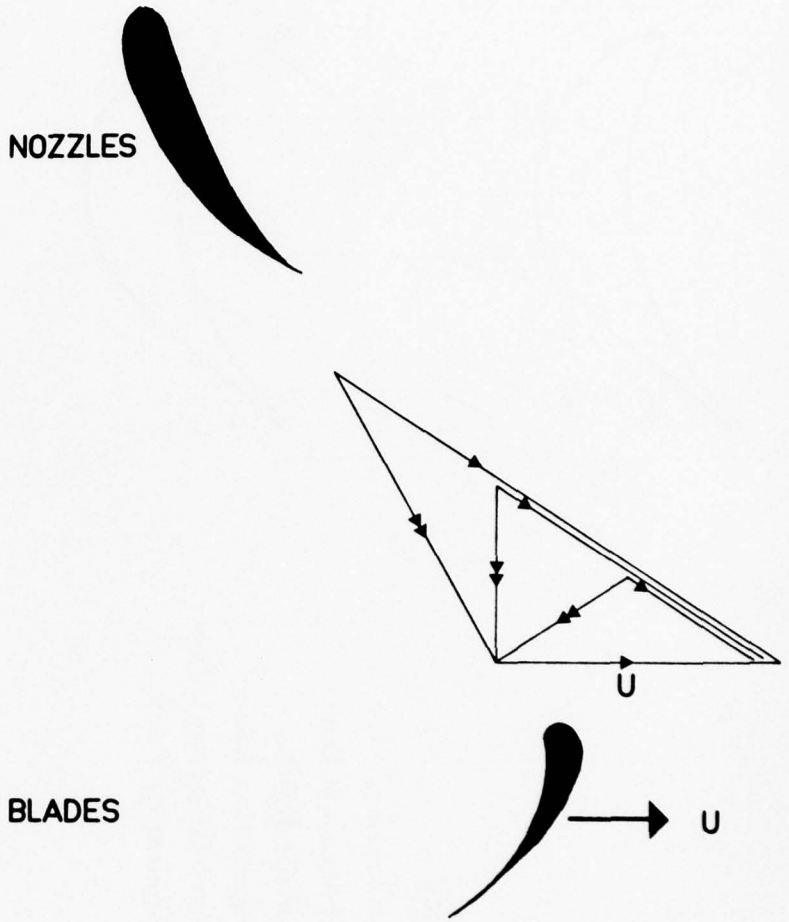
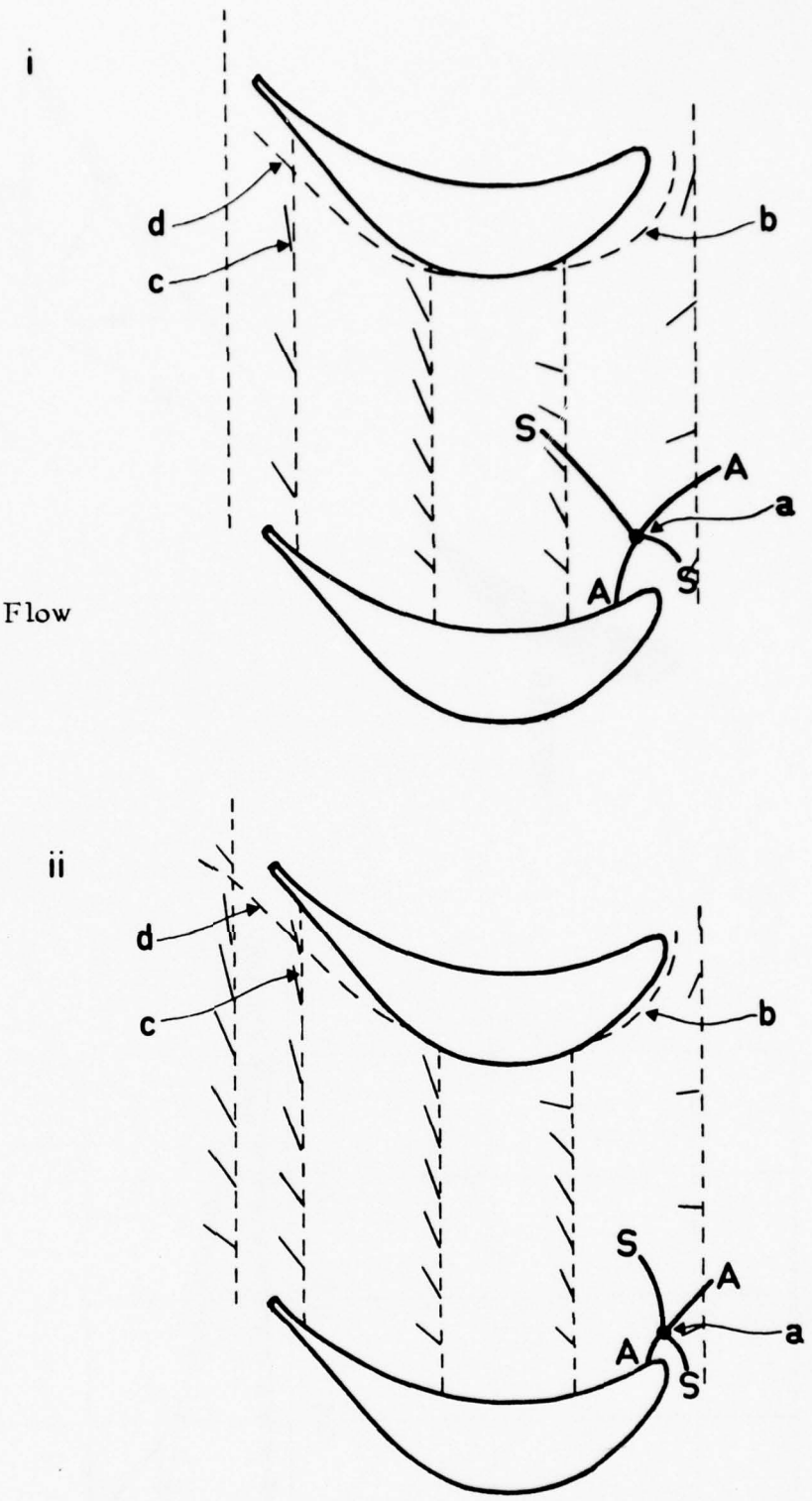


Fig.9 Skewed relative velocities at entry to turbine rotor blades



key

A Attachment Line
S Separation Line
a Saddle Point
b Separation Zone
c Near Tangential Flow
d Separation Zone

Fig.10 Surface flow in turbine cascade (Carrick)
(i) With zero entry skew
(ii) With high entry skew

CALCULATIONS CONCERNING THE SECONDARY FLOWS IN COMPRESSOR BLADINGS

F. LEBOEUF[1], A. COMTE[2], K.D. PAPAILIOU[3]
ECOLE CENTRALE DE LYON
Laboratoire de Mécanique des Fluides
36, route de Dardilly, 36
Boîte Postale 163
69130 ECULLY (France)

1 Assistant, Ecole Centrale de Lyon
2 Boursier C.N.R.S.
3 Maître de Conférences Associé, Ecole Centrale de Lyon

SUMMARY

The behaviour of secondary flows in compressors is analysed by using an integral method of calculation based on MELLOR's theory and a radial equilibrium calculation method. The comparison of theory with experiment is finally discussed.

NOMENCLATURE

c_f	skin friction coefficient
F	blade force
H	shape factor
g	gap
h	enthalpie
K	empirical constant
M	mach number
R	radius
R_g	perfect gas constant
S	entropy
U	axial velocity
U_w	velocity of the end wall
V	velocity relative to the blades
W	circumferential velocity
β	relative angle
γ	specific heat ratio
γ_s	stagger angle
δ	boundary layer thickness
δ_c	clearance
δ^*	displacement thickness
ε	blade forces angle parameter
θ	momentum thickness
ρ	density
σ	solidity
Σ	density function
ϕ	function of the stream function derivations
τ_w	wall shear stress

SUBSCRIPTS

e	external condition
m	meridional direction
n	transversal direction
o	reference condition
s	longitudinal direction
t	total condition
x	axial direction
y	radial direction
z	circumferential direction
1	upstream condition
2	downstream condition

LIST OF FIGURES

Fig. 1. The function $\Phi(\Sigma)$

Fig. 2. Comparison between theory and experiment for the axial and tangential values of the wall shear layer integral quantities. Nominal conditions.

Fig. 3. Comparison between theory and experiment for the axial and tangential values of the wall shear layer integral quantities. Conditions near surge.

Fig. 4. Comparison between theory and experiment for the free stream flow at station 2. Meridional velocity, nominal conditions.

Fig. 5. Comparison between theory and experiment for the free stream flow at station 2. Meridional velocity, conditions near surge.

Fig. 6. Comparison between theory and experiment for the free stream flow at station 2. Absolute angle, nominal conditions.

Fig. 7. Comparison between theory and experiment for the free stream flow at station 2. Absolute angle, conditions near surge.

Fig. 8. Comparison between theory and experiment for the free stream flow at station 2. Total pressure, nominal conditions.

Fig. 9. Comparison between theory and experiment for the free stream flow at station 2. Static pressure, nominal conditions.

Fig. 10. Comparison between theory and experiment for the free stream flow at station 3. Total pressure, nominal conditions.

Fig. 11. Comparison between theory and experiment for the free stream flow at station 3. Static pressure, nominal conditions.

Fig. 12. Comparison between theory and experiment of the longitudinal and transversal velocity profiles at the rotor hub exit. Nominal conditions.

Fig. 13. Comparison between theory and experiment of the longitudinal and transversal velocity profiles at the rotor hub exit. Conditions near surge.

1. INTRODUCTION

Looking back in recent years, one may realize that, in most cases, the equations used for the calculation of a wall shear layer are the turbulent Navier-Stokes equations circumferentially averaged, as they were first introduced by Railly[1] and later by Mellor[2] and Horlock[3]. Besides the new unknowns (turbulent stresses) introduced by the statistical averaging of the Navier-Stokes equations, some more unknowns are introduced through the circumferential averaging : (a) the "fluctuation terms" expressing the deviation of the velocity components from their mean values in the circumferential direction, and (b) the blade force terms.

The boundary layer approximation is used then (the variation of the axial pressure gradient in the direction normal to the wall being conserved sometimes) and an integral formulation is conceived for the equations, the different quantities being expressed as deficits in respect to their freestream values.

The closure of the problem passes through the modelization of the new unknowns introduced by the successive integrations. Lack of knowledge concerning the behaviour of these terms has lead Mellor to perform an additional integration in the axial direction (equal to an axial chord length) obtaining closure through a number of crude assumptions concerning the global behaviour of the different quantities.

Horlock[3] on the contrary doesn't perform this last integration and obtains closure based on inviscid secondary flow considerations. His method is thus applicable inside the blade passage. Although the present authors believe that it is necessary to calculate the flow in the passage in order to arrive to a sufficiently good accuracy, the comparison of Horlock's method to measurements, presented in ref.(4) revealed that it is not possible to neglect the axial force deficit term and thus considerably simplify the calculation procedure. On the contrary, it was found that Horlock's expressions are surprisingly accurate as far as the force deficit terms are concerned.

In this paper, the measurements that have already been presented in reference (5) will be further discussed in connection with a calculation procedure which is based on the interaction of an end wall shear layer calculation method and a radial equilibrium calculation method. This procedure is described in the next section. Then the experimental results are presented and the comparison of theory with experiment is finally discussed.

2. DESCRIPTION OF THE METHOD USED

The method of calculation used in this paper derives from the combination of two calculation methods : (a) one, which calculates the freestream quantities . (b) Another one, which calculates the hub and tip wall shear layers.

The freestream calculation method

The freestream calculation method is based on the matrix solution of the radial equilibrium equations, habitually used in turbomachinery. Two forms of the basic equations were used. The first one as developed by Horlock[9] and Marsh and Bosman[10] (the later version of the basic equation was used). Solutions were obtained by both forms. The matrix solution is the one developed originally by Davis[8]. A certain number of modifications were introduced to it in order to obtain better numerical stability and allow for supersonic mean relative velocities with subsonic meridional ones. In addition, the formulation was slightly changed in order to allow for wall shear layer blockage effects. This last effect is taken into

account in the following way :
The physical boundaries are conserved and the stream function is given the appropriate values on these boundaries, so that the mass flow is conserved in the "inviscid" part of the flow. In this respect, the calculated mass deficit in the wall viscous layers is taken into account.

Better numerical stability was obtained by introducing the calculated profile losses and the end wall blockage progressively in the calculation.

Supersonic mean relative to the blading velocities are allowed, if the value of the product RVu is known[11]. Then the equation exhibits an elliptic character (as far as the meridional velocities are subsonic). The way the solution is obtained in our case is described briefly below :

Following a streamline (see also Marsh[12]) a relationship is established between the density function Σ and the function of the stream function derivatives Φ, as :

$$\Sigma = \left(1 - \frac{\Phi}{\Sigma^2}\right)^{\frac{1}{\gamma-1}} \tag{1}$$

where

$$\Sigma = \frac{\rho}{\rho_{c_0}} \left(\frac{h_{c_0}}{h_c - \frac{W^2}{2}}\right)^{\frac{1}{\gamma-1}} e^{\frac{s-s_0}{R_g}} = \left(1 + \frac{\gamma-1}{2} M_m^2\right)^{-\frac{1}{\gamma-1}} \tag{2}$$

and

$$\Phi = \left[\frac{(\rho U)^2 + (\rho V_g)^2}{2 \rho_{c_0}^2 h_{c_0}}\right] \left(\frac{h_{c_0}}{h_c - \frac{W^2}{2}}\right)^{\frac{\gamma+1}{\gamma-1}} e^{\frac{2(s-s_0)}{R_g}} \tag{3}$$

These functions are used in our case for the duct flow, stator, and rotor. The curve $\Phi = \Phi(\Sigma)$ as given by equation (1) has the general form given in figure (1) with the subsonic and supersonic meridional flow solution corresponding to one value of Φ. In fact equation (1) can be written as :

$$\Phi = \Sigma^2 \left(1 - \Sigma^{\gamma-1}\right) \tag{1a}$$

or

$$\Phi = A \cdot \Sigma^2 \tag{1b}$$

where A depends on the meridional Mach number.

Some of the parabolas $\Phi = A \Sigma^2$ for different meridional Mach numbers are given in figure (1). Of course, the correct solution is given by the intersection of such a curve with the curve representing equation (1).

The subsonic solution is generally accepted, but in the program the value of the $(i)^{th}$ iteration is taken to be on the same branch as the one of the $(i-1)^{th}$. During the course of the successive iterations it is possible that $\Phi > \Phi^* = 0.06698$. For that case the value of Σ is taken to be equal to the one given by the previous iteration, as long as the corresponding M_m is lower than 1.2. For M_m values higher than 1.2, the value of Σ is taken to be equal to the one corresponding to the intersection of Φ = const. and the A = const. curve for $M_m = 1.2$.

This happens quite often during successive iterations, even for relatively low converged meridional Mach numbers and in this way the solution passes momentarily from the supersonic meridional Mach number branch (lower than $M_m = 1.2$) without observing any particular signs of instability. In fact the convergence to the solution seems to be improved.

The end wall shear layers calculation method

The end wall shear layer calculation method is based on the work at Mellor and Wood[2]. A slightly different formulation is used (given in appendix A) which avoids a certain number of inconveniences present in the original formulation of Mellor. Axial and post axial absolute or relative velocities are allowed (in principle, this formulation accepts turbine configurations). The entrainment equation of Head[13] is used in addition, for the calculation of the behaviour of the momentum form factor.

The two methods coupled form the calculation procedure.

3. COMPARISON OF THE CALCULATION PROCEDURE WITH EXPERIMENTAL RESULTS

Some of the experimental results coming out of the same series of measurements as the ones presented and discussed in reference (5) are used in the present comparison. They are presented along with the prediction method in figures (2) to (13). A comparison of the theory and experimental integral quantities for the hub and tip wall shear layers is presented in figures (2) and (3) for two operating points. One near nominal conditions and one near surge. Figures (4) to (11) give some comparisons of the free-stream measured quantities with the calculated ones, by the usual radial equilibrium equations and Marsh's formulation.

Horlock's formulation[14] for the calculation of the transversal velocity profile was used to estimate the exit transversal velocity profile at hub. The exit transversal velocity profile at the tip was not calculated as the tip clearance effects invalidate Horlock's formulation.

For the hub, the transversal velocity profile was used in relation to a Coles'profile which was matched to the longitudinal experimental velocity profile. The results of the calculation are presented

in figures (4) to (7). In fact a slightly different formulation than the one proposed by Horlock was used for the transversal velocity profile. This expression was derived by requiring that the transversal velocity equals to zero at a distance from the wall equal to 2 δ. The resulting expression is

$$V_n = A(V_e - V_s) - \frac{6AV_e}{k g^2}\left[\frac{-I_1(\delta)e^{-k\lambda} + I_2(\delta)}{1+e^{-k\lambda}} - I_1(\gamma)\right]e^{-k\gamma} - \frac{6AV_e}{k g^2}\left[\frac{-I_1(\delta)e^{-k\lambda} + I_2(\delta)}{1+e^{-k\lambda}} - I_2(\gamma)\right]e^{k\gamma} \quad (4)$$

with

$$A = 2(\beta_{e_2} - \beta_{e_1})$$

and

$$I_1(\gamma) = \int_0^{\gamma}\left(1 - \frac{V_s}{V_e}\right)e^{-k\gamma}\,d\gamma$$

$$I_2(\gamma) = \int_0^{\gamma}\left(1 - \frac{V_s}{V_e}\right)e^{+k\gamma}\,d\gamma$$

$$k = \frac{2\sqrt{3}}{g} \qquad \lambda = 2\delta$$

4. DISCUSSION AND COMPARISON BETWEEN THEORY AND EXPERIMENT

From figures (2) and (3) it can be seen that the agreement between Mellor's theory coupled with an"inviscid" radial equilibrium calculation method is acceptable for engineering applications. It gives the possibility, using a meridional calculation, to predict in a satisfactory way the behaviour of the bulk of the flow. In order to appreciate better the accuracy of the prediction one has to say that the predicted quantities, at least for the rotor, result as the difference of two quantities. The dissipation of the kinetic energy inside the passage and the addition of energy corresponding to the work of the blade forces. It can also be seen that the quantity θ_{zx} is particularly well predicted.

The difference in the calculation results of the two formulations used for the prediction of the "inviscid" flow came as a surprise. One would expect that the formulation of Marsh would be more accurate, being formally more accurate, than the usual *radial equilibrium equations*, which are derived from Euler's equations. No explanation was found up to now for this discrepancy. Horlock's formulation gives fair agree ment with the experimental results (see figures (12) and (13)), giving at the same time a good idea of the angle variation inside the viscous layer (see figures (6) and (7)).

In this sense, it is only fair to say that the upstream conditions weren't well established inside the region wall shear layer, as it was quite difficult to approach the rotating hub at a distance less than 1.5 to 2.0 mm. One may see, however, that the trends are there. The accuracy with which the longitudinal velocity profile is represented by Coles'velocity profile family is quite acceptable for engineering purposes.

5. CONCLUSIONS

Some comparisons were presented between a through-flow calculation method coupled with a calculation method for the wall viscous layer and the experimental results presented in reference (5). The agreement was found to be acceptable for engineering purposes as far as the integral quantities of the wall shear layers were concerned. Horlock's theory was further used in order to calculate the transversal velocity profile at the rotor hub outlet station. The agreement was fair, although it seems that such a prediction in order to replace the collateral-boundary-layer-at-the-exit condition could improve its accuracy.

6. ACKNOWLEDGMENTS

This work was supported by SNECMA (Société Nationale d'Etude et de Construction de Moteurs d'Aviation).

The authors wish to express their thanks to the staff of the Department of Ensembles Tournants of SNECMA for his help and encouragement throughout this work.

LIST OF REFERENCES

1. J.W. RAILLY, J.G. HOWARD : Velocity profile development in axial flow compressors. Journal of Mechanical Engineering Science, Vol. 4, 1962, p. 166-76.

2. G.L. MELLOR, G.M. WOOD : An axial compressor end-wall boundary layer theory. Journal of basic engineering, Vol. 93, p. 300-316.

3. J.H. HORLOCK, H.J. PER.INS : Annulus wall boundary in turbomachines. AGARDograph 10-185, 1974.

4. K.D. PAPAILIOU, R. FLOT, J. MATHIEU : Secondary flows in compressor blading. A.S.M.E. Paper 76-GT-57, 1976.

5. G. BOIS, F. LEBOEUF , A. COMTE, K.D. PAPAILIOU : Experimental study of the behaviour of secondary flows in a transonic compressor. AGARD 49th Meeting on secondary flows in turbomachines 20-30 March 1977, The Hague, Netherlands.

6. C.H. WU : A general theory of three dimensional flow in subsonic and supersonic turbomachines of axial, radial, and mixed flow types (NACA TN 2604).

7. M.H. VAVRA : Aero-thermodynamics and flow in turbomachines. John Wiley & Sons, 1974.

8. W.R. DAVIS, D.A.J. MILLAR : Axial flow compressor analysis using a matrix method. Carleton University ME/A73-1.

9. J.H. HORLOCK : On entropy production in adiabatic flow in turbomachines. Journal of Basic Engineering, Trans. A.S.M.E., series D, 1971-73.

10. H. MARSH, C. BOSMAN : An improved method for calculating the flow in turbomachines, including a consis tent lors model. Journal of Mechanical Engng. Science, 1974, Vol. 16, n°1, p. 25-31.

11. J.M. THIAVILLE : Modèles de calcul de l'écoulement dans les turbomachines axiales. Agard 47th Meeting on "Through flow calculations in axial turbomachines".

12. H. MARSH : A digital computer program for the through flow fluid mechanics in an arbitrary turbomachine using a matrix method. ARC RM n°3509, 1968.

13. M.R. HEAD, V.C. PATEL : Improved entrainment method for calculating turbulent layer development. A.R.C. RM n°3643, 1970.

14. J.H. HORLOCK : Cross Flows in bounded three-dimensional turbulent boundary layers. Journal of Mechanical Engineering Science, vol. 15, n°4, 1973.

Appendix A

The new equations will be developped in the same way the ones Mellor[2] developped starting from equations (71) and (72) of his paper. They are written below

$$\frac{1}{\rho_e r}\frac{d}{dx}\left(\rho_e r U_e^2 \Theta_x\right) + H \Theta_x U_e \frac{dU_e}{dx} = \frac{d}{dx}\left(\frac{V_e^2}{2} F_x\right) + \frac{\tau_{wx}}{\rho_e} \tag{A1}$$

$$\frac{1}{\rho_e r}\frac{d}{dx}\left(\rho_e r U_e W_e \Theta_z\right) + H \Theta_x U_e \frac{dW_e}{dx} = \frac{d}{dx}\left(\frac{V_e^2}{2} F_z\right) + \frac{\tau_{wz}}{\rho_e} \tag{A2}$$

By multiplying the first equation by $\rho_e r U_e dx$ and the second by $(1-\varepsilon)\rho_e r W_e dx = (1-\varepsilon) R W_e dx$ and by adding together we have, taking into account that

$$U_e \frac{d}{dx}\left(\frac{V_e^2}{2} F_x\right) + (1-\varepsilon) W_e \frac{d}{dx}\left(\frac{V_e^2}{2} F_z\right) = 0 \tag{A3}$$

$$U_e d\left(R U_e^2 \Theta_x\right) + H R U_e^2 \Theta_x dU_e + (1-\varepsilon) W_e d\left(R U_e W_e \Theta_z\right) + (1-\varepsilon) R U_e^2 \Theta_x H \frac{W_e}{U_e} dW_e = \frac{R}{\rho_e}\left[U_e \tau_{wx} + (1-\varepsilon) W_e \tau_{wz}\right] dx \tag{A4}$$

Defining :

$$\Theta_x = R U_e^2 \Theta_x$$
$$\Theta_z = R U_e W_e \Theta_z \tag{A5}$$

we have :

$$U_e d\Theta_x + H \Theta_x dU_e + (1-\varepsilon) W_e d\Theta_z + (1-\varepsilon) H \Theta_x \frac{W_e}{U_e} dW_e = \frac{R}{\rho_e}\left(U_e \tau_{wx} + (1-\varepsilon) W_e \tau_{wz}\right) dx \tag{A6}$$

Taking into account that

$$d\left(|U_e|^H \Theta_x\right) = |U_e|^{H-1}\left[U_e d\Theta_x + H \Theta_x dU_e\right] \operatorname{sign}(U_e)$$

and

$$d\left(|w_e|^H \left(\frac{w_e}{u_e}\right)\Theta_x\right) = |w_e|^{H-1}\,\mathrm{sign}(w_e)\left[w_e\, d\left[\left(\frac{w_e}{u_e}\right)\Theta_x\right] + H\left(\frac{w_e}{u_e}\right)\Theta_x\, d w_e\right]$$

we have

$$|u_e|^{1-H}\,\mathrm{sign}(u_e)\, d\left(|u_e|^H \Theta_x\right) + (1-\varepsilon)\,|w_e|^{1-H}\,\mathrm{sign}(w_e)\, d\left(|w_e|^H \frac{w_e}{u_e}\,\Theta_x\right)$$

$$+ (1-\varepsilon)\, w_e\, d\left(\Theta_z - \left(\frac{w_e}{u_e}\right)\Theta_x\right) = R\left[u_e \frac{\tau_{wx}}{\rho_e} + (1-\varepsilon)\, w_e \frac{\tau_{wz}}{\rho_e}\right] dx \qquad \text{(A6.a)}$$

Integrating over an axial spacing as Mellor does and considering that H takes an average value H and that

$$R\left[u_e \frac{\tau_{wx}}{\rho_e} + (1-\varepsilon)\, w_e \frac{\tau_{wz}}{\rho_e}\right] = \frac{R}{\rho_e}\left\{u_e^2 + (w_e - u_w)^2\right\}^{1/2}\left[u_e^2 + (1-\varepsilon)\, w_e\,(w_e - u_w)\right]\frac{C_f}{2}\, dx$$

we have

$$\Theta_{x_2}\left\{|u_{e_2}|^{\bar H}\,|\bar u_e|^{1-\bar H}\,\mathrm{sign}(\bar u_e) + (1-\varepsilon)\,|\bar w_e|^{1-\bar H}\,|w_{e_2}|^{\bar H}\frac{w_{e_2}}{u_{e_2}}\,\mathrm{sign}(\bar w_e)\right\}$$

$$-\Theta_{x_1}\left\{|u_{e_1}|^{\bar H}\,|\bar u_e|^{1-\bar H}\,\mathrm{sign}(\bar u_e) + (1-\varepsilon)\,|\bar w_e|^{1-\bar H}\,|w_{e_1}|^{\bar H}\frac{w_{e_1}}{u_{e_1}}\,\mathrm{sign}(\bar w_e)\right\}$$

$$+ (1-\varepsilon)\,\bar w_e\left[\left(\Theta_{z_2} - \frac{w_{e_2}}{u_{e_2}}\Theta_{x_2}\right) - \left(\Theta_{z_1} - \frac{w_{e_1}}{u_{e_1}}\Theta_{x_1}\right)\right]$$

$$= \frac{\bar R}{\rho_e}\left\{\bar u_e^2 + (\bar w_e - \bar u_w)^2\right\}^{1/2}\cdot\left\{\bar u_e^2 + (1-\varepsilon)\,\bar w_e\,(\bar w_e - u_w)\right\}\cdot\frac{\bar C_f}{2}\,(x_2 - x_1) \qquad \text{(A7)}$$

This equation which is used for the calculation of Θ_{x_2}, is combined with equation (42) of Mellor's paper, which takes the following form

$$R_2\, u_{e_2}\, w_{e_2}\left(\vartheta_{z_2} - \vartheta_{x_2}\right) = \frac{k\,\delta_c\, R_2\, u_{e_2}}{\cos\gamma_B}\left[\frac{v_e}{\sigma}\left(w_{e_2} - w_{e_1}\right)\right]^{1/2}\mathrm{sign}\left(w_{e_2} - w_{e_1}\right)$$

$$= \Theta_{z_2} - \frac{w_{e_2}}{u_{e_2}}\,\Theta_{x_2} \qquad \text{(A8)}$$

Using now equation (A2) for the calculation of F_z we can write it in the following form

$$w_e\, d\,\Theta_z + H\,\Theta_x\,\frac{w_e}{u_e}\, d\,w_e = R\, w_e\, d\left(\frac{V_e^2}{2} F_z\right) + R\, w_e\,\frac{\tau_{wz}}{\rho_e}\, dx \qquad \text{(A9)}$$

from which we have

$$F_z = \frac{\left(\Theta_{z_2} - \Theta_{z_1}\right) + \frac{\bar H\,\Theta_x}{\bar u_e}\left(w_{e_2} - w_{e_1}\right) - \bar R\,\frac{\bar\tau_{wz}}{\bar\rho_e}\left(x_2 - x_1\right)}{\bar R\left(\bar u_e^2 + \bar w_e^2\right)/2.} \qquad \text{(A10)}$$

and

$$F_x = \frac{(1-\varepsilon)\,\bar w_e}{\bar u_e}\, F_z \qquad \text{(A11)}$$

The bars used in the previous equations designate mean arithmetic values of the upstream and downstream quantities.

The above formulation presents the following advantages.

a) The quantities Θ_x and Θ_z are independent of the system of coordinates (the jump conditions are automatically satisfied)

b) The quantities Θ_x and Θ_z are never infinite.

c) No quantity in the denominator becomes zero.

d) The present formulation may be used as well for turbines as for compressors.

NOTE: FOR DISCUSSION ON THIS PAPER, SEE END OF PAPER 3.

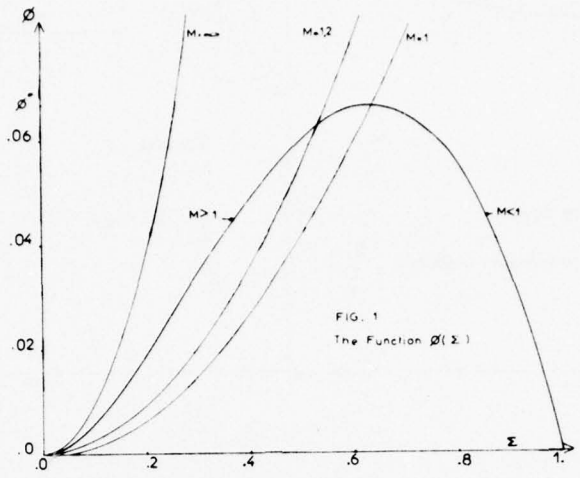


FIG. 1
The Function Ø(Σ)

FIG. 2

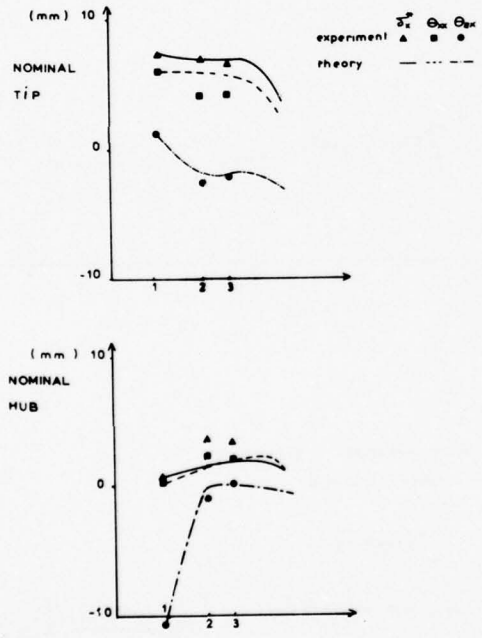
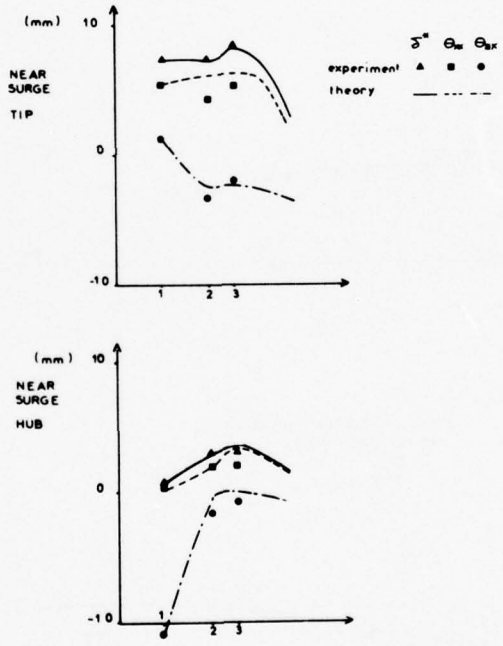
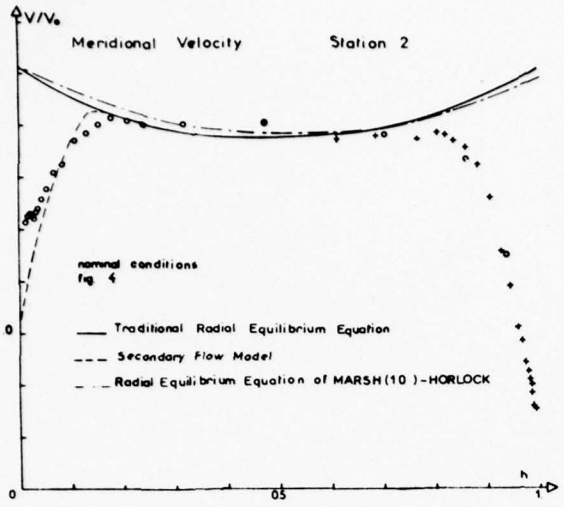
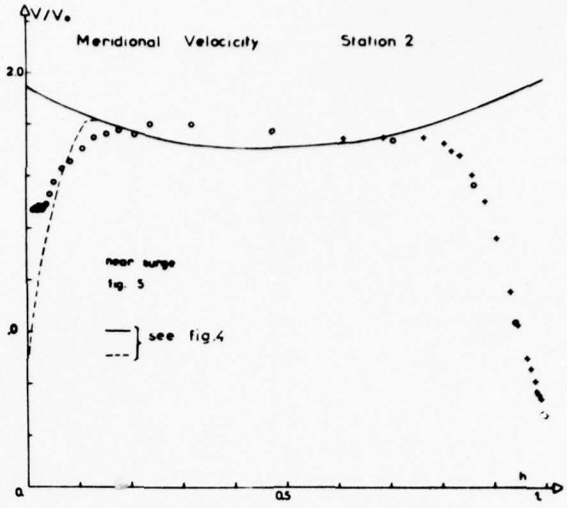
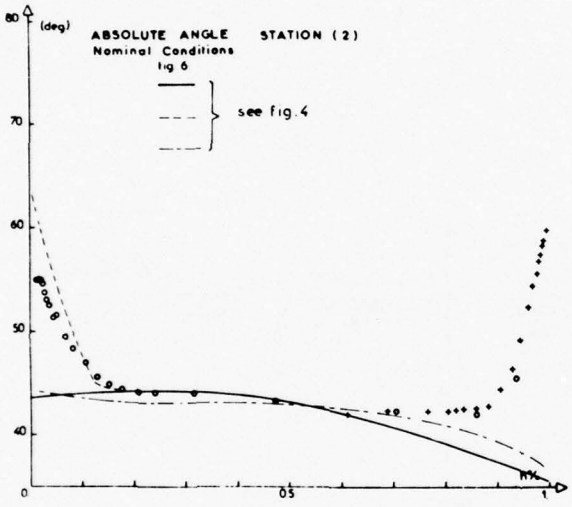


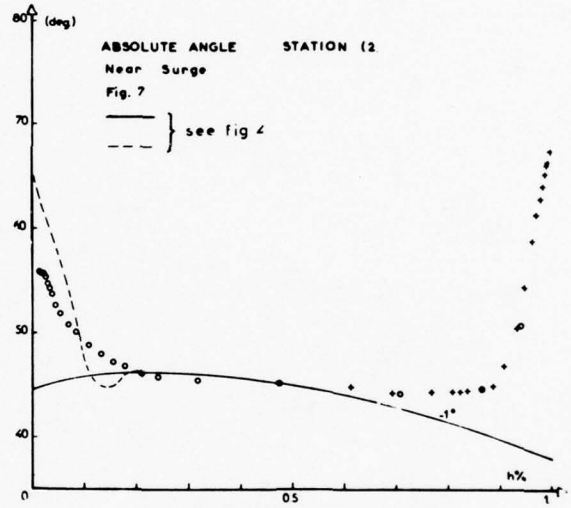
FIG. 3

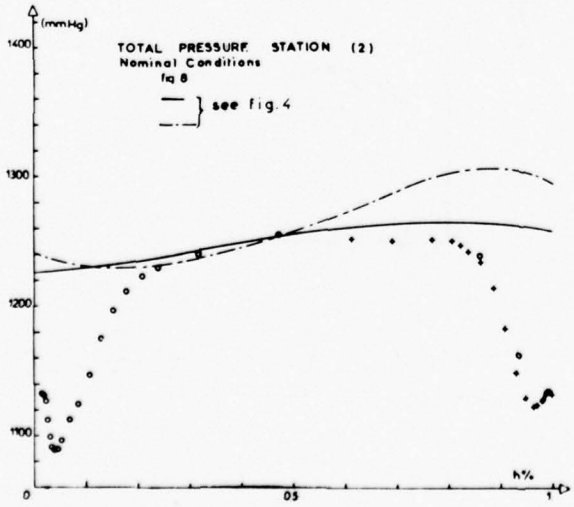


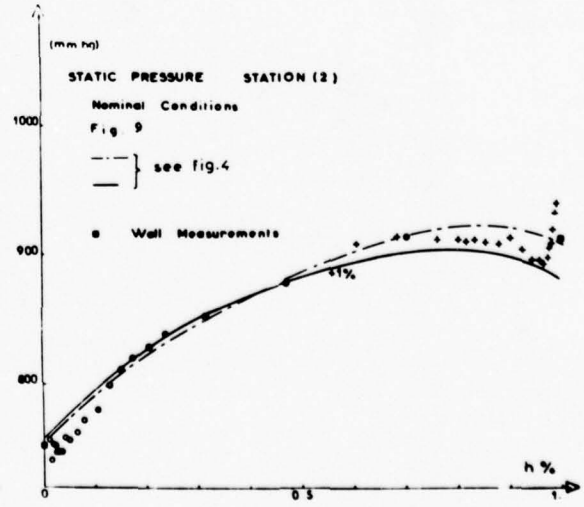

V/Vo
Meridional Velocity
Station 2
nominal conditions
fig. 4
Traditional Radial Equilibrium Equation
Secondary Flow Model
Radial Equilibrium Equation of MARSH(10)-HORLOCK
h
0
0.5
1

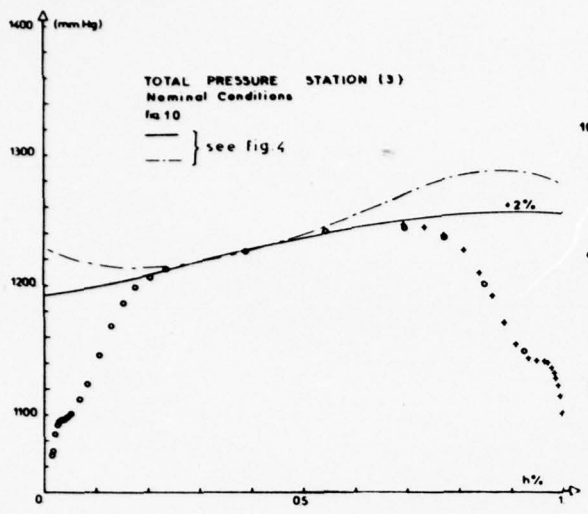

V/Vo
Meridional Velocicity
Station 2
2.0
near surge
fig. 5
see fig.4
h
0
0.5
1


(deg.)
ABSOLUTE ANGLE STATION (2)
Nominal Conditions
fig. 6
see fig. 4
80
70
60
50
40
h%
0
0.5
1


(deg.)
ABSOLUTE ANGLE STATION (2
Near Surge
Fig. 7
see fig 4
80
70
60
50
40
h%
0
0.5
1


(mmHg)
TOTAL PRESSURE STATION (2)
Nominal Conditions
fig. 8
see fig. 4
1400
1300
1200
1100
h%
0
0.5
1


(mm hg)
STATIC PRESSURE STATION (2)
Nominal Conditions
Fig. 9
see fig.4
Wall Measurements
1000
900
800
h %
0
0.5
1


1400
(mm Hg)
TOTAL PRESSURE STATION (3)
Nominal Conditions
fig 10
see fig 4
1300
1200
1100
+2%
0
05
1
h%

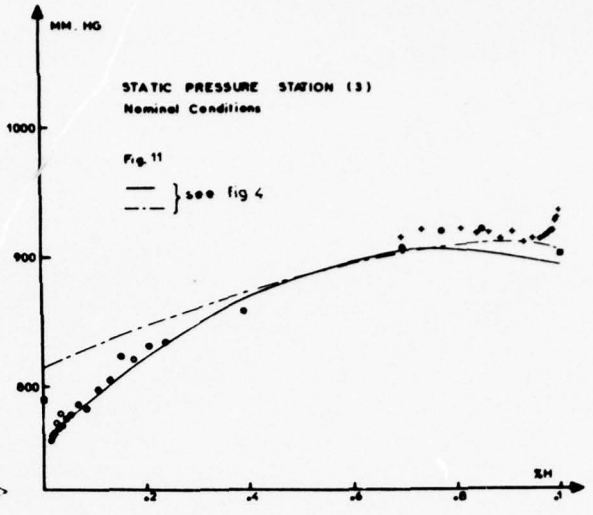

MM. HG
STATIC PRESSURE STATION (3)
Nominal Conditions
Fig. 11
see fig 4
1000
900
800
%H

FIG - 12

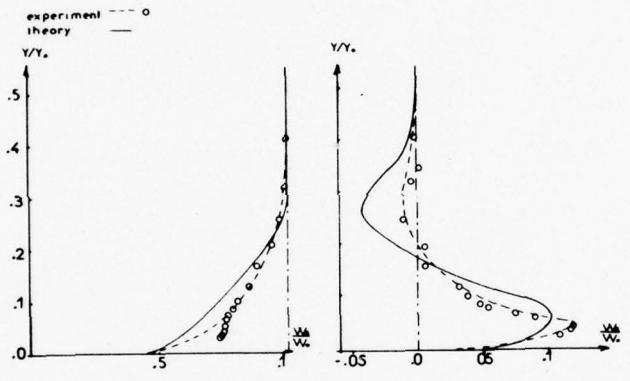
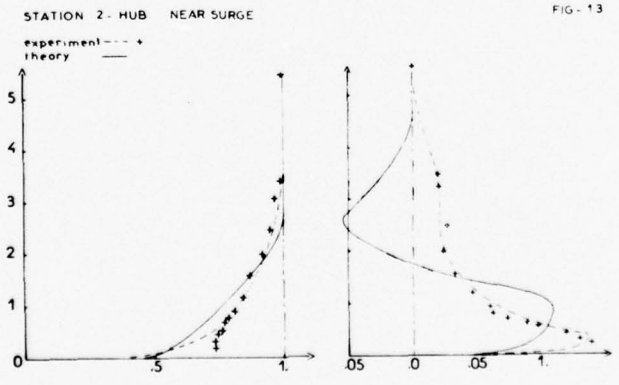

STATION 2 - HUB NOMINAL
experiment o
theory
Y/Y.
.5
.4
.3
.2
.1
.0
.5
1
Y/Y.
-.05
.0
.05
.1

FIG - 13


STATION 2 - HUB NEAR SURGE
experiment +
theory
5
4
3
2
1
0
.5
1.
.05
.0
.05
1.

EXPERIMENTAL STUDY OF THE BEHAVIOUR OF SECONDARY FLOWS IN A TRANSONIC COMPRESSOR

G. BOIS[1], F. LEBOEUF[2], A. COMTE[3], K.D. PAPAILIOU[4]
ECOLE CENTRALE DE LYON
Laboratoire de Mécanique des Fluides
36, Route de Dardilly, 36
Boîte Postale 163
69130 ECULLY (France)

[1] Ingénieur, Sté Metraflu
[2] Assistant, Ecole Centrale de Lyon
[3] Boursier C.N.R.S.
[4] Maître de Conférences Ass., Ecole Centrale de Lyon

SUMMARY

Detailed measurements in the secondary flow regions in a transonic one-stage compressor have been performed for different values of the inlet boundary layer and tip clearance. The behaviour of the secondary flows in examined in the light of these measurements.

NOMENCLATURE

V	absolute velocity
W	relative velocity
y	normal distance to the wall
h	relative distance to the wall

SUBSCRIPTS

o	reference condition
s	longitudinal direction
n	transversal direction

1. INTRODUCTION

The importance of the secondary flows has been recognized in recent years and a considerable effort has been made towards developping methods for their calculation. Accurate experimental results are, however, lacking, which will contribute to the understanding of the phenomena and help to the modelisation of the unknown terms in the equations.

Detailed measurements were performed on an experimental transonic compressor of S.N.E.C.M.A. (given schematically in figure (1)), for different values of the upstream wall boundary layer and different tip clearance values.

In this paper some of these measurements will be presented. They will be first analysed and subsequently used to discuss some general notions and hypotheses concerning the secondary flow calculations.

2. THE PROBES AND THEIR CALIBRATION

Combined probes for total pressure, static pressure, one direction, and total temperature were conceived in order to diminish the measuring time in a costly installation.

Two probes were used (see photo (1)) : a cylindrical-wedge-type probe ("tip" probe, figure (2)) which permitted us to approach the tip end wall of the compressor and a cobra-type probe ("hub" probe, figure (3)) which permitted us to approach the hub end wall of the compressor. Small diameter tubes were used in order to diminish the probe dimensions as much as possible. Besides the directional holes, which were calibrated for static pressure measurements, one more possibility was added for the measurement of the static pressure :

a) For the "hub" probe a static hole was drilled on an extra tube under the probe stem (see figure (3))

b) For the "tip" probe a static hole was drilled on the ending hemisphere of the probe. Different backward positions of this hole were examined in order to find if one could obtain a stable response for the static pressure with varying pitch angle.

The probes were calibrated at the Von Karman Institute for different Mach numbers up to 0.8 and for varying pitch and yaw angles (pressure measurements) and at S.N.E.C.M.A. statically and dynamically for the temperature measurements.

The following remarks can be made as far as probe behaviour is concerned :

a) The static pressure measurements through the bottom hole for the "hub" probe is nearly independant of the pitch angle (± 9°). However, the static pressure measurements through the directional holes depend strongly on the pitch angle.

b) The static pressure measurements through the bottom hole for the "tip" probe are strongly dependant on the pitch angle, whatever the position of the hole. The static pressure measurements through the directional holes are independant of the pitch angle.

c) The total pressure measurements for the "hub" probe are slightly but appreciably dependent on the pitch angle.

d) The total pressure measurements for the "tip" probe are practically independent of the pitch angle.

e) Good recovery coefficients were found for the total temperature measurements.

3. THE PROBE BEHAVIOUR IN THE ENVIRONMENT OF THE COMPRESSOR

Using the two probes (put at an angle of 90°), measurements were performed in a transonic compressor of S.N.E.G.M.A.. In figure (1) the three measuring stations discussed here are presented : One upstream and two downstream of the compressor rotor.

Typical measurements of the total pressure, the static pressure, the yaw direction, the total temperature and resulting radial distribution of the meridional velocity are presented in figures (4) to (31). Care was taken to ensure that for a certain radial distance, measurements were taken by both probes (overlapping region).

The data reduction of these measurements was done using the calibration curves of the probes. It was found necessary to introduce the value of the pitch angle in order to obtain correct results. The value of the pitch angle (which was not measured) was taken equal to the one given by a theoretical through flow calculation in the meridional plane, which will be described briefly later.

Although the probes present some geometrical imperfections that result into asymetric calibration curves, it seems that coherent results are obtained for every quantity measured, as can be seen from the presented experimental results in the overlapping region. This is confined also by the fact that the continuity equation is satisfied for the three stations within ± 0.25 %.

Some remarks can be made concerning the measurement of the static pressure which is put often in doubt. From our measurements it can be seen that the static pressure measured from the static pressure taps at the compressor end walls agrees well with the static pressure measurements of the probes.

Many investigators, not believing in the static pressure measurements given by probes, often use the values of the wall statics and interpolate in between. From the results presented here it seems that this may be dangerous. On the other hand another method to avoid static pressure measurements is to use the continuity equation and the simple radial equilibrium equations (the curvature terms neglected). In this case the experimental total pressure, total temperature and yaw angle distributions are used. Such a data reduction was performed and the results are compared with the experimental static pressure and meridional velocity distributions. It can be seen that only fair agreement can be obtained.

In fact it can be seen that the agreement is better in the plane (3) where the curvature influence is much smaller. This seems to indicate that the radial equilibrium equations give an acceptable accuracy in the secondary flow region, if the losses are evaluated correctly. In order to obtain further information in this direction, a data reduction computer program was used which analyses the flow using as data the experimental absolute angle and total pressure distributions and the value of the mass flow rate. In this program the radial equilibrium equations are used with the curvature terms taken into account. Difficulties, however, were encountered when the experimental total pressure gradients near the wall were used and convergence was not obtained.

The results of the through flow calculation at our disposal, which combines a modified version (1) of the matrix method solution of Davis' (2) for the meridional plane and a modified version (3) of Mellor's theory (4) for the wall boundary layer calculation are given on the cited figures. It can be easily seen that the predicted static pressure distribution comes closer to the measured one for both stations (2) and (3). It seems then, that taking into account of the streamline curvature effects in a data reduction program using as input the total pressure, the total temperature and the yaw angle distributions, may result in a good approximation of the static pressure distribution.

A question, which comes up frequently, concerns the response of a probe which is introduced in a non-stationary environment as in the case for the measurements we have at hand behind the rotor. A typical comparison of total pressure measurements for the stations (2) and (3) (which is located more than a chord behind the rotor) are given in figure (32). Noting that the measurements were not done simultaneously and that they are only referred to the same operating point, it can be deduced that the differences of the order of 1 % present, can be considered to be within the error of measurements.

It seems, so, that for our case there is little influence of the nonstationary field on the probe response. This fact is confirmed by the already mentionned continuity considerations between upstream and downstream of the rotor measuring stations. In our opinion this result must be attributed to the small size of the probe tube diameters used.

4. THE DISCUSSION OF THE EXPERIMENTAL RESULTS

We shall discuss the experimental results on the basis of the following statements :

a) There exist a part of the flow which is not influenced by the presence of the secondary flows but indirectly through the defect of the mass in the viscous layers which can be accounted for by the introduction of the displacement thickness. Thus we admit the three zone model.

b) The secondary flows will be defined as the difference between the real flow and the extrapolation of the "free stream" flow inside the viscous layer according to the laws of the radial equilibrium which takes into account only profile losses.

For this two statements we implicitely addmit (if not in theory, certainly in practice) that there exists a radial equilibrium calculation method which allows us to define the "free stream" zone as well as the extrapolated "free stream" flow in the secondary flow region necessary to the definition of the secondary flow quantities.

The results of the calculations performed with the through flow calculation at our disposal are presented along with the measurements.

Some differences can be observed in the calculated values which may result from defects in the deviation angle correlations, the profile loss correlations or the secondary flow calculation. The calculation of the flow at the compressor inlet plane presents some difficulties. It was found that the calculation results for the upstream of the rotor plane were greatly influenced by the values of the different parameters downstream of the rotor (especially loss distribution and curvature). However, no valid explanation was found for the differences present between measurements (which seem to be coherent) and different ways of data reduction or calculations.

The important result of these calculations is that on the whole the gradients of the radial distributions of the flow quantities are calculated correctly and, thus, that we may proceed in the analysis of the secondary flow problem on the basis of the two statements we made.

It must be noted that small discrepencies between theory and experiment in the "free stream" zone may result in large errors in the definition of the secondary flow integral quantities.

One important result of the comparison of the theoretical calculation and the experimental results is the agreement between the calculated and the measured static pressure distribution at least behind the rotating wheel : The matching of the shear layer and the external flow is based on the identity of the static pressure distribution.

In figure (33) to (44) we have presented typical velocity profiles for the six measuring stations (hub and tip) and for two operating points : one, near the nominal conditions and another one near surge. The measurements are presented in a deficit form on the basis of the radial equilibrium calculation. It is assumed that this calculation represents well the free stream radial equilibrium and its extrapolation inside the viscous layers. In this respect one has to have in mind that small deviations from the above stated assumption result to considerable errors in the deficit quantities. The coordinate system used is the implicit one, that is, in the direction of the external flow and normal to it, as it is presented in figure (45). As has already been mentionned (3), only this coordinate system has a physical meaning, so that it is in this coordinate system that a representation of the physical quantities must be sought. One, however, must decide whether to use the absolute intrincic coordinate system or the relative one, or if one can, as would be more convenient, use both. In order to be able to interpret the longitudinal and normal velocity profiles one must follow intuitively the following rules.

a) Analyse the wall region in a coordinate system relative to the wall (moving or not).

b) Analyse the outer region in a coordinate system relative to the blading.

c) Avoid to mix the longitudinal profile which is described on the basis of boundary layer considerations and the transversal profile which is described on basis of inviscid flow considerations.

We shall try to discuss the available data on the basis of the above intuitive rules. We shall consider first the tip wall shear layer. The inlet wall layer must be examined in the absolute system, according to the established "rules". The longitudinal velocity profile, given in figure (33) seems to be reasonably represented by a two-dimensional turbulent boundary layer profile. A weak transversal velocity profile exists (given in figure (33)), which probably been induced by the influence of the rotating wheel upstream.

Considering the same profile in the relative system, given in figure (34), we immediatelly become aware that the region near the wall does not correspond to the traditional boundary layer concepts. The influence to the external part of the velocity profile due to the contribution of the normal profile in the absolute system is small in this case. It has to be stressed, however, that in view of the difference in nature of the two profiles (longitudinal and transversal) in the absolute system, it doesn't seem plausible that the same laws apply to profiles in the relative system, which are the outcome of their combination. This becomes quite evident at the exit of the rotating wheel, which is now considered.

The velocity profiles are given in figures (35) and (36) for the immediatelly after the rotor station and in figures (37) and (38) for the station one chord downstream. It can be seen that a reorganisation of the flow has taken place inside the rotating passage so that the external part of the velocity profile is better described according to the traditional boundary layer concepts in the relative to the blade system. It is evident that the near to the wall region is better described in the absolute system, in respect to which the velocity at the wall is zero. However, the wall region, which is due to the tip clearance, seems to be rather small (in the longitudinal direction) so that a theoretical representation of the velocity profile seems to be more plausible in the relative coordinate system than in the absolute one, in respect to which it is completely distorded by the contribution of the relative transversal velocity profile.

Further downstream, the wall layer becomes, more important and a representation of the profile in either of the two systems (relative or absolute) seems rather difficult. This state of affaires seems to favor a differential formulation of the problem. However, many questions have to be answered before such a formulation becomes possible.

The same behaviour is observed for the hub at the compressor inlet, the rotating hub gives a certain positive prerotation to the flow and from the velocity profiles we can see that the external part is equally well behaved in the relative and absolute system, although the relative system would be prefered, as the transversal velocity profile is better represented in respect to the moving wall.

The inner part of this velocity profile is not quite well described as measurements very near the rotating hub were not possible. At the exit for both stations a conventional representation is obtained in the relative to the blade system for both velocity profiles. Near the wall the flow is perturbed by the injected recirculation flow, as the measurements were performed at the clearance between the rotating hub and the stationary part of the shrouded stator.

As far as the change in coordinate system is concerned, the same remarks can be made for the two downstream hub stations as the ones already made for the tip stations. Considering again the tip wall layer in the relative system we can immediatelly remark the decrease of the importance of the shear layer zone from upstream to downstream due to the reenergetization process at the exit the transversal relative velocity profile is quite reduced (except near the wall, where the action of the tip clearance is felt), a fact which tends to confirm Mellor's hypothesis for collateral boundary layers at the exit.

The action of the tip clearance is felt in developing a transversal velocity profile in the direction of the rotating wall relative to the blading. Note that the tip clearance effect is felt much more in the transversal direction than in the longitudinal one.

Looking at the hub in the relative coordinate system we observe an increase of the wall shear layer inside the rotating wheel. The action of the rotating hub is such that it hinders large relative angles to be developped near the wall. Thus, downstream, the overturning process inside the viscous layer results to an overturning in angle near the wall in respect to the free stream flow. This phenomenon hinders the formation of s-shape transversal velocity profiles.

5. CONCLUSION

Measurements were performed in a one stage transonic compressor with emphasis on the wall shear layers. The analysis of these measurements shows that :

a) Data reduction on the basis of simple radial equilibrium considerations may result into serious errors. On the contrary, indications exist that taking into account the curvature terms, radial equilibrium considerations may give a good approximation even inside the wall viscous layers.

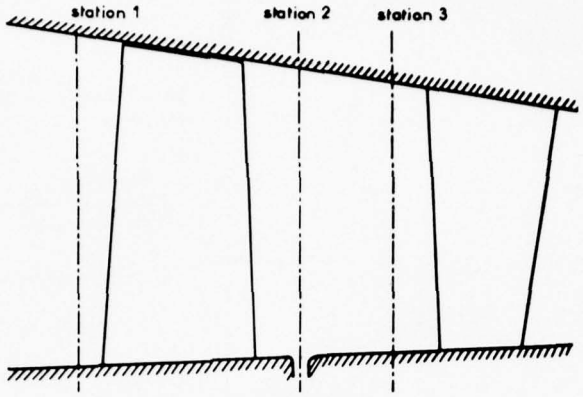
b) Agreement was obtained between a radial equilibrium calculation and the experimental results in the free stream part of the flow. This fact confirms the three zone model, when there is no interaction of the two wall boundary layers, even if they are considerably thick.

c) Agreement was obtained between experimental static pressure distributions and theoretical free stream radial equilibrium calculations even inside the viscous layer. This means that the basis for the matching of the viscous wall layer and the free stream flow is sound.

d) The general trends of the velocity profiles are those expected. It seems, however, that difficulties exist when an analytical representation of the velocity profiles is sought in both absolute and relative systems of reference. This fact would favor differential calculations for the wall shear layer, although this seems rather difficult for the moment because of lake of detailed information of the flow behaviour inside the blade passage.

REFERENCES

1. F. LEBOEUF : "Calcul de l'écoulement dans le plan méridien d'une turbomachine", (en préparation, Ecole Centrale de Lyon).
2. W.R. DAVIS, D.A.J. MILLAR : "Axial flow compressor using a matrix method", (Carleton Univ. ME/A73-1).
3. K.D. PAPAILIOU : "Remarques supplémentaires sur le calcul des pertes secondaires", (Compte-rendu S.N.E.C.M.A. YKB n° 24/74).
4. G. MELLOR, G. WOOD : "An axial compressor end-wall boundary layer theory", (A.S.M.E. paper 70-GT-80).



SNECMA EXPERIMENTAL COMPRESSOR Fig. 1

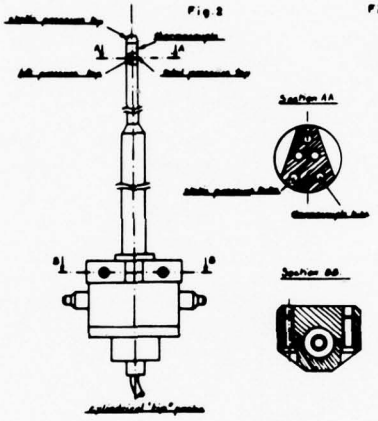


Fig. 2

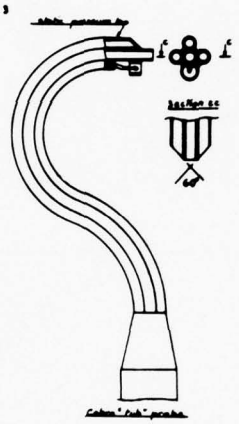
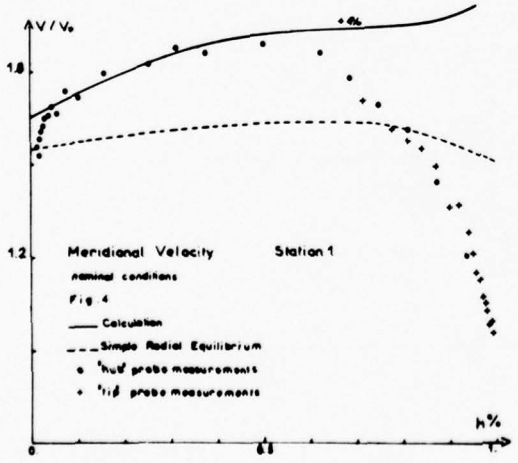
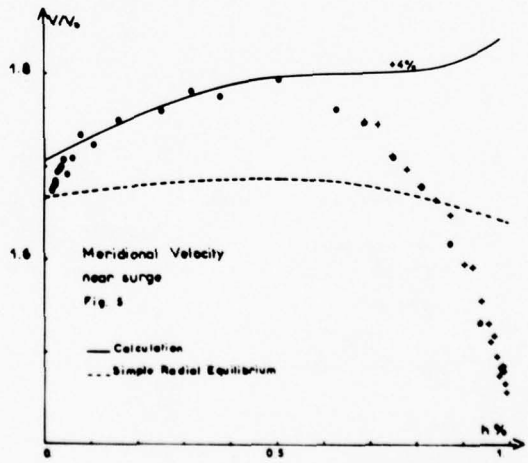


Fig. 3

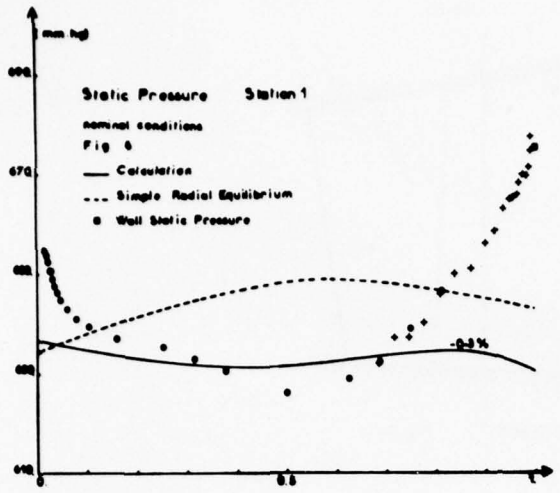


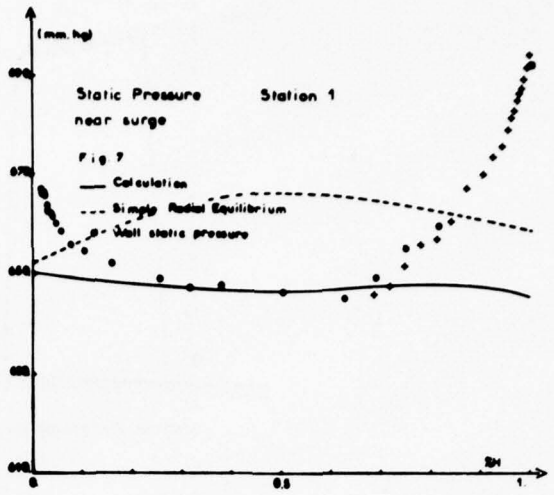


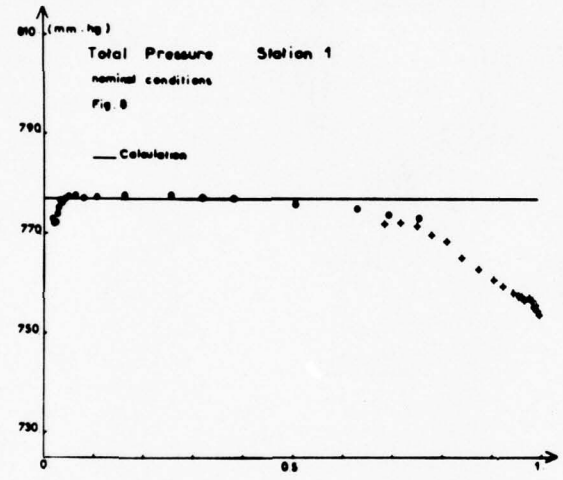
Author's Reply

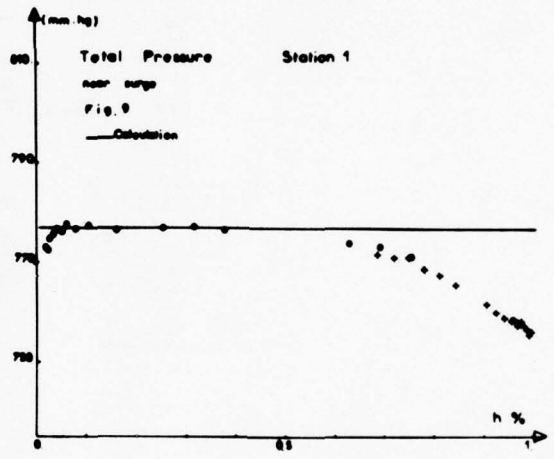
The blade passing frequency was:

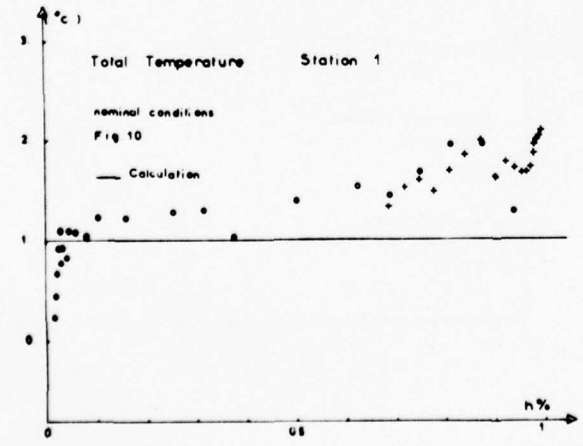
$$f_B = 7500 \text{ HZ}$$

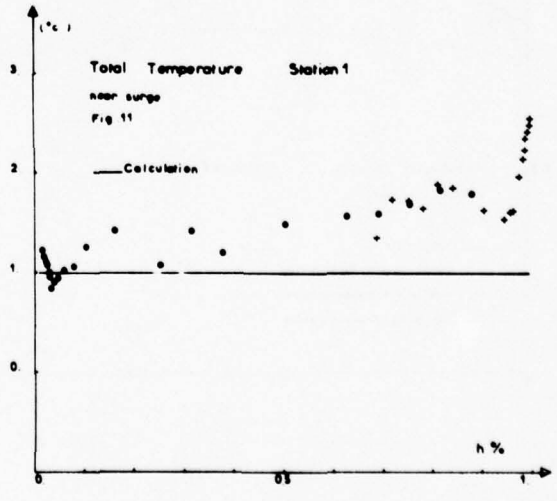

mm hg
Static Pressure Station 1
nominal conditions
Fig 6
Calculation
Simple Radial Equilibrium
Wall Static Pressure
-0.3 %

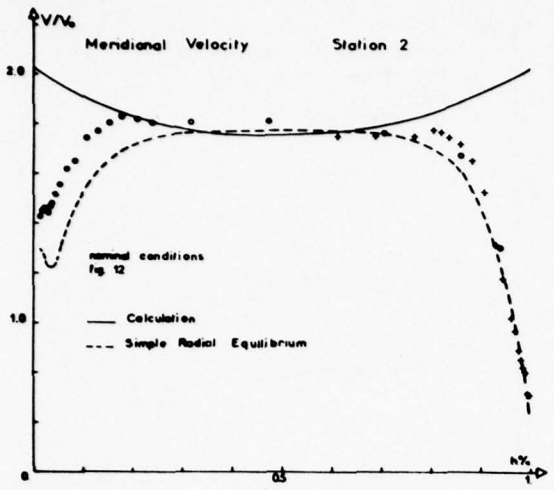

(mm. hg)
Static Pressure Station 1
near surge
Fig 7
Calculation
Simple Radial Equilibrium
Wall static pressure
0.5
1

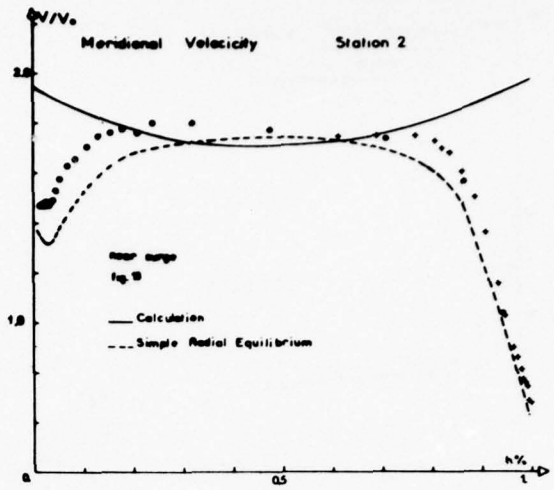

(mm. hg)
Total Pressure Station 1
nominal conditions
Fig. 8
Calculation
790
770
750
730
0.5
1

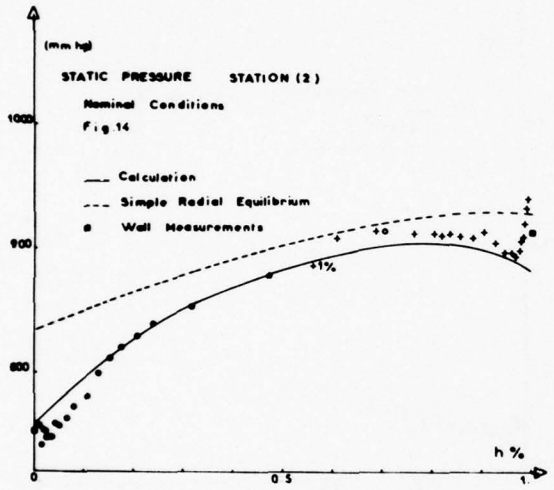

(mm. hg)
Total Pressure Station 1
near surge
Fig. 9
Calculation
790
770
750
h %
0.5
1

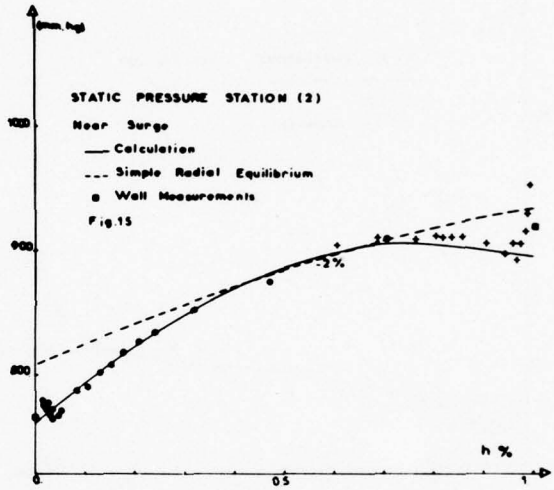

(°c)
Total Temperature Station 1
nominal conditions
Fig 10
Calculation
3
2
1
0
h %
0.5
1

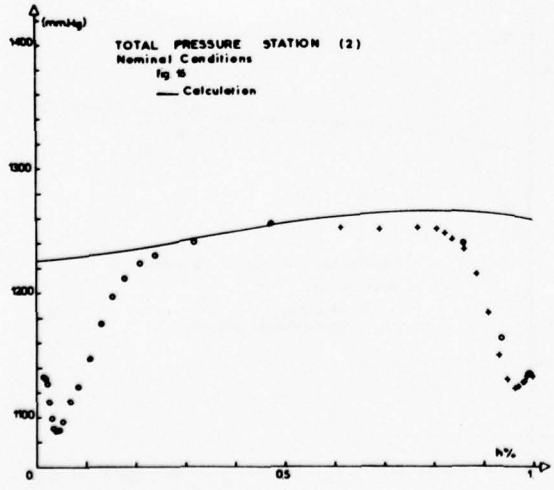

(°c)
Total Temperature Station 1
near surge
Fig 11
Calculation
3
2
1
0.
h %
0.5
1

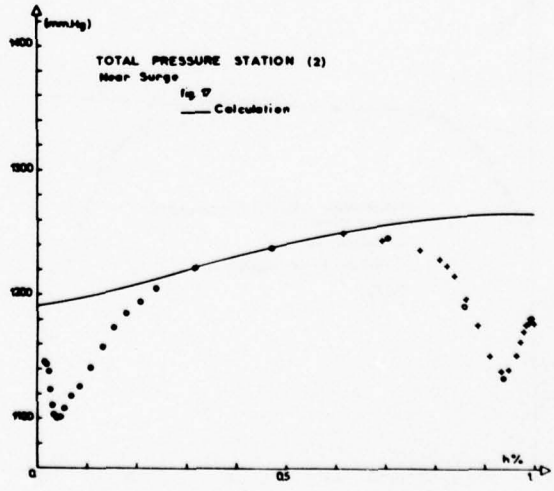

V/V₀
Meridional Velocity
Station 2
2.0
1.0
0
0.5
1
h%
nominal conditions
fig. 12
Calculation
Simple Radial Equilibrium

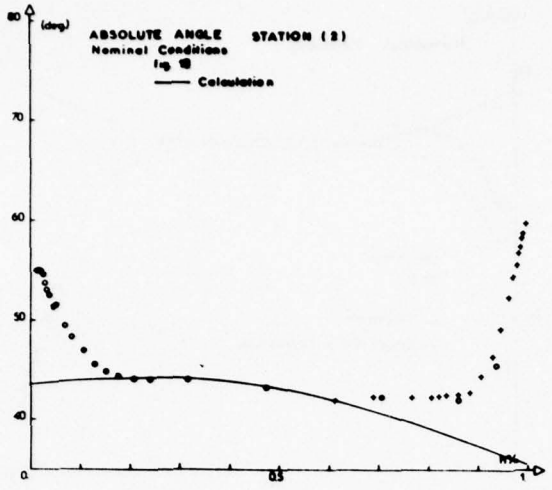

V/V₀
Meridional Velocity
Station 2
2.0
1.0
0
0.5
1
h%
Calculation
Simple Radial Equilibrium

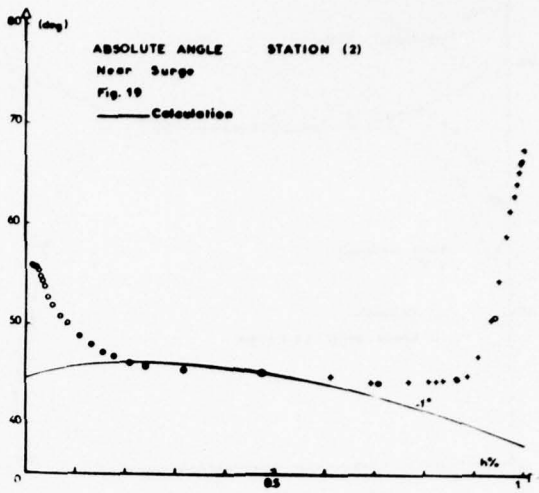

(mm hg)
STATIC PRESSURE STATION (2)
Nominal Conditions
Fig 14
Calculation
Simple Radial Equilibrium
Wall Measurements
1000
900
800
0
0.5
1
h %

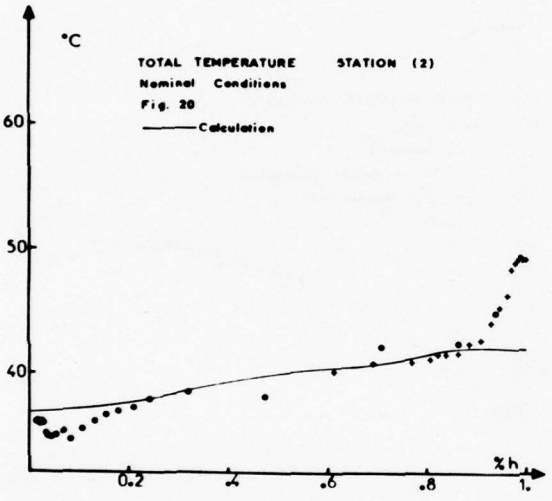

STATIC PRESSURE STATION (2)
Near Surge
Calculation
Simple Radial Equilibrium
Wall Measurements
Fig.15
1000
900
800
0
0.5
1
h %

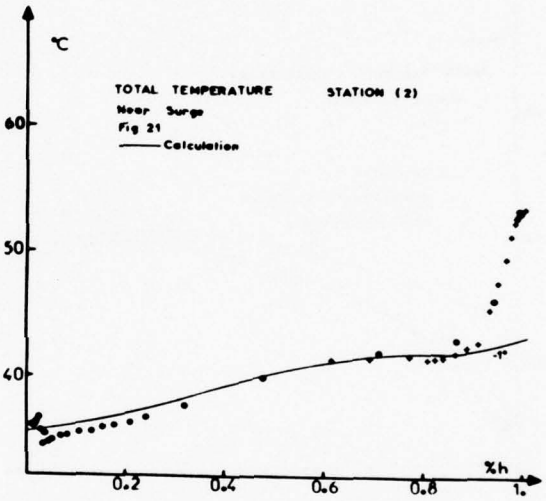

(mm Hg)
TOTAL PRESSURE STATION (2)
Nominal Conditions
fig 16
Calculation
1400
1300
1200
1100
0
0.5
1
h%

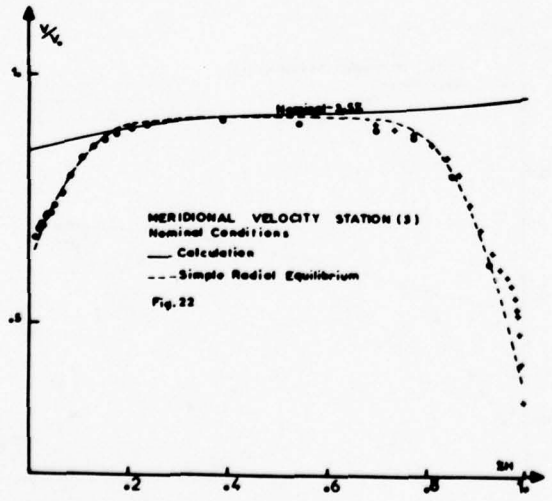

(mm Hg)
TOTAL PRESSURE STATION (2)
Near Surge
fig 17
Calculation
1400
1300
1200
0
0.5
1
h%

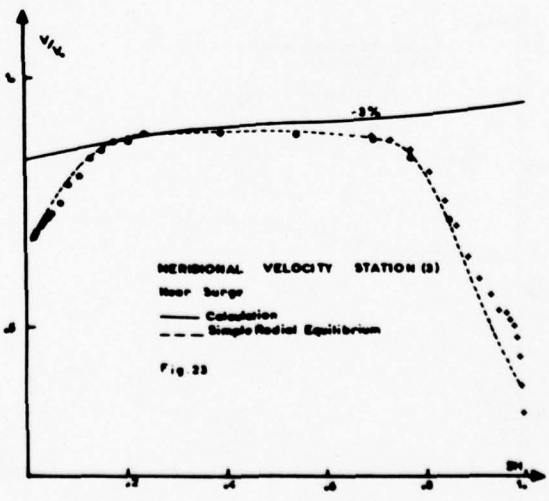

(deg)
ABSOLUTE ANGLE STATION (3)
Nominal Conditions
Fig. 18
Calculation
80
70
60
50
40
0
0.5
1
h%

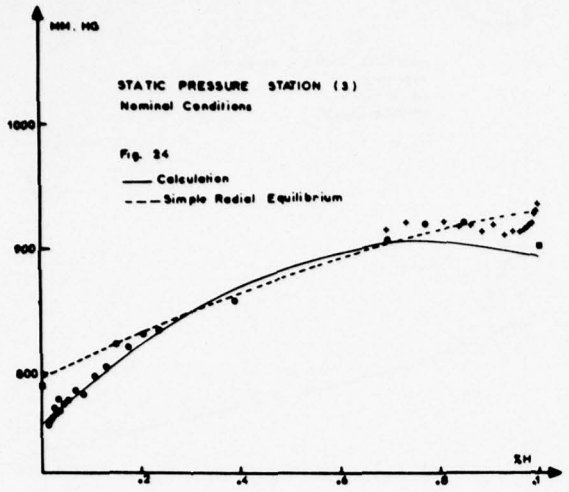

(deg)
ABSOLUTE ANGLE STATION (2)
Near Surge
Fig. 19
Calculation
80
70
60
50
40
0
0.5
1
h%

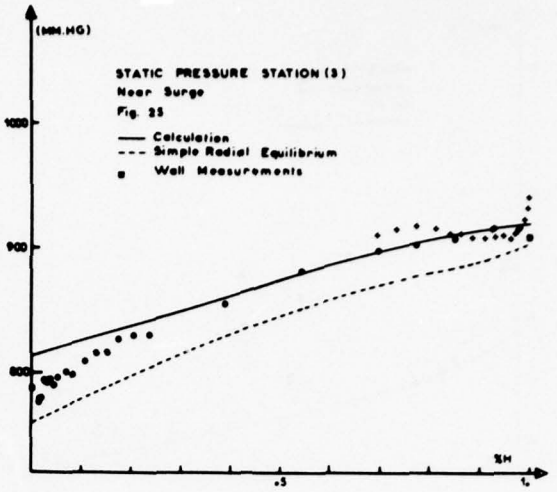

°C
TOTAL TEMPERATURE STATION (2)
Nominal Conditions
Fig. 20
Calculation
60
50
40
0.2
0.4
0.6
0.8
1.
%h

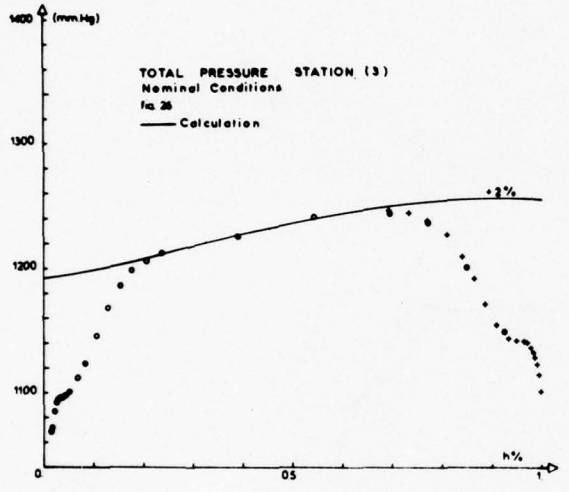

°C
TOTAL TEMPERATURE STATION (2)
Near Surge
Fig. 21
Calculation
60
50
40
0.2
0.4
0.6
0.8
1.
%h

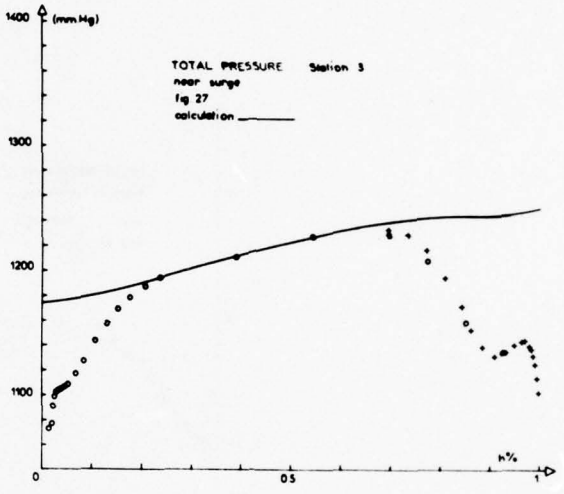

V/Uc
Nominal -0.5%
MERIDIONAL VELOCITY STATION (3)
Nominal Conditions
Calculation
Simple Radial Equilibrium
Fig. 22
.8
.2
.4
.6
.8
1.
%H

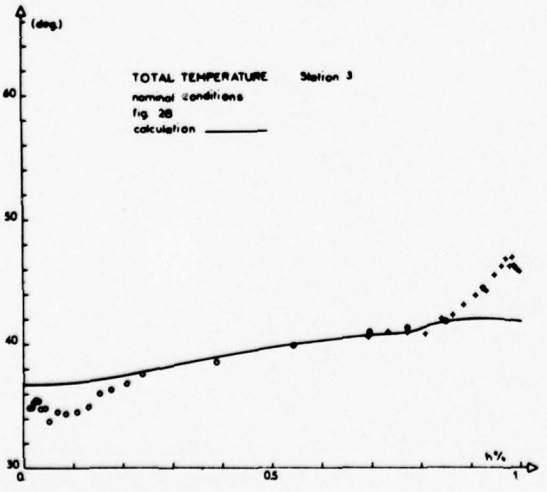

V/Uc
-3%
MERIDIONAL VELOCITY STATION (3)
Near Surge
Calculation
Simple Radial Equilibrium
Fig. 23
.8
.2
.4
.6
.8
1.
%H

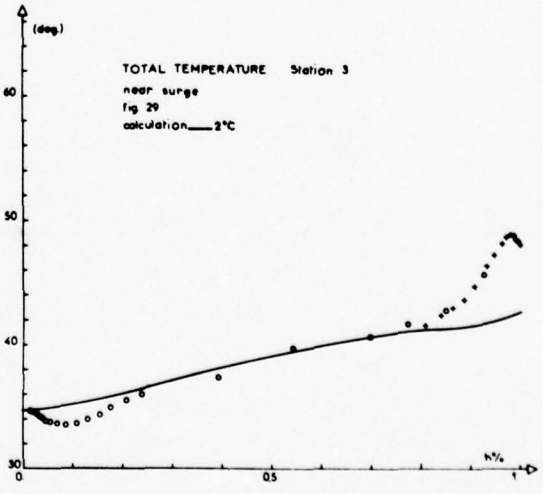

MM. HG
STATIC PRESSURE STATION (3)
Nominal Conditions
Fig. 24
Calculation
Simple Radial Equilibrium
1000
900
800
%H
.2
.4
.6
.8
1

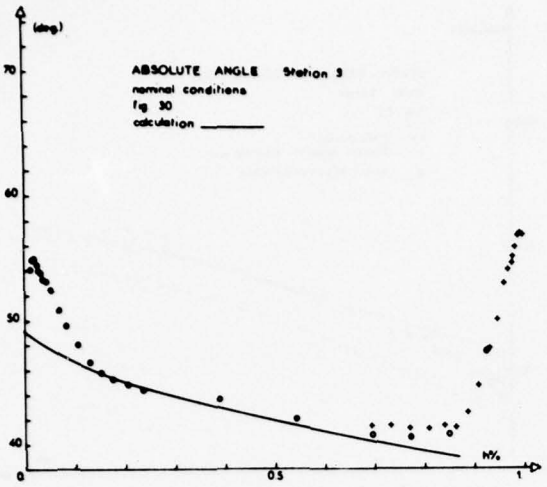

(MM.HG)
STATIC PRESSURE STATION (3)
Near Surge
Fig. 25
Calculation
Simple Radial Equilibrium
Wall Measurements
1000
900
800
%H
.5
1

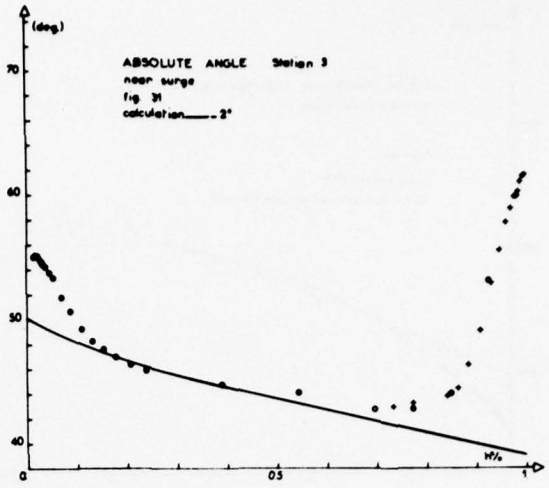

1400
(mm.Hg)
TOTAL PRESSURE STATION (3)
Nominal Conditions
fig. 26
Calculation
+2%
1300
1200
1100
h%
0
0.5
1

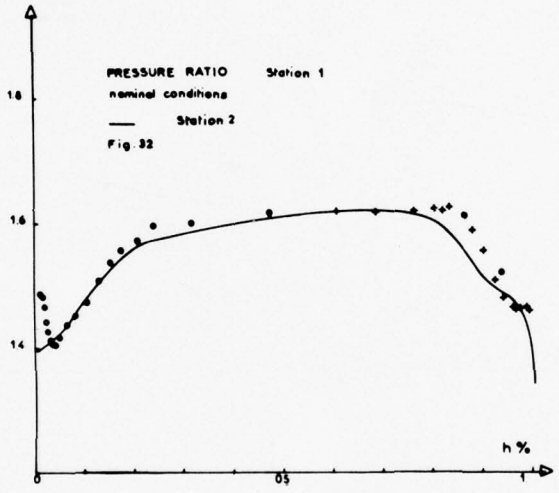

1400
(mm.Hg)
TOTAL PRESSURE Station 3
near surge
fig. 27
calculation
1300
1200
1100
h%
0
0.5
1


(deg.)
TOTAL TEMPERATURE Station 3
nominal conditions
fig. 28
calculation
60
50
40
30
h%
0
0.5
1


(deg.)
TOTAL TEMPERATURE Station 3
near surge
fig. 29
calculation 2°C
60
50
40
30
h%
0
0.5
1


(deg)
ABSOLUTE ANGLE Station 3
nominal conditions
fig 30
calculation
70
60
50
40
0
0.5
1
H%


(deg)
ABSOLUTE ANGLE Station 3
near surge
fig 31
calculation - 2°
70
60
50
40
0
0.5
1
H%


PRESSURE RATIO Station 1
nominal conditions
Station 2
Fig. 32
1.8
1.6
1.4
0
0.5
1
h %

STATION 1 TIP

fig. 33

o nominal

+ near surge

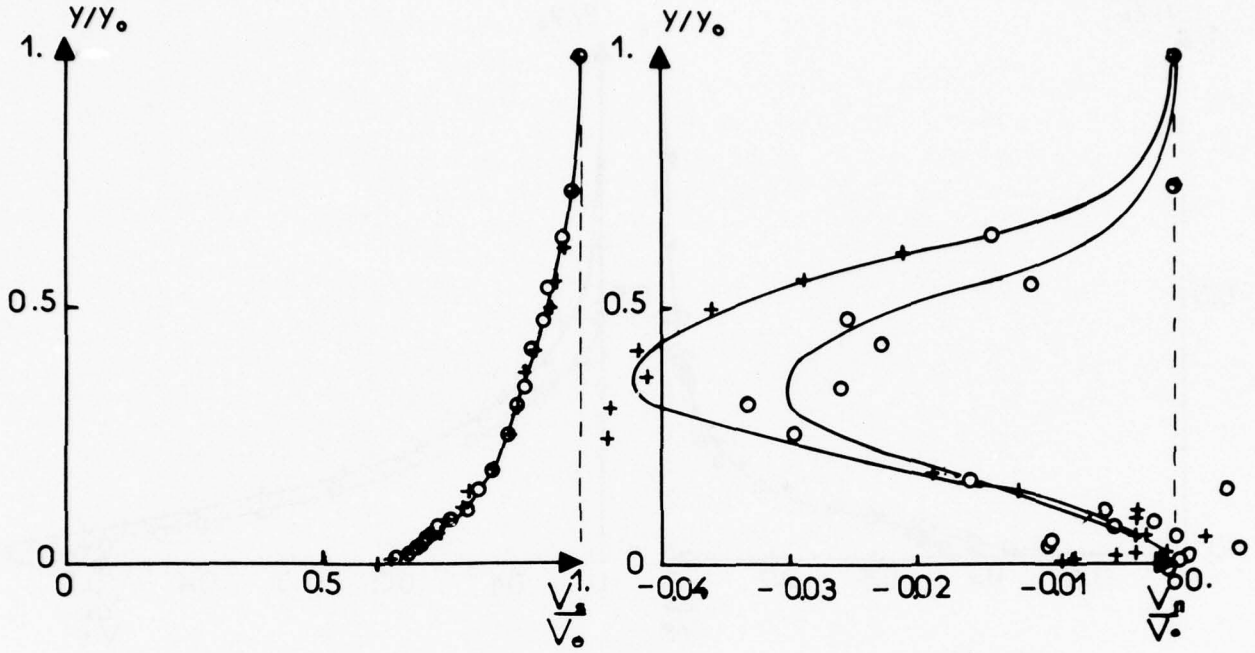
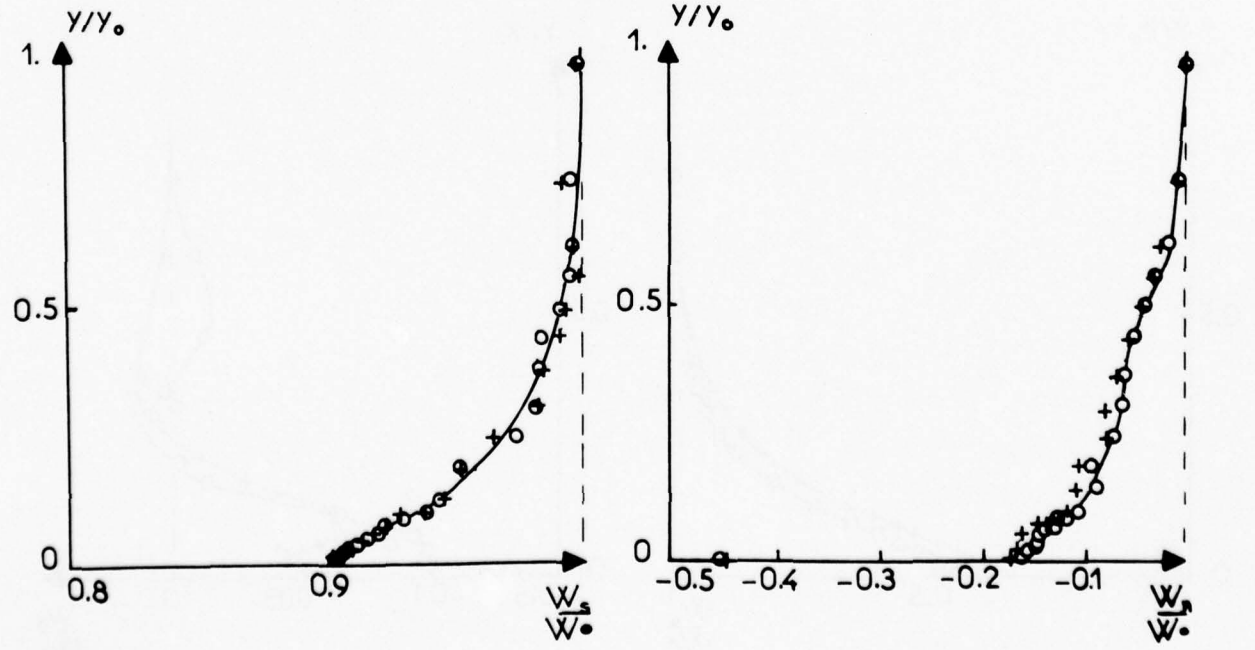


fig. 34

STATION 1 TIP

o nominal

+ near surge

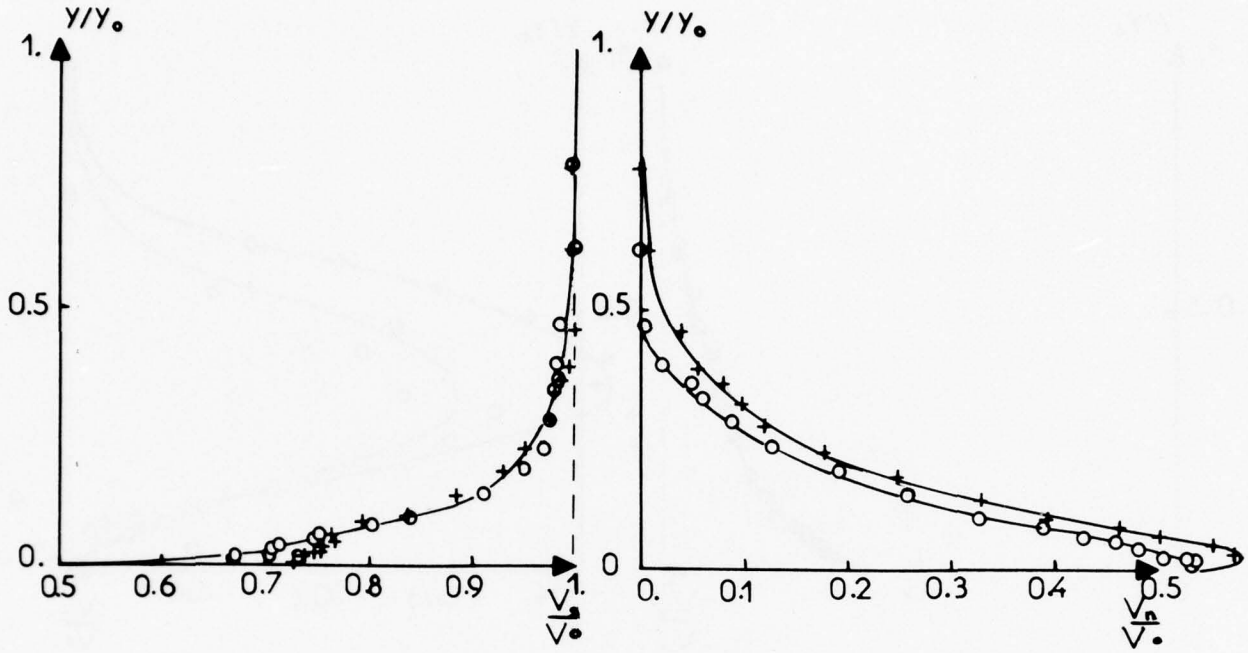


STATION 2 TIP

o nominal

+ near surge

fig. 35

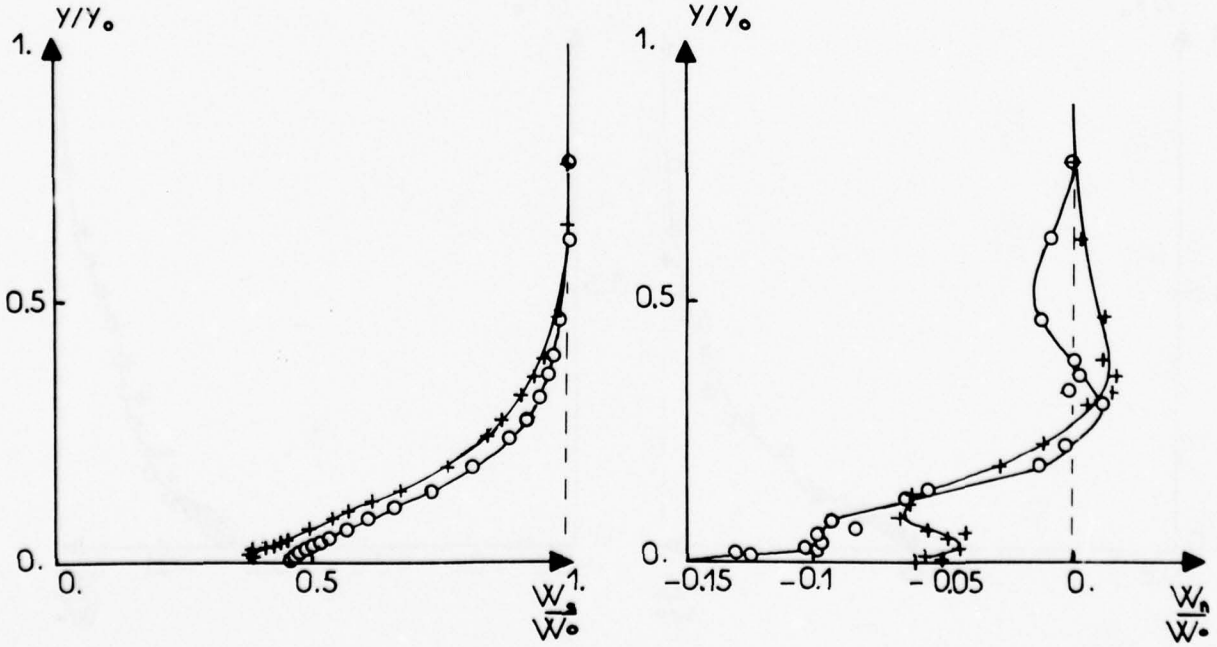


STATION 2 TIP

o nominal

+ near surge

fig. 36

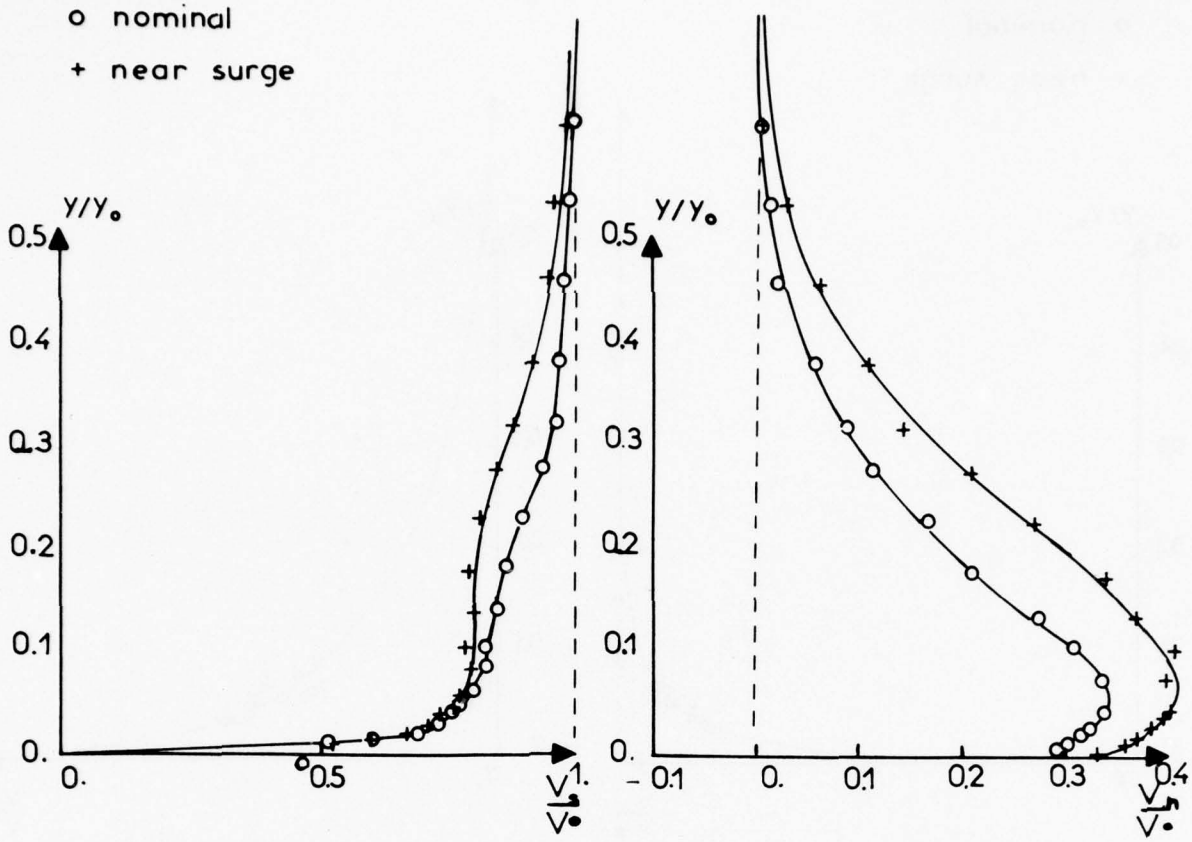


STATION 3 TIP

o nominal

+ near surge

fig. 37

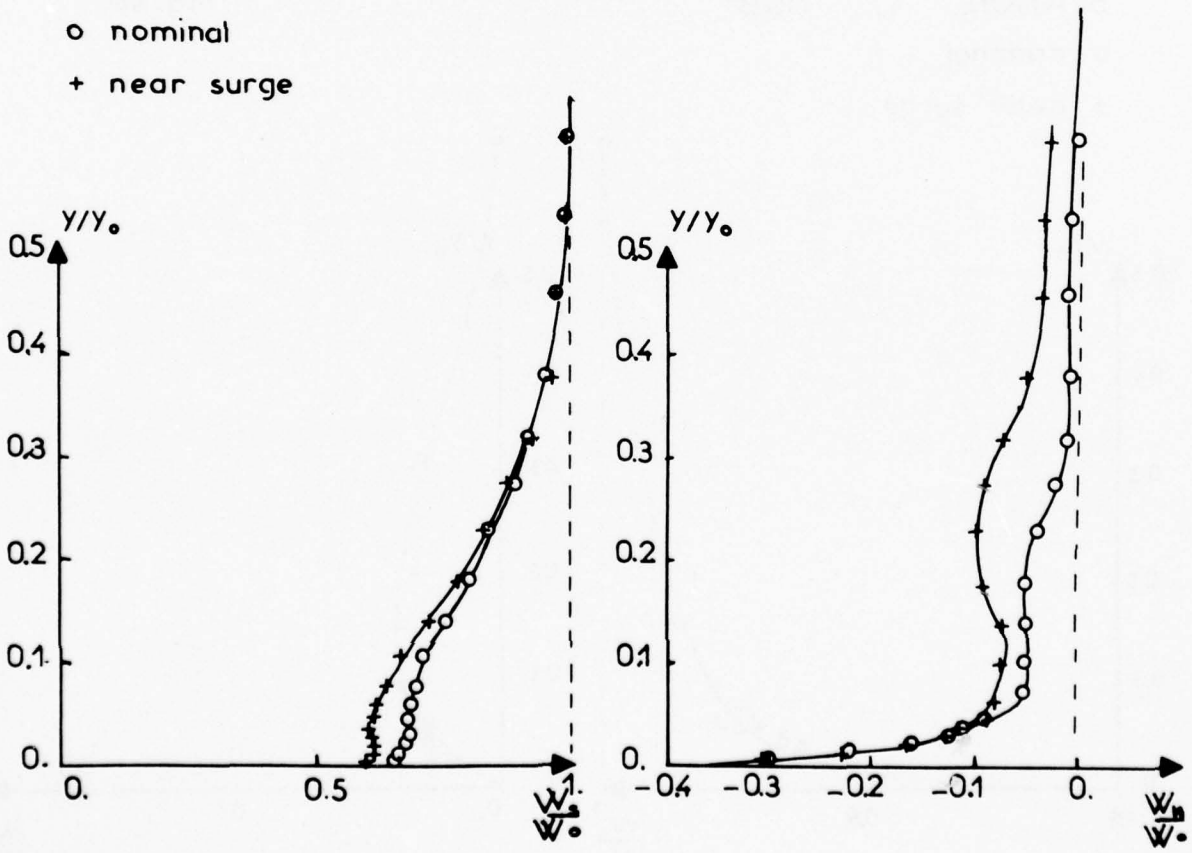


STATION 3 TIP

o nominal

+ near surge

fig. 38

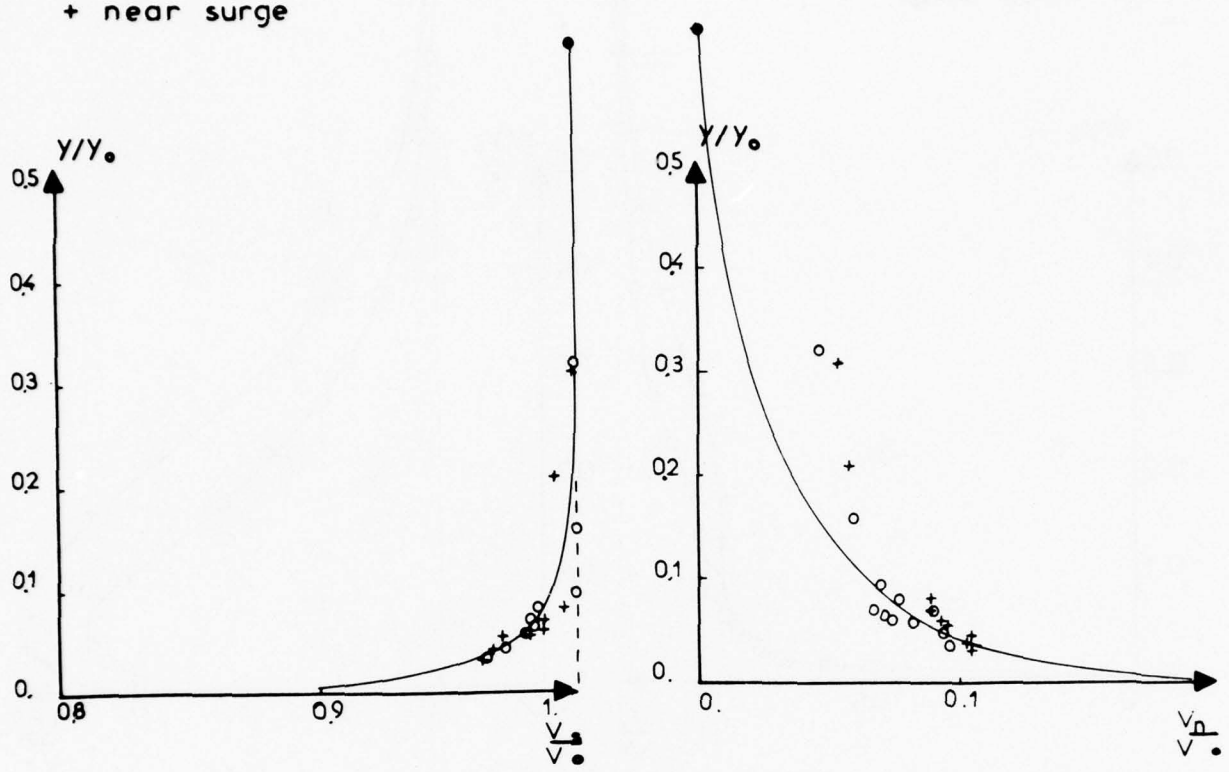


STATION 1 HUB

o nominal

+ near surge

Fig. 39

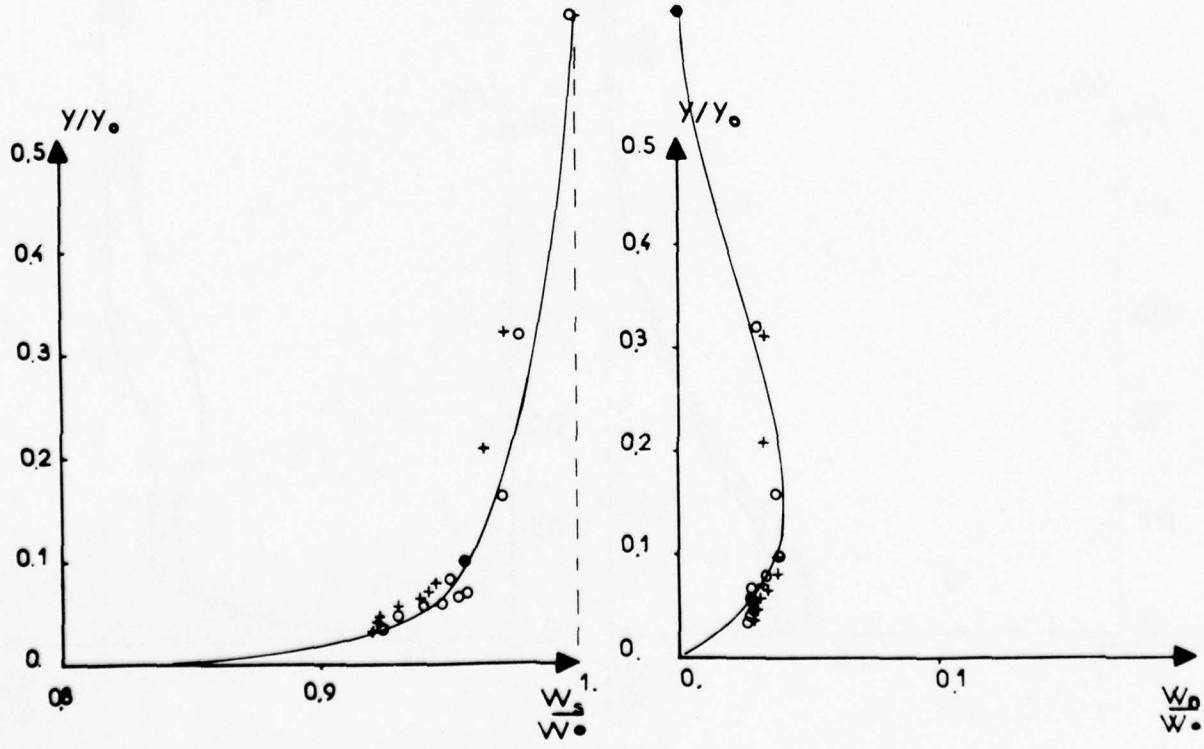


STATION 1 HUB

o nominal

+ near surge

Fig. 40

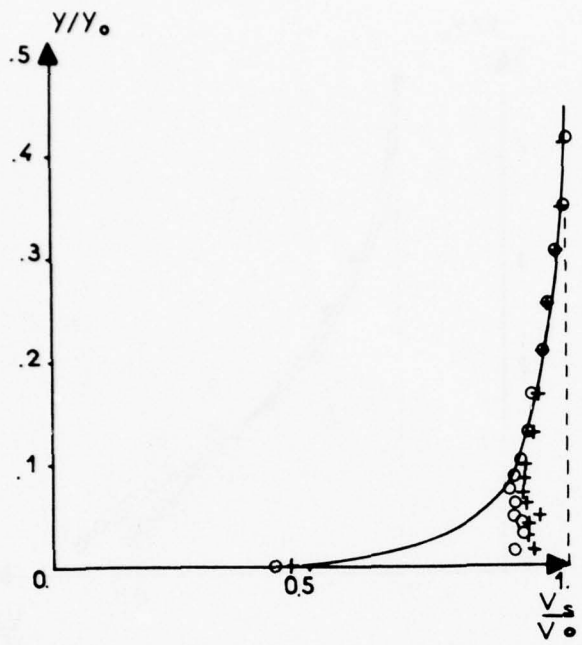


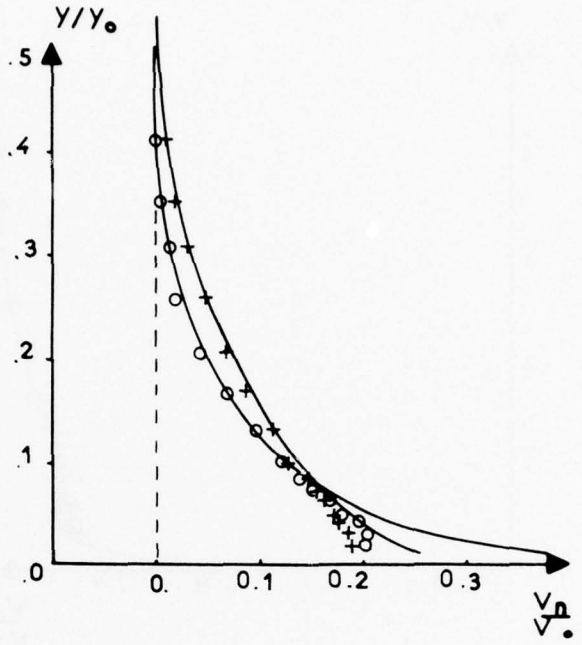
STATION 2 HUB

fig. 41

o nominal

+ near surge



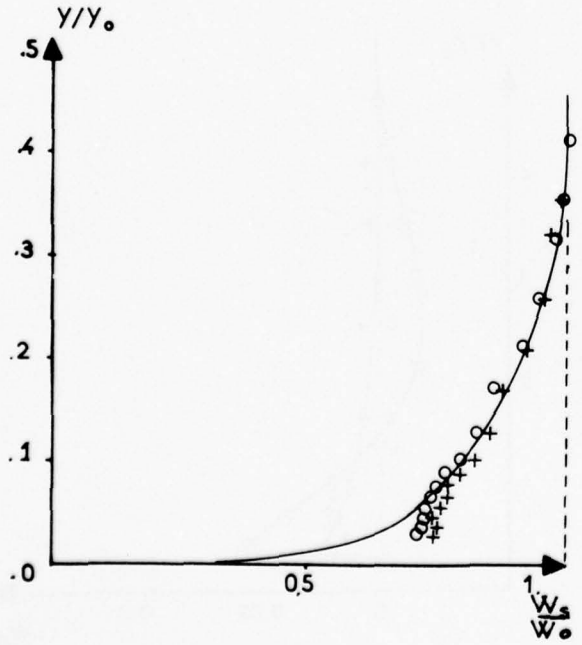


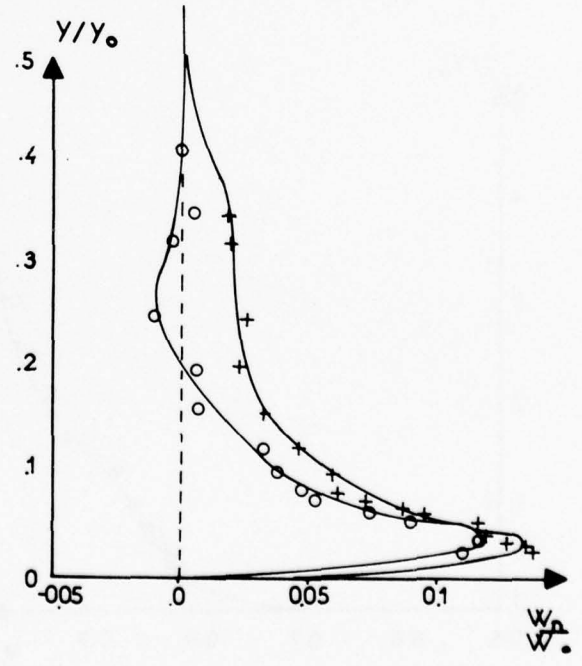
STATION 2 HUB

fig. 42

o nominal

+ near surge



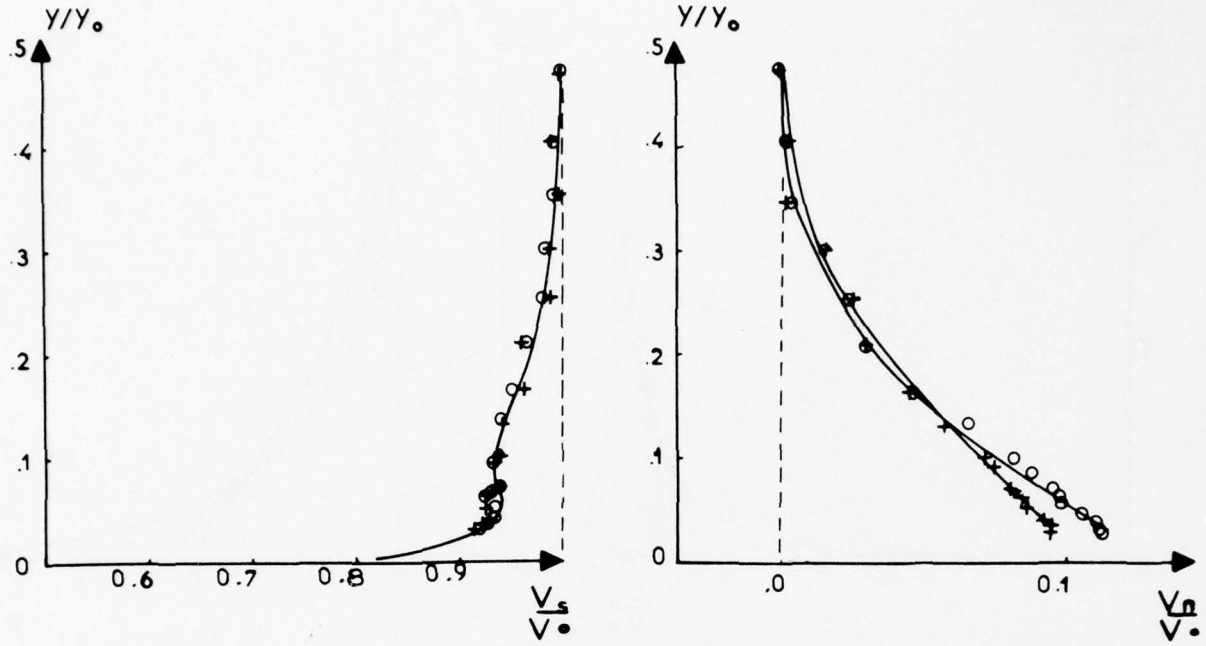


STATION 3 HUB

fig.43

o nominal

+ near surge



STATION 3 HUB

fig.44

o nominal

+ near surge

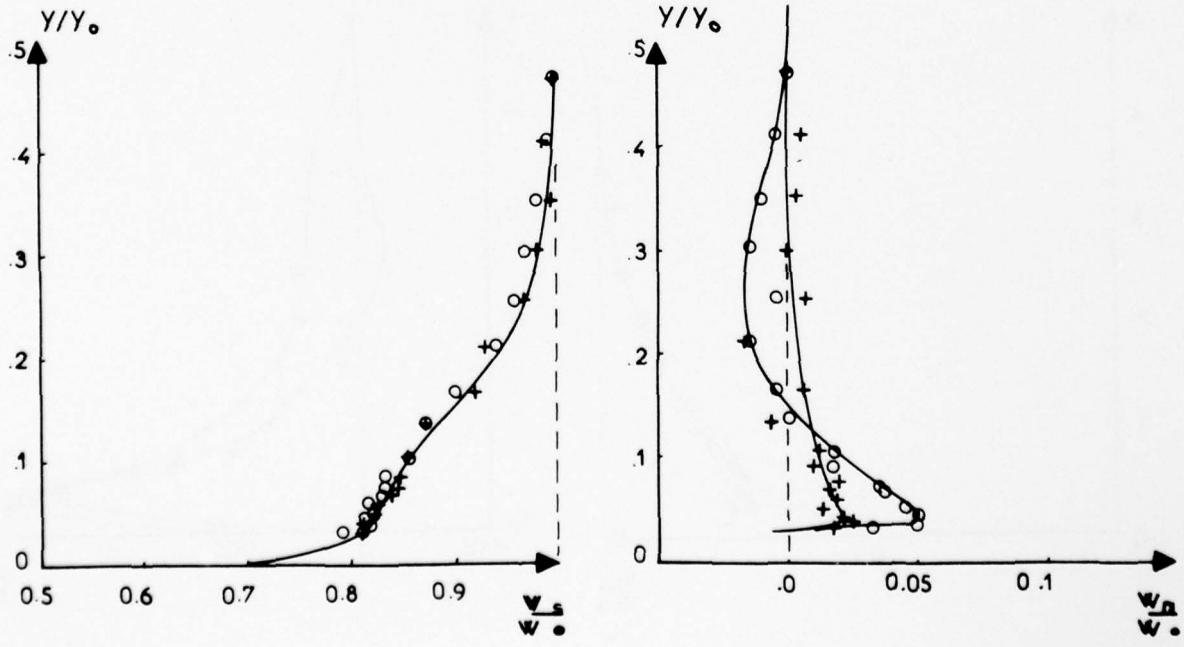
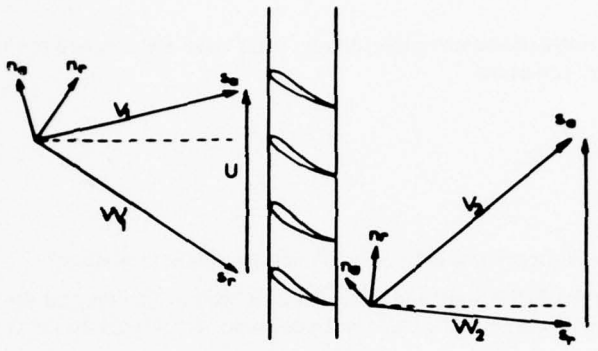


Fig. 45



a : absolute direction

r : relative direction

DISCUSSION OF PAPER 2 AND PAPER 3

H.Marsh

Will the authors describe the two loss models which have been used for the two calculation methods?

Author's Reply

The loss model was the same for the two forms of the radial equilibrium equation used. In both cases we have only taken the profile losses into account, disregarding the correlations for secondary losses. The main difference between the two equations used, is the additional term, which appears in Marsh's equations and which takes into account (correctly) the entropy increase. We were surprised to see that the usual radial equilibrium formulation gave more consistent results and that was the reason we reported them. Of course, one has to bear in mind that these results are depending on loss and deviation angle correlations, which are questionable.

J.W.Railly

In the application of the end-wall boundary layer theory what value was assigned to the factor $(1 - \epsilon)$ which appears in the "normality" condition?

Author's Reply

It is unity in our case.

J.H.Horlock

What increased value of wall shear stress did you use in applying Mellor's method?

How can you use the Wu/Marsh/Davis method (essentially an "elliptic" method) if the flow relative to the blades is supersonic – i.e. characteristics from the blade surfaces cannot get through to the upstream flow?

Author's Reply

We used the same value as Mellor did. $Cf = 0.01$ for the casing and $Cf = 0.003$ for the hub.

It is well established now (see for instance "Through Flow Calculations in Axial Turbomachinery, AGARD CP-195: Thiaville – modèle de calcul de l'écoulement dans les turbomachines axiales") that if one defines the quantity RVu in the equations and not the angle of the blading, the equations of radial equilibrium become elliptic for subsonic meridional velocities. Then one has, of course, to iterate on the relative flow angle. This presents, maybe, some numerical difficulties, but in principle it is correct.

E.E.Covert

We have had some problems obtaining a reasonably accurate measurement of average pressure and temperature in unsteady flow? Was a calibration procedure developed? What procedure did you use to validate the data? i.e. what averages do your probe data represent?

Author's Reply

Probes calibrations were done in a flow facility at the von Kármán Institute for pressure measurements.

For temperature calibration a cylindrical tube tunnel was used.

No calibration of the probes in unsteady flow was done. However, some indirect proof exists that the measurements were correct.

(a) Measurements at two different distances behind the trailing edge (planes 2 and 3, the first one just behind the rotor, the second one a chord behind) gave the same results in total pressure and total temperature within measurement errors.

(b) Check of the continuity at the three measuring planes (one in front and two behind the rotor) gave deviations of the order of $\pm 0.25\%$.

We feel that the fact that no differences exist between the two planes is probably due to the small size of the probes:

"tip" probe cylindrical $\emptyset$ 3mm
pressure holes $\emptyset$ 0.3mm

"hub" probe cobra type $\emptyset$ 8mm
pressure tubes $\emptyset$ 3.5mm

size of the thermocouple $\emptyset$ 2.5mm (or less)

E.E.Covert

What is blade passing frequency with respect to instrumentation?

Author's Reply

The blade passing frequency was:

$$f_B = 7500 \text{ HZ}$$

Bosman

I would like to make a comment on the matter which Professor Horlock has just raised, concerning the use of the Matrix method to calculate any form of supersonic flow. I am not sure, whether you said axially supersonic because within the blade row this method would normally fail if the flow itself was supersonic, rather than the axial component, but we developed the method ourselves at Manchester and we played with it for several years. We have never successfully been able to produce a converged solution even with a small supersonic patch and the stability analysis which I did, very clearly showed that there was a limit on convergence at Mach 1 within a blade channel. I've had cases where apparent convergence occured apparently up to Mach 1.2. We have always found that if you reduced the convergence criterion and the coarseness of the mesh it eventually comes down to Mach 1. So, I too am very surprised you were able to use this program usefully to predict the velocity profile in this area.

Author's Reply

See answer to Professor Horlock.

J.Dunham

Please give some details of your compressor, in particular the tip clearance?

You refer in your introduction to changes in inlet boundary layer and in "tip" clearance, but they are not mentioned again. What results were obtained? What was the effect of inlet boundary layer changes on efficiency?

Author's Reply

The only details that we can give about the experimental compressor, which was a S.N.E.C.M.A. compressor are the following:

hub to tip ratio = 0.597
tip clearance to height ratio = 0.021
external diameter at inlet = 0.780

Unfortunately, this is propriatory work and no more details can be given. The measurements varying tip clearance and inlet boundary layer were done. The series of measurements presented here are selected from them and they aim to present experimental evidence concerning the basic assumptions currently used for the development of secondary flow calculation methods and their matching with the "inviscid" flow calculation methods.

H.Marsh

What is the meaning of the figures given in the diagrams such as + 4% in Figure 4?

Author's Reply

These figures represent the translation of the different calculation results, so as to adjust their levels with those of the experimental results. In this sense we admit that the main effect of the wall boundary layers on the inviscid flow exists through the influence of the displacement thickness which was not always predicted accurately.

H-J.Heinemann

(1) What is the value of the recovery factor for the total temperature measurements?

(2) Is this value constant over the Mach number range?

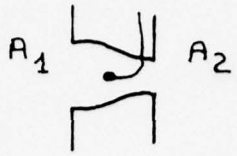
(3) Are the calibration curves the same coming from low Mach numbers to higher ones and coming from high Mach numbers to lower ones?

Author's Reply

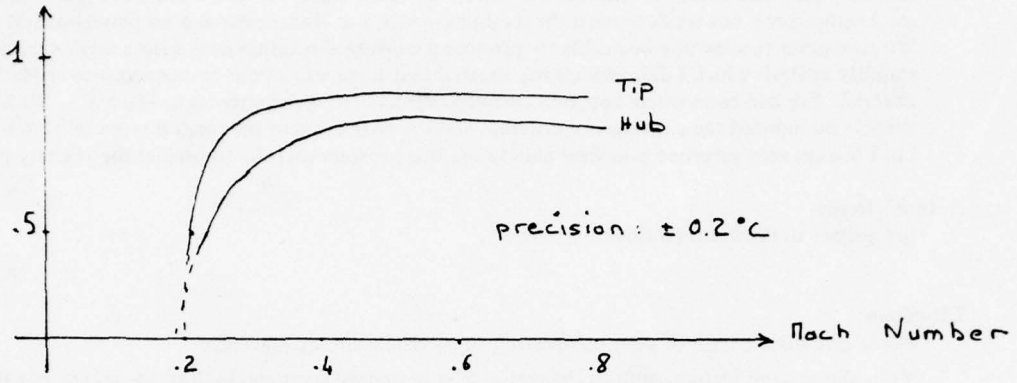
(1)

K = .9 for "Tip" probe
K = .85 for "Hub" probe

$$\frac{A_1}{A_2} = \frac{\text{Entrance area}}{\text{Outlet area}} = 2.$$



(2)



(3) No influence, but a systematic variation of mach numbers up and down have not really been made.

SECONDARY FLOWS AND ANNULUS WALL BOUNDARY LAYERS IN AXIAL-FLOW COMPRESSOR AND TURBINE STAGES

by
Prof. Dr.-Ing. H. E. Gallus and
Dr.-Ing. W. Kümmel
at
"Institut für Strahlantriebe und Turboarbeitsmaschinen", Technische Hochschule Aachen
D-5100 Aachen, Templergraben
Germany

Summary

The complex interdependencies of the various loss sources in axial turbomachines require very complicated correlations in the prediction of the total losses. Thus, it is worth proving the question how the really occurring total losses can be predicted by more simplified and idealized loss models. In this paper, an appropriate method is presented. In a first attempt, this method is demonstrated by the calculation of only three essential loss components in an axial-flow compressor stage and their comparison with the measured total losses. The loss components taken into account, are: profile losses, losses by the collateral wall boundary layer, and a certain part of losses caused by secondary flows.

In the stator of the axial compressor stage mentioned before, systematical measurements in the casing wall boundary layer were performed. Some results such as streamline patterns, pressure distributions and velocity profiles are presented.

At last, experimental investigations aiming at the reduction of secondary flow losses in an axial-flow turbine stage are dealt with. A considerable reduction was achieved by boundary layer grooves or fences for the very small aspect ratio of 0.25.

List of Symbols

A	area
b_p	axial width of cascade
c	absolute velocity
c_D	dissipation coefficient
c_p	specific heat at constant pressure
c^p	dimensionless pressure
c_u	dimensionless blade force in circumferential direction
D	diameter
F	force
g	dimensionless velocity distribution
H, h	enthalpie, specific enthalpie
J, j	dissipation, specific dissipation
l	blade height
M	Mach number
$\dot{m}$	mass flow
n	polytropic exponent, rotational speed
p	static pressure
Q, q	heat, specific heat
R	gas constant
r, φ, z	cylindrical coordinate system
s	chord length, specific entropy
s, n, z	orthogonal curvilinear coordinate system
T	temperature
u	blade velocity
V, v	volume, specific volume
w	relative velocity
y, Y	spec. flow energie, flow energie
z	blade number
z'	axial profile coordinate
α	absolute flow angle
β	relative flow angle
δ	boundary layer thickness
δ_1	displacement thickness
δ_2	momentum loss thickness
δ_3	energy loss thickness
η	polytropic efficiency
η^*	dimensionless measuring distance from the wall
λ	loss ratio
Π	sum of laminar and turbulent viscosity
ν	hub-to-tip ratio
π	pressure ratio
φ	flow coefficient
ρ	density
τ	shear stress

Subscripts

A, a	outlet, axial direction
C, c	calculated, collateral
D	pressure surface
DS	direct secondary flow loss
E	inlet
H	hub
INA	international normal atmosphere
IS	indirect secondary loss
N	after changing reference frame
P	profile
R	rest
r, φ, z	r, φ, z direction
S	secondary, suction surface
St	stage
s, n, z	s, n, z direction
T	tip, turbine
t	spacing, total
u	circumferential direction
V	before changing reference frame
W	annulus wall
Δ, δ	difference, edge of the boundary layer
$-$	mean value
0	before entrance guide vanes
1	before rotor
2	behind rotor
3	behind stator
$\cdot$	per time unit

1. Introduction

Further progress in the development of turbomachines essentially depends on an improved determination of the influence of losses on the internal flow. For a more powerful use of modern computer-aided design methods, there is an increasing need of qualified loss models that are compatible with such design methods. Models of that kind are expected to deliver the integral losses at design point and in the off-design region. On the other hand, it should be possible to correlate the integral losses to each of all loss-producing sources as well as to analyse and optimise the parameters of influence. Obviously, systematical experiments will play an important part for both checking appropriate loss models and improving the internal flow-behaviour.

2. Flow Losses in Axial-Flow Turbomachines

2.1 Definition of Flow Losses

The influence of the viscosity of all technical fluids is taken into account by the friction terms in the fundamental equations of the three-dimensional flow and prevents a general solution of the flow field in turbomachines. In the following, the flow losses are defined by the specific "dissipation j", i.e., the entropy production by irreversibilities of the flow. By this definition, according to the second law of thermodynamics there is always valid

$$j \geq 0 \tag{1}$$

Thus, the total dissipation can be determined by summing up all individual loss components.

2.2 Determination of Losses by Measurements

The energy conversion for a part $d\dot{m}$ of the mass flow passing from E to A in Fig. 1 can be described by the integral form of Gibbs' fundamental equation

$$d\dot{m} \int_E^A T\,ds = q_{EA}\,d\dot{m} + j_{EA}\,d\dot{m} = \Delta h_{EA}\,d\dot{m} - y_{EA}\,d\dot{m} \tag{2}$$

On condition that the inner and outer annulus walls of the flow channel do not move relatively to the blades and can be regarded adiabatic, there is valid for the whole channel between two adjacent blades:

$$\int_{\dot{m}} q_{EA}\,d\dot{m} = \dot{Q}_{EA} = 0 \tag{3}$$

Applying Eq. (2) to the whole channel and taking into account Eq. (3), delivers the losses in the flow channel:

$$\dot{J}_{EA} = \Delta\dot{H}_{EA} - \dot{Y}_{EA} \tag{4}$$

For this, the measured values are needed only in the entrance area E and the exit area A. As enthalpy is a state variable, its change can be determined from the difference $\Delta\dot{H}_{EA} = \dot{H}_A - \dot{H}_E$ on the areas in front and behind the channel, with (for a perfect gas):

$$\dot{H}_E = \frac{\bar{c}_p}{R} \int_{r_{HE}}^{r_{TE}} \int_0^{\varphi_t} p_E(r_E, \varphi_E)\, c_{aE}(r_E, \varphi_E)\, r_E\, d\varphi_E\, dr_E \tag{5}$$

$$H_A = \frac{\bar{c}_p}{R} \int_{r_{HA}}^{r_{TA}} \int_0^{\varphi_t} p_A(r_A, \varphi_A)\, c_{aA}(r_A, \varphi_A)\, r_A\, d\varphi_A\, dr_A\,, \tag{6}$$

The specific flow energy y_{EA} is dependent on the path of the change of state along the channel. Assuming polytropic change of state and rotational-symmetric entrance conditions on rotational-symmetric flow surfaces, the flow energy can be determined from measured values according to Eq. (7). For this, the radii r_E and r_A are known as $r_E = r_E(r_A)$ from mass flow integration:

$$\dot{Y}_{EA} = \int_{r_{HA}}^{r_{TA}} \int_0^{\varphi_t} \left(\frac{n}{n-1}\right)\Big|_{r_A,\varphi_A} \left[1 - \frac{T_E(r_E(r_A))}{T_A(r_A, \varphi_A)}\right] p_A(r_A, \varphi_A)\, c_{aA}(r_A, \varphi_A)\, r_a\, d\varphi_A\, dr_A \tag{7}$$

with

$$\left(\frac{n}{n-1}\right)\Big|_{r_A,\varphi_A} = \frac{\ln\left[p_A(r_A, \varphi_A) / p_E(r_E(r_A))\right]}{\ln\left[T_A(r_A, \varphi_A) / T_E(r_E(r_A))\right]} \tag{8}$$

From measured values, Eqs. (4) ... (8) permit the determination of the losses occurring in the flow channel.

2.3 Calculation of Component Losses

2.3.1 Introduction of Loss Models

The deformation work by frictional forces on the surface of a volume element causes dissipation. For the element, this process can be described mathematically. For getting quantitative results, the integration over all elements in the entire channel would have to be required. This can hardly be realized, as the distributions of the local flow properties within the channel are unknown, in general. Thus, the prediction of losses cannot be prosecuted in such a desirable general validity.

Other possibilities for the prediction of losses are given by empirical relations, e.g. the well-known diffusion factor /1/, or, for only small changes in size or design, by practical experiences.

This paper deals with an attempt for a detailed prediction of some essential loss components. To reveal the relations between the losses and the various design parameters, is

an important aim for optimizing already during the design phase. For this purpose, the introduction of a simplified model of the mode of loss formation seems to be unavoidable. The relation

$$\dot{J} = \dot{J}_P + \dot{J}_W + \dot{J}_S \tag{9}$$

defines the simplified model presented in this paper. The loss components $\dot{J}_P$ and $\dot{J}_W$ are considered to be caused by the surface friction along the blade profiles ($\dot{J}_P$) and on the annulus walls between them ($\dot{J}_W$) for the idealized assumption of a quasi-steady flow without secondary flow components. The secondary losses $\dot{J}_S$ consist in all other loss components, such as direct and indirect secondary flow losses (see 2.4.3), losses by unsteady flow, mixing losses, local shocks and other effects. In the following sections, both well-known and new approaches to the calculation of the idealized loss components $\dot{J}_P$, $\dot{J}_W$, and $\dot{J}_{DS}$ ("direct secondary flow losses") are dealt with. These three components are determined within the proposed model. Thus, the calculated losses $\dot{J}_C$ are represented by

$$\dot{J}_C = \dot{J}_P + \dot{J}_W + \dot{J}_{DS}. \tag{10}$$

All remaining losses were not calculated for this comparison and are comprehended as "rest losses $\dot{J}_R$" in the following. For checking both the usefulness of this extremely reduced loss model and the applied computation methods, the losses of the axial-flow compressor described in section 3.1, were calculated for the design point and a wide range below,and compared with measured total losses ($\dot{J}$). Thus, the rest losses

$$\dot{J}_R = \dot{J} - \dot{J}_C \tag{11}$$

were determined, too.

2.3.2 Profile Losses $\dot{J}_P$

The prediction of the profile losses for steady flow can be regarded as a solved problem. They were determined here only for getting the sum of the calculated losses and the ratios of the various component losses.

After the unrolling of the cylindrical profile section into a plane the computation of the potential flow field round the blade profiles was performed according to the singularity method of Oellers /2/.

The following computation of the boundary layers according to Walz /3/ delivers the dissipation in the boundary layers of suction and pressure side. The mixing losses in the wake behind the profile are determined by a modified method in accordance with Traupel /4/. Fig. 2 shows the calculated profile losses of each cascade of the test compressor (see 3.1), plotted for the whole range of operation. Flow separation at off-design operation could not be taken into account. Additionally, profile losses including separation were extrapolated from NACA-data for comparable profiles /5/ and marked by dashed lines.

2.3.3 Annulus Wall Losses $\dot{J}_W$

Other than the profile losses, the annulus wall losses cannot be determined analytically till now without considerable simplifications and using empirical data, as the occurring three-dimensional boundary layer flow is very complicated. Here, a method is proposed taking into account the non-rotational flow within the cascade. Empirical data are needed only in so far as they are inherent in nowaday boundary layer computation methods. Machine-bound empirical data are not used.

For the development of an appropriate approximation, the flow conditions near the side wall are considered (Fig. 3). Assuming that only velocity gradients normal to the wall contribute to dissipation, and on the understanding that the radial velocity $c_z \approx 0$, the dissipation in a volume element near the wall becomes

$$d\dot{J} = \tau_{nr} \frac{\partial c_n}{\partial z} dV + \tau_{sr} \frac{\partial c_s}{\partial z} dV \tag{12}$$

As was pointed out in Section 2.1, a splitting of the dissipation is possible due to its formation. The second term on the right side of Eq. (12) represents the dissipation occurring in an idealized side wall boundary layer on the following assumptions:

a) no secondary flows,

b) no interaction with the boundary layers on the profiles in the corners between side walls and profile surfaces,

c) quasi-steady flow conditions.

This fictive flow configuration is called "collateral side wall boundary layer". The losses in this boundary layer are defined as isolated side wall friction losses $\dot{J}_W$. This chapter aims at the determination of this component loss.

The first term on the right side of Eq. (12) represents further losses on the side wall originated by secondary flows. Their computation will be discussed in Chapter 2.3.4.

The fluid particles of the collateral side wall boundary layer move on flow surfaces extending between streamlines of the adjacent main flow and their projection normal to the side wall. Fig. 4 shows the conditions for an axial cascade developed into a plane. The streamlines of the main flow are calculated with the singularity method of Oellers /2/. Then, the discrete flow surfaces of the collateral side wall boundary layer are unrolled into the z,s-plane, in which a two-dimensional boundary layer computation after Walz /3/

is carried through. The calculation delivers the distribution of the integral dissipation coefficient

$$c_D = \frac{d\dot{J}/dA}{\rho_\delta c_\delta^3} \tag{13}$$

along the flow surfaces. The numerical integration of the loss distribution on the side-wall surface (Fig. 1) determines the side-wall friction losses at the hub (J_{WH}), at the casing wall (J_{WT}) and by summing up, for the cascade (J_W):

$$\dot{J}_{WH,T} = z \int_0^{\varphi_t} \int_E^A c_D \, \rho_\delta \, c_\delta^3 \, dz \, d(r_{H,T}\varphi) \tag{14}$$

$$\dot{J}_W = \dot{J}_{WH} + \dot{J}_{WT} \tag{15}$$

There must be regarded that unrolling an axial cascade into the plane leads to errors which are negligible only for a small boundary layer thickness compared with the radii of the side walls. As secondary flows had been excluded by definition, the side walls are assumed not to move relatively to the blade channel. For the low Mach numbers of the example, the calculation was done for incompressible flow. This is also in accordance with Truckenbrodt /6/, who stated the conformity between the friction coefficients for compressible subsonic flow through smooth pipes and those for incompressible flow.

For the flow calculation in an axial turbomachine, there has to be considered the change between rotating and not moving reference systems. With the change of the system, a three-dimensional twisted boundary layer profile is built up in the following cascade out of the collateral side-wall boundary layer of the preceding cascade. Fig. 5 demonstrates these conditions for the change of the reference system. In order to continue the two-dimensional boundary layer computation on collateral flow surfaces in the following cascade, there has to be established a collateral start profile by projecting the vectors of the twisted starting profile into the direction of the main streamline at cascade entrance. According to Fig. 5, the relation for the collateral velocity at rotor entrance of the compressor can be written as follows for the change from stator to rotor:

$$w_{1c} = \frac{c_{a1} w_{1\delta}}{c_{a1\delta}} + (u - c_{a1} \tan \alpha_1 - c_{a1} \frac{u - c_{a1\delta} \tan \alpha_1}{c_{a1\delta}}) \frac{u - c_{a1\delta} \tan \alpha_1}{w_{1\delta}} \tag{16}$$

Division of Eq. (16) by the velocity $w_{1\delta}$ at the edge of the boundary layer delivers the dimensionless start profile $g_N = w_{1c} / w_{1\delta}$ at the entrance of the following cascade.

By use of the relations in Fig. 5, there is generally valid (compressor; turbine; change from rotor to stator and from stator to rotor):

$$g_N = \frac{g_V \varphi^2 + (1 - z\, g_V)\, k}{\varphi^2 + k^2} \tag{17}$$

If there is used an integral method for the calculation of the boundary layers, the thickness parameters have to be transformed, too. Assuming constant density and blade velocity within the boundary layer, the thickness parameters after change of reference system result in

$$\delta_{1N} = \delta_{1V} \frac{\varphi^2 - k\,z}{\varphi^2 + k^2} \tag{18}$$

$$\delta_{2N} = \frac{\delta_{2V} (\varphi^2 - k\,z)^2 + \delta_{1V} \left[k (\varphi^2 - k\,z)\right]}{(\varphi^2 + k^2)^2} \tag{19}$$

$$\delta_{3N} = \frac{\delta_{3V} (\varphi^2 - k\,z)^3 + \delta_{2V} \left[3k (\varphi^2 - k\,z)^2\right] + \delta_{1V} \{k \left[\varphi^4 + 2\varphi^2 k^2 - k^2 z (2 - z)\right]\}}{(\varphi^2 + k^2)^3} \tag{20}$$

The transformation equations permit the computation of the side-wall friction losses in the cascades of the axial-flow compressor under consideration in the whole range of operation. The results are plotted in Fig. 6.

2.3.4 Secondary Losses $\dot{J}_S$

The secondary losses $\dot{J}_S$ introduced in Chapter 2.3.1, comprehend the losses caused by the various components of secondary flow:

a) cross flow in the side-wall boundary layers between pressure and suction side of adjacent blades,

b) radial secondary flow in the boundary layer on the blade surface between the side-walls,

c) clearance flow at free blade ends,

d) relative secondary flow by relative motion between side walls and blade channel.

After all, secondary losses comprehend all rest losses which are not included in the profile or side-wall friction losses defined before, e.g., losses by unsteady flow effects due to rotor-stator interaction, mixing losses, losses by local shocks, etc. Out of the losses directly generated by the secondary flows a) to d), the components a) and b) are determined by an approximation explained in the following. They are called "direct" secondary flow losses and are denoted by $\dot{J}_{DS}$. The subsequent losses caused by secondary flows, the so-called "indirect" secondary flow losses denoted by $\dot{J}_{IS}$, e.g., separation losses etc., are not determined in this contribution, nor the losses according to c) and d). These component losses not calculated in this example are comprehended in the following by the rest losses $\dot{J}_R$ (Eq. (11)).

The losses in a volume element dV of the side-wall boundary layer are described by Eq. (12); see also Fig. 3. The shear stresses τ_{ik} can be represented by Newton's approach with the aid of a turbulent total viscosity $\bar{\mu}$. Considering a volume element dV = h·ds·dn extending from the wall to an area distanced by h, Eq. (21) will yield the losses in the three-dimensional wall boundary layer

$$d\dot{J} = d\dot{J}_{DS} + d\dot{J}_{W} = \int_{o}^{h} \bar{\mu} \left(\frac{\partial c_n}{\partial z}\right)^2 dz\, ds\, dn + \int_{o}^{h} \bar{\mu} \left(\frac{\partial c_s}{\partial z}\right)^2 dz\, ds\, dn \qquad (21)$$

where $h > \delta$.

Because of the considerable uncertainty in the determination of the turbulent total viscosity $\bar{\mu}$, the loss rate λ is introduced by Bitterlich /6/ as follows:

$$\lambda = \frac{d\dot{J}_{DS}}{d\dot{J}_{W}} = \int_{o}^{h} \bar{\mu} \left(\frac{\partial c_n}{\partial z}\right)^2 dz \Big/ \int_{o}^{h} \bar{\mu} \left(\frac{\partial c_s}{\partial z}\right)^2 dz \qquad (22)$$

In this expression, the viscosity appears both in numerator and denominator. Thus, the influence of the uncertain turbulent total viscosity is weakened. In the calculations of the example, there were used a power law for the collateral flow profile c_s and an approximation according to Bitterlich /6/ for the cross-flow profile c_n. The viscosity distribution was adapted to results of flow measurements by Nikuradse /7/ in pipes. Numerical checks for various viscosity distributions revealed a small influence on the loss rate λ. After the determination of λ, the direct secondary flow losses according to a) can be calculated:

$$\dot{J}_{DS} = \int_{A} \lambda\, d\dot{J}_{W} \qquad (23)$$

resp.

$$\dot{J}_{DS} = \bar{\lambda}\, \dot{J}_{W} \qquad (24) \qquad \text{with} \qquad \bar{\lambda} = \int_{A} \lambda\, d\dot{J}_{W} \Big/ \dot{J}_{W} \qquad (25)$$

The λ-rate is relatively insensitive to changes of the empirical viscosity distribution. The losses $\dot{J}_W$ in the collateral side-wall boundary layer are calculated with sufficient exactness by the aid of a two-dimensional boundary layer computation method /3/, whose dissipation coefficients are experimentally checked. Thus, the direct secondary flow losses can be regarded sufficiently proved, too. Analogous considerations are valid for the three-dimensional profile boundary layer. In this way, the direct secondary flow losses in a cascade according to a) and b) are covered by the relation

$$\dot{J}_{DS} = (\bar{\lambda}_{WH}\, \dot{J}_{WH} + \bar{\lambda}_{WT}\, \dot{J}_{WT}) + (\bar{\lambda}_{PS}\, \dot{J}'_{PS} + \bar{\lambda}_{PD}\, \dot{J}'_{PD}) \qquad (26)$$

In this Eq., $\dot{J}'_{PS}$ and $\dot{J}'_{PD}$ are representing the profile losses in the boundary layers of the profiles (without mixing losses in the wakes). Figs. 7 and 8 show the distribution of the loss rates λ_{WT} and λ_{PS} for the guide vanes in front of the compressor stage. The loss rates on the side-walls are plotted in Fig. 9 for the whole range of operation.

3. Measurement of Losses and Investigation of Annulus Wall Boundary Layers in an Axial-Flow Compressor Stage

3.1 Test Rig and Instrumentation

The experiments for the determination of the losses and the measurement of the side-wall boundary layer were carried through in a one-stage subsonic axial-flow compressor with entrance guide-vanes in front of the rotor. All the details are dealt with in /8/. Some characteristic data of the stage are as follows:

tip diameter	$D_T = 0.428$ m	values at design point (n = 9500 rpm):	
hub-to-tip ratio	$\nu = 0.38$	blade velocity at the tip	$u_{2T} = 210$ m/s
maximum speed	$n_{max} = 12000$ rpm	axial-flow velocity	$c_{ao} = 115$ m/s
		difference of total enthalpy	$\Delta h_{to3} = 10060$ J/kg
		pressure ratio	$\pi = 1{,}11$
		polytropic efficiency	$\eta = 0.88$

The compressor is provided with an extremely long inlet pipe (21.7 D_T) for the realisation of thick side-wall boundary layers.

The construction of the compressor is demonstrated in Fig. 10. There, the essential measuring device for the investigation of quasi-steady flow is pointed out, too:

A: Five-hole pressure probes connected with NTC-temperature probes for the determination of the properties $\vec{c}$, T, and p in the axial clearances 0, 1, 2, and 3. Probe motion by computer-governed device.

B: Pressure probe for measuring in the boundary layer of the stator casing wall.

C: Adapting piece for use of B in the axial clearances 0 to 3.

D: Wall segment with 33 holes, to allow the measurement of wall pressure distribution and boundary layer flow field, and to permit also colour injection.

E: Plugs provided with static wall pressure holes.

F: Stator blade and wall segment for measuring pneumatically the distributions of static pressure on the casing wall and on the profile within the side-wall boundary layer.

G, H: Revolving guide-vanes and stator blades with static wall pressure tappings each at 24 positions around the profile and at 25 (23) different radii along the blade.

I: Pick-up for digital speed measurement.

For the investigation of the casing-wall boundary layer a special wall segment was developed (Fig. 11) being mounted from outside. The 33 holes of the segment are closed by plugs, each provided with a static pressure measuring tapping. Each of these plugs can be replaced one after the other by the device B (Fig. 10) carrying an extremely small pressure probe of a special type shown in Fig. 12 for measuring the flow field within the side-wall boundary layer. The device B permits radial shifting of this probe and turning about its axis. Firstly, the two-hole part of this probe is directed upstream and revolved until the two holes indicate the same pressure. Thus having met the flow angle, the probe is turned by 180 degrees to measure the local total pressure by the tiny Pitot-tube at the other side of this probe. After having removed this probe and having replaced it by the plug for the measurement of the static wall pressure p_T, the latter is determined. From this one and from the knowledge of local flow angle and total pressure the static pressure distribution within the boundary layer is determined taking into account the simplified condition of radial equilibrium. This measuring procedure owns two advantages:

a) The special probe fulfils the requirements of a normal three-hole probe but needs only the cross-section for two tubes. The compact construction of the two-hole part guarantees minimum sensitivity to gradients.

b) The static wall pressure can be measured, while the probe is removed. Thus, the measured results are not falsified by the influence of the probe-body.

3.2 Determination of Losses for the Entire Range of Operation

Fig. 13 shows the compressor map. The various points of operation are defined by the key number KFELD, where the first and second figures are denoting the speed in r.p.m. divided by 100, and the third, fourth and fifth figures are representing certain throttling positions (000 ... 700). In Fig. 14, there are plotted the total flow losses determined by measurements in the whole operation field of the compressor. These measured data are compared with the calculated component losses J_W, J_{DS}, and J_P. It is evident that at a throttling position near design point, the rest losses J_R between measured and calculated data are relatively small. With increasing throttling, the rest losses progressively increase due to flow separation effects. The latter were not taken into account for the determination of the component losses but for the profile losses.

3.3 Boundary Layer on the Annulus Wall of the Stator Casing

3.3.1 Streamlines and Pressure Distributions

Fig. 15 shows the $(33 + 2 \cdot 6) \cdot 11 = 495$ measuring positions within the casing-wall boundary layer of the stator. To support the measurement by the probe, the directions of the wall streamlines (surface 1) were determined by colour injection. That was done via the static wall pressure tappings in the 33 wall plugs. Leaving the small hole, the colour droplet traces the tangent to the streamline just at the hole. These tangents were measured at each of the 33 holes. From their field the wall streamlines could be determined by numerical integration according to Runge-Kutta-Butcher /9/. In the same way, the streamlines in the boundary layer were calculated from the field of angles measured by the two-hole probe. For this, the flow was considered to stream on co-axial cylindrical surfaces. In Fig. 16, there are composed the stream lines for the various flow surfaces 1 ($\eta^* = 0$); 2 ($\eta^* = 0.023$); 4 ($\eta^* = 0.063$); 7 ($\eta^* = 0.178$); and 12 ($\eta^* = 1.0$ wall distance = 30.4 mm) at operation point KFELD 50100. Because of the preceding rotor the streamlines in the wall boundary layer of the stator show an increasing incidence angle the nearer they are to the wall (see Fig. 5). As a consequence, there occurs flow separation at the casing wall ($\eta^* = 0$) near the suction side. Thus, the stagnation point is shifted downstream along the compression side of the profile. This results in larger pressure gradients and deflection towards the suction side of the adjacent profile. After all, there is to be observed a divergence of the streamlines near the suction side and a convergence near the compression side of the profiles. At a distance of 0.7 mm from the wall ($\eta^* = 0.023$) the same tendencies are still ruling, but there is already noticeable the influence of higher velocities. On surface 4, the kinetic energy of the fluid particles is as high that they are not turned enough by the pressure field at the compression side and hit the surface, there. At the suction side, there is still separation but the deflection is increasing. At $\eta = 0.178$, the stagnation point of that streamline nearest to compression side moves downstream because of the decreasing incidence.

Near the suction side, the flow is re-attached. The flow pattern has already assimilated to that of the main flow ($\eta^* = 1.0$). Moreover, the direction field of surface 2 ($\eta^* = 0.023$) is represented additionally to the streamline pattern of the main flow ($\eta^* = 1$) in Fig. 16. This kind of representation permits a survey of magnitude and direction of the maximum twist of the velocity profile in the boundary layer. At cascade inlet, a positive cross-flow component generated by the rotary motion of the rotor, can be noticed (Fig. 5). This cross-flow is reduced by the superposition with secondary cross-flow (from compression to suction side). Thus, there is to be found a boundary layer with only small secondary flow components at the cascade outlet. At cascade inlet near the suction and compression side, a sudden change in the velocity profile takes place because of the big pressure gradients dominating there. Whereas Fig. 16 represents a throttled point of operation of the compressor, there are plotted the corresponding streamline patterns for design flow-coefficient (KFELD 80000) in Fig. 17. Here, the incidence angle is considerably smaller. Therefore, the wall streamlines neither show such an extreme difference between convergent and divergent patterns, nor accurs there any flow separation.

The streamlines rapidly assimilate to the main flow with increasing distance from the wall. For this point of operation, the fluid leaves the cascade nearly without secondary flow components, as well.

Moreover, pressure distributions on the stator profile were measured at different distances from the wall within the casing-wall boundary layer. They were made dimensionless by the inlet dynamic head at the edge of the boundary layer:

$$c_p = \frac{p(z') - p_2}{\left(\frac{\rho}{2} c^2\right)_{2,\eta = 1}} \tag{27}$$

Fig. 18 shows the pressure distribution for the point of operation KFELD 50100. For increasing distance from the wall, there can be noticed a growing pressure drop at the suction side and a movement of the stagnation point towards the leading edge.

The pressure distributions for the operation point KFELD 80000 are plotted in Fig. 19. The pressure difference along the profile is smaller than above but the pressure drop along the suction side can be observed with increasing distance from the wall, as well.

In Fig. 20, the coefficient of the circumferential force of the stator blade

$$c_u = \frac{dF_u}{dr} \frac{1}{b_p \left(\frac{\rho}{2} c^2\right)_{2,\eta^* = 1}} = \int_0^1 \left[c_{p_D} - c_{p_S} \right] d\left(\frac{z'}{b_p}\right) \tag{28}$$

is represented for different operation points as a function of the distance from the wall.

3.3.2 Velocity Profiles of the Annulus Wall Boundary Layer

A survey of the three-dimensional boundary layer flow near the stator casing wall is given by Figs. 21 and 22. The dimensionless collateral and cross-flow profiles (see Fig. 3) are plotted for several mainstream surfaces (see Fig. 4) and for five different axial positions on each one. The cross-flow component at the entrance of the cascade, generated by the preceding rotor, is diminished on its path through the cascade. Comparing the two operating points represented, it is obvious that the cross-flow at the entrance plane is smaller when the compressor is running at the design flow coefficient (KFELD 80000).

Within the casing wall boundary layer the distributions of certain dimensionless velocity components at five subsequent axial positions are displayed in Figs. 23 and 24. The streamsurfaces, these profiles are attached to, are indicated with "5" in Figs. 21 and 22 respectively. The difference between the real velocity ratio c/c_δ and the collateral velocity ratio c_s/c_δ is recognized to be very small.

4. Some Remarks on the Reduction of Secondary Flow Losses in an Axial-Flow Turbine Stage

4.1 Test Rig and Instrumentation

The investigations aiming at a reduction of secondary flow losses were carried out by Pruemper /10, 11/ in an axial-flow turbine stage. With a constant outer diameter of D_T = 0.4 m, the stage allows the realisation of different hub-to-tip ratios of ν = 0.6; 0.75; 0.84; and 0.9. The test equipment is shown in Fig. 25. The symbols are explained as follows:

A: Pitot probe for radial traversing of total pressure p_{to}
B: NTC-temperature probe for measuring total temperature T_{to}
C: stator, circumferentially adjustable by 360 degrees
D: miniature "flag probe" for measuring p_{t1} and α_1
E: shifting device for "flag probe"
F: three-hole probe synchronously rotating with the rotor
G: planetary gear for shifting the rotating probe circumferentially during operation
H: transmitter for static pressures out of the rotating system

4.2 Experimental Results

To achieve reduction of secondary flow losses, numerous tests using boundary layer overflow slots, boundary layer blow out, boundary layer fences, and boundary layer grooves were carried through systematically. As criterion for checking the success of the different methods served the integral improvement of the total pressure loss, at first in the stator. The best results were obtained by application of boundary layer grooves along the suction side of the stator blades. The investigations were mainly made with a hub-to-tip ratio of ν = 0.9. As most important geometry parameter proved the depth of grooves (about $2 \cdot \delta_{1E}$). The optimal distance between side wall and groove edge was found to be about $(0.7 \ldots 0.8) \cdot \delta_E$. This configuration of grooves proved less sensitive to changes of the Mach number. Fig. 26 shows the measured improvement of the total polytropic stage efficiency when using optimal boundary layer grooves in the stator blades. The gain of maximum efficiency amounts to about 1 % at a mean stator outlet Mach number of $\overline{M}_{1A}$ = 0.5. The improvement increased with rising Mach number and reached 2 % at $\overline{M}_{1A}$ = 0.8. Most advantage is achieved in the overload region with rising flow coefficients ϕ_{St}. For partial-load flow coefficients a significant gain is noticed, too, though in this region the difference is not so obvious because of the steep slope of the efficiency curves. Two main effects are contributing to the increasing stage efficiency when using boundary layer grooves in the stator:

a) the mixing of boundary layer material from the suction side of the stator blade with the main-flow yields an integral improvement of stator efficiency. The deflection is increased.

b) The more favourable flow conditions downstream the stator imply a reduction of rotor losses.

The reduction of secondary flow effects in the turbine rotor by adequate measures in the rotor blading was studied, too. In this case, boundary layer fences with enlarged distance from the wall were most successful. Blade geometry and radial distribution of dissipation (assuming $dq(r) / dr = 0$) are shown in Fig.27. The dashed line refers to a rotor blading with attached fences, the full line refers to the normal blading. The dissipation grows with the radius, reaching the maximum value immediately above the mean diameter: the boundary layer on the blades moves towards the tip, leading to separation. Near the tip section, part of the boundary layer may be exhausted over the shroud causing a considerable reduction of losses. Similar as in stator, the fences in the rotor diminish the boundary layer on the suction side by mixing with the main flow. This results in an overall decrease of dissipation.

The influence of the aspect ratio l/s on the reduction of stator losses is estimated in Fig. 28. This Figure is valid on the assumption that the losses occurring in the side wall regions are independent of the aspect ratio. Obviously, the improvements are growing with decreasing aspect ratio.

5. Conclusions

A considerable part of the losses occurring in turbomachines is due to flow effects in the side wall regions. Thus, for design tasks, it is very urgent to improve the prediction of these phenomena by theoretical models. To reach this aim, systematical experiments on secondary flows are extremely useful. The hopeful results of secondary flow reduction in an axial-flow turbine stage should encourage to adequate endeavours for all types of turbomachines /12; 13/.

6. References

1. Johnsen, Bullock: "Aerodynamic Design of Axial-Flow Compressors", I-III, NACA RM E 56 B03, 03a, 03b, Washington, 1956

2. Oellers: "Ein Beitrag zur Berechnung der inkompressiblen Unterschallströmung in ebenen Profilgittern auf elektronischen Digitalrechnern", Forschungsbericht des Landes Nordrhein-Westfalen, Nr. 1127, Köln, Opladen: Westdeutscher Verlag, 1963

3. Walz: "Strömungs- und Temperaturgrenzschichten", Karlsruhe: Braun 1966

4. Traupel: "Thermische Turbomaschinen", Band 1, 2. Auflage, Berlin, Heidelberg, New York: Springer 1966

5. Herrig, Emery, Erwin: "Systematic Two-Dimensional Cascade Tests of NACA 65-Series Compressor Blades at Low Speeds", NACA Technical Note 3916, 1957

6. Bitterlich, Rubner: "Theoretical and Experimental Investigation of the Three-Dimensional Frictional Flows in an Axial-Flow Compressor Stage", Mitteilung Nr. 74-04 des Instituts für Strahlantriebe und Turboarbeitsmaschinen der Technischen Hochschule Aachen, 1974

7. Nikuradse: "Gesetzmäßigkeit der turbulenten Strömung in glatten Rohren", Forsch. Arb. Ing.-Wes. Heft 356 (1932)

8. Kümmel: "Untersuchung der verlustbehafteten räumlichen Strömung in einem Axialverdichter mit besonderer Berücksichtigung der Seitenwandgrenzschichten", Dissertation, Technische Hochschule Aachen, 1976

9. Zurmühl: "Praktische Mathematik für Ingenieure und Physiker", 5. Auflage, Berlin, Heidelberg, New York: Springer 1965

10. Pruemper: "Application of Boundary Layer Fences in Turbomachinery", AGARDograph Nr. 164, pp. 311-331

11. Pruemper: "Verbesserung des Wirkungsgrades axialer Turbinenstufen durch Reduzierung der Sekundärverluste", Dissertation, Technische Hochschule Aachen, 1975

12. Gallus, Adams: "Experimentelle Untersuchung und Beeinflussung der Sekundärströmung in einem Radialverdichterlaufrad", Jahresbericht 1975 des Sonderforschungsbereichs 83 'Strömungsmechanik und Thermogasdynamik' an der Technischen Hochschule Aachen, 1976

13. Gallus, Subramanian: "Experimentelle Untersuchung und Beeinflussung der Sekundärströmung in einem Radialverdichterlaufrad", Jahresbericht 1976 des Sonderforschungsbereichs 83 'Strömungsmechanik und Thermogasdynamik' an der Technischen Hochschule Aachen, 1977

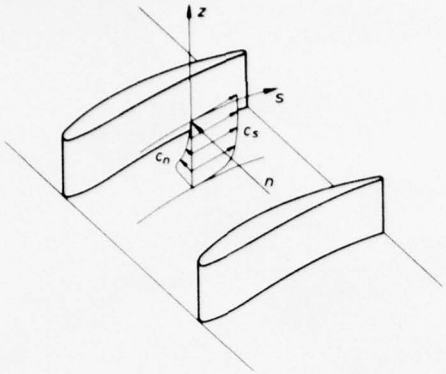


Fig. 3: Flow conditions near the side wall

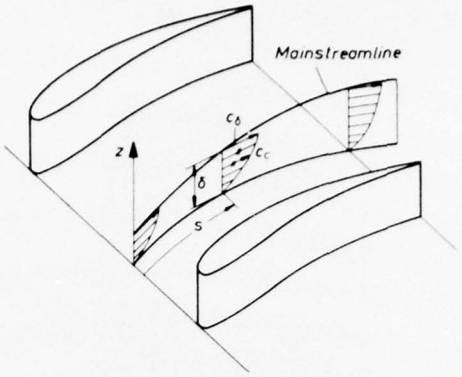


Fig. 4: Streamsurface of the collateral wall boundary layer

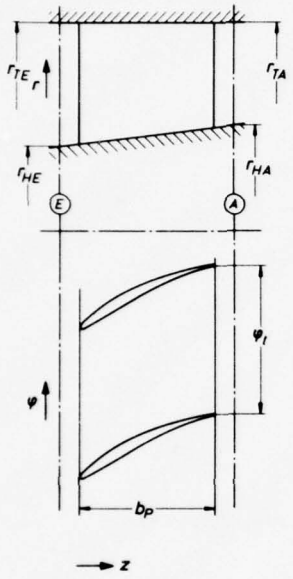
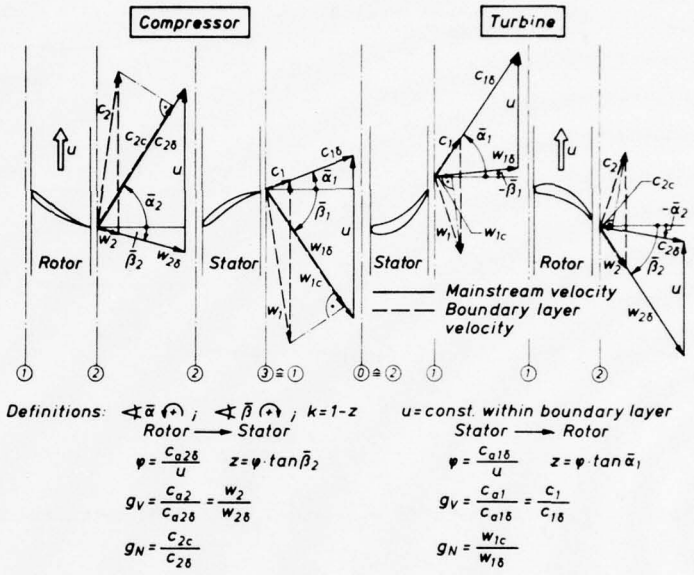


Fig. 1: Geometry of flow channel



Definitions: $\sphericalangle\bar{\alpha}$ ↻ ; $\sphericalangle\bar{\beta}$ ↻ ; k=1-z

Rotor → Stator

$\varphi = \frac{c_{a2\delta}}{u}$ $z = \varphi \cdot \tan\bar{\beta}_2$

$g_V = \frac{c_{a2}}{c_{a2\delta}} = \frac{w_2}{w_{2\delta}}$

$g_N = \frac{c_{2c}}{c_{2\delta}}$

u=const. within boundary layer

Stator → Rotor

$\varphi = \frac{c_{a1\delta}}{u}$ $z = \varphi \cdot \tan\bar{\alpha}_1$

$g_V = \frac{c_{a1}}{c_{a1\delta}} = \frac{c_1}{c_{1\delta}}$

$g_N = \frac{w_{1c}}{w_{1\delta}}$

Fig. 5: Flow conditions in compressor and turbine stages

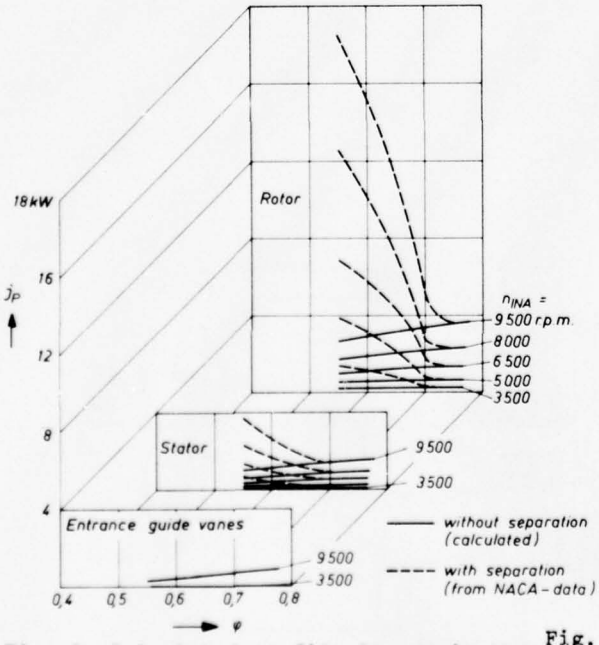


Fig. 2: Calculated profile losses in the cascades of the axial-flow compressor

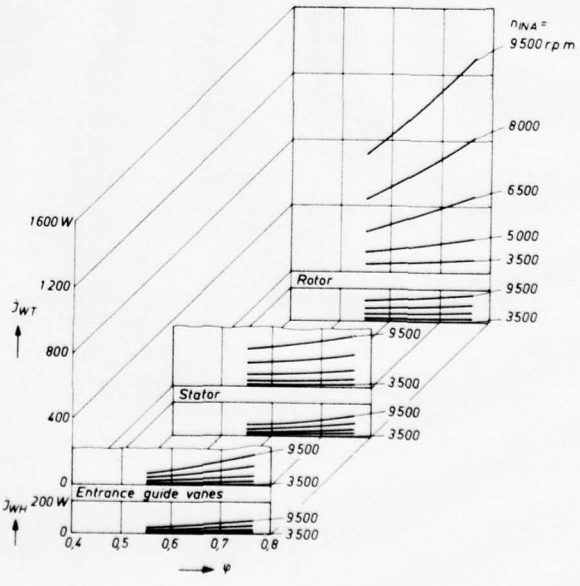


Fig. 6: Calculated annulus wall losses in the cascades of the axial-flow compressor

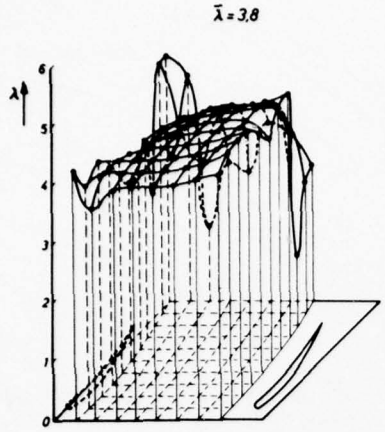


Fig. 7: Distribution of the loss rate λ_{WT} at the casing wall of the entrance guide vanes

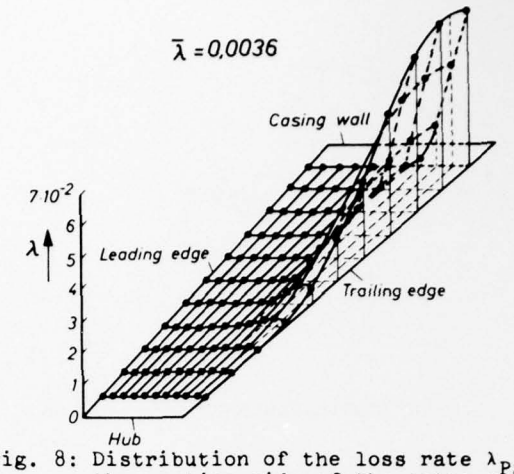


Fig. 8: Distribution of the loss rate λ_{PS} at the suction side of the entrance guide vanes

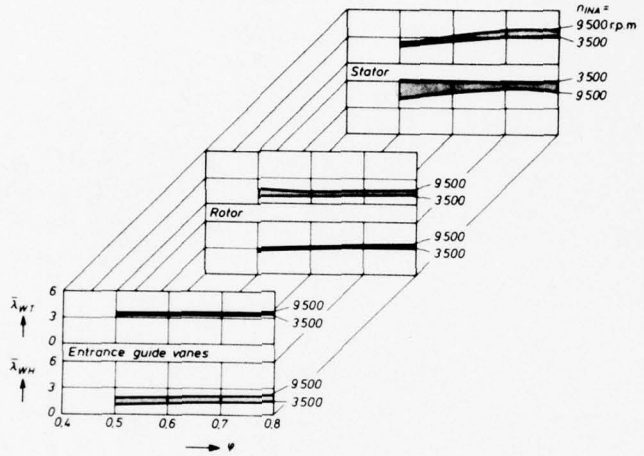


Fig. 9: Mean loss rates $\bar{\lambda}_{WH}$ and $\bar{\lambda}_{WT}$ in the cascades of the axial-flow compressor

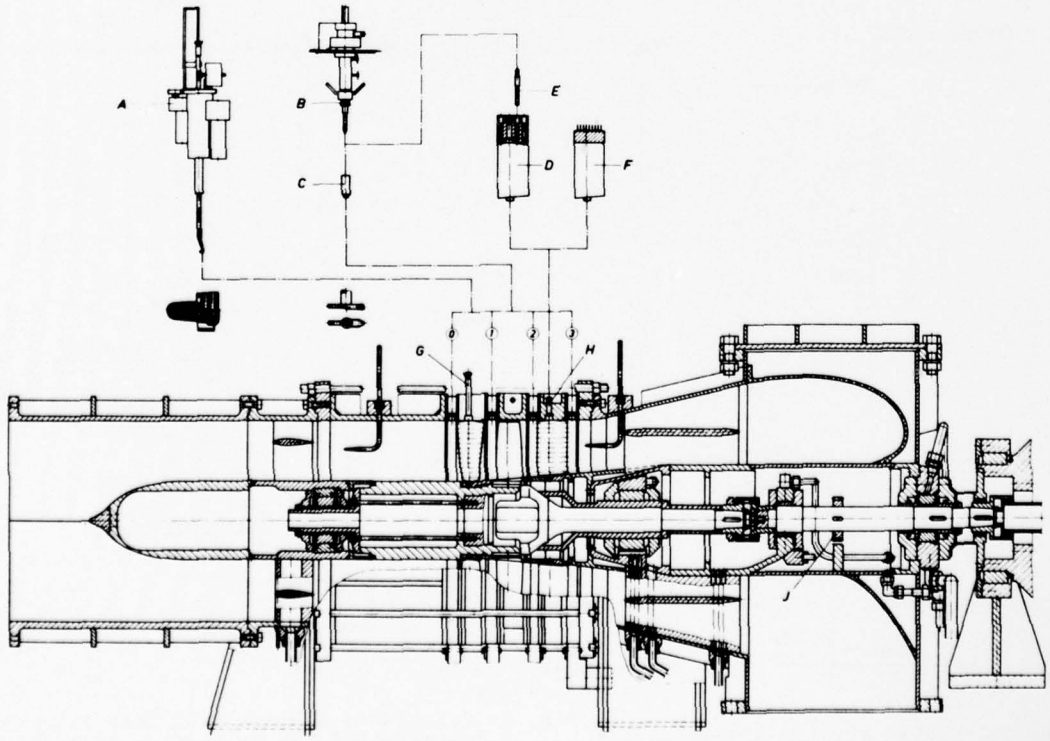


Fig. 10: Axial-flow compressor stage

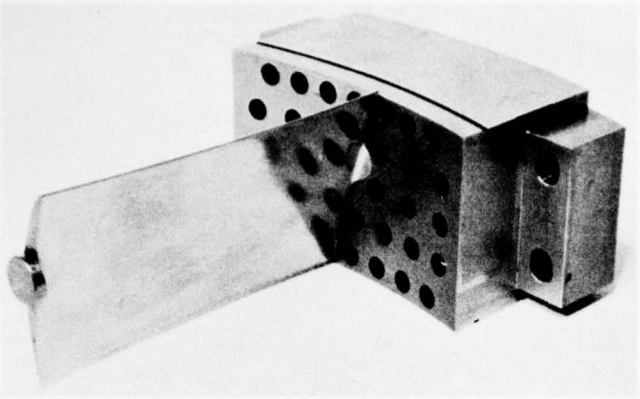


Fig. 11: Casing wall segment

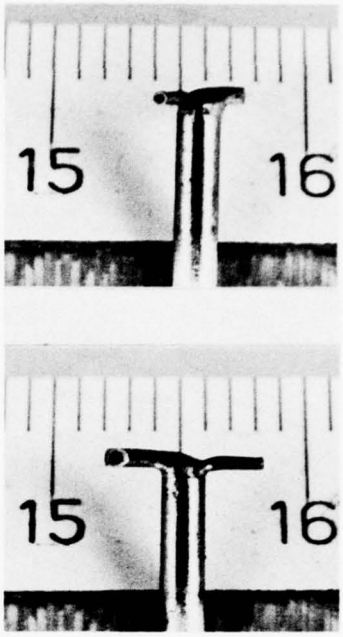


Fig. 12: Views of the boundary layer probe compared with a mm-scale

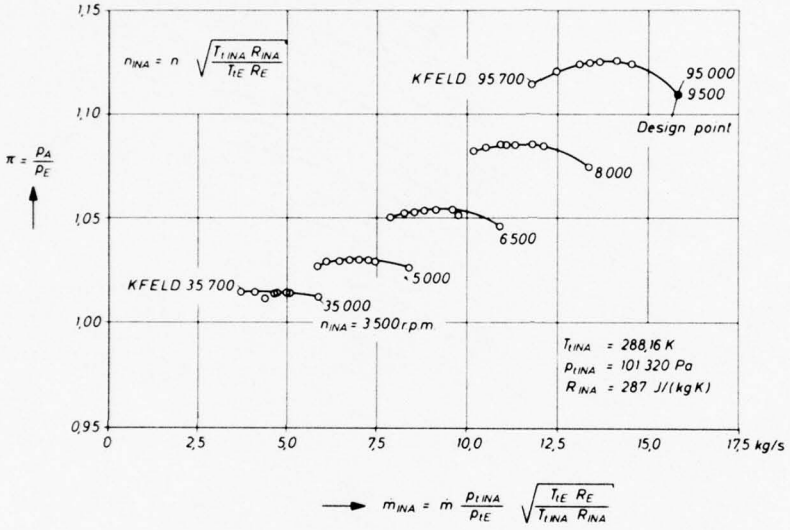


Fig. 13: Performance map of the axial-flow compressor

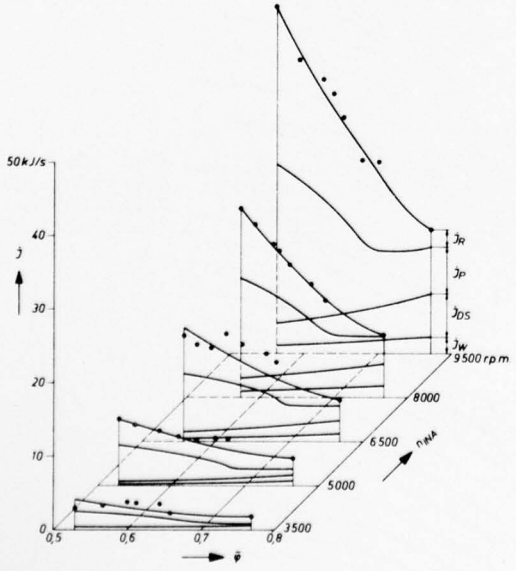
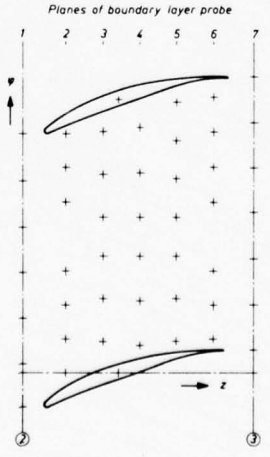


Fig. 14: Confrontation of measured and calculated losses of the axial-flow compressor



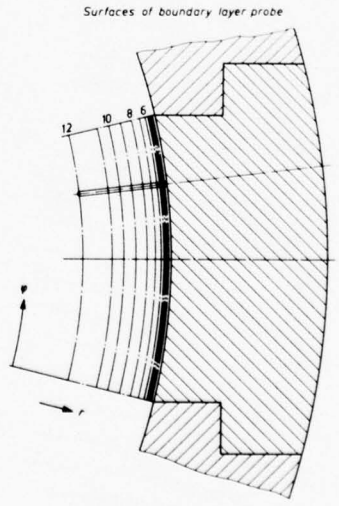


Fig. 15: Measuring positions in the annulus wall boundary layer at the stator casing

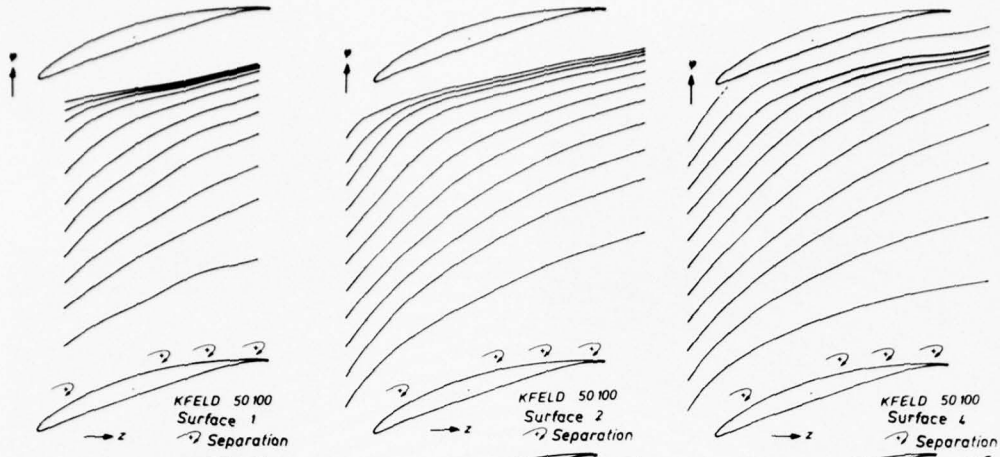
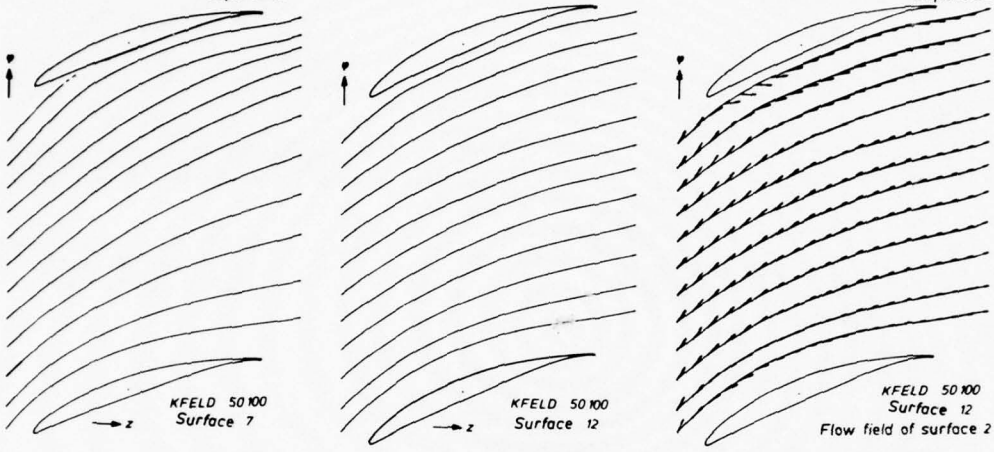


Fig. 16:
Operating point
KFELD 50100
(throttled)



Streamlines in
the annulus wall
boundary layer
at the stator
casing

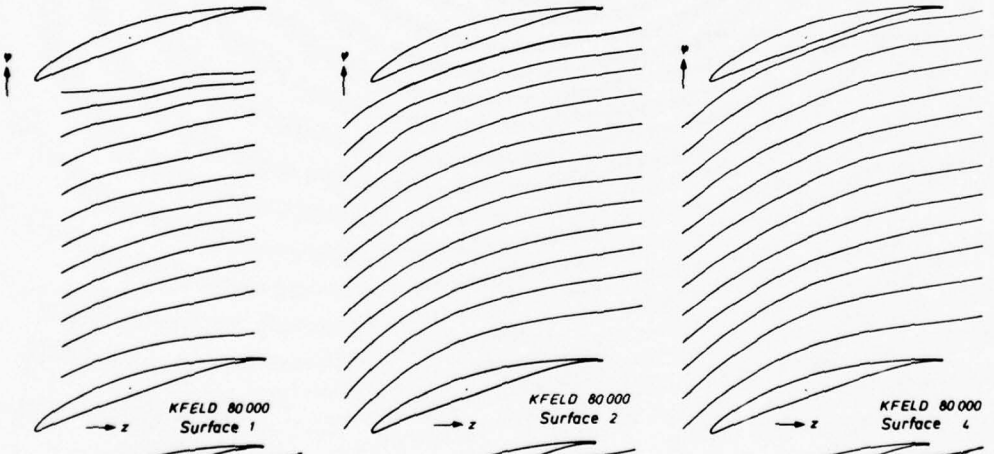
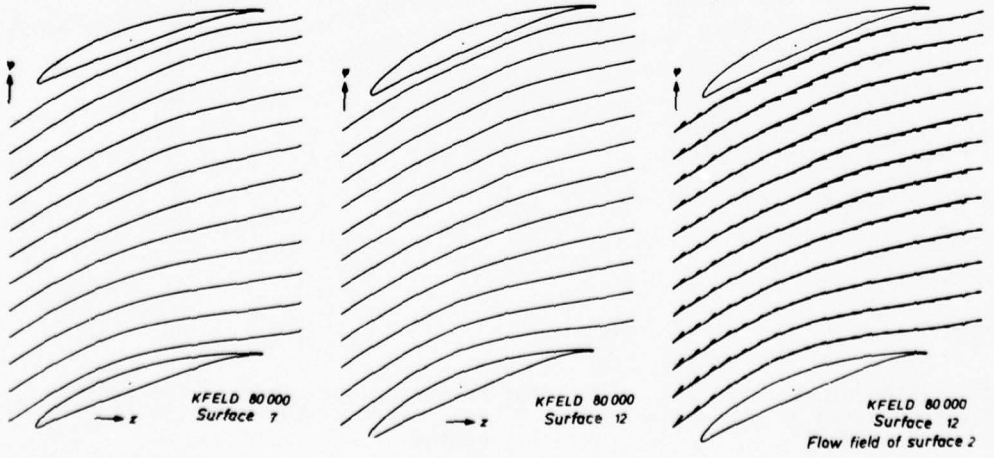


Fig. 17:
Operating point
KFELD 80000
(unthrottled)



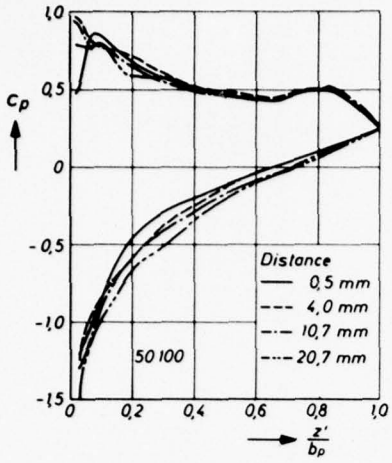


Fig. 18: Dimensionless profile pressure distributions at different distances from the casing wall, operating point KFELD 50100

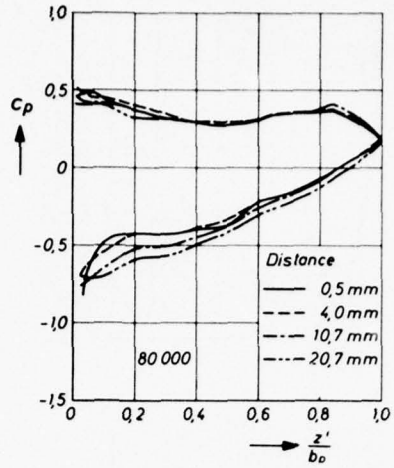


Fig.19: Dimensionless profile pressure distributions at different distances from the casing wall, operating point KFELD 80000

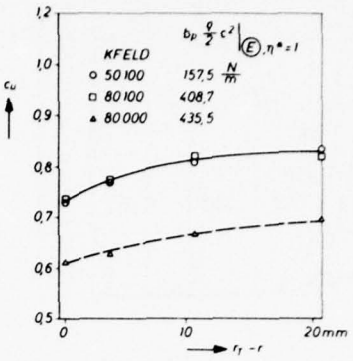


Fig.20: Dimensionless circumferential stator blade force versus distance from the casing wall

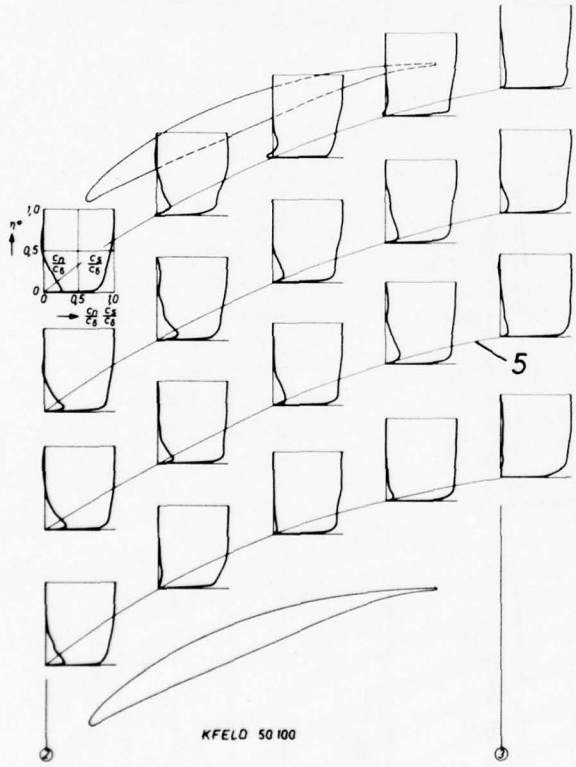


Fig. 21: Collateral and crossflow velocity profiles in the annulus wall boundary layer, operating point 50100

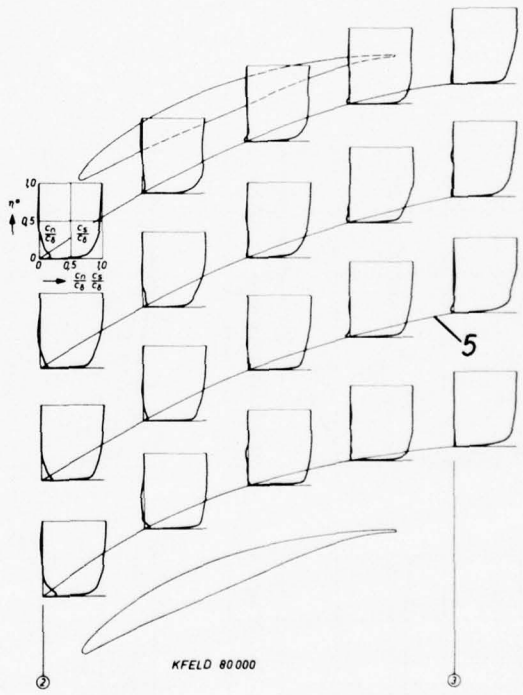
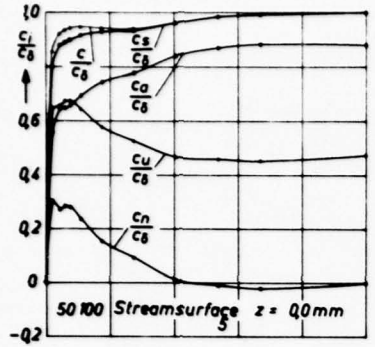
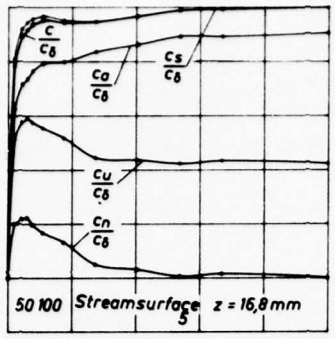
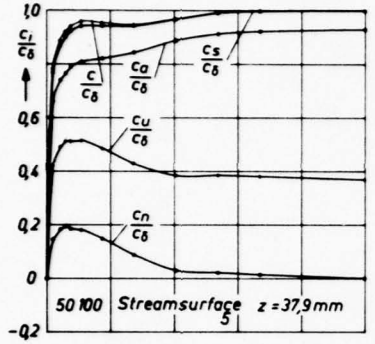
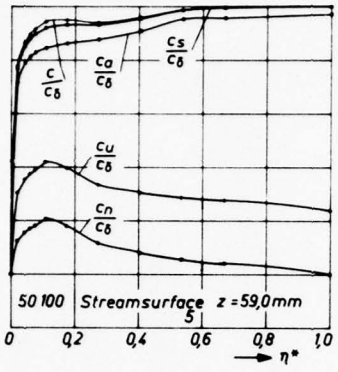


Fig. 22: Collateral and crossflow velocity profiles in the annulus wall boundary layer, operating point 80000









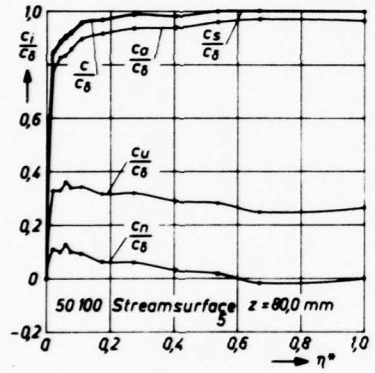
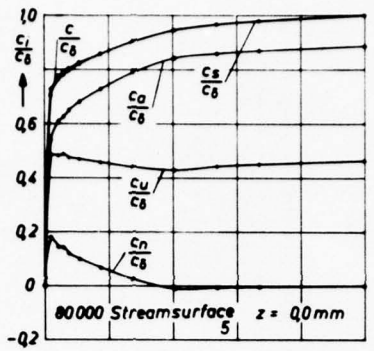
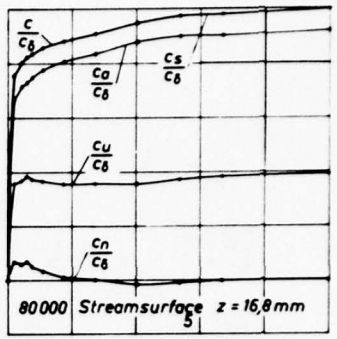
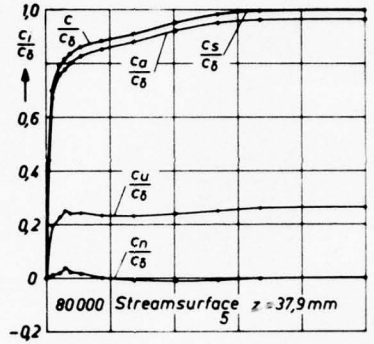
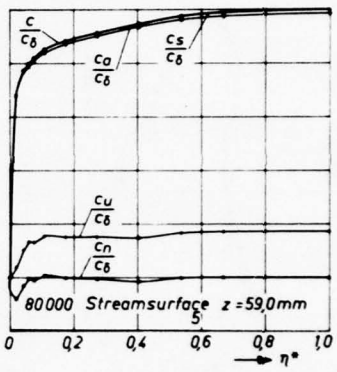


Fig. 23: Velocity components in the annulus wall boundary layer, streamsurface 5, operating point 50100









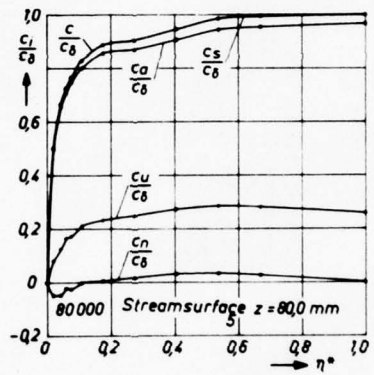


Fig. 24: Velocity components in the annulus wall boundary layer, streamsurface 5, operating point 80000

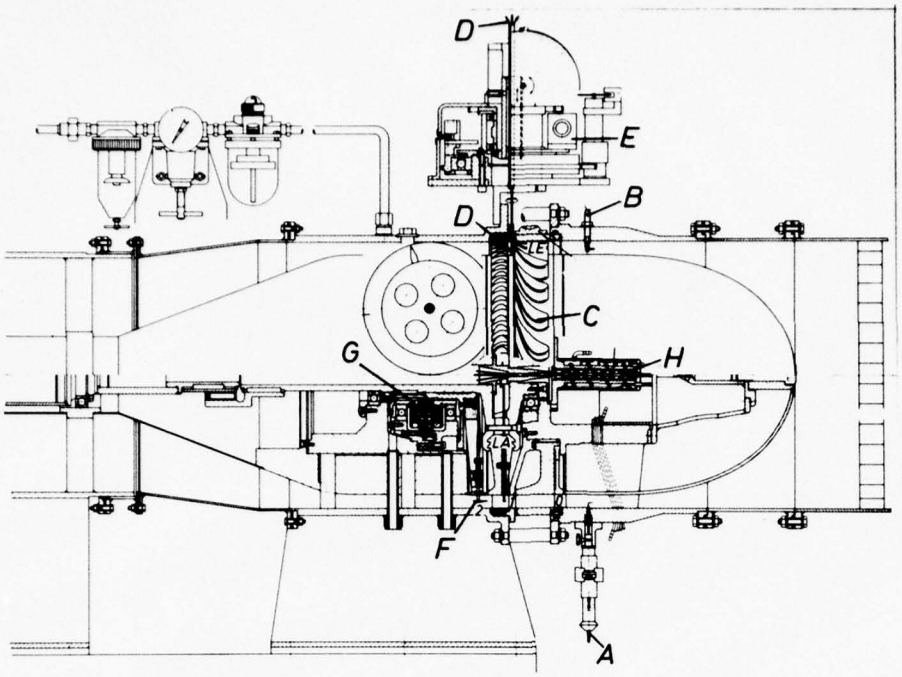


Fig. 25:
Axial-flow turbine stage

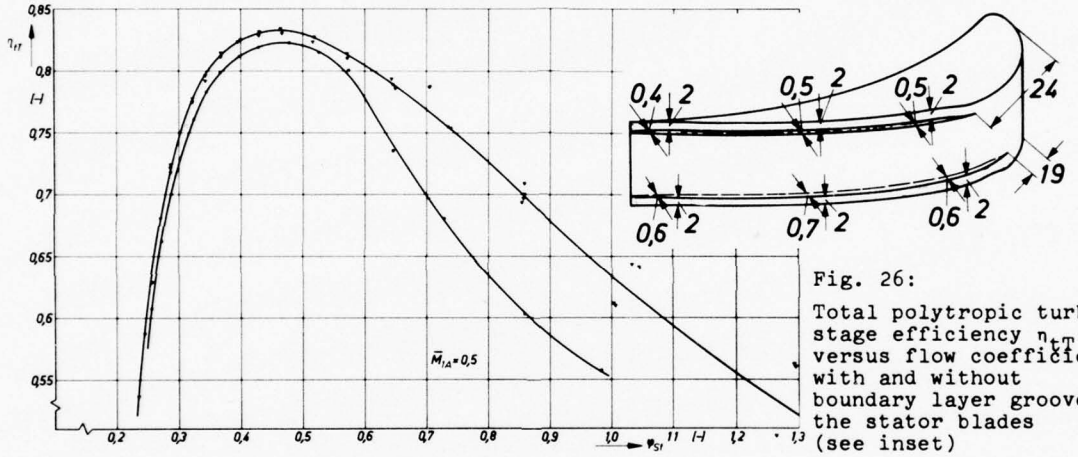
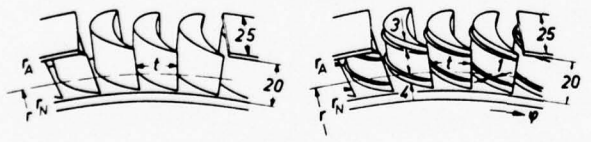


Fig. 26:
Total polytropic turbine stage efficiency η_{tT} versus flow coefficient φ_{St} with and without boundary layer grooves in the stator blades (see inset)



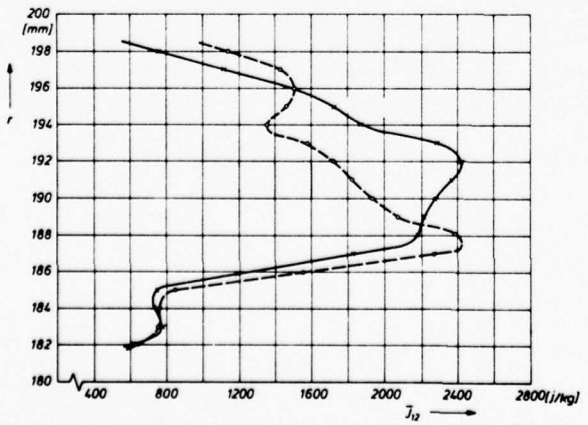


Fig. 27: Radial loss distribution with (dashed lines) and without (full lines) boundary layer fences on the rotor blading

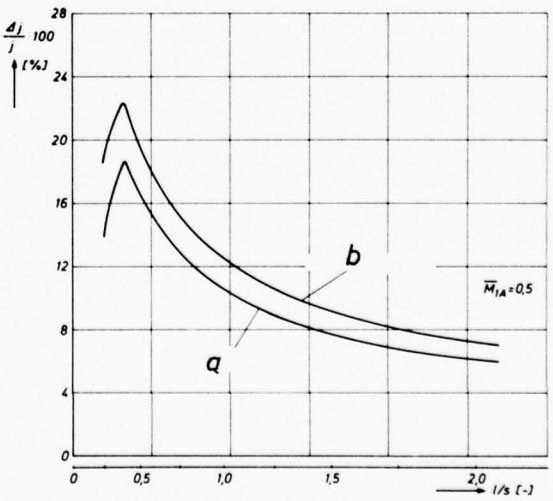


Fig. 28: Diminishing of losses in the stator versus aspect ratio. a): fences b) grooves

SECONDARY FLOWS IN AXIAL FLOW COMPRESSORS WITH TREATED BLADES

by

Meherwan P. Boyce, Ph.D., P.E.
Director, Gas Turbine Laboratories
Texas A&M University
College Station, Texas 77840
U.S.A.

SUMMARY

As a means of increasing the performance and surge margin of axial flow compressors, boundary layer control in many forms have to be applied. This paper deals with a technique which controls the flow in the separation region. The technique deals with the treatment of the suction surface of the blade.

The overall goals of the program were to extend the surge-to-stall margin; and to accomplish this, an extensive test program of flow visualization was conducted, using a different cascade model. These results were then compared with various theoretical models to understand the complex flow field in an axial compressor. The results indicate that blade treatment is effective in controlling the onset of surge, and thus increases the surge-to-stall margin by creating a stable flow situation.

SYMBOLS

$\dot{m}$	mass flow rate in one streamtube
P	static pressure
r	radial distance from axis of rotation
R_e	machine Reynolds number
r_c	radius of curvature of a streamline
T	static temperature
t	time
U	blade velocity
u	velocity in the x direction
V	absolute fluid velocity
W	relative fluid velocity
w	nondimensional relative fluid velocity
x	direction of boundary layer growth
y	direction normal to boundary layer growth
z	axial direction

GREEK SYMBOLS

α	angle meridional streajline forms with axis of rotation
β	blade angle
μ	dynamic viscosity
θ	direction of rotation of impeller
ρ	density
τ_0	wall shear stress
ω	rotative speed of impeller
ν	kinematic viscosity

SUBSCRIPTS

r radial component

x component in direction of boundary layer

y component perpendicular to boundary layer

z axial component

∞ free stream value

INTRODUCTION

Axial flow compressors have a characteristically narrow surge-to-stall margin. To increase this margin, various concepts of boundary layer techniques have been devised.

Interest in application of boundary layer control to axial flow turbomachinery first began in the early fifties [1, 2]. Previous investigation has taken the form of analytical studies and some experimental cascade work. Except in one instance, where an axial flow blower was tested, there is no indication that boundary layer control has been applied to any actual production or experimental type of axial flow compressor [3].

Compressor designers have had considerable interest in the slotted axial flow compressor blade for some time. The benefits of the slotted compressor blade were first demonstrated by Sheets [3] in the test of an axial flow blower. More recent work, including a comparison of analytical and experimental cascade results, has been reported by Mikolajczak, Weingold, and Nikkanen [4], indicating a potential improvement in axial flow compressor performance.

The other technique of boundary layer control in axial flow turbomachinery that has had considerable investigation is that of optimizing the blade shape to delay or prevent the transition to turbulent flow. Several computational methods of designing blades to accomplish this are cited in the literature [2, 5, 6]. Although most of the work published on this subject is theoretical in nature, Papailiou [5] has made a notable contribution in that he has discussed a method of optimizing the blade shape and has also compared cascade test results with analytically predicted performance. The performance of Papailiou's cascade was somewhat better than an equivalent NACA cascade.

Some work has also been done in the area of jet-flap cascades. This principle has been investigated theoretically by Stark [7] and experimentally by Clark and Ordway [8]. Although an increase in incidence range is realized with this technique of boundary layer control, the potential for increased pressure loading per stage is offset by the energy consumed in supplying the jet air.

In the case of casing treatments in axial flow compressors, initial work in this area has been linked to acoustical studies of compressors. Casing treatments, which have resulted in changing the flow characteristics in the passage between the impeller and casing, have also led to reduction in sound attenuation. Early work in this area was conducted by C. C. Koch [9] and Hartman et al [10]. Further work was done by Boyce and Schiller [11], which indicated that casing treatment increased the surge-to-stall margin by delaying the onset of surge.

An axial flow compressor has a surge line for very much the same reason an aircraft wing stalls. As the incidence angle of the flow on the blade row is increased with increased stage loading, the pressure rise for the stage will continue to increase until some critical value of incidence is obtained. At that point, the stage can no longer maintain flow against the back pressure behind it; the boundary layer separates, and the flow pattern breaks down. In high performance compressors, this creates, in effect, an instantaneous and massive blockage of the passage. If the fluid medium is gaseous, the incoming flow will be discharged violently back through the inlet of the compressor because of compressibility. The demand on the stalled stage is relieved by this flow reversal, and it becomes unstalled. It then begins to pump flow again only to repeat the process. This flow oscillation is violent and rapid, the frequency being perhaps several cycles per second. Because of the limited mechanical strength of the compressor blading, it is highly desirable, imperative in fact, that this surging phenomenon be avoided. This explains the necessity for surge margin.

The objective of this research program was to seek and to investigate a technique of axial flow compressor blade treatment which will delay the separation of the boundary layer on the compressor blades. If the boundary layer separation can be effectively delayed through some increased incidence range, compressor surge can also be delayed to higher pressure ratios and flows. The effect of this higher surge line would be to either create an additional surge margin at the initial design point or to provide greater design point performance with no change in surge margin.

Compressor blade treatment is proposed here as an alternative concept. Figure 1 shows a perspective view of a compressor blade with the proposed treatment. The reasoning behind this concept is that an airfoil, whether it is a wing section or an axial flow compressor blade, derives its lift from the greater acceleration and deceleration of the flow over the suction surface compared to the pressure surface. To increase the lift of a given airfoil section, the angle of incidence can be increased, resulting in still greater acceleration over the suction surface and increased dynamic lift on the pressure surface. At some critical incidence, however, the increased deceleration of the flow in the face of an unfavorable pressure gradient will cause the boundary layer on the suction surface to separate, resulting in sharply reduced lift and increased drag. If the acceleration and deceleration on the suction surface can be reduced by modifying the blade cross section, it is intuitive that the likelihood of boundary layer separation is reduced.

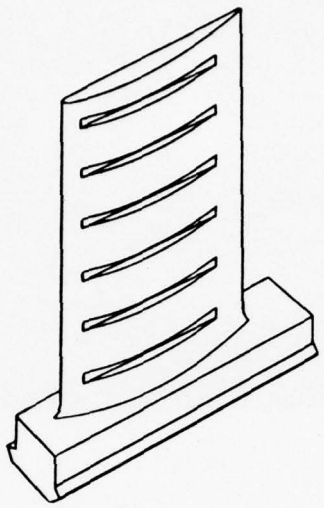


Figure 1 Perspective of Compressor Blade with Treatment

EXPERIMENTAL ANALYSIS

The flow visualization studies in both cases used water as a fluid medium. Globules of dibutyl phthalate and kerosine were used as tracers for the flow. This mixture, whose density was made to equal that of the medium (water), was used, since in previous tests it had been found not to coagulate but follow the streamlines closely.

An impeller designed for air can be tested using water as the medium if the dimensionless parameters, Reynolds number, and specific speed are held constant:

$$\text{Reynolds Number} = \frac{\rho_{air} V_{air} D}{\mu_{air}} = \frac{\rho_{water} V_{water} D}{\mu_{water}}$$

$$\text{Specific Speed} = \frac{Q_{air}}{N_{air} D^3} = \frac{Q_{water}}{N_{water} D^3}$$

where ρ = density of medium, V = velocity, D = diameter of impeller, μ = viscosity, and N = speed. Using this assumption, we can apply this method of flow visualization to any working medium.

The general apparatus consists of two large tanks on two different levels. The lower tank is constructed entirely out of Plexiglas and is maintained at a constant head of flow from the upper tank. The flow entering the lower tank comes through a large rectangular opening which houses a number of screens so that no turbulence is created by water entering the lower tank. In the center of the lower tank can be fitted various boxes for the various flow visualization problems to be studied. This modular concept enables us to interchange models rapidly and enables us to work on more than one concept at a time.

For the blade treatment cascade rig experiment, a Plexiglas cascade was designed and built. Figure 2 shows the cascade. This cascade was then placed in the bottom tank, which is maintained at a constant head. Figure 3 shows the entire setup.

The cascade model was designed such that the flow incidence angle on the cascade was variable and the subject blades could be removed and interchanged easily. For ease of observation and for strength and rigidity, the main body of the cascade model was fabricated from 1/2" clear sheet Plexiglas. It consisted of an oversized base piece,

sides to form a rectangular channel, and a cover piece having the same dimensions as the base. The major structure of the main body was formed by the base piece and the stationary sides of the channel downstream of the cascade. After the appropriate positions for the cascade blades had been determined and clearance holes drilled for the attachment screws and injection tube of each blade, chloroform was used to permanently cement the stationary sides to the base of the cascade model. The cover piece was then attached to the main body of the model. This permitted easy removal of the cover for access to the blades of the cascade. On the forward end of the cascade model, additional strength was provided by two small supports between the base and cover having the same height as the sides. As with the stationary sides, they were permanently attached to the base with drilled and tapped holes for the cover attachment screws.

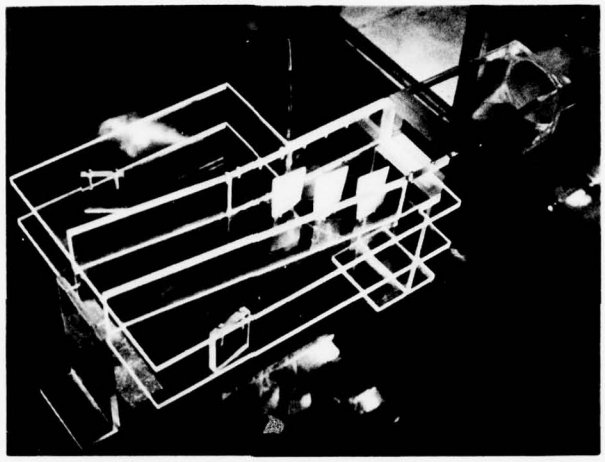


Figure 2 Cascade Model in Axial Flow Test Tank

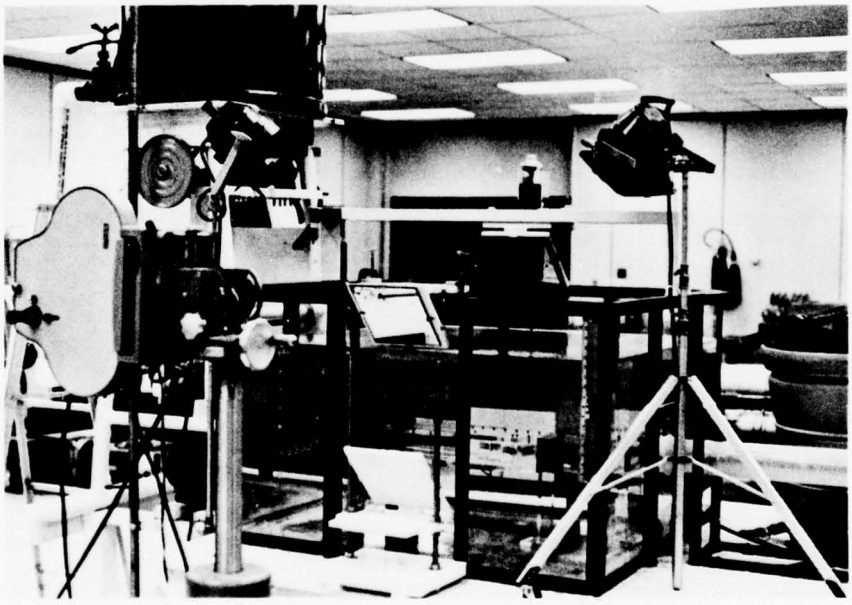


Figure 3 Apparatus for Testing Axial Flow Cascade Model

To allow the upstream channel direction to be variable, the sides of the model forming the channel upstream of the cascade were hinged to the stationary sides. These hinge points were located at the point of intersection of the stationary side and a line along the leading edge of the cascade blade row. To minimize leakage, the hinge joints were constructed by machining a 1/2" diameter concave semicircle into the forward edge of the stationary sides and a 1/2" diameter convex semicircle into the rear edge of the movable sides. Each movable side was then held in place by a single number 8-32 x 3/4" brass screw in a hole which was drilled and tapped through the cover into the center of

the semicircle. On the forward end of the cascade model, each movable side of the channel was held in position by a 4" C-clamp, which clamped the side between the base and cover surfaces. For setting the channel direction, a protractor scale for each movable side was scored into the surface of the base. These scales provided for a range of incidence angles between -10° and +20° in one-degree increments.

The blades placed in the cascade were actual castings of an NACA 65 series blade used in a high-pressure compressor. Holes were drilled in the leading edge of the blade so that die could be propelled out of them to show the flow patterns in the blades. Figure 4 shows an NACA 65 series blade prepared in such a fashion. A total of seven cascade blades were fabricated in the manner described above. Of these seven, three were left unmodified for use as a control or reference cascade, and the remaining four were modified to incorporate some form or configuration of the compressor blade treatment.

In an attempt to investigate the influence of number and width of the slots, these configurations included different combinations of slot widths and number of slots. One configuration had six wide (0.090") slots that were uniformly distributed along the blade length; another configuration had six narrow (0.030") slots uniformly distributed; a third configuration had twelve narrow slots uniformly distributed; and another configuration had no slots but a continuous flat cut to the depth of the proposed slots and extending across the same portion of the blade as the slot treatment. The cascade blade specimens are shown in Figures 5 - 8.



Figure 4 Standard NACA 65 Series Blade



Figure 5 Treatment Configuration with Six Wide Slots

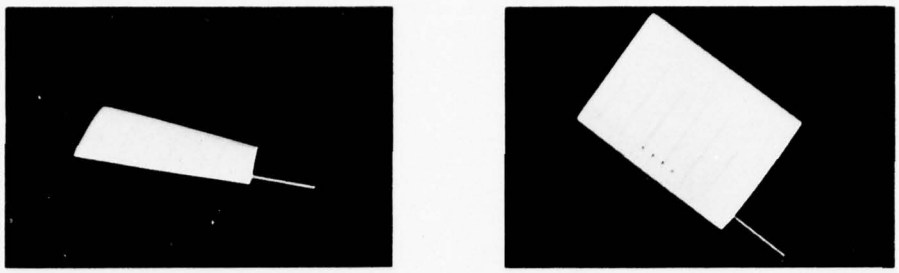


Figure 6 Treatment Configuration with Six Narrow Slots



Figure 7 Treatment Configuration with Twelve Narrow Slots

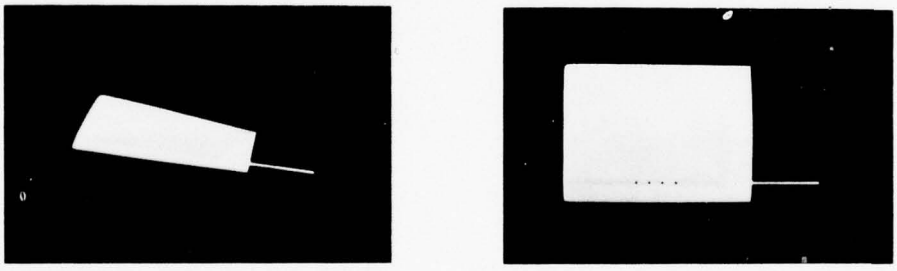


Figure 8 Treatment Configuration with Continuous Flat

DISCUSSION OF EXPERIMENTAL RESULTS

The cascade for the treated blade program consisted of three blades, two of which were untreated NACA 65 series compressor blades. The third blade was either an untreated blade for a reference cascade or one of the treated blades. The treatment configurations were first tested in the center blade position of the cascade model which was most representative of a blade in an infinite cascade. After it was learned that the blade in the downstream position was particularly susceptible to early separation of the boundary layer, the treatment configurations were also tested in that position. It was reasoned that if a treatment configuration made an obvious improvement in the performance of the blade in the downstream position, it would certainly do the same or more for the blades in the other two cascade positions.

In evaluating the performance of the different cascade configurations, one of the observed flow characteristics was the extent of the laminar flow boundary layer. Typically, the boundary layer flow on an axial flow compressor blade will begin as a laminar boundary layer at the leading edge, and further downstream it will, depending on the blade chord Reynolds number, undergo a transition to a turbulent boundary layer. Since the laminar boundary layer has less viscous drag than the turbulent, and the turbulent boundary layer is less susceptible to separation under adverse pressure gradients, the ideal condition would have a large extent of laminar boundary layer followed by a transition to the turbulent boundary layer just prior to an impending laminar separation. Consequently, in comparing the performance of the different cascade configurations under identical test conditions, the cascade of blades that maintained the greatest extent of laminar flow before successfully making the transition to a turbulent flow boundary layer or separating from the blade surface was judged to be operating at the highest efficiency.

The estimated blade chord Reynolds number for these cascade tests was $Re_c = 72000$. The boundary layer flow on the suction surface of each blade was laminar over a significant percentage of the chord length. In the photographs and the motion pictures using the ink injection technique of flow visualization, the laminar flow regions were easily identified by the tendency of the ink streams to remain stable and undiffused. The large extent of the laminar flow regions, particularly at the lower incidence angles, is evident in Figure 9 and Figure 10, the composite summaries of the 35 mm test results for the treatment configurations in the center blade position and the downstream blade position, respectively.

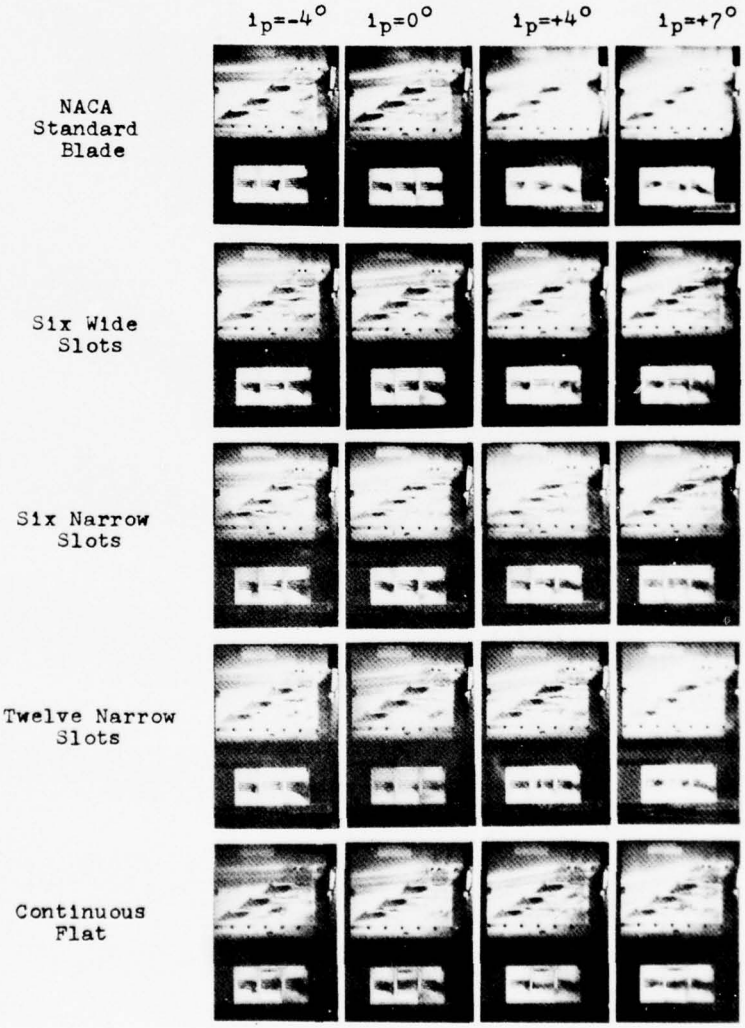


Figure 9 Treatments on Center Cascade Blade

For all cascade configurations, it was observed that the extent of the laminar flow region on each blade was progressively reduced with increasing incidence angle. From Figure 9 and Figure 10, and from the summary of observations made from the high-speed motion pictures in Table 1, it was observed that the earliest and greatest reduction

occurred on the blade in the downstream position, while the center blade position was only moderately affected and the upstream blade position was affected only slightly.

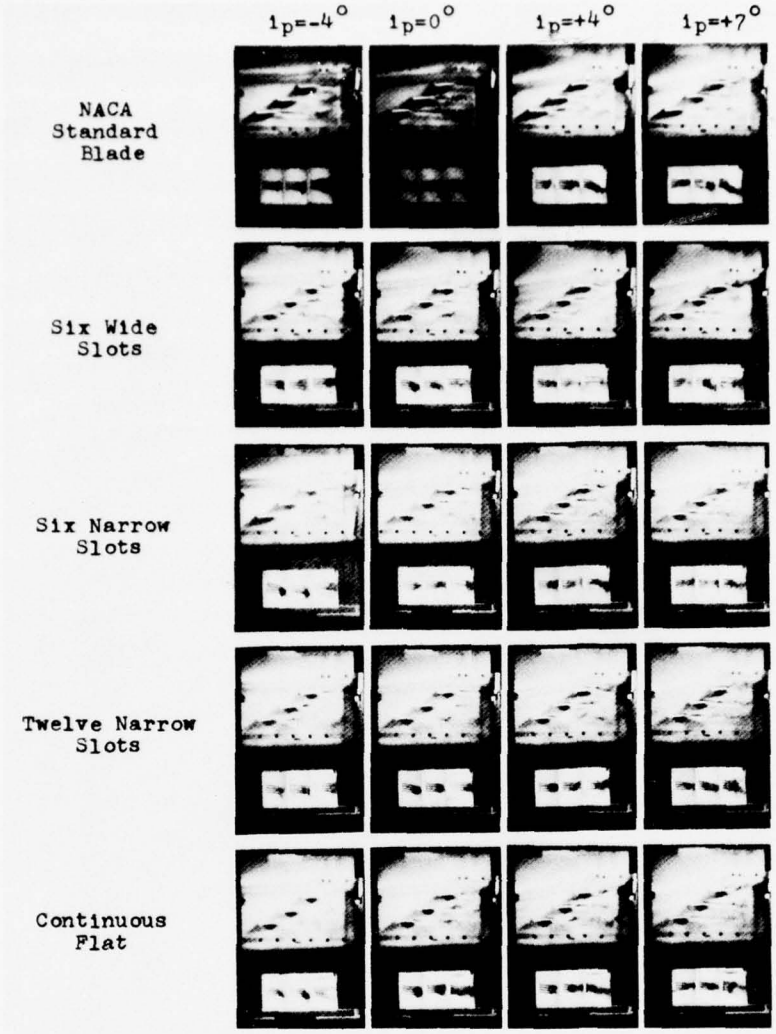


Figure 10 Treatments on Downstream Cascade Blade

From the observations summarized in Table 1, and also from comparing the test results presented in Figure 9 and Figure 10, it is evident that, in the center blade position, the treatment configuration having six wide slots has been more successful than either the standard blade or any other treatment configuration in maintaining stable laminar flow over a greater percentage of the blade suction surface. This observation appears to be true for all incidence angles up to and including +4°, and marginally true for the highest incidence value of +7°. Although the ink streams are becoming slightly diffused at an incidence angle of +7°, they remain fairly distinct, and it is concluded that this represents the initial stage of transition to a turbulent boundary layer which remains attached to the blade surface.

Table 1 Extent of Laminar Region in Fraction of Blade Chord

i_p	Standard			Six Wide			Six Narrow			Twelve Narrow			Continuous Flat		
	Up	Ctr	Dn	Up	Ctr	Dn	Up	Ctr	Dn	Up	Ctr	Dn	Up	Ctr	Dn
-4°	.55	.55	.45	.65	.70	.45	.55	.70	.35	.75	.75	.35	.65	.25	.45
0°	.55	.50	.35	.55	.70	.35	.55	.65	.35	.55	.65	.35	.65	.10	.45
+4°	.55	.45	.25	.55	$\frac{.25^*}{.75}$	.25	.55	$\frac{.35^*}{.65}$	.25	.55	.65	.35	.55	.10	.25
+7°	.45	.35	.15	.45	$\frac{.25^*}{.75}$	.25	.45	.30**	.25	.45	$\frac{.25^*}{.55}$	.25	.45	.10	.25

*Top number is for blade surface between slots; bottom number is for slot.
**For entire blade including slots.

The laminar region on the downstream cascade blade, as seen in Figure 10, appears to be approximately the same as before except at 3° less incidence; that is, the treatment configuration having six wide slots again appears to have improved on the standard blade and the other treatment configurations in extending the laminar flow region and maintaining an attached boundary layer up to and including the +4° incidence angle, with perhaps some very slight improvement at +7° incidence. Some of the other treatment configurations seem to have made similar improvements, except that, upon closer examination, the boundary layer on these blades actually appears to have already separated. As indicated earlier, the blade in the downstream position was particularly susceptible to early separation of the boundary layer.

A notable exception to this discussion of the laminar flow region is the treatment configuration having the continuous flat surface. When this treatment configuration was tested in either the downstream blade position, or in the center blade position, it was observed to have virtually no laminar flow region at any of the higher incidence angles. This fact in itself is not a liability, since the turbulent boundary layer will remain attached to the blade surface better than the laminar boundary layer. However, it was also observed during the cascade testing, and later in the motion pictures, that the turbulent boundary layer was accompanied by severe buffeting and flow instability, and on that basis it was concluded that the continuous flat would not perform as well as the other configurations, and it was given secondary consideration thereafter.

Depending on the circumstances, it was observed from the cascade test results that immediately following the region of laminar flow, the boundary layer would undergo transition to a turbulent boundary layer, which might be subject to separation further downstream, or it would separate from the blade surface while still in the laminar flow regime.

At the lower incidence angles of -4° and 0°, for example, it was observed that for all the cascade configurations, the laminar flow regions on the blades generally ended with a diffusion and dispersion of the ink streams with no appreciable increase in the boundary layer thicknesses. This behavior, which was observed in the 16 mm high-speed motion pictures and is also evident in Figure 9 and Figure 10, suggests that at this incidence angle the boundary layer generally undergoes a transition to turbulent flow without separation.

From the high-speed movies, it was further observed that for all cascade configurations at the -4° incidence angle, the boundary layer on the downstream cascade blade occasionally appeared thickened, and infrequently it would separate over the last 50 percent of the blade suction surface. At the same time, the boundary layers on the other two cascade blades appeared, for the most part, very thin and completely attached. At the 0° incidence angle, however, the boundary layers on the upstream cascade blade and the center cascade blade were also observed to be occasionally thickened; and the downstream cascade blade, which was observed to be thickened more often, was again infrequently separated over the last 50 to 70 percent of the blade surface. At these low incidence values the performance of all the treatment configurations in terms of boundary layer attachment was observed to be approximately the same as that of the standard NACA 65 series blade.

At the +4° incidence setting, it was observed from the high-speed motion pictures that the boundary layer on the downstream cascade blade of all cascade test configurations was moderately thickened and showing deviation at the trailing edge of the blade. The boundary layer on the downstream cascade blade was also separated over the last 50 to 75 percent of the blade surface. This separation of the boundary layer was observed to occur directly from the laminar flow regime. In addition to this occasional separation, bumps or projections very similar in appearance to the initial stage of a laminar separation appeared sporadically on the suction surface of the downstream cascade blade, and also on the center cascade blade, but more infrequently.

The upstream cascade blade, and the center cascade blade in particular, appeared to have an occasional thickening of the boundary layer, but in general the boundary layers on these blades were relatively thin and well attached along the entire blade surface. At this incidence angle, a careful study of the high-speed motion pictures and of Figure 9 and Figure 10 indicated that, in either the center blade position or the downstream blade position, the treatment configuration with six wide slots was slightly better than the standard blade or any of the other treatment configurations in maintaining an attached boundary layer on the blade surface.

At the highest incidence angle of +7°, it was observed from the high-speed motion pictures that all of the cascade blades of each cascade configuration were intermittently showing signs of operating at too great an incidence angle. The blade in the chronically weak downstream cascade position was frequently separated over 75 percent of its suction surface, while the treatment configuration in the center cascade position was occasionally separated over the last 50 percent of the blade suction surface. When the boundary layer did separate on the center cascade blade, the effect of this separation was also observed on the downstream cascade blade in the form of a boundary layer separation. This flow behavior appeared very similar to the mechanism that causes a rotating stall cell to propagate around an axial flow compressor rotor blade row. The boundary layer on the upstream cascade position was observed to thicken occasionally and to have the sporadic projections that were discussed earlier. None of the treatment configurations that were tested seemed to have made a significant and obvious improvement in maintaining an attached boundary layer at a flow incidence angle of +7°. There may have been some

evidence in the high-speed motion pictures of a slight improvement by the treatment configurations with six wide slots and with six narrow slots, and a very careful examination of Figure 9 seems to verify this conclusion.

A very close examination of Figure 10, particularly of the boundary layer thicknesses and wake behavior, indicates that the treatment configuration with six wide slots has also made some slight improvement in the performance of the downstream cascade blade at higher incidence angles. The wake downstream of the blade, however, may indicate that, even with this slight improvement, the blade continues to operate intermittently in and out of a stalled condition. None of the other treatment configurations appear to have made any perceptible improvement in the performance of the downstream cascade blade.

Another flow characteristic that was initially considered to be a factor in the performance of the cascade configurations over the incidence range was that of down-wash flow on the suction surface of the cascade blades -- the downstream blade in particular. At the low and intermediate incidence angle settings, it was observed that there was a very slight tendency for the ink streams to down-wash on the upstream and center cascade blades, and a slight to moderate tendency for the ink streams to down-wash on the down-stream cascade blade. In all cascade configurations, it was observed that the tendency for the flow to down-wash on the downstream cascade blade increased to a moderate to an occasionally severe down-wash as the incidence angle increased to the largest incidence value, +7°.

THEORY

The flow phenomena in an axial compressor is very complicated. To better understand this flow, it is necessary to obtain a clear understanding of some of the physical concepts involving the separation of flow in the boundary layer. At the point of separation,

$$\left.\frac{\partial u}{\partial y}\right|_{y=0} = 0 \quad , \tag{1}$$

the tangent to the velocity profile is vertical at the boundary surface. Separation of the boundary layer occurs only in decelerated flow where the pressure gradient, $\frac{\partial P}{\partial x}$, is positive. In the simplified boundary layer theory,

$$\mu \left.\frac{\partial^2 u}{\partial y^2}\right|_{y=0} = \frac{dP}{dx} \quad , \tag{2}$$

the curvature of the velocity profile is a function of only the pressure gradient, as shown in Figure 11. In the case of a decelerated flow, however, the pressure gradient at the wall is positive, $dp/dx>0$, and the curvature of the velocity profile in the vicinity of the wall is also positive, $(\partial^2 u/\partial y^2)_{y=0}>0$. Since the curvature of the velocity profile must again be negative at some distance from the boundary surface, it follows that under these conditions there must be a point of inflexion somewhere in the velocity profile, as shown in Figure 12. Thus, it follows that the velocity profile will always display a point of inflexion in a region of retarded flow. Since a point of inflexion is required for the velocity profile to have a zero tangent at the point of separation, separation of the boundary layer can therefore occur only when the flow is retarded.

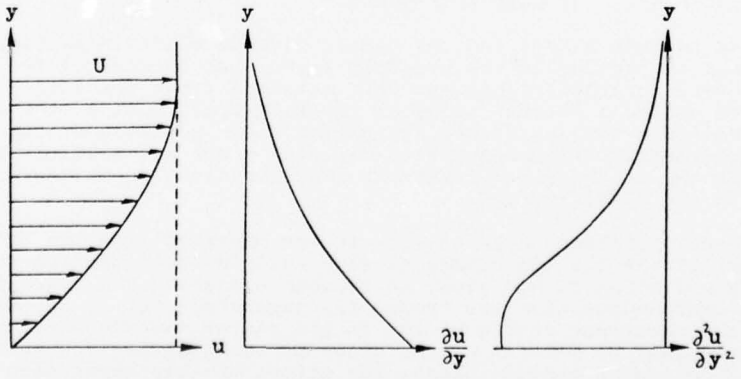


Figure 11 Velocity Profile with Negative Pressure Gradient

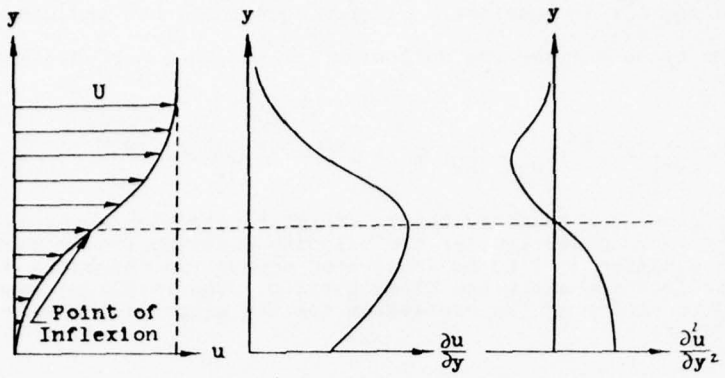


Figure 12 Velocity Profile with Positive Pressure Gradient

In axial flow compressor blades which are treated by the addition of slots, the high energy fluid from the main stream flow is injected tangentially along the blade surface into the decelerating boundary layer in the critical region near the blade surface. This results in a negative pressure gradient being imposed over the unfavorable positive pressure gradient and causes the velocity profile in the boundary layer to be modified, as shown in Figure 13. From the previous discussion, it seems clear that a velocity profile of the form shown in Figure 16 can have no zero tangent at the blade surface, and therefore separation of the boundary layer will not occur without further modification of the velocity profile.

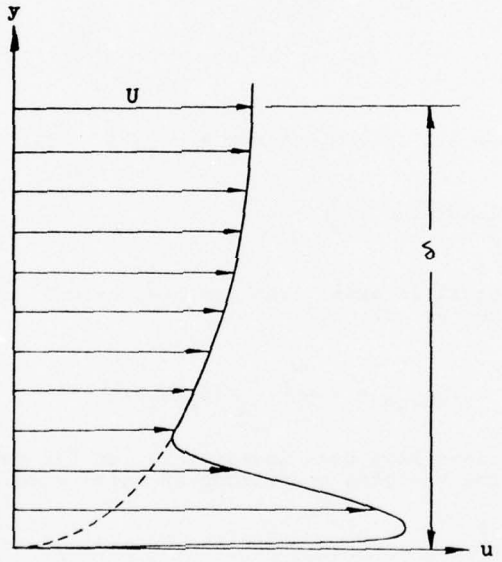


Figure 13 Velocity Profile with Tangential Blowing

To further describe the flow as accurately as possible, the Navier-Stokes' equations have been modified into a natural coordinate system, as shown in Figure 14. The modified form of the combination of these equations written for the boundary layers in a viscous compressible fluid can be given as:

$$W_x \frac{\partial W_x}{\partial x} + W_y \frac{\partial W_x}{\partial y} - \sin\alpha \cdot \cos\beta \cdot \omega^2 r = -\frac{1}{\rho}\frac{\partial P}{\partial x} + \nu \left[C_1 \frac{\partial^2 W_x}{\partial y^2}\right] \quad , \quad (3)$$

where

$$C_1 = \cos^2\beta + \sin^2\beta \cdot \cos\beta \left[\sin\beta + \cos\beta\right] \quad .$$

The continuity equation is

$$\frac{\partial W_x}{\partial x} + \frac{\partial W_y}{\partial y} + \left[\frac{\sin\alpha \cdot \cos\beta}{r} + \frac{1}{\rho}\frac{\partial \rho}{\partial x}\right] W_x = 0 \quad (4)$$

Substituting for $\frac{\partial W_x}{\partial x}$ in equation (3) from equation (4), and assuming negligible flow normal to the blade surface the following second order second degree differential equation results:

$$\frac{\partial^2 W_x}{\partial y^2} + \left[\frac{\sin\alpha \cdot \cos\beta}{r\nu C_1} + \frac{1}{\rho\nu C_1}\frac{\partial\rho}{\partial x}\right] W_x^2 + \left[\frac{\sin\alpha \cdot \cos\beta \cdot \omega^2 r}{\nu C_1} - \frac{1}{\rho\nu C_1}\right] = 0 \qquad (5)$$

Existence of turbulent boundary layers at relatively high Reynolds' number permits the use of the one-tenth power law for the velocity distribution in these layers. This assumption allows equation ( ) to be integrated across the thickness of the boundary layer at any given location along the blade surface. The resulting boundary layer thickness is used to arrive at the expression for the slope of the velocity profile at the edge of the layer:

$$\frac{\partial W_x}{\partial y}\Big| = W_{x\infty}/\left[10\left\{\frac{B}{A}\left(1 - e^{\{1+c\}Ax}\right)\right\}^{\frac{1}{1+c}}\right] , \qquad (6)$$

where the constants A and B are functions of the blade geometry and stage location.

$$A = \frac{10}{W_{x\infty}}\frac{dW_{x\infty}}{dx} - C_2 - \frac{13.2 \sin\alpha \cdot \cos\beta\, \omega^2 r}{W_{x\infty}^2} + \frac{13.5}{W_{x\infty}^2 \rho}\frac{dP}{dx}$$

$$B = -0.155608\, W_x^2\, C_1 \left(\frac{\nu}{W_x}\right)^c$$

$$c = \frac{2}{11}$$

$$C_1 = \cos^2\beta + \sin^2\beta \cos\beta(\sin\beta + \cos\beta)$$

$$C_2 = \frac{\sin\alpha \cdot \cos\beta}{r} + \frac{1}{\rho}\frac{d\rho}{dX}$$

In order to predict stall in axial fans and compressors, a new criterion is developed by defining the surge factor as [12, 13]:

$$\tau_{surge} = \nu \frac{\partial W_x}{\partial y}\Big|_{\delta} / [N_s\{U_2/\sqrt{\theta}\}^2] \qquad (7)$$

A limited number of cases have been investigated so far wherein a value of 0.03 for the surge factor signals the stalling conditions in axial machines operating in adverse pressure gradients.

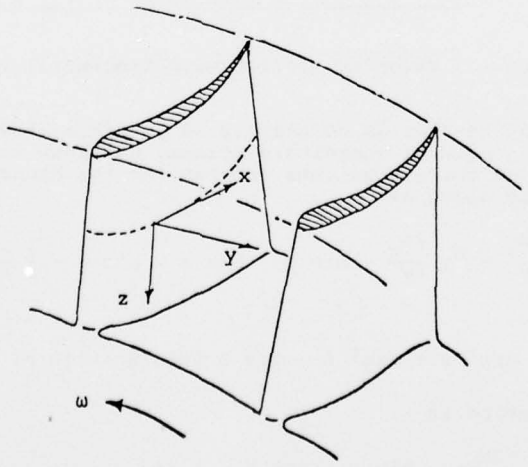


Figure 14 Natural Coordinate System

CONCLUSIONS

The technique outlined for controlling the separation shows considerable promise. The major points of the flow visualization study are:

1. The flow stays attached for a longer period of time on the treated blades than it does on the untreated blades.

2. For all cascade test configurations, the extent of the laminar flow boundary layer was found to be progressively reduced as the flow incidence angle was increased. This effect is concluded to be the result of earlier separation of the boundary layer with increased incidence angle. The treatment configuration having six 0.090" slots was found to be the most successful in maintaining a greater extent of laminar flow boundary layer on the suction surface of the cascade blades.

3. At the lower incidence angles, it was found that the performance of all the cascade test configurations in terms of boundary layer attachment were not appreciably different. At the +4° incidence angle, however, the treatment configuration with six 0.090" slots was found to be slightly superior to the standard NACA 65 series blade and the other treatment configurations. This treatment configuration and the treatment configuration with 0.030" slots also appeared to make some improvement over the standard blade and the other treatment configurations at the +7° incidence angle.

4. The treated blade with the continuous flat was prone to separate much earlier and had a marked tendency to induce a down-wash.

The analysis presented describes the flow using the viscous Navier-Stokes' equation. A calculation for boundary layer thickness in the blade is presented. The surge factor introduced may become a bench factor in signaling surge after more compressors can be tested against it. The author wishes to acknowledge the contribution of Mr. Sangerhausen [14] during the experimental phase of this program.

REFERENCES

1. Sinnette, J. T., Jr., and Costello, G. R., "Possible Application of Blade Boundary-Layer Control to Improvement of Design and Off-Design Performance of Axial-Flow Turbomachines," NACA TN 2371, May 1951.

2. Costello, G. R., "Method of Designing Cascade Blades with Prescribed Velocity Distributions in Compressible Potential Flows," NACA Report 978, 1950.

3. Sheets, H. E., "The Slotted-Blade Axial-Flow Blower," Trans. ASME, Vol. 78, No. 8, Nov 1956, pp. 1683-1690.

4. Mikolajczak, A. A., Weingold, H. D., and Nikkanen, J. P., "Flow Through Cascades of Slotted Compressor Blades," Journal of Engineering for Power, Trans. ASME, Vol. 92, Ser. A., No. 1, Jan 1970, pp. 57-64.

5. Papailiou, K. D., "Boundary Layer Optimization for the Design of High Turbine Axial-Flow Compressor Blades," Journal of Engineering for Power, Trans. ASME, Vol. 93, Ser. A., No. 1, Jan 1971, pp. 147-155.

6. Schwering, W., "Design of Cascades for Incompressible Plane Potential Flows with Prescribed Velocity Distribution," Journal of Engineering for Power, Trans. ASME, Vol. 93, Series A, No. 3, July 1971, pp. 321-331.

7. Stark, U., "A Theoretical Investigation of the Jet-Flap Compressor Cascade in Incompressible Flow," Journal of Engineering for Power, Trans. ASME, Vol. 94, Ser. A, No. 4, Oct 1972, pp. 249-260.

8. Clark, E. L., Jr., and Ordway, D. E., "An Experimental Study of Jet-Flap Compressor Blades," Journal of the Aero/Space Sciences, Vol. 26, No. 11, Nov 1959, pp. 698-702.

9. Koch, C. C., "Experimental Evaluation of Outer Case Blowing or Bleeding of Single Stage Axial Flow Compressor," Part IV, Rep. R 69AEG256, General Electric Company, NASA CR 54592, Jan 1970.

10. Hartmann, M. J., Benser, W. A., Hauser, C. H., and Ruggeri, R. S., "Fan and Compressor Technology," NASA SP259, pp. 1-36.

11. Boyce, M. P., Schiller, R. N., and Desai, A. R., "Study of Casing Treatment Effects in Axial Flow Compressors," ASME Paper No. 74-GT-89.

12. Elchuri, V., "A Method of Predicting Surge in Centrifugal Compressors," M. S. Thesis, Texas A&M University, Dec 1975.

13. Boyce, M. P., "Method and Apparatus for Compressor Surge Control," United States Patent, 3,901,620, Aug 1975.

14. Sangerhausen, C. R., "An Investigation of Axial-Flow Compressor Blade Treatments," M. S. Thesis, Texas A&M University, Dec 1974.

DISCUSSION

J.Fabri

In parallel to your experimental work, did you also make computations on the flow in the grooves and did you publish them?

Author's Reply

Yes, the flow between the tips of the compressor and the casing was computed and the results were published in an ASME paper presented at the Zurich conference in 1974. The paper is also published in the Journal of Engineering for Power. Another paper which deals with similar theory was presented at a Lubrication Society meeting and printed in the Journal of the American Society of Lubrication Engineers in October 1972.

K.Papailiou

(a) You didn't speak of losses in your paper. Could you comment on them?

(b) Did the slots affect the slip factor value for the radial compressor case and, if so, by how much?

Author's Reply

(a) The losses were reduced on an experimental centrifugal compressor using boundary layer slots. Our qualitative data on axial flow compressor also indicated that the losses would be reduced since separation was reduced and consequently a reduction in secondary flows. Our computations indicate an increase in efficiency of about 3%.

(b) The slots affected the flow at the exit of the compressor. The flow was closer to the blade shape with these slots than without them. The initial slip factor was about .76, after the boundary slots the slip factor was increased to .82.

$$\text{Slip factor} = \frac{V_{\sigma_2}}{u_2}$$

J.H.Horlock

Does not the introduction of slots or fences only lead to increased efficiency if the efficiency of the basic compressor or turbine is low to begin with, i.e. if there is initially a flow separation present which is removed by the device?

Author's Reply

Well, the compressors which we were checking were those of turbochargers. The engineering for those compressors is relatively inefficient. We more are looking to a unit which is a 4 to 1 pressure ratio compressor. This would be a Ford gas turbine, where the compressor is rather well designed. We are going to test this compressor and if we do show any increase, we will know we have better results. The turbocharger had low efficiencies to start with.

J.Fabri

The advantage of grooves is to increase the surge margin?

Author's Reply

The main advantage of the grooves was to increase the surge margin. Experimental results performed on a centrifugal compressor indicated a fifteen percent increase in surge to stall margin. Efficiency increase was about 2-3 percent. The major advantage of the grooves is to enable you to extend the surge line thus being able to operate closer to the present surge point and therefore at higher efficiencies.

INFLUENCE DE DISTORSIONS INITIALES SUR LES ECOULEMENTS SECONDAIRES DANS UNE GRILLE D'AUBES ANNULAIRE FIXE *

par Jacques HUARD

Office National d'Etudes et de Recherches Aérospatiales (ONERA)
92320 Châtillon (France)

♦

Résumé

Cette étude expérimentale a été effectuée sur un montage comportant dans un canal cylindrique de hauteur constante une grille accélératrice induisant un écoulement giratoire de nombre de Mach subsonique élevé et une grille réceptrice, représentant le redresseur d'un compresseur axial, qui renvoie le fluide dans la direction axiale.

La configuration de référence comporte un écoulement azimutalement uniforme à l'entrée de la première grille. Au moyen de secteurs angulaires de grillages à perméabilités différentes on crée en amont de la grille distributrice une perte de charge. L'exploration de l'écoulement entre les deux grilles fait apparaître une forte perturbation au voisinage du moyeu où la variation azimutale de la composante tangentielle a pour effet de transformer un écoulement initialement à pression statique radialement et azimutalement variable en un écoulement à pression statique variable le long du rayon seulement. C'est cet écoulement qui attaque la grille décélératrice, ce qui amplifie les effets secondaires au voisinage du moyeu où des décollements intenses apparaissent.

L'étude expérimentale de l'effet d'une distorsion amont de l'écoulement a permis de mettre en évidence une forte amplification de celle-ci dans le domaine d'écoulement secondaire.

INFLUENCE OF INITIAL DISTORTIONS ON SECONDARY FLOWS IN A FIXED ANNULAR CASCADE

Summary

This experimental study was carried out on a test rig comprising, in a cylindrical duct of constant height, an accelerating cascade providing a girating flow at high subsonic Mach number and a receiving cascade representing the downstream stator of an axial compressor deflecting the flow back to the axial direction.

In the reference configuration, the flow is uniform in azimuth at inlet. By means of angular sectors of screens with different permeabilities, a pressure drop is created upstream of the first cascade. The exploration of the flow between the two cascades reveals a strong perturbation near the hub, where the azimuthal variation of the tangential component induces the transformation of the flow, whose static pressure was initially variable in both radius and azimuth, into one with only radial pressure variation. It is this flow that impinges the decelerating cascade, which amplifies the secondary effects near the hub, where intense flow separations take place.

A strong amplification of initial flow distortions has thus been brought to light, as regards secondary flows.

* *Travail effectué sous contrat DRME.*

NOTATIONS

h	:	hauteur de l'aube
M	:	nombre de Mach absolu
M_a	:	composante axiale du nombre de Mach
M_u	:	composante tangentielle du nombre de Mach
p	:	pression statique
p_i	:	pression d'arrêt
r	:	rayon
u_s	:	composante longitudinale de la vitesse dans la couche limite
V	:	vitesse absolue
w_n	:	composante transversale de la vitesse dans la couche limite
y	:	distance à la paroi externe
α	:	position azimutale
β	:	angle de l'écoulement avec la direction axiale
δ	:	épaisseur de la couche limite de carter.

Indices :

e se rapportant à l'écoulement moyen calculé
0 plan infini amont
1 plan de sondage en amont du distributeur
2 plan de sondage en aval du distributeur
3 plan de sondage en aval de la grille décélératrice
( ) valeur moyennée azimutalement.

I – INTRODUCTION

De nombreuses études, tant expérimentales que théoriques, ont été effectuées sur les écoulements secondaires [1 à 5]. Généralement, celles-ci se limitent aux grilles planes et aux compresseurs. Une étude expérimentale en grille annulaire se plaçait donc comme une étape intéressante pour la compréhension de ces écoulements.

Cette étude en grille d'aubes annulaire fixe a été effectuée sur un montage comportant dans un canal cylindrique de hauteur constante une grille accélératrice induisant un écoulement giratoire de nombre de Mach subsonique élevé réglagle par variation de la pression génératrice de l'écoulement et une grille décélératrice qui renvoie le fluide dans la direction axiale.

La configuration de référence comporte un écoulement azimutalement uniforme à l'entrée de la grille distributrice.

L'exploration de l'écoulement en amont et en aval de la grille décélératrice a permis de déterminer l'influence du nombre de Mach moyen et de l'angle d'incidence à l'entrée de cette grille, les variations de cet angle ont été obtenues par l'emploi de différentes grilles inductrices.

Ces études ont été complétées par l'analyse de la réponse de l'écoulement à des distorsions de formes variées imposées en amont de la grille distributrice et notamment de l'effet de ces distorsions sur les écoulements secondaires.

Au moyen de secteurs angulaires de grillages à perméabilités différentes on induit en amont de la grille distributrice un écoulement azimutalement non uniforme. Au cours des essais décrits la variation azimutale de la pression d'arrêt est sensiblement sinusoïdale d'amplitude dix pour cent de la pression génératrice moyenne. On s'est limité à l'étude d'une seule période azimutale.

II – MONTAGE EXPÉRIMENTAL

Le dispositif expérimental mis en place fonctionne d'une façon continue à l'air comprimé et comprend essentiellement un canal cylindrique à section constante équipé d'une grille distributrice, analogue à un distributeur de turbine, suivie de la grille d'essais proprement dite (fig. 1).

Les caractéristiques aérodynamiques de la soufflerie sont présentées au tableau I.

Tableau I

Diamètre extérieur	206 mm
Diamètre intérieur	110 mm
Débit m	$\leqslant$ 7 kg/s
Pression génératrice p_{io}	$\leqslant$ 2,4 bars
Température génératrice T_{io}	$\leqslant$ 325 K
Nombre de Mach à l'entrée du distributeur	$0{,}2 < M < 0{,}4$
Nombre de Mach à l'entrée de la grille d'essais	$0{,}3 < M < 0{,}8$

II.1 – Distributeurs

Les trois distributeurs utilisés assurent à l'entrée de la grille un écoulement giratoire. Ceux-ci dénommés $\Delta 3$, $\Delta 4$ et $\Delta 5$ sont réalisés avec des aubes en tôle mince de profil circulaire et les déflexions obtenues au rayon moyen sont présentées au tableau II.

Tableau II

Distributeur	Déflexion obtenue
$\Delta 3$	47,5°
$\Delta 4$	48°
$\Delta 5$	53,5°

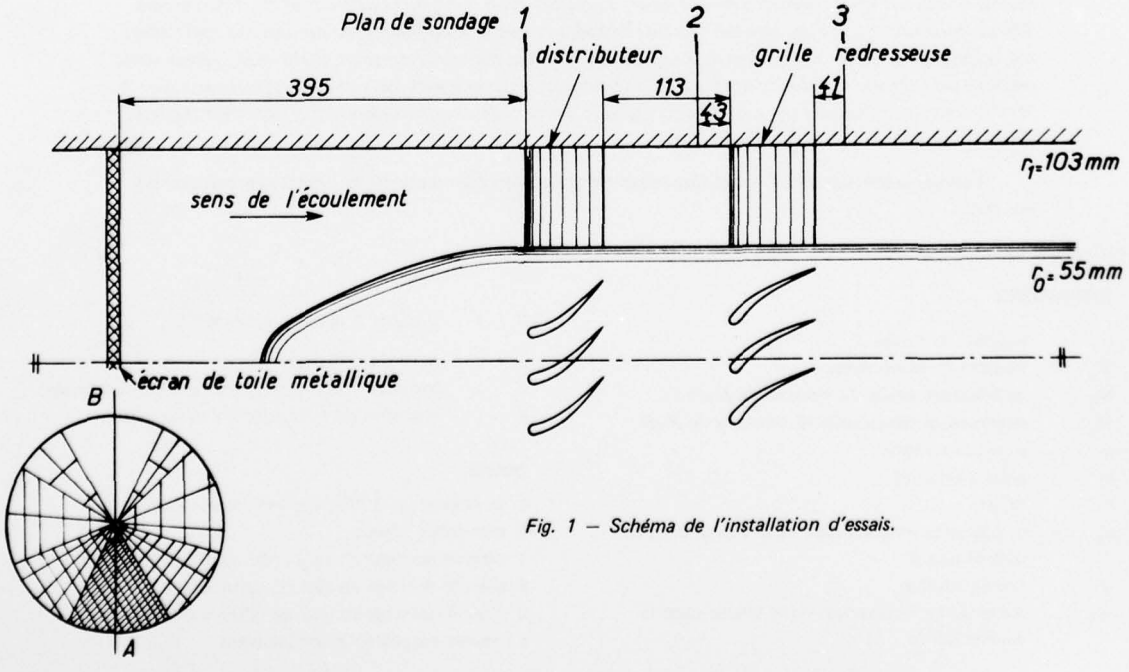


Fig. 1 – Schéma de l'installation d'essais.

II.2 – Grille redresseuse

La grille redresseuse est constituée de 34 profils paraboliques non vrillés de type industriel.

L'angle de la tangente à la ligne moyenne au bord d'attaque de la grille avec la direction axiale étant de 55 degrés, l'incidence de l'écoulement attaquant celle-ci varie donc de $-1,5°$ à $-7,5°$ à mi-hauteur de veine. La direction de sortie théorique est sensiblement axiale.

II.3 – Instrumentation de mesures

Dans le plan de sondage 1 en amont du distributeur des mesures de pression d'arrêt ainsi qu'un contrôle de la direction axiale de l'écoulement ont été effectués (fig. 1).

Une exploration de l'écoulement en direction et intensité de la vitesse a été effectuée à l'entrée de la grille redresseuse (plan de sondage 2) et à la sortie (plan de sondage 3).

Une sonde directionnelle type NACA a été utilisée à cet effet par déplacement radial et azimutal sur un pas de la grille.

Les sondes sont automatiquement mises en direction grâce à un dispositif qui permet d'effectuer rapidement les mesures. Lorsqu'elles sont dans la direction de l'écoulement, une chaîne d'acquisition enregistre instantanément les informations sur ruban perforé.

III – MÉTHODE DE DÉPOUILLEMENT

Les mesures étant effectuées sur le pas d'un canal inter-aubes, chaque information recueillie est fonction du rayon r et de la position azimutale α. Il faut donc définir l'écoulement moyen équivalent.

Les valeurs moyennes ont été définies par pondération suivant le Mach débitant :

- pression d'arrêt :

$$\overline{p_i}(r) = \frac{\int_0^{\alpha_0} p_i\,(r,\alpha)\, M\,(r,\alpha) \cos\beta\,(r,\alpha)\, d\alpha}{\int_0^{\alpha_0} M\,(r,\alpha) \cos\beta\,(r,\alpha)\, d\alpha} \quad ;$$

- pression statique :

$$\overline{p}(r) = \frac{\int_0^{\alpha_0} p\,(r,\alpha)\, M\,(r,\alpha) \cos\beta\,(r,\alpha)\, d\alpha}{\int_0^{\alpha_0} M\,(r,\alpha) \cos\beta\,(r,\alpha)\, d\alpha} \quad .$$

ainsi que les composantes axiale moyenne $\overline{M_a}(r)$ et tangentielle moyenne $\overline{M_u}(r)$.

Le secteur angulaire α_0 correspond à un pas de la grille en l'absence de distorsion et est réduit au voisinage du rayon de pression maximale ou minimale dans le cas de l'étude de la distorsion, mais même dans ce cas, il importe de définir des valeurs moyennes afin d'éliminer l'effet du sillage des aubes distributrices.

Connaissant la pression d'arrêt et la pression statique moyenne, on calcule le nombre de Mach absolu moyen $\overline{M}(r)$.

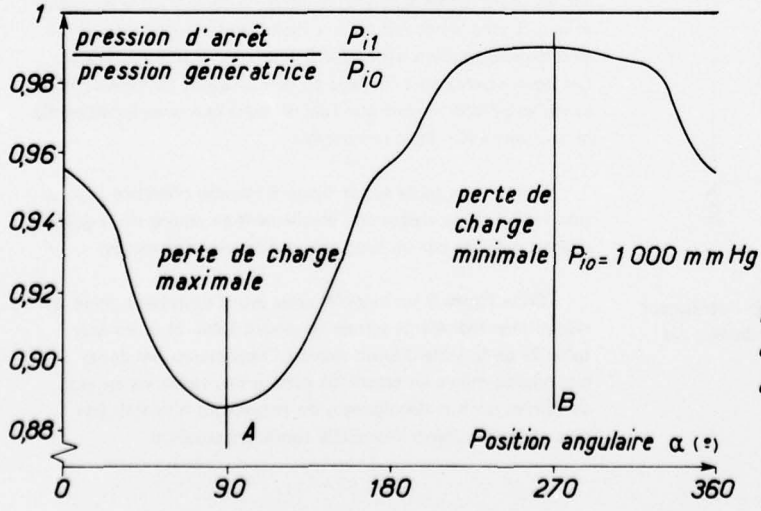
L'angle moyen $\overline{\beta}(r)$ de l'écoulement avec la direction axiale est déterminé par la relation :

$$\overline{\beta(r)} = \text{Arc tg}\ \frac{\overline{M_u}(r)}{\overline{M_a}(r)} \quad .$$

Le programme de dépouillement des valeurs moyennes permet en outre de calculer l'équilibre radial des filets fluide à partir de l'équation simplifiée, la comparaison avec l'expérience met éventuellement en évidence l'existence de vitesses radiales.

IV – RÉSULTATS EXPÉRIMENTAUX

Des mesures de pression d'arrêt ont été effectuées dans le plan de sondage 1, à mi-hauteur de veine afin d'ajuster les secteurs angulaires de grillage pour réaliser une évolution azimutale sinusoïdale de la pression d'arrêt initiale (fig. 2). Nous avons relevé de légères variations de la direction de l'écoulement toutefois celles-ci ne dépassent pas plus ou moins deux degrés.



Cette figure repère les deux positions azimutales A et B présentant le maximum et le minimum de perte de charge due à la distorsion et dans lesquelles les mesures ont été effectuées.

Fig. 2 – Evolution azimutale à mi-hauteur de la pression d'arrêt, P_{i1}, en amont du distributeur.

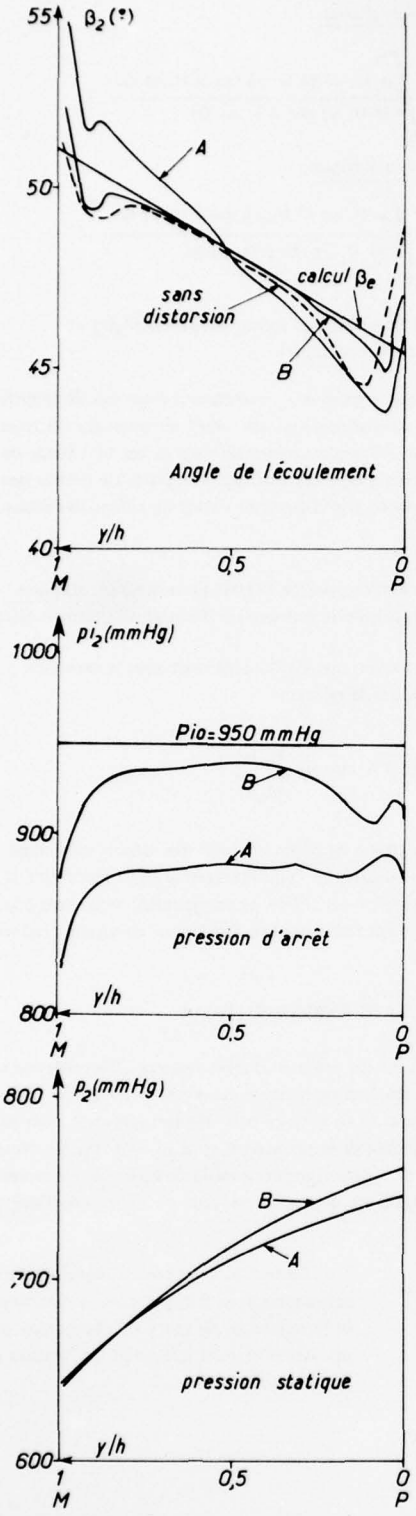


Fig. 3 – Exploration de l'écoulement entre le distributeur et la grille d'essais (plan de sondage 2). Distributeur Δ4.
Perte de charge maximale : A
Perte de charge minimale : B

IV.1 – Plan de sondage en aval du distributeur

Les caractéristiques aérodynamiques de l'écoulement en aval du distributeur Δ4 (plan de sondage 2) sont rassemblées sur la figure 3. L'étude de l'évolution radiale de la direction de l'écoulement met en évidence une surdéflexion de deux degrés au moyeu dans la position A, maximum de perte de charge, alors que près de la périphérie nous notons une sous déflexion de un degré par rapport à la position B, minimum de la perte de charge.

Nous relevons une bonne concordance dans la zone d'écoulement sain entre les évolutions radiales des angles avec (zone B) et sans distorsion, néanmoins on remarque que les régions d'écoulements secondaires se trouvent légèrement altérées par la distorsion amont.

L'évolution radiale de la pression statique pour les positions A et B montre que la pression est pratiquement uniforme azimutalement sur une fraction importante de la veine au voisinage du moyeu.

La variation azimutale de la composante tangentielle de la vitesse a pour effet de transformer l'écoulement initialement à pression statique radialement et azimutalement variable en un écoulement près du moyeu à pression statique variable le long du rayon seulement. C'est cet écoulement hétérogène qui attaque la grille décélératrice.

IV.2 – Plan de sondage en aval de la grille d'essais

La figure 4 montre pour le distributeur Δ4 les caractéristiques aérodynamiques de l'écoulement en aval de la grille décélératrice. L'évolution radiale de la pression d'arrêt met en évidence au voisinage du moyeu un décollement intense qui affecte 30 % de la hauteur de la veine.

On observe d'autre part qu'il ne s'opère plus de transfert tangentiel de débit en aval de la grille d'essais.

V – COMPARAISON DES ZONES D'ÉCOULEMENT SECONDAIRE AVEC ET SANS DISTORSION

Afin de cerner valablement les effets de la distorsion amont sur les phénomènes secondaires, nous ne comparerons les essais effectués sans distorsion qu'aux mesures effectuées avec distorsion dans la position azimutale B (perte de charge minimale). Ces deux essais ayant été faits au même niveau de vitesse. Nous avons vu précédemment que l'écoulement sain avec (position B) et sans distorsion était comparable.

Nous avons porté sur la figure 5 comme référence l'évolution radiale de la vitesse de l'écoulement en amont de la grille d'essais calculée par un programme d'écoulement moyen.

Cette figure 5 sur laquelle nous avons également porté les répartitions radiales de vitesse en amont (plan 2) et en aval (plan 3) de la grille d'essais montre l'importance des zones secondaires même en amont de cette grille, tandis qu'en aval de celle-ci un fort décollement de moyeu qui n'existait pas sans distorsion, rend impossible toute comparaison.

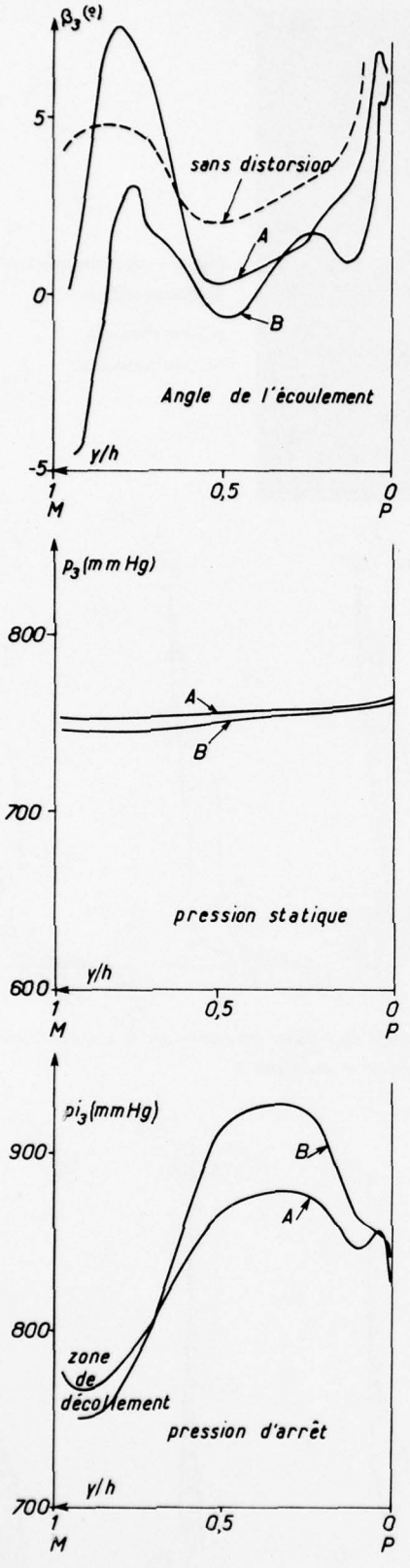


Fig. 4 — Exploration de l'écoulement en aval de la grille d'essais (plan de sondage 3). Distributeur Δ4.
Perte de charge maximale : A
Perte de charge minimale : B.

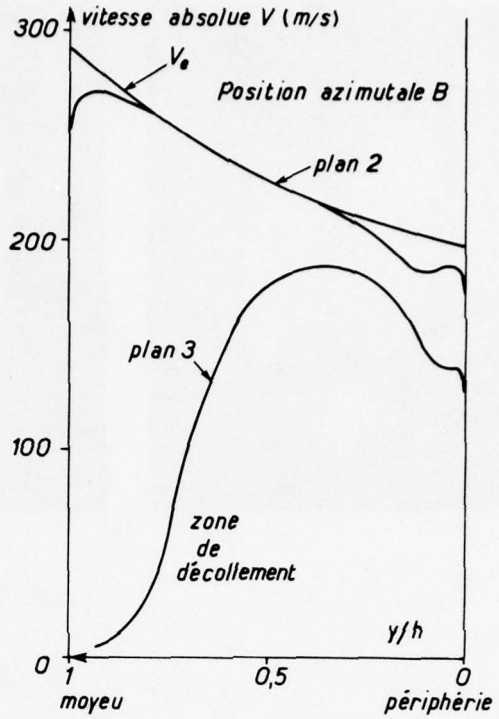


Fig. 5 — Evolution radiale de la vitesse de l'écoulement. Position azimutale B. Distributeur Δ4.

L'apparition de ce décollement de moyeu dû à la distorsion a été confirmé par visualisation hydraulique (fig. 6) [6].

La figure 7 sur laquelle nous avons porté la répartition de vitesse dans le domaine secondaire confirme que la distorsion de l'écoulement n'amplifie pas les pertes dues aux écoulements secondaires en périphérie.

Les distributions de vitesses à la périphérie dans un système de coordonnées lié à la ligne de courant de l'écoulement sain sont présentées figure 8.

Le système d'axes choisi est tel qu'une composante transversale positive correspond à une diminution de la direction de l'écoulement par rapport à l'écoulement sain.

Les composantes longitudinale U_s et transversale W_n sont donc définies par :

$$U_s = V_e \cos(\beta_e - \beta)$$

$$W_n = V_e \sin(\beta_e - \beta) .$$

En aval du distributeur (plan 2) on remarque que la distorsion atténue le vrillage de la couche limite.

L'hétérogénéité de l'écoulement impose en effet un transfert de quantité de mouvement tangentiel du minimum de perte de charge vers la position azimutale A de maximum de perte de charge.

Des résultats très semblables ont été obtenus avec les deux autres distributeurs Δ3 et Δ5 qui induisent des écoulements attaquant les aubes d'essais de part et d'autre de la direction optimale.

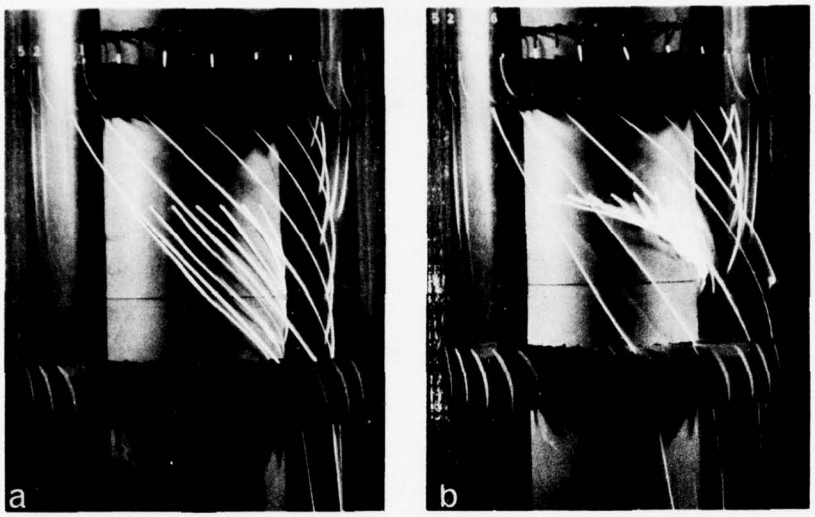


Fig. 6 – Visualisation au tunnel hydrodynamique.

a) sans distorsion

b) avec distorsion

avec distorsion { ○ plan 2 amont de la grille ; △ plan 3 aval de la grille

sans distorsion ——

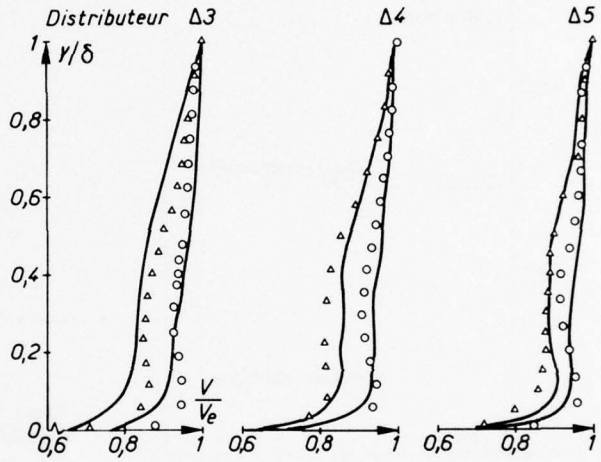


Fig. 7 – Profil de vitesses résultantes de la couche limite de carter. Position azimutale B.

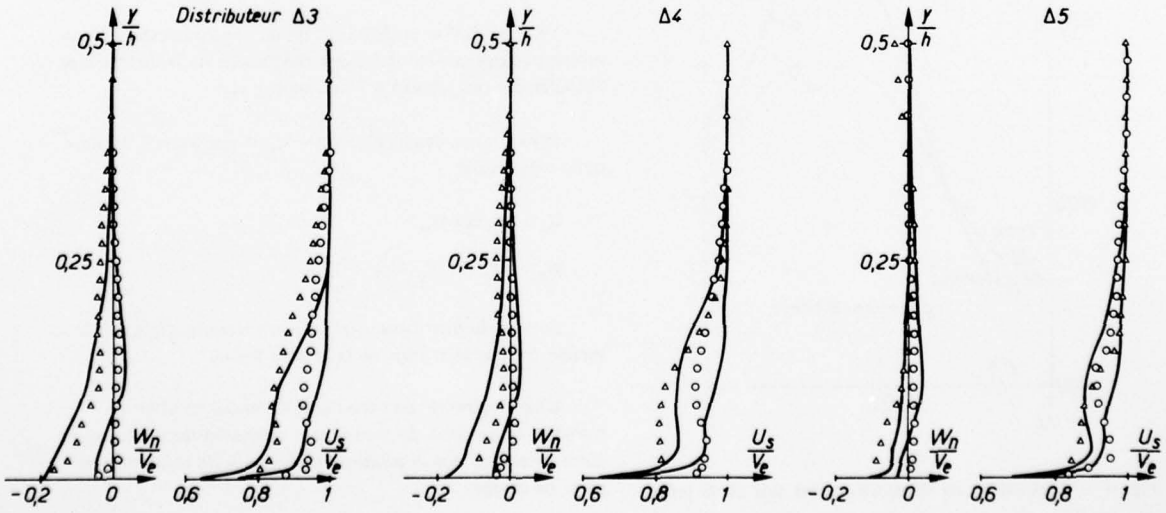


Fig. 8 – Profils de vitesse transversal et longitudinal dans la couche limite de carter.

Position azimutale B.

avec distorsion : ○ plan 2 amont de la grille △ plan 3 aval de la grille ; sans distorsion : ——

VI – CONCLUSION

L'étude expérimentale de l'effet d'une distorsion de l'écoulement amont sur les performances d'une grille d'aubes annulaire et notamment sur les zones secondaires de l'écoulement a mis en évidence un effet très important des hétérogénéités amont sur le domaine d'écoulement secondaire.

Bien qu'au voisinage du carter externe dans la zone à faible perte de charge on retrouve en aval de la grille distributrice les répartitions de vitesse caractéristiques de l'écoulement azimutalement uniforme, le déficit de débit du domaine à forte perte de charge conduit à une modification profonde du champ de vitesse au voisinage de la paroi externe.

A l'aval de la grille décélératrice qui donne une forte recompression de l'écoulement, un décollement intense apparaît au moyeu aussi bien dans la zone à forte perte de charge que dans celle à faible perte de charge, conduisant à un écart notable avec le fonctionnement sans distorsion.

Les modifications de l'écoulement sain dues à une distorsion azimutale de l'écoulement amont sont donc fortement amplifiées dans le domaine d'écoulement secondaire.

RÉFÉRENCES

1. Hawthorne W.R. – *Rotational flow through cascades.* Part I, the components of vorticity. Quarterly Journal of Mechanics and Applied Mathematics, V. 8 (1955), p. 266-279.

2. Horlock J.G. – *Cross flows in bounded three dimensional turbulent boundary layers.* Cambridge Univ. CUED/A Turbo/TR 28, 1971.

3. Horlock J.G. and Perkins H.J. – *Annulus wall boundary layers in turbomachines.* AGARDograph 10. 185 (1974).

4. Mellor G.L. and Wood – *An axial compressor end-wall boundary layer theory.* J. of Basic Eng., V. 93 (June 1971), p. 300-316.

5. Papaillou K., Flot R., Mathieu J. – *Secondary flows in compressor bladings.* ASME Paper No 76-GT-57 (1976).

6. Werlé H., Huard J. – *Article à paraître* – Rech. Aérosp.

DISCUSSION

J.Dunham

Was your blading free vortex or solid body rotation?

Author's Reply

It was a solid body blading.

HOT-WIRE MEASUREMENTS IN AN AXIAL COMPRESSOR AND CONFRONTATION WITH THEORETICAL PREDICTIONS OF SECONDARY FLOWS.

by

J. DE RUYCK [1], Ch. HIRSCH [2], P. KOOL [3]

VRIJE UNIVERSITEIT BRUSSEL
Dept. of Fluid Mechanics
1050 Brussels
Belgium

ABSTRACT

Measurements of the three-dimensional flow field behind a single stage compressor rotor are presented and a brief description of the measurement technique is given.
Components of vorticity are extracted from the experimental data and compared with secondary flows theory.

INTRODUCTION

Theoretical formulations of secondary flows based on inviscid considerations has been the subject of a great deal of work in the past 25 years since the early paper of Squire and Winter. Detailed developments due to Hawthorne, Horlock and Laksminarayana, Marsh and many others, have clarified in recent years aspects of secondary flows in rotating blades, effects of compressibility and of blade twisting as well as the separation of the different components of streamwise vorticity, trailing shed vorticity and filament vorticity.
Secondary flow theories introduce essentially a connection between an inlet transverse component of vorticity, caused by a sheared flow generally produced by a viscous, turbulent, boundary layer, and the outlet streamwise vorticity without taking into account any viscous effect. However, the three-dimensional flow at outlet of a compressor rotor is influenced by various viscous effects and by tip leakage flows and it seems interesting to compare the experimentalstreamwise vorticitywith the theoretical prediction of inviscid secondary flow theories.
In order to reduce the amount of theoretical input, the transverse vorticity at inlet of the IGV preceding the rotor is deduced from the experimental transverse vorticity at rotor outlet and used as input to the theoretical calculation of secondary flows.

1. EXPERIMENTAL RESULTS

A detailed experimental study of the three-dimensional flow behind a rotor of an axial compressor has been performed with a hot-wire instrumentation.
Figure (1) is a sketch of the open return blowing facility R1 at the Von Karman Institute. The driving motor is a 75-HP dc motor, continuously variable in speed.
Air enters the settling chamber, goes through a set of dust filters with decreasing mesh size, the inlet guide vane, the rotor, the diffuser and the throttle valve. The air speed and flow direction is conventionally measured using Naca short prism Pitot static three-hole probes. Pressures are measured with Statham strain gauge pressure transducers, with direct readout on galvanometer. The three-dimensional flow is determined with a single hot-wire in the absolute reference frame.

---

1) Research Assistant I.W.O.N.L.
2) Professor
3) Research Assistant N.F.W.O.

The technique of periodic sampling and averaging [2], [7] is used to extract the periodically varying flow induced by the rotor at the hot-wire location from the overall signal (periodic part plus turbulent fluctuations). The hot-wire probe is introduced radially and different angular positions are realised at a fixed radius. A survey from inner to outer casing is made by traversing the hot-wire radially.

1.1. Hot-wire technique for three-dimensional flow measurement

To determine a three-dimensional flow field with a single hot-wire the wire must be located in at least three different orientations with respect to the flow direction. To resolve a velocity vector use is made of the directional sensitivity of slanted hot-wires to obtain a different sensitivity to changes in flow direction and velocity magnitude in each of these positions. The most easy way to obtain this is to rotate the wire about the probe axis. Quite generally a position is available where the wire is primarily influenced by the absolute velocity only, and other positions where the sensitivity to changes in flow angle is largely increased with respect to this first position. As can easily be deduced from a velocity triangle modifications in the magnitude of the relative velocity primarily induce changes in the absolute flow. As the hot wire is very sensitive to these changes an accurate measuring system is available. Two methods to determine the three-dimensional flow field with any slanted hot-wire rotated about its axis into different positions are presented in reference [1].

The first method makes use of as many equations as unknown velocity components, the second method is a least squares method and allows to use more data than necessary. The basic equations relating the anemometer voltage to the velocity magnitude at different orientations of the flow are obtained by calibrating the wire in a known flow field. Three of these non-linear equations are solved in an iterative way in the first method, whereas the second method minimizes the difference between the measured and computed effective velocities. The latter method therefore does not require the solution of the equations and is less restrictive for the choice of the different orientations of the hot-wire than the former.

With the hot-wire geometry of figure (2), the following relation is obtained between the yaw-angle ϕ and the angles α_p, α_R and α_o

$$\sin \phi = \cos \alpha_o \cos \alpha_R \cos \alpha_p + \sin \alpha_o \sin \alpha_R \qquad (1)$$

The angle α_o is characteristic for the slanted hot-wire, whereas the radial angle α_R and the probe-angle α_p uniquely define the orientation of the velocity vector $\bar{V}$ in a reference frame connected to the hot-wire. The probe-angle α_p changes by the amount of turning of the probe-axis, whereas α_R is not changed by turning the probe. Therefore, in each position of the probe the following equation can be written down :

$$\sin \phi_i = \cos \alpha_o \cos \alpha_R \cos (\alpha_p + a_i) + \sin \alpha_o \sin \alpha_R \qquad (2)$$

where a_i represents the amount of turning with respect to a reference position.

The yaw-angles ϕ_i are related to the measured effective velocity V_{ei} and the absolute velocity by a calibration law, the exact form of which does not matter here

$$\phi_i = \phi_i (V_{ei}, V) \qquad (3)$$

The three unknown parameters V, α_p, α_R uniquely define the velocity vector in a hot-wire reference frame, and can be determined iteratively from a set of three equations as (2), or by optimization from more than three equations.

The optimum can be defined as the minimum of the expression

$$\sum_{i=1}^{N} \left(V_{ei} - V_e\left(\alpha_{pi}, \alpha_R, V\right)\right)^2 \qquad (4)$$

with $$N > 3 \qquad (5)$$

where V_{ei} represents the measured effective velocity and V_e the calculated effective velocity, N being the number of positions of the hot-wire.

1.2. Performance curves

The investigations reported herein are shown in figure (3) on the performance curves. Case T75 corresponds to the occurrence of stall in the rotor. Case TC3 is lying on a different set of characteristics not identical to the previous one, due to differences of geometry and inlet filter blockage.
Case T95 is also close to stall.

1.3. Typical results

The periodic variation of different flow variables downstream of the rotor at various blade height is given in figures (4) and (5). One period corresponds to a single blade pitch. The results have been obtained by averaging the flow of all blade channels in a plane parallel to the exit plane. In the absolute reference frame large flow angle changes are seen to occur.
The radial flow angle which is positive when directed to the rotor hub indicates that the wake fluid is directed upwards with respect to the free-stream fluid. At blade heights approaching the rotor tip a second viscous region appears. This has been attributed to the strong influence of the tip clearance in this region.
The clearance flow is opposite to the secondary flow in this region and is swept towards the pressure side of the blade.
A view of the axial velocity (case TC3) in the measuring plane from hub to tip and spanning one blade pitch is given in figure (6) as lines of constant velocity. The blade wake is easily recognizable as well as the tip boundary layer. The axial velocity is fairly constant outside these regions.
A three-dimensional projection of the axial velocity profile (case T75) is shown in figure (7).

2. SECONDARY FLOW ANALYSIS

Our purpose is to compare recent theories about non viscous secondary flows with the above mentioned measurements made in a real turbomachine, where usual simplifying assumptions about secondary flows lose much of their validity.
Important effects are leakage flow in the rotor stage and the twisting of blades and stream surfaces.

2.1. Expression for streamwise secondary vorticity

The expression used is that proposed by A.G. Smith [4] valid for an inviscid uniform density flow in a rotating system :

$$\frac{\partial}{\partial s'}\left[\frac{\omega_{s'}}{W}\right] = \frac{2}{W^2 R'}\left|\frac{\nabla I}{\rho}\right| \sin\varphi + 2\frac{\Omega}{W^3}\left|\frac{\nabla I}{\rho}\right| \cos\delta \qquad (6)$$

$$\frac{\nabla I}{\rho} = \vec{W} \wedge \vec{\omega} \qquad (7)$$

where φ is the angle between the normal of the Bernouilli surfaces and the principal normal

of the streamline ; δ, the angle between $\frac{\nabla I}{\rho}$ and $\vec{\Omega}$, and $\omega_{s'}$, the projection of $\vec{\omega}$ (always absolute) in the direction s' of the relative streamline.

$$\omega_{s'} = \bar{\omega} \cdot \bar{1}_{s'} \tag{8}$$

To obtain an available expression, the following assumptions are introduced :

i) Secondary flow occurs in surfaces normal to the mainstream and can be considered as a two-dimensional flow superimposed on the main flow.

ii) Distorsion of the Bernouilli surfaces is small enough to assume $\left|\frac{\nabla I}{\rho}\right|$, δ and φ nearly constant.

iii) $V \cos \alpha = v_x \simeq$ constant through a blade row.

If the inlet flow has no velocity and vorticity components in the radial direction, $\frac{\nabla I}{\rho}$ is radial, and its magnitude is W times the projection of $\bar{\omega}$ on the normal of the relative streamline. Equation (6) becomes, see [5] :

$$\left|\frac{\nabla I}{\rho}\right| = W \cdot \omega_{n'} \cong cte \tag{9}$$

$$\left(\frac{\omega_{s'}}{W}\right)_2 - \left(\frac{\omega_{s'}}{W}\right)_1 = 2 \frac{W\omega_{n'}}{v_x^2} \int_1^2 \cos^2\beta \, d\beta \tag{10}$$

or

$$\omega_{s'2} = \omega_{s'1} \frac{\cos \beta_1}{\cos \beta_2} + \omega_{n'1} \frac{\frac{1}{2}[\sin 2\beta_2 - \sin 2\beta_1] + \beta_2 - \beta_1}{\cos \beta_1 \cos \beta_2} \tag{11}$$

If trailing shed and trailing filament vorticities are introduced, the pitch averaged value of $\omega_{s'2}$ becomes [8]

$$\tilde{\omega}_{s'2} = \tilde{\omega}_{n'1} \operatorname{tg} \beta_2 \left[\frac{\cos \beta_2}{\cos \beta_1} - \frac{\cos \beta_1}{\cos \beta_2}\right] \tag{12}$$

2.2. Calculation of streamwise vorticity at outlet of the compressor

As the measurements are done only in the exit plane 2, we have to assume $\frac{\omega_n}{\cos \alpha} = ct$ to apply the expression for $\omega_{s'2}$. This assumption is in accordance with $\left|\frac{\nabla I}{\rho}\right| \simeq ct$.
Since the compressor contains two blade rows, the calculation must be split up into two parts. The system of equations between the various vorticity components, assuming no streamwise vorticity at inlet of the IGV, is : (see figure 9)

$$\omega_{s1} = \omega_{no} \left[\sin \alpha_1 + \frac{\alpha_1}{\cos \alpha_1}\right] \qquad [\alpha_o = 0] \tag{13}$$

$$\omega_{n1} = \omega_{no} \cos \alpha_1 \tag{14}$$

$$\omega_{s'1} = \bar{\omega}_1 . \bar{1}_{s'1} \tag{15}$$

$$\omega_{n'1} = \bar{\omega}_1 . \bar{1}_{n'1} \tag{16}$$

$$\omega_{s'2} = \omega_{s'1} \frac{\cos \beta_1}{\cos \beta_2} + \omega_{n'1} \frac{\frac{1}{2}[\sin 2\beta_2 - \sin 2\beta_1] + \beta_2 - \beta_1}{\cos \beta_2 \cos \beta_1} \tag{17}$$

$$\omega_{n'2} = \omega_{n'1} \frac{\cos \beta_2}{\cos \beta_1} = \bar{\omega}_{(exp)} \cdot \bar{1}_{n'2} \tag{18}$$

A primary flow has to be defined in order to compare experimental and theoretical values of vorticities. From the three-dimensional experimental velocity profiles it is not possible to define without ambiguity a primary flow. Therefore the blade angles α and β are taken as representative of the primary flow direction.
The experimental vorticity $\bar{\omega}_{exp}$ is calculated from the experimental velocity vector V_2.

$$\omega_x = \frac{1}{r} \frac{\partial v_r}{\partial \theta} - \frac{1}{r} \frac{\partial r v_\theta}{\partial r} \tag{19}$$

$$\omega_\theta = \frac{\partial v_x}{\partial r} - \frac{\partial v_r}{\partial x} \tag{20}$$

Since $\frac{\partial v_r}{\partial x}$ is unknown, we assume that

$$\frac{\partial v_r}{\partial s'} \simeq 0 \quad \rightarrow \quad \frac{\partial v_r}{\partial x} \simeq - tg\, \beta \frac{1}{r} \frac{\partial v_r}{\partial \theta} \tag{21}$$

Since no information is available about the inlet transverse vorticity, equations (13) to (18) are used with the experimental outlet transverse vorticity as input to the theoretical calculations.
If the shed and filament vorticities are considered only equations (18) (averaged over a pitch) and equation (12) are used, since equation (12) is independant of $\omega_{s'1}$, and $\omega_{n'1}$ is only function of the known $\omega_{n'2}$.

2.3. Twisting and tip leakage flow

Since the rotor blades are twisted, an extra vorticity is induced, caused by a different $\frac{\partial v_{n'}}{\partial r}$ along the blade span at in and outlet.
Following the idea of Ehrich [6] we evaluate this vorticity by

$$(\omega_{s'})_{tw} = - \frac{1}{r} \frac{\partial}{\partial r} r\, v_{s'}\, (\varepsilon - \varepsilon_o) \tag{22}$$

$$(\omega_{s'}) = (\omega_{s'})_{sec} - (\omega_{s'})_{tw} \tag{23}$$

where ε is the deflection, ε_o the mean deflection and $(\omega_{s'})_{sec}$ is given by equation (17).
This extra term is found to be of the same order of magnitude as $(\omega_{s'})_{sec}$.
Since little information is available for calculating vorticity caused by the leakage flow, contributions from tip leakage vortices have not been taken into account.

2.4. Secondary streamfunction definition at rotor outlet

Separation between primary and secondary flow can be defined by [9] :

$$\bar{V} = \bar{V}_{pr} + \bar{v} \tag{24}$$

$$\bar{W} = \bar{V}_{pr} + \bar{v} - \bar{\Omega} \wedge \bar{r} = \bar{W}_{pr} + \bar{v} \tag{25}$$

where $\bar{v}$ is the perturbation velocity and is the same for both relative and absolute systems, but is defined in a relative system as normal to $\vec{W}_{pr}$. Thus, the perturbance $\bar{v}$ can be found by defining a streamfunction ψ in a plane normal to $\vec{W}_{pr}$. It is to be noted that the secondary flow considered here is defined as the flow induced by the absolute vorticity component in the direction of $\vec{W}_{pr}$.

A difficulty which raises is that, since the s' and n' lines are not lines of curvature on the cylinder, and according to the theorem of Dupin [10], a coordinate system s',n',r defined in this surface is not orthogonal, even if $\frac{\partial \beta}{\partial s} = \frac{\partial \beta}{\partial r} = 0$. So it is complicated to calculate the $\vec{\nabla}$ operator in the plane r,n'.

A solution to this problem is proposed by Dixon [5], who defines a streamfunction in a plane x=ct, and considers the components of the perturbation vector $\vec{v}$ in the coordinate system x,θ,r.

$$v_r = \frac{1}{r} \frac{\partial \psi}{\partial \theta} \tag{26}$$

$$v_\theta - v_x \, tg \, \beta = - \frac{\partial \psi}{\partial r} \tag{27}$$

and solves :

$$\Delta \psi = \frac{v_x}{r} \frac{d}{dr} r \, tg \, \beta - \frac{\omega_{s'}}{\cos \beta} \tag{28}$$

In our case, this method cannot be used to solve directly for ψ, since v_x in the r.h.s. of equation (28) is a component of the searched secondary flow, and is unknown. An approximation for ψ is found by defining it in a surface normal to a mean flow direction β_o. In this system, the principal curvature of the s' and n' lines are found to be respectively $\frac{\sin^2 \beta_o}{r}$ and $\frac{\cos^2 \beta_o}{r}$, and the torsion $\frac{\sin \beta_o \cos \beta_o}{r}$ (see figure 9).

The approximation consists in neglecting the torsion by developping this surface into a plane. In this plane the n' lines still have a curvature $\frac{\cos^2 \beta_o}{r}$ and a length dn' is given by

$$dn' = r \, d\theta \cos \beta_o$$

Since the radii of curvature of all n' lines are proportional to r, a polar coordinate system r',θ' can be defined in this plane by :

$$r' = \frac{r}{\cos^2 \beta_o} \tag{29}$$

$$\theta' = \theta \cos^3 \beta_o \tag{30}$$

with $$r' \, d\theta' = r \, d\theta \cos \beta_o \, . \tag{31}$$

The streamfunction is defined in these coordinates as follows :

$$v_{n'} = - \frac{\partial \psi}{\partial r'} \tag{32}$$

$$v_r = \frac{1}{r'} \frac{\partial \psi}{\partial \theta'} \tag{33}$$

$$\Delta \psi = \omega_{s'} = \frac{1}{r'^2} \frac{\partial^2 \psi}{\partial \theta'^2} + \frac{1}{r'} \frac{\partial}{\partial r'} r' \frac{\partial \psi}{\partial r'} \tag{34}$$

Equation (34) is solved with a finiteelement method using curved elements in order to simulate correctly the curved boundaries of the secondary flow surface.

3. DISCUSSION OF EXPERIMENTAL AND THEORETICAL RESULTS

From the measured three-dimensional flowfield, a streamwise vorticity has been calculated, as indicated in the previous sections, and the corresponding secondary flow field determined by solving equation (34). The same equation has also been solved with the theoretical expression for streamwise vorticity along the line indicated in section 2.2 and 2.3.

Comparisons have also been made between experimental and theoretical pitch-averaged secondary vorticities and between corresponding values of pitch-averaged secondary cross-flows (n' component of secondary velocity field).

A first general observation is that the detailed secondary flow turns in the direction opposite to the direction induced by the transverse pressure gradient. In fact, the direction of the secondary flow at exit is not obvious, since the transverse vorticity component ω_n, at exit of the IGV, combined with the created streamwise vorticity through the IGV, has a large component in the direction of the relative inlet velocity of the rotor. Due to the structure of the velocity triangle, the major contribution to $\omega_{s'1}$ is due to ω_{n1} (see figure 9).

The streamwise components at rotor inlet turn in the same direction as those found at rotor exit. Thus if the deflection of the rotor is not important enough, the sign of the mainstream vorticity is not defined. In reference [5], Dixon found a similar result in his test-case.

3.1. Pitch-averaged values

Figures 10 to 12 contain the pitch-averaged values of the experimental streamwise vorticities, and those found using equations (11) and (12), resp. without and with contributions from trailing shed and filament vorticities. In all cases, both equations give fair agreement with experimental data in the hub-region of the rotor outlet. Near the tip, equation (11), which contains only the secondary vorticity, yields a vorticity of opposite sign to the experimental one. Taking into account the trailing shed and filament vorticities (eq. (12)) a qualitative agreement is found with experimental data. However the calculated contributions are underestimated. The observed difference in the tip-region may be attributed to the tip leakage vortices which should contribute to a reduction of the observed difference. Better agreement is probably difficult without taking this tip effects into account. Similar conclusions can be drawn from the pitch-averaged secondary cross-flow in figure 13 to 15.

3.2. Secondary flow pattern

Figures 16 to 18 show the secondary flow distribution induced by the experimental streamwise vorticity for the three test-cases considered here. Figure 19 is a contour plot of the experimental streamwise vorticity for test-case T75. The velocities induced at the center of the observed vortices are rather small, but at the boundaries of the blade channel large secondary velocities are induced. This leads to important changes in flow angle near the end-walls and large radial velocities in the blade-wake regions. The patterns of cases T75 (fig. 16) and T95 (fig. 17) show both an important flow at tip. This is due to the leakage flow, which is reinforced since these two cases are close to stall. Case TC3 (fig. 18) has vorticities lower than the two previous ones, and its pattern does not show any more two distinct vortices.

The figures 20 to 22 show a pattern of the secondary flows using eq. (11). Only one vortex is found in the passage, and this vorticity is induced by a mainstream velocity profile which has a dominant gradient from tip to hub (see fig. 8). These patterns give no agreement with the experimental ones on figures 16 to 18. In fact, the measuring plane lies at a distance .34 of a chord from the exit of the rotor for cases T75 and T95 and .56 chord for TC3, and the wakes are spread on an important part of the pitch (see fig. 4 and 5). This means that trailing shed and trailing filament vorticities are also spread, and since they have an important contribution to the total vorticity, it is reasonable to take them into account. An approximation is made by spreading these vorticities over the whole pitch, giving patterns of fig. 23 to 25 as results. Better agreement is reached in this way, using equation :

$$\omega_{s'2} = \omega_{n'1} \, tg \, \beta_2 \left(\frac{\cos \beta_2}{\cos \beta_1} - \frac{\cos \beta_1}{\cos \beta_2} \right) \qquad (35)$$

CONCLUSIONS

From the measurements of the three-dimensional flow field behind an axial compressor rotor, vorticities and secondary flow patterns have been estimated and three test-cases have been analysed.
Theoretical evaluation of streamwise secondary vorticities have been obtained using as input the experimental transverse vorticity component at outlet, since no information was available about the flow at IGV inlet.
Two main conclusions can be drawn from this analysis :

i) Trailing shed and filament vorticities seem to have an important contribution.

ii) Tip leakage vortices have to be taken into consideration.

Main shortcomings are the assumptions about Bernouilli surfaces and leakage flow. The importance of including trailing shed and trailing filament vorticity in theoretical prediction methods is also stressed.

LIST OF VARIABLES

I rothalpy, $\frac{I}{\rho} = \frac{p}{\rho} + \frac{1}{2}[W^2 - (\Omega r)^2]$
n transverse to mainstream coordinate
R principal radius of curvature
r radial coordinate
s mainstream coordinate
$\vec{V}$ absolute velocity
v velocity component
$\vec{v}$ perturbation velocity
$\vec{W}$ relative velocity
X axial coordinate
α absolute flow angle
β relative flow angle
θ angular coordinate in polar coordinate system
ϕ yaw angle
ω vorticity
Ω angular rotation frequency
ψ streamfunction

Subscripts
0 at inlet IGV
1 at inlet rotor
2 at outlet rotor
pr primary flow
n,θ,r cylindrical coordinate system
s,n,r streamline coordinate system
s',n',r relative streamline coordinate system
e effective
p probe
R radial in wire system

Superscripts
' *in relative system*

REFERENCES

[1] KOOL, P. : "Experimental Investigation of the Three-dimensional Flow Field Downstream of Axial Compressors", Ph.D. Thesis, Vrije Universiteit Brussel, January 1977.

[2] HIRSCH, Ch. ; KOOL, P. : "Application of a Periodic Sampling and Averaging Technique to Flow Measurements in Turbomachines", Report V.U.B.-Str.-4, Sept. 1973, Vrije Universiteit Brussel.

[3] HIRSCH, Ch. ; KOOL, P. : "Measurements of the Three-dimensional Flow Field behind an Axial Compressor Stage", ASME Paper, No 76 - GT - 18.

[4] SMITH, A.G. : "On the Generation of the Streamwise Component of Vorticity for Flows in Rotating Passages", Aeronaut. Quart. 8 : 369, 1957.

[5] DIXON, S.L. : "Fluid Mechanics and Design of Turbomachinery", NASA SP304, Part I, 1974.

[6] EHRICH, F. : "Secondary Flows in Cascades of Twisted Blades", Journal of Aeronaut. Sciences, 22, 51, 1955.

[7] WHITFIELD, C.E. ; KELLY, J.C. ; BARRY, B. : "A Three-dimensional Analysis of Rotor Wakes", Aeronautical Quarterly, 23, Part 4, 1972.

[8] HAWTHORNE, W.R. : "Rotational Flow through Cascades". Part 1 : The Components of Vorticity. Q. Journal Mech. Appl. Math., vol. 8, pt.3, 1955.

[9] HORLOCK, J.H. ; LAKSMINARAYANA, B. : "Secondary Flows Theory, Experiment and Application in Turbomachinery Aerodynamics", Annual Review of Fluid Mechanics 5, 247, 1975.

[10] SMIRNOV, V.J. : "A Course of Higher Mathematics", Vol. 2, Pergamon Press, Oxford, 1964.

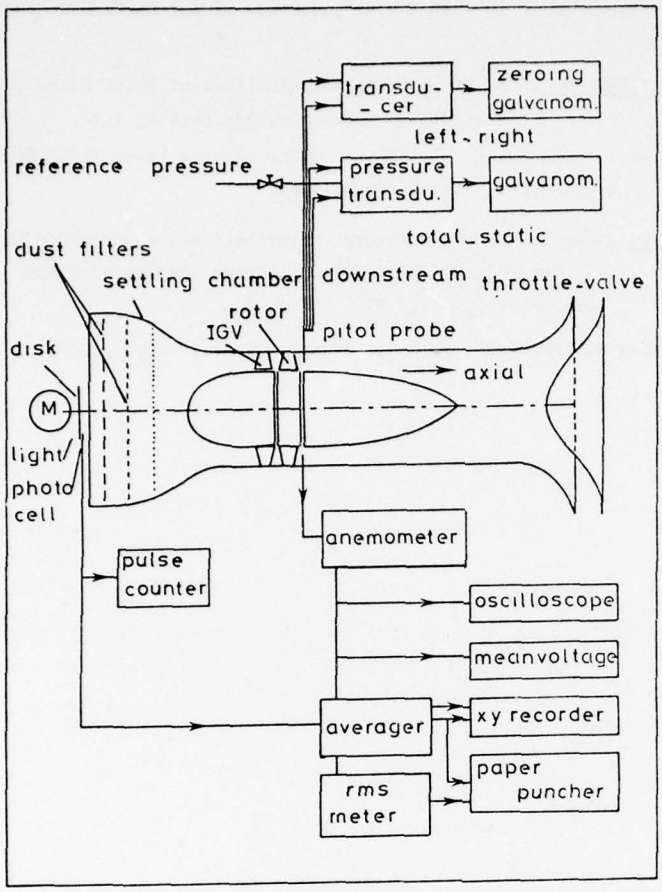
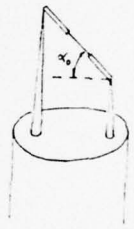


Figure 1: Sketch of R1 blowing facility at the Von Karman Institute and experimental set-up.



Slanted hot-wire

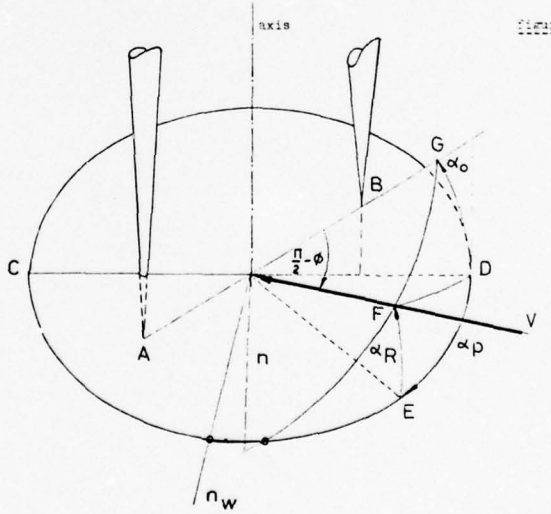


Figure (2.1)

Hot wire configuration showing hot wire sensor AB, and wire angle α_o. The velocity vector is characterized by the modulus V, the radial angle α_R and the probe angle α_p. The yaw angle is ϕ.

Figure (2.2)

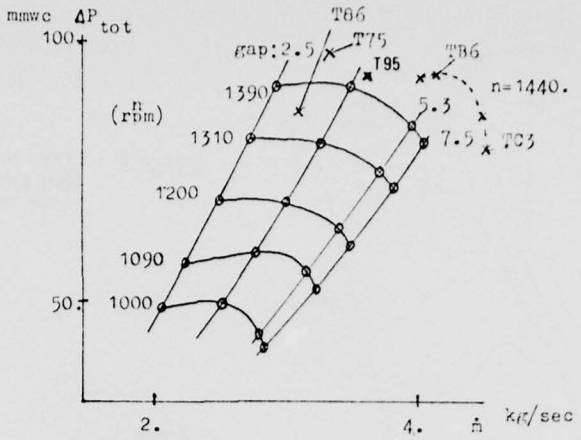


Figure 3 : Performance curves of R1 compressor.

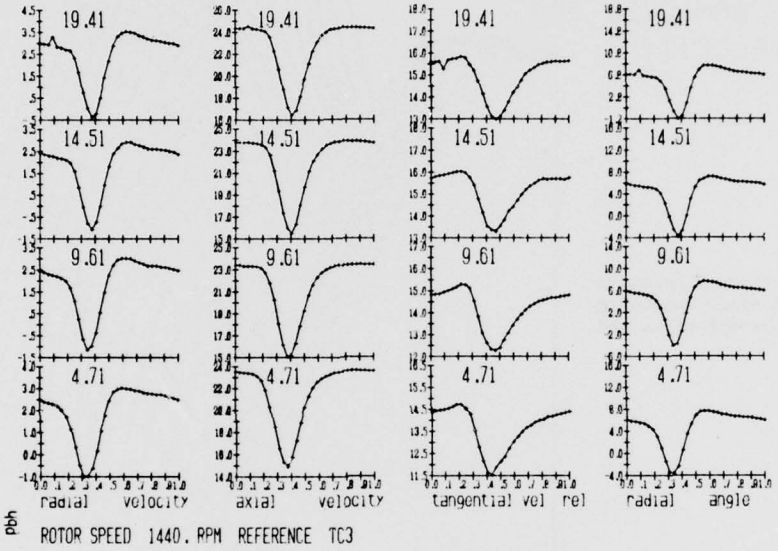


Figure 4 : Pitchwise distribution of radial, axial and tangential velocity and radial angle at 4.71, 9.61, 14.51, 19.41 % height.

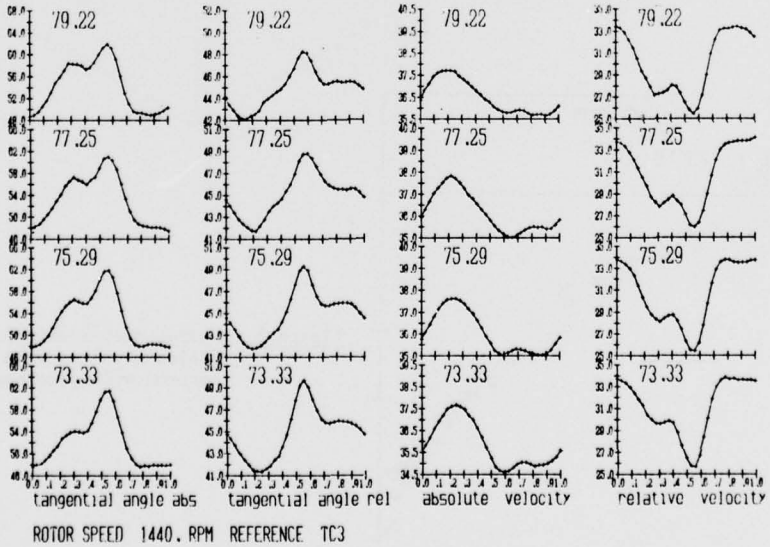
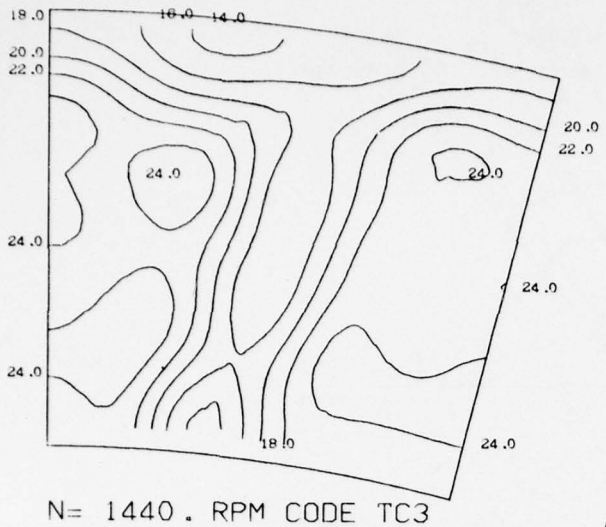
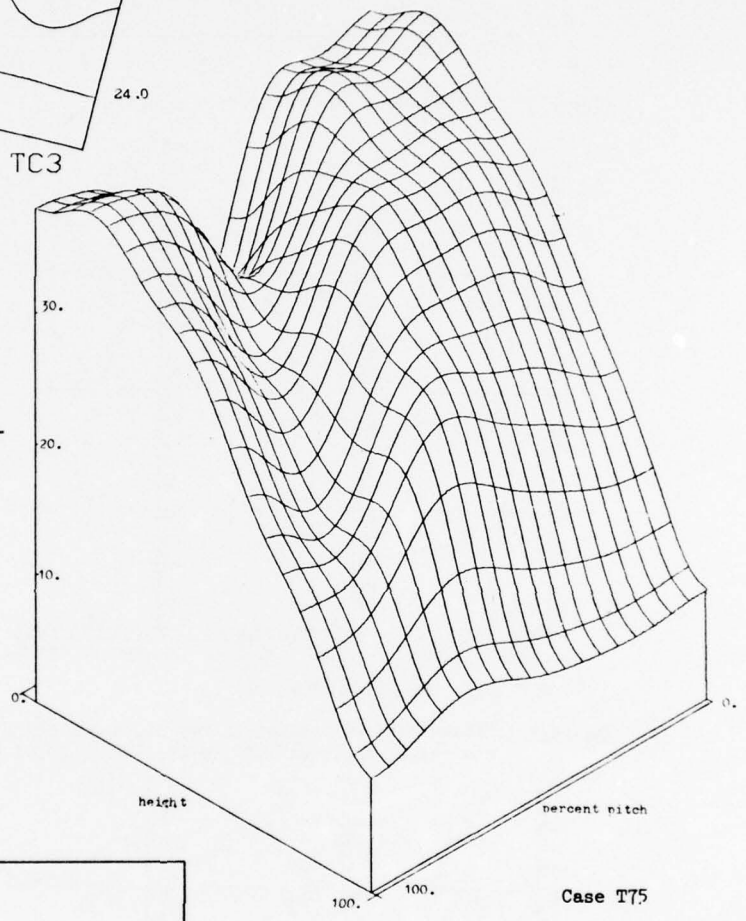


Figure 5 : Pitchwise distribution of absolute and relative flow angle and velocity at 73., 75., 77. and 79. % height from hub.



N= 1440. RPM CODE TC3
AXIAL VELOCITY

Figure 6 : Lines of constant axial velocity from hub to tip from blade-to-blade in the measuring plane.



Case T75

Figure 7 : Projection of axial velocities obtained after smoothing along lines of constant pitch and constant height.

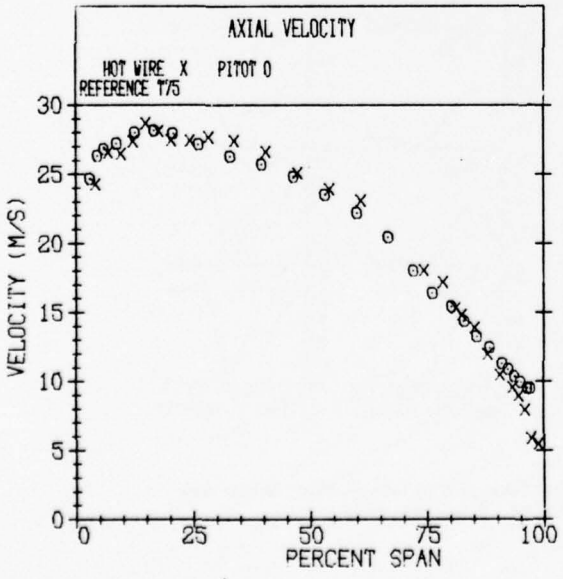


Figure 8 : Radial distribution of mean axial velocities obtained with hot-wire and comparison with pitot-results.

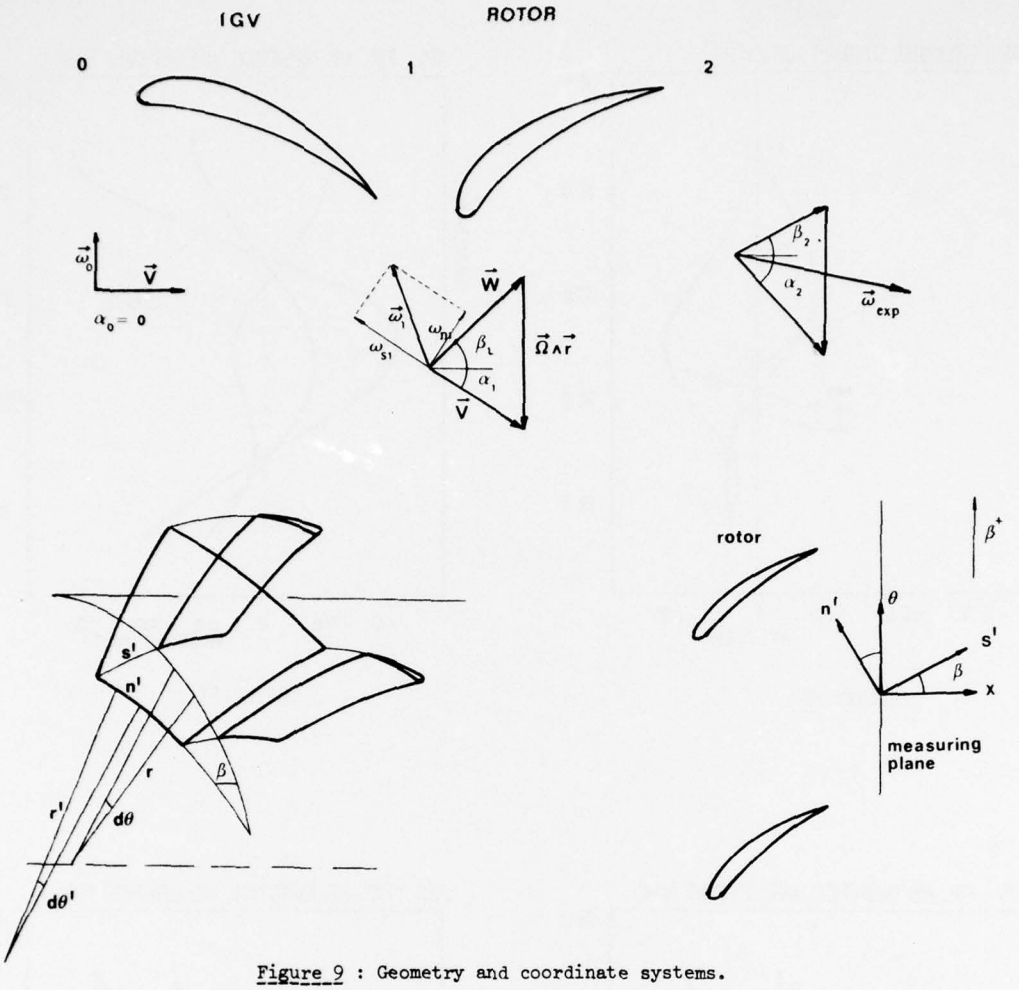


Figure 9 : Geometry and coordinate systems.

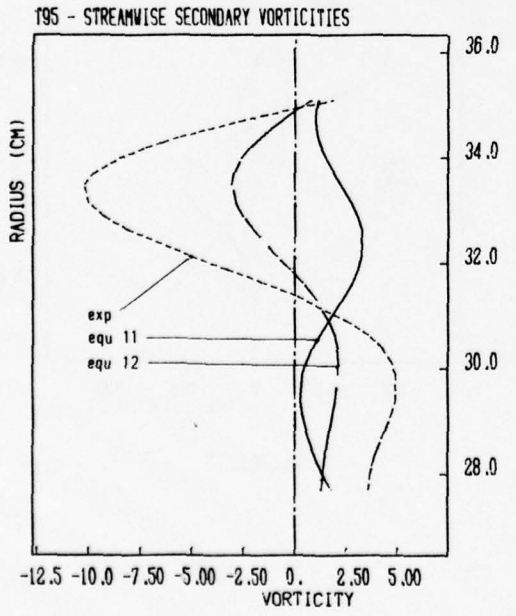


Figure 10 : Pitch-averaged vorticities.

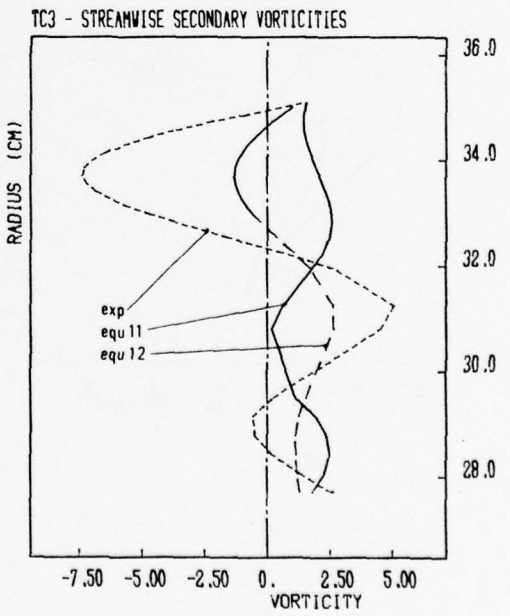


Figure 11 : Pitch-averaged vorticities.

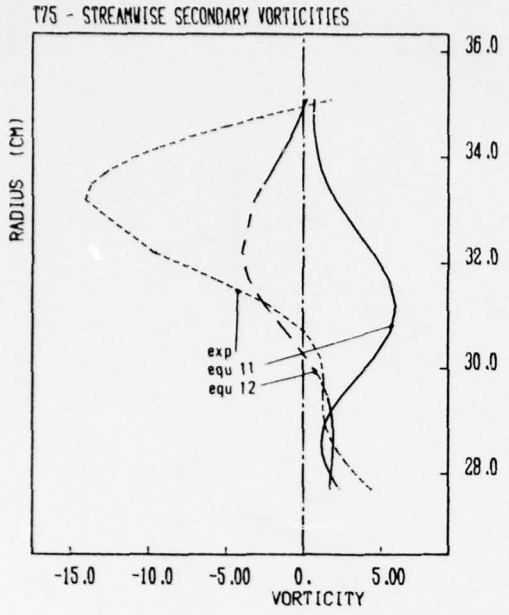


Figure 12

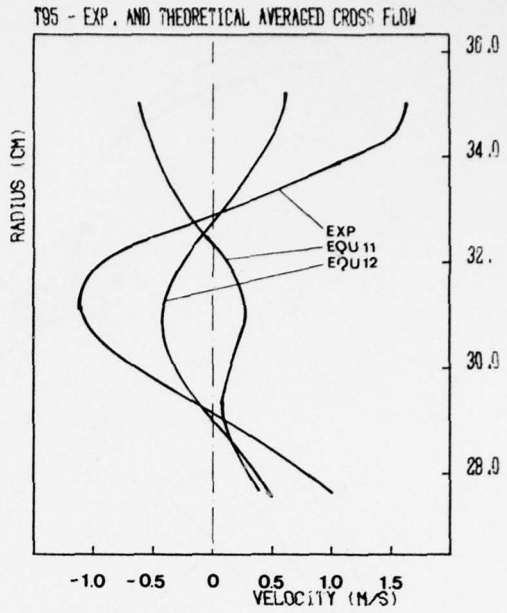


Figure 13

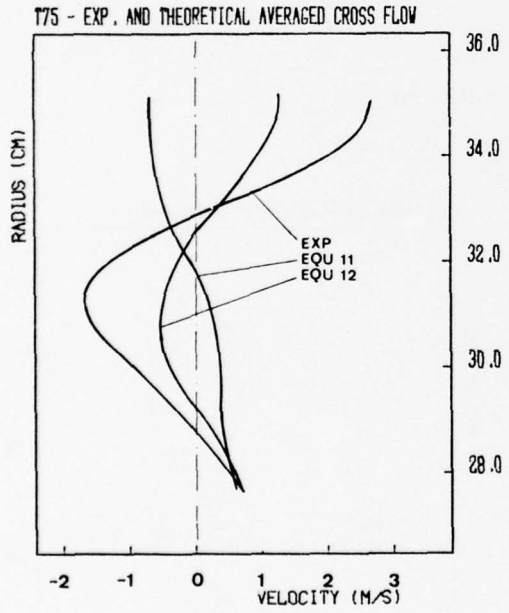


Figure 14

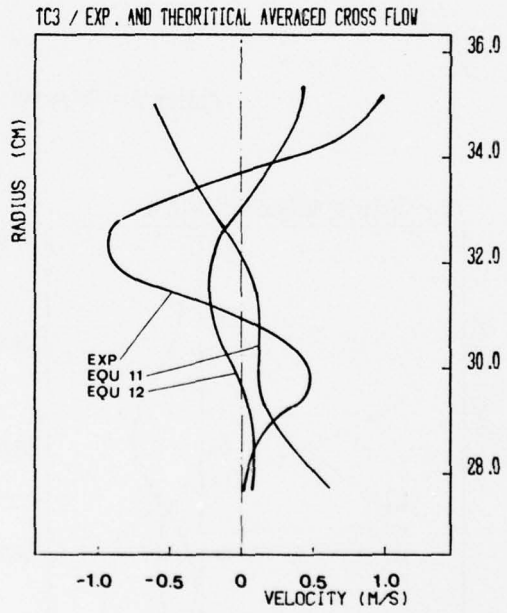


Figure 15

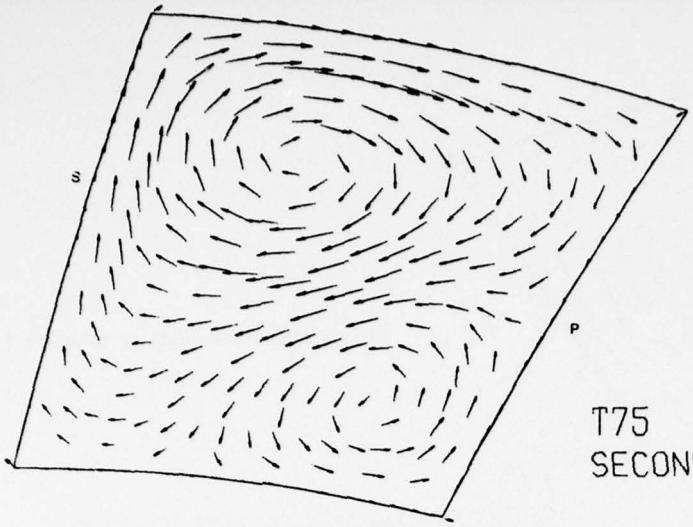


Figure 16 :

T75 EXP CASE
SECONDARY VELOCITY FIELD

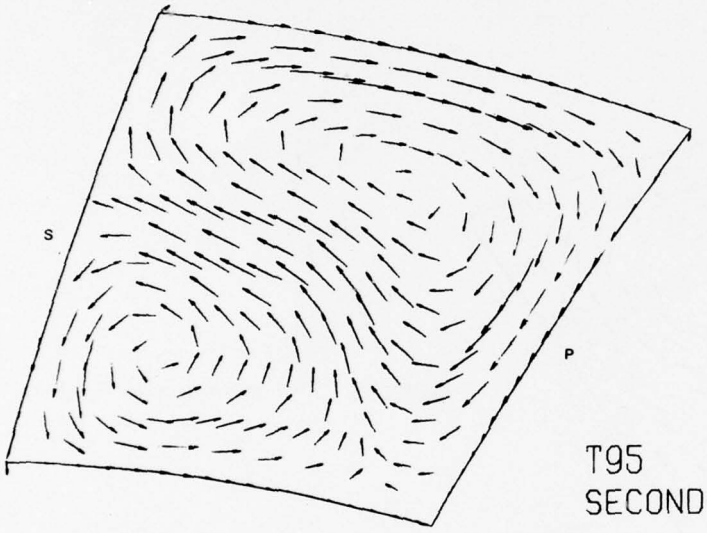


Figure 17 :

T95 EXP CASE
SECONDARY VELOCITY FIELD

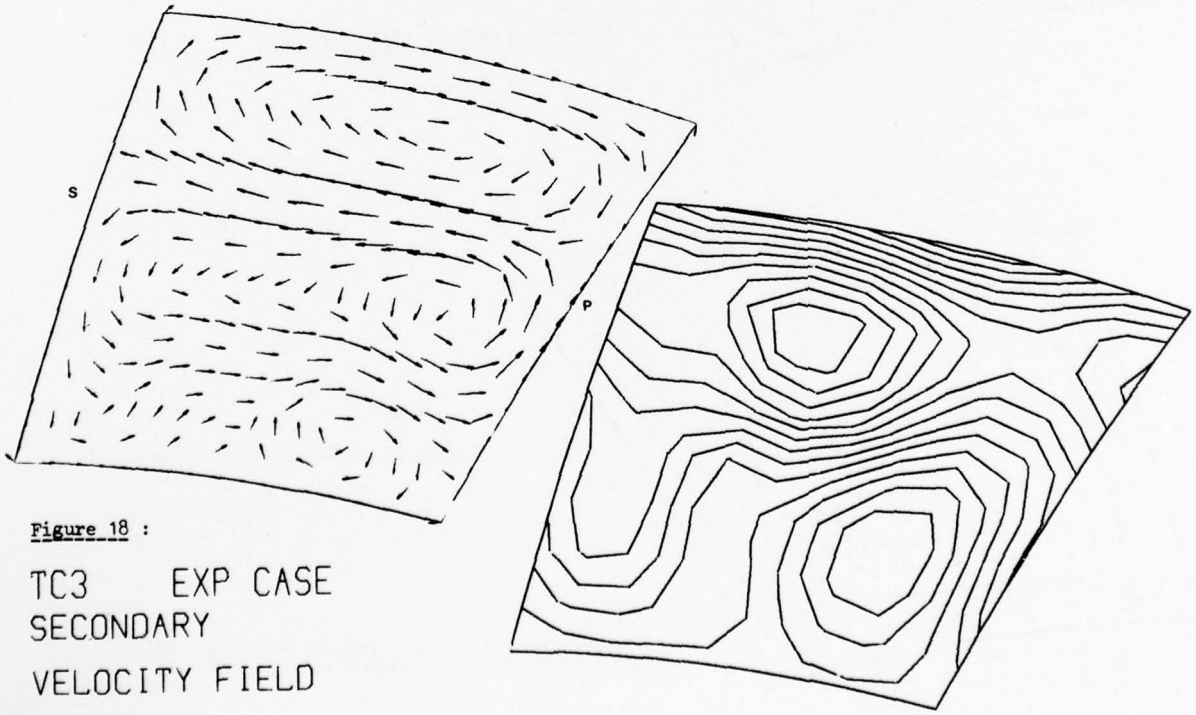


Figure 18 :

TC3 EXP CASE
SECONDARY
VELOCITY FIELD

Figure 19 : T75 EXP CASE
Contourlines of mainstream vorticity.

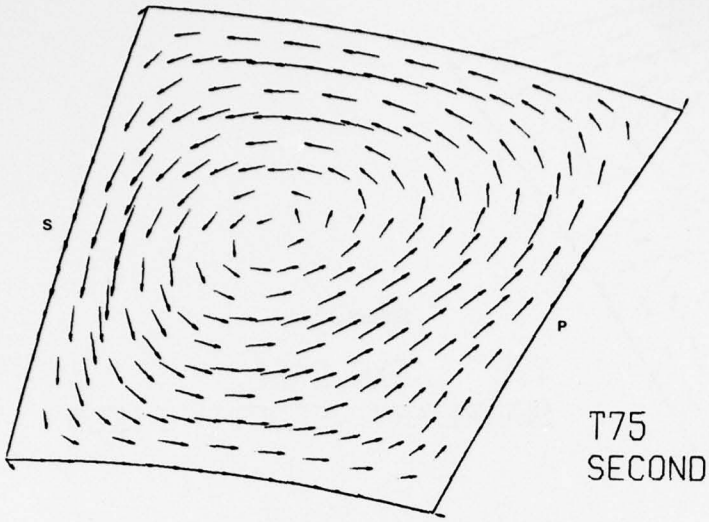


Figure 20 : Flow pattern using eq.(11).

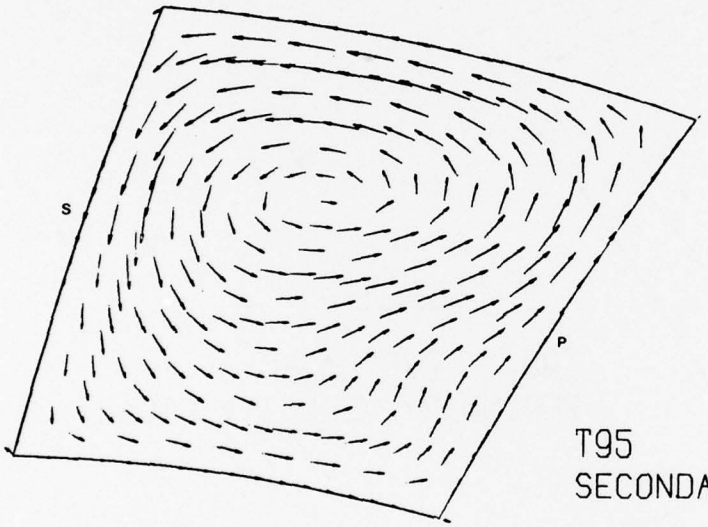


Figure 21 : Flow pattern using eq. (11).

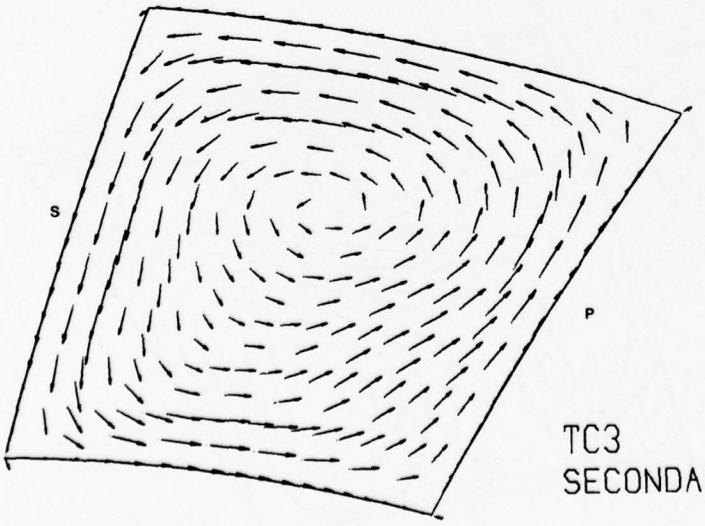


Figure 21 : Flow pattern using eq. (11).

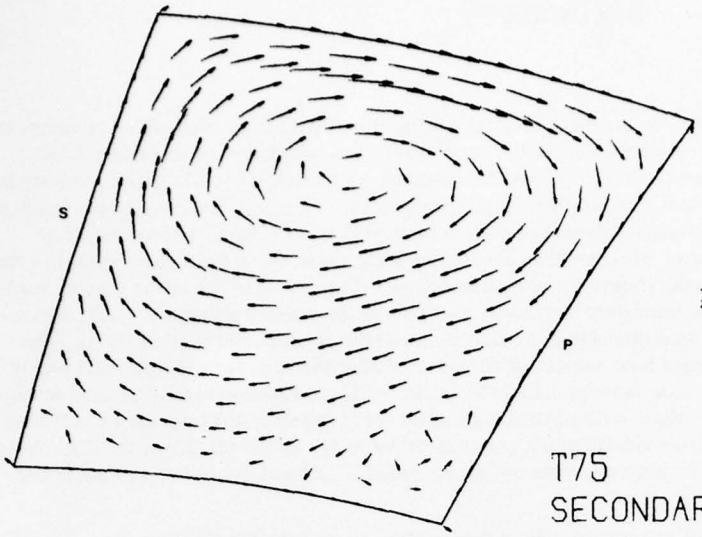


Figure 23 : Flow pattern using eq. (35).

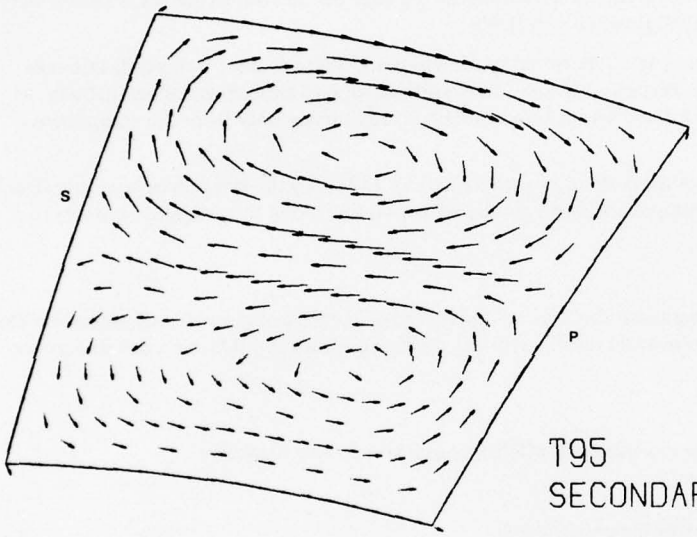


Figure 24 : Flow pattern using eq. (35).

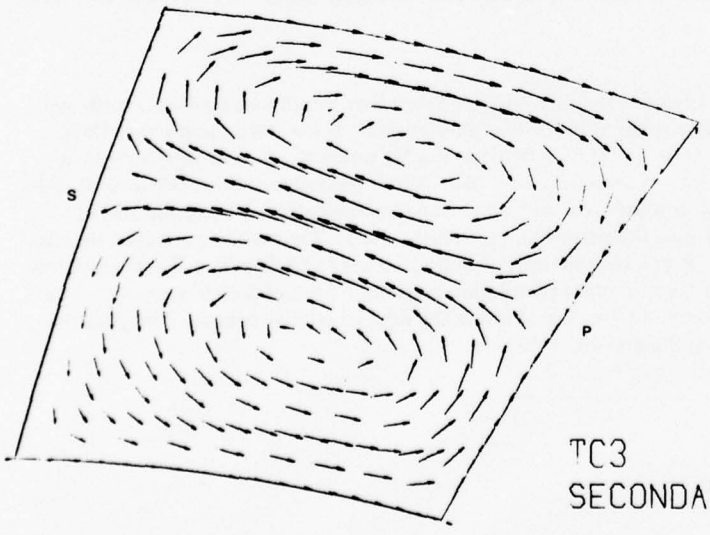


Figure 25 : Flow pattern using eq. (35).

DISCUSSION

J.W.Railly

I would like to raise the same question that Professor Horlock raised this morning, namely, that which concerns the correctness of using just the absolute vortex component in the equation for the calculation of secondary flow contours. In our paper (Railly and Howard (1962))* we used the resolved component of total relative vorticity in a similar calculation that employed the method of Smith to obtain the absolute vorticity. This procedure worried me subsequently but the problem, I think, was resolved by Smith in discussion of the case of a rotor where no (absolute) deflection of the flow takes place. This question has also been discussed by Dr Fairbairn, present in this room, in his recent Ph.D. thesis (1976) at the University of Newcastle-upon-Tyne. It is to the effect that we ought to include (for the purpose of determining secondary flow) only that part of the relative vorticity, -2Ω, which is not satisfied by the boundary conditions on either side of a blade channel (the pressure and suction sides). The short answer, I think (and Dr Fairbairn might have something to add) is that in the case, for example, of a purely axial rotor blade (e.g. the central portion of an impulse rotor) the entire -2Ω component should be used to obtain the secondary flow (in the situation where there is no upstream absolute vorticity) since the boundary conditions over the sector (hub, tip, pressure and suction sides) require zero normal velocity. In the middle of the blade height (for a large aspect ratio passage) the relative eddy velocities are purely radial, equal and opposite on pressure and suction sides.

In the case of a rotor row which consists of an array of helices representing an undeflected absolute flow, Vz, the relative flow in a radial plane (normal to the rotor axis) obviously has no eddying character. The apparent contradiction is resolved when it is realised that the boundary conditions at the edge of the sector (the blade traces) have exactly the correct angle to match the relative flow, i.e. $-\Omega r/Vz$.

In the more general case the determination of the 'relative eddy' flow is more difficult since it depends critically upon the blade shape as well as stream-wise vorticity. Under the conditions of zero (initial) absolute vorticity, as Fairbairn has shown, it is possible to deduce the contribution to relative eddy arising only from the component, -2Ω.

In conclusion, therefore, secondary flow contours should be calculated by adding to the streamwise absolute (free) vorticity a definite portion of the -2Ω component, both components pointing along the averaged (primary) relative flow direction.

H.Marsh

The calculations for the pitch averaged streamwise vorticity are based on the conventional version of secondary flow theory. Has the author compared the experimental results with the predicted values of pitch averaged streamwise vorticity?

Author's Reply

On slide No.9 the dotted line represents the experimental pitch averaged streamwise vorticity.

H.Marsh

The theory does not give good agreement with the experiments.

Author's Reply

We have here some qualitative agreement, and this effect is a strong stream blockage effect which we have not taken into account at all.

J.H.Horlock

I don't understand Professor Railly's point. I refer to the presentation which Roy Smith uses to illustrate his argument that you should use the absolute vorticity resolved in the relative direction. If you take the primary flow, which is the axisymmetric flow, the velocity is $\bar{V}$ and the vorticity is $\nabla \times \bar{V}$, which is $\bar{\omega}$. The relative flow is $\bar{V} - \bar{\Omega} \times \bar{R}$ and the relative vorticity is then $\nabla \times \bar{W}$, which is $\bar{\omega} - 2\bar{\Omega}$. That's the primary flow. We now consider a secondary perturbation of the primary flow in which you introduce a small perturbation $\bar{V}'$ and the curl of $\bar{V} + \bar{V}'$ is the original primary vorticity $(\bar{\omega})$ plus the perturbation vorticity $(\bar{\omega}')$. The relative perturbed flow is $\bar{W} + \bar{W}'$ which is equal to $\bar{V} + \bar{V}' - \bar{\Omega} \times \bar{R}$. If you take the curl of that, it comes to be $\nabla \times \bar{W} + \nabla \times \bar{V}'$, which is the relative vorticity in the primary flow plus the absolute perturbation vorticity. So that Smith argues that what you should do when you calculate the secondary relative flow is to use the original relative primary flow plus the absolute perturbation vorticity. I can't see anything wrong with this.

---

* Railly, J.W. and Howard, J.H.G., (1962), *Velocity Profile Development in Axial Flow Compressors*, J. Mech. Eng. Sci., Vol.4, p.166.

DUAL BEAM LASER ANEMOMETRY STUDY OF THE FLOW FIELD IN A TRANSONIC COMPRESSOR

by

H.B. Weyer

and

R. Dunker

DFVLR-Institut für Luftstrahlantriebe
Linder Höhe, 5 Köln 90, W.Germany

ABSTRACT

An advanced laser anemometer (L-2-F-technique) was used to study in detail the internal flow of a transonic axial flow compressor at tip Machnumbers of 0.9 and 1.4 (corresponding to 70 and 100% speed). This investigation having yielded quite complete data on the span- and gap-wise velocity profiles reveals a good survey on the real flow pattern even in the high-speed transonic rotor: detailed informations are available on the flow deceleration at subsonic and supersonic inlet velocities, on the 3-dimensional shock-waves, on transition phenomena from subsonic to supersonic flow along the blade height, on blade wakes, and flow unsteadiness.

In this paper experimental results will be submitted to discuss some primary characteristics of transonic rotor flow.

INTRODUCTION

The worldwide R and D activities on turbomachines are focused on increasing the performance capability and the economy as well as on improving the current design techniques. Both aspects of the work require intensive experimental studies to accomplish the today's experience on the real flow phenomena in turbomachines as e.g. boundary-layers, shock wave-boundary-layer interaction, secondary flows, flow unsteadiness etc. This is the only chance to establish complete flow models and to come up with new ideas to push further the performance and economy of turbomachines.

In the near past, great progress has been achieved by the development of new high-response testing techniques, which now allow the compressor flow field being analysed in great detail [1 - 5]. Primarily the noninstrusive optical velocimeters have been proved as a very useful tool to investigate the compressor's internal flow. These techniques enable us to measure the velocity vectors as well as the flow fluctuations at any point inside of a turbomachine which is accessible by laser light from outside. This is true even for the rotating blade channels [6 - 11].

The "Laser-2-Focus" velocimeter (L2F) developed at DFVLR [9 - 11], was applied to detailed flow studies in a transonic axial compressor rotor. This paper deals primarily with the results obtained to discuss some high lights of real flow pattern in transonic compressors.

TEST COMPRESSOR AND INSTRUMENTATION

The test compressor is a single-stage transonic compressor without inlet guide vanes designed for a total pressure ratio of 1.51 and a mass flow of 17.3 kg/s at a tip speed of 425 m/s. The isentropic efficiency was estimated to be about 80.5 %. The rotor inlet diameter is 400 mm, the hub tip ratio 0.5. MCA-profiles are selected for the rotor blading from hub to tip. 28 blades with a tip chord length of about 60 mm yield quite usual blade solidities between 1.34 and 2.0 for the rotor. The maximum inlet Machnumber to rotor blading reaches up to 1.37; whereas the maximum diffusion factor is estimated to be 0.53. Fig.1 demonstrates the compressor annulus geometry. Hub and outer wall are shaped to adapt the flow path to the stage pressure rise, to achieve nearly constant axial velocity over the annulus height, and to balance rotor and stator diffusion factors properly [12].

This compressor has been investigated using both conventional measuring techniques and the far advanced "Laser-Two-Focus" velocimeter. To carry out the optical measurements in the fast moving rotor blade channels the velocimeter operates stroboscopically controled by a trigger and time delay unit which also allows to shift the measuring volume stepwise from blade pressure to suction side or vise versa.

The axial and radial position of the measuring volume within the flow channel can easily be changed by moving the whole optical apparatus. The circular symbols in Fig.1 indicate the various probe volume settings on the rotor's meridional plane; each symbol thereby represents up to 15 distinct points over the circumference from blade to blade. This figure furthermore illustrates that measurements in the vicinity of the hub and casing walls can be performed.

The accuracy of the optical measurement is quite satisfying: the error of the flow velocity analysis does not exceed ±1 percent whereas the flow direction can be determined with an accuracy of ±1 deg.

EXPERIMENTAL RESULTS AND DISCUSSION

Just to introduce the compressor tested Fig.2 shows its overall performance map. The speed lines are quite typical of a single stage transonic compressor; at design speed a maximum pressure ratio of 1.65 and a maximum efficiency of 85% - based on temperature rise - are achieved. There is a slight increase in maximum efficiency from 85 to 100% speed due to long term operation at 85% speed associated with severe rotor and stator blade contamination. The tests at 100% speed were carried out with the compressor cleaned up [13].

The rotor internal flow investigation using the "Laser-Two-Focus" velocimeter has been carried out at 70 and 100% speed at mass flows corresponding to the point of maximum efficiency. Thus, all the experimental data shown in following graphs are concerned with these test conditions.

At 70% speed the relative entrance Machnumber is always subsonic along the blade span; however, in the outer blade sections small supersonic bubbles appear on the blade suction sides as it is illustrated in Fig.3 which presents the flow field at 89% blade height. Lines of constant relative Machnumber are plotted over two rotor blade channels revealing the already reasonable effect of the blade row on its upstream flow, which here enters the rotor at a mean Machnumber of 0.86. The upstream effect increases considerably when approaching sonic or even supersonic velocities because now expansion waves and shock waves start travelling upstream. However, the small supersonic flow bubble on SS with a peak Machnumber of 1.1 does not yet contribute to the static pressure rise due to its very local limitation. Smooth and steady subsonic flow turning throughout the blade element produces all the static pressure rise observed. No considerable flow separation seems to occur on the blade suction side as pointed out by the very narrow blade wake.

In order to complete this flow pattern at 89% blade height Fig.4 contains the analogous presentation of the corresponding relative flow angles defined with respect to the compressor axis. This plot demonstrates another great advantage of optical velocimetry which is of course providing useful informations on the local flow turning inside of rotor and stator blading. Again the upstream effect of the blade row becomes evident from this graph; it leads to periodic flow angle fluctuations of 3 to 4 deg which extend about one blade pitch in front of the rotor. This figure particularly reflects to the uncertainties of current incidence angle prediction methods.

A similar situation exists with the downstream air angles which also vary within 3 to 4 deg, associated with the well known problem of defining equivalent deviation angles. Within the blade channel the flow turning varies from about 7 deg at the pressure side to 10 deg at the suction side. Near the almost flat blade pressure side the 7 deg turning occurs in the blade front part due to high mean positive incidence ($\sim$ 8 deg), whereas near the suction side the turning is concentrated mainly in the rear portion of the blade with high surface camber. (The mean flow studied with the help of conventional probes turns from 70.5 deg at inlet to 59 deg at outlet with a 4 deg deviation). Summarizing the data presented in the last two figures one may conclude that no characteristic difference appears between the rotor flow pattern and the flow in equivalent two-dimensional cascades.

Increasing the speed to 100% leads to fully supersonic inlet flow at 89% blade height as illustrated in Fig.5. The entrance Machnumber is now about 1.3; an attached shock wave appears at the blade leading edge travelling upstream and interfering with expansion waves originated on the blade suction surface. As typical for low to medium back pressure an oblique shock exists within the blade channel extending from leading edge to 80% chord of adjacent blade. This shock wave contributes already considerably to the overall static pressure rise of the blade section, however - and this is the striking detail of the flow pattern - the supersonic flow is not decelerated by a normal shock as usually observed in two-dimensional cascades but by supersonic diffusion which probably results from the very smooth stream tube convergence. Downstream of Machnumber line 1 a remarkable subsonic diffusion takes place around the rear part of the blade suction side; no severe boundary layer separation happens, and thus very tight blade wakes are found behind the rotor.

Fig.6 presents the corresponding relative flow angle distribution. There is a few degree turning around the blade leading edge due to supersonic expansion, followed by a 6 deg supersonic turning along the suction side associated with an equivalent Machnumber increase. The internal oblique shock wave turns the flow another 3 to 4 deg until the subsonic diffusion ends up at 55 deg near the suction side in the rear part of the blade. The mean outlet angle is around 58.5 deg which corresponds quite well to the averaged value of 59.3 deg ($\delta \sim 4.3$ deg) taken by a conventional flow direction probe (inlet mean angle: 69 deg $\hat{=}$ i $\sim$ 6.5 deg).

The flow pattern at 45% blade height is characterized by the transition from subsonic to supersonic inlet flow, Fig.7. The Machnumber is slightly supersonic (M $\sim$ 1.05); a detached bow shock appears in the entrance portion of the blade channel having a quite large distance to the leading edge which marks considerable spilling flow at inlet. The internal normal branch of the bow shock retards the supersonic flow to subsonic state followed by a smooth subsonic diffusion. Neither shock wave impingement nor subsonic deceleration lead to noticeable boundary layer separation on the blade suction surface.

The Machnumber and air angle plots presented here more or less isolated do not reveal the evident existance of strong 3-dimensional flow effects. However there are some 3-d phenomena, for instance Machnumber decrease, pressure rise, and turning within the shock waves are not compatible with the one-dimensional theory due to stream tube convergence and flow interference on adjacent blade sections. In transonic compressors this interaction is believed to arise primarily from the 3-dimensional shock wave at rotor inlet, as illustrated in Fig.8. The entrance shock wave is shown at 45, 63, and 89% blade height with respect to the corresponding profiles at right stagger to give an idea on the complicated 3-d shock wave surface.

Inlet and outlet flow conditions, blade and cascade geometry varying over the blade

height initiate this flow pattern which obviously leads to strong radial gradients of the static pressure and to strong radial components of the flow vectors behind the shock wave. Thus the radial equilibrium of the rotor flow is more complex than predicted by today's usual theories which do not account for these flow phenomena.

Coming back to the local flow study Fig.9 illustrates the axial chordwise distribution of the relative flow angle throughout the rotor at 89% blade height and 100% speed. The curve on top represents the flow situation near the blade suction side; within the forward portion the flow vector follows quite well to the surface angle, which is really characteristic of supersonic flow. The small but constant distance of about 1 deg is probably due to an incorrect estimation of the blade untwist. From the experimental data a weak boundary layer separation may be expected to occur just upstream of the blade trailing edge.

In midchannel the whole flow turning is completed within the forward 60% of axial chord; beyond that point a slightly negative turning as in turbine operation is observed. This figure outlines a considerably stronger flow separation than really happens as describe above. (The test data are compared to camber line angle).

Near the blade pressure side again the flow vector follows quite accurately to the surface angle, although the probable untwist effect is here also evident. Some flow turning takes pla[illegible] in the rear portion of the blade and around the leading edge due to pressure sid[illegible]nce flow.

Fig.10 pr[illegible] corresponding data for 70% speed. In general an adequate flow situation is [illegible]r, higher incidence angles at inlet lead to higher turning around the le[illegible]rticularly on the blade pressure side.

The follow[illegible]l to 13 illustrate the flow pattern behind the rotor along the blade span. Th[illegible] in 100%. The plane where the test data were taken is situated about 25% of blade [illegible]ownstream of the rotor.

Fig.11 reproduces the relative Machnumber distribution over one blade channel; the geometry of the blade trailing edge is noted in the figure just for reference. The region of lower velocities extending from hub to tip identifies clearly the blade wake. Its circumferential position varies considerably along the blade span because the tangential velocity component changes with radius and because the distance between rotor outlet and measuring plane increases over the blade height. Outside the blade wake the relative Mach number grows smoothly from hub to tip; data on the velocity profiles in the Rear vicinity of the walls are not yet available because the intensive background radiation in the wall regions prevents often successful measurements with the Two-Focus velocimeter. Thus the momentary informations on corner and secondary flow as well as on gap flow effects are rather limited. However, a new fluorescent technique which is just going to be used in addition to the laser velocimeter will help to extend the measuring range very close to the wall (a few tenth of a millimeter).

Fig.12 shows the corresponding relative flow angle distribution - always with respect to compressor axis. This plot reveals the blade wake as a region of relatively high flow particularly near hub and tip; its maximum of 85 deg - not noted in the figure - is achieved at the blade tip. Outside the blade wake the flow angle increases along the blade span as the Machnumbers do (Fig.11).

Fig.13 is a perspective view to illustrate the air angle defect within the blade wake. The difference between the local angle and the mean flow direction* is plotted against the blade pitch at different blade heights. At mid span the angle defect is rather small, about ± 3 to 4 deg. But it grows up very rapidly when approaching hub or tip. Furthermore, the positive angle defect is here always dominant, which means, that the flow component from blade pressure to suction side preponderates the adverse component in the mixing process. This flow procedure agrees correctly with the pressure gradient at trailing edge. Near midspan positive and negative angle defect corresponds to each other; obviously no boundary layer separation happens associated with narrow blade wakes and small pressure drops across the wake at trailing edge. Thus, a "normal" mixing takes place characterized by equal flow components on both sides of the wake. However, in the hub sections and at blade tip more intense boundary layer separation leads to larger blade wakes and higher pressure drops across the wake. Therefore a downstream mixing is initiated which is primarily controled by a flow component from pressure to suction side.

CONCLUSIONS

The detailed investigation by means of the L2F-velocimeter here described reveals useful informations on the internal flow in a transonic axial compressor rotor at sub- and supersonic speeds.

The results obtained demonstrate the capability of the technique for experimental studies of the complex real flow pattern: The shock-wave-system within the blade row was analysed concerning its position and intensity. Effects of flow turning, of flow deceleration, and of blade wakes were recognized. It seems realistic to study also boundary layers and flow separation in the near future, although today measurements directly inside of the blade and wall boundary layers are yet difficult.

The comparison with calculated data proves the today's theoretical methods being insufficient for the appropriate analysis of the internal flow field in blade rows. More accurate methods for estimating the flow losses, for calculating the boundary layer development, and for predicting the secondary flows are needed as well as more sophisticated mathematical models of the internal compressor flow are required. Experimental investigations like this will help to prove computational techniques and to develop step by step more realistic and reliable flow models as the basis of future theoretical work.

* measured by conventional probe

List of References

[1] WEYER,H.B. "The Determination of Time-Weighted Average Pressures in Strongly Fluctuating Flows, Especially in Turbomachines," Technical Translation ESRO TT-161,1974,p.141.

[2] WEYER,H.B. HUNGENBERG,H.G. "Analysis of Unsteady Flow in a Transonic Compressor by Means of High-Response Pressure Measuring Techniques," AGARD-CP-177,1976.

[3] ECKARDT,D., "Advanced Experimental Techniques for Centrifugal Compressor Development," Presented to the AMSE Fluid Dynamics Institutes, Radial Flow Turbomachinery Course, Aug. 23.-27.,1976,p.135.

[4] HANTMAN,R.G.,et al.,"The Application of Holography to the Visualization of Shock Pattern in a Transonic Compressor," AIAA 74-637,1974.

[5] EPSTEIN,A.H., "Quantitative Density Visualization in a Transonic Compressor Rotor," PhD thesis, M.I.T., Sept.1975.

[6] WISLER,D.C., MOSSEY,P.W., "Gas Velocity Measurements Within a Compressor Rotor Passage Using the Laser Doppler Velocimeter," JOURNAL OF ENGINEERING FOR POWER, TRANS. ASME,Series A, Vol.95, Apr.1973,p.91.

[7] WALKER,D.A., WILLIAMS,M.C., HOUSE,R.D., "Intrablade Velocity Measurements in a Transonic Fan Utilizing a Laser Doppler Velocimeter," Minnesota Symp. on Laser Anemometry, University of Minnesota, Minneapolis, Oct.22-24,1975.

[8] WISLER,D.C., "Shock Wave and Flow Velocity Measurements in a High Speed Fan Rotor Using the Laser Velocimeter," ASME Paper No. 76-GT-49.

[9] SCHODL,R., "Laser Dual-Beam Method for Flow Measurements in Turbomachines," ASME Paper No.74-GT-157.

[10] WEYER,H.B., SCHODL,R., "Unsteady Flow Measurements in Turbomachines," Modern Methods of Testing Rotating Components of Turbomachines, AGARD-AG-207,1975.

[11] SCHODL,R., "On the Extension of the Range of Applicability of LDA by Means of the Laser-Dual-Focus (L2F)-Technique," LDA-Symp.1975, Technical University of Denmark,Copenhagen,Aug.25-28.1975.

[12] STRINNING,P.E., DUNKER,R.J., "Aerodynamic- and Blade-Design of a Transonic Axial Compressor Stage," (in German),DFVLR, Institute for Air Breathing Engines, Internal Report No.IB-352-75/7, 1975,p.87.

[13] WEYER,H.B., "Compressor Design and Experimental Results",

WEYER,H.B., DUNKER,R.J., Comparison between the Calculated and the Experimental Results of the Compressor Test cases in: Through-flow Calculations in Axial Turbomachinery, AGARD-CP-195,1976.

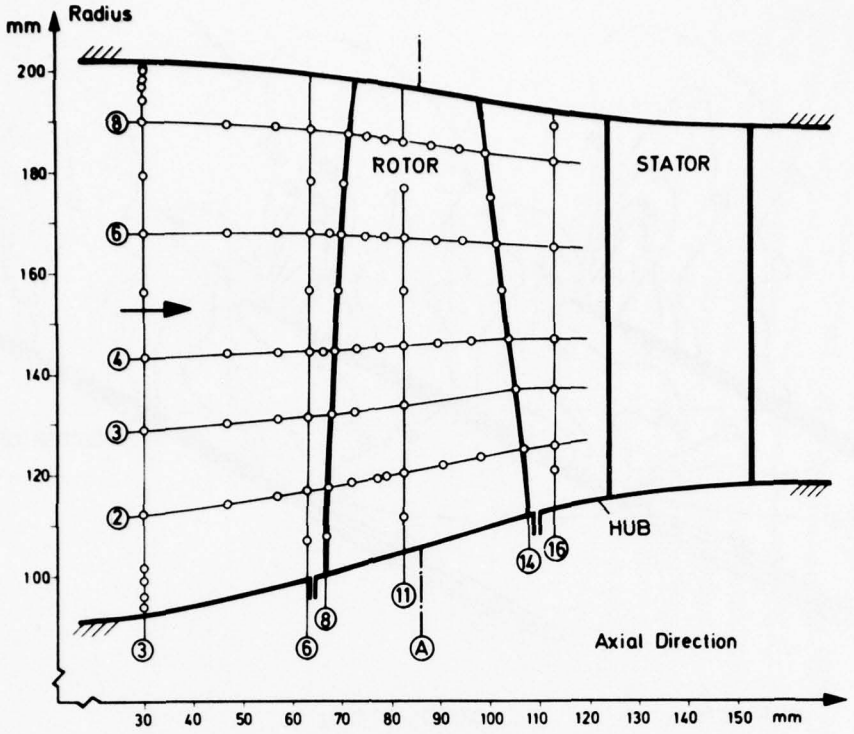


Fig. 1: Compressor annulus geometry and L-2-F measuring locii

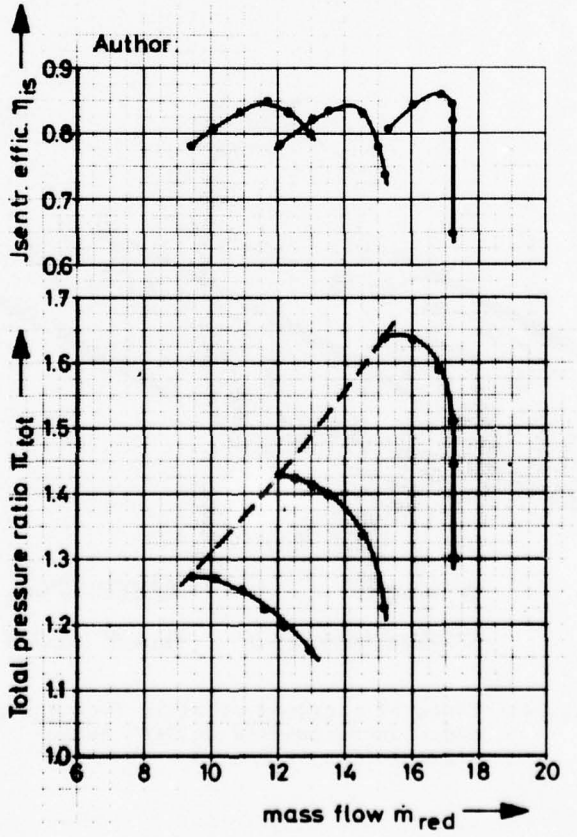
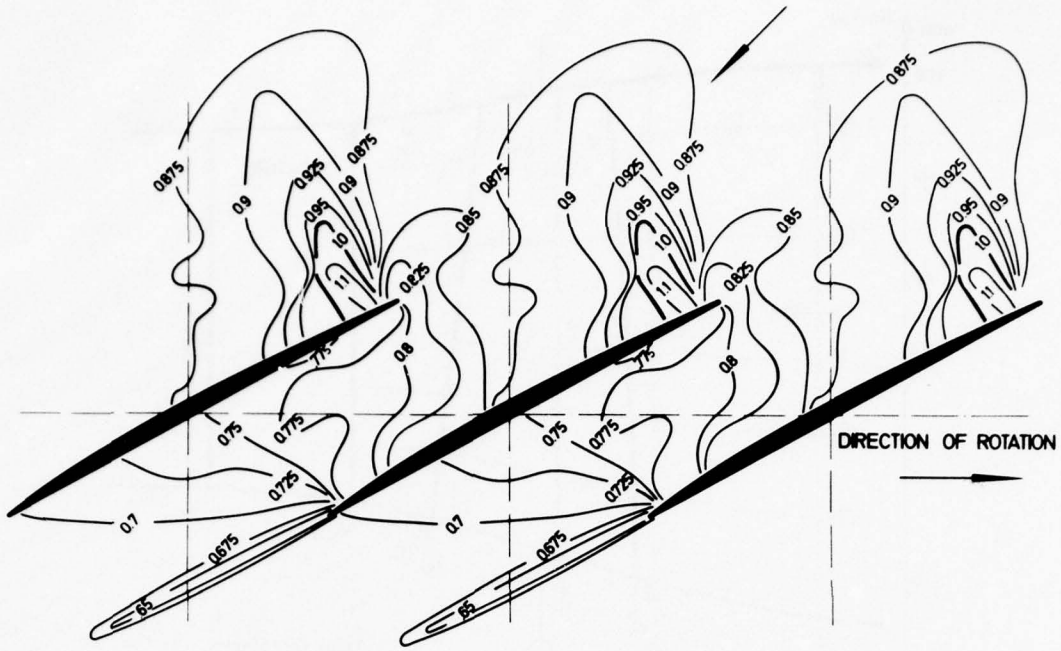


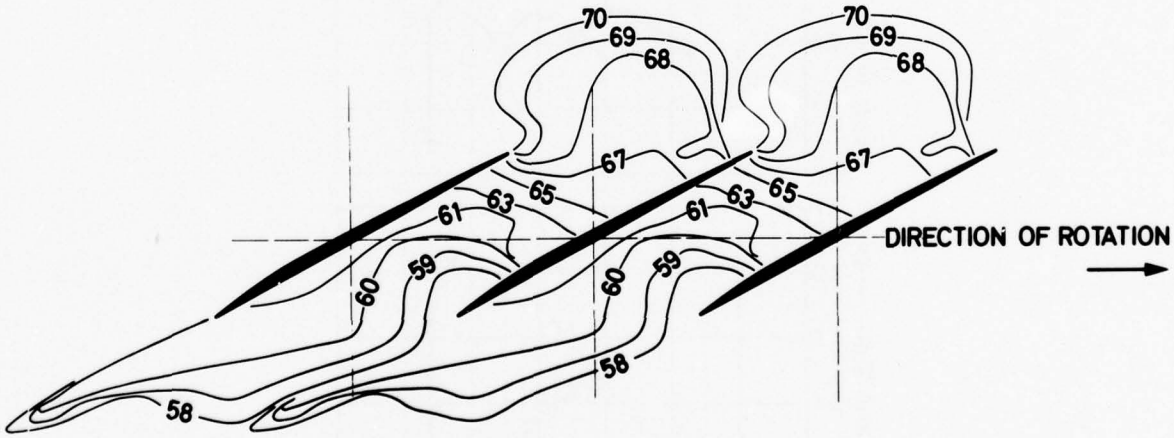
Fig. 2: Compressor overall performance



ṁ: 11.7 kg/s SPEED: 70 % n_A

STREAMSURFACE : 8 BLADE HEIGHT: 89 %

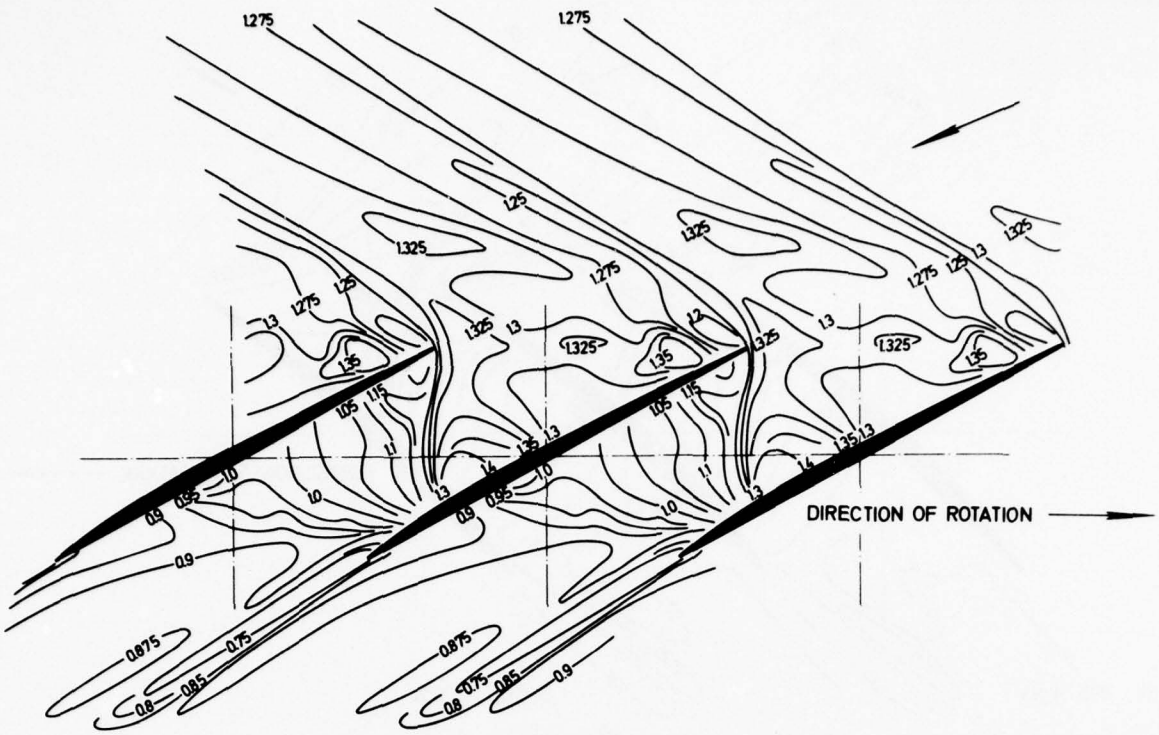
Fig. 3: Lines of constant relative Mach number on rotor blade section at 89% blade height; 70% speed, max. efficiency



ṁ: 11.7 kg/s SPEED: 70% n_A

STREAMSURFACE: 8 BLADE HEIGHT: 89%

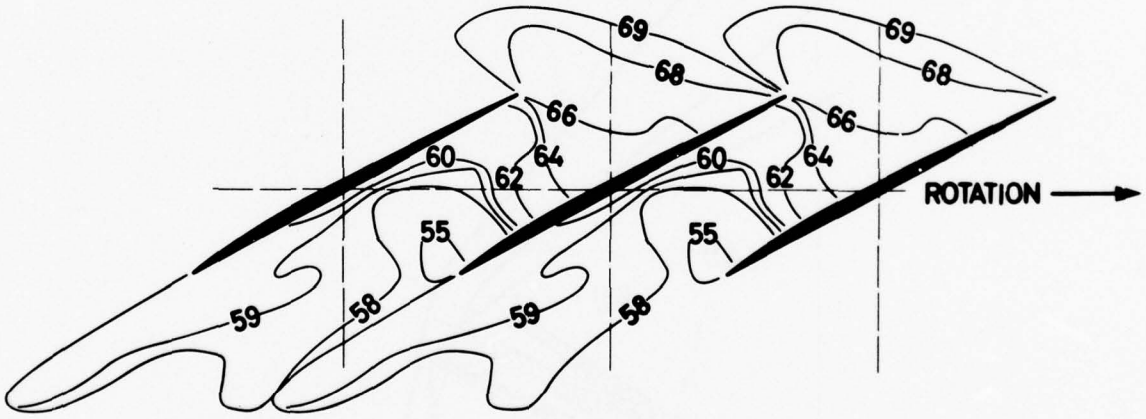
Fig. 4: Lines of constant relative flow angle, deg., corresponding to Mach number distribution in Fig. 3



ṁ : 16.8 kg/s SPEED : 100 %

STREAMSURFACE : 8 BLADE HEIGHT : 89 %

Fig. 5: Mach number distribution as in Fig. 3, however at 100% speed, max. efficiency



ṁ: 16.8kg/s SPEED: 100%n_A

STREAMSURFACE: 8 BLADE HEIGHT: 89%

Fig. 6: Relative flow angle distribution, deg., corresponding to the Mach number plot of Fig. 5

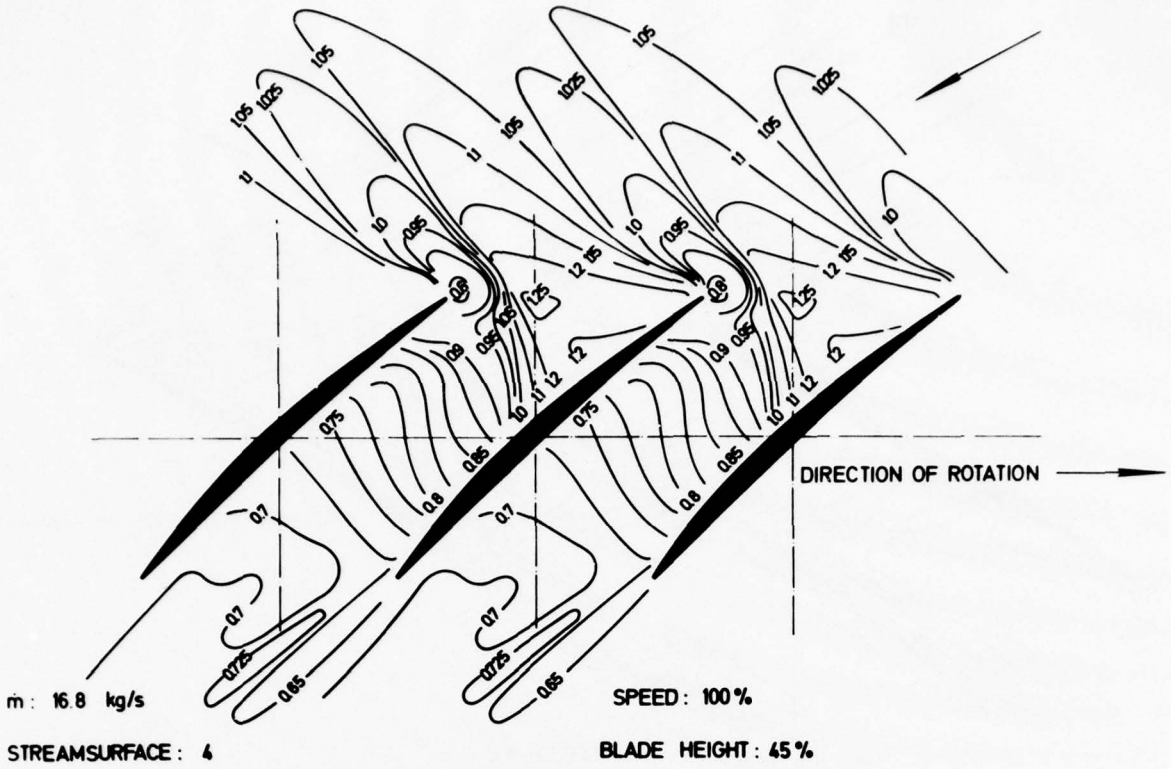


Fig. 7: Relative Mach number lines on rotor blade section at 45% blade height; 100% speed, max. efficiency

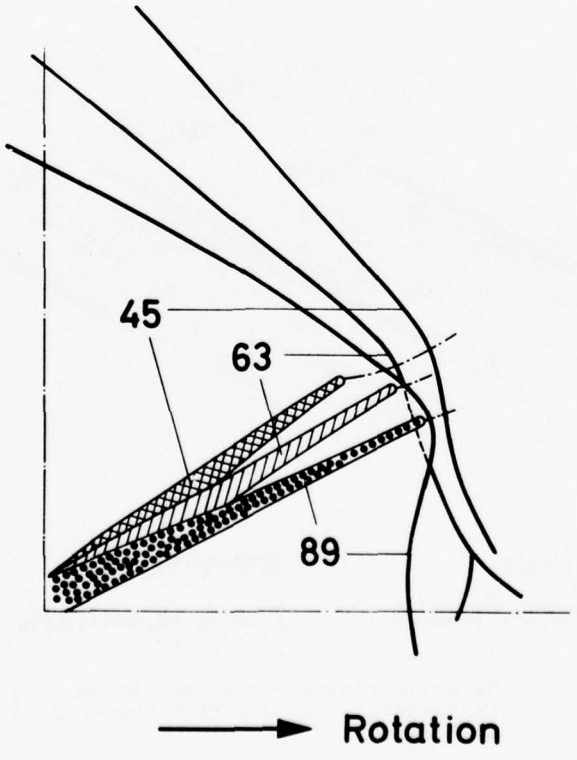


Fig. 8: Entrance shock wave at 45, 63 and 89% blade height; 100% speed, max. efficiency

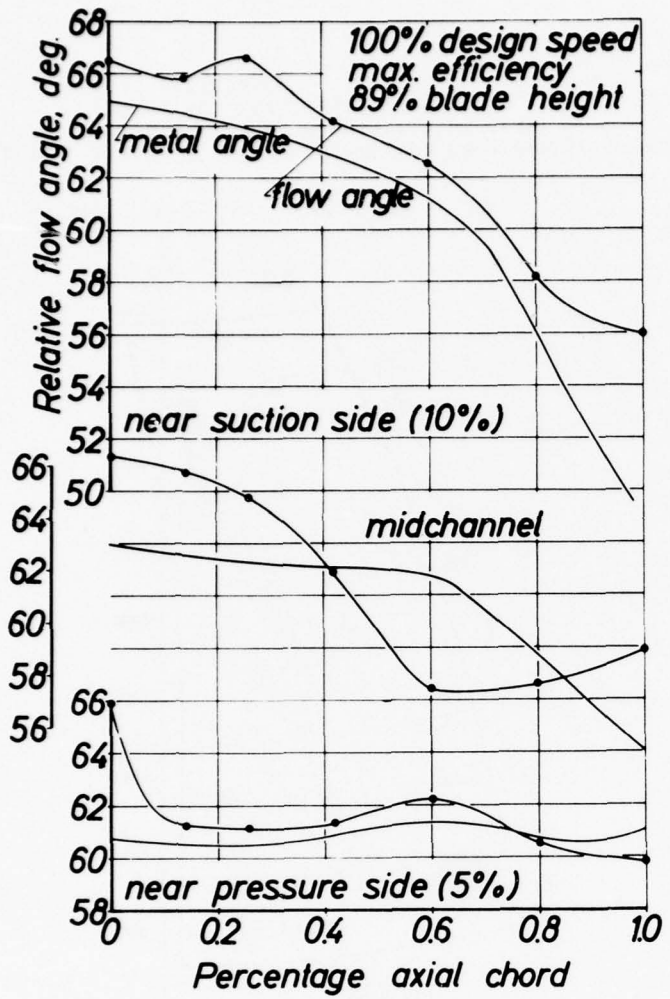


Fig. 9: Axial chordwise distribution of relative flow angle, deg., throughout the rotor at 89% blade height; 100% speed, max. efficiency

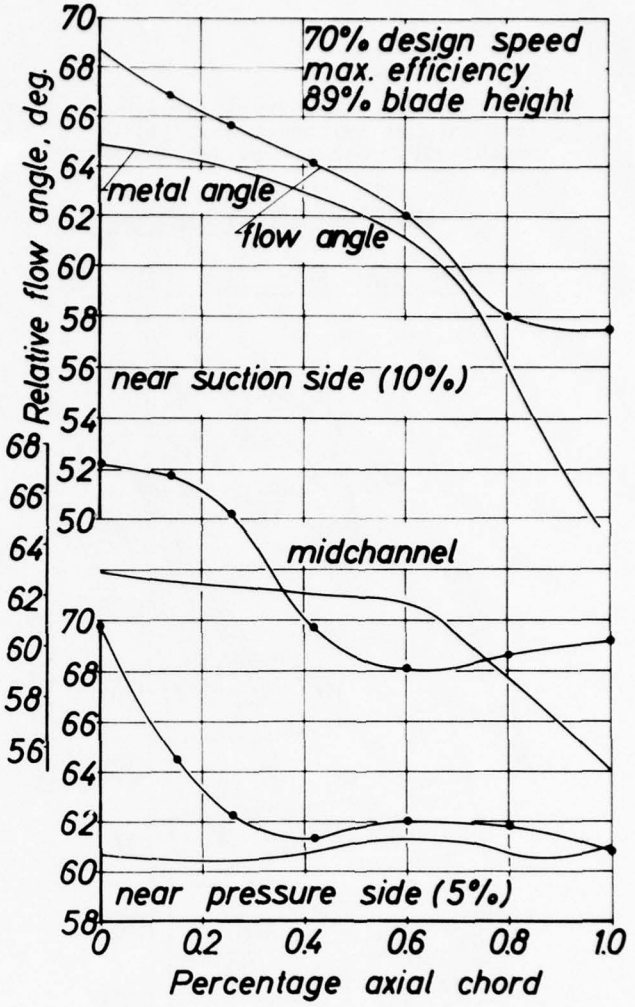


Fig.10: Cont., 70% speed, max. efficiency

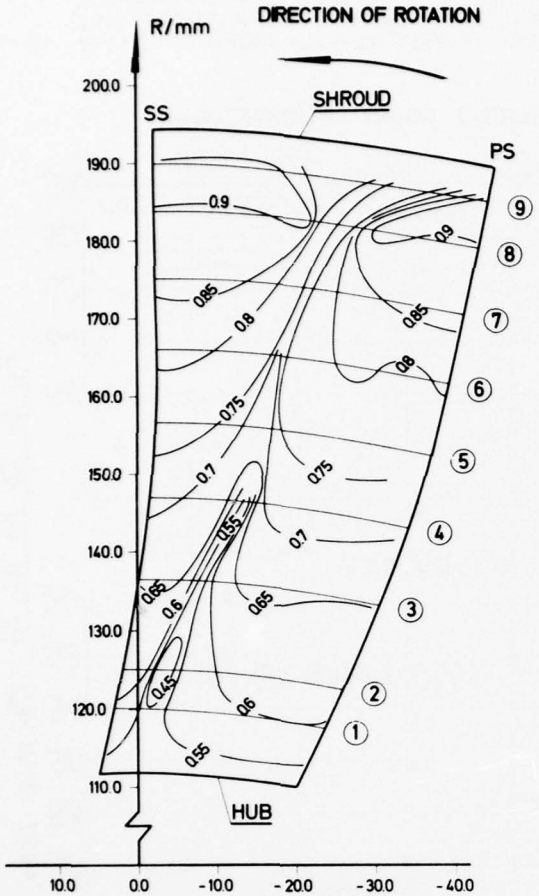


Fig.11: Lines of constant relative Mach number over 1 blade channel downstream of rotor (plane 16, Fig. 1); 100% speed, max. efficiency

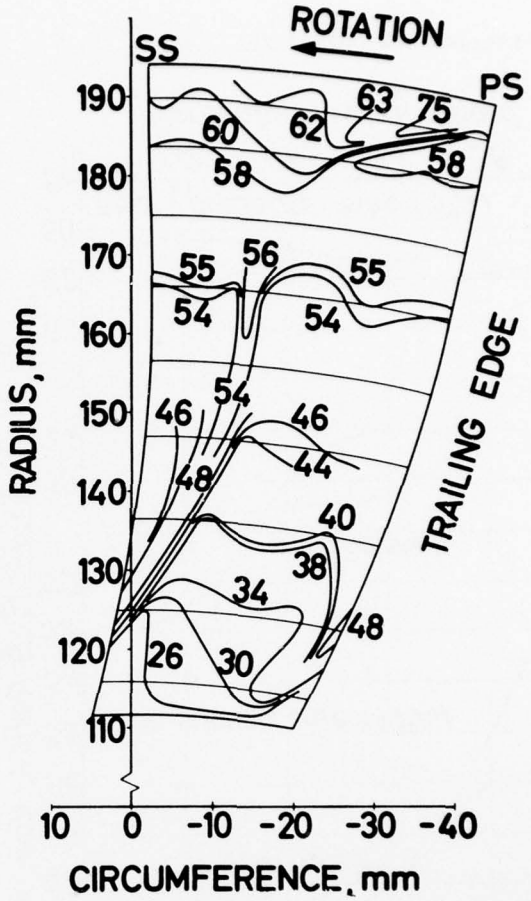


Fig.12: Relative flow angle distribution, deg., corresponding to Mach number plot of Fig. 11

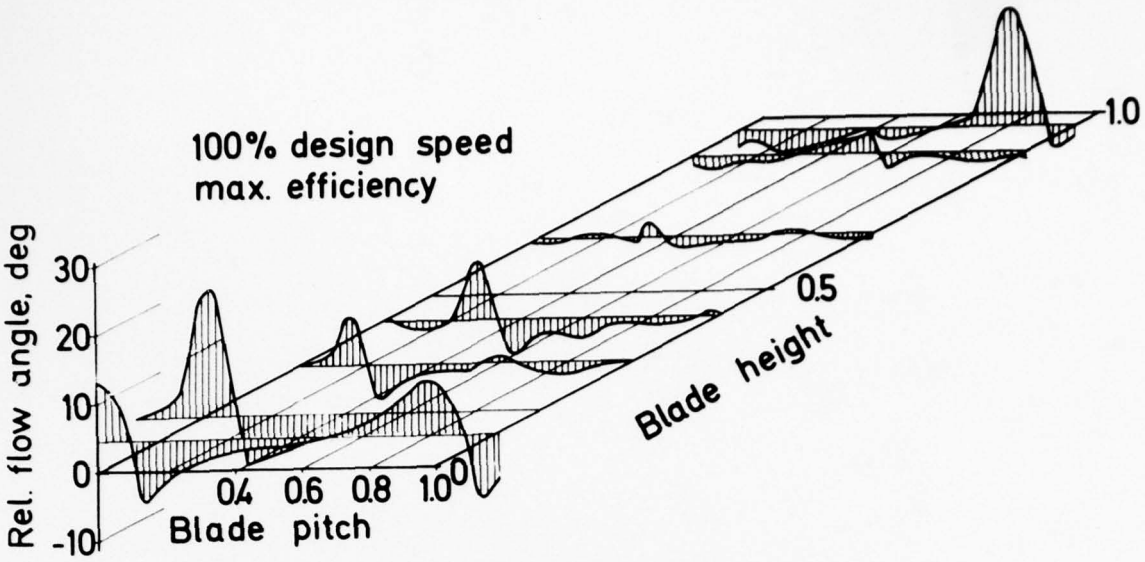


Fig.13: Perspective view of relative flow angle defect, deg., (local minus mean data) downstream of rotor (plane 16), plotted against blade span and pitch

DISCUSSION

P.Came

I would like to congratulate Dr. Weyer on an excellent set of measurements in a transonic fan. These measurements, as well as giving valuable insight into the nature of the flow in a fan rotor, could provide most useful detailed data for comparison with theoretical flow methods which are now being used in attempts to predict these mixed subsonic/supersonic flow situations. Does the written paper* contain sufficient geometric data to enable predictions of the flow to be attempted?

Author's Reply

No, due to contract restrictions detailed geometric data of the compressor are not released for publication.

J.Fabri

How close to the walls can you make your velocity measurements?

Author's Reply

With the standard L-2-F apparatus measurements are generally possible to 1.5mm close to a scattering wall, in turbomachines, however, only 2 to 3 mm could be realized primarily due to machine vibration. With the additional fluorescent techniques, distances around 0.5 mm are realistic even in turbomachines as proved experimentally in our axial compressor.

A.R.Eves

From the experimental work reported today has the author been able to make any conclusions regarding the validity in a three dimensional flow situation, of the unique incidence treatment of (say) Lichtfuss and Starken? If no conclusions have as yet been made in this respect, what does the author believe should be done experimentally to demonstrate this phenomena in a three-dimensional flow situation?

Author's Reply

Up to now we did not check for the validity of the unique incidence concept in 3-d flows, because there is not a calculation technique available accounting for the outer wall convergence starting upstream of the rotor leading edge. Thus, we are just planning to carry out wind-tunnel tests on a cascade which is equivalent to the 89% rotor blade section. These tests will be performed with the correct stream tube convergence. Comparing with the rotor data we hope to get the information of interest.

---

* Not available at time of Conference.

"SECONDARY FLOW AND LOSSES IN TURBINE CASCADES WITH INLET SKEW"

H B Carrick, M.A., Ph. D.
Imperial Chemical Industries Limited
Petrochemicals Division
Nylon Chemical Works
Wilton, Middlesbrough, Cleveland, England

SUMMARY

A skewed boundary layer was produced upstream of an impulse turbine cascade, using a moving belt. Measurements of the flow field upstream, downstream and within the cascade passage were made with pressure probes. Typical results for total pressure, velocity and static pressure are presented, and the effect of the skewed inlet boundary layer on the secondary losses and flow pattern within the cascade is discussed.

Three numerical methods were used to calculate the endwall flow field, a passage averaged boundary layer method, a three-dimensional boundary layer method for a cascade passage, and a three-dimensional inviscid method. Typical results of these methods are displayed and their advantages and disadvantages discussed.

ACKNOWLEDGEMENT

This work was carried out in the Turbomachinery laboratory, Cambridge University Engineering Department, and was supported by a contract administered by the Procurement Executive, UK Ministry of Defence. Throughout the course of the research the author was the recipient of a Post First Degree Award from ICI Ltd.

S Y M B O L S

c	blade chord
H	boundary layer shape factor
Re	Reynolds number
V_B	rotor or belt speed
V_{IN}	air velocity at inlet to cascade
Y_S	secondary loss (non-dimensionalised by $\frac{1}{2} \rho V_{IN}^2$)
α_B	measure of boundary layer skew at inlet to a blade row
α_{IN}	air angle at inlet to cascade
δ_S^*	displacement thickness
E_o	crossflow parameter
θ_{SS}	steamwise momentum thickness
ρ	density
μ	viscosity

1 INTRODUCTION

In axial flow turbines the high deflections which are imposed on the casing boundary layers, especially at rotor hubs, result in significant secondary losses. Many investigators have measured secondary losses in stationary turbine cascades and correlated these losses in terms of blade geometry, aerodynamic loading and inlet boundary layer thickness (4). One factor which is not normally reproduced in such tests is the skew which may exist in the boundary layer at inlet to the blade row.

In the case of the turbine rotor, if the annulus boundary layer is produced on a stationary hub, then this boundary layer will be skewed with respect to the mainstream at entry to the rotor. This is illustrated in figure 1 where the velocity triangles are used to construct the polar plot of the velocity within the boundary layer relative to a rotating reference frame. In turbines this skew, due to relative motion, is always in the same sense as the conventional passage secondary flow and may therefore be expected to cause an increase both in the secondary flow itself and its effects: loss, overturning within the boundary layer and midspan deviation.

In the experimental work a skewed boundary layer was produced by a moving belt upstream of an impulse turbine cascade. The effect of inlet skew due to relative motion on the secondary flow and losses of that cascade have been measured. The results are used here to illustrate the type of flow pattern and the effects of inlet skew.

For theoretical work three numerical methods were used to calculate the endwall flow field. These methods are not described here but typical results are presented for discussion in order to indicate what can be achieved with currently available calculation methods.

Details of the work are given in Carrick (3).

2 APPARATUS AND EXPERIMENTAL CONDITIONS

The apparatus used is shown in figure 4. The belt is mounted parallel with and upstream of the cascade. A steel framework supports the belt, pulleys and cascade, and the whole unit is attached to a conventional low speed cascade wind tunnel.

The cascade was that used by Armstrong (1) at an inlet air angle of 40° C., giving an incidence of -8° and a turning of approximately 79°. The principal dimensions of the cascade with a drawing of the profile are shown in figure 2.

Experiments were carried out at constant Reynolds number based on blade chord and inlet velocity $Re_c = \rho \frac{V_{IN}\, c}{\mu}$

The belt was run at a constant fraction of the inlet velocity V_{IN}.

The experimental conditions used are shown in the table.

Inlet boundary layer displacement thicknesses are shown in figure 7.

Re_c	V_B/V_{IN}	Title
4.0×10^5	0.0	ZS/HR
2.5×10^5	0.0	ZS/LR
2.5×10^5	0.5	IS/LR
2.5×10^5	0.9	HS/LR

Within the cascade measurements were taken using a five-hole and a three-hole pressure probe. Traverse stations are shown in figure 3. Static pressure was measured on the endwall and on a blade surface. Downstream of the cascade a simple shielded total pressure probe was used to measure overall losses.

3 EXPERIMENTAL RESULTS

The effect of skew on the overall performance of the cascade can be seen in figure 5 which shows the contours of total pressure defect in a plane one chord axially downstream of the trailing edge. The defect contours are deeper and further from the endwall with increasing inlet skew. This is also demonstrated in figure 6 which shows the pitch averaged total pressure defects at the same plane.

Figure 7 shows the effect of skew on the secondary loss by plotting $\frac{Y_S\ (\alpha_B)}{Y_S\ (\alpha_B = 0)}$ against B.

Y_S is defined as in Came (2), namely as the change in total pressure defect across the blade row minus the profile loss. B is defined in figure 1 and is used as a suitable measure of inlet skew.

Also plotted in figure 7 are the results of Klein (5) for an annular turbine nozzle row. The skewed inlet boundary layer has a substantial effect in increasing secondary loss.

The measurements within the endwall region of the cascade passage were used to study the flow pattern in greater detail. Velocity vectors were processed on the computer for display on a cathode ray tube and then photographed. Overall views of these vectors are shown in figures 8a-8d. One advantage of this type of display is the facility of resolving the velocity components along any given direction without additional computation. Figure 9 shows the velocity vectors in a place just upstream of the trailing edge, viewed by looking upstream along the mid-pitch mainstream velocity. This reveals approximate secondary velocities. The suction side of the passage is on the right and the magnitude of these "secondary" velocities should be compared with the inlet freestream velocity indicated underneath.

The total pressure contours for the same plane, both with and without inlet skew, are shown in figure 10 (a + b). Additional contours within the passage are shown in figures 15-18. Profiles of static pressure on the suction surface of the blade, figure 11, clearly show the influence of the low total pressure fluid which passes onto the blade surface and moves away from the endwall. This fluid is passing through a region of large adverse pressure gradient from the suction peak on the blade to the trailing edge, but in fact diffuses more slowly than the surrounding fluid.

4 ANNULUS WALL BOUNDARY LAYER THEORY

This theory, which is based on the pitch-averaged equations of motion, is aimed at predicting the development of the average boundary layer parameters along the mean streamline in a turbomachine. The pitch averaging process, coupled with the use of momentum integral techniques for the boundary layer, simplifies the calculation procedures and makes the results compatible with the commonly available axisymmetric models of the mainstream flow. The main problem rests with the terms in the equations which simulate the actual non-axisymmetric flow.

Secondary flow theory was used by Lindsay (6) to develop expressions for these terms. He used this method to obtain satisfactory agreement with experimental results in cascades of low deflection. Lindsay's method was revised by the present author to include the effects of inlet skew in these non-axisymmetric terms. However, none of these terms, when tested against the experimental results of this higher turning cascade, would give a reasonable prediction. The conclusion reached was that in its present form the pitch-averaged boundary layer approach is inadequate for the high turning blade row, with or without inlet skew.

5 THREE-DIMENSIONAL BOUNDARY LAYER METHOD FOR A SINGLE PASSAGE

A three-dimensional boundary layer calculation was attempted, based on the momentum integral method of P D Smith (8) for compressible aerodynamic boundary layers. The unknowns are θ_{ss} the streamwise momentum thickness, H the streamwise shape factor, and E_o the crossflow parameter. Once the boundary conditions are prescribed, the solution can proceed by numerical integration over an arbitrary non-orthogonal grid.

One boundary is that with the freestream, and Dr D J Smith kindly provided the results of his computer programme (7) for the two-dimensional freestream velocity in the experimental cascade.

The boundary layer method was modified to allow the calculation of a periodic (cascade) solution upstream of the blade row, and secondary flow effects were also incorporated in a simple way by modifying the freestream input to the calculation.

Typical results are shown in figures 12-14 compared with the experimental results of the ZS/HR case. The upstream perodicity is quite successfully predicted. The wave in the calculated results (figure 14) appears in a more subdued form in the experimental results for the crossflow displacement thickness (figure 14).

It was found that for mathematical reasons values of the variables θ_{ss}, H, E_o had to be provided on the high pressure side of the passage. This input has a significant effect on the calculated results within the passage and experimental results were used to obtain these boundary values. This represents a major limitation on the predictive ability of the method.

The comparison between theory and experiment was less satisfactory for the experiments with skew. This was partly because the boundary layer was thicker and partly because the disturbance of the freestream was greater with the stronger secondary flow.

6 THREE-DIMENSIONAL INVISCID THEORY

The basic method used was described by Stuart and Hetherington (10) and by Stuart (9) and is a fully three-dimensional method which is not subject to any order of magnitude limitations. The method is capable of treating arbitrary cascade geometries but this generality is made possible principally by the inviscid flow assumption.

In a manner analogous with two dimensional streamline curvature methods, the set of equations (1 continuity, 3 momentum) is replaced by the set (1 continuity, 2 momentum, 1 Bernoulli) and the anomalous variable pressure is eliminated. The solution is obtained by iterating between two solutions for one major velocity component which come from the two momentum equations. The total pressure is obtained by tracing the calculated streamlines back to the initial plane.

The limitations of the method are associated with the loss model and the resolution which is practical on existing computers. For a grid of 9 x 8 x 19 the computer storage requirement was 180 k-bytes and a time per iteration of 3.5 seconds on an IBM 370/165 was achieved. The number of iterations required for good convergence may be 60 - 100, after a number of trial runs to determine suitable choices for the two principal numerical convergence factors.

The assumption of inviscid flow was relaxed by the present author through the inclusion of a simple loss model. This altered the total pressure along a streamline in a manner matched to the gradient of turbulent kinetic energy (Q). In order to allow the calculation to proceed without great additional complication, the turbulent kinetic energy was calculated from a simple conservative equation $\frac{DQ}{Dt} = 0$

The results of calculations for the HS/LR case are compared with experiment in figures 15-18. The flow pattern and position of the total pressure contours are predicted quite well within the blade row.

7 CONCLUSIONS

One objective of the experimental work was to establish the effect of boundary layer skew without the radial pressure gradients present in annular cascades. For this reason the skew was produced by a moving belt in one wall of a conventional cascade wind tunnel. The measurements of overall losses show a considerable increase in secondary loss with inlet skew. The present results are compared with those of Klein in figure 7. It appears that the impulse turbine cascade used in the present work is more sensitive than the annular nozzle cascade tested by Klein, however the trends are very similar.

In addition to the measurement of overall secondary loss with varying inlet skew, the end-wall flow pattern was investigated by taking measurements within a blade passage. These detailed measurements have shown that the secondary flow (for the particular inlet boundary layer thicknesses used) is of the same order as the primary (inlet) flow and is intensified by the inlet skew. This is shown by the velocities and by the total pressure contours which are highly distorted, especially near the wall. This distortion occurs nearer the inlet of the cascade with inlet skew. The strong distortion rules out analytical calculations of the flow and makes numerical methods essential. The static pressure was found to be substantially constant through the endwall boundary layer except in the suction side corner. This observation supports the use of boundary layer analysis. However the corner region becomes larger with inlet skew and the application of a boundary layer analysis is more doubtful at high inlet skews.

Boundary layer analyses are permissible provided the inlet boundary layer is thin, perhaps for δ^*/blade spacing < 0.05. Where the inlet boundary layer is thick or there is high inlet skew, the other calculation which was attempted was the three-dimensional inviscid procedure. This is a very powerful tool and it is evident that good qualitative comparisons can be obtained with an inviscid model. However the development of improved representations of the effects of viscosity and turbulence are necessary, at least for the end-wall problem, if quantitative comparisons are to be obtained.

REFERENCES

1 ARMSTRONG W D : "The non-uniform flow of air through cascades of turbine blades" - Ph. D. thesis, Cambridge (1954).

2 CAME P M : "Secondary loss measurements in a cascade of turbine blades" - Inst. of Mechanical Engineers, Conference Publication 3 (1973).

3 CARRICK H B : "Secondary flow and losses in turbine cascades with inlet skew" - Ph. D. thesis, Cambridge (1975).

4 DUNHAM J : "A review of cascade data and secondary loss in turbines" - Jnl Mech. Engg Sci. 12, 1, 48 (1970).

5 KLEIN A : "Investigation of the effect of the entry boundary layer on the secondary flows in blading of axial flow turbines" - BHRA Translation 1004 (1969).

6 LINDSAY W L : "Tip clearance effects in the growth of annulus wall boundary layers in turbomachines" - Ph. D. thesis, Cambridge (1974).

7 SMITH D J : "Calculation for the flow past turbomachine blades" - Proc. Inst. of Mechanical Engineers, 184, Pt 3G (1970).

8 SMITH P D : "An integral prediction method for three-dimensional compressible turbulent boundary layers" - ARC R&M 3739 (1974).

9 STUART A R : "A numerical solution of the three-dimensional problem of internal aerodynamics" - Ph. D. thesis, Univ. of Aston (1970).

10 STUART A R and HETHERINGTON R : "A solution of the three variable duct flow equations" - Proceedings of a Conference at Penn State 1971, NASA SP 304 (1974).

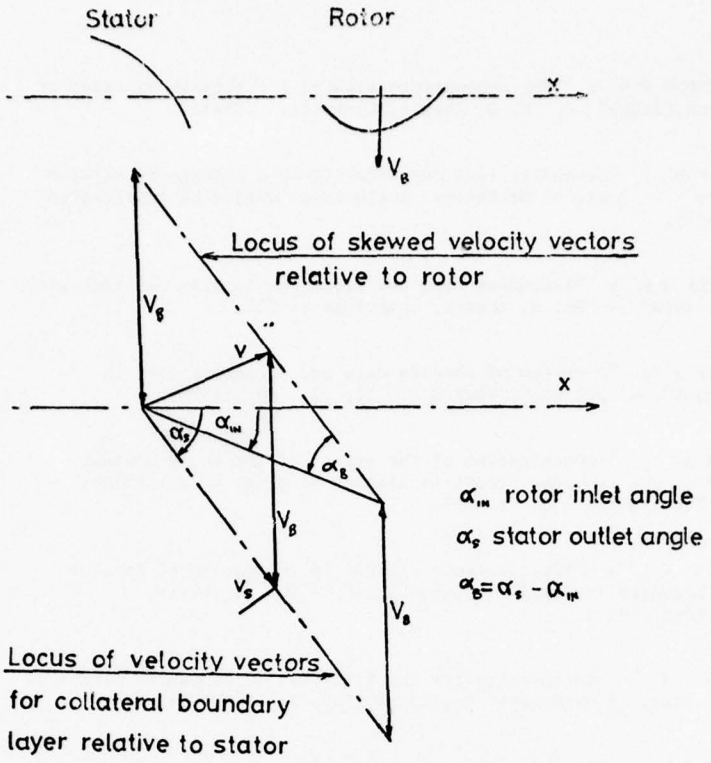


Fig.1 Polar plot for boundary layer at inlet to rotor

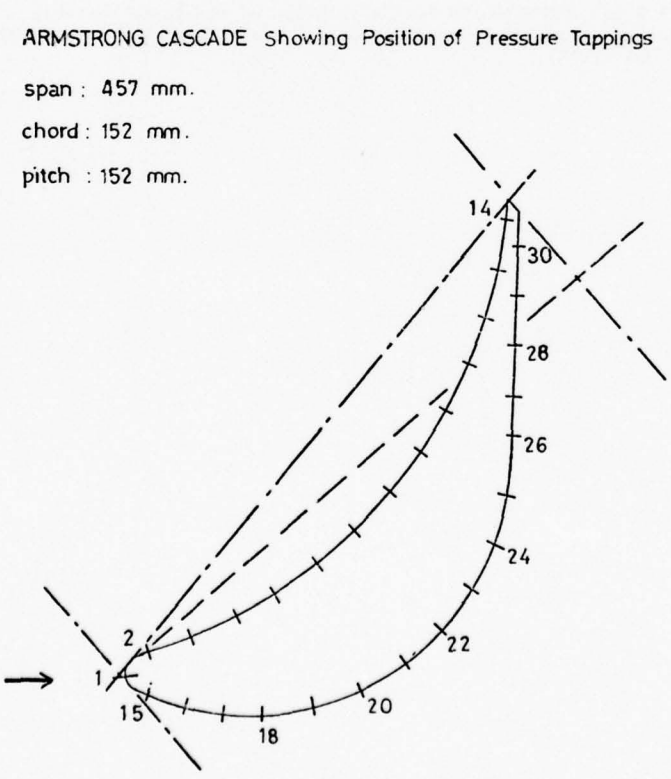


Figure 2

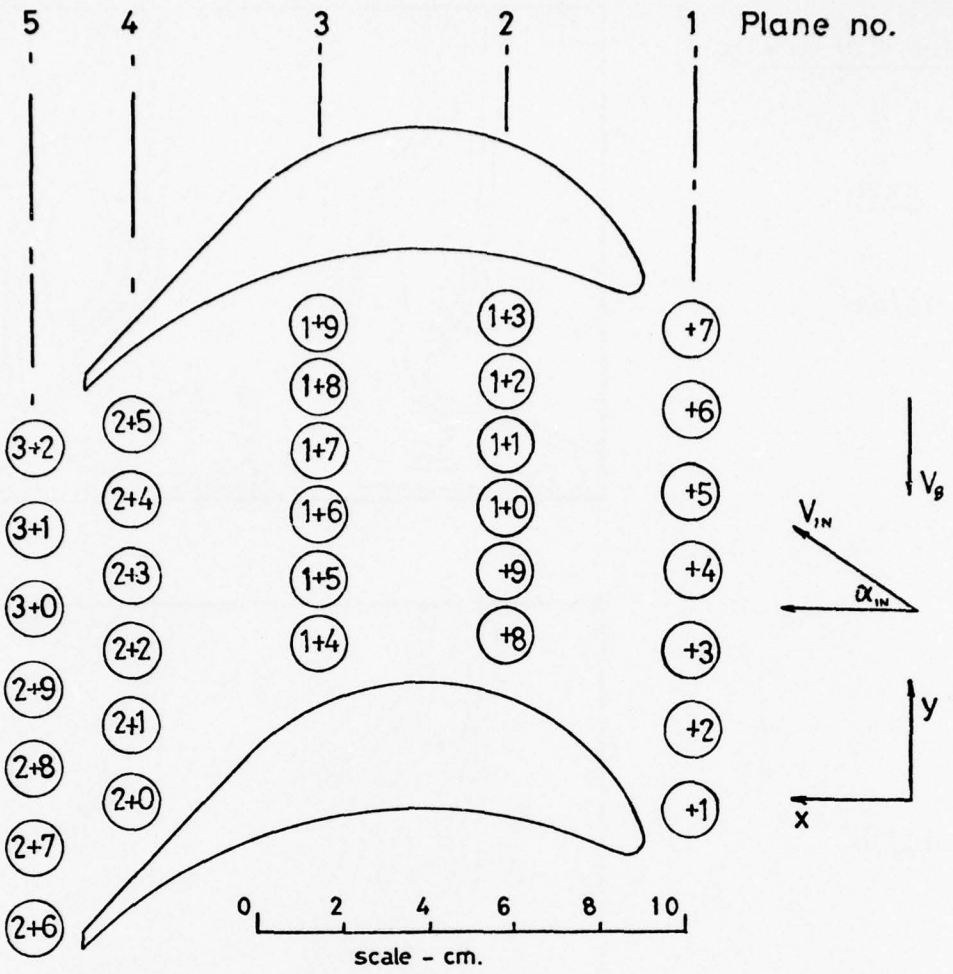


Fig.3 Traverse positions

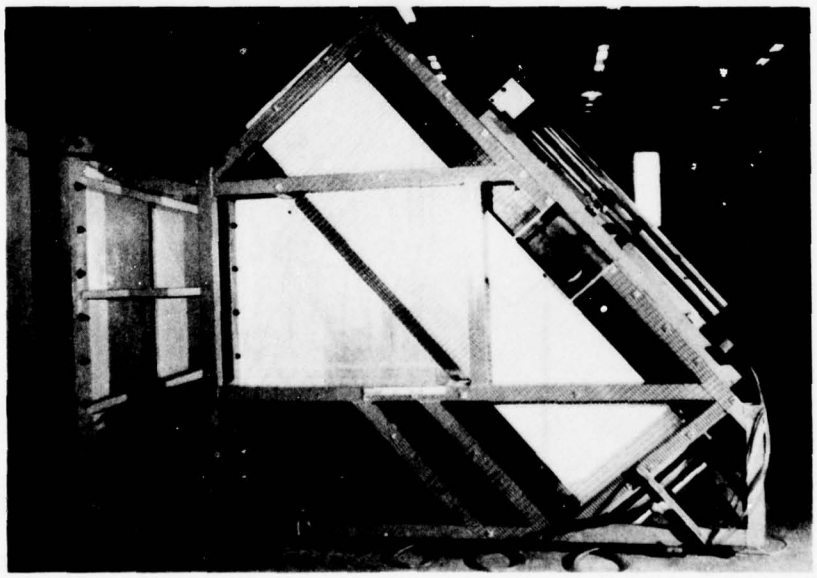
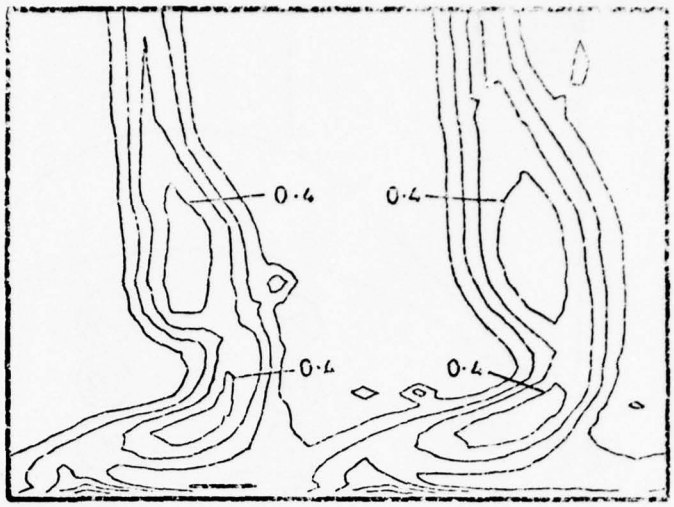


Fig.4 Plate 1 – Experimental apparatus

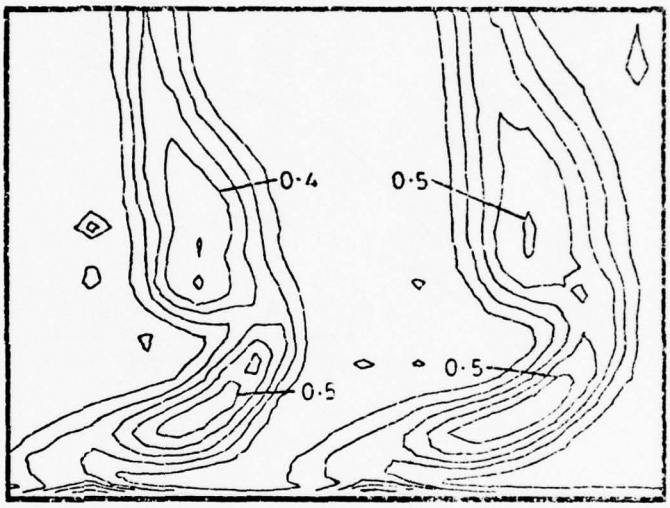
Contours at $0.1 \times Q_{IN}$

EXPT.

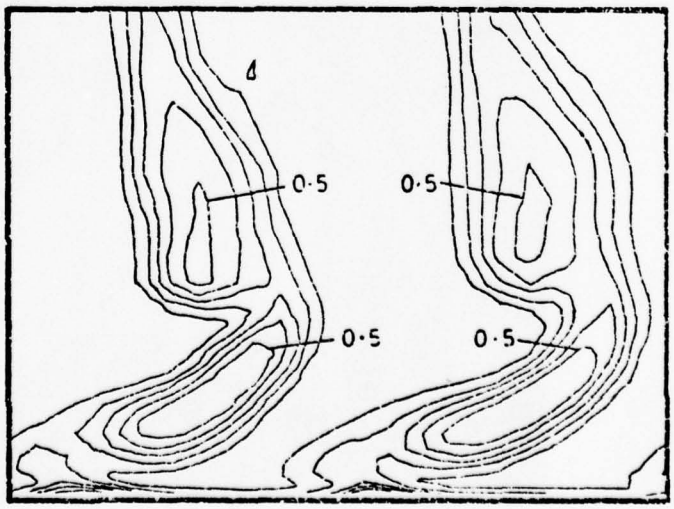
ZS/LR



IS/LR



HS/LR



P_o DEFECT, 1 CHORD DOWNSTREAM of T.E.

Figure 5

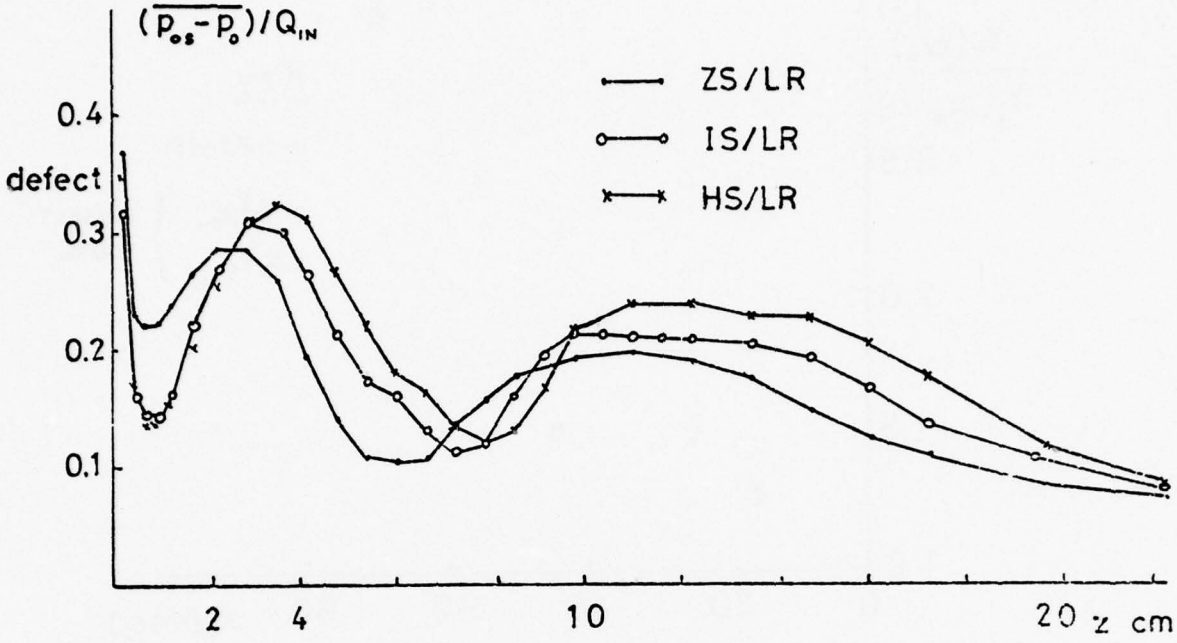
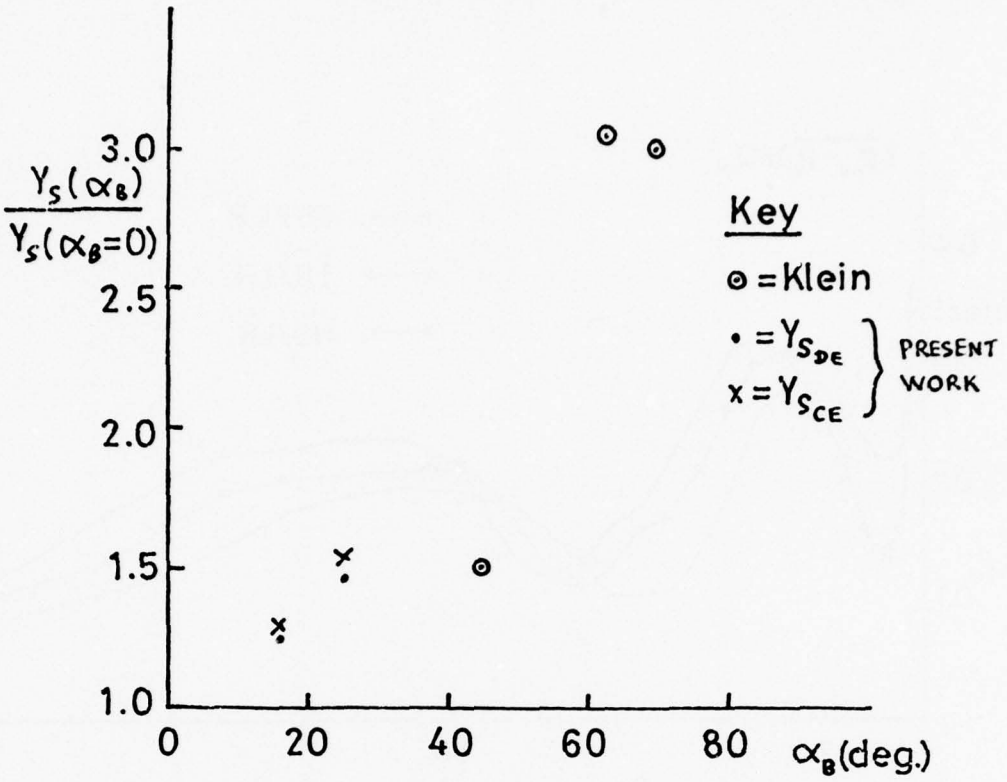


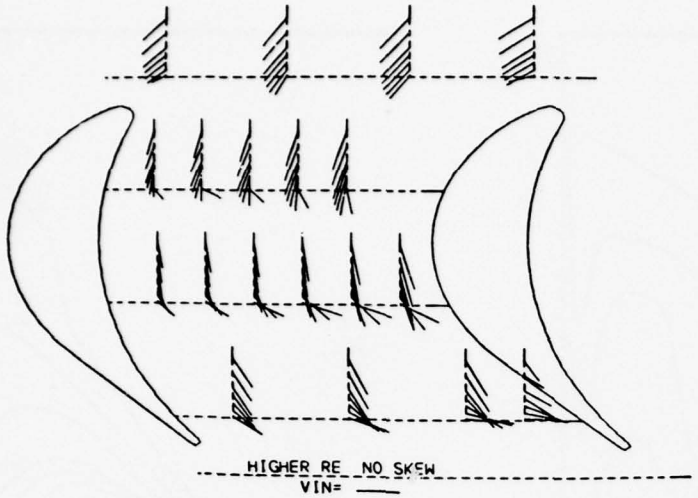
Fig.6 Pitch averaged P_o defect



Inlet Displacement Thicknesses

α_B	δ_s^*/c	δ_n^*/c	source
0.0	0.044	0.0	Present Work
16.2	0.047	0.0063	
23.6	0.057	0.015	
0.0	0.0122	0.0	Klein
45.0	0.0194	0.0215	
63.4	0.0260	0.0501	
69.7	0.0294	0.0931	

Fig.7 Effect of skew on secondary loss



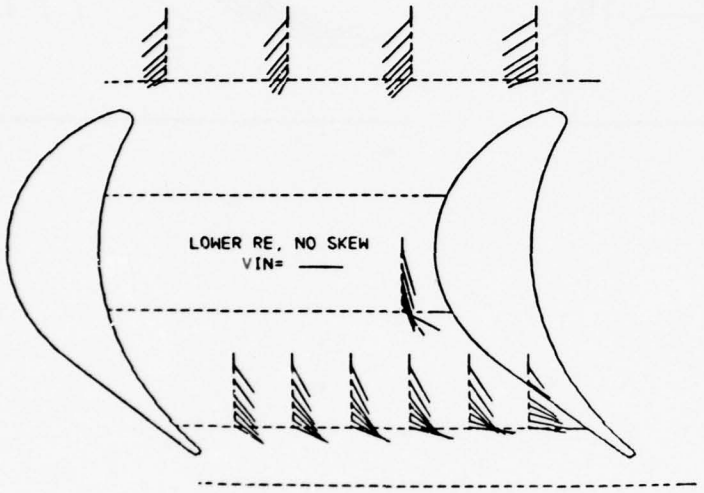
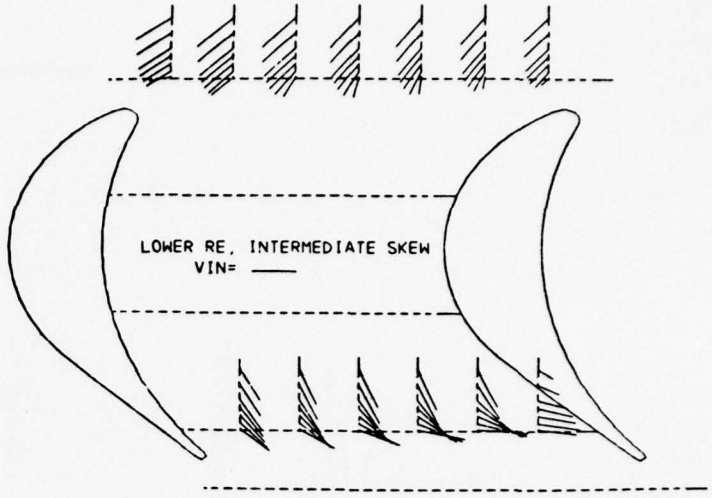


Fig.8(a),(b) Velocities, General view



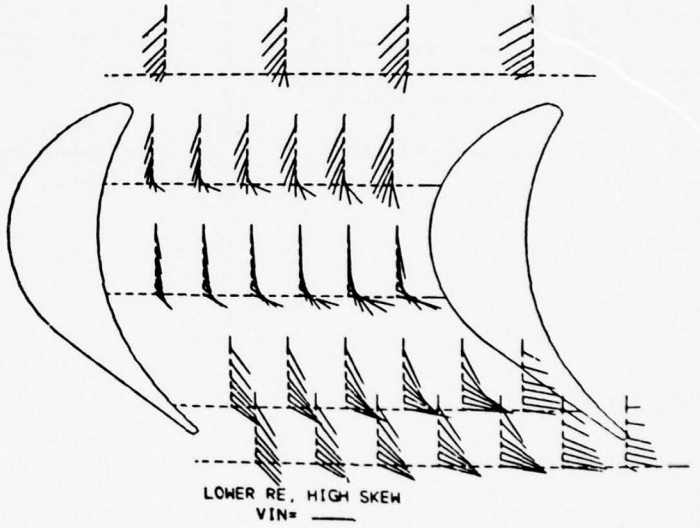


Fig.8(c),(d) Velocities, General view

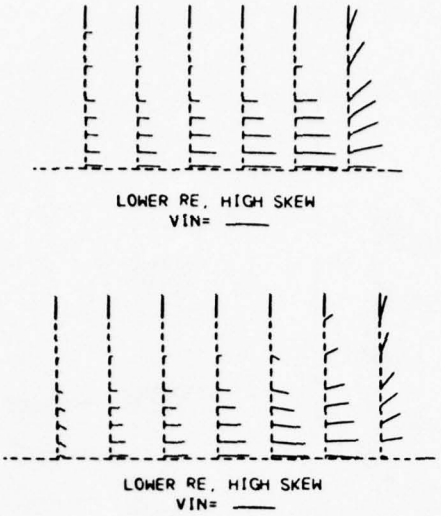


Fig.9 Approx. secondary velocities, Planes 4,5

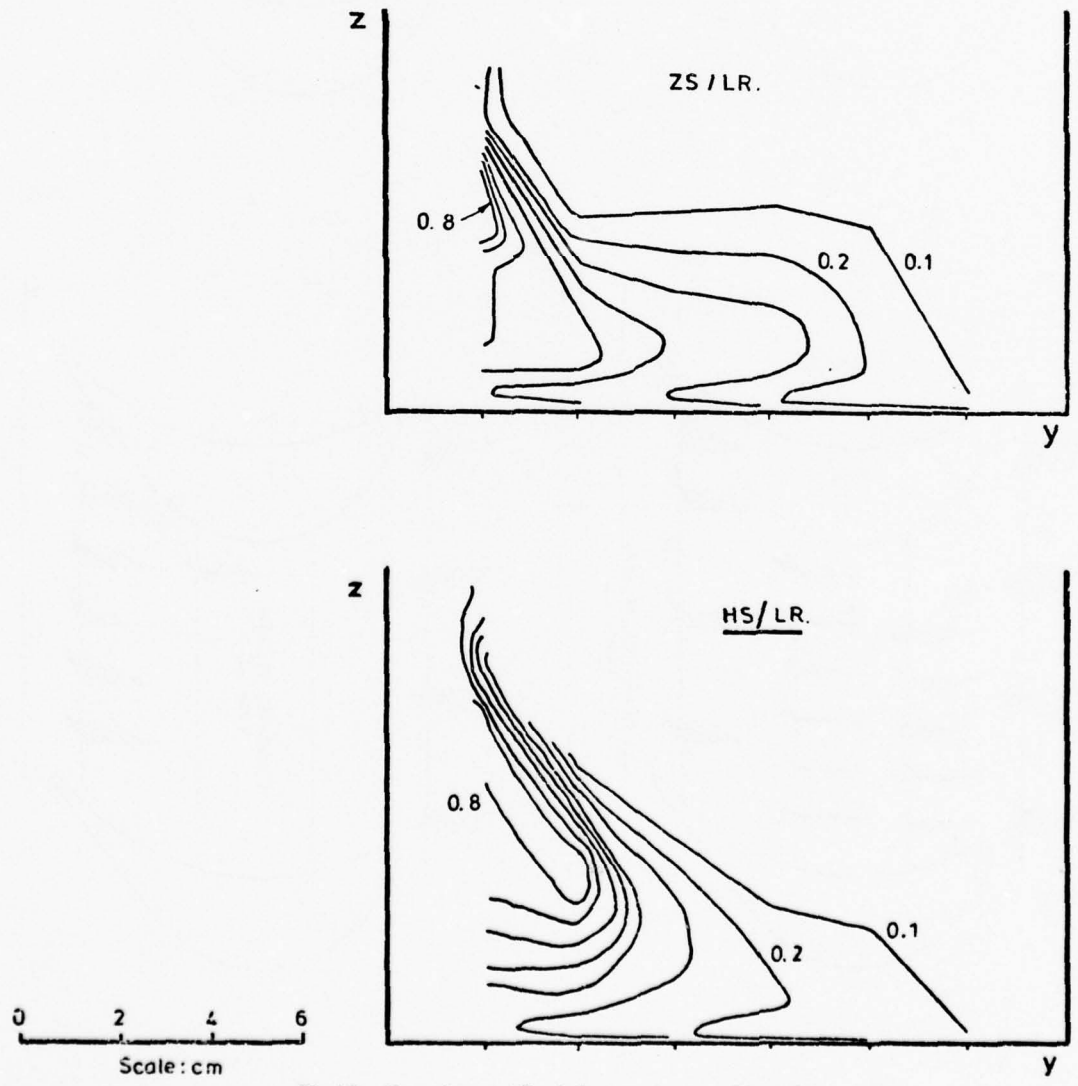


Fig.10 Experimental P_o defect contours – Plane 4

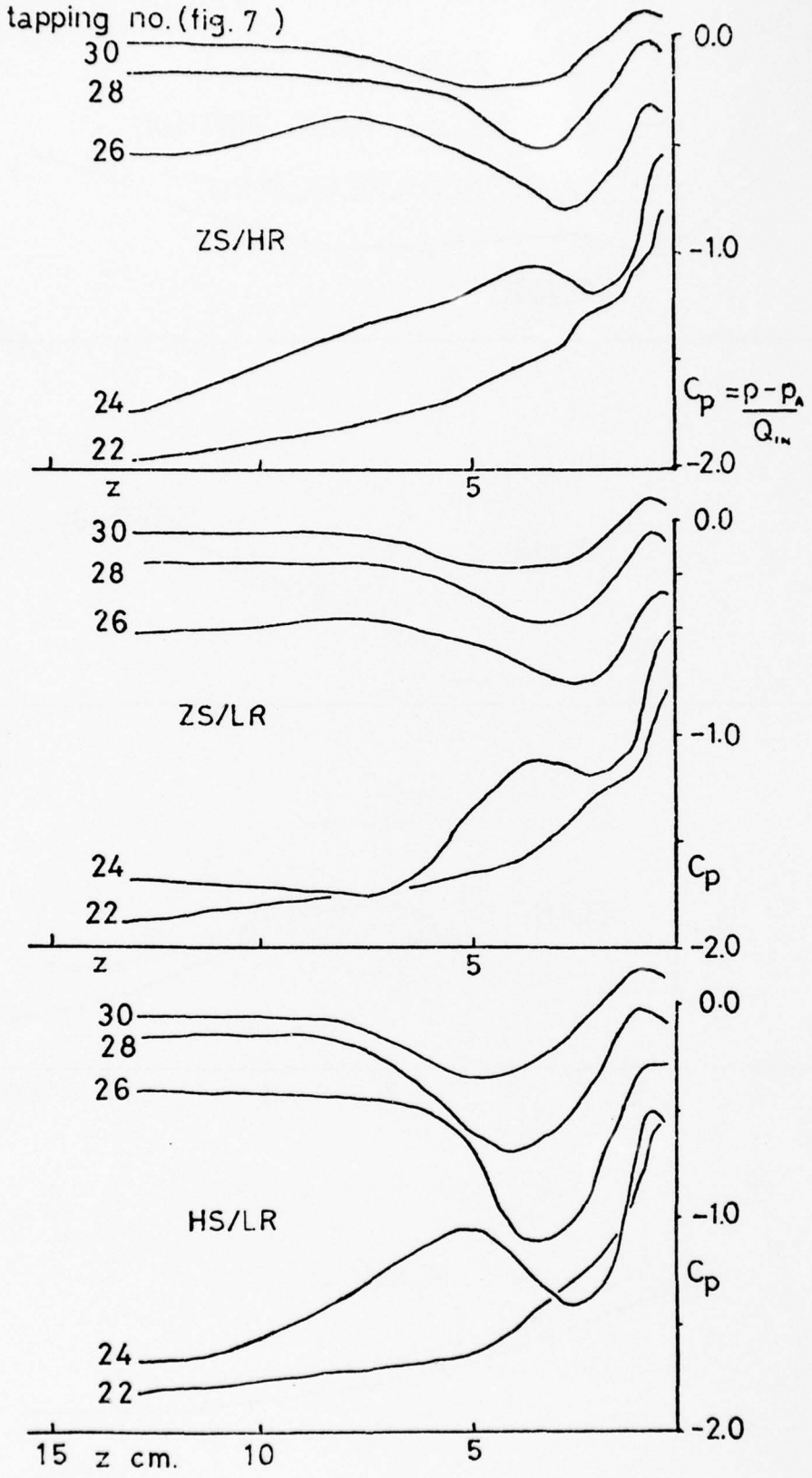


Fig.11 Suction surface pressures

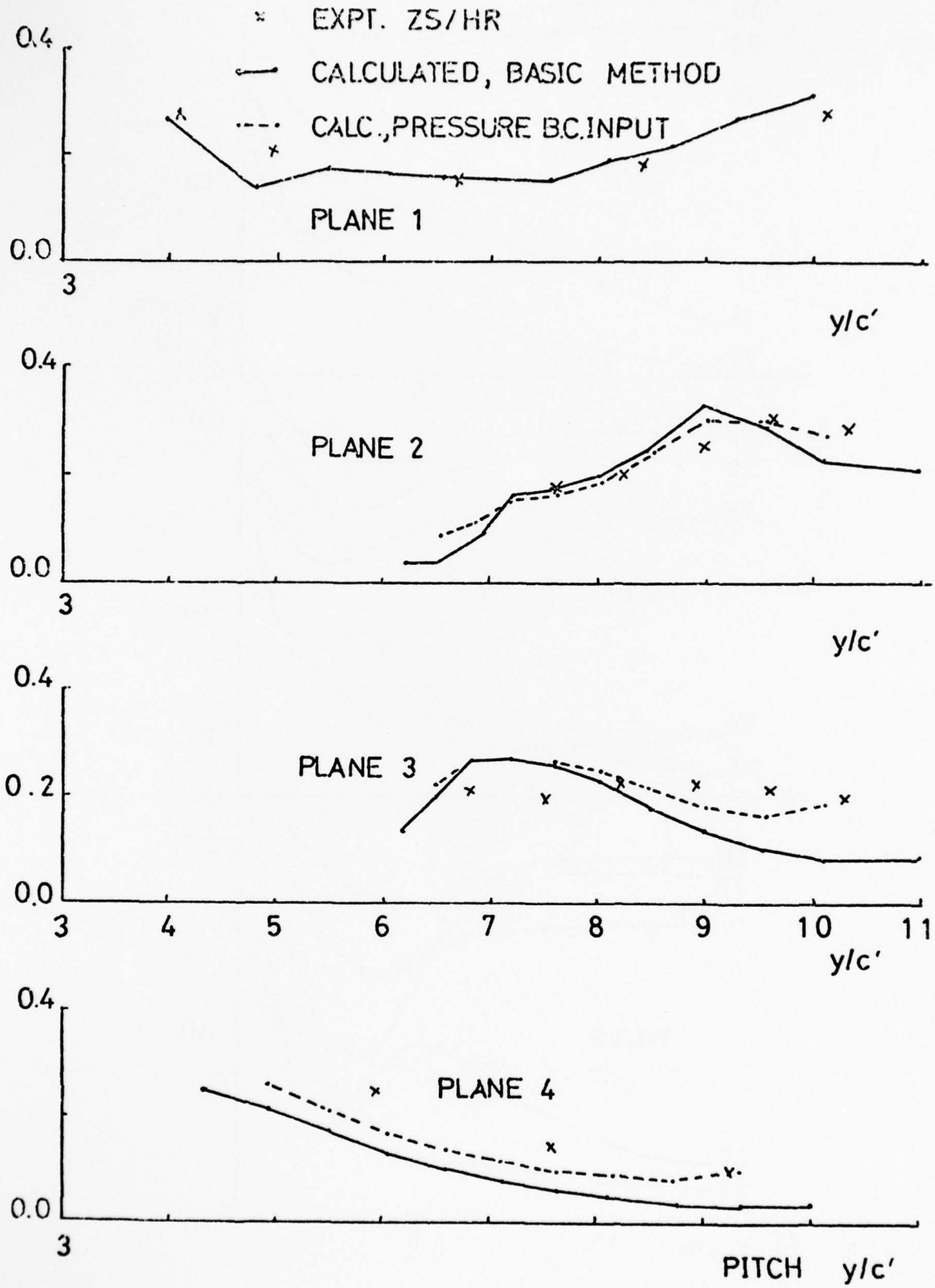


Fig.12 Single passage analysis, expt. ZS/HR, δ^*_s/c'

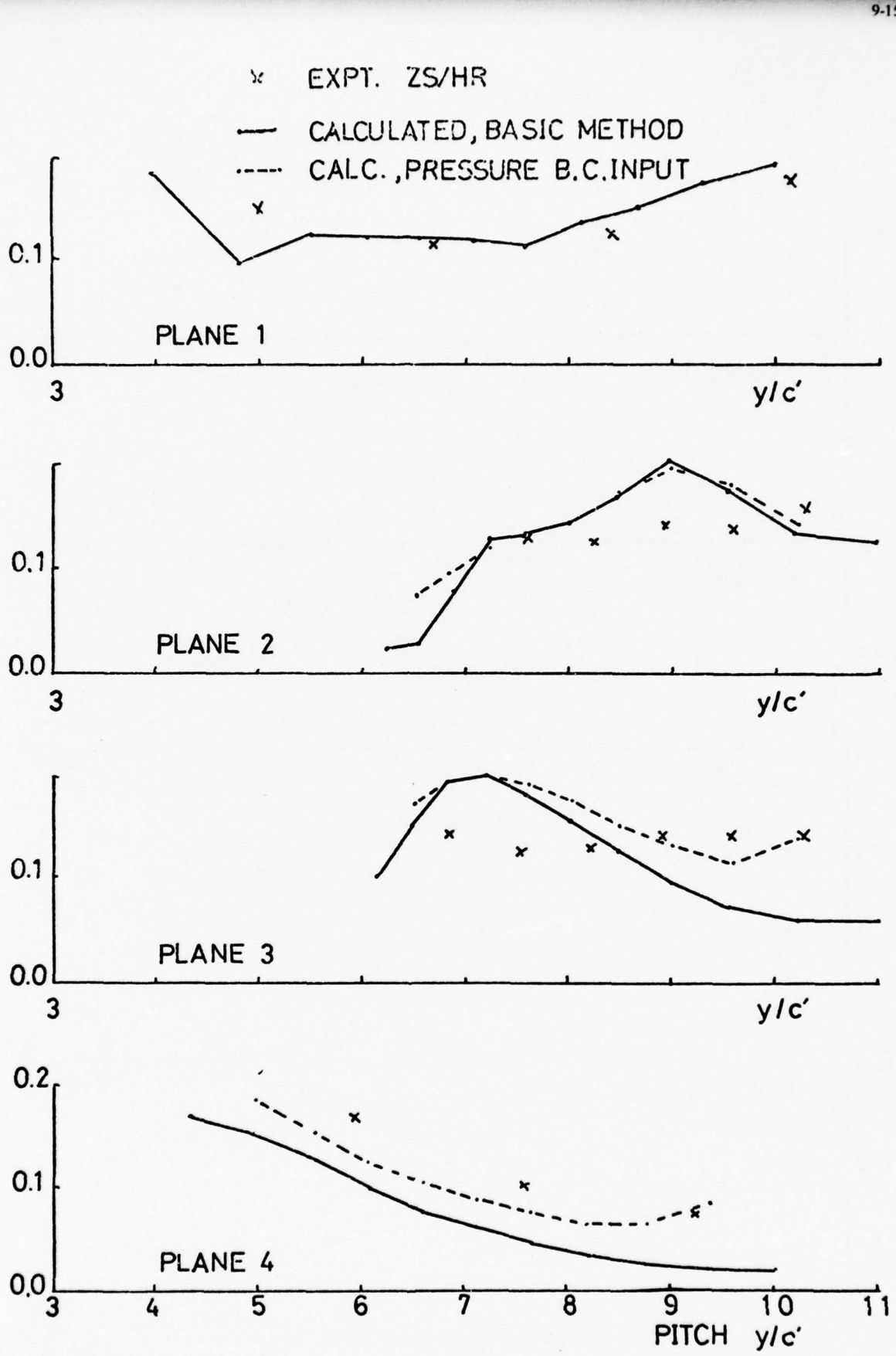


Fig.13 Single passage analysis, expt. ZS/HR, θ_{ss}/c'

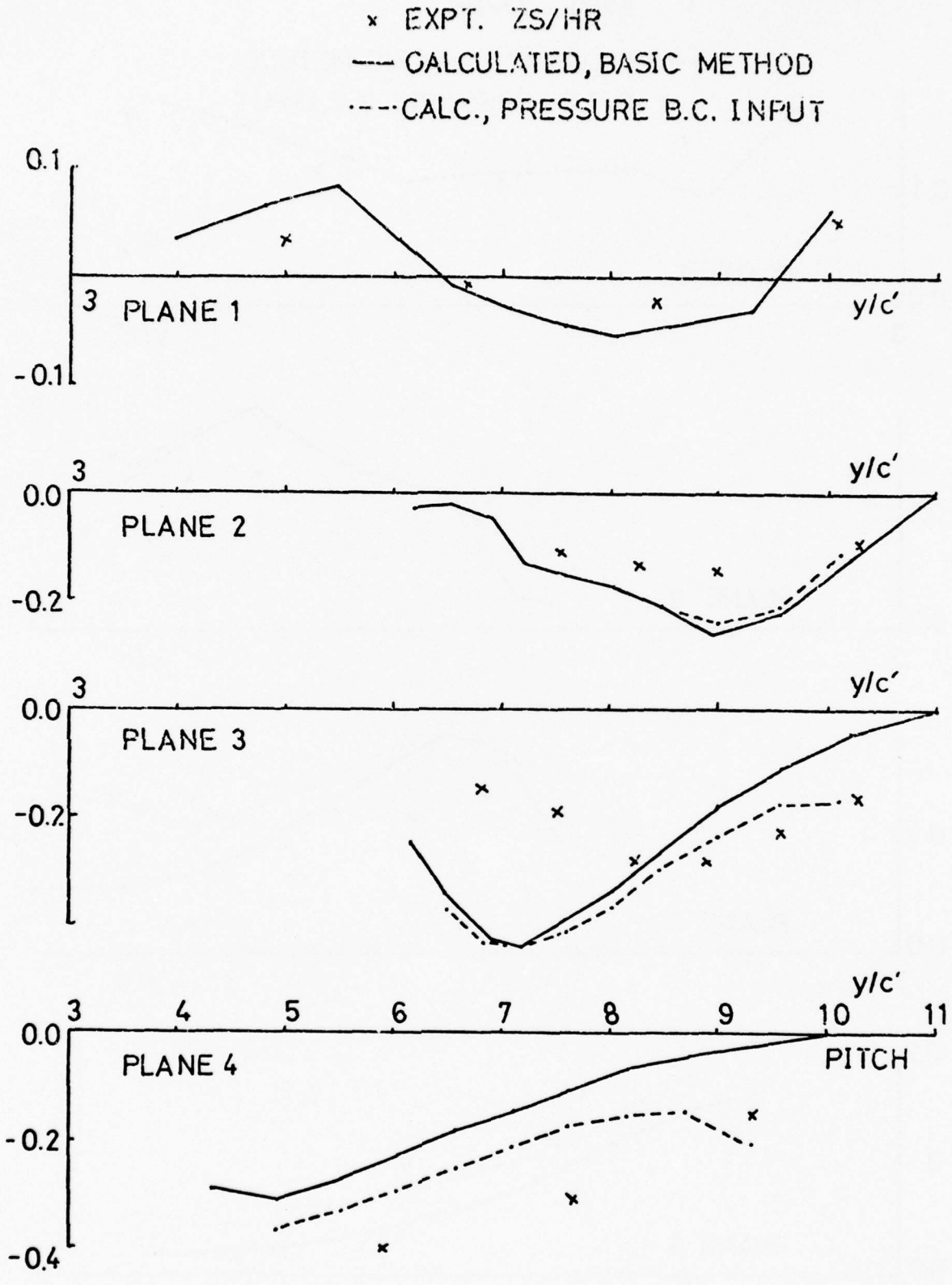


Fig.14 Single passage analysis, expt. ZS/HR, δ^*_n/c'

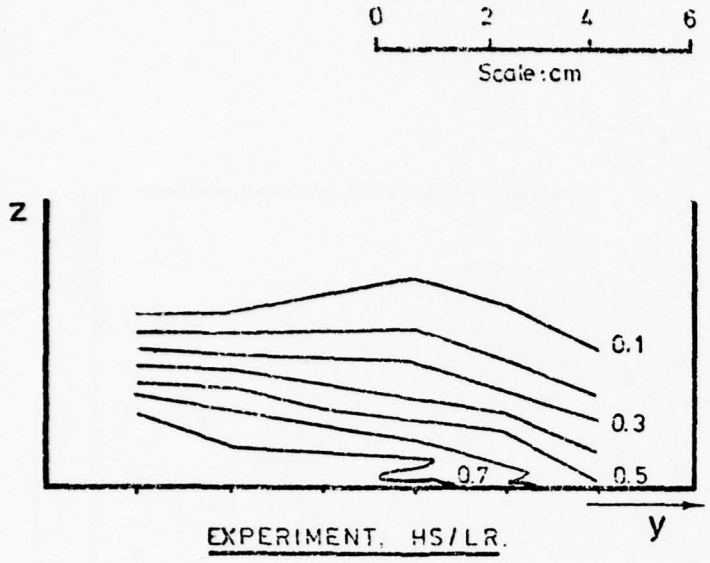


Fig.15 Contours of P_o defect, Plane 2

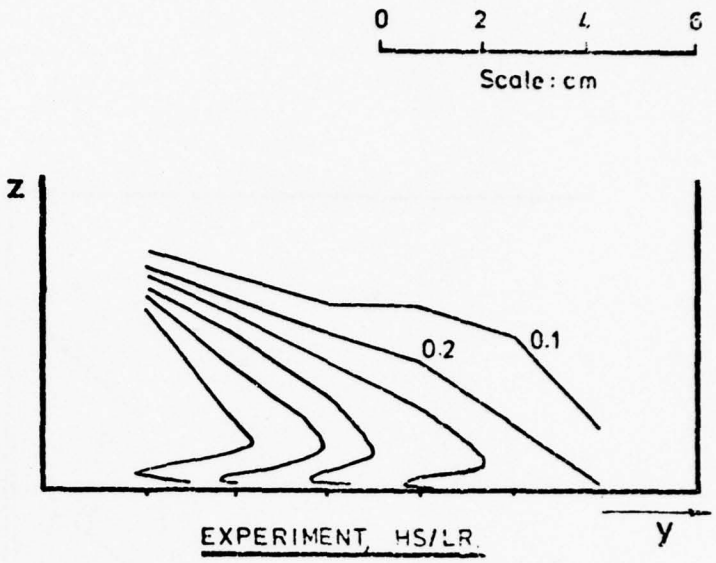


Fig.16 Contours of P_o defect, Plane 3

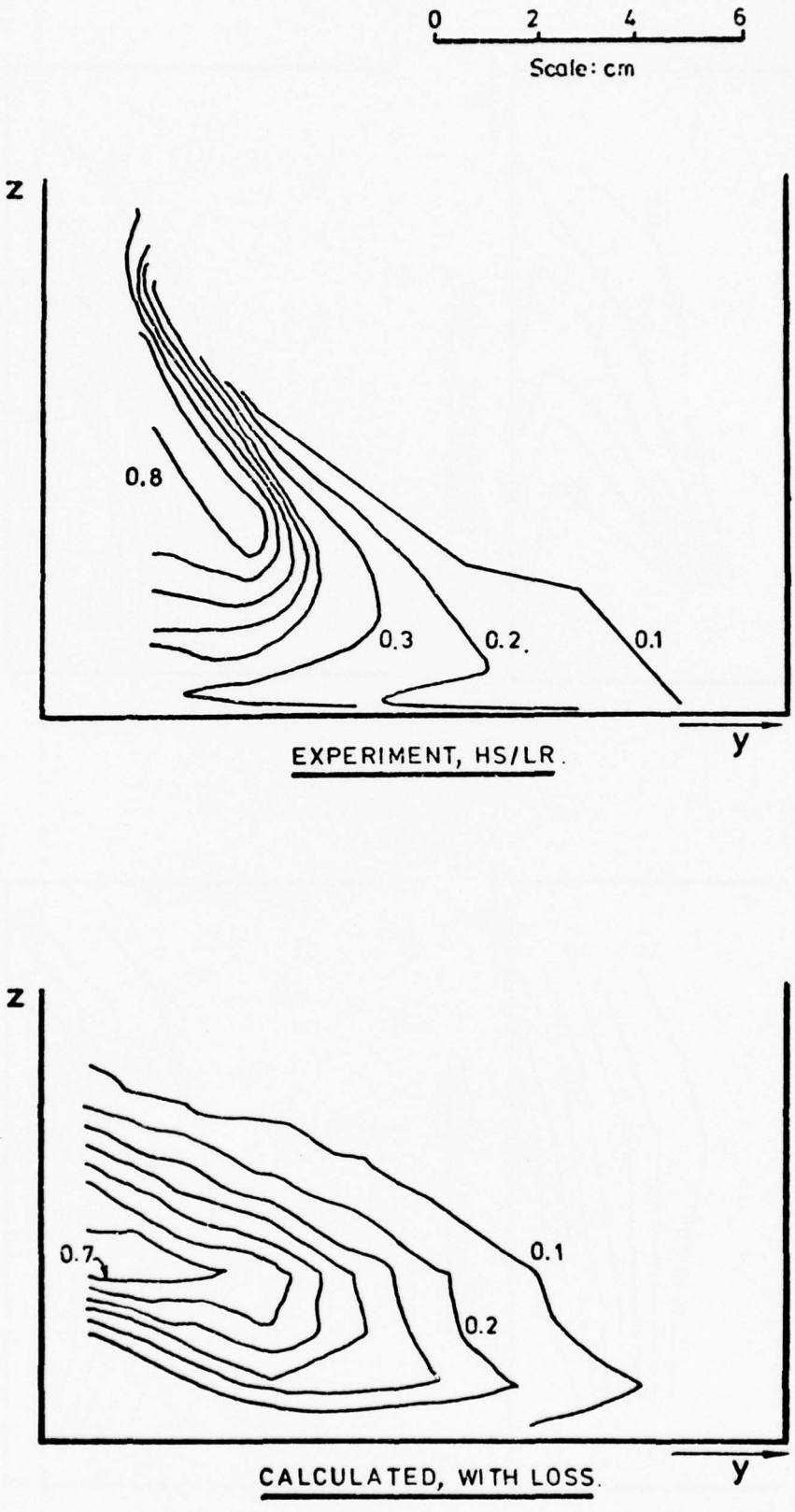


Fig.17 Contours of P_o defect, Plane 4

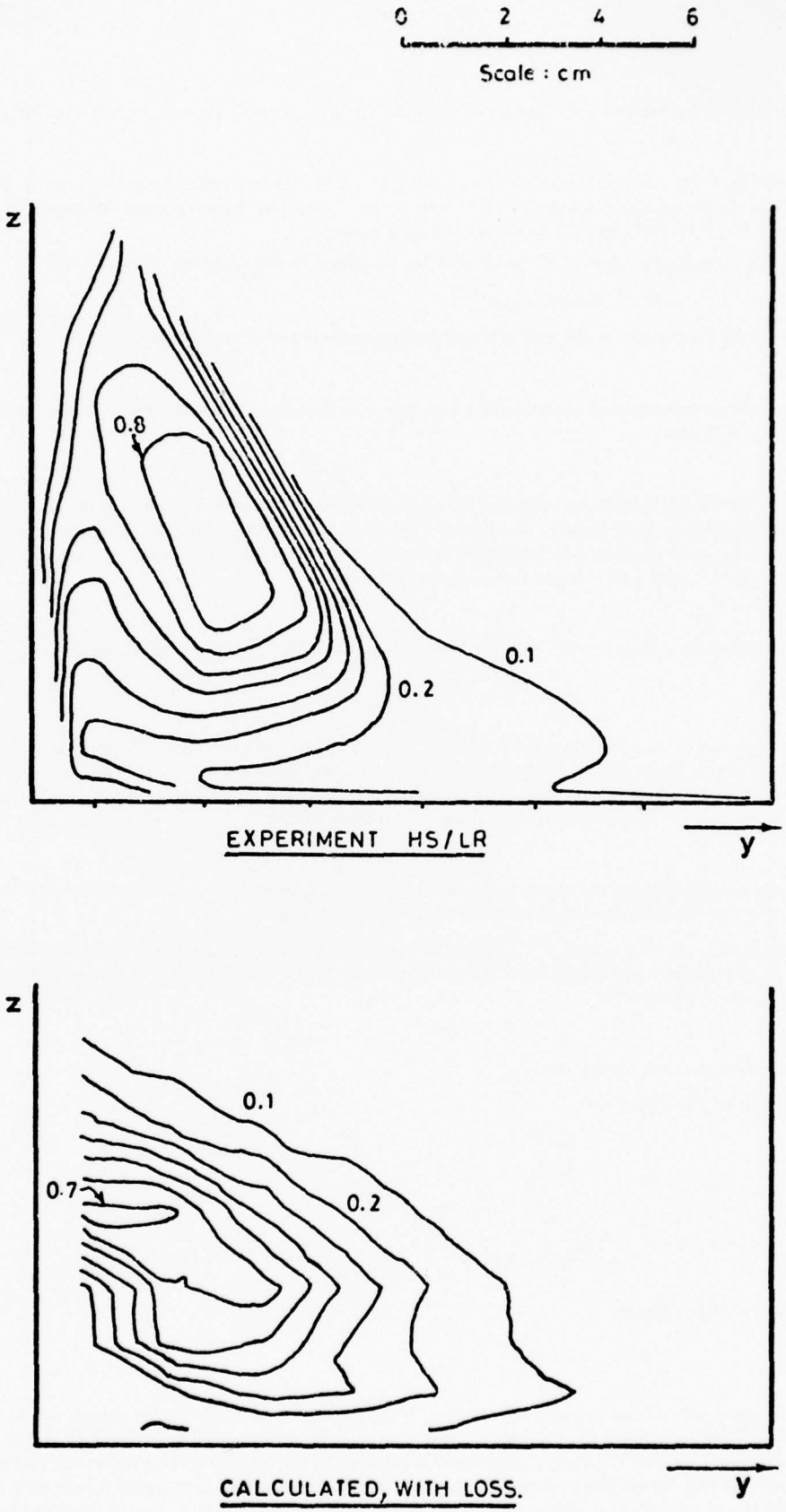


Fig.18 Contours of P_o defect, Plane 5

DISCUSSION

A.E.Fuhs

Would you comment on adequacy of the turbulent boundary layer model? How do you determine wall shear stress?

Author's Reply

The turbulent boundary layer method used (due to Dr P.D.Smith) is a momentum integral method. Since the strongest effect on the boundary layer flow is the turning i.e. an inertial effect, this was considered as an appropriate starting point. The wall shear stress was determined by assuming

(a) that the streamwise component of the shear stress was given by the Ludwieg-Tillman relation

$$C_f = 0.264\,(Re_\theta)^{-0.268}$$

(b) that the total shear stress at the wall acts along a line inclined at ϵ_0 to the free streamline.

C.H.Sieverding

What is the spanwise extension of the secondary loss region downstream of the cascade with respect to the inlet boundary layer thickness?

Author's Reply

The secondary flow itself extends to midspan, the region of intense secondary flow is very close to the wall. The majority of the boundary layer is swept away from the wall so the boundary layer downstream of the cascade is very thin. The region of the flow which contains vorticity extends off the wake and depending on the aspect ratio of the cascade the secondary flow might not extend to mid-span.

C.H.Sieverding

What interpretation do you give to the existence of the two loss peaks which you measured downstream of the cascade?

Author's Reply

This double peak was of course shown by Armstrong's results for the same cascade. He plotted the secondary velocities (rotation) in the outlet or, if you want, in the measuring plane one chord downstream superimposed in the total pressure contours. That shows that the rotations of the two peaks are in fact opposite in direction and they identify both with the different signs of the passage and trailing vorticity.

K.Papailiou

Could you give some details on the velocity profiles used in your integral calculation method? Could you also explain the way you treat the boundary conditions on the blade surface?

The comparison of three-dimensional charts does not give a clear idea of the accuracy of the calculation. Could you, please, give the comparison between theory and experiment of the circumferentially mean averaged quantities (total pressure and angle, for instance)?

Author's Reply

Boundary layer integral calculation method

(a) Streamwise profile (Spence)

$$\frac{v_s}{V_s} = \left(\frac{Z}{Z_\delta}\right)^{1/n}$$

where

$$\frac{1}{n} = \frac{H-1}{2}$$

(b) Crosswise profile (Mager)

$$\frac{v_n}{V_s} = \left(1 - \frac{2}{2\delta}\right)^2 \tan \epsilon_0$$

(c) On the suction side of the passage the boundary layer fluid is allowed to leave the region, i.e. no boundary condition is prescribed and the fluid is regarded physically as passing on to and collecting on the blade surface. On the pressure side of the passage some input is required to the calculations. A collateral boundary layer calculation in this corner although used in the basic method was proved to be inconsistent with the boundary layer equations and the experimental results were used for this input (see the dotted lines on Figures 12–14) in later calculations.

Three-dimensional calculation

As stated in the paper, the comparison between calculated and experimental results is qualitative rather than quantitative and no attempt was made to integrate these total pressure or angle results for comparison with experiment. This was because the grid used (see Section (6) of the paper) is too coarse to make a fair comparison. It must also be pointed out that blade boundary layer effects are not included and hence comparisons downstream of the cascade are anomalous.

P.Came

I too have a question concerning the two observed loss concentrations downstream of the cascade (Fig.6). Both peaks are seen to be increased by the effect of skew. Since skew-induced vorticity is in the same sense as the passage vorticity which may be associated with the loss concentration nearer the wall, would you not have expected this one only to have been increased by skew, rather than both peaks?

Author's Reply

My understanding of the source of the second low total pressure region (that which is further from the endwall) is that it comes mainly from blade boundary layer fluid. Since the convergence of blade boundary layer on the suction side of the blade is stronger with inlet skew I would expect the outer loss defect also to become deeper.

EFFETS DES ÉCOULEMENTS SECONDAIRES DANS LES GRILLES D'AUBES RECTILIGNES

par Georges MEAUZÉ

Office National d'Etudes et de Recherches Aérospatiales (ONERA)
92320 Châtillon - France

Résumé

Le rôle des écoulements secondaires dans les grilles d'aubes rectilignes est considérable et nuit à la validité des essais, surtout à fort taux de compression statique où l'écoulement secondaire peut remplir une partie notable des canaux inter-aubes.

Afin de pallier ces difficultés, un système d'aspiration des couches limites pariétales a été mis au point. Il permet d'éliminer le flux secondaire et de reconstituer un écoulement primaire pratiquement sain sur toute l'envergure de la grille. Les résultats obtenus sont satisfaisants que l'écoulement soit subsonique, transsonique ou supersonique, avec simulation ou non de la convergence de veine.

EFFECTS OF SECONDARY FLOWS IN STRAIGHT CASCADES

Summary

Secondary flows in straight cascades play a considerable role, and jeopardize the validity of the tests performed on this experimental set-up, especially at high compression rate, when the secondary flow may fill a relatively important part of the interblade channels.

In order to palliate this difficulty, a system of lateral boundary layer suction has been developed. It permits the elimination of the secondary flow and the definition of a primary flow practically uniform over the whole cascade width. The results obtained are satisfactory in subsonic, transonic and supersonic flow, with or without simulation of section convergence.

I - INTRODUCTION

Du fait de la présence de parois fixées rigidement aux aubes, le développement de l'écoulement secondaire dans les grilles d'aubes rectilignes pose des problèmes différents de ceux rencontrés dans les compresseurs. Les effets secondaires sont d'autant plus marqués que la contrepression est plus élevée et dans certains cas le domaine secondaire peut occuper toute la veine fluide.

Il est bien évident que dans ces conditions, la validité et l'exploitation des essais de grilles deviennent très douteuses, dans la mesure où l'on cherche à simuler l'écoulement dans une coupe donnée de roue mobile ou fixe.

Pour s'affranchir de ces inconvénients, un dispositif d'aspiration des couches limites a été mis au point et appliqué avec succès comme le montrent les résultats présentés ici, qui mettent en évidence la disparition de ces effets secondaires, et l'obtention d'un écoulement bidimensionnel.

Par ailleurs, en vue d'améliorer la représentativité des essais de grilles rectilignes, il convient de simuler la variation de convergence de veine qui existe dans la machine à la coupe considérée. Cette convergence qui est créée à l'aide d'un remplissage des parois latérales a pour effet de réduire le ralentissement comme dans la machine. Cela diminue les effets secondaires mais une aspiration des couches limites sur les parois latérales est toujours nécessaire, sauf dans le cas particulier d'une grille supersonique avec une forte convergence de veine où il semble qu'il n'y a plus de formation d'écoulements secondaires.

Nous allons décrire les phénomènes rencontrés dans les différents cas, subsonique ou supersonique avec ou sans convergence de veine, et montrer les effets favorables des aspirations de couches limites

II - GRILLES RECTILIGNES A PAROIS LATERALES PARALLELES

Ce type de configurations qui présente une "géométrie" bidimensionnelle est essentiellement destiné à des essais effectués en vue de confirmer les méthodes de calculs d'écoulements visqueux ou non, dans la grille.

II-1 - Ecoulement amont subsonique

La compression, fournie par la grille, est obtenue grâce à la déviation de l'écoulement qui crée un accroissement de la section de passage donc un ralentissement. L'apparition d'écoulements secondaires, au raccordement de la paroi et de la grille, est essentiellement due à la présence des gradients de pression statique dans la grille et à leur action sur les couches limites des parois des aubes et sur celle des parois latérales de la soufflerie. En effet, le champ d'écoulement dans les canaux inter-aubes est complexe. Le long d'une ligne de courant, il existe évidemment un gradient de pression positif puisque l'écoulement est ralenti ; par ailleurs, la courbure des lignesde

courant qui résulte de la déviation induite par les aubes, impose un gradient de pression transversal. Ainsi, la couche limite initialement bidimensionnelle et relativement épaisse qui s'est développée sur les parois latérales de la soufflerie, va être profondément bouleversée en présence de ces gradients à la traversée de la grille :

- d'une part la compression longitudinale a tendance à l'épaissir encore plus sinon à provoquer un décollement,

- d'autre part, sous l'effet du gradient transversal, le fluide à basse vitesse près des parois a tendance à être drainé de l'intrados (forte pression) d'une aube à l'extrados (faible pression) de l'aube immédiatement adjacente. Il en résulte un "vrillage" de la couche limite ; dans le cas d'aubes fortement chargées, où les gradients transversaux sont très importants, les filets de courant s'enroulent sur eux-mêmes à la paroi et donnent naissance à un tourbillon qui va partir de cette paroi et se développer au sein de l'écoulement. Le phénomène a pu être mis en évidence au moyen d'une méthode de visualisation. La figure 1 représente un schéma des lignes de courant pariétales obtenu à l'aide d'une visualisation par enduit visqueux, dans le cas d'une grille de redresseur constituée d'aubes DCA de 65° de cambrure pour un nombre de Mach amont de 0,85 et un angle d'attaque de l'écoulement de 65° par rapport à la direction normale au front de grille.

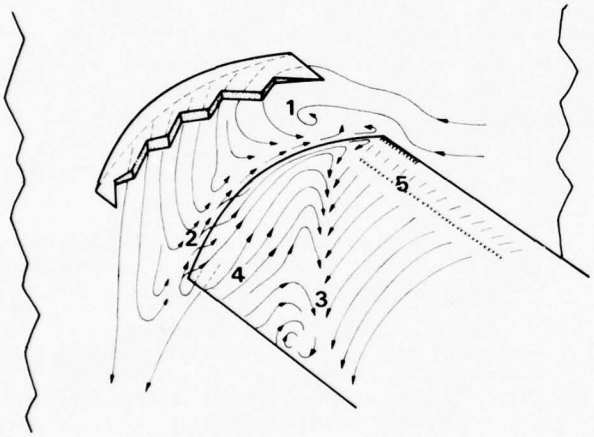


Fig. 1 — Visualisation de l'écoulement pariétal.

L'enduit déposé sur les parois latérales de la soufflerie fait apparaître la naissance du tourbillon (1). Il existe sur cette paroi, une zone décollée (2) s'écartant assez peu de l'extrados de l'aube ; hors de cette zone l'écoulement pariétal se dirige de l'intrados vers l'extrados de l'aube adjacente. Par ailleurs, sur l'extrados de l'aube elle même, deux importantes lignes d'accumulation de bouillie (3), (une seule est présentée sur la figure 1) symétriques par rapport au plan médian, issues des parois vers l'amont et prenant une inclinaison de 45° vers le bord de fuite indiquent les frontières de deux décollements symétriques. Dans les zones décollées (4), les lignes de courants remontent à partir du bord de fuite. On remarquera, en outre, la discontinuité des lignes de courant (5) à environ 15% du bord d'attaque, causée par la présence d'un bulbe de décollement laminaire.

Une telle configuration d'écoulement est tridimensionnelle comme le confirme la cartographe reportée figure 2, qui est obtenue à partir de sondages en pression d'arrêt effectués à une demie corde en aval de la grille, selon la direction du front de grille et pour diverses positions en envergure.

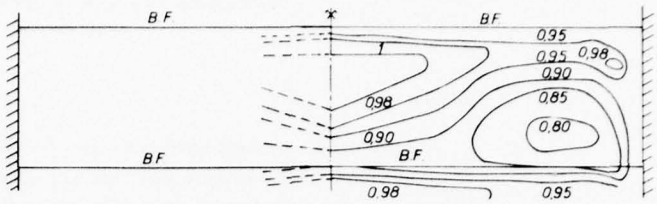


Fig. 2 — Cartographie en iso-pressions d'arrêt en aval de la grille.

Cette cartographie montre l'effet des écoulements secondaires qui envahissent la presque totalité de l'écoulement, ainsi que le niveau de pertes qui en résulte.

L'aspect tridimensionnel de l'écoulement est aussi caractérisé par la valeur du coefficient de contraction défini comme étant le rapport du débit amont au débit aval dans une même tranche infiniment mince, comprise entre 2 plans parallèles aux parois latérales. Dans le plan médian, et pour le cas correspondant à la figure 1, la valeur de ce coefficient est de l'ordre de 0,76 au lieu de 1 pour un écoulement bidimensionnel. Cela montre que les écoulements secondaires créent une forte convergence de veine, et les essais effectués dans ces conditions ne caractérisent plus le fonctionnement bidimensionnel de la grille.

Pour s'affranchir de ces effets secondaires, il est nécessaire d'apporter un traitement approprié aux couches limites pariétales. Diverses techniques ont été essayées, dont les principales sont rappelées ci-après :

- Elimination de la couche limite à l'entrée de la grille

Cette technique permet de réduire les effets secondaires mais non pas de les éliminer complètement car à l'entrée de la grille, à la paroi, il se développe une couche limite mince mais le plus souvent laminaire qui est alors très sensible aux gradients de pression, de plus le phénomène de drainage et le vrillage qui en résulte n'est pas évité.

- Aspiration continue de la couche limite au niveau de la grille

Cette technique peut permettre d'éliminer les effets secondaires, mais elle apporte dans ce cas de fortes perturbations au champ de l'écoulement. En effet, la majeure partie du débit aspiré provient des zones à forte pression c'est-à-dire de tout le long de l'intrados, et de toute la partie aval du canal. Dans ces conditions, si l'on veut supprimer les écoulements secondaires qui se créent dans une zone à plus faible pression, le débit aspiré est beaucoup trop important et, l'écoulement principal n'est plus bidimensionnel. Si le débit aspiré est réduit, il y a des risques de recirculations, ce qui perturbe le champ de l'écoulement.

- Aspiration localisée à travers des lumières

Pour éviter les inconvénients évoqués ci-dessus, l'ONERA à mis au point un dispositif

d'aspiration localisée à travers des lumières affleurantes à la paroi fig.3 . Ce piège à couche limite est placé dans la région où commence la recompression et est orienté suivant les courbes isobares ce qui nécessite le calcul de tout le champ de l'écoulement théorique avant la mise en place du piège à couche limite.

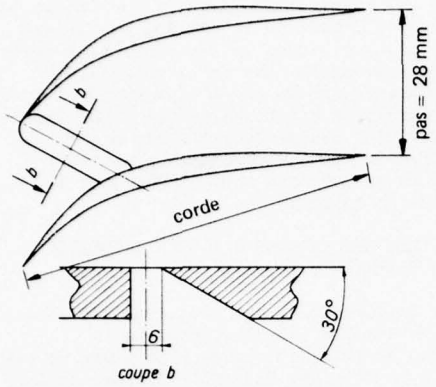


Fig. 3 – Définition du piège à couche limite.
envergure = 120 mm

Ce dispositif a été utilisé sur plusieurs types de redresseurs et a donné toute satisfaction. Les résultats présentés ici correspondent à une grille à profil MCA de 57° de cambrure.

L'aspiration de la couche limite latérale, à travers les pièges, réduit les phénomènes secondaires et diminue la convergence artificielle de la veine ; en particulier dans le plan médian de la grille, le coefficient de contraction croît continuellement avec le débit aspiré. La figure 4 montre son évolution en fonction du taux d'aspiration. On notera aussi l'évolution du rapport de pression d'arrêt aval/amont moyen ainsi que celui mesuré au centre. Ces rapports ont des valeurs très voisines quand le coefficient de contraction devient égal à 1.

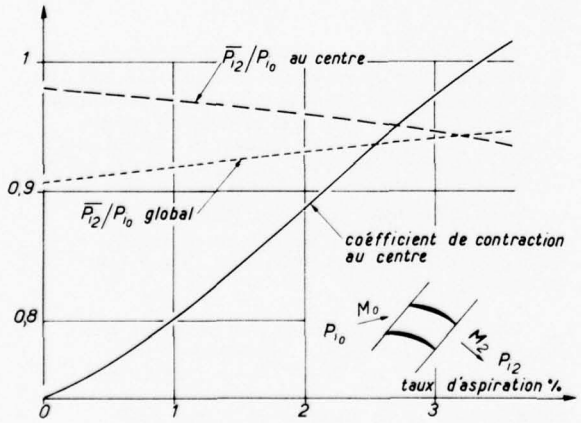


Fig. 4 – Evolution du coefficient de contraction et des pressions d'arrêt moyenne et au centre.

On remarquera que la mise en oeuvre de l'aspiration diminue notablement les pertes globales, ce qui est évidemment associé à une augmentation du taux de compression de la grille.

La cartographie des pressions d'arrêt (fig.5) obtenue à l'aval de la grille dans ces conditions montre bien que l'écoulement est devenu bidimensionnel sur toute l'envergure de la grille sauf au voisinage immédiat des parois.

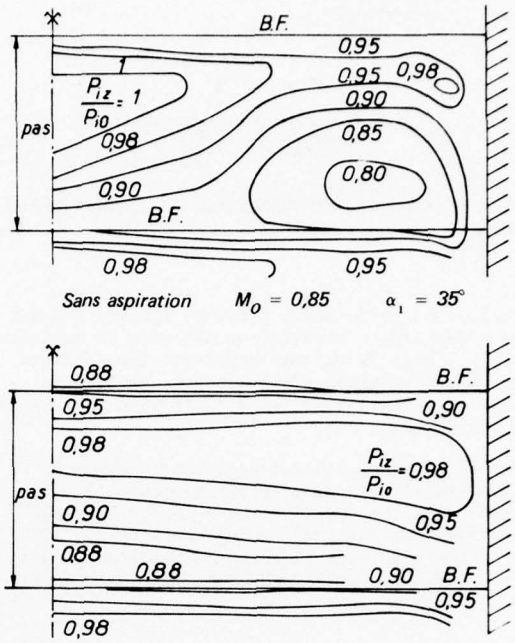


Fig. 5 – Effet d'aspiration de la couche limite.

- Soufflage de la couche limite

Un dispositif de soufflage des couches limites pariétales a été essayé et a donné des résultats satisfaisants quant à la réduction des effets secondaires, mais il a été rapidement abandonné pour deux raisons principales :

1) Pour que le soufflage soit efficace il faut que la fente de soufflage soit le plus tangentielle possible, et par suite sa réalisation est délicate et coûteuse ;

2) en toute rigueur il est impossible d'avoir un coefficient de contraction égal à 1 puisque le débit est plus important à l'aval qu'à l'amont de la grille. Celà s'ajoutant à l'épaississement des couches limites pariétales. Cet inconvénient n'existe pas dans le cas de l'aspiration puisque la réduction du débit à l'aval peut être compensée par le développement des couches limites sans décollement dans le canal à la paroi en aval du piège.

II-2 - Ecoulement amont supersonique

Il s'agit de configuration simulant une coupe de roue mobile.

La compression est obtenue ici par un système de chocs et il n'y a presque plus de courbure des lignes de courant, donc l'effet de vrillage est atténué. Par contre l'accroissement de pression à travers les ondes de choc fait décoller la couche limite des parois latérales, d'où des pertes considérables.

La suppression de ces effets secondaires est obtenue ici aussi par une aspiration des couches limites des parois latérales à travers des lumières aménagées au niveau où se situe théoriquement le choc principal pour la plus forte contrepression - Figure 6.

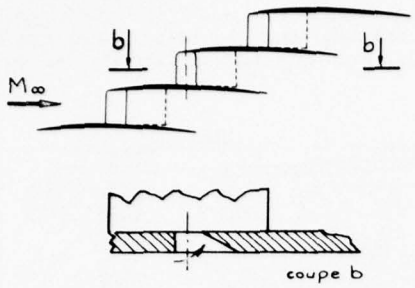


Fig. 6 – Schéma de grille d'aubes supersonique avec piège à couche limite.

En absence de piège à couche limite, l'importance des effets secondaires est mise en évidence par la figure 7a où sont reportées des sondages en pression d'arrêt effectués près du bord de fuite, sur deux canaux et à différentes positions en envergure.

Une cartographie des pressions d'arrêt à l'aval aurait été plus explicite, mais elle aurait nécessité un plus grand nombre de plans de sondage en envergure pour être bien définie. De toute façon, les différences importantes des répartitions de pressions montrent bien l'effet des décollements latéraux.

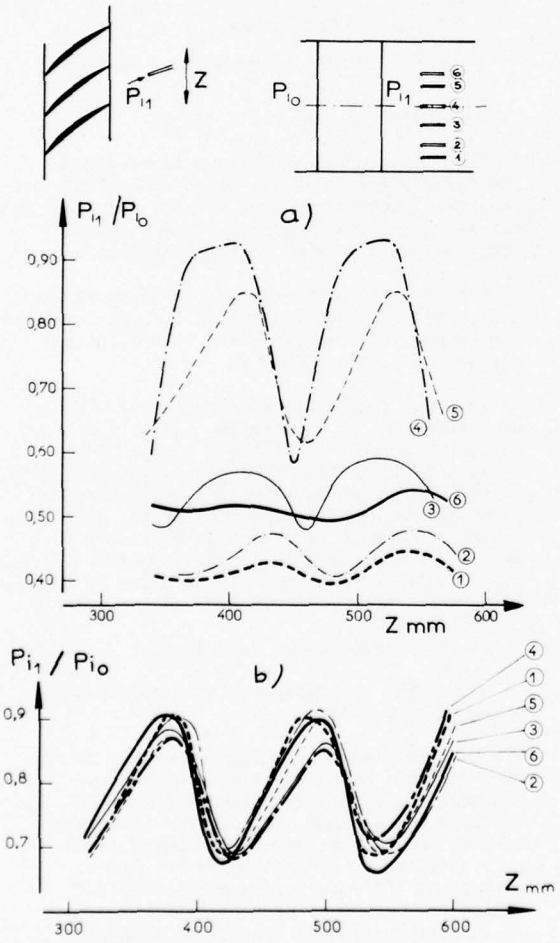


Fig. 7 – Répartition de pression totale le long de deux canaux interaubes pour 6 positions en envergue (n° 1 à 6). M_o = 1,5. (a) sans aspiration ; (b) avec aspiration.

La mise en oeuvre de l'aspiration latérale modifie considérablement ces répartitions de pression d'arrêt, en envergure, (Fig.7b) qui présentent alors un aspect tout à fait semblable. Les effets secondaires sont ainsi pratiquement éliminés, mais il n'est pas possible d'affirmer que l'écoulement est parfaitement bidimensionnel car la mesure du coefficient de contraction nécessite une connaissance précise de l'angle de l'écoulement à l'aval de la grille, ce qui est difficile à obtenir dans le cas présent, à cause des variations importantes de la vitesse. Il faut en outre remarquer que l'élimination des effets secondaires s'accompagne ici d'une importante diminution des pertes, associé à une augmentation du taux de compression statique (2,2 au lieu de 1,6 sans aspiration, pour la contrepression maximum).

III - GRILLES RECTILIGNES A PAROIS LATERALES CONVERGENTES -

Cette configuration est plus réaliste que la bidimensionnelle car elle respecte la convergence du tube de courant à la coupe considérée dans la machine. En grille d'aube, cette convergence résulte d'une évolution de la forme des parois latérales définie de manière à recréer dans la tranche centrale, où sont faites les mesures, l'évolution de convergence recherchée.

III-1 - Ecoulement amont subsonique

Au point de vue effets secondaires, on retrouve les mêmes phénomènes que dans le cas des parois parallèles. Toutefois la convergence de veine ayant pour effet de réduire le ralentissement, les gradients sont plus faibles et les pertes dues aux écoulements secondaires sont atténués. Si l'on veut s'affranchir de ces effets secondaires, il est nécessaire comme précédemment d'aspirer les couches limites latérales. La disposition des lumières d'aspiration est, cette fois encore, définie à partir du champ des pressions à la paroi, qu'il est nécessaire de calculer tout spécialement, l'écoulement dans la grille étant tridimensionnel.

Rappelons qu'à cet effet, une méthode approchée du calcul tridimensionnel dans une grille d'aube a été mise au point .

Cette méthode dérive du schéma classifié du calcul quasi-tridimensionnel proposé par Wu [1] pour les compresseurs axiaux. Du fait du nombre limite des aubes et de l'existence de parois latérales non parallèles la notion d'écoulement moyen a dû être adaptée à ce type de montage [2] et le calcul consiste à définir d'une part les surfaces de courant moyennes calculées en l'absence d'aubes et d'effectuer un calcul d'aubes à aubes du type Katsanis [3]sur ces surfaces de courant.

Les résultats expérimentaux montrent que pour éliminer les effets secondaires, et obtenir à l'aval de la grille un coefficient de contraction égal au taux de convergence géométrique, il ne faut qu'un faible débit d'aspiration (1% du débit de la grille, alors que en bidimensionnel, des taux de l'ordre de 3 % sont nécessaires).

III-2 - Ecoulement amont supersonique

Les essais de mise au point dans des configurations simulant une coupe de roue mobile supersonique avec convergence de veine, ont été effectués à un nombre de Mach supersonique modéré Mo = 1,3.

L'allongement des aubes est de 1,5 et le rapport de contraction géométrique est de 0,7.

Pour les premiers essais la forme des parois latérales était linéaire (fig.8a)

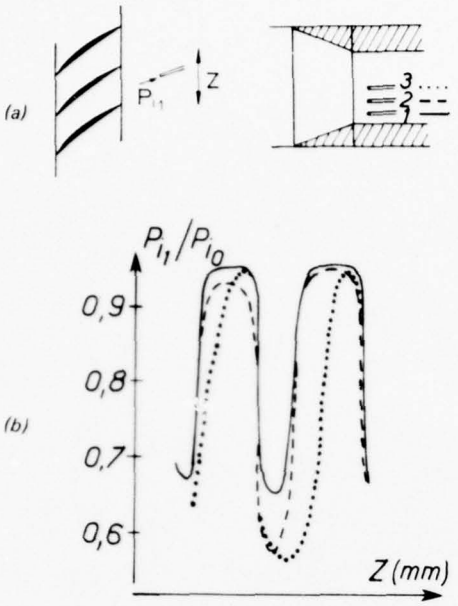


Fig. 8 – Répartition de pression totale le long de deux canaux interaubes avec convergence de veine. M_o = 1,3.

En absence de tout traitement des couches limites sur les parois latérales, les répartitions de pression en envergure présentent l'aspect de la figure 8 b, pour la contre pression maximum.

On constate une dégradation des pressions d'arrêt vers le centre de l'aube, du côté extrados, mais vers les parois, les répartitions correspondent à celles d'un écoulement "sain" après traversée d'un choc, et avec des sillages classiques. Celà est à l'opposé des effets habituellement rencontrés ; il semble que le champ de l'écoulement au voisinage des parois latérales ne soit pas favorable à la formation d'écoulements secondaires.

Une aspiration des couches limites latérales ne modifie d'ailleurs en rien l'aspect des répartitions de pressions d'arrêt.

Les essais ont été repris avec une forme de paroi convergente à variation continue de courbure, mais avec la même convergence globale (fig.9).

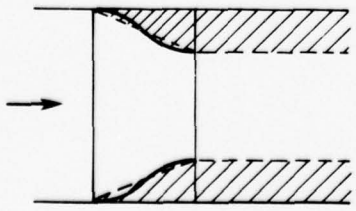


Fig. 9 – Schéma de la convergence des parois latérales.

--- *1ère forme (linéaire)*
—— *2e forme*

Les résultats obtenus avec cette nouvelle veine ne diffèrent pas de façon sensible de ceux correspondant à la première veine.

Les visualisations par enduit visqueux montrent la présence d'un décollement sur l'extrados de l'aube : la ligne de séparation qui se trouve à un quart de corde du bord d'attaque au centre de l'aube, rejoint le bord de fuite quand on s'approche des parois latérales. En revanche au voisinage des parois, il n'apparait aucune trace de décollement, pas plus que sur l'intrados ou sur les parois latérales de la soufflerie.

Par ailleurs, on constate que les pressions statiques à la paroi dans le plan de sortie de la grille restent insensibles à la variation de la contre-pression. Quant aux prises de pressions situées plus en aval, ainsi que celles situées dans le plan médian de la grille, elles suivent bien la variation de pression et l'on peut noter la remontée du choc principal quand la contre-pression croît. Il semble que l'écoulement étant fortement tridimensionnel, le désamorçage des tranches centrales se produise avant que le choc principal aux parois ne pénètre dans la grille à l'aval.

Mais il est difficile d'expliquer ce phénomène et seul un calcul tridimensionnel de l'écoulement complet dans une grille supersonique avec convergence permettra d'apporter une réponse satisfaisante.

CONCLUSION

Les écoulements secondaires, qui prennent naissance sur les parois latérales dans les soufflerie de grilles d'aubes rectilignes, perturbent l'écoulement et nuisent considérablement à la validité des essais. Une aspiration des couches limites latérales localisée, à travers des lumières orientées suivant les courbes isobares, juste au début de la recompression de l'écoulement dans la grille, permet d'éliminer ces effets secondaires. L'application de ce dispositif donne de bons résultats que l'écoulement relatif soit subsonique ou supersonique en veine bidimentionnelle ou subsonique en veine convergente.

Par ailleurs, dans le cas d'une coupe de roue mobile supersonique, les essais montrent qu'une forte convergence de veine semble éviter la formation d'écoulement secondaire, mais ce phénomène est encore mal expliqué.

REFERENCES

[1] WU C.H. - A general through flow theory of fluid flow with subsonic or supersonic velocity in turbomachines of arbitrary hub and casing shapes. NACA TN 2302 (1951).

[2] A method for testing cascades with converging side wall - G.MEAUZE
CIMAC 77 TOKYO (à paraître)

[3] KATSANIS T. - Computer program for calculating velocities and streamlines on a blade to blade stream surface of revolution . NACA TN D 4529 (1968).

DISCUSSION

R.Flot

Dans les premiers essais sans convergence des parois latérales, quand vous calculez le champ de pression (mi-hauteur) tenez-vous compte de la convergence?

Réponse d'auteur

Je fais un calcul purement bi-dimensionnel.

SECONDARY FLOWS WITHIN TURBOMACHINERY BLADINGS

Ph. Marchal, Research Fellow and C.H. Sieverding, Associate Professor

von Karman Institute for Fluid Dynamics
Chaussée de Waterloo, 72
B-1640 Rhode Saint Genèse, Belgium

SUMMARY

Because of the complexity of secondary flows in turbomachinery bladings and the difficulty to describe these in a theoretical sound formulation, detailed experimental investigations of the boundary layer development within the blade passages have been started recently at VKI.

The paper recalls first the VKI contribution in the field of secondary flows in compressor cascades and then presents the results of the experiments which are carried out presently on turbine cascades. The paper describes the secondary flow development under the influence of a variation of the inlet boundary layer thickness and the blade loading. Particular attention is devoted to the role of the leading edge vortex. The experimental techniques used include three-directional pressure probes, oil flow visualizations and smoke visualizations combined with the light sheet technique using illumination by laser.

LIST OF SYMBOLS

AR	aspect ratio $\frac{h}{c}$
c	chord
H_{12}	boundary layer form factor $\frac{\delta^*}{\delta^{**}}$
h	blade height
M	Mach number
P	pressure
q	dynamic head
q_{ref}	reference dynamic head $= q_{1,MS}$ for compressor cascades $= (P_{01}-P_2)_{MS,M}$ for turbine "
Re	Reynolds number
s	blade spacing
T	temperature
T_u	turbulence level
V	magnitude of absolute velocity
x	coordinate in the direction of the mid-span flow
y	coordinate normal to the wall
z	coordinate normal to x and y directions
o	throat
β	flow angle with rcspect to axial direction
γ	blade stagger angle with respect to axial direction
δ	boundary layer thickness
δ^*	boundary layer displacement thickness $\int_0^{h/2} (1-\frac{V}{V_{MS}})\, dy$
δ^{**}	boundary layer momentum thickness $\int_0^{h/2} (1-\frac{V}{V_{MS}})\frac{V}{V_{MS}}\, dy$
ϕ	blade camber angle
θ	flow turning $\beta_1 - \beta_2$
ν	kinematic viscosity
σ	cascade solidity, $\frac{c}{s}$
ω	total pressure loss coefficient $\frac{P_{01_{MS}}-P_{0_\ell}}{q_{ref}}$
ω'	total pressure loss coefficient $\frac{\overline{\overline{P_{01}}}-P_{0_\ell}}{q_{ref}}$

Subscripts

o	total or stagnation conditions
1	upstream conditions
2	downstream conditions
a	axial component
A	area averaged value
ℓ	local value
M	mass averaged value
MS	mid span
s	secondary
x,y,z	denote a component in the x,y,z direction

Superscripts

(-)	a pitchwise averaged value at a given spanwise station
(=)	an average over the entire measuring plane

1. INTRODUCTION

The lack of reliable secondary flow prediction methods, which hampers considerably the optimization of any compressor and turbine design presents in the particular case of small aspect ratio machines an insuperable difficulty for any further significant improvement of the efficiency. Every designer is faced with the discouraging problem of selecting one loss correlation between a great variety of correlations for which the loss levels differ by a factor of up to 3 and more (Refs. 1, 2). The wide scatter in the data and the heavy contradictions as to the importance of parameters like inlet boundary layer thickness, cross channel gradients and Reynolds numbers make a judicious choice impossible. The failure of the secondary loss correlations is due to the fact that, as Salvage (Ref. 2) states :"The correlations are not close enough to the fundamentals of what is essentially a boundary layer problem".

In the last years there exists an increased tendency of replacing conventional profile loss correlations by correlations based on theoretical boundary layer calculations for well specified blade profile families (e.g., Ref. 3). A similar reorientation is also very much needed for the secondary loss correlations. However, due to the difficulty of calculating the real three dimensional flow in plane cascades by the Navier-Stokes equation, one has to use at present still simplified flow models. An urgent task is therefore to obtain a better physical understanding of secondary flows in order to check the validity of the assumptions involved in such simplified calculation methods. The conventional approach of performing flow surveys only upstream and downstream of the cascade is insufficient for this task. Detailed surveys of the endwall boundary layer development throughout the whole cascade are indispensable.

Salvage's work on compressor cascades at VKI is a typical example of how a comprehensive test program, involving both overall performance tests and complete endwall boundary layer surveys, can lead not only to an improved understanding of the fundamentals of secondary flows but also provide the basis for a partial solution of the practical problem of determining loss and turning angle in three dimensional cascade flows. Due to the importance of his work a short summary of his results will be given below with the intention to confront his findings on compressor blades with the results of a similar investigation on turbine cascades which is carried out at present at VKI.

2. SALVAGE'S WORK ON SECONDARY FLOWS IN COMPRESSOR CASCADES

The blades chosen for his investigation were taken mainly from the NACA 65-series thickness distribution employed with the A_{10} camber line. The bulk of the test programme was concerned with overall performance tests for the following cascade geometries and flow conditions:

- aspect ratio, h/c : 1.0
- solidity, σ : 0.667, 1.0, 2.0
- blade camber angle, ϕ: 10°, 20°, 30°, 45°
- blade stagger angle, γ: from negative to positive stall
- inlet flow angle, β_1: 45°, 60°
- endwall boundary layer thickness to chord ratio, δ_1/c : $0.06 \leq \delta_1 \leq 0.3$
- Reynolds number based on chord and inlet velocity, Re : $2.4\times10^5 \leq Re \leq 3.3\times10^5$
- incompressible flow.

Some additional tests were carried out on blades with different blade shapes.
The detailed analysis of the endwall boundary layer development was carried out on 2 of the above NACA blades with 10° and 45° camber angle. For this purpose, 80 boundary layer traverses were made for each cascade. The main conclusions drawn by the author are summarized below :

- The mass averaged total pressure loss coefficient $\bar{\omega}'_M = \dfrac{P_{01,M}-P_{02,M}}{q_{1,MS}}$ is independent of the inlet wall boundary layer. The dependence on δ_1^* of the more classical loss coefficient $\bar{\omega}_M = \dfrac{P_{01,MS}-P_{02,M}}{q_{1,MS}}$ comes from the fact that in the balance of total pressure across the blading, the deficit of inlet total pressure due to the inlet boundary layer is considered as part of the blading loss.
- Except for the cases with low aspect ratio effects the mass averaged total pressure loss ω'_M is best predicted by Stewart et al. (Ref. 4), who relates the total loss to the profile loss via the ratio of the total wetted passage area to the wetted blade surface area.
- The loss attributable to interaction effects between sidewall and blade boundary layer was generally negligable. Exception is made for instance for cascades with a cross channel gradient that is very high near the leading edge and decreases rapidly towards the trailing edge. It is believed that severe endwall separation ("corner stall") occurs for those cascades, leading to increased losses.
- The passage vortex primarily controls the spanwise distribution of the outlet flow angle. Cascade inviscid secondary flow theory may be used to determine the distribution of the outlet flow angle because the passage vortex is an inviscid flow phenomenon.
- The conditions that are presently termed "low aspect ratio" effects (severe disturbance of mid-span flow by secondary flows) are shown to be dependent on the ratio of the inlet boundary layer thickness to blade height and on the turning of the cascade, rather than on the aspect ratio. The following criteria is proposed for the appearance of "low aspect ratio" effects :

$$\frac{\delta_1}{h} \geq .5\left(1 - \theta\,\frac{c}{h}\right) \qquad \text{with } \theta \text{ in radians.}$$

The passage vortex is the mechanism which creates effectively low aspect ratio conditions by redistributing low energy boundary layer material.

- Within the passage the resultant and streamwise velocity profile of the endwall boundary layer were observed to be fairly well described by a two dimensional turbulent boundary layer velocity profile family, except in the corner region. On the other hand, the cross flow velocity profile is not well represented by Johnston's triangular model. A three regions model seems to be required.
- When the mid-span flow field is known, it is possible to use two dimensional boundary layer methods to determine the viscous loss of the endwall flow. A simple calculation method is described in Ref. 2.

3. SECONDARY FLOWS IN TURBINE CASCADES

3.1 Experimental apparatus

3.1.1 Wind tunnels

Two different wind tunnels were used for the present investigation. The overall tests as well as the detailed survey of the three dimensional flow throughout the cascade by means of 5-hole pressure probes are performed in the large VKI low speed cascade tunnel C-1, while the flow visualization tests were made for convenience in the much smaller VKI high speed cascade tunnel C-3, which allows an easier flow observation.

The low speed tunnel is an open cycle configuration with exhaust to atmosphere at the exit of the test section. The maximum test section dimensions are 600 mm × 127 mm. For the present test series the tunnel was equipped with one movable side wall allowing blade height variations from 117 mm to 50 mm. The side wall opposite to the movable wall is equipped with exchangable rectangular steel plate inserts with provision for a probe traversing system. This arrangement allows to make endwall boundary layer traverses at various axial planes upstream of, within and downstream of the cascade (in total 14 planes).

The high speed cascade tunnel is a blowdown tunnel with exhaust to atmosphere via a diffuser. The maximum test section dimensions are 260 × 100 mm^2. The test section is formed by two circular transparent perspex side walls between which the blades are mounted. The top wall and the wall behind the trailing edge are also made from perspex blocks to enable the viewing from different directions. The test section is laid out for blades with a chord length between 30 mm and 60 mm. In the present case the test section had to accept blades from the low speed wind tunnel with 120 mm and 127 mm chord length, which entailed that only 4 blades could be accommodated. This is, however, sufficient for visualization tests.

3.1.2 Blade and cascade geometry

The tests were carried out on two gas turbine blade sections : a nozzle blade with axial inlet and a rotor blade section designed for 30° inlet angle (with respect to axial direction). The blade sections are presented in Fig. 1. The cascade geometry is given in the following table :

	Nozzle blade	Rotor blade
Chord length c	120 mm	127 mm
Space to chord ratio s/c	0,725	0,685
Stagger angle γ	-42°5	-38°5
Inlet blade angle β_1'	10°	40°
Inlet air angle	0°	30°
Arc sin (o/S)	67°7	69°8
Blade height h	100 mm	100 mm
Aspect ratio	0.83	0.79

Note : angles are measured with respect to axial direction.

3.1.3 Flow visualizations

Oil flow visualizations were made with a mixture of medium grade oil and titanium dioxyd powder which was applied evenly to both the blades and the side walls. After each blowdown, the test section (side walls with blades) was taken out off the tunnel in order to take detailed photographs of the flow patterns. Very good quality pictures were obtained at medium and high speed flow. At very low speed (below 50 m/s), two problems exist : (a) gravity influences strongly the side wall patterns and (b) bubbles of paint remain in the regions of separated flows, e.g., at the trailing edge and spread out over the blade and the side wall as soon as the test is finished.

Smoke visualizations by use of the light sheet technique is the perfect complementary test to the oil flow technique. Contrary to the oil flow technique, which visualizes flow patterns on the tunnel wall and blade surfaces, the light sheet technique allows to take sectional views of the flow in selected planes of the passage. Oil smoke is used to get a sufficient density of reflecting particles in the test section. Details about the experimental set up are given in Ref. 5. Figure 2 shows the principle of the optical system. Photographs inside the passage are difficult to obtain because of the curved channel. In order to avoid any pertubation of the inlet flow field the smoke was introduced into the settling chamber. The tests were done at very low speed (V_2 = 8 to 10 m/s). The flow visualization study on the rotor blade was made at an inlet angle of β_1 = 45° instead of 30° at which all the pressure measurements, presented herein, were made. The simple reason for this difference is that the test arrangement allowed a much better photographing of the light planes inside the passage at a higher inlet angle. For comparison reasons, the oil flow pictures were than taken at the same angle. It can be expected that a variation from β_1 = 30° to 45° does not change fundamentally the flow patterns. Hence, the qualitative results from the rotor blade visualization at 45° are also applicable to the inlet

flow angle $\beta_1 = 30°$ at which the flow field measurements are made.

3.1.4 Measuring technique

A miniaturized 5-hole probe (probe head diameter 1.2 mm, see Fig. 3) was used for the present investigation. The pressures measured by the probe are sensed by strain gauge transducers; the signals from these transducers are applied to a digital voltmeter, the output of which is punched on paper tape. This paper tape is then processed on a MITRA 15 computer.

The estimated experimental uncertainties associated with the 5-hole probe measurements are as follows :
linear position : ± .2 mm
flow angles : ± 1.0°
total pressure : ± .25 mm of H_2O ≈ 0.4% of q_{ref}.

3.2 Test program

Figures 1a and 1b show the selected measurement planes for the nozzle and the rotor cascades respectively. In each of those planes, 13 equidistant spanwise traverses were made, except for plane n° 0 (upstream plane), where only 5 traverses were made, and planes n° 10N (nozzle blade) and 9R (rotor blade), where 15 traverses were made. In each spanwise traverse, 17 measuring points were taken, from .7 mm from the wall to mid-span.

A complete flow field survey was performed in both cascades, for an inlet wall boundary layer resulting from natural development between the settling chamber and the cascade : this case will be referred to as the "thin boundary layer" case ($2\delta_1/h = .17$). The nozzle cascade was tested in addition with an artificially thickened boundary layer. This thickening was achieved by the use of vortex generators placed upstream of the cascade, just at the outlet of the settling chamber. This case will later be referred to as the "thick boundary layer" one ($2\delta_1/h = .62$). The corresponding inlet wall boundary layer velocity profiles are plotted in Fig. 4.

In order to avoid laminar separation on the rear part of the blade suction side, tripping wires ($\emptyset$ = .22 mm) were placed as indicated in Figs. 1a and 1b.

The test conditions are summarized in the following table :

	Nozzle Blade (Thin BL)	Nozzle Blade (Thick BL)	Rotor Blade
Inlet wall BL integral parameters :			
δ_1 (mm)	8.4	31.1	16.2
δ_1^* (mm)	1.10	3.75	2.05
H_{12}	1.48	1.36	1.39
Upstream total pressure P_{01} (mm H_2O)	70	70	70
Upstream total temperature T_{01} (°K)	291	291	291
Inlet air angle β_1 (°)	0.	0.	30
Outlet air angle β_2(°)	-67.8	-68.3	-69.6
Outlet velocity V_2 (ms^{-1})	32.2	32.5	32.6
Outlet Mach number M_2	.10	.10	.10
Reynolds number cV_2/ν_2	2.61×10^5	2.64×10^5	2.80×10^5
Turbulence intensity Tu (%)	.5	.5	.5

Note : angles are measured with respect to the axial direction

3.3 Test results

3.3.1 Qualitative description of secondary flows on the basis of flow visualizations

The smoke and oil flow visualizations were made at different cascade outlet velocities. The optimum speed for the smoke visualization was 8-10 m/s, while the oil flow visualizations had to be made at considerable higher velocities in order to reduce the influence of the gravity on the flow patterns. Minimum velocities were of the order of 20 to 50 m/s. depending on the blade type and the surface flow to be visualized, i.e., on the side wall or on the blade. The oil flow visualizations were extended to higher outlet velocities (up to 160 m/s) in order to check the validity of the low speed secondary flow models in the compressible flow range. In addition, the quality of the oil flow patterns improves with increasing velocities.

Langston (Ref. 6) and Sjolander (Ref. 7) were probably the first who demonstrated experimentally the importance of the leading edge vortex in turbine cascades. The present tests confirm basically their results. The light sheet technique adds, however, a new dimension, which allows a much improved interpretation of the secondary flow patterns. We shall start with the description of the flow in the rotor blade because of the stronger secondary flow effects.

Figures 5a,b,c show three smoke visualizations of the inlet flow. Figures a and b present light planes parallel to the incoming flow. These planes are situated slightly above and below the saddle point (see Fig.5d). Hence, photograph (a) is a picture of the vortex leg, which swings around the leading edge towards the blade suction side (denoted as suction side leg hereafter) while photograph (b) shows the pressure side leg which moves to the suction side of the adjacent blade. Both photographs indicate the existence of a low energy region between the first lift off point of the side wall boundary layer from the tunnel wall and the separation of the leading edge vortex from the tunnel wall.

The light plane (c) of Fig. 5 , which is taken parallel to the side wall at 5 mm distance from it, cuts nearly through the center of the leading edge vortex. The vortex core as well as the limiting streamline for the low energy region ahead of the vortex are clearly seen. The photograph shows also the nearly 90° deflection of the incoming streamlines in front of the low energy region.

The side wall oil flow patterns in Fig. 5d complete the information obtained from the smoke visualizations. Both the suction side leg of the leading edge vortex and the separation zone in front of it are reduced rapidly in size under the influence of the transverse pressure gradient. The side wall separation line of the vortex interfers with the blade suction side shortly behind the leading edge. The vortex leg continues on the blade suction side where its dark characteristic separation line is slightly visible (see Fig. 5f). The smoke visualization in Fig. 5e which is taken in the cascade outlet plane just ahead of the trailing edge demonstrates clearly the existence of this vortex on the mid-span side of the passage vortex. Its sense of rotation is opposite to the one of the passage vortex.

The pressure side leg of the leading edge vortex turns in the same sense as the passage vortex. The question is whether we can identify right from the beginning the passage vortex with the pressure side leg of the leading edge vortex or whether both exist at the beginning separately due to their different origin; the leading edge vortex exists independently of the transverse pressure gradient, while the passage vortex is due to the transverse pressure gradient and does theoretically not need the existence of a leading edge vortex (see passage vortex in curved ducts). If the second hypothesis is correct, we can nevertheless assume that both vortices cannot continue to exist separately next to each other. They will combine to form one single vortex which we shall call passage vortex. On the basis of a great quantity of smoke visualizations in Ref. 5 it seems, however, that we deal from the beginning with one single vortex only with a strong excentric vortex core formed by the leading edge vortex. An indication for this is already given by the smoke visualization in Fig. 5a and the oil flow visualization of the blade pressure side in Fig.5g. The smoke visualization shows in fact that the spanwise motion of the incoming streamlines is not limited to the near wall region, but starts almost from mid-span. This is confirmed by the oil flow pictures which show an important downwash of the pressure side streamlines towards the side wall starting from mid-span. The downwash effect is so big that we can observe a small corner separation which is indicated by a separation line on the pressure surface near the wall (see Fig. 5g). The quality of the oil flow visualization is, however, not sufficient to indicate also the corresponding reattachment line on the side wall.

The question "pressure side leg of leading edge vortex - passage vortex" will be raised again in the discussion of the secondary velocity charts. For the moment we conclude that this problem is certainly confined to the immediate leading edge zone and outside of this zone it is the passage vortex which is entirely responsible for the endwall cross flow.

Similar to the pressure side - endwall corner separation there exists a suction side - endwall corner separation. The dark lift off line of the passage vortex on the endwall along the suction side and the reattachment line on the suction side are clearly visible (Fig. 5f). For both corners we must expect the existence of small corner vortices. The origin of the suction side - endwall corner vortex lies probably in the interaction zone of the low energy region upstream of the pressure side leg of the leading edge vortex with the blade suction side.

The smoke visualization near the outlet plane in Fig. 5e shows the passage vortex center at almost half way between the suction side and pressure side. The oil flow visualizations of the blade suction surface (Fig. 5f) indicate a low energy region between the separation lines of the passage vortex and the reminder of the suction side leg of the leading edge vortex.

The above discussion concerned the rotor blade at 45° inlet flow angle (the reasons for the angle difference between the flow visualizations and the flow field measurements ($\beta_1 = 30°$) are explained in chapter 3.1.3). Figure 6 shows the corresponding flow pictures for the nozzle blade ($\beta_1 = 0°$). The flow phenomena are basically the same, but due to the smaller transverse pressure gradient, the characteristic limiting streamlines are much less pronounced.

3.3.2 Flow field measurements

Growth of losses through cascade

The losses are presented in Fig. 7 under the form

$$\bar{\bar{\omega}}_M = \frac{\overline{P_{01}}_{MS,M} - \overline{\overline{P_{01}}}_{,M}}{q_{ref}} \qquad \text{and} \qquad \bar{\bar{\omega}}'_M = \frac{\overline{\overline{P_{01}}}_{,M} - \overline{\overline{P_{0\ell}}}_{,M}}{q_{ref}} \quad .$$

The first expression includes the losses due to the inlet boundary layer while the second expression presents only the additional losses downstream of the inlet plane. Both coefficients present mass averaged values.

Due to the impossibility to traverse close enough to the blade surface, the measurements include only partially the profile losses (starting with plane 8 for the nozzle and plane 7 for the rotor blade; for position of planes see Fig. 1). In order to be consistent, Fig. 7 presents only the secondary losses which were obtained by deducing from the total measured losses the profile losses measured at mid-span.

The most interesting feature from Fig. 7a is that, after a slight increase near the leading edge plane, the secondary losses remain practically constant (within the experimental uncertainty) up to approximately 75% of the axial chord behind the leading edge, while a rapid increase of the losses is observed over the rear part of the blade. Downstream of the trailing edge the secondary losses continue to rise at the same rate up to the last measuring plane situated at a distance equivalent to ~30% of the axial chord behind the trailing edge plane. This loss variation is nearly the same for all 3 cases, i.e., nozzle blade with thin and thick inlet boundary layer and rotor blade, although the losses for the rotor blade increase at a slightly higher rate. A comparison with the flow visualizations indicates that, if the rise of secondary losses is linked to the interference of the endwall boundary layer with the suction side boundary layer, this interference effect takes only significant proportions in the decelerating zone, i.e., downstream of the throat.

The variation of the inlet boundary layer thickness from $2\delta_1/h = 0.17$ to 0.63 has no visible effect on the secondary losses $\bar{\bar{\omega}}'_M$ in the nozzle blade (Fig. 7). The effect on the profile losses measured at mid span in plane 10 remains within the measuring error.

$\bar{\bar{\omega}}_{MS} = 0.035$ thin BL $\qquad\qquad$ $\bar{\bar{\omega}}_{MS} = 0.037$ thick BL

The mid-span profile losses for the rotor blade amount to $\bar{\bar{\omega}}_{MS} = 0.052$ in the corresponding measuring plane 9 ($0.3 \times C_{ax}$ downstream of trailing edge plane).

Spanwise variation of losses and flow angles

The results are plotted in form of a pitchwise mass averaged loss coefficient

$$\omega(y) = \frac{\overline{P_{01}}_{MS,M} - \overline{P_{0\ell(y),M}}}{q_{ref}}$$

and a pitchwise mass averaged angle

$$\Delta\beta(y) = \overline{\beta_{\ell,MS}} - \overline{\beta_{\ell(y)}}$$

which presents the flow deviation with respect to the flow direction at mid-span.

The loss coefficient $\omega(y)$ is presented for the test case "nozzle blade with thin inlet boundary layer" in the Fig. 8a for the planes 0, 7, 8, 9 and 10. As already indicated before, an essential deviation from the inlet plane loss distribution starts only at plane 7 (at 75% of the axial chord behind the leading edge plane), where a single loss peak appears close to the side wall. In the trailing edge plane (plane 9), the spanwise loss distribution is characterized by two distinct loss peaks at $2y/H = 0.24$ and 0.08 and very low losses immediately at the side wall. The existence of such double peaks was already observed by Came (Ref. 8). By comparison with the suction side oil flow visualizations in Figs. 5 and 6, it appears that the first peak (starting from mid-span) can be associated with the low energy region which is visible on the photographs as white line on the blade suction side between the separation lines of the passage vortex and the suction side leg of the leading edge vortex. Downstream of the trailing edge plane, a reorganization of the losses occurs. In the last measuring plane (plane 10) the first peak has shifted towards mid-span from $2y/H = 0.24$ to 0.36 while the second peak has disappeared due to a new increase of the losses in the immediate neighbourhood of the endwall. A slight kink in the curve at $2y/H = 0.08$ remains as reminder of the second peak.

The flow deviation angle $\Delta\beta(y)$ for the nozzle blade with thin inlet boundary layer is plotted in Fig. 8b for the planes 0, 3, 5, 8 and 10. The evolution of $\Delta\beta(y)$ through the cascade is characterized up to plane 4 by an increasing overturning (positive $\Delta\beta$) near the side wall. Starting with plane 5 ($0.33\ C_{ax}$ behind the leading edge), the overturning region near the side wall is preceeded by an underturning region as a result of the increasing intensity of the passage vortex. The shift of the minimum $\Delta\beta$ from $2y/H = 0.4$ in plane 5 to 0.23 in plane 8 indicates a shift of the vortex core towards the wall, while downstream of the trailing edge an inverse trend is observed corresponding to the shift of the loss peak towards mid-span.

A comparison of $\omega(y)$ and $\Delta\beta(y)$ in plane 9 for the nozzle with thin and thick inlet boundary layer is made in Fig. 9a and 9b. The agreement of the spanwise location of the 2 loss peaks for both curves as well as their general evolution is remarkable in spite of the different loss levels. Furthermore, the variation of the inlet boundary layer thickness does in no means affect the spanwise location of the maximum underturning which differs by hardly 0.5°. It is worth noting that in an earlier test series with two dimensional pressure probes on the same blade, a variation of the aspect ratio from $h/c = 1$ to 0.4 had also no influence on the absolute distance of the maximum underturning point from the side wall, (Ref. 9).

The corresponsing results for the rotor blade are as follows (Fig. 10) :

- appearance of the first loss peak in plane 5, at 55% of the axial chord behind the leading edge plane (note that the numeration of the measuring planes is different for the nozzle blade and rotor blade, see Fig. 1);
- double peak loss in plane 7 near the outlet;
- reorganization downstream of the trailing edge plane with one single loss peak from plane 8 onwards and shift of this maximum towards mid-span. In the last measurement plane (plane 9, 0.22 C_{ax} downstream of the trailing edge plane), the loss peak is situated at the spanwise location $2y/H = 0.46$, compared to $2y/H = 0.36$ for the nozzle blade in the corresponding measuring plane;

- due to the high transverse pressure gradient both the overturning and the underturning measured with respect to the midspan flow direction) are more pronounced than for the nozzle blade;
- between plane 2 (near leading edge) and plane 5 ($0.55 \times C_{ax}$ downstream of it), the point of maximum overturning moves towards the wall, $2y/H = 0.3$ in plane 5, and moves away from it further downstream. It reaches $2y/H = 0.46$ in the last measuring plane (plane 9), which corresponds again to the position of maximum losses.

Flow charts

The evolution of local losses and velocities from cascade inlet to outlet is demonstrated at the example of the nozzle blade with thin boundary layer for which loss contour plots and secondary velocity charts are presented for several measuring planes . The loss contour plots are obtained by linear interpolation between the experimental measurement points. Iso-loss lines are plotted for ω = 1, 2, 5, 10, 15, 20 and 25%, where ω is defined as

$$\omega = \frac{\overline{P_{01}}_{MS,M} - P_{0\ell(y,z)}}{q_{ref}}$$

For the defintion of the secondary losses let us refer to Fig. 11. Use is made of a coordinate system in which in a given point P the x-axis is aligned with the midspan velocity at the same pitchwise position, y points into the spanwise direction and the coordinate z is normal to the x-y plane such that the x,y,z coordinates form a right handed system. Then, the secondary velocity vector $\vec{V}_s$ at point P will be defined as the projection of the velocity vector $\vec{V}$ at point P onto the plane y-z. For the presentation in Fig. 12 the secondary flow vector $\vec{V}_s$ is turned around the y-axis until it lies in the measuring plane such that the secondary velocity charts show the real secondary velocities and not a projection of the secondary flow velocity from the y-z plane onto the measuring plane.

Plane 3N: the two legs of the leading edge vortex are clearly apparent from the secondary velocity chart (Fig.12a). In order to simplify the interpretation of the chart, dotted lines have been drawn along a line at which the estimated dividing stream surface associated with the lift off of the incoming wall boundary layer cuts the measuring plane. The suction side leg of the leading edge vortex rotates in the opposite sense to the secondary flow generated by the cross channel pressure gradient (the "passage vortex") while the pressure side leg rotates in the same sense. An important effect of the leading edge vortex is to initiate the development of the passage vortex. Indeed, inspite of the fact that plane 3 is located just upstream of the leading edge, one can already observe the characterietic fluid motion from the pressure side to the suction side along the side wall (see also flow visualizations).

Plane 4N: two vortices are still clearly visible in Fig. 12b (approximate trajectories of the secondary velocity vectors are traced in dashed lines to facilitate the interpretation). The vortex located in the end wall suction side corner is the suction side leg of the leading edge vortex. The other one covers a much larger area and will be referred to as the passage vortex. It is characterized by an eccentric core, reminding us that it was initialized by the pressure side leg of the leading edge vortex. The loss contour plot (Fig. 12b) shows that the low energy material forming the boundary layer is entrained by the vortical motions leading to :
- a reduction of the endwall viscous layer near the blade surfaces, especially near the pressure side;
- a thickening of this viscous layer at mid pitch.

A small area of slightly higher losses (> 10%) appears in the region of converging secondary velocities at the end wall. Apart from this effect, no significant viscous forces are associated with the secondary flow, as shown by the evolution of the mass averaged, plane averaged loss factor (Fig. 7b).

Plane 6N : at this axial position, the passage vortex is centered at mid pitch and extends over the whole passage. The suction side leg of the leading edge vortex has been pushed onto the blade suction surface and its presence is only indicated by perturbations of the secondary velocity field (see Fig. 12c). The main effect of the passage vortex on the local loss distribution (Fig. 12c) is still the transport of the low energy material : the end wall viscous layer is swept from the pressure side to the suction side. A low total pressure region develops in the end wall suction side corner, where the flow separates from the wall to reattach on the blade suction side (see oil flow visualizations).

Plane 8N (Fig.12d) : it is worth noting that in this plane, located at .85 axial chord from the blade leading edge, the passage vortex is still centered at mid-pitch (and not near the suction corner). In fact, this has shown to be true up to the trailing edge plane.

A region of high losses occurs on the blade suction surface, at ~10% from the blade height from the wall (Fig. 12d). Two contributions to these losses have to be considered:
- the accumulation of low energy material originating from the end wall and blade suction side boundary layers;
- supplementary losses due to the inetraction of the secondary flow with the suction surface boundary layer. The strong convergence of the wall streamlines in the vicinity of the passage vortex separation line (see suction surface flow visualization Fig. 5f), occurring in a region where the accelerating streamwise pressure gradient has relaxed (downstream of the throat), is likely to cause severe local separation.

This last contribution is thought to be the main factor responsible for the rapid increase of the loss coefficient $\bar{\omega}'_M$ downstream of plane 7N.

The same figure reveals that the end wall viscous layer near the pressure side has been nearly completely removed by the passage vortex.

Plane 9N : the contour plot of Fig.12e shows the same features than that of plane 8N, but in an even more pronounced way. In particular, the removal of the end wall boundary layer material by means of the passage vortex, at proximity of the wall, explains why the pitchwise averaged loss in Fig. 8a decreases when approaching the wall, leading to a second maximum for the loss coefficient (the first one, closer to mid span, is associated with the interaction zone on the blade suction side).

Plane 10N : this plane is located 28% of the axial chord downstream of the trailing edge plane in the axial direction. It intersects with the blade wake and the secondary velocity chart of Fig.12f shows that, besides the passage vortex, a second vortex with opposite rotation exists in the wake. This vortex is supposed to be associated to both the trailing shed vorticity and the vorticity remaining from the suction side leg of the "leading edge" vortex.

The plots obtained from the nozzle blade tests performed with a thick inlet end wall boundary layer do not present qualitative differences from those with a thin boundary layer.

An example of the results obtained from the rotor cascade is given in Fig. 13 ("trailing edge" plane). Due to the higher flow turning, the secondary flows are stronger in this case, and one can observe that :
- the center of the passage vortex is shifted towards the suction side. It is, however, interesting to note that in the preceeding measuring station (plane 7R), the center of the passage vortex is still situated at 40% of the passage width from the blade suction surface;
- a secondary corner vortex is visible in the suction corner (dashed lines);
- the high loss region on the suction surface is bigger than for the nozzle cascade and is shifted towards midspan;
- the removal of the end wall viscous layer by the passage vortex is more pronounced in this case. The loss contour pattern approaches that of Langston et al. (Ref. 6).

3.5 Comparison with inviscid secondary flow theory

3.5.1 The inviscid secondary flow model

The inviscid secondary flow theory, where a primary potential flow convects the vortex filament that simulates the inlet end wall boundary layer, has reached the status of a classical area of fluid mechanics (e.g., Ref. 10). For this reason, we shall only briefly review those fundamental aspects of the theory which are needed for the interpretation of our results.

The computation of the secondary velocities in a plane perpendicular to the main stream direction, downstream of the cascade, requires a two step approach :
a) an estimation of the streamwise component of distributed vorticity $\xi_{s,2}$
b) the solution of the equation for the secondary stream function

$$\Delta\psi_s = \xi_{s,2}$$

A finite element method was used to deal with the second step. The secondary velocities were computed by numerical derivation.

As far as the firt step is concerned, many expression for the streamwise secondary vorticity are given in the literature, see for instance Refs. 10 or 11. For the purpose of our numerical tests, the simple expression of Squire and Winter $\left(\xi_{s,2} = 2\theta\ (dV_1/dx)\right)$ was chosen (Ref. 12).

3.5.2 Discussion of the numerical tests

In Fig. 14, the spanwise distributions of the calculated pitchwise averaged secondary velocities $V_{s,2}$ are compared with the measured ones, for the two nozzle test cases (thin and thick boundary layer). Some interesting features are apparent from this figure :
a) the general shape is well predicted;
b) the tendency of obtaining a reduced underturning when thickening the inlet wall boundary layer is well indicated; the predicted magnitude of this underturning is, however, not correct (thick boundary layer case);
c) the predicted point of maximum underturning is located at a distance from the wall equal to the inlet wall boundary layer thickness δ_1

The last feature is a general result confirmed by many numerical tests, and constitutes perhaps the most severe limitation of the simple inviscid secondary flow approach. Actually, the outlet flow patter, was experimentally found to be largely independent of δ_1. This failure of the theory is in fact not surprising, since most of the hypotheses needed for its application are violated (high turning angle, skewing of stream surfaces, viscous effects, etc.).

Having this in mind it must be noted that the surprisingly good agreement between the predicted and measured magnitude of the maximum underturning in Fig.14a has to be considered as a coincidence, since the expression used for $\xi_{s,2}$ (Squire and Winter, Ref. 12) is in principle not valid for a large turning cascade.

The next step in the theoretical approach will be the fully tridimensional inviscid flow field computation. Although it does not take into account any viscous effect, it has the advantage of not being restricted to small perturbations. The three dimensional program is currently under development at VKI and is based on the solution of the Euler equations using a time marching procedure.

4. SECONDARY FLOWS IN COMPRESSOR AND TURBINE CASCADES - A PRELIMINARY COMPARISON

In the following, the main results of the herein presented tests are confronted with the conclusions of Salvage's work on compressor cascades :

- the secondary losses for both turbines and compressor cascades seem to be independent of the inlet boundary layer;
- contrary to the compressor cascades, the interaction effects between end wall boundary layer and suction side boundary layer are not negligible;
- the passage vortex controls the outlet angle distribution for both types of cascades, however, in the case of turbine cascade the simplified secondary flow theory does not predict correctly the position and intensity of the passage vortex. Hence, the outlet angle distribution is not well predicted. Cases with good agreement are due to a fortunate combination of inlet boundary layer thickness and turning angle;
- the skewing of the end wall boundary layer is much more important for turbine than for compressor cascades;
- the flow phenomena associated with the leading edge vortex are found to be significant in turbine cascades with thick leading edges. Similar observations have not yet been made for compressor bladings.

5. CONCLUSIONS

An experimental investigation of the three dimensional flow field in turbine cascade was performed. The use of the light sheet technique in addition to oil flow visualizations and 5-hole probe measurements allowed for an improved interpretation of the flow patterns :

- due to the presence of the blade leading edge, the inlet end wall boundary layer separates from the wall in front of the blade nose and rolls up into a vortical motion : it is the so-called leading edge vortex. The vortex leg wrapping along the suction side of the blade rotates in the opposite direction to the secondary flow generated by the cross channel pressure gradient. Therefore, its size rapidly diminishes as soon as it penetrates into the blade passage, while it is in the same time pushed on the blade suction surface where it continues on the mid-span side of the passage vortex. On the other hand, the pressure side leg of the leading edge vortex initiates the passage cross flow and rapidly develops into the passage vortex. The center of the passage vortex in the trailing edge plane moves from mid-channel width for the nozzle blade towards the blade suction side for the rotor blade. Downstream of the cascade, the vorticity associated with the suction side leg of the leading edge vortex combines with the trailing shed vorticity into a single vortical motion, centered in the blade wake, and rotating in opposite sens to the passage vortex.
  The existence of two corner vortices of very small extension appears from the close examination of the experimental data.
- a low energy region exists between the primary separation line of the inlet end wall boundary layer and the following lift off line of the leading edge vortex. The importance of this low energy region depends strongly on the cross channel pressure gradient. Within the blade passage the main effect of the leading edge vortex and the subsequent passage vortex on the end wall boundary layer is to remove it from the end wall. The low energy material is transported from the pressure side to the suction side, allowing a new boundary layer to grow. No significant losses are associated with this process. However, downstream of the throat, the interaction of secondary flows with the blade suction side boundary layer results in a rapid rise of the loss. It is worth noting that within the limit of our tests this rise was independent of the inlet boundary layer thickness, but increased slightly with increasing load;
- the outlet flow angle is controlled by the passage vortex. The inviscid tbeory of secondary flows gives a reasonable qualitative agreement, but fails to give the correct position and magnitude of the maximum underturning. The next step must be the solution for the full three dimensional inviscid flow field.

REFERENCES

1. CHAUVIN, J.: Turbine cascade end wall losses - a review.
   von Karman Institute, LS 72 "Secondary Flows in Turbomachines", January 1975.
2. SALVAGE, J.W.: Investigation of secondary flow behaviour and the end wall boundary layer development through compressor cascades.
   VKI TN 107, June 1974.
3. DENTON, J.D.: A survey and comparison of methods for predicting the profile loss on turbine blades.
   Inst. Mech. Engrs, Conf. Publ. 3, 1973, pp 204-212.
4. STEWART, W.L.; WHITNEY, W.J.; WONG, R.Y.: A study of boundary layer characteristics of turbomacbinery blade rows and their relation to overall blade loss.
   ASME Transact., Series D "J. of Basic Engrg", Vol. 82, 1960, pp 588-592.
5. SIEVERDING, C.; GODDARD, M., YEUNG, : Visualization study of the flow in plane cascades by use of the light sheet technique.
   VKI - in preparation.
6. LANGSTON, L.S.; NICE, M.L.; HOOPER, R.M.: Three dimensional flow within a turbine cascade passage.
   ASME Paper 76 GT 50, 1976.
7. SJOLANDER, S.A.: The end wall boundary layer in an annular cascade of turbine nozzle guide vanes.
   Carleton U., Dept. Mech. & Aeron. Engrg, Ottawa, Canada, TR ME/A 75-4, December 1975.
8. CAME, P.M.: Secondary loss measurements in a cascade of turbine blades.
   Inst. Mech. Engrs, Conf. Publi. 3, 1973, pp 75-83.
9. SIEVERDING, C. & MARCHAL, Ph.: Film cooled small turbine research. Vol. 1 - Aerodynamic study of secondary flows.
   VKI June 1976.

10. HORLOCK, J.H. & LAKSHMINARAYANA, B.: Secondary flows: theory, experiment and application in turbomachinery aerodynamics.
Annual Review of Fluid Mechanics, Vol. 5, 1973, pp 247-280.
11. CAME, P.M. & MARSH, H.: Secondary flow in cascades : two simple derivations for the component of vorticity.
J. Mech. Engrg Sc., Vol. 16, No 6, 1974, pp 391-401.
12. SQUIRE, H.B. & WINTER, K.G.: The secondary flow in a cascade of airfoils in a non uniform stream.
J.Aeron. Sc., April 1951, pp 271-277.

ACKNOWLEDGEMENTS

This work was partially sponsored by the European Research Office of the US Army under Grant Number DA-ERO-75-G-074.

The authors whish to express their gratitude to J.P. Craissac who did much of the experimental work.

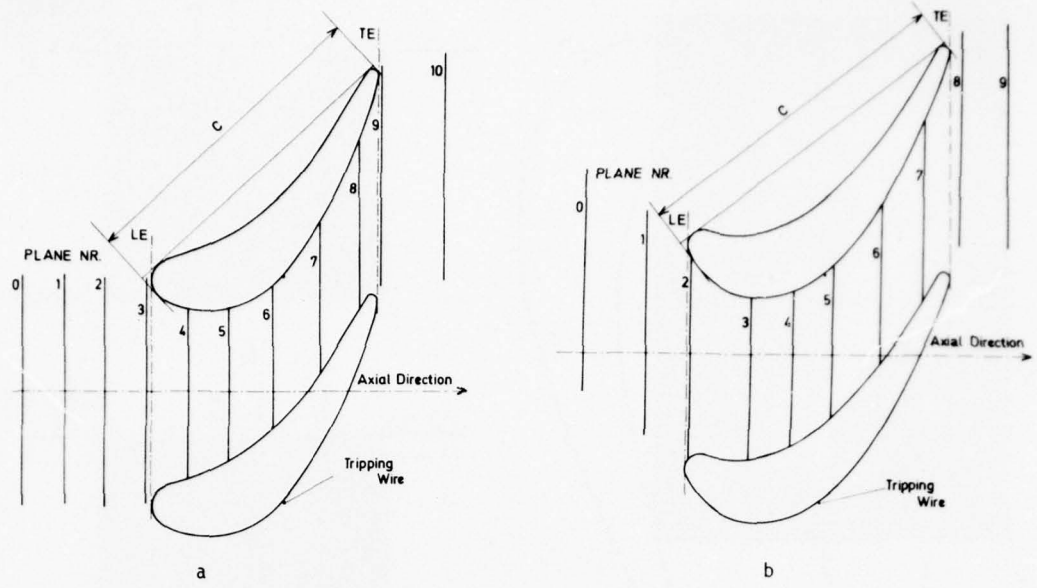


FIG. 1 BLADE PROFILES WITH MEASURING PLANES

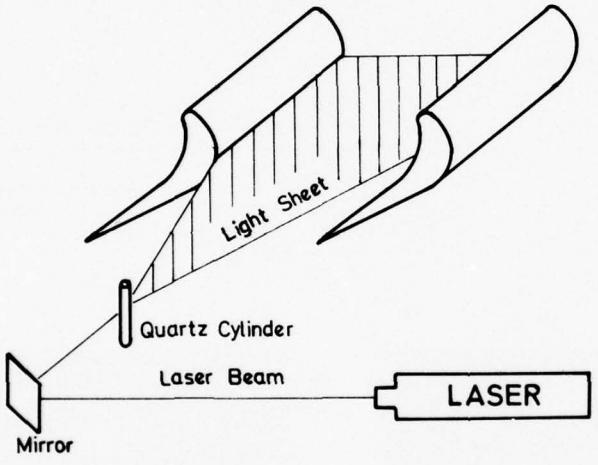


FIG. 2 SET UP FOR LIGHT SHEET TECHNIQUE

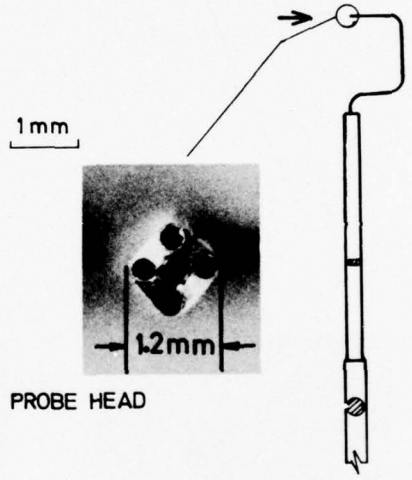


FIG. 3 FIVE HOLE PROBE

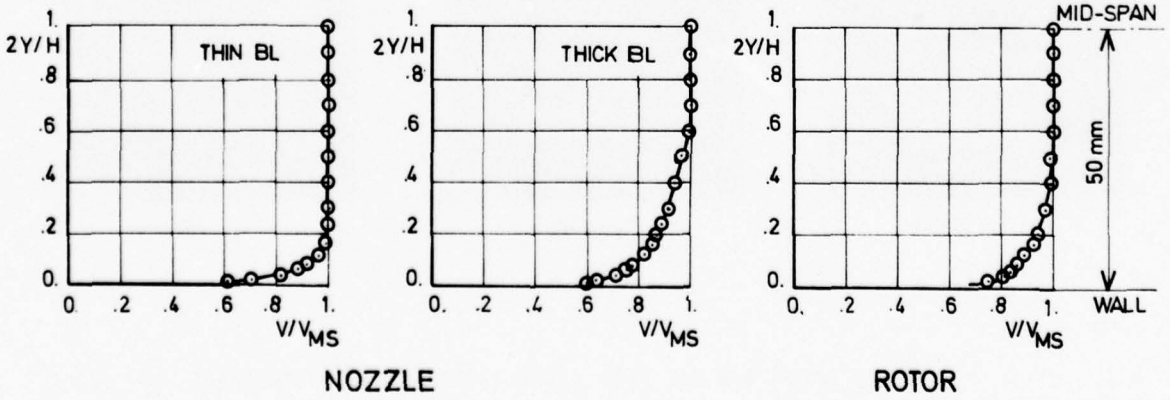
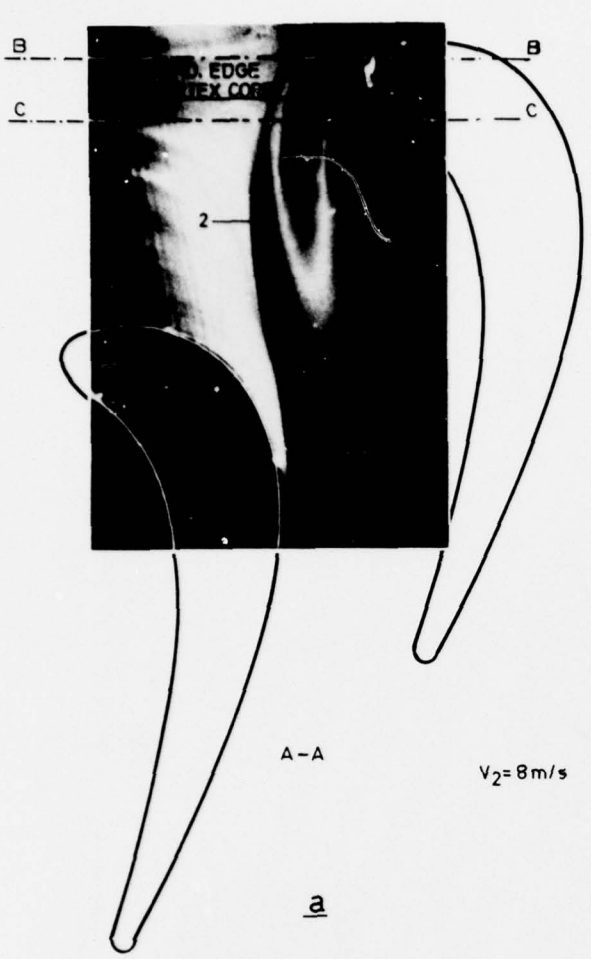
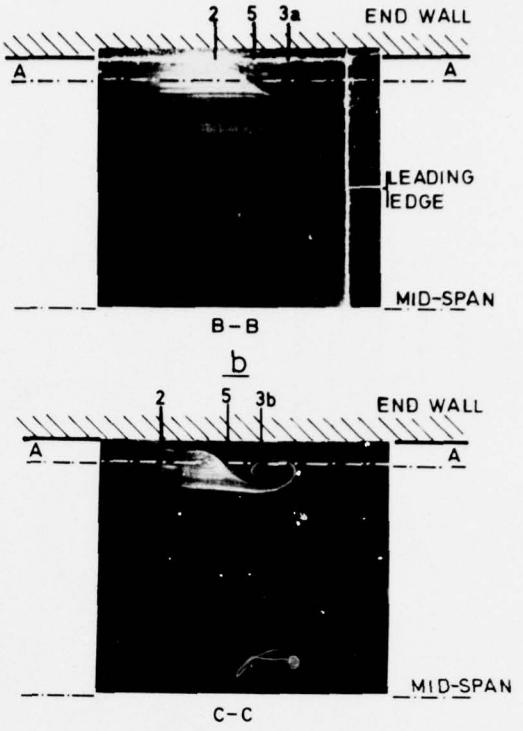


FIG. 4 INLET END WALL BOUNDARY LAYER PROFILES





1. Saddle point
2. Separation line of inlet end wall boundary layer
3a. End wall separation line of suction side leg of leading edge vortex
3b. End wall separation line of "pressure side leg of leading edge vortex" and or passage vortex
4. Start of suction side end wall corner vortex
5. Low energy region



FIG. 5 SMOKE AND OIL FLOW VISUALIZATIONS FOR ROTOR BLADE

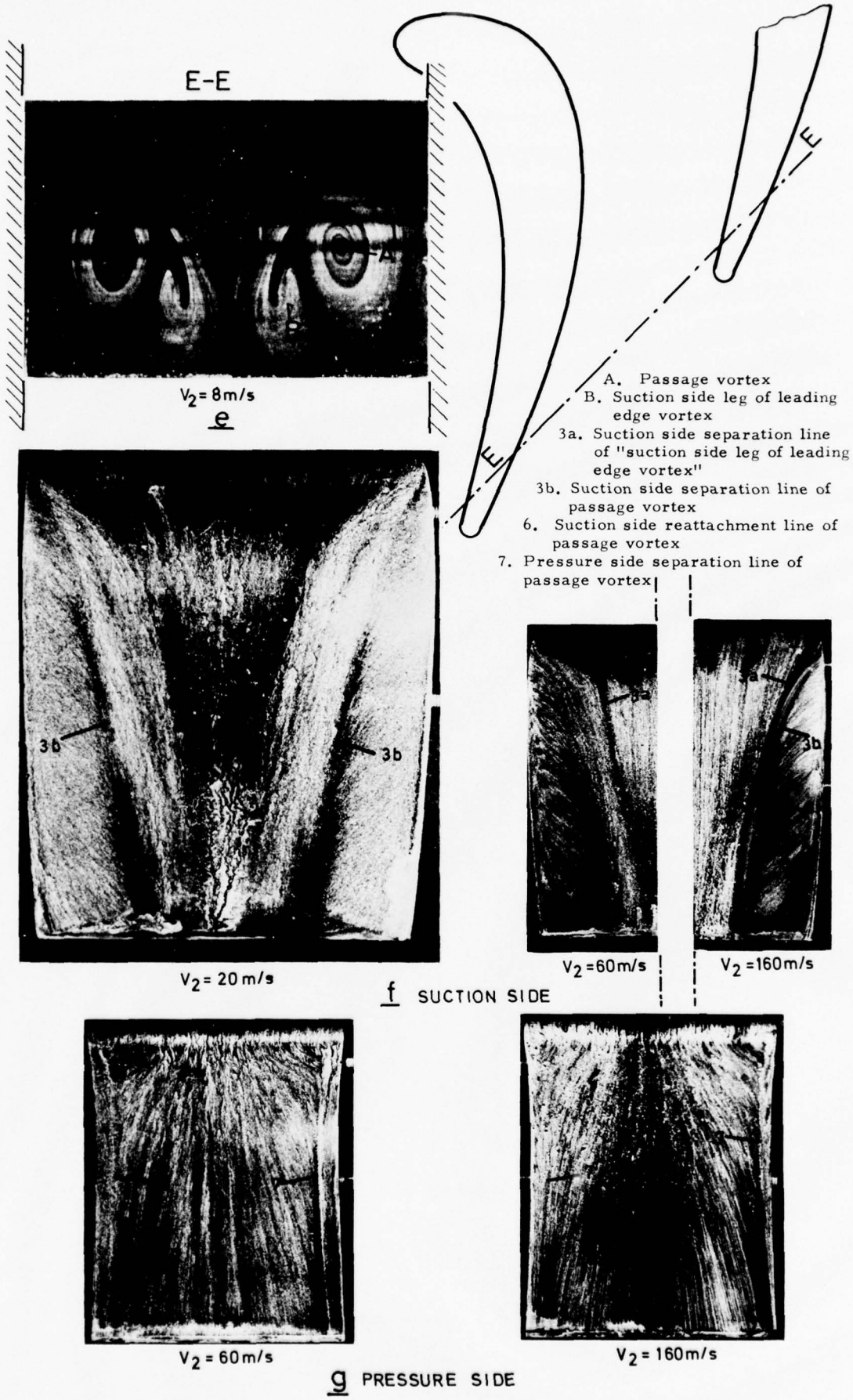
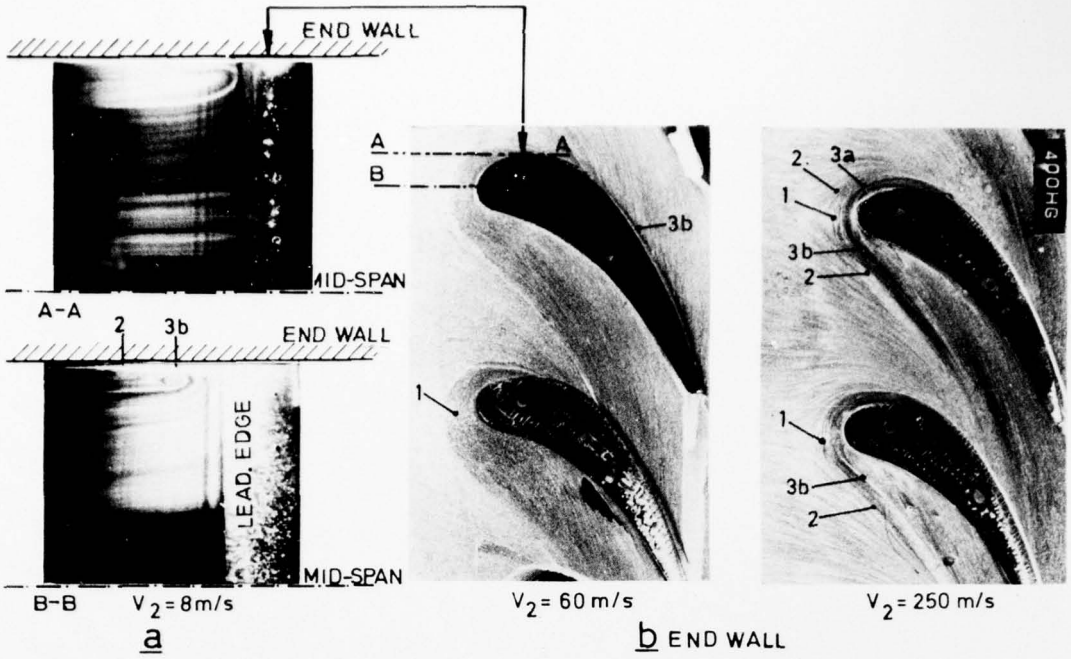
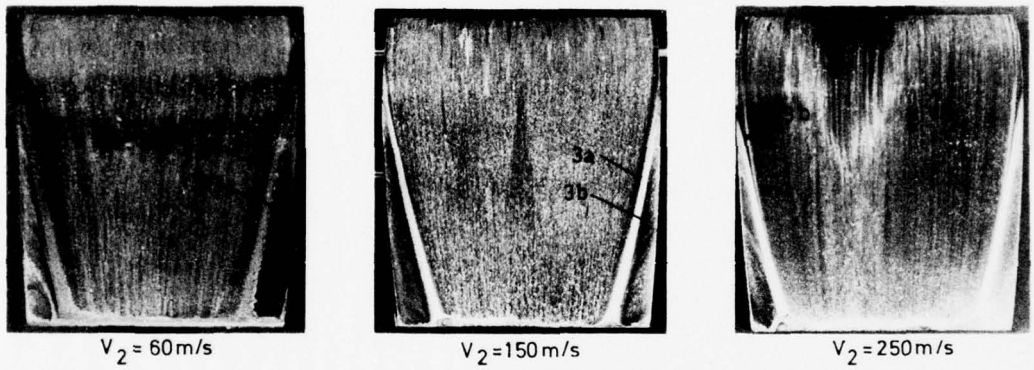
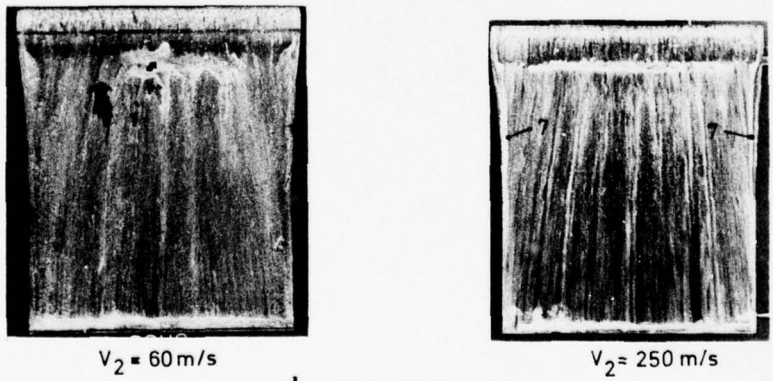


FIG. 5 SMOKE AND OIL FLOW VISUALIZATIONS FOR ROTOR BLADE (continued)







1. Saddle point
2. Separation line of inlet end wall boundary layer
3a. End wall separation line of suction side leg of leading edge vortex
3b. End wall separation line of "pressure side leg of leading edge vortex" and/or passage vortex
7. Pressure side separation line of passage vortex

FIG. 6 SMOKE AND OIL FLOW VISUALIZATIONS FOR NOZZLE BLADE

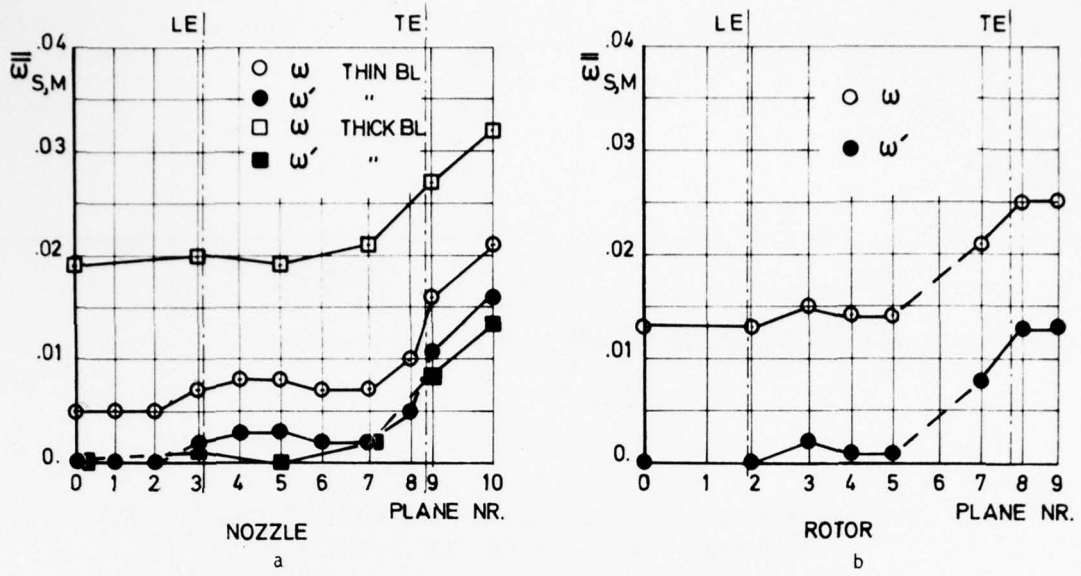
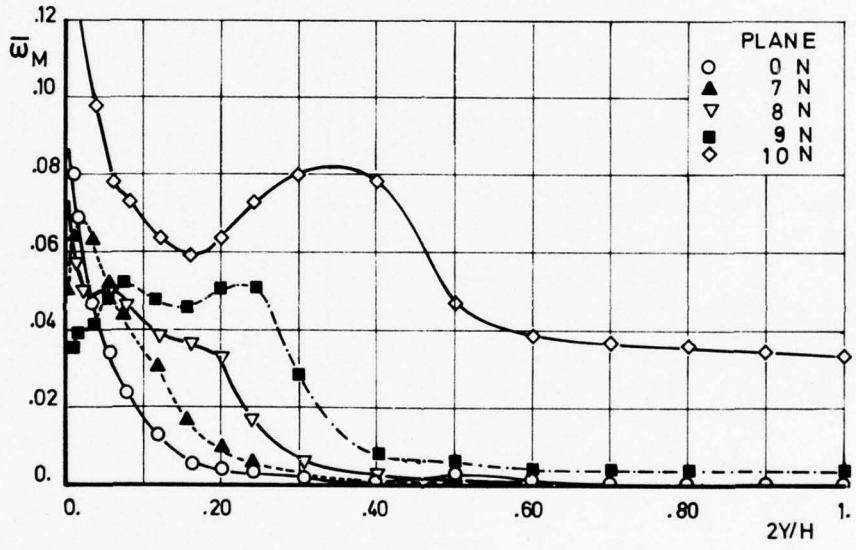


FIG. 7 GROWTH OF LOSSES THROUGH THE CASCADES



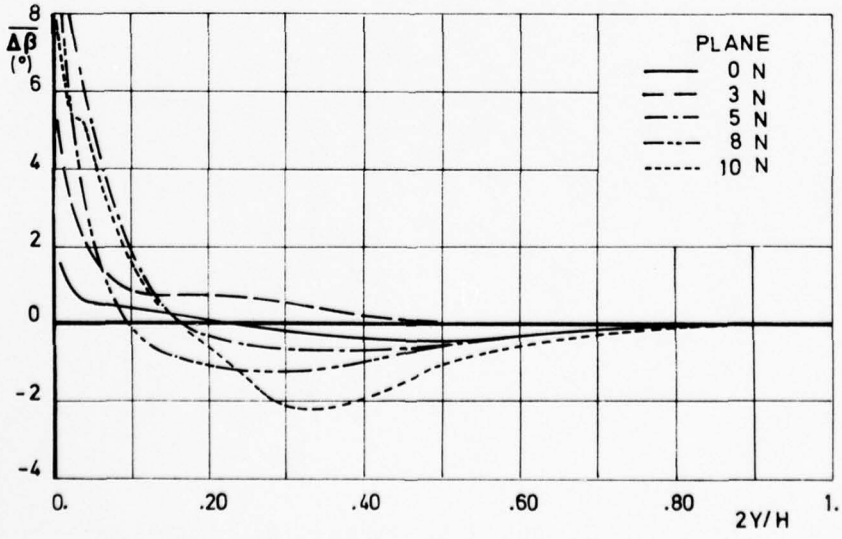
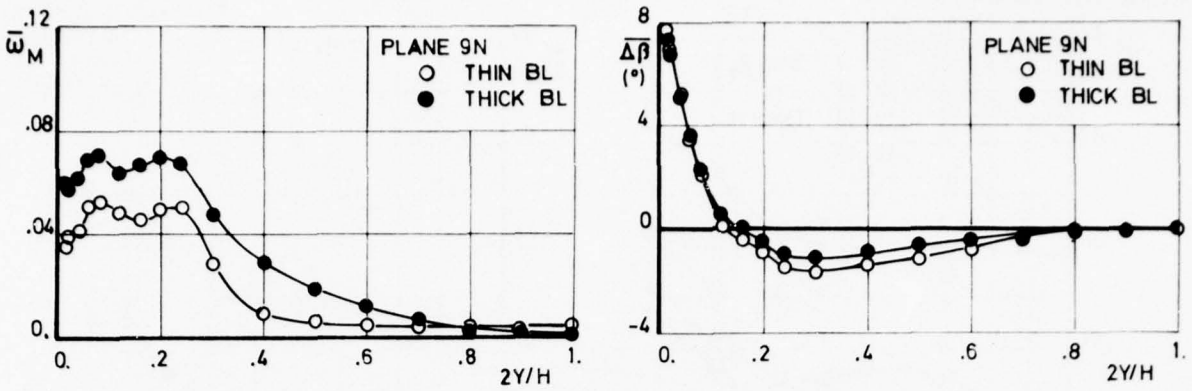
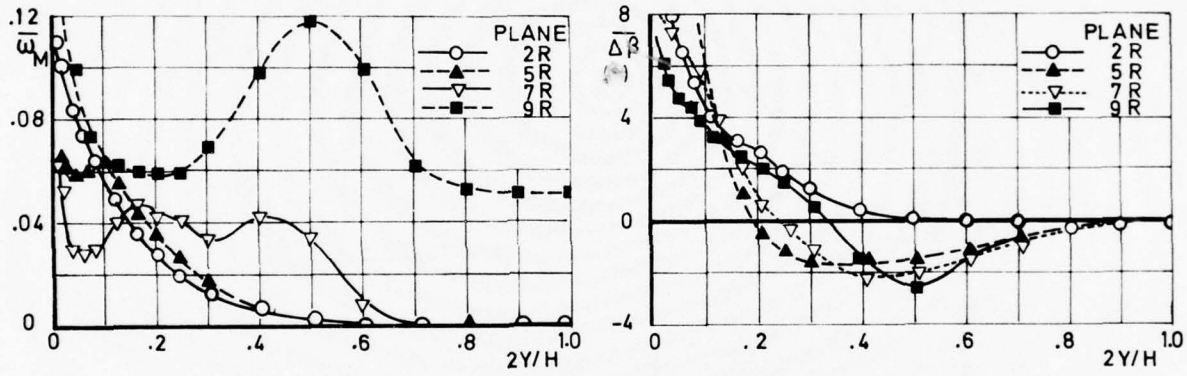


FIG. 8 SPAN-WISE LOSS AND ANGLE DISTRIBUTIONS FOR NOZZLE BLADE



a b

FIG. 9 COMPARISON OF SPAN-WISE LOSS AND ANGLE DISTRIBUTION FOR TWO BOUNDARY LAYER THICKNESSES (NOZZLE BLADE)



a b

FIG. 10 SPAN-WISE LOSS AND ANGLE DISTRIBUTIONS FOR ROTOR BLADE

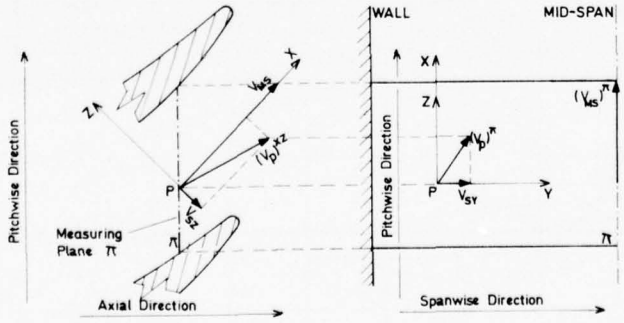
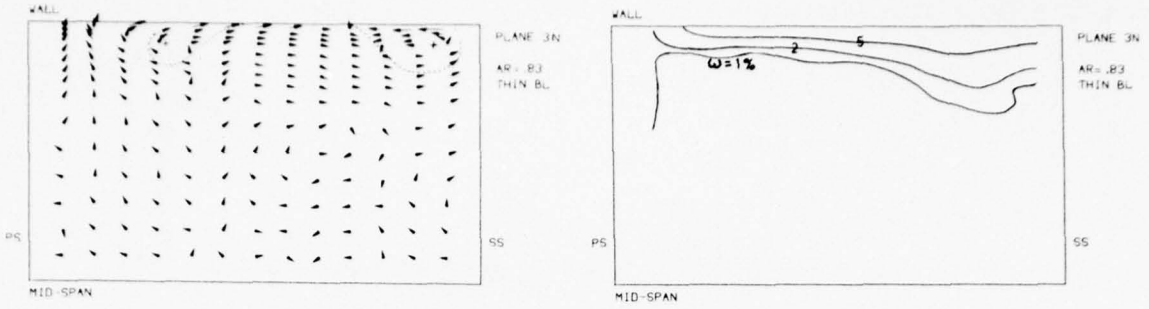
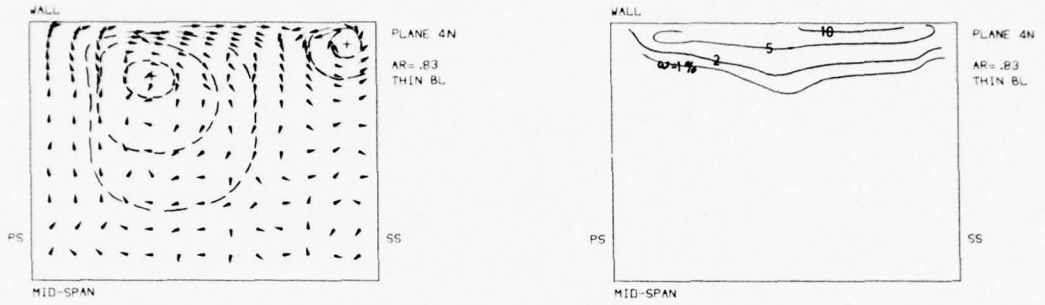


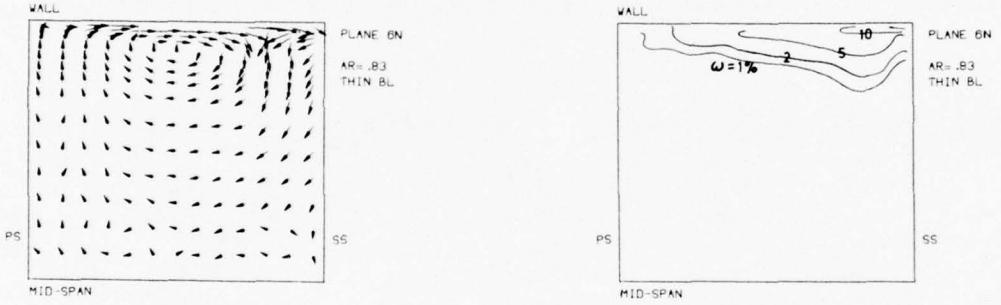
FIG. 11 DEFINITION OF SECONDARY VELOCITY COMPONENTS



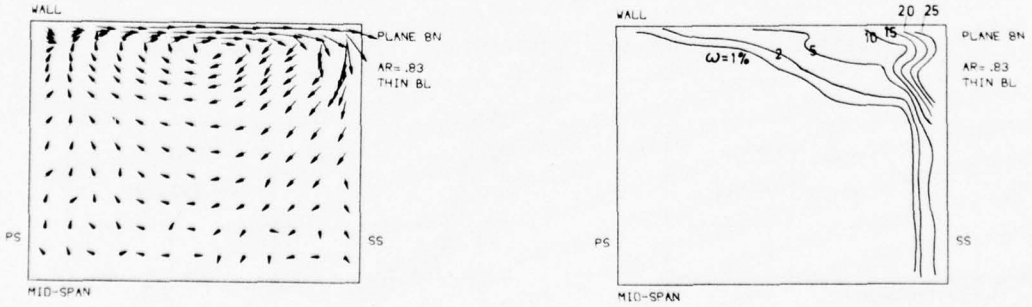
a



b

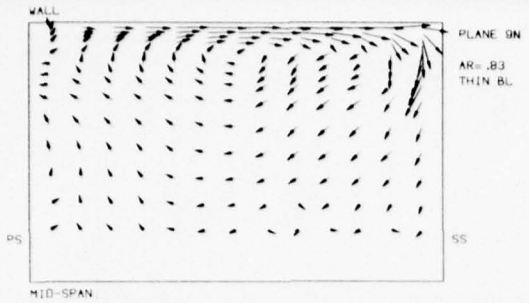


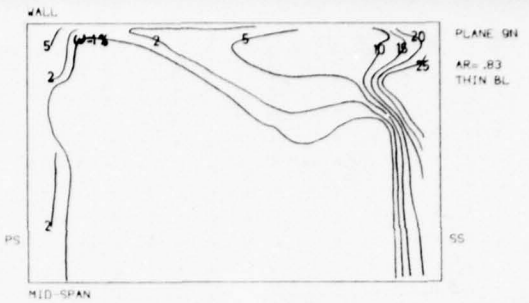
c



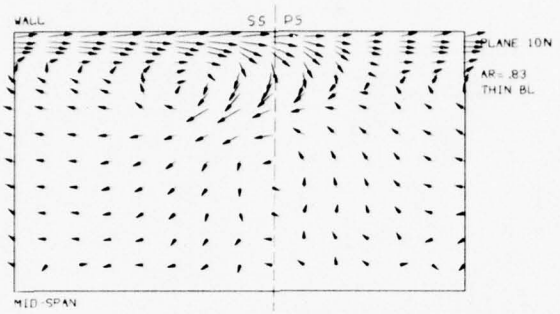
d

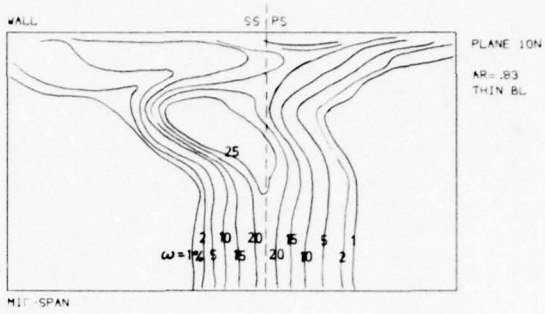
FIG. 12 SECONDARY FLOW CHARTS AND LOSS CONTOUR PLOTS FOR NOZZLE BLADE





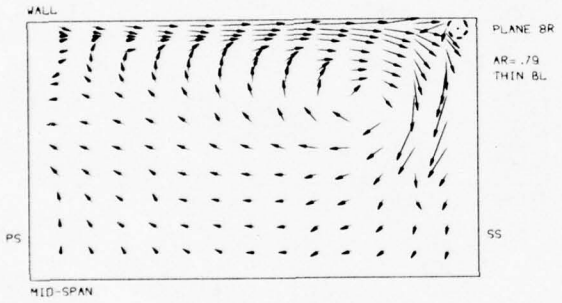
e





f

FIG. 12 SECONDARY FLOW CHARTS AND LOSS CONTOUR PLOTS FOR NOZZLE BLADE (continued)



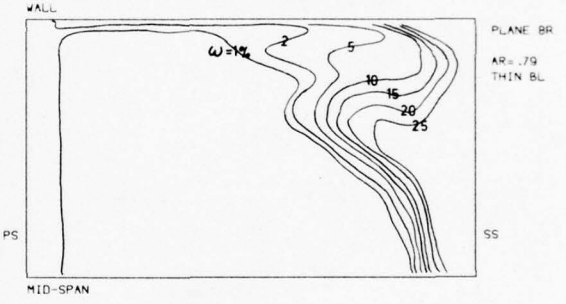
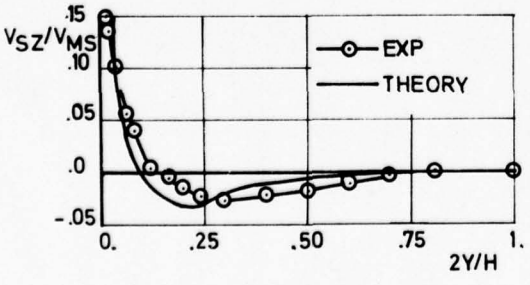
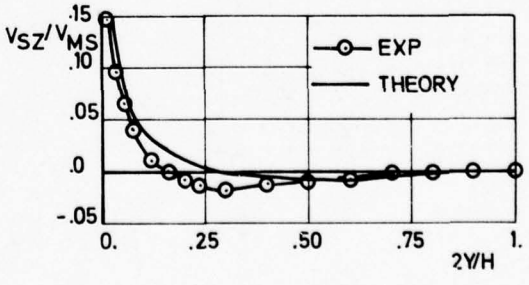


FIG. 13 SECONDARY FLOW CHART AND LOSS CONTOUR PLOT FOR ROTOR BLADE



a- thin boundary layer



b - thick boundary layer

FIG. 14 COMPARISON OF THEORETICAL AND EXPERIMENTAL SPAN-WISE VELOCITY DISTRIBUTION FOR NOZZLE BLADE

DISCUSSION

N.A.Cumpsty

I compliment you on superb flow visualization – we can learn more from this than many quantitative measurements.

Were losses on an area average basis?

Author's Reply

The losses are calculated on a mass average basis.

G.Servoy

Please comment on the relationship between the cascades geometries, the qualitative information and the quantitative results obtained in these experiments, and the results reported by N.A.C.A. between 1950 and 1953 (Hansen, Herzig, Costello, Kofskey, and others. .).

Author's Reply

The studies mentioned by Serovy are presented in NACA Report 1163, as far as plane cascades are concerned. They consisted in flow visualizations in low turning compressor cascades and higher turning sheet metal bends and cascades (45° and 60°).

The highest turning is still less than the lowest turning used in the present tests. Moreover, sheet metal blades lack the presence of the rather blunt trailing edge of our blades which is an important parameter with respect to the leading edge vortex. Any detailed comparison is still further impaired by the use of different smoke visualization techniques. However, it is worth noting that the NACA authors do mention that the boundary layer flows in cascades are noticeably different from those in bends as a result of what the authors call the "nose effect", which can be looked at as an effect of the leading edge vortex.

K.Papailiou

Where is the peak velocity on the blade suction side of the experimental cascades?

Could you give the complete velocity distribution?

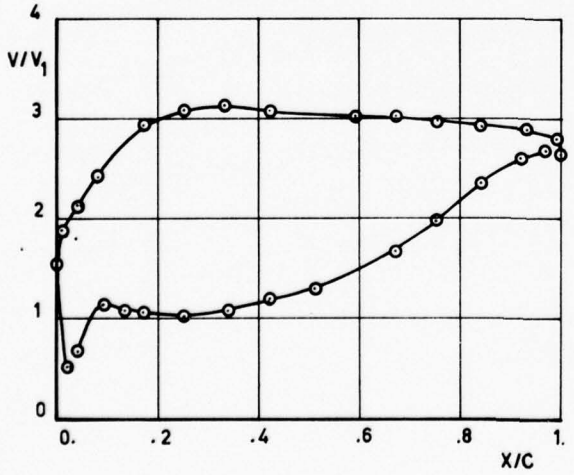
Author's Reply

The experimental velocity distributions at mid-span are given in the following two figures for the two blade profiles. The measurements were made for an aspect ratio of about 1 and an inlet velocity of about 10 ms^{-1}.

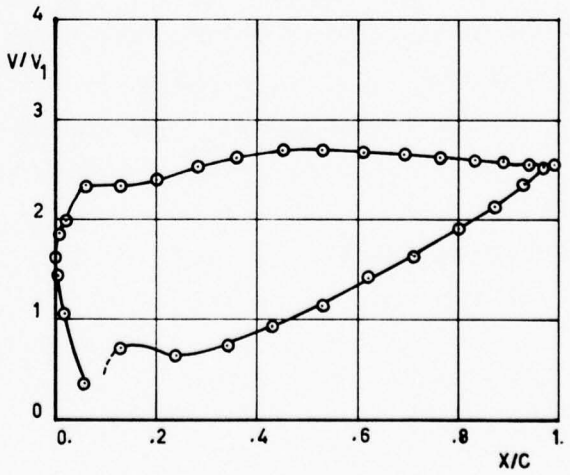
V_1 : inlet velocity

C : Chord length

X : Distance from the leading edge, measured along the blade chord.



NOZZLE



ROTOR

W.Schlachter

You were talking about the two branches of the leading-edge vortex; the first one passing along the suction side and turning *opposite* to the passage vortex; the second one passing from the pressure side to the suction side and turning in the same direction as the passage vortex.

You made the statement that the last-mentioned vortices cannot be distinguished. Is this due to a lack of flow visualization or is it reality? Could you comment more on that?

Author's Reply

The question of the undistinguishability of the pressure side leg of the leading edge vortex and the passage vortex is already partially discussed in the written version of the paper. It is mentioned there that those vortices are generated by different causes, and hence we can imagine that the pressure side leg of the leading edge vortex and the passage vortex can temporarily exist separately next to each other. On the other hand, it could be argued that the pressure field associated with the curved channel will simply amplify the secondary flows generated by the presence of the leading edge.

The question remains open.

C.H.Sieverding

We have been for a long time discussing the possibility of two vorticies rotating side by side in the same sense. Physically this doesn't seem to be possible to exist for a long distance. From close examination of several light planes close to each other we have been able to trace only one single vortex center which moved rapidly away from the pressure side and the end wall. If you look for instance, on the secondary flow chart (first picture we showed) you will notice that the passage vortex has still a very eccentric core which is located in the corner of the pressure side end wall.

P.Runstadler

The flow visualization work of this paper is excellent and the authors should be praised for their efforts. In the techniques used, the results obtained at a plane downstream depend upon a change in the density of particles. If a pattern changes locally, then the techniques will take some time for the new density variations to be evident in the flow (i.e. some distance in the downstream direction for the flow changes to be apparent).

I am not suggesting that changes are taking place in the flows shown in the paper – in fact the multiple plane photos plus the pressure data suggest otherwise – but rather that one should be aware and on the lookout for such an effect in the visualization technique used.

INFLUENCE OF SECONDARY FLOW EFFECTS ON BLADE SURFACE PRESSURE MEASUREMENTS IN 2-D TRANSONIC TURBINE CASCADES

Dipl.-Ing. Hans-J. Heinemann
DFVLR-AVA
Bunsenstraße 10
D - 3400 Göttingen

SUMMARY

In the case of a turbine cascade with high deflection, surface pressure measurements are carried out in different planes of the blade height. The height of the instrumented blade is twice as much as usual and the blade can be moved through the end-walls. Thus it is possible to take measurements in different planes with the same tappings. The ratio of the blade height to the blade length is slightly larger than two.

The tests were performed in the DFVLR-AVA plane cascade tunnel for a subsonic, transonic and supersonic Mach number. The inlet angle and the pitch/chord ratio is varied. The flow is visualized by oil flow pictures of the blade surface taken during the windtunnel runs. This method is also used for motion pictures in which the flow behaviour on the blade surface is observed for a high-turning rotor cascade and a stator cascade.

LIST OF SYMBOLS

β_1	inlet angle	p_{01}	upstream total pressure
b	height of the blade	p (x/c)	local pressure on the blade surface
c	chord length of the blade	x	coordinate in chord length direction
γ	stagger angle	s	blade contour coordinate
g	pitch length	$\varkappa$	isentropic exponent
M_1	upstream Mach number	β_2	outlet angle
M_2	downstream Mach number (isentropic)		
c_{p1}^*	pressure coefficient		

1. INTRODUCTION

On the problem of secondary flow effects in turbomachines and cascades a large amount of theoretical and experimental work has been published (see for example [1, 2, 3, 4, 14]. The investigations were carried out for compressor stages [5] and deceleration cascades [6] as well as for turbine stages [7] and acceleration cascades [8, 9] . Also flow visualisation experiments are done for a better physical understanding of the flow through the blade passage [10] .

The aim of the experimental investigations, which are described here, is to show the influence of the end-walls for surface pressure measurements of a turbine cascade of high deflection. This is of interest particularly for transonic flow - i.e. subsonic flow at the inlet-plane and supersonic flow at the outlet-plane -, because the calculation methods of such flows are nowadays at a satisfactory standard, mainly in the case of calculating the pressure distribution. If theoretical results are compared with the experiments, it is necessary to know how reliable those measurements really are.

2. EXPERIMENTAL FACILITY

2.1 WINDTUNNEL FOR 2-DIMENSIONAL CASCADES

The cascade-windtunnel of the DFVLR-AVA is a blow down tunnel. A detailed description of the facility is given in [11] . There is a rectangular nozzle upstream of the cascade and either a free jet or in some cases a tail-board downstream. The test section can accomodate up to about 16 blades (figure 1) depending on the geometry of the cascade and on the inlet angle β_1. In general the blade chord, c, is 60 mm and the blade height, b, is 125 mm. Thus the height/chord ratio, b/c, is 2.08. For taking Schlieren pictures the blades are fixed within the glass-wall with the aid of two pins at each side of the blade.

2.2 SURFACE PRESSURE MEASUREMENTS

In the case of surface pressure measurements the glass-walls are replaced by steel-walls. Usually the instrumented blade is fixed with two pins in the one steel-wall and in the other steel-wall by a steel plate. Figure 2 shows the profile used and the locations of the 26 tappings. To measure the surface pressure always with the same tappings the length of the instrumented blade is twice as much as usual and it is led at the end-walls through holes, which were casted with casting resin. Between the casting resin and the instrumented blade there is a sealing, which is pressed by a plate against the steel-wall. Figure 3 shows a picture of the cascade with the instrumented blade and also the mechanism by which it is possible to move the blade to the different planes of its height. A gauge shows the position of the tapping plane.

The surface pressure is measured with a pressure transducer, digitalized, punched on tape, and plotted.

2.3 OIL FLOW PICTURES

For a better physical understanding of the flow on the blade surface oil flow pictures are taken. The behaviour of the oil mixture photographed by a camera with 25 frames per second shows the development from starting the windtunnel during the running time to the turn off. These experiments can give a qualitative impression of the flow behaviour. The method is used for two different turbine cascades, a stator and a rotor turbine cascade. The first one has a deflection of about 60 degrees and the second one a deflection of about 110 degrees. In figure 4 a sketch shows how the oil flow pictures are photographed. In the case of the rotor blades the cascade is turned upside down for better observation.

3. SURFACE PRESSURE MEASUREMENTS IN DIFFERENT PLANES OF THE BLADE HEIGHT

3.1 TEST PROGRAMM

The investigated cascade is shown in figure 1 and the instrumented blade with the positions of the tappings in figure 2. The geometry of the cascade is given by the stagger angle $\gamma = 70^{\circ}$ and the pitch/chord ratio $g/c = 0.5$ and 0.6 . The inlet angle β_1 is 115°, 130° and 147°. Three different down-stream Mach numbers M_2 are investigated: a subsonic, transonic and supersonic one. The computation of the Mach number is based on the pressure in the test chamber. Thus the losses of the cascade are not included. The maximum deflection is about 110° at the inlet angle of $\beta_1 = 147^{\circ}$.

The measurements are carried out in six ($g/c = 0.5$) or respectively seven ($g/c = 0.6$) different planes of the blade height (figure 5). In all cases the construction did not allow to take measurements in the middle of the blade height. The first plane is 12 mm out of the mid-span. All the following planes are spaced at 8 mm distance. The closest distance of the plane to the end-wall is 2.5 mm ($g/c = 0.6$). It is supposed that the flow is symmetrically to the mid-span plane. So the experiments are performed only on one half of the blade height.

3.2 TEST RESULTS

The non-dimensional pressure coefficient, which is given in figures 6 to 9, is defined by:

$$c_{p1}^{*} = \frac{p(x/c) - p_1^{*}}{p_1^{*}} \qquad (1)$$

$$p_1^{*} = \left(\frac{2}{\varkappa + 1}\right)^{\frac{\varkappa}{\varkappa - 1}} \cdot p_{01}$$

This means that sonic velocity occurs at $c_{p1}^{*} = 0$. $c_{p1}^{*} > 0$ represents a subsonic velocity and $c_{p1}^{*} < 0$ a supersonic velocity. All possible values of c_{p1}^{*} are within

$$-1 < c_{p1}^{*} < \left(\frac{\varkappa + 1}{2}\right)^{\frac{\varkappa}{\varkappa - 1}} - 1$$

In the case of air:

$$-1 < c_{p1}^{*} < 0.892$$

The pressure coefficient is plotted versus the blade contour coordinate, s. The three-dimensional plots are divided into the pressure side (tapping 1 to 11) and the suction side (tapping number 12 to 26).

The third coordinate represents the blade height, beginning at the mid-span plan and ending at the end-wall. The positions of the different planes are indicated in the diagrams.

3.2.1 PRESSURE SIDE

Figure 6 shows the results of the pressure side for the investigated flow conditions in the case of $g/c = 0.6$. It can be seen that only in the case of the largest inlet angle $\beta_1 = 147^o$ a variation of the pressure distribution from the third to the fourth plane appears. This means that for this inlet angle the pressure distribution on the blade is not influenced by the end-walls for about 50 percent of the blade height. At all other flow conditions a significant variation appears only close to the end-wall, in most cases only at the last plane. The strength of variation depends mainly on the inlet angle, while the influence of the Mach number for constant inlet angle (for example $\beta_1 = 130^o$) is small. The same effect is observed in the case of pitch/chord ratio $g/c = 0.5$ which is not shown in the diagrams.

3.2.2 SUCTION SIDE

The results for the three different Mach numbers for the inlet angle $\beta_1 = 115^o$ ($g/c = 0.5$) are given in figure 7 together with the corresponding Schlieren pictures. Also for the suction side an influence of the end-walls is only realized at the measuring planes closest to the end-wall. For more than 50 percent of the blade height the flow is sufficiently uniform for all Mach numbers. The Schlieren pictures show a thickening of the boundary layer on the suction side starting at $x/c \approx 0.55$. At $M_2 = 0.921$ a local supersonic flow field occurs on the blade, c_{p1}^* is smaller than zero in this area.

Figure 8 shows the results of the measurements for the lowest Mach number and the different inlet angles $\beta_1 = 115^o$, 130^o and 147^o ($g/c = 0.6$). Only at $\beta_1 = 147^o$ spanwise variations of the pressure distribution are observed, for all other inlet angles the variations are small. But even at $\beta_1 = 147^o$ the first three planes are apparently not affected. The Schlieren pictures are shown for $\beta_1 = 130^o$ and 147^o. At $\beta_1 = 147^o$ a supersonic flow region appears close to the leading edge at the suction side, due to a very high acceleration of the flow around the leading edge. The flow seems to separate at this position. This phenomenon can be seen better in the Schlieren picture of figure 9, showing the results for the highest Mach number. The Schlieren picture for $\beta_1 = 147^o$ shows a very strong separation, which starts on the suction side of the leading edge. In such cases a good two-dimensionality of the flow cannot be expected. At $\beta_1 = 115^o$ and 130^o a separation does not occur. The influence of the inlet angle on the separation is shown in a motion picture which is produced in the DFVLR-AVA [12]. The diagrams in figure 9 show that the flow on the blade surface is not much influenced in the first three planes even at $\beta_1 = 147^o$.

Figures 7 and 8 show the results for the highest Mach number for $\beta_1 = 115^o$ and $g/c = 0.5$ and $g/c = 0.6$. In both cases the spanwise variations are small and begin at about the same plane. Analogous results are obtained for $\beta_1 = 130^o$ and 147^o, which are omitted here.

3.2.3 OIL FLOW PICTURES

Figure 4 shows schematically how the oil flow pictures were obtained. The construction shown allows to take pictures of the suction side of the blade which is the most important to observe. The motion picture, which is part of the investigations described here, shows this part of the suction side for both cascades. In order to get best results with the oil flow technique it is necessary to obtain a uniform distribution of the oil mixture. It is the author's experience, that the photographs should be taken when the tunnel is still running. If for example a separation bubble exists on the profile, the oil mixture within this bubble is spread non-uniformly over the blade surface when the tunnel is shut off. It is useful to watch the surface flow when the tunnel is running, to see whether a significant change of the flow pattern occurs when the windtunnel is shut off. The change of the flow pattern depends on different flow conditions as e.g. thick boundary layers or large bubbles. In the pictures shown in figures 10 and 11 the effect of the tunnel shut off is negligible.

In figure 10 the pressure side and the suction side of the stator cascade blade is shown. The photographs are taken outside of the test section in order to show both sides of the blade. The black line on the suction side represents the region where the shock wave of the adjacent profile is reflected. It can be seen that the oil flow traces on the blade are parallel except at the ends where the blade is fixed to the end-walls. The white part on the pressure side downstream of the leading edge shows an area of low speed. Figure 11 shows the photos of the high turning cascade for two different inlet angles ($g/c = 0.6$; $\beta_1 = 130^o$ and 147^o). The influence of the end-walls is larger than in the case of the stator blade. Comparing the figures for the different inlet angles, it is obvious that in the case of $\beta_1 = 147^o$ there is on the suction side only a small region close to the trailing edge where the traces are parallel. In the forward part of the blade the traces are not parallel, even in the middle part of the blade. This is the region where the flow completely separates, as can be seen in the Schlieren pictures of figures 7 and 8. The picture for $\beta_1 = 130^o$ shows that parallel traces exist on the profile from the leading to the trailing edge and the area of end-wall influence is smaller. The photos of the pressure side show that about 50 percent of the blade height is not influenced by the end-walls, and the influence is larger for the inlet angle $\beta_1 = 147^o$.

All these figures, which give only a qualitative impression - as mentioned already -, are in satisfactory agreement with the results of the surface pressure measurements. For the stator turbine cascade surface pressure measurements are not performed, since the qualitative results of the oil flow method show that the two-dimensionality of the flow on the blade surface is even better than in the case of a high turning cascade. An inlet angle β_1 which is larger than 100^o as shown in figure 10 is not of interest for such a cascade. So it seems to be sufficient - for the cascade-tunnel used here - to check the two-dimensionality of the flow only for extreme turning conditions.

3.3 COMPARISON WITH THEORY

Figure 12 shows the comparison between a theoretical calculation and the experiments. The theoretical result is based on a time-marching method described by LEHTHAUS [13] , which is a two-dimensional method not including boundary layer effects. The comparison shows very good agreement between theory and experiment for the planes 1, 2, and 3. For plane 7, which is 2.5 mm apart from the end-wall, there are larger deviations. Results of the plane 4, 5, and 6 are not plotted to obtain greater clearness of the drawing. The experimental points would fall between the results of the third and seventh plane. The Schlieren photo of this flow (figure 8) shows a shock system on the suction side at about $0.3 < x/c < 0.6$. In this area there are some differences between the theoretical and experimental results, which may be caused by not including boundary layer effects in the theory.

4. CONCLUSION

In the 2-D cascade-windtunnel of the DFVLR-AVA Göttingen surface pressure measurements in different planes of the blade height are performed for a high turning turbine rotor cascade. The height/chord ratio of the blade is 2.08 . Three different Mach numbers - a subsonic, transonic and supersonic Mach number - are investigated for two different pitch/chord ratios and three different inlet angles. Also oil flow pictures of the flow are taken. Motion pictures show the flow on the blade surface for two different cascades, one of high deflection and one of low deflection. The development of the surface flow is shown beginning with no flow and ending with the turning off of the tunnel.

The results show that the inlet angle is the most sensitive parameter regarding two-dimensionality of the flow. If this angle becomes larger, the area of two-dimensional flow on the blade surface decreases. There is no remarkable influence of the Mach number on two-dimensionality. For the pitch/chord ratios investigated a difference could not be stated. In the cases of inlet angles $\beta_1 = 115^o$ and 130^o there are only small span-wise variations of the flow, except at planes close to the end-wall: more than 50 percent of the blade height (mid-span symmetry is supposed) show uniform flow. This value decreases for an inlet angle $\beta_1 = 147^o$, but even in this case about 40 percent of the blade height have uniform flow. The oil flow pictures, which only give qualitative results, confirm the measurements. The comparison of two cascades shows that for the cascade of less turning (about 60 degrees) the two-dimensionality is better than for the high turning (about 110 degrees) cascade. It is advantageous to photograph the painted blade during the running of the tunnel, because the shut off process may influence the flow pattern. The surface pressure measurements are compared with a theoretical result, based on a two-dimensional theory. The agreement is good, if the measurements close to mid-span are compared, and becomes worse for measurements in planes near the end-wall.

5. LIST OF REFERENCES

[1] Secondary Flows in Turbomachines
Lecture Series 72, von Karman Institute, Brüssels, Belgium, January 1975

[2] Carrick, H. B. Calculation of End-Wall Flow in Turbine Cascades
Polska Akademia Nauk, Transactions of the Institut of
Fluid-Flow Machinery, 70 - 72, Warszawa-Poznan (1976)

[3] Hawthorne, W. R.
Armstrong, W. D. Shear Flow Through a Cascade
The Aeronautical Quarterly, Vol. VII, February 1965 - November 1956,
pp 247 - 274, published by the Royal Aeronautical Society

[4] Horlock, J. H. Cross Flows in Bounded Three-Dimensional Turbulent Boundary Layers
Journal Mechanical Engineering Science, pp 274 - 284
Vol. 15, No. 4, 1973

[5] Rubner, K. Messung der räumlichen Strömung und der Schaufeldrücke
in einem Axialverdichter unter Berücksichtigung der wandnahen
Strömung mit Hilfe einer digitalen Datenerfassung und Versuchsablaufsteuerung
Dissertation TU Aachen, West-Germany, 1970

[6] Armstrong, W. D. — An Experimental Investigation of the Secondary Flow Occuring in a Compressor Cascade
The Aeronautical Quarterly, Vol. VIII, February 1957 - November 1957, pp 240 - 256, published by the Royal Aeronautical Society

[7] Prümper, H. — Methoden zur Verminderung der Sekundärverluste in axialen Turbinenstufen
Zeitschrift für Flugwissenschaften 20 (1972), Heft 1/2, pp 60 - 70

[8] Langston, L. S.; Nice, M. L.; Hooper, R. M. — Three-Dimensional Flow within a Turbine Cascade Passage
ASME Paper No. 76 - GT - 50

[9] Senoo, Y. — The Boundary Layer on the End Wall of a Turbine Nozzle Cascade
TRANS. ASME, Vol. 80, Nov. 1958, pp 1711 - 1720

[10] Herzig, H. Z.; Hansen, A. G.; Costello, G. R. — A Visualization Study of Secondary Flows in Cascades
NACA Report 1163, 1954

[11] Lawaczeck, O. — Der Prüfstand für ebene Schaufelgitter der Aerodynamischen Versuchsanstalt Göttingen
DFVLR-AVA-Bericht 70 A 46 (1970)

[12] Lehthaus, F. — Transonic Flow in a Turbine Cascade with high Deflection (Colour-Schlieren-Film with High-Speed-Passages)
DFVLR-AVA-Bericht 251 74 A 24 (1974) and
Polska Akademia Nauk, Transactions of the Institute of Fluid-Flow Machinery, 70 - 72, Warszawa-Poznan (1976)

[13] Lehthaus, F. — Anwendung eines Zeit-Schritt-Verfahrens zur Berechnung der transsonischen Durchströmung ebener Turbinengitter und experimentelle Überprüfung
DFVLR-AVA-Bericht 251 77 A 01 (1977)

[14] Hubert, G.; Bauermeister, K.J. — Probleme der Sekundärströmung in axialen Turbomaschinen
VDI-Forschungsheft 496, Ausgabe B, Band 29 (1963), VDI-Verlag, Düsseldorf, W-Germany

LIST OF FIGURES

Figure 1: Turbine cascade of high deflection

Figure 2: Instrumented blade (locations of the tappings)

Figure 3: Photo of the cascade with the instrumented blade

Figure 4: Sketch of the high and less turning cascade

Figure 5: Measurement planes

Figure 6: Surface pressure measurements: results of the pressure side ($g/c = 0.6$)

Figure 7: Surface pressure measurements: results of the suction side ($g/c = 0.5$; $\beta_1 = 115^{\circ}$)

Figure 8: Surface pressure measurements: results of the suction side ($g/c = 0.6$; $M_2 < 1$; $\beta_1 = 115^{\circ}, 130^{\circ}, 147^{\circ}$)

Figure 9: Surface pressure measurements: results of the suction side ($g/c = 0.6$; $M_2 > 1$; $\beta_1 = 115^{\circ}, 130^{\circ}, 147^{\circ}$)

Figure 10: Oil flow pictures: turbine stator cascade

Figure 11: Oil flow pictures: turbine rotor cascade

Figure 12: Surface pressure distribution: comparison of theoretical and experimental results

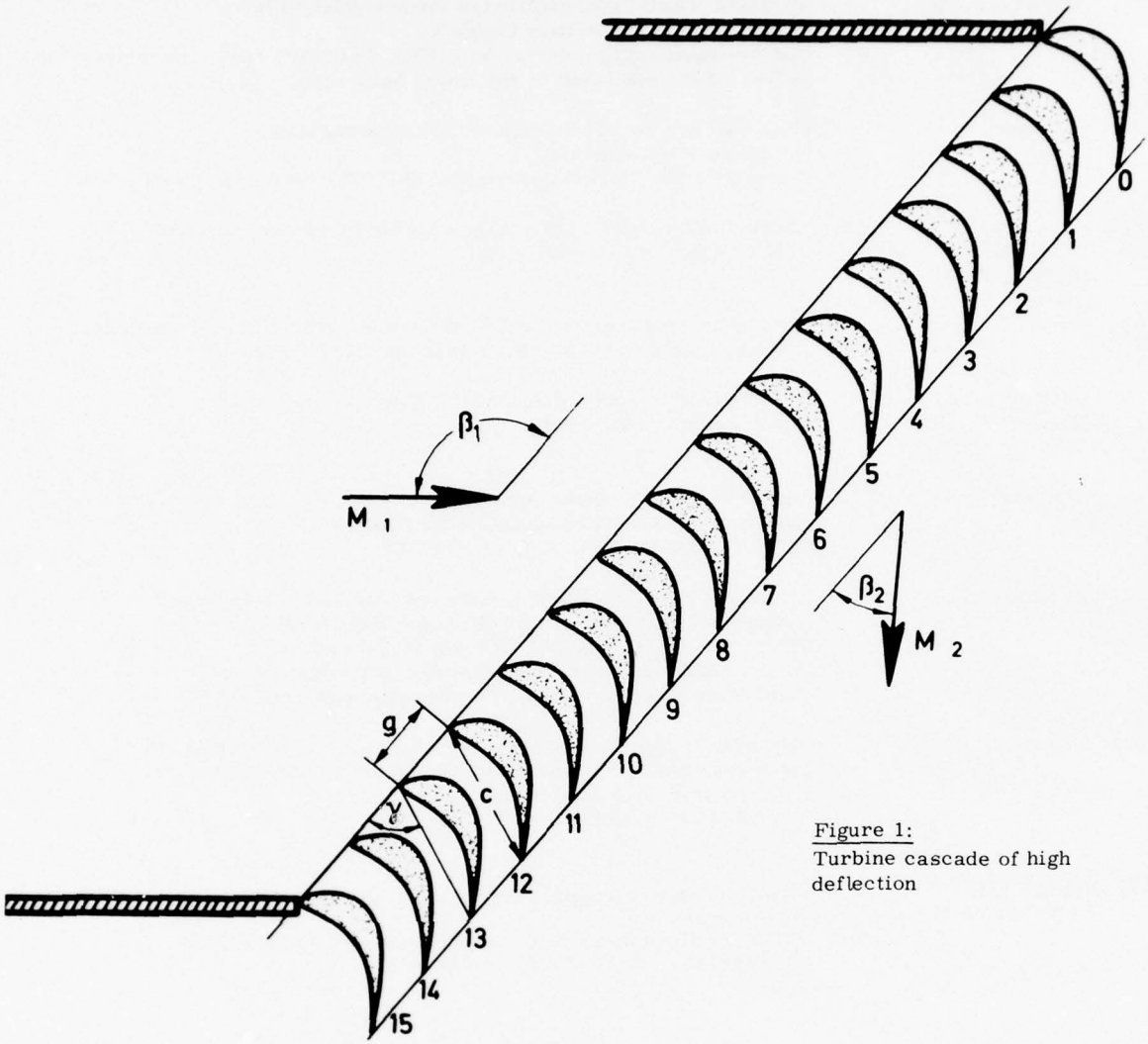


Figure 1:
Turbine cascade of high deflection

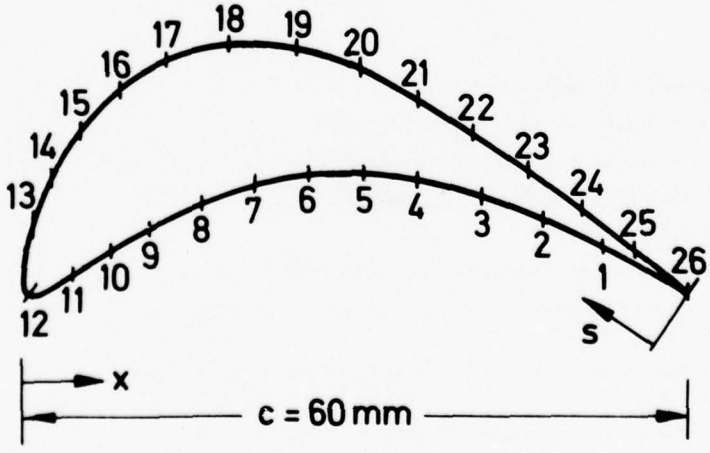


Figure 2: Instrumented blade (locations of the tappings)

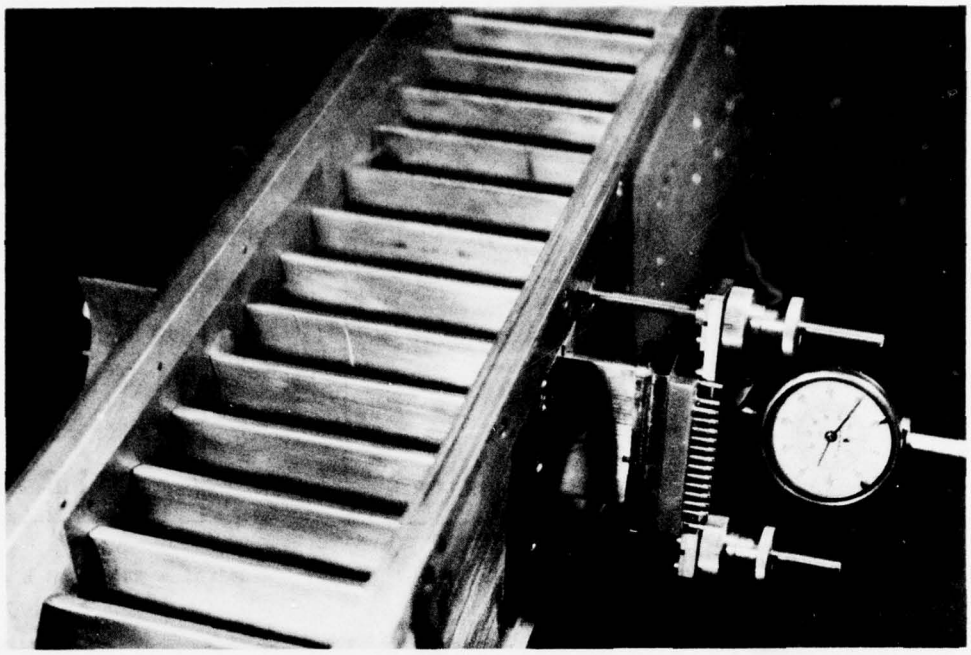


Figure 3: Photo of the cascade with the instrumented blade

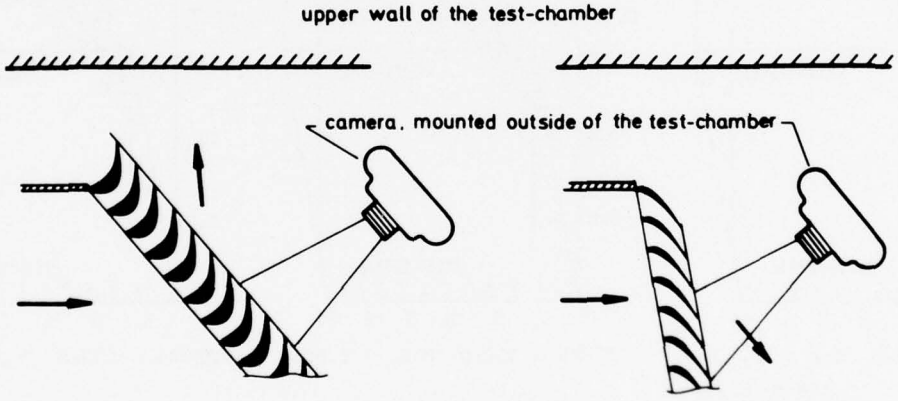


Figure 4: Sketch of the high and less turning cascade

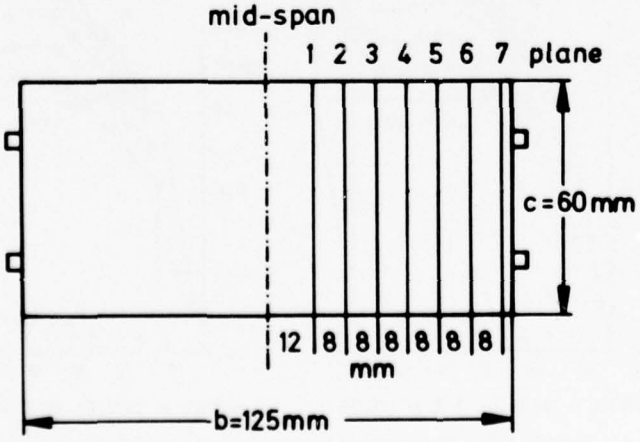


Figure 5:
Measurement planes

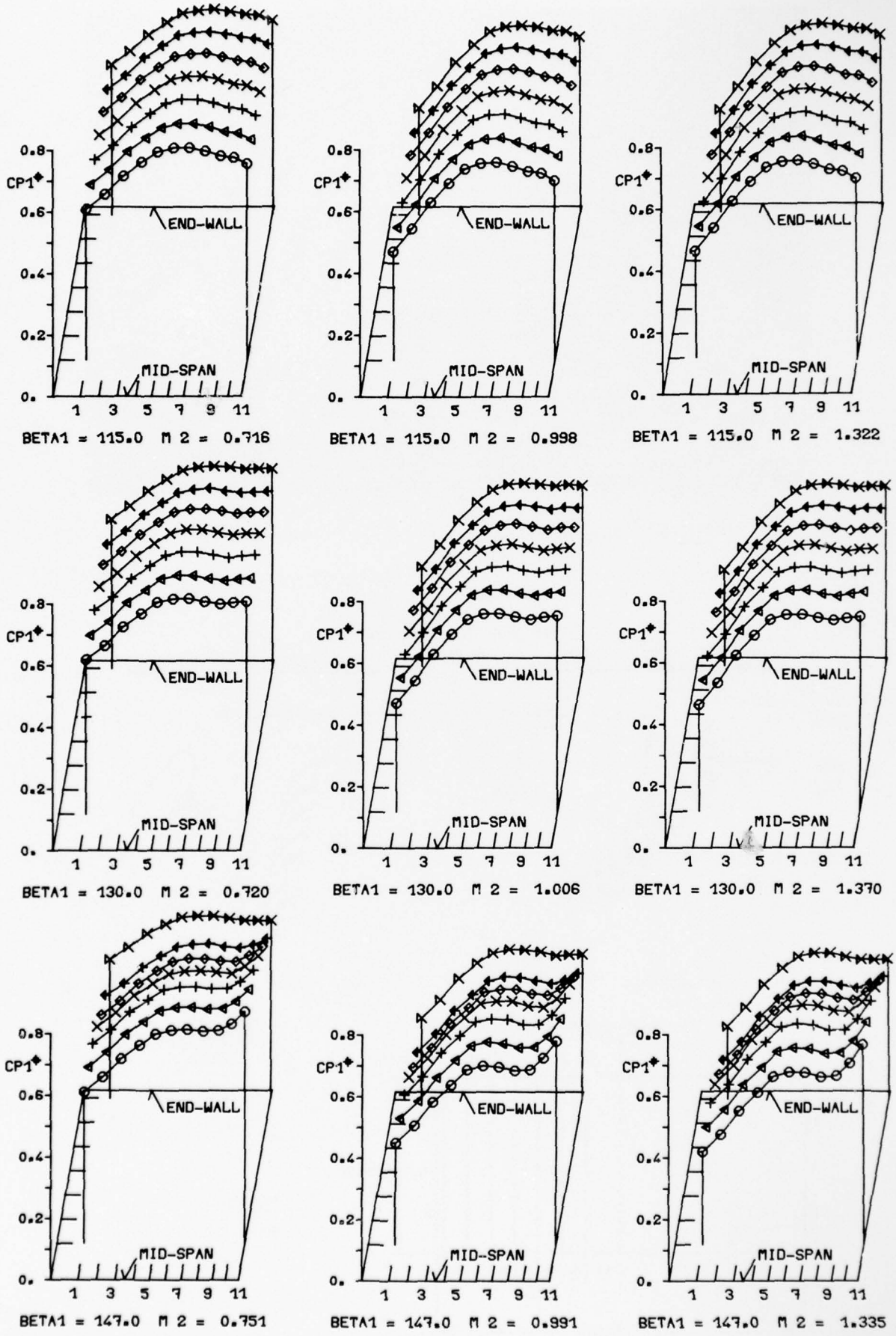
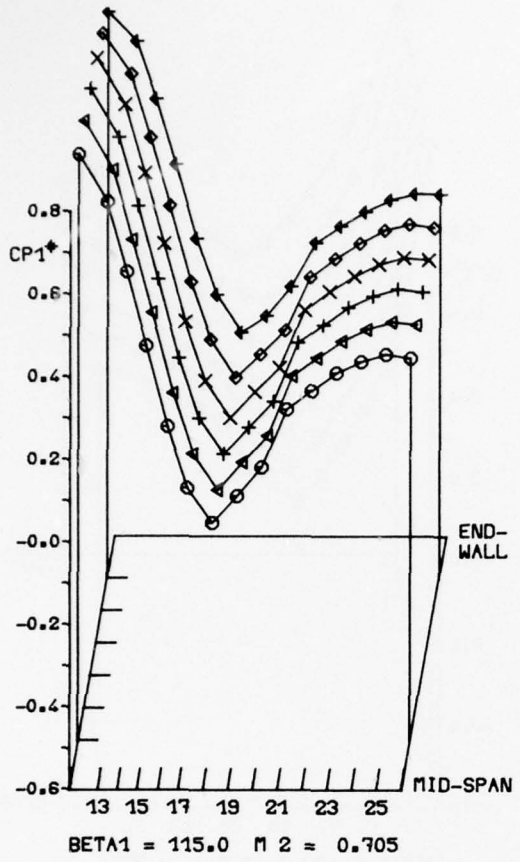
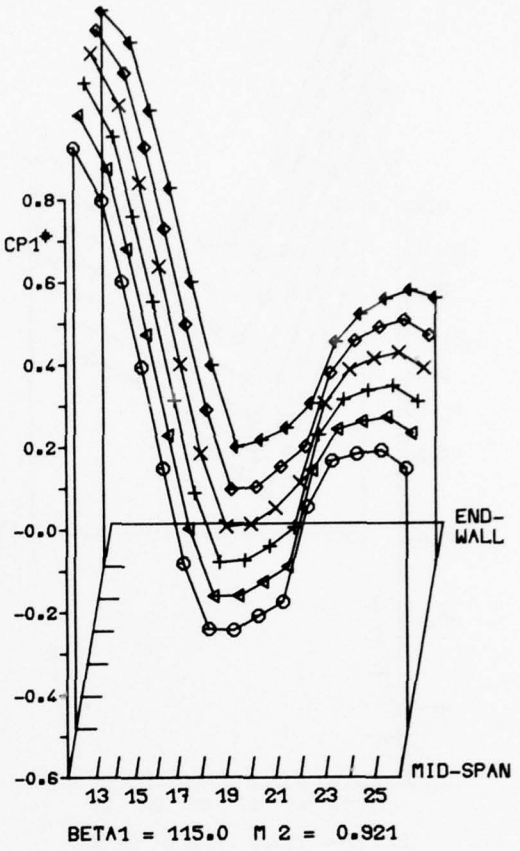
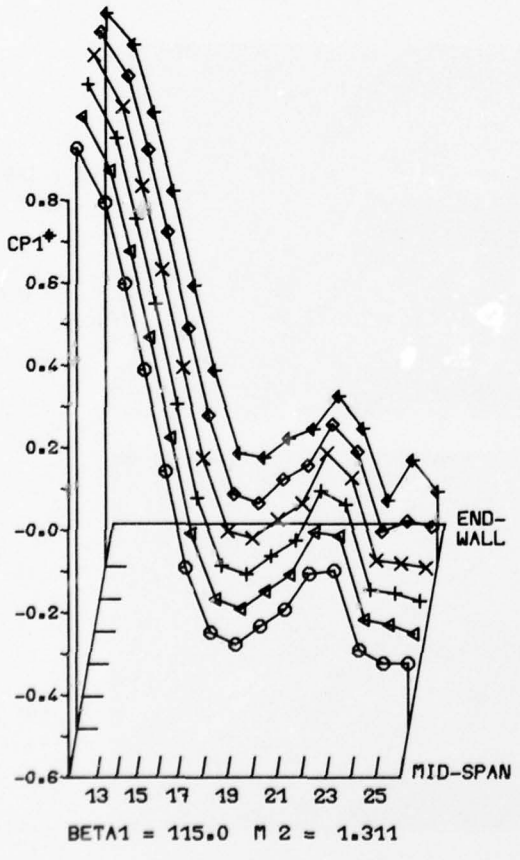


Figure 6: Surface pressure measurements: results of the pressure side (g/c = 0.6)







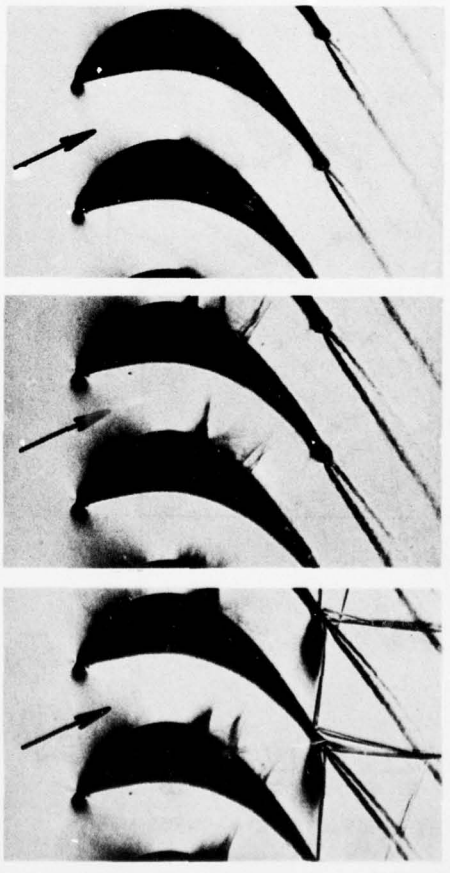
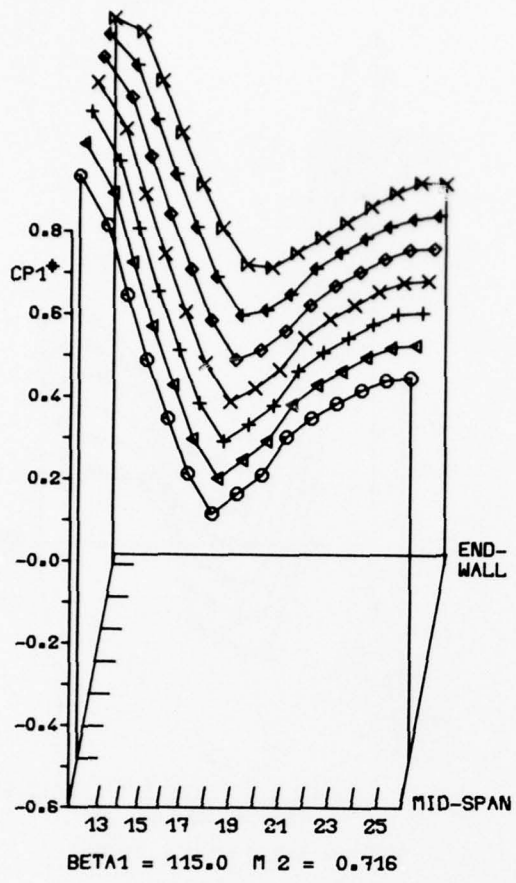
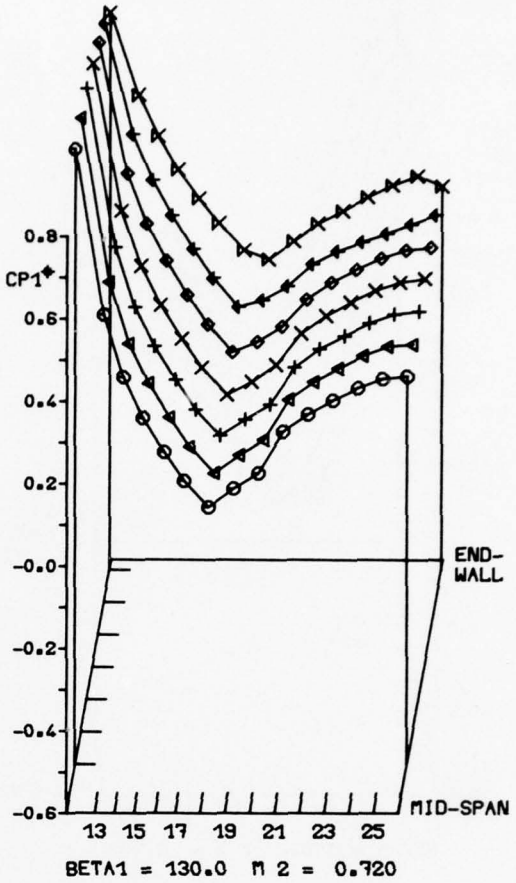
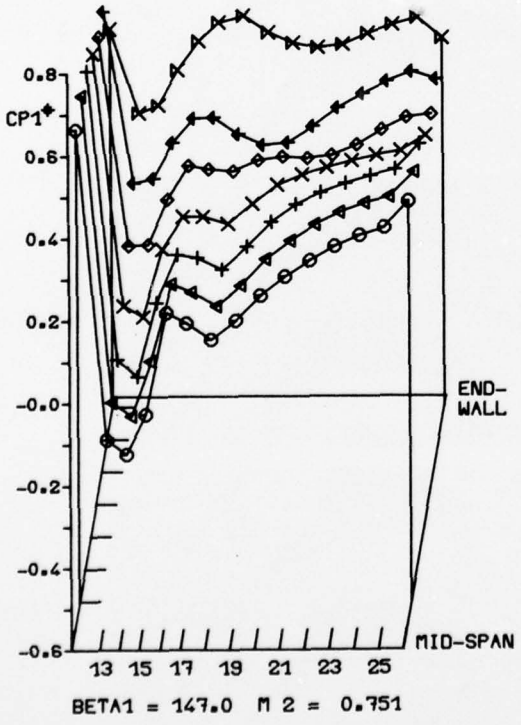
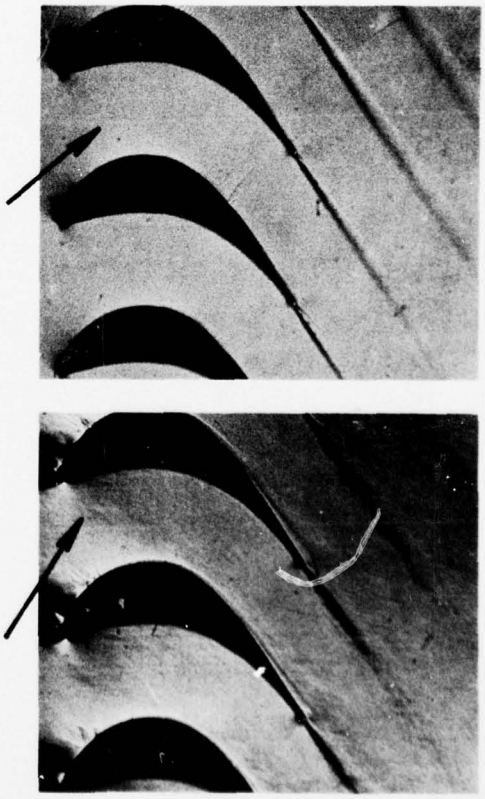


Figure 7: Surface pressure measurements: results of the suction side ($g/c = 0.5$; $\beta_1 = 115^{\circ}$)









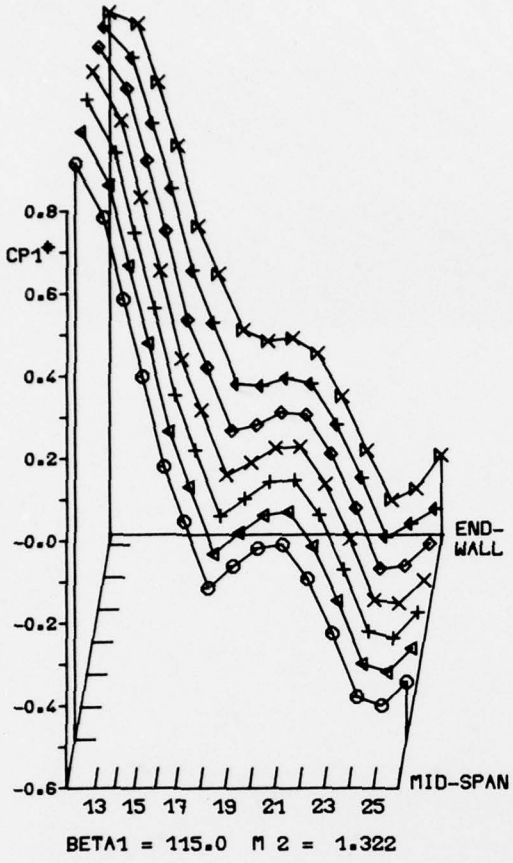
$\beta_1 = 130^{\circ}$

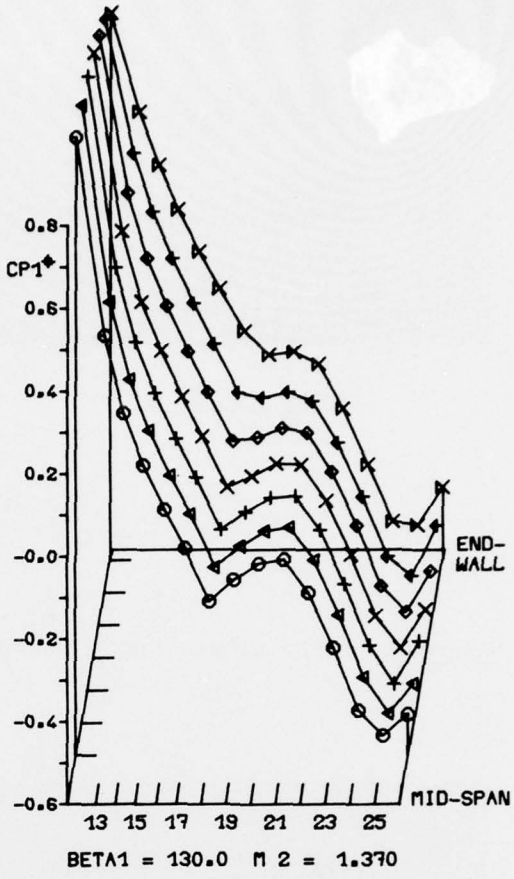
$M_2 = 0.720$

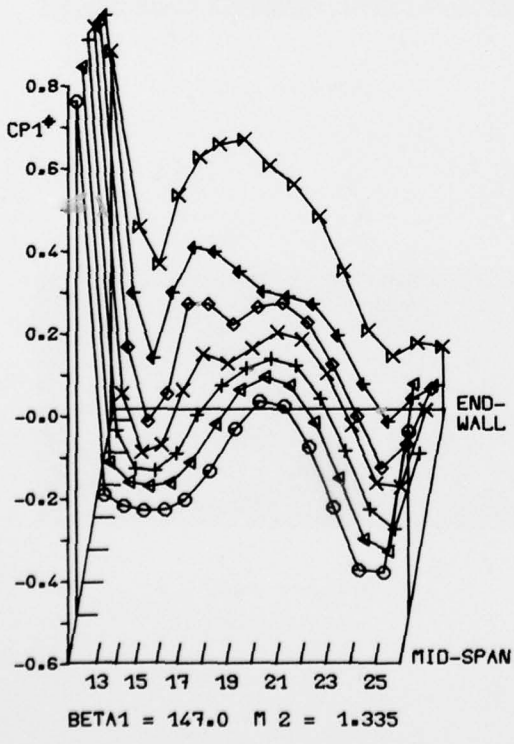
$\beta_1 = 147^{\circ}$

$M_2 = 0.751$

Figure 8:
Surface pressure measurements: results of the suction side ($g/c = 0.6$; $M_2 < 1$; $\beta_1 = 115^{\circ}, 130^{\circ}, 147^{\circ}$)







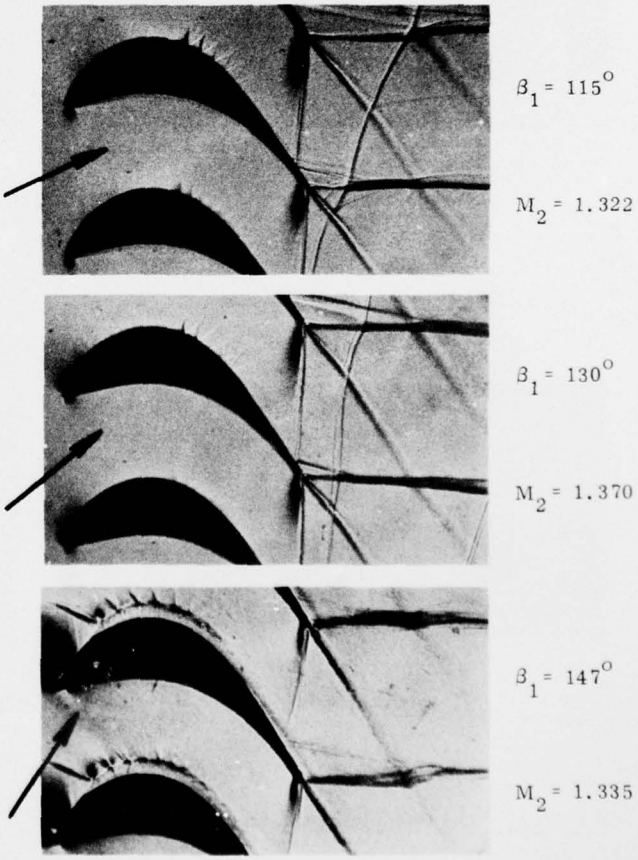
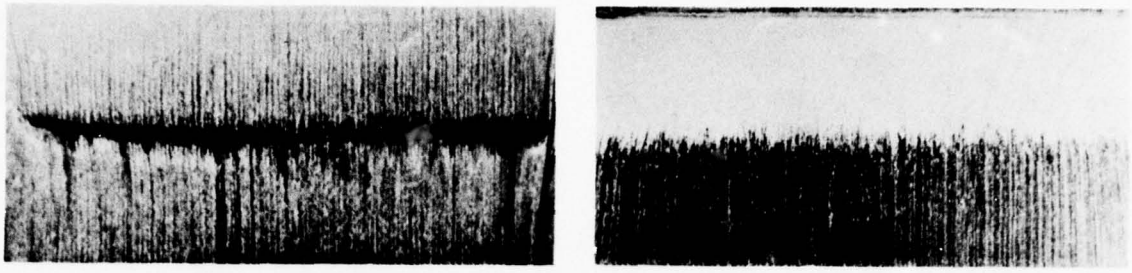


Figure 9:
Surface pressure measurements: results of the suction side ($g/c = 0.6$; $M_2 > 1$; $\beta_1 = 115^o$, 130^o, 147^o)

leading edge

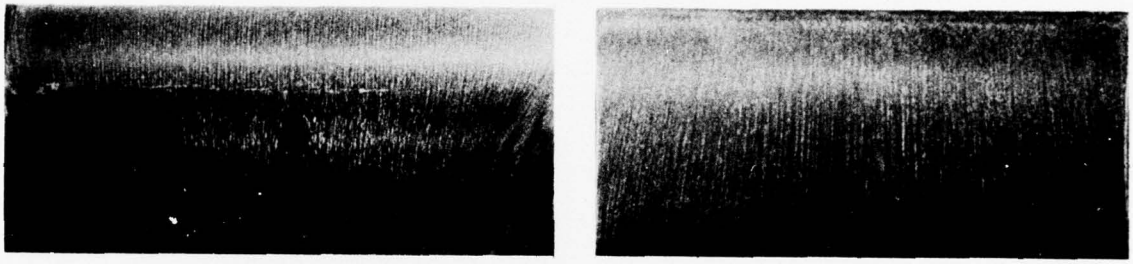


suction side trailing edge pressure side

$\beta_1 = 100^o$ $M_2 = 1.1$

Figure 10: Oil flow pictures: turbine stator cascade

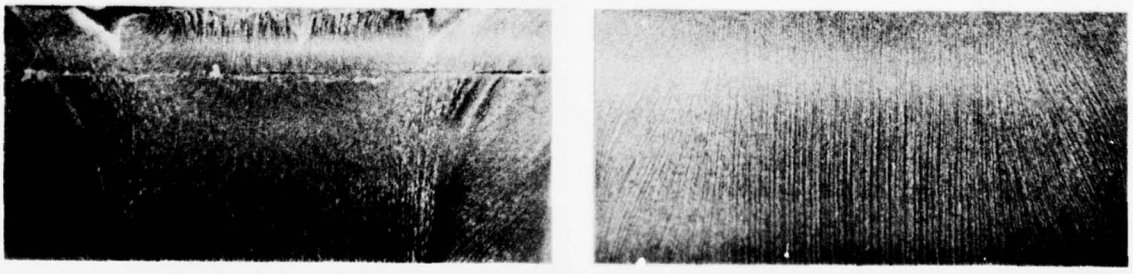
leading edge



suction side trailing edge pressure side

$\beta_1 = 130^o$ $M_2 = 1.1$

leading edge



suction side trailing edge pressure side

$\beta_1 = 147^o$ $M_2 = 1.1$

Figure 11: Oil flow pictures: turbine rotor cascade

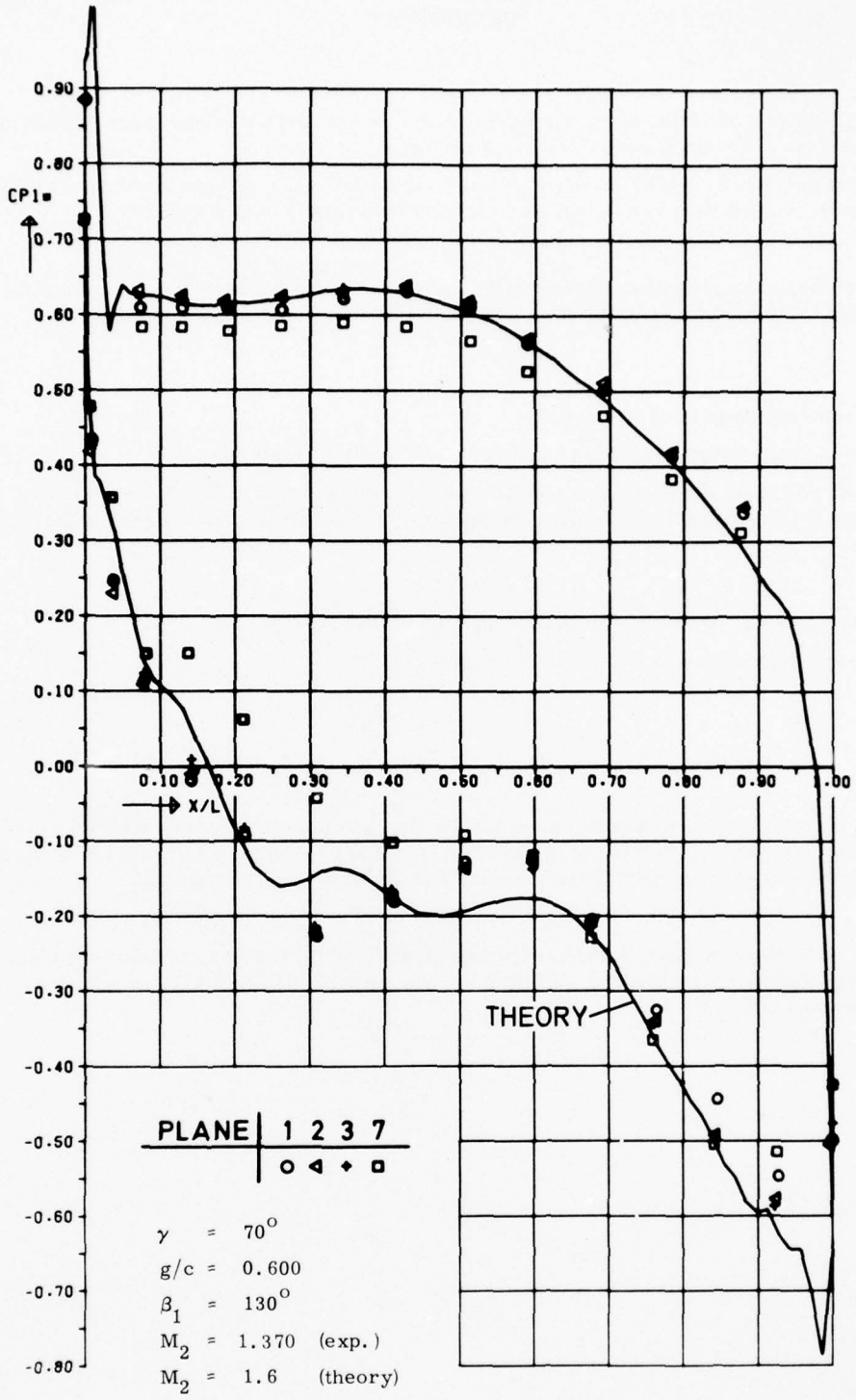


Figure 12: Surface pressure distribution: comparison of theoretical and experimental results

DISCUSSION

C.H.Sieverding

Referring to Figure 11, which shows that the shock interference line does not extend to the endwalls, my question is whether the flow is still supersonic or subsonic in this region.

Can you relate the extension of the secondary flow zones indicated by the oil flow visualizations to the point where the pressure distribution starts to deviate from the pressure distribution at midspan?

Author's Reply

The results of the surface pressure measurements indicate that there is supersonic flow also in the plane closest to the endwall. Both results are in satisfactory agreement concerning the location of changing.

N.A.Cumpsty

What is the rotor and stator blade inlet angle?

This angle is important to appreciate what β_1 of 110°, 130° and 147° really means.

I disagree with Prof. Sieverding's comments on the appearance of a shock in surface flow visualisation. Even though it may not be apparent from wall flow visualisation it may be present and detectable in the pressure distribution.

Author's Reply

The turbine rotor cascade is designed for an inlet angle $\beta_1 = 147°$.

The turbine stator cascade is designed for an inlet angle $\beta_1 = 90°$.

P.Runstadler

Do you have similar wall flow pattern visualization pictures for the trailing edge shock foot pattern at $M = 1.3$?

If these pictures also show the shock pattern not going to the wall (while the pressure trends seem to indicate supersonic flow – see Fig. 12) then it is most likely that Dr. Cumpsty's remark is true that the secondary vorticity near the wall is obscuring the imprint of the shock at this location near the wall.

Author's Reply

The oil-flow visualization pictures of $M = 1.3$ show (more or less) the same pattern as to be seen in Figure 11, where the result for $M = 1.1$ is shown. The black line indicating the reflection of the shock from the adjacent blade does also not extend to the wall.

SECONDARY FLOW IN CASCADES

by

D. Glynn
A. Spurr
and
H. Marsh
Department of Engineering Science
University of Durham
Durham
DH1 3LE
England

SUMMARY

The paper describes recent work on secondary flow in linear cascades. The use of a power law profile for the end wall boundary layer is shown to lead to a discontinuity in the slope of the variation of exit angle across the span of the blades. The change in the shape of the wall boundary layer across a cascade is estimated and the corresponding change in axial velocity is included in the secondary flow theory. An iterative scheme is proposed where the distributed secondary vorticity is based on the predicted outlet angle rather than the mainstream flow angle. The pitch averaged streamwise vorticity is calculated at exit from the cascade and is shown to be in close agreement with experimental results.

NOTATION

H	boundary layer shape factor
n	power law exponent
q	local velocity
Q	mainstream velocity
s	pitch
s^1	$s^1 = s \cos \alpha_2$
u	axial velocity
v_n	secondary velocity across the blade passage
w	secondary velocity along the span of the blades
y_n	direction across the blade passage
z	spanwise direction
α	flow angle
δ	thickness of the boundary layer
ξ_n	normal component of vorticity at inlet
ξ_s	streamwise component of vorticity at inlet
ξ_{sec}	distributed secondary vorticity
ξ_{fil}	trailing filament vorticity
ξ_{shed}	trailing shed vorticity
$\bar{\xi}$	pitch averaged streamwise vorticity

SUBSCRIPTS

1	upstream
2	downstream

INTRODUCTION

When a non-uniform flow is turned in a linear cascade, secondary flow is produced and at exit from the cascade, there is a variation of flow angle along the span of the blades. In a turbomachine, secondary flow leads to a variation in the exit flow angle from a blade row and this effect should be included in the design procedure. In the past, secondary flow theory has been based on an analysis which is relatively complex and a comprehensive review has been given by Horlock and Lakshminarayana (1). More recently, Came and Marsh(2) have shown that there are simple derivations for the governing equations which can be obtained by considering the flow through a many bladed cascade.

Hawthorne (3) has considered the flow of a fluid with a non-uniform velocity through a cascade and has identified three components of vorticity in the direction of flow at exit from the cascade. One component is distributed in the passage flow while the other two components form the trailing vortex sheet leaving the blade trailing edge. The first component is the distributed secondary vorticity, ξ_{sec}, caused by turning the shear flow in the cascade. Hawthorne has called the second component the trailing filament vorticity, ξ_{fil}, this being caused by the stretching of the vortex filaments as they move over the surface of the blades. The third component is the trailing shed vorticity, ξ_{shed}, which is caused by the variation of circulation along the span of the blades. Hawthorne derived expressions for the three streamwise components of vorticity and these have been widely used over the past 25 years. The variation of exit flow angle can be predicted from the distributed secondary vorticity and many papers have been published showing good agreement between experimental results and the predictions based on secondary flow theory.

Came and Marsh (2) have provided an alternative approach to the theory of secondary flow. An expression is obtained for the difference in the time taken for fluid particles to travel over the two surfaces of the blade and this is used in the derivation of the governing equations for ξ_{sec}, ξ_{fil} and ξ_{shed}. The equations for ξ_{sec} and ξ_{fil} are the same as those obtained many years earlier by Hawthorne (3), but the two approaches lead to different expressions for the trailing shed vorticity. Since the two methods of analysis give the same distributed secondary vorticity, they predict the same secondary velocities and the same variation in exit angle along the span of the blades. Came and Marsh show that their expression for the strength of the trailing vortex sheet is consistent with the secondary velocities.

In a turbomachine, a shear flow, such as a wall boundary layer, may be turned by a stationary blade row, producing changes in the streamwise and normal components of vorticity, and this flow is then passed downstream into a moving blade row. In this situation, it is essential that the basic theory of secondary flow for the stationary cascade and blade row should be fully understood and confirmed experimentally before attempting to predict secondary flow in the rotor row. Experimental data is required to test the theory of secondary flow for linear and annular cascades, including both the variation of outlet flow angle and the components of vorticity at exit from the cascade. A suitable test case is provided by the data given by Dunham (4) which summarises experimental results obtained by Dr. S.L. Dixon with a linear cascade of turbine nozzle blades, the N.G.T.E. cascade.

SECONDARY FLOW THEORY

Hawthorne (3) has given the following expressions for the three streamwise components of vorticity at exit from a cascade:

(a) distributed secondary vorticity, ξ_{sec},

$$\xi_{sec} = \xi_s \frac{\cos\alpha_1}{\cos\alpha_2} + \frac{\xi_n}{\cos\alpha_2}\left\{-Q_1 \oint \frac{dl}{q} + \frac{s(\sin 2\alpha_2 - \sin 2\alpha_1)}{2\cos\alpha_1}\right\} \tag{1}$$

(b) trailing filament vorticity, ξ_{fil},

$$\xi_{fil} = \xi_n Q_1 \oint \frac{dl}{q} \tag{2}$$

(c) trailing shed vorticity, ξ_{shed},

$$\xi_{shed} = -s\xi_n \cos\alpha_1 \left[\tan\alpha_2 - \tan\alpha_1\right] - s\xi_s \cos\alpha_1 \tag{3}$$

where ξ_s and ξ_n are the streamwise and normal components of vorticity at inlet to the cascade, Q_1 is the velocity at inlet and q is the local velocity on the blade surface. The integral $\oint dl/q$ is taken from the leading edge of a blade along the suction surface to the trailing edge and back along the pressure surface. In general, there is no simple expression for this integral, which represents the difference in the time taken for fluid particles to pass over the suction and pressure surfaces of the blade.

Came and Marsh (2) have applied Kelvin's circulation theorem to the flow through a many bladed cascade and have shown that for this model, the integral is given by

$$\oint \frac{dl}{q} = -\frac{s}{u}(\alpha_2 - \alpha_1) \tag{4}$$

where u is the velocity normal to the cascade. If this expression is substituted into Hawthorne's analysis, then

$$\xi_{sec} = \xi_s \frac{\cos\alpha_1}{\cos\alpha_2} + \frac{\xi_n}{\cos\alpha_1 \cos\alpha_2}\left\{\alpha_2 - \alpha_1 + \tfrac{1}{2}(\sin 2\alpha_2 - \sin 2\alpha_1)\right\} \tag{5}$$

$$\frac{1}{s}\xi_{fil} = -\xi_n \frac{(\alpha_2 - \alpha_1)}{\cos\alpha_1} \tag{6}$$

and the trailing shed vorticity remains

$$\frac{1}{s}\xi_{shed} = -\xi_n \cos\alpha_1 (\tan\alpha_2 - \tan\alpha_1) - \xi_s \cos\alpha_1 \tag{7}$$

With the equations in this form, it can be seen that secondary flow theory predicts that all cascades which have the same inlet and exit flow angles produce the same distributed secondary vorticity and the same

strength per unit pitch for the trailing filament and trailing shed vortex sheets. If the many bladed cascade has the same inlet and exit flow angles as the real cascade, then it will have the same values for ξ_{sec}, $\xi_{fil/s}$ and $\xi_{shed/s}$.

The use of the many bladed cascade model is discussed in detail in ref. (2) where it is shown that it leads to the same expressions for ξ_{sec} and ξ_{fil} as had been derived many years earlier by Hawthorne. However, the use of Kelvin's circulation theorem leads to a different expression for the trailing shed vorticity

$$\frac{1}{s}\xi_{shed} = -\frac{\xi_n}{2\cos\alpha_1}\left[\sin 2\alpha_2 - \sin 2\alpha_1\right] - \xi_s \cos\alpha_1 - q_2 \cos\alpha_2 \frac{d\alpha_2}{dz} \tag{8}$$

where z is the direction along the span of the blades. The strength of the trailing shed vortex sheet is dependent on the variation of exit flow angle produced by the secondary flow.

THE CALCULATION OF SECONDARY FLOW

Following the work of Hawthorne and Armstrong (5), the secondary velocity components v_n and w are defined in a plane normal to the mainstream flow at exit from the cascade, fig. 1, and the secondary flow stream function ψ is introduced where

$$\left.\begin{aligned} v_n &= -\frac{\partial\psi}{\partial z} \\ w &= \frac{\partial\psi}{\partial y_n} \end{aligned}\right\} \tag{9}$$

The distributed secondary vorticity is related to v_n and w by

$$\frac{\partial w}{\partial y_n} - \frac{\partial v_n}{\partial z} = \xi_{sec} \tag{10}$$

or, in terms of ψ,

$$\frac{\partial^2\psi}{\partial y_n^2} + \frac{\partial^2\psi}{\partial z^2} = \xi_{sec} \tag{11}$$

The secondary flow is determined by the distributed secondary vorticity and the boundary conditions imposed by the blade geometry.

Hawthorne (6) has provided a series solution for the stream function ψ and from this, the change in the mean outlet angle can be calculated as a function of the distance from the end wall, z. The series solution is particularly simple when the inlet velocity profile can be represented by a power law,

$$0 < z \leq \delta \qquad \left(\frac{q}{Q}\right)_1 = \left(\frac{z}{\delta_1}\right)^n$$

$$z > \delta \qquad \left(\frac{q}{Q}\right)_1 = 1$$

If the distributed secondary vorticity is written as

$$\xi_{sec} = 2\epsilon' \xi_n$$

where

$$\epsilon' = \frac{1}{2\cos\alpha_1 \cos\alpha_2}\left[\alpha_2 - \alpha_1 + \tfrac{1}{2}(\sin 2\alpha_2 - \sin 2\alpha_1)\right] \tag{12}$$

then the solution for the variation of the exit flow angle is,
for $0 < z \leq \delta$

$$\frac{\Delta\alpha_2}{\epsilon'} = \frac{16n\cos\alpha_2}{\delta\cos\alpha_1}\left(\frac{\delta}{z}\right)^n \sum_{m=1,3,} \left\{ \frac{\cosh\left(\frac{m\pi z}{s'}\right)}{(m\pi)^2} \int_z^{\delta} \left(\frac{\lambda}{\delta}\right)^{n-1} e^{-\frac{m\pi\lambda}{s'}}\, d\lambda \right.$$

$$\left. - \frac{e^{-\frac{m\pi z}{s'}}}{(m\pi)^2} \int_0^z \left(\frac{\lambda}{\delta}\right)^{n-1} \sinh\left(\frac{m\pi\lambda}{s'}\right) d\lambda \right\} \tag{13}$$

and for $z > \delta$

$$\frac{\Delta\alpha_2}{\epsilon'} = -\frac{16n\cos\alpha_2}{\delta\cos\alpha_1} \sum_{m=1,3,} \frac{e^{-\frac{m\pi z}{s'}}}{(m\pi)^2} \int_0^{\delta} \left(\frac{\lambda}{\delta}\right)^{n-1} \sinh\left(\frac{m\pi\lambda}{s'}\right) d\lambda \tag{14}$$

where $s^1 = s\cos\alpha_2$. Equation (14) is slightly different to that given in ref. (6) where the power law profile appears to have been used outside of the boundary layer when calculating $\Delta\alpha_2$. The series solution assumes that the velocity profile at exit from the cascade obeys the same power law as the velocity profile at inlet and the validity of this assumption will be discussed later. In the computer program for the

series solution, the summation of the series is terminated when two successive sums differ by less than 0.01 per cent.

The alternative method of solution is to define a rectangular grid in the plane normal to the flow at exit from the cascade and to obtain a numerical solution for Ψ, v_n and w by means of a finite difference technique. The solution can be based on matrix inversion or on an iterative technique such as Gauss-Seidel. The advantage of the numerical solution is that it can easily deal with any velocity profile at inlet, but care must be taken to ensure that the variation of ξ_n is smooth.

CALCULATIONS FOR THE N.G.T.E. CASCADE

The cascade at N.G.T.E. tested by Dr. Dixon has an inlet angle of $\alpha_1 = 0$ and a mean exit flow angle of $\alpha_2 = -62.4^o$. The blade pitch is 90.8 mm, the thickness of the boundary layer at inlet is $\delta = 25.4$ mm and the inlet velocity profile can be approximated by

$$\frac{q}{Q} = \left(\frac{z}{\delta}\right)^{1/7}$$

For this profile, the normal component of vorticity at inlet is given by

$$\xi_n = \frac{Q}{7\delta}\left(\frac{\delta}{z}\right)^{6/7} \quad \text{for} \quad 0 < z < \delta$$

and

$$\xi_n = 0 \quad \text{for} \quad z > \delta$$

The variation of exit flow angle can be calculated from Hawthorne's series solution or the finite difference approach. The two solutions give identical results and in fig. 1, they are compared with the experimental data.

THE NEED FOR A SMOOTH INLET PROFILE

The series solution and the finite difference method both give a variation of exit flow angle which shows a discontinuity in slope at the edge of the boundary layer. This discontinuity in $d\alpha_2/dz$ is not shown in most papers dealing with secondary flow and it has therefore been investigated in more detail. At a position just within the boundary layer, z = A in fig. 2,

$$\frac{\partial w}{\partial y_n} - \frac{\partial v_n}{\partial z} = \xi_{sec}$$

so that integrating across the plane normal to the flow,

$$(w_2 - w_1)_A - \left(\frac{\partial \bar{v}_n}{\partial z}\right)_A s\cos\alpha_2 = \left(\xi_{sec}\right)_A s\cos\alpha_2 \qquad (15)$$

Now consider the flow at z = B where B lies just outside the boundary layer,

$$\frac{\partial w}{\partial y_n} - \frac{\partial v_n}{\partial z} = 0$$

and

$$(w_2 - w_1)_B - \left(\frac{\partial \bar{v}_n}{\partial z}\right)_B s\cos\alpha_2 = 0 \qquad (16)$$

The secondary velocity component w must vary continuously across the edge of the boundary layer, so that

$$w_{1A} = w_{1B} \quad , \quad w_{2A} = w_{2B} \qquad (17)$$

and from equations (15) and (16),

$$\left(\frac{\partial v_n}{\partial z}\right)_B - \left(\frac{\partial v_n}{\partial z}\right)_A = \left(\xi_{sec}\right)_A \qquad (18)$$

Hence, if there is a discontinuity in the value of ξ_{sec} at the edge of the boundary layer, then there will be a discontinuity in dv_n/dz and in $d\alpha_2/dz$.

The discontinuity in $d\alpha_2/dz$ which is shown in fig. 1 can be removed by taking a better approximation to the inlet velocity profile which has zero slope at the edge of the boundary layer. In approximating the inlet profile, it is more important to maintain the same value for the displacment or momentum thickness, rather than the less easily defined boundary layer thickness. It is found that the outer part of the (1/7)th power law profile can be closely approximated by a parabola which has the same gradient as the power law at z = 10 mm and zero gradient at 29.5 mm, these values being chosen to maintain the same displacment thickness. Fig. 1 shows the predicted variation of exit flow angle for this smoothed profile. The use of the smoothed profile removes discontinuity in $d\alpha_2/dz$ and the maximum underturning now occurs at a value of $z \approx 24$ mm. This example demonstrates the need for a smooth variation of the normal component of vorticity when calculating secondary flow; the use of a power law to represent the velocity profile leads to a discontinuity in $d\alpha_2/dz$

at the edge of the boundary layer.

THE EXIT VELOCITY PROFILE

When a shear layer passes through a cascade, there is a change in the normal component of vorticity and the velocity profile is changed. By applying Kelvin's circulation theorem to the flow on a mean stream surface passing through a cascade, it is found that

$$\left[q \frac{\partial q}{\partial \psi'} \right]_{\text{upstream}} = \left[q \frac{\partial q}{\partial \psi'} \right]_{\text{downstream}} \qquad (19)$$

where ψ^1 is the stream function for the flow on the mean stream surface. This is a generalisation of the analysis given in ref.(2) for the change in ξ_n across a cascade. Equation (19) can be obtained by assuming that there is no spanwise variation of pressure in the flow upstream and downstream of the cascade and then differentiating Bernoulli's equation with respect to ψ^1

$$Q_1^2 - q_1^2 = Q_2^2 - q_2^2 \qquad (20)$$

so that

$$q_1 \frac{\partial q_1}{\partial \psi'} = q_2 \frac{\partial q_2}{\partial \psi'} \qquad (21)$$

where Q_1 and Q_2 are the mainstream velocities upstream and downstream of the cascade. Equation (20) assumes that there is no loss of stagnation pressure along each streamline and this may be a reasonable approximation for the outer part of the boundary layer.

The velocity profile for the outer part of the boundary layer can be calculated directly from equation (20). However, it may be more useful to represent the inlet and outlet boundary layers by simple power law profiles and then attempt to relate the boundary layer parameters for the two flows. If it is assumed that viscous effects are confined to the inner boundary layer, say $\psi^1 = 0$ to $\psi^1 = 0.1\ \psi^1_\delta$ where ψ^1_δ is the value of ψ^1_δ at the edge of the boundary layer, then

$$\int_{0.1\,\psi'_\delta}^{\psi'_\delta} (Q_1^2 - q_1^2)\, d\psi' = \int_{0.1\,\psi'_\delta}^{\psi'_\delta} (Q_2^2 - q_2^2)\, d\psi' \qquad (22)$$

The velocity profiles at inlet and exit from the cascade are approximated by

$$\left(\frac{q}{Q}\right)_1 = \left(\frac{z}{\delta_1}\right)^{n_1} = \left(\frac{\psi'}{\psi'_{\delta_1}}\right)^{\frac{n_1}{1+n_1}}$$

and (23)

$$\left(\frac{q}{Q}\right)_2 = \left(\frac{z}{\delta_2}\right)^{n_2} = \left(\frac{\psi'}{\psi'_{\delta_2}}\right)^{\frac{n_2}{1+n_2}}$$

These two profiles can be substituted into equation (22) and this leads to

$$Q_1^2\, \psi'_{\delta_1}\, f(n_1) = Q_2^2\, \psi'_{\delta_2}\, f(n_2)$$

$$\text{where} \quad f(n) = 0.9 - \frac{1+n}{1+3n}\left[1 - (0.1)^{\frac{1+3n}{1+n}}\right] \qquad (24)$$

Since there is no loss of stagnation pressure, the streamline $\psi^1_{\delta_1}$ which is at the edge of the inlet boundary layer remains the edge of the boundary layer at outlet,

$$\psi'_{\delta_1} = \psi'_{\delta_2}$$

or

$$\frac{Q_1 \delta_1 \cos\alpha_1}{1+n_1} = \frac{Q_2 \delta_2 \cos\alpha_2}{1+n_2} \qquad (25)$$

and equation (23) reduces to

$$Q_1^2 f(n_1) = Q_2^2 f(n_2) \qquad (26)$$

If the inlet profile and Q_2 are known, then the exponent n_2 for the outlet boundary layer is given by equation (26) and the thickness δ_2 is obtained from equation (25). Calculations indicate that the solutions for n_2 and δ_2 are not sensitive to the extent of the boundary layer over which the integration is taken in equation (22).

To demonstrate the use of this analysis, consider a compressor cascade with an inlet flow where the wall boundary layer can be represented by a 1/7th power law, $H_1 = 1.286$. If the exit flow angle is chosen to cause separation of the end wall boundary layer, then at exit from the cascade $H_2 = 1.8$, or $n_2 = 0.4$. From equation (26), the mainstream velocities are related by

$$Q_2 = 0.7\, Q_1$$

The analysis suggests that the end wall boundary layer will separate when the exit velocity is less than 0.7 of the inlet velocity, which is essentially the same as de Haller's criterion for the stalling of a cascade.

THE EFFECT OF AXIAL VELOCITY RATIO IN THE BOUNDARY LAYER

If there is a change of velocity profile across the cascade, then there is a change of axial velocity for the streamlines which lie within the boundary layer. The theory of secondary flow has been extended to include a change in axial velocity across a cascade, ref. (7) and this can now be applied locally using the predicted change in the velocity profile. The method of calculation proceeds as follows:

1. given the inlet profile parameters n_1 and δ_1, calculate n_2 and δ_2 for the exit flow,
2. the position of the streamlines is determined upstream and downstream of the cascade and the local change of axial velocity is found,
3. the normal component of vorticity at inlet is found for each streamline using the smoothed profile,
4. the distributed secondary vorticity at exit from the cascade is calculated for each streamline, including the effect of the local change of axial velocity,
5. the secondary flow stream function and the variation of outlet flow angle are determined

This analysis has been applied to the N.G.T.E. cascade and fig. 3 shows the predicted variation in outlet angle for the smoothed inlet profile. The overall effect of including the local change of axial velocity is to move the position of maximum underturning to a lower value of z, but there is no significant improvement in the level of agreement with the experimental results.

SECONDARY FLOW BASED ON THE PREDICTED EXIT ANGLE

In equation (5), the distributed secondary vorticity is based on the assumption that the flow in the shear layer is turned through the same angle as the mainstream flow, $\alpha_2 - \alpha_1$. In practice, the flow turns through an angle $(\alpha_2 + \Delta\alpha_2 - \alpha_1)$ where $\Delta\alpha_2$ is the spanwise variation of the exit flow angle. It can be argued that the value of ξ_{sec} should be based on the predicted exit flow angle $\alpha_2 + \Delta\alpha_2$. The calculation for the secondary flow would be made in a plane normal to the mainstream flow and it would be based on the vorticity normal to the plane. The calculation procedure is iterative and takes the following form:

1. calculate the distributed secondary vorticity for a specified outlet flow angle α_2, allowing for the change in velocity profile,
2. determine the variation of exit flow angle, $\Delta\alpha_2$,
3. re-calculate ξ_{sec} and the normal component of vorticity at outlet, ξ_{n2}, using the predicted outlet angle $\alpha_2 + \Delta\alpha_2$,
4. resolve ξ_{sec} and ξ_{n2} in the direction of the mainstream flow to obtain the vorticity normal to the calculating plane,
5. re-calculate the variation of α_2,
6. return to step 3 and repeat until the process converges

This scheme has been applied to the N.G.T.E. cascade and fig. 3 shows a comparison with the experimental results. The use of the predicted flow angle in this iterative process leads to a slight improvement in the level of agreement.

THE PITCH AVERAGED STREAMWISE VORTICITY

The flow leaving a stationary blade row will usually form the inlet flow to a rotor row. It is therefore important to calculate not only the variation of exit flow angle, but also the pitch averaged streamwise vorticity, the streamwise vorticity at inlet to the following blade row. Dunham (4) has calculated the pitch averaged streamwise vorticity at outlet from the N.G.T.E. cascade and this forms a valuable test case to

check the predictions of secondary flow theory.

The pitch averaged streamwise vorticity $\bar{\xi}$ is given by

$$\bar{\xi} = \frac{1}{s \cos \alpha_2} \left[\xi_{sec} s \cos \alpha_2 + \xi_{fil} + \xi_{shed} \right] \tag{27}$$

If conventional secondary flow theory is used to evaluate ξ_{sec}, ξ_{fil} and ξ_{shed}, then from equations (5), (6) and (7).

$$\bar{\xi} = \xi_n \tan \alpha_2 \left[\frac{\cos \alpha_2}{\cos \alpha_1} - \frac{\cos \alpha_1}{\cos \alpha_2} \right] \tag{28}$$

However, if the alternative expression for ξ_{shed} is used, equation (8), then

$$\bar{\xi} = -q_2 \frac{d\alpha_2}{dz} \tag{29}$$

Differentiation of α_2 can be avoided by noting that for small shear

$$q_2 \frac{d\alpha_2}{dz} = \frac{d\bar{v}_n}{dz} \tag{30}$$

Now within the boundary layer

$$\frac{\partial w}{\partial y_n} - \frac{\partial v_n}{\partial z} = \xi_{sec}$$

and integrating across the flow, fig. 2,

$$(w_2 - w_1) - s \cos \alpha_2 \frac{d\bar{v}_n}{dz} = \xi_{sec} s \cos \alpha_2$$

The pitch averaged streamwise vorticity can then be expressed as

$$\bar{\xi} = -\frac{d\bar{v}_n}{dz} = \xi_{sec} + \frac{(w_1 - w_2)}{s \cos \alpha_2} \tag{31}$$

This is a more useful expression for $\bar{\xi}$ in that it avoids the need to differentiate the exit flow angle. Furthermore, comparison with equation (26) shows that

$$\xi_{fil} + \xi_{shed} = w_1 - w_2 \tag{32}$$

thus confirming that the strength of the trailing vortex sheet is consistent with the values of w calculated from the distributed secondary vorticity.

Fig. 4 shows a comparison between the values of $\bar{\xi}$ calculated by Dunham from the experimental data and the values given by equations (28) and (31). Equation (29) has been used as a check and it gives almost identical results to equation (31). The very small difference between the solutions from equations (29) and (31) may be caused by numerical errors introduced in differentiating α_2. It is clear from fig. 4 that conventional secondary flow theory, as represented in equation (28), is incorrect, while the new expression for $\bar{\xi}$, equation (29) or (31), gives good agreement with the experimental results. Since the two theories only differ in the expression used for ξ_{shed}, this example suggests that equation (8) is the better approximation for the trailing shed vorticity.

PREDICTION OF THE AXIAL VELOCITY PROFILE

The theory of secondary flow and the simple analysis for the end wall boundary layer can be combined to predict the variation of exit flow angle and the velocity profile in the direction of the mainstream flow. The axial velocity is given by

$$u_2 = q_2 \cos \alpha_2 - v_n \sin \alpha_2 \tag{33}$$

or using $v_n = q_2 \Delta\alpha_2$,

$$u_2 \approx q_2 \cos (\alpha_2 + \Delta\alpha_2)$$

The axial velocity profile downstream of the cascade is a combination of the mainstream velocity profile and the variation of the outlet angle α_2.

For the N.G.T.E. cascade, the inlet profile can be approximated by a 1/7th power law and the simple theory for wall boundary layers predicts that with an exit angle of -62.4°, the exit velocity profile is given by

$$\left(\frac{q}{Q}\right)_2 = \left(\frac{z}{\delta_2}\right)^{n_2}$$

where $\delta_2 = 0.91\delta_1$ and $n_2 = 0.025$. The shape factor for this theoretical flow is extremely low, 1.05. The

experimental data does not provide sufficient information to check this prediction, but the evidence suggests that the shape factor at exit may be far less than the value of 1.29 at inlet.

When this theoretical velocity profile is combined with the outlet angle predicted from secondary flow theory, then the axial velocity profile is as shown in fig. 5. The theory gives a remarkably accurate prediction for the shape of the axial velocity profile, including the unusual 'hump' in the experimental results. However, the theory is not sensitive to the shape of the velocity profile in the mainstream direction and the 'hump' in the axial velocity profile is mainly associated with the region of underturning.

CONCLUSIONS

The theory of secondary flow has been applied to predicting the flow at exit from a linear cascade, including the variation of exit flow angle, the pitch averaged streamwise vorticity and the axial velocity profile. It has been shown that if a power law is used to represent the inlet velocity profile, then secondary flow theory predicts a discontinuity in $d\alpha_2/dz$ at the edge of the boundary layer. A smooth variation of exit flow angle is obtained by using a smooth profile to remove the discontinuity in the normal component of vorticity. With this smooth profile, the predicted variation in α_2 is in fair agreement with the experimental results, the maximum underturning being about 70 per cent of the experimental value.

When a shear layer is turned in a cascade, the shape of the velocity profile may change and a simple analysis has been given for estimating the outlet velocity profile. This analysis assumes an inviscid adjustment of the flow so that the kinetic energy deficit of the outer part of the boundary layer remains constant across the cascade. For a compressor cascade, this simple model predicts separation of the end wall boundary layer when the velocity at outlet is less than 70 per cent of the inlet velocity, a result which is very close to de Haller's criterion for the limiting diffusion in a cascade.

The theory for the end wall boundary layer can be used to estimate the exit velocity profile and the local change in axial velocity across the cascade. The theory of secondary flow with an axial velocity change can then be applied and the variation of exit flow angle can be calculated. Comparison with the experimental results shows that there is no significant improvement in the prediction of the exit flow angle. However, when the exit velocity profile is combined with the variation of α_2, then it is possible to obtain a very good prediction for the axial velocity profile.

The theory of secondary flow is based on the shear flow being turned through the same angle as the mainstream flow. This can be regarded as a first approximation in an iterative scheme where the distributed secondary vorticity is based on the predicted exit flow angle $\alpha_2 + \Delta\alpha_2$ and the vorticity in the mainstream flow direction is re-calculated on each iteration. This iterative process converges to a solution for the exit flow angle which is in closer agreement with the experimental results.

The pitch averaged streamwise vorticity $\bar{\xi}$ has been calculated and compared with the values obtained from Dixon's experimental results. It has been shown that conventional secondary flow theory gives a value for $\bar{\xi}$ which has the opposite sign to the experimental values over most of the shear layer. When the new expression for the trailing shed vorticity is used, there is close agreement with the experimental results. This comparison is important in that it indicates that the new expression for the trailing shed vorticity is a good approximation for the behaviour of a real cascade.

This review of recent work on secondary flow in linear cascades shows that with the improved expression for the trailing shed vorticity, good agreement is obtained with the experimental results for the variation in exit flow angle, the pitch averaged streamwise vorticity and the axial velocity profile. The N.G.T.E. cascade is a severe test case with high deflection and for this example, many of the assumptions of secondary flow theory may not be satisfied. With the wall boundary layer, the shear is not small, the Bernoulli surfaces may twist and much of the inlet boundary layer may be swept onto the suction surface of the blades. In these circumstances, it would be unreasonable to expect very close agreement with the experimental results and the predictions shown in this paper are perhaps better than might have been expected. With the development of methods for calculating three dimensional inviscid flows in cascades, it will be interesting to see whether better agreement with the experimental results is obtained, or whether the differences in figures 1 to 5 are caused by viscous effects.

REFERENCES

1. Horlock, J.H. and Lakshminarayana, B., Secondary flows, Annual review of fluid mechanics, no 5, 1973.

2. Came, P. and Marsh, H., Secondary flow in cascades: two simple derivations for the components of vorticity, I.Mech.E. Jnl. Mech.Eng.Sci., Vol 16, no. 6, 1974.

3. Hawthorne, W.R. Rotational flow through cascades. Part 1: The components of vorticity, Q. Jnl.Mech. Appl.Math., vol 8, pt. 3, 1955.

4. Dunham, J. Private communication.

5. Hawthorne, W.R. and Armstrong, W.D., Rotational flow through cascades, Part 2: The circulation about the cascade, Q.Jnl.Mech.Appl.Math., vol 8, pt. 3, 1955.

6. Hawthorne, W.R. , Some formulae for the calculation of secondary flow in cascades, A.R.C. Report No. 17519, 1955.

7. Marsh, H. Secondary flow in cascades: the effect of axial velocity ratio, I.Mech.E. Jnl.Mech.Eng.Sci. vol 16, no. 6, 1974.

ACKNOWLEDGEMENTS

The work described in this paper forms part of a research project at Durham University on secondary flow and it has been supported by the National Gas Turbine Establishment.

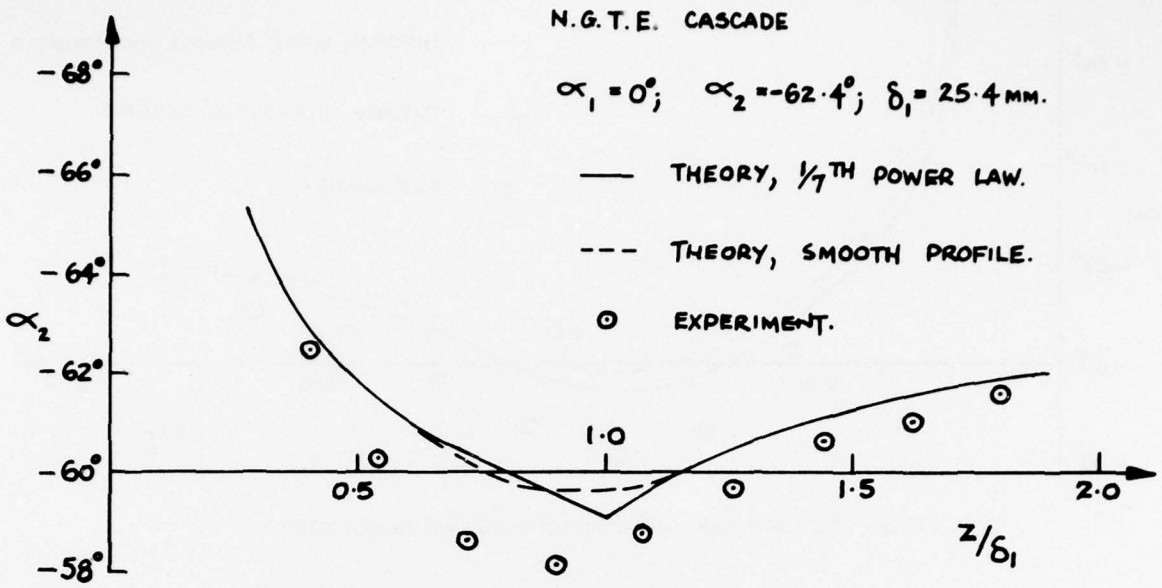


Fig. 1 Exit flow angle, effect of inlet profile

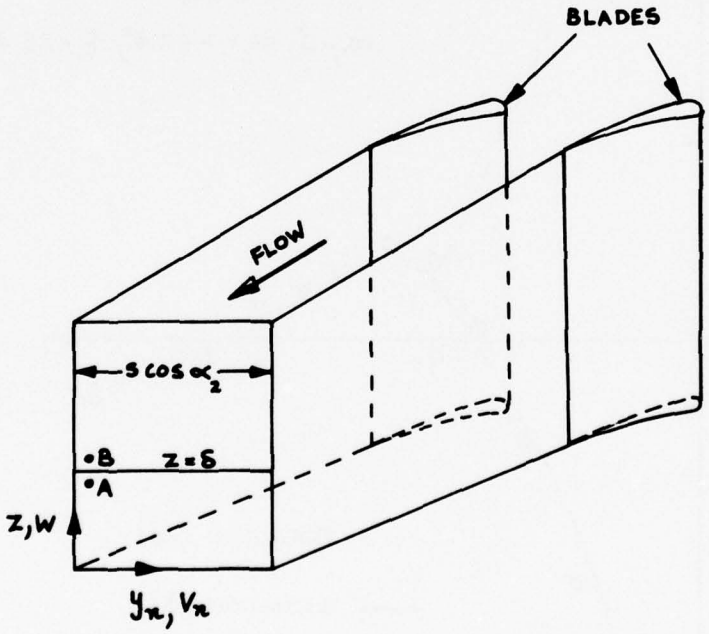


Fig. 2 Flow downstream of the cascade

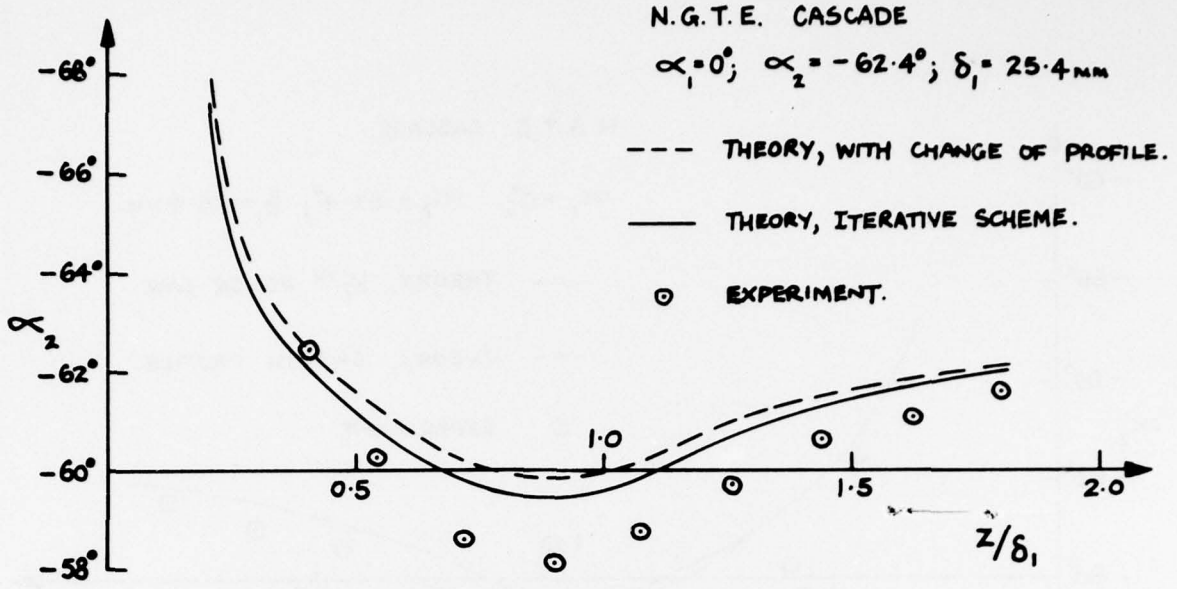


Fig.3 Exit flow angle, with change of profile and iterative scheme

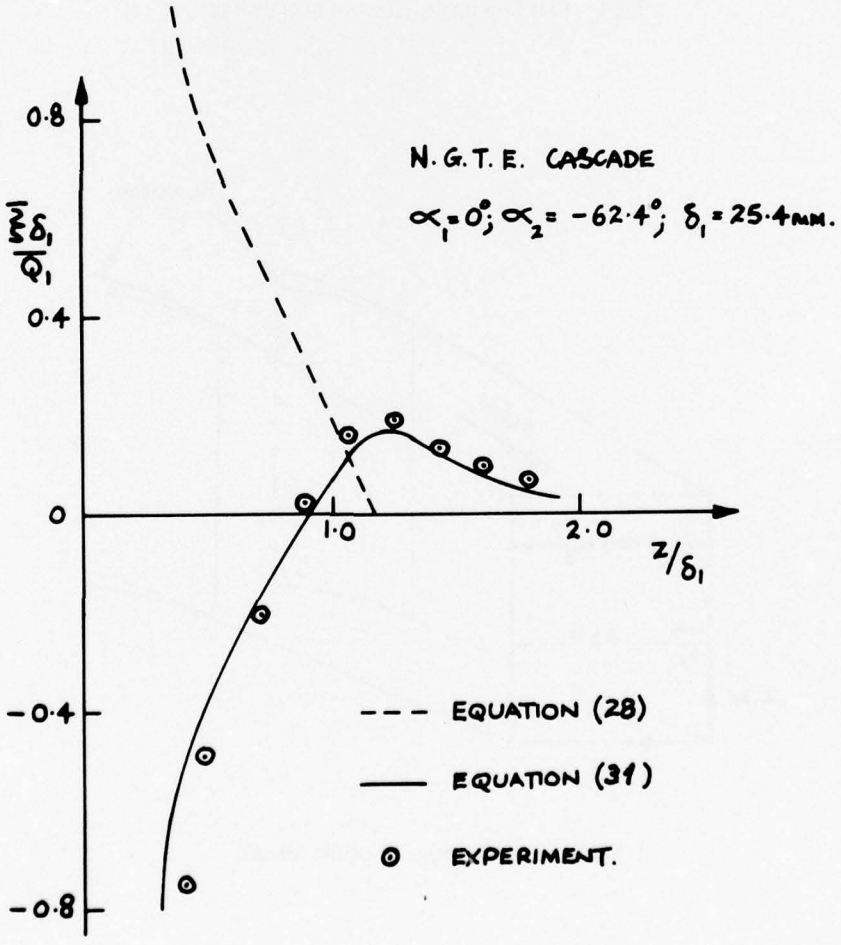


Fig.4 Pitch averaged streamwise vorticity

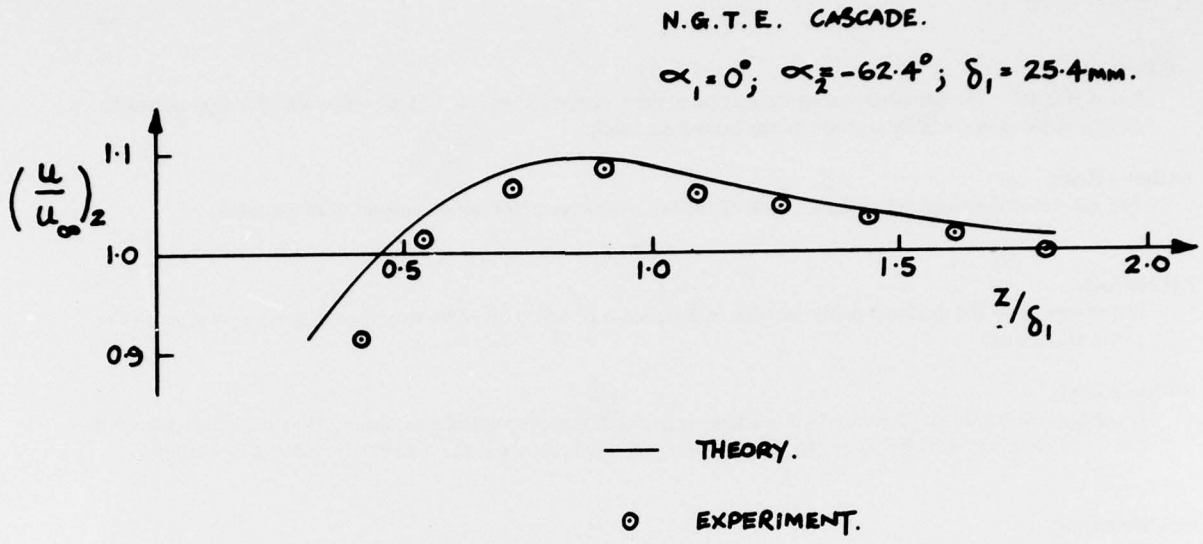


Fig.5 Axial velocity profile at outlet

DISCUSSION

Author

Equation 3 uses Hawthorne's expression for the trailing shed vorticity and it therefore assumes that there is not trailing shed vorticity outside the boundary layer. It is the expression for the trailing shed vorticity which is incorrect, Equation 3 in the paper, also the assumption that the trailing shed vorticity occures only within the shear layer. If the secondary velocity components are calculated from the distributed secondary vorticity, then spanwise velocities are found outside of the boundary layer and the secondary flow extends out to the mid-span of the blades.

J.H.Horlock

But if you solve the equations using Reference 6, the Current Paper No. 17519, these will give you non-zero pitchwise average vorticity outside of the boundary layer.

Author's Reply

The predicted spanwise velocities outside of the boundary layer are not consistent with Equation 3.

J.H.Horlock

But if you solve the problem using analysis of Reference 6, will it give you exactly the same answer as you've got in this paper?

Author's Reply

If the expression for the trailing shed vorticity is ignored, then the correct secondary flow is obtained from the numerical solution of the flow in the passage using the expression for the distributed secondary vorticity.

C.H.Sieverding

Refering to Figure 3 of your paper. You have a difference of the order of half a degree. My question is really directed towards the engine manufacturers: what kind of accuracy would you like to have for the prediction over the height within the secondary flows? Is two or three degrees sufficient (encountered in the comparisons between theories and experiments)?

B.Barry

I think we will be very pleased to have $\pm 0.5°$. We have very often to be content with rather less. I would have thought that ± 1 to 2 degrees is the best we can achieve in some of our turbine test experiments. In the cascade experiment we would certainly look for that sort of degree of accuracy.

Author's Reply

I would describe the level of agreement in Figure 3 as encouraging rather than good. The maximum underturning is $4°$ and the predicted value is about $2.5°$.

U.Stark

How can the vortex line behind the cascade have the correct inclination when at the same time the calculated time difference of fluid particles does not compare with experimental results.

Author's Reply

In the theory it is necessary to calculate the inclination of a vortex filament to the mainstream flow at exit from the cascade. For the many bladed cascade model, the inclination can be obtained from the estimate for the time difference for particles passing over the pressure and suction surfaces of the blades. In the real cascade, it is possible that the estimate for the inclination remains accurate, even though it was derived for the many bladed cascade model, but at the same time, the estimate for the time difference may not be so accurate, probably as a result of the effects of blade thickness.

UNDERSTANDING TURBINE SECONDARY FLOW

by

Wayne A. Tall
United States Air Force
Aero-Propulsion Laboratory
Wright-Patterson AFB, Ohio 45433, USA

SUMMARY

Practical utilization of high temperature technology in a gas turbine engine commands careful control of the flow in three dimensions, particularly in low aspect ratio, axial flow turbines. A review of the literature of radial fluid motion and three-dimensional viscous flow in such cascades discloses many contradictory interpretations which cannot lead to improved understanding of low aspect ratio cascade flow. More recent experiments demonstrate that earlier experiments were guided by a false understanding of such flows, especially near the cascade endwalls. A recent effort using annular cascades and a three-dimensional, viscous flow analysis to improve stage performance rather than merely to correlate cascade results, demonstrates the tremendous potential of three-dimensional viscous flow analysis techniques to help us understand this flow problem.

SYMBOLS

g -- gravitational constant

Δh -- enthalpy drop

J -- mechanical equivalent of thermal energy

δ -- referenced pressure (ratio to standard atmospheric pressure)

θ -- referenced temperature (ratio to standard atmospheric temperature)

U_m -- mean wheel speed

$\dot{\omega}$ -- air flow

INTRODUCTION

In appendix 1 of his paper (Ref 1), Dunham lists several experimental investigations of radial fluid motion in annular and flared turbine cascades, yet radial effects were not included in the secondary flow loss model proposed in his paper. Rather, that model proposed to correlate turbine endwall losses to turbine geometry and inlet boundary layer thickness. Dunham based his correlation on the prevailing belief that the mechanisms of secondary flows were understood, yet the magnitude of the losses that his formula correlated were larger than could be explained by the prevailing understanding of secondary flows. Meanwhile, some workers -- particularly those manufacturing small, cooled engines -- voiced their concern that small engine problems were not understood (Ref 2). Dunham concluded that the influence of inlet boundary layer thickness required more study in order to quantify losses. He also concluded that a fresh approach was needed to better understand endwall losses, especially the part played by the radial motion of the fluid, although he maintained that the basic mechanisms were understood.

Hosney and Tabakoff (Ref 3) conducted an extensive study of loss calculation and secondary flow analysis procedures. They suggested a change to Dunham's formula so that positive secondary flow loss is calculated at zero flow deflection through the cascade. Hosney and Tabakoff addressed the small engine problem and recommended more study of very small low aspect ratio cooled turbines and further suggested that viscosity inside the channel be considered in secondary loss models. They expected that these models would provide more uniform flow into the rotor, further improving turbine performance. Hosney and Tabakoff then developed an endwall loss model based on the Johnston triangular model for inner sublayer shear flow. This model was checked against data from a large sharp-edged impulse airfoil section (Ref 4). The agreement with endwall cross-flow pathlines was good. But, the sharp leading edge and the large scale resulted in minimum radial flow. Their paper concluded with a discussion of Deich's airfoil tilting and endwall meridional constriction concepts. Hosney and Tabakoff provided neither guidelines nor suggestions for coping with radial flows beyond their review of Deich. No specific attempt to provide assistance to small engine turbine designers was presented in spite of their stated recognition of problems peculiar to small engine turbines.

Booth (Ref 5) developed an endwall model using Johnston's triangular velocity model and accounting for losses other than friction. He stated that his model was incorporated into a turbine design system to be used for endwall cooling studies and designs. That design system, although not described in the paper, addressed some effects of cross flow on the core flow. However, it still represented a "patch" approach of partial solutions -- the blade to blade, the endwall, and the streamline analysis. The fact remained that radial gradients had not been accurately accounted for.

CONTROL OF FLOW IN TURBINES

The initial effort to control or influence endwall flow behavior was reported by Dorman, Welna, and Lindlauf (Ref 6). Dorman et al called their concept "controlled vortex" aerodynamics. Simply, the radial reaction distribution was changed from that which keeps the product of radius and swirl velocity a constant so that reaction was increased at the inner wall and decreased at the outer wall. An effort sponsored by the U.S. Air Force Aero-Propulsion Laboratory (AFAPL) developed this concept further on a fan-drive, high aspect ratio turbine (Ref 7). The airfoils were designed with lower endwall camber (and specific work) near the inner wall while more camber and specific work was designed into the mean diameter section of the foil; therefore, lower endwall losses were expected. Figure 1 shows the radial specific work gradients employed. Figure 2 shows the performance compared to previous free vortex designs.

Several subsequent efforts to develop this technique were never reported.* In one such effort Schlegel, Liu, and Waterman (Ref 8) reported on the application of this technique to a low aspect ratio small turbine. They concluded that stage losses were reduced by better control of the nozzle exit flow and the reduced solidity required by the endwalls (Fig 3), and that more investigation was needed to determine how specific work should be radially distributed.

Some insight into the general state-of-the-art of controlling flow in turbines may result from a comparison of the results and conclusions from Schlegel et al with those of Ewen, Huber, and Mitchell (Ref 9). Table 1 provides some pertinent parameters.

TABLE 1

	Schlegel, et al Ref 8 Turbine	Ewen, et al Ref 9 Turbine
Corrected Airflow $\dot{w}\sqrt{\theta/\delta}$	1.02 lbm/sec ~.5 Kg/sec	1.02 lbm/sec ~.5 Kg/sec
Corrected Specific Work $\Delta h/\theta$	32.5 BTU/lbm 75,500 Joules/Kg	30.8 BTU/lbm 71,500 Joules/Kg
Mean Velocity Ratio $Um/\sqrt{2gJ\Delta h}$	0.53	0.65
Blade Height	0.54 in. ~1.37 cm	0.57 in. ~1.45 cm
Exit Mach Number } Nozzle	1.19	0.88
Exit Mach Number } Rotor	1.06	1.04
Rotor Tip Clearance	0.010 in. ~0.025 cm	0.010 in. ~0.025 cm
Design Point Efficiency (Actual)	85%	84+%

Ewen, Huber, and Mitchell concluded in their paper that:

(1) high reaction was beneficial, especially at low solidity, and

(2) the contoured outer diameter endwall was effective in reducing secondary losses.

In view of the velocity ratio and cascade row exit Mach number differences, Ewen's design must be higher reaction; it is a fairly common argument that increased reaction is a prime method of increasing stage efficiency. Presentation of dissimilar data hinders comparison, since Ewen presented radial distribution of efficiency and Schlegel did not. Further, Schlegel presented nozzle exit angle distribution and Ewen did not. Finally, the design of Ewen, Huber, Waterman featured the inflection endwall meridional constriction and Schlegel, Liu, Mitchell design featured a bellmouth endwall constriction. According to Ewen, Huber, and Mitchell the Schlegel, Liu, and Waterman design should have developed up to four counts less efficiency (Fig 4); but the efficiencies are nearly equal and the latter design, as mentioned, showed superior control of nozzle exit angle. These results do not support the arguments that reaction or inflection endwall constriction necessarily improve performance. (The author is aware that the higher reaction of the Ewen design produces exit swirl similar to the swirl of the low velocity ratio design of Schlegel.)

The paper by Okapuu (Ref 10) provides another interesting comparison. His work is compared to an even smaller diameter, lower hub radius/tip radius ratio turbine with higher inlet relative blade Mach numbers designed by Helton, Lueders, and Arvin (Ref 11). Neither of these turbines should be considered a coolable design in their test form. Pertinent data are tabulated in Table II.

Okapuu used the controlled vortex concept of Dorman et al to achieve his performance. Helton employed the further refinement of radial work distribution (Ref 7) and a recent development in endwall loss modeling (Ref 5). Neither Okapuu's standard design nor Helton's design used endwall meridional constriction. Okapuu did use the inflection endwall in an alternate design of the nozzle, but found little improvement at design point (Fig 5). The performance of Okapuu's turbine was improved somewhat for lower overall pressure ratios at design speed, but these conditions correspond to negative rotor hub reaction plus a subsonic turbine nozzle exit Mach number. Okapuu also found

*Based on private communications

TABLE II

	Okapuu Ref 10 Turbine	Helton, et al Ref 11 Turbine
Corrected Airflow $\dot{\omega}\sqrt{\theta}/\delta$	2.4 lbm/sec 1.2 Kg/sec	1.5 lbm/sec 0.75 Kg/sec
Corrected Specific Work $\Delta h/\theta$	36.0 BTU/lbm 83,500 Joules/Kg	33.4 BTU/lbm 77,500 Joules/Kg
Mean Velocity Ratio $U_m/\sqrt{2gJ\Delta h}$	0.58	0.48
Blade Height	1.14 in ~2.90 cm	0.94 in ~2.39 cm
Rotor Relative Inlet Mach Number } Hub	N/A	0.68
Rotor Relative Inlet Mach Number } Mean	0.45	0.56
Rotor Tip Clearance	0.019 in ~0.048 cm	0.007 in ~0.018 cm
Rotor Tip Diameter	8.96 in ~22.75 cm	6.61 in ~16.80 cm
Hub radius / Tip Radius Ratio (rotor)	0.745	0.71
Hub Reaction	6-17%	16%
Efficiency Design Point	<90%	89%

negligible peak performance changes with change in reaction. Reaction changes did cause change in the overall pressure ratio at which maximum efficiency occurred. These data complement the previous comparison, specifically: reaction and meridional constriction (especially the inflection shape) are over-emphasized as means to improve performance, especially to improve the exit flow condition from transonic stators.

The point of the foregoing is simply this: Control of the fluid in three dimensions is required for good efficiency and in turn, control of the fluid in three dimensions requires the analysis capability to predict, or design, for the behavior desired. The controlled vortex approach was a start, the radial work distribution concept was an improvement, and a three-dimensional viscous analysis will offer more improvement.

Controlling fluid signifies some minimization of randomness. This fact is important in the calculation method. Not all details of every endwall flow situation requires modeling. For example, it may be possible to ignore reversed flow. If the calculation procedure indicates separation, and proceeds as though the flow did not reverse, the designer must search for those designs that do not separate. Under these restrictions, the three-dimensional analysis is a useful and adequate design tool. The important result from the analysis should be enough detail of the flow for competent designers to understand the underlying mechanisms and determine how to modify the cascade geometry to obtain the desired flow.

To separate this approach from the previous assumption of a core flow with boundary layer match, a review of some experimental work is presented. Simultaneously, some serious limitations of two-dimensional, low-speed cascade testing can be considered.

Carter and Lenherr (Ref 12) tested leaned airfoils in their experiments. This data was obtained from a high-speed, two-dimensional (planar) cascade. A qualitative argument was presented to interpret the results and define how to use blade leaning. Their qualitative argument must have been sound, since another investigator eventually produced these results analytically. But nowhere in the data nor in the argument was there a method for determining the proper lean for an annular cascade. In a verbal presentation in March 1976, Waterman (Ref 14) presented results of a three-dimensional, viscous, incompressible analysis used to define the proper lean distribution of two different turbine nozzle airfoils. One was a first-stage nozzle with a bellmouth shaped endwall, the other was a middle-stage nozzle with endwall divergence (flare). The intriguing piece of information was the prediction of different methods of leaning as optimum for the two cases. These were high subsonic or transonic cascades and were designed using incompressible theory in the three-dimensional viscous flow analysis.

Perhaps the best piece of experimental work on secondary flow definition remains that of Langston, Nice and Hooper (Ref 13). This work was conducted on a very large, low-speed, two-dimensional cascade. Axial chord was about 30 cm. The clear presentation of the leading edge endwall stagnation vortex, its position and path, streamlines resulting therefrom, the flow coming off the concave surface onto the endwall near the leading edge, the resultant boundary layer establishment and growth, and the downstream -- in and out of the channel -- behavior of the vortices on the convex side near the endwall make this a landmark experiment. It certainly dispells any remaining notions that secondary flows in cascades are understood.

Two conclusions from their work are pursued here because they help illustrate the limited usefulness of planar cascades in the study of endwall flow:

(1) conclusion number 4 states a net reduction of lift is realized because convex side diffusion did not occur near the endwalls, possibly because of the vortices there, and

(2) conclusion number 5 states that in the first half of the passage, the potential core remains two dimensional, but in the downstream half of the passage, this core is disturbed (skewed).

In a similar but less detailed experiment, Waterman and Tall (Ref 14) achieved near design lift near the endwalls in part annular, 0.3 Mach number tests. The airfoils were designed using the radially distributed work concept. Welna and Dahlberg (Ref 7) report that their part-annular cascade experiments showed a loss of lift for the airfoil near the inner diameter endwall. However, near the opposite endwall, the airfoil showed increased lift. Without downstream turning airfoils, Welna and Dahlberg agreed that the exit static pressure gradient could not be established for the cascades. Waterman and Tall used this information to design the downstream test section sidewalls to continue the desired static pressure gradients past the measurement station.

Several factors may have helped retain lift near the endwalls. Either the sidewalls and radial gradients reduced the diffusion on the outer endwall or increased meridional pressure gradients reduced the channel crossflow at the endwall. Since their primary goal was to demonstrate the usefulness of a three-dimensional viscous analysis in the design of a low aspect ratio turbine, Waterman and Tall accomplished insufficient testing or analysis to define which of the two phenomena was more important.

Their paper concluded that a three-dimensional viscous, incompressible flow analysis method agreed well with experimental data. This method is from Dodge (Ref 15). Because the agreement was good, the effect on cascade losses of vane solidity, vane stacking and endwall contouring could be analyzed.

In a continuation of the study, a stage was designed from a new turbine nozzle predicted to produce very low losses. Two rotor designs were included in the stage design. Incidence and actual rotor foil camber were varied in the rotor designs, but the same velocity triangles were maintained for the stage.

The goal of the nozzle design was reduced endwall losses and a minimum of radial fluid transfer. Minimum radial fluid transfer was believed to maintain design conditions into the rotor and reduce rotor entrance losses.

The design was developed as follows: A two-dimensional, blade-to-blade transonic flow analysis defined the desired two-dimensional turbine nozzle profiles for several radial sections. The three dimensional, viscous, incompressible analysis predicted cascade losses for each of two solidities. The lower solidity design was predicted to produce lower cascade losses. That design was refined with various endwall shapes and turbine nozzle leans again to produce lowest calculated cascade loss.

The rationale for using an incompressible flow analysis method to design a transonic turbine is two-fold:

(1) The method properly orders the overall cascade loss levels, even in the transonic flow region (Ref 14), and

(2) The initial section of the nozzle passage is subsonic and much is nearly incompressible; this is the region in which the channel cross-flow is established (Refs 13 and 14).

This second reason finds partial agreement with Langston's fifth conclusion. The consequences of the magnitude of "core skewing" seem much less important at larger turbine nozzle channel exit Mach numbers.

Preliminary test results on this stage indicate very low nozzle cascade losses, especially at the endwalls and very good stage efficiency (Fig 6 and 7), thereby justifying the design procedure. Table III compares design and test parameters.

TABLE III

LOW ASPECT RATIO PHASE II DESIGN PARAMETERS

	Phase I Design	Phase II Test
Corrected Flow $\omega\sqrt{\frac{\theta}{\delta}}$	6.559 lbm/sec ~ 3.0 Kg/sec	6.515 lbm/sec ~3.0 Kg/sec
Pressure Ratio	3.28	3.09
Specific Work	31.5 BTU/lbm 73,000 Joules/Kg	32.5 BTU/lbm 75,500 Joules/Kg
Clearance	--	0.013 in. 0.033 cm
Velocity Ratio	.54	--
Efficiency	--	92%

Hub Radius Tip Radius Ratio		0.84	--
Inlet Critical Mach Number	Hub	0.65	--
	Mean	0.51	

Since the nozzle endwall and lean are calculated to be largely responsible for this stage performance, a description seems in order.

The stage is designed for an unshrouded rotor and as mentioned, two rotors were designed. Table IV defines the incidence variations. These rotors were designed for the same velocity triangles and to have distributed radial work. The same two-dimensional time dependent transonic solution used for the nozzle airfoil profile design was used for the rotor airfoil profile design. No three-dimensional viscous flow analysis was available for the rotor design. The profiles of each design were stacked with their centers of gravity on a radial line, thus giving each rotor a conventional trailing edge appearance but a curvilinear leading edge appearance.

The motivation for these two incidence designs was the observation of data from Welna and Dahlberg (Ref 7) that negative incidence improved performance. The rotors in their work were higher aspect ratio, shrouded airfoil designs with lower rotor inlet Mach numbers. Those rotors also used somewhat smaller negative incidence angles. Test results from the continuation design indicate somewhat lower performance for the negative incidence rotor. Indeed, the negative incidence rotor tests really ask more questions than were answered:

(1) Would negative incidence angle provide better performance?

(2) Does negative incidence only at the endwall with zero incidence at midspan provide best performance?

(3) Does negative incidence at the unshrouded rotor tip provide improved performance?

This very uncertainty exemplifies the value of even a crude three-dimensional, viscous calculation procedure. Availability of such a procedure could have established trends and been useful to interpret such questions regarding the test results.

THE FUTURE

Future items of investigation should include:

(1) compressible analysis

(2) rotor analysis

(3) rotor tip clearance analysis, and

(4) rotor-to-nozzle interaction analysis

These items require additional investigation and only limited, and perhaps misleading, results can be expected from low-speed, two-dimensional testing. Experimentation alone cannot expeditiously study turbine stage three-dimensional flow problems. Analysis in three dimensions, wit viscosity, will become an integral part of future investigations. Details of cascade geometry will become important items for consideration -- leaning, solidity, fillet radii, axial spacing, endwall shaping, modification of airfoil camber distribution at endwalls, and rotor tip geometry for thick, cooled airfoils. Such items must be analytically modeled if the ambiguous and sometimes contradictory history of secondary flow investigation is not to be continued.

REFERENCES

1. Dunham, J., "A Review of Cascade Data on Secondary Losses in Turbines," J. of Mechanical Engineering Sciences, Vol 12, No 1, 1970.

2. Benstein, Eli H., "Small Flying Engines ARE Different," AIAA Paper No. 74-1185.

3. Hosney, W. and Tabakoff, W., "An Analysis of Losses and Secondary Flow in Turbine Cascades," Project Themis Report No. 71-23, December 1971.

4. Woods, J.R., Jr., "An Investigation of Secondary Flow Phenomena and Associated Losses in a High-Deflection Turbine Cascade," Thesis, Naval Postgraduate School, Monterey, California, September 1972.

5. Booth, T.C., "An Analysis of the Turbine Endwall Boundary Layer and Aerodynamic Losses," ASME Paper 75-GT-23.

6. Dorman, E.E., Welna, H., and Lindlauf, R.W., "The Application of Controlled Vortex Aerodynamics tc Advanced Axial Flow Turbines," ASME Paper No. 68-GT-4, March 1968.

7. Welna, H. and Dahlberg, D.E., "Investigation of a Highly Loaded Two-Stage Fan-Drive Turbine," AFAPL-TR-69-92, Vol VI, November 1971.

8. Schlegel, J.C., Liu, H.C., and Waterman, W.F., "Reduction of Endwall Effects in a Small, Low-Aspect-Ratio Turbine by Radial Work Distribution," ASME Paper No. 75-GT-7.

9. Ewen, J.S., Huber, F.W., Mitchell, J.P., "Investigation of the Aerodynamic Performance of Small Axial Turbines," ASME Paper No. 73-GT-3.

10. Okapuu, U., "Some Results from Tests on a High Work Axial Gas Generator Turbine," ASME Paper No. 74-GT-81.

11. Helton, D.J., Lueders, H.G., and Arvin, J.R., "An Experimental Investigation of a Subscale Variable Pressure Ratio High Thru Flow Turbine," AFAPL-TR-77-7.

12. Carter, A.F., and Lenherr, F.K., "An Investigation of Efficiency Limits for Small, Cooled Turbines", USAAVLABS Technical Report 70-14, August 1970.

13. Langston, L.S., Nice, M.L., and Hooper, R.M., "Three-Dimensional Flow Within a Turbine Cascade Passage," ASME Paper 76-GT-50.

14. Waterman, W.F., and Tall, W.A., "Measurement and Prediction of 3-D Viscous Flows in Low-Aspect-Ratio Turbine Nozzles," ASME Paper No. 76-GT-73.

15. Dodge, P., "A Numerical Method for 2-D and 3-D Viscous Flows", AIAA Paper No 76-425.

STAGE WORK VS PERCENT SPAN

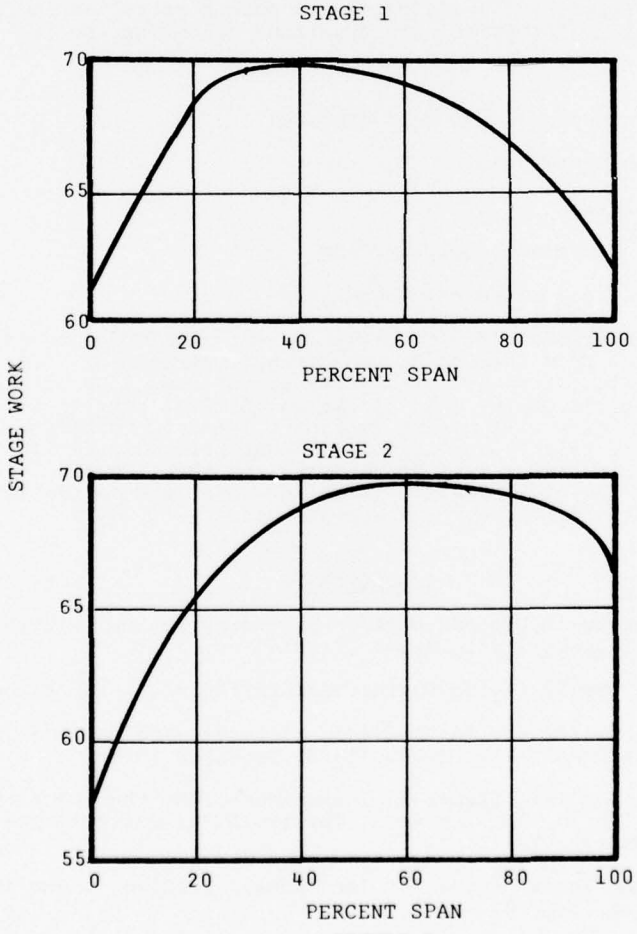


FIGURE 1

COMPARISON OF RADIAL WORK DISTRIBUTION
AND FREE VORTEX DESIGN METHODS

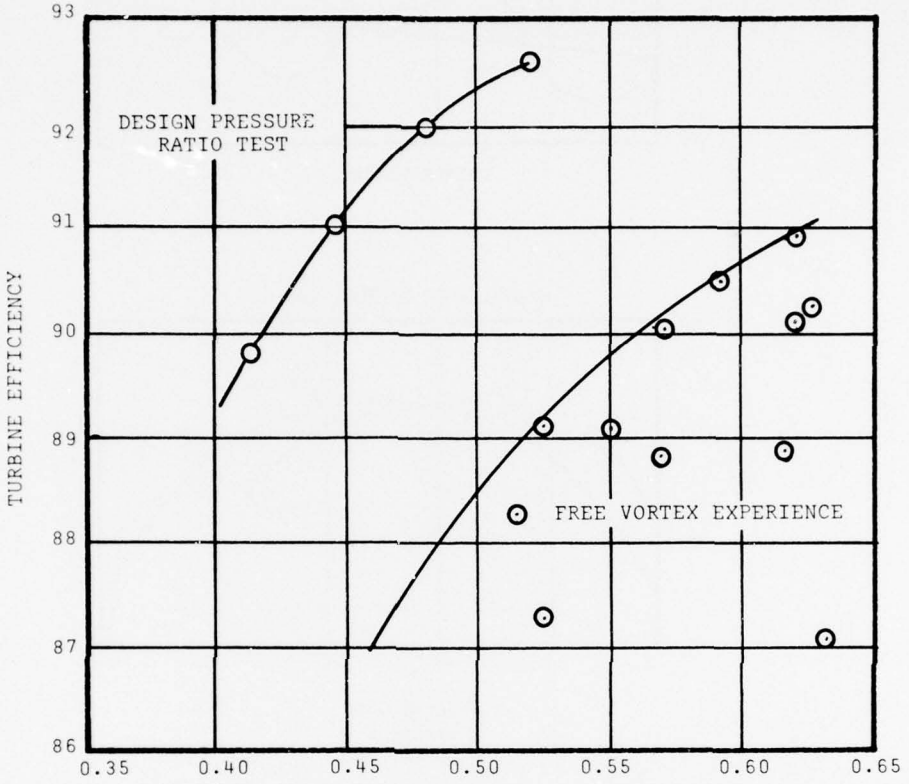


FIGURE 2

Nozzle Exit Angle Control

RADIAL WORK DISTRIBUTION
vs
FREE VORTEX DESIGN METHODS
(AFTER SCHLEGEL)

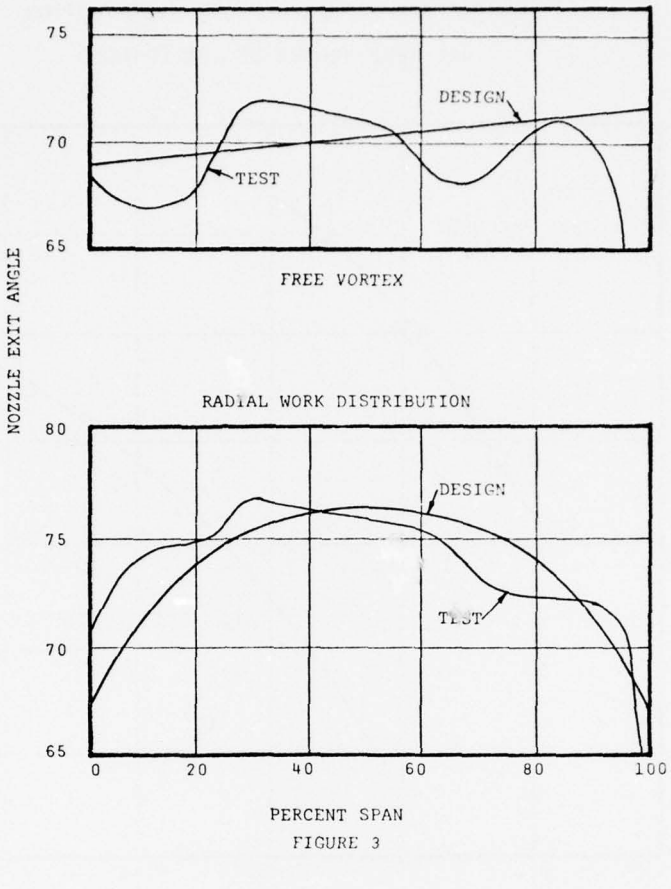


FIGURE 3

Turbine Performance

(AFTER EWEN, HUBER, MITCHELL)

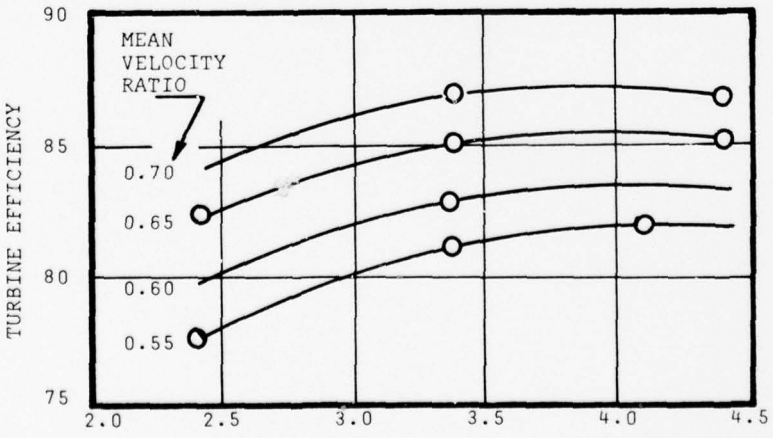
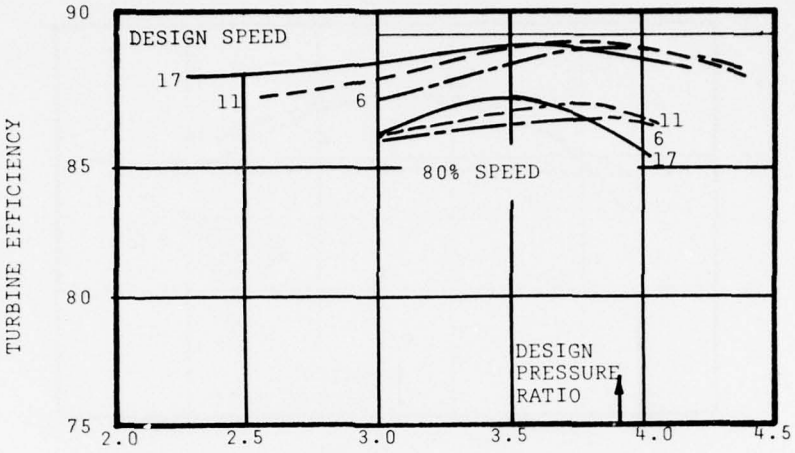


FIGURE 4

Turbine Performance
After Okapuu

EFFECT OF REACTION ON EFFICIENCY

VALUE IS ROOT REACTION
AT DESIGN PRESSURE RATIO AND SPEED



TURBINE PRESSURE RATIO

FIGURE 5

Low Aspect Ratio Turbine
Nozzle Losses

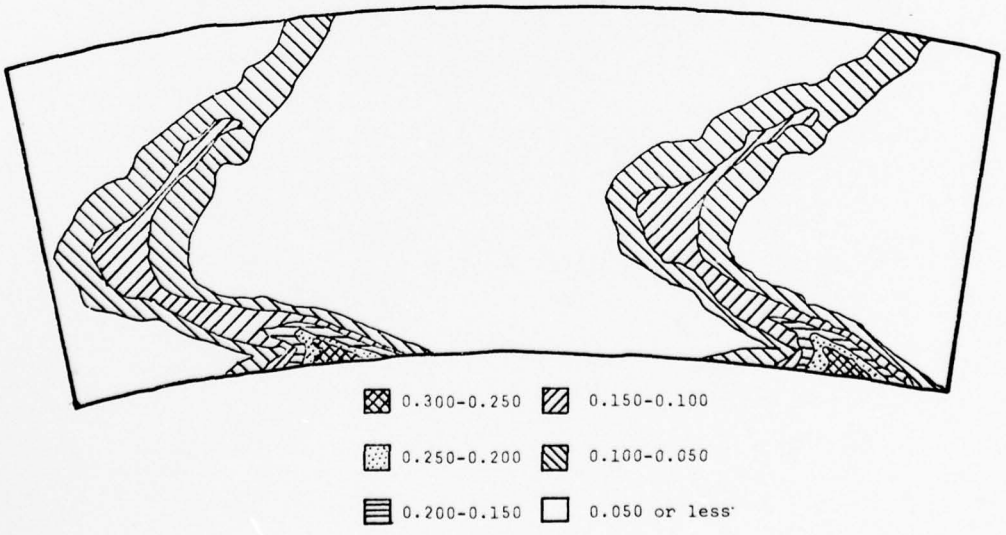
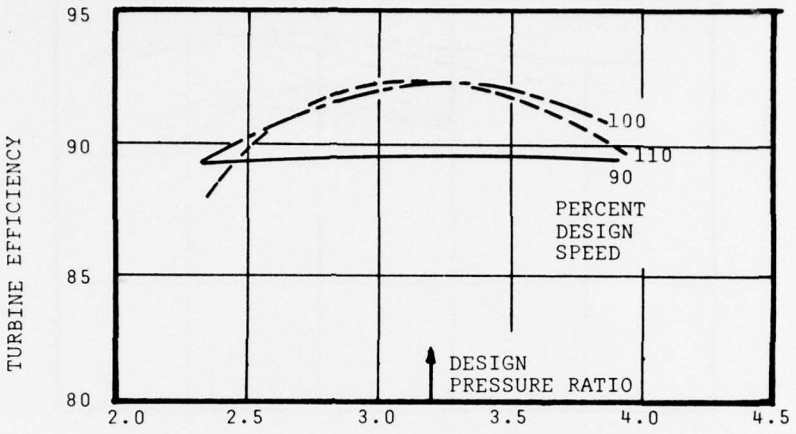


FIGURE 6

Low Aspect Ratio Turbine

MEASURED PERFORMANCE



TURBINE PRESSURE RATIO

FIGURE 7

DISCUSSION

J.Dunham

May I assure you that my correlation of secondary losses was purely empirical, not based on the belief that secondary flows were understood.

You have achieved very high efficiencies. How do they compare with predictions by Ainley and Mathieson's method? In short, how much efficiency have you gained by your careful design?

You state that your Reference 14 nozzle design goal was to minimize radial fluid transfer, presumably by minimizing the radial pressure gradient, in order to reduce rotor entrance losses. Do you believe this was successful and should it be used in future?

Author's Reply

Some indication of the improvement due to the careful design may be indicated by the following considerations.

The overall cooled efficiency goal was about 85%, requiring about 87% or so for the initial uncooled (adiabatic) efficiency. This was based on usual global parameter estimation of efficiency. A more refined analysis, taking account of the improvements of radially distributed work, endwall contouring, solidity optimization, etc. . . resulted in a predicted efficiency of 89% (adiabatic, total to total).

The careful design (leaning and endwall contour optimization) predicted about 15% reduction in overall stator losses.

The fact that the test efficiency was higher than predicted, while nozzle losses were near predicted in magnitude and distribution, allows one to conjecture that the uniformity of the flow presented to the rotor by the turbine nozzle may be responsible for the higher efficiency attained. This attitude was prevalent during the final stator and the rotor designs. Only more work can affirm this conjecture or supposition.

Of course, there are cases, as Waterman pointed out, where radial motion may be required. In these cases, *uniform* radial motion would be desired.

W.Schlachter

How are your turbine efficiencies defined? Are those isentropic total to total efficiencies?

Author's Reply

Those are isentropic total to total efficiencies and it is a cold air rig. The downstream section is insulated and is very near ambient temperatures, so there is almost negligible heat loss as far as measuring efficiency is concerned. The efficiencies were checked with temperatures and with torque meters and they agreed within half a percent in either case.

P.Came

Do you have a figure for the stage loading of the turbine?

Author's Reply

The stage loading is around 1.7.

P.Came

Is there any reason why the 100% and 110% speed lines in Figure 7 are dashed as opposed to the solid line at 90% speed?

Author's Reply

No. That is only for clarification of following the lines. Those are data points.

C.H.Sieverding

What are your estimations as to the beneficial effect of endwall shaping on the turbine efficiency?

Author's Reply

Analytically, the proper analog finally accounted for about 10 to 15% reduction in overall losses (of overall stage losses).

B.Barry

You emphasize the use of 3-D viscous methods for successful design of high efficiency turbine components. Most advanced propulsion engines now include substantial coolant ejection. Would you include coolant ejection in your 3-D design process?

Author's Reply

We will. We are working on that.

EFFECT OF ENDWALL COOLING ON SECONDARY FLOWS IN TURBINE STATOR VANES

Louis J. Goldman and Kerry L. McLallin

National Aeronautics and Space Administration
Lewis Research Center
Cleveland, Ohio, 44135

SUMMARY

An experimental investigation was performed to determine the effect of endwall cooling on the secondary flow behavior and the aerodynamic performance of a core-turbine stator vane. The investigation was conducted in a cold-air, full-annular cascade, where three-dimensional effects could be obtained. Two endwall cooling configurations were tested. In the first configuration, the cooling holes were oriented so that the coolant was injected in line with the inviscid streamline direction. In the second configuration, the coolant was injected at an angle of 15° to the inviscid streamline direction and oriented toward the vane pressure surface. In both cases the stator vanes were solid and uncooled so that the effect of endwall cooling could be obtained directly.

Total-pressure surveys were taken downstream of the stator vanes over a range of cooling flows at the design, mean-radius, critical velocity ratio of 0.778. Changes in the total-pressure contours downstream of the vanes were used to obtain the effect of endwall cooling on the secondary flows in the stator. Comparisons are made between the two cooled-endwall configurations and with the results obtained previously for solid (uncooled) endwalls. The results presented in this paper are the first part of a comprehensive program of endwall cooling studies currently in progress at NASA.

SYMBOLS

C_p specific heat at constant pressure, J/kg-K (Btu/lbm-°R)

E energy parameter, eq. (4)

g force-mass conversion constant, 32.174 lbm-ft/lbf-sec^2

J mechanical equivalent of heat, 778.0 ft-lbf/Btu

J_z axial momentum parameter, eq. (2)

J_θ tangential momentum parameter, eq. (3)

M Mach number

$\bar{m}$ mass flow parameter at radius r, eq. (1)

$\bar{\bar{m}}$ total mass flow per passage, kg/sec (lbm/sec)

p pressure, N/m^2 (lbf/ft^2)

$\bar{p}$ circumferentially mixed pressure at radius r, N/m^2 (lbf/ft^2)

p_c inlet pressure of coolant, N/m^2 (lbf/ft^2)

p_0 inlet pressure of primary flow, N/m^2 (lbf/ft^2)

R gas constant, J/kg-K (ft-lbf/lbm-°R)

r radial direction, m (ft)

T temperature, K (°R)

T_c inlet temperature of coolant, K (°R)

T_0 inlet temperature of primary flow, K (°R)

V velocity, m/sec (ft/sec)

y mass flow fraction

z axial direction, m (ft)

α flow angle measured from axial direction, deg

γ ratio of specific heats

$\bar{\bar{\eta}}$ overall efficiency based on kinetic energy

θ vane angular spacing, deg

θ circumferential direction, deg

ρ density, kg/m^3 (lbm/ft^3)

Subscripts:

c coolant flow

cr flow condition at Mach 1

h hub

i survey position closest to inner (hub) wall

id ideal or isentropic process

L lower or pressure surface

o survey position closest to outer (tip) wall

p primary flow

s solid (uncooled)

T thermodynamic

t tip

U upper or suction surface

z axial direction

θ tangential direction

0 station at inlet plane of cascade bellmouth, fig. 2

1 station at vane inlet, fig. 2

2 station at vane trailing edge, fig. 2

3 station downstream of vane trailing edge where survey measurements were taken, fig. 2

3M station far downstream of vane trailing edge where flow was assumed to be circumferentially mixed (uniform), fig. 2

Superscript:

' total-state condition

INTRODUCTION

Experimental investigations are being conducted at the NASA Lewis Research Center (refs. 1 to 3) and under contract (ref. 4) to obtain the aerodynamic performance of air-cooled blading and endwalls for high-temperature, core-engine turbines. As part of this effort, the performance of a solid (uncooled) version of the core stator has been determined in a full-annular cascade (ref. 3). These results form the basis of comparison for the cooled versions of the core stator and endwalls. Downstream of the solid vanes and endwalls, two vortex cores of high loss concentration are located at the corners formed by the endwalls and the vane suction surface (ref. 3). Because of the low aspect ratio of these vanes (the ratio of vane height to vane axial chord is 1.0), these losses were expected and were identified with the secondary flows present in the stator. The secondary flow loss for the solid vanes and endwalls was estimated (ref. 3) to be a significant portion (about 28 percent) of the total loss. For cooled stators, one possible method of reducing these losses is to use the injected endwall coolant to modify the secondary flows in the stator vanes.

A test program was, therefore, undertaken to study the effect of endwall cooling on these secondary flows. Parameters to be investigated in the endwall cooling program include cooling hole location, cooling hole size, blowing rate, and coolant injection angle. The first part of this study, and the subject of this paper, is the effect of endwall coolant injection angle on these secondary flows and on the vane aerodynamic performance.

Two similar endwall cooling configurations were experimentally studied. In the first configuration, three rows of cooling holes were oriented so that the endwall coolant was injected in line with the inviscid streamline direction. In the second configuration, the coolant was injected at an angle of 15° to the inviscid streamline direc-

tion and oriented toward the vane pressure surface. In both cooled-endwall configurations, the coolant was injected at an angle of 15° to the endwall surface and the stator vanes were solid (uncooled), so that the effect of endwall cooling could be obtained directly. The coolant was injected at 15° to the inviscid streamline direction in the second configuration in an attempt to impede the crossflows that occur in the endwall boundary layers and thereby to decrease the secondary flow losses. In addition, flow visualization studies on flat plates (ref. 5) have shown that coolant injected at an angle to the streamwise flow direction tends to prevent the cooling film from separating from the surface even at high blowing rates. It might be possible, therefore, to reduce the secondary flow losses and by the same means increase the film cooling effectiveness.

The cooled-endwall investigation was conducted at the vane design, mean-radius, aftermixed, critical velocity ratio of 0.778. Annular total-pressure surveys were taken downstream of the vanes over a range of coolant to primary inlet total-pressure ratios from 1.0 to 2.0. This corresponds to coolant flow rates from 0.9 to 3.1 percent of the prima[illegible]low. All tests were conducted with primary air at ambient conditions at the case[illegible] and with a primary to coolant total-temperature ratio of 1.0. It was tho[illegible] comparison of the two cooled-endwall configurations could be made at t[illegible]ratio. In addition, the cold-test data can be used to predict the perfo[illegible]al engine temperature ratios by the method described in reference 6.

Th[illegible]scribes the two endwall cooling configurations tested and the results obtained. [illegible]tal-pressure contours downstream of the vanes are presented for selected coolant to primary total-pressure ratios. Changes in these total-pressure patterns are used to obtain the effect of endwall cooling on the secondary flow in the stator. How the vane aftermixed total pressure varies with radial position is shown for these coolant to primary total-pressure ratios. The percent change in aftermixed efficiency (from the solid endwalls) per percent coolant is also shown over the range of total-pressure ratios tested. The cooled-endwall results are compared, where applicable, with the results obtained for the solid (uncooled) endwalls. Comparisons are also made between the two endwall configurations tested. This paper also includes a description of future work planned in the endwall cooling program.

APPARATUS, INSTRUMENTATION, AND PROCEDURE

Cascade Facility

The full-annular cascade facility consists primarily of an inlet section, a test section, and an exit section. The actual facility and a cross-sectional view of the facility are shown in figures 1 and 2, respectively. In operation, primary or mainstream air (at ambient conditions) is drawn from the test cell through the inlet section, the blading, and the exit section and then is exhausted through the laboratory exhaust system. Cooling air at room temperature and 27.58 N/cm^2 (40 psig) is supplied by the laboratory combustion air system and is routed to the individual coolant circuits as shown in figures 1 and 2. For this investigation, only the hub and tip endwall cooling air was used since the vanes were solid (uncooled).

Inlet section. - The inlet, consisting of a bellmouth and a short straight section, was designed to accelerate the flow to uniform axial flow at the vane inlet. The bellmouth was designed to provide a smooth transition to the straight section and to minimize the boundary layer growth.

Test section. - The test section consists of a section of five vanes that are part of the full-annular ring of 36 vanes. As seen in figure 2, the vanes pass through two hollow vane rings (endwalls). This allows cooling air to be independently supplied to both the vanes and the endwalls. For the endwall cooling investigation reported herein, all the vanes were solid (uncooled). Only the four endwall passages between the five test vanes were cooled.

The stator vane geometry (same aerodynamic profile as in refs. 1 to 4) is shown in figure 3. The untwisted vanes, of constant profile from hub to tip, have a height of 3.81 centimeters (1.50 in.), an axial chord of 3.823 centimeters (1.505 in.), and a trailing-edge radius of 0.089 centimeter (0.035 in.). The vane aspect ratio and solidity at the mean section are 1.00 and 0.93, respectively, based on axial chord. The stator hub-to-tip radius ratio is 0.85 and the mean radius is 23.50 centimeters (9.25 in.).

Exit section. - The exit section consists primarily of a diffusing section and a flow straightening section (fig. 2). The diffusing section decelerates the flow downstream of the 3M station. The flow straightening section turns the swirling flow back to the axial direction prior to its entering the laboratory exhaust system. The straightener consists of a bundle of short tubes with centerlines parallel to the cascade axis (fig. 2).

Endwall Cooling Configurations

Two similar endwall cooling configurations were tested. A schematic representation of the configurations is shown in figure 4 for the hub endwall. In the first configuration, three rows of cooling holes were oriented so that the endwall coolant was injected in line with the inviscid streamline direction. In the second configuration, the coolant (within the vane passage) was injected at an angle of 15° to the inviscid streamline di-

rection and oriented toward the vane pressure surface. This was done in an attempt to impede the crossflows that occur in the endwall boundary layers and thereby to decrease the secondary flow losses.

The endwall cooling geometry and coordinates are presented in figure 5 and in table I. The in-line coolant injection configuration was designed for NASA under contract (ref. 4). This design had a row of cooling holes upstream of the vane leading edge, on both the hub and tip endwalls, which could not be fabricated in our hollow vane rings. In addition, as noted in table I, a number of cooling holes (primarily in the first row of holes) on the hub endwall could not be fabricated. This was caused by the shallow coolant injection angle (15° to the endwall surface) and the excessive hub endwall thickness that occurred during fabrication. To make comparison of the two configurations easier, the holes that could not be machined in the second configuration were filled with epoxy in the first configuration. In this way both configurations had the same number (and location) of open cooling holes (fig. 4). The row of cooling holes downstream of the vane trailing edge, on the tip endwall, were 0.038 centimeter (0.015 in.) in diameter and were aligned near the design flow angle for both configurations. All other cooling holes were 0.051 centimeter (0.020 in.) diameter. The actual hub and tip hollow vane rings for the first configuration (with all cooling holes open) are shown in figure 6.

Instrumentation

Instrumentation was provided to measure inlet total temperature and pressure, wall static pressures upstream and downstream of the test section, survey data of vane exit total pressure, and coolant supply conditions. All pressures were measured with calibrated strain-gage transducers, and all temperatures were measured with copper-constantan thermocouples. Figure 2 shows the station nomenclature used for the instrumentation.

Inlet total conditions. - The total temperature of the primary air was measured by four thermocouples located 90° apart circumferentially at the bellmouth inlet (station 0). The ambient pressure was measured by a transducer located near the cascade inlet. Prior to the subject investigation, boundary layer measurements of total pressure were made near the vane inlet (station 1).

Wall static pressures. - Static pressures were measured at various locations in the cascade by 0.051-centimeter (0.020-in.) diameter pressure taps located on both the hub and tip walls. At a distance of one axial chord length upstream of the vane inlet (station 1), four taps were located 90° apart circumferentially. These taps were used primarily to check the uniformity of the flow entering the vanes. At the vane exit survey plane (station 3), eight taps (on both the hub and tip endwalls) spanned the test section and were spaced circumferentially as shown in figure 7. These pressures were used to estimate the variation of static pressure with radius for use in the aerodynamic performance calculations. Two static taps (hub and tip wall) were also located 10.2 centimeters (4.0 in.) axially downstream of the vanes, where the flow would probably be mixed to relatively uniform conditions (station 3M). This hub static pressure was used to set the primary airflow conditions in the cascade.

Survey probe. - Vane aerodynamic performance data were obtained with the two-element, total-pressure probe shown in figure 8. This type of fixed-position probe allows survey data to be taken near both the hub and tip walls. The hub element (fig. 8) was used for measurements in the region that extended from near the hub wall up to a radial position of 75 percent of the vane span. The tip element was used in the remaining tip region. The survey plane (station 3, fig. 7) was 1.3 centimeters (0.5 in.) axially downstream of the vane trailing edge with the probe positioned at a fixed angle of 67° from the axial direction (design flow angle). Survey data were taken over three vane wakes to check for periodicity.

The probe elements were made of stainless-steel tubing having an outside diameter of 0.051 centimeter (0.020 in.) and an inside diameter of 0.038 centimeter (0.015 in.). The total-pressure tubes had inside bevels of 30°, which reduce the sensitivity of the total-pressure measurement to flow angle variations (ref. 7). The loss in total pressure was measured with a differential pressure transducer referenced to atmospheric pressure.

Coolant flow conditions. - The coolant flow rate was measured with calibrated venturi meters of various sizes. The venturi meters and runs conformed to ASME specifications and were calibrated before installation. The endwall coolant total pressures and temperatures were assumed to be equal to the static measurements made before the coolant entered the hollow vane rings (fig. 1). Errors of less than 1 percent resulted from this assumption because of the small coolant flow velocities (Mach numbers less than 0.1) in the supply tubing.

Test Procedure

To operate the full-annular cascade facility, atmospheric air from the test cell was drawn through the cascade and exhausted into the laboratory exhaust system. The primary airflow conditions were set by controlling the pressure ratio across the stator vanes with a throttle valve located in the exhaust system. The hub static-pressure tap located at station 3M downstream of the vane exit was used to set this pressure ratio.

Cooling air, at room temperature and 27.58 N/cm^2 (40 psig), was supplied by the

laboratory combustion air system. The desired coolant flow rate was obtained by setting the pressure upstream of the venturi with a pressure regulator and controlling the venturi pressure ratio with a throttle valve located downstream of the venturi run.

The two endwall cooling configurations were tested at an exit static- to inlet total-pressure ratio that corresponded to the design, mean-radius, ideal, aftermixed, critical velocity ratio of 0.778. Nominal coolant to primary inlet total-pressure ratios p'_c/p'_0 of 1.0, 1.2, 1.4, 1.6, 1.8, and 2.0 were set by varying the coolant flow rates from 0.9 to 3.1 percent of the primary flow. For any given test, this pressure ratio was maintained the same for the hub and tip endwall coolants, as this would correspond to usual engine operation.

At a given flow condition, probe survey data were obtained at a number of different radii (typically 23) from hub to tip. At any fixed radius, the probe moved circumferentially in a continuous manner behind the middle three vanes of the five-vane test section, with survey data being recorded at 0.08-degree increments (fig. 7). The vane spacing θ of 10° results in about 125 measurement points per vane. The output signals of the thermocouples and pressure transducers were digitized for all the data and recorded on magnetic tape for permanent record.

Data Reduction

The cooled aerodynamic performance presented herein was calculated from the measurement of the survey probe total pressure, the wall static pressures at the survey plane (station 3), and the probe position. Data from the middle test vane (of the three vanes that were surveyed) were used in these calculations. Since only the vane exit total pressure was measured for these tests, the following assumptions were made for data reduction purposes:

(1) The static pressure at the survey plane (station 3) is constant circumferentially and varies linearly with radius. The hub and tip wall static pressures at station 3 were used for this interpolation.

(2) The flow angle at the survey plane is constant circumferentially and radially. The design value of 67° was used for the performance data presented herein.

(3) The total temperature at the survey plane is constant and equal to the total temperature at the bellmouth inlet (station 0).

The calculated vane performance was compared in reference 3 with data obtained from a total-pressure probe (similar to the one used in this paper) by using the previous assumptions and from a combination probe (measuring total pressure, static pressure, and flow angle). Excellent agreement was found in the results obtained for the two probe types. The main advantage of the probe type used herein is that measurements close to both walls can be made without changing probes.

The calculation of vane performance is based on the determination of a hypothetical state where it is assumed that the flow has mixed to a circumferentially uniform condition. The application of the conservation equations to an annular-sector control volume to obtain this aftermixed state, at each radius, has been described fully in reference 8 and is summarized in the appendix. The aftermixed vane efficiency, based on kinetic energy, is used herein because it is theoretically independent of the location of the survey measurement plane. In addition, the aftermixed state represents the "average" conditions seen by the rotor. Note that the aftermixed efficiency contains not only the solid boundary friction losses but also the mixing losses.

RESULTS AND DISCUSSION

Presented in this section are the experimentally determined, survey plane, total-pressure contours, the variation of aftermixed total pressure with radius, and the overall vane aerodynamic performance. Comparisons are made between the two cooled-endwall configurations and the solid endwall. The solid-endwall performance, which serves as a basis of comparison for the cooled endwalls, is discussed first.

Solid (Uncooled) Endwalls

For test program flexibility, two physically distinct sets of hollow vane rings (endwalls) and vanes were used for the endwall cooling investigation reported herein. With this arrangement, one configuration could be tested while the other configuration was being fabricated. Having two distinct endwall sets did, however, lead to some difficulties as it was observed that there were some small geometric differences in the two sets. Because of this the performance of the solid (uncooled) version of each endwall set had to be experimentally determined. These results then formed the basis of comparison for the corresponding cooled version of each vane and endwall set.

The survey plane total-pressure p'_3 characteristics for the solid (uncooled) endwall sets are compared in figure 9. The higher loss regions in figure 9 (i.e., $p'_3/p'_0 \leq 0.93$) have been crosshatched for easier comparison of the two configurations. Two cores of high loss, centered at approximately 10 and 80 percent of vane height, are located on

the suction side of the trailing-edge projection, for each endwall set. As discussed in reference 3, these loss regions are associated with the movement of secondary flows within the endwall boundary layers from the pressure surface to the suction surface in the vane passage. This flow is then turned away from the endwalls and rolls up to form passage vortices in the corners formed by the endwalls and the vane suction surface. Close inspection of figure 9 shows that the losses are somewhat higher and extend further into the mean section (fig. 9) for the endwall set that was subsequently used for the in-line coolant ejection tests. This can be more easily seen in the next figure.

Another comparison of the two solid endwall sets is shown in figure 10, where the aftermixed to inlet total-pressure ratio $\bar{p}'_{3M}/p'_0$ is presented as a function of vane height. The wall static to inlet total-pressure ratios (at the survey plane) were 0.65 and 0.73 for the hub and tip walls, respectively. The solid endwall set used for the in-line coolant injection tests again shows higher losses, particularly, in the vortex core regions. The overall aftermixed efficiency $\bar{\eta}_{3M,s}$ for this endwall set was 96.17 percent, while that for the solid endwall set used for the coolant injected at 15° to the in-line direction was 96.53 percent.

Also shown in figure 10 is the vane inlet to bellmouth inlet total-pressure ratio p'_1/p'_0 as a function of vane height, which was determined for the in-line configuration only. The inlet boundary layer probe was removed prior to obtaining the vane exit survey data to prevent any interference effects. The calculated displacement and momentum thickness per percentage of vane height were 1.51 and 0.56, respectively. Because of the small difference between p'_0 and p'_1 and the negligible effect on the results, the bellmouth total pressure p'_0 has been used as a basis of comparison in all figures and calculations.

Endwall Coolant Flow Characteristics

The coolant flow characteristics for the two endwall configurations are shown in figure 11. The hub, tip, and total endwall coolant flows as percentages of primary flow are shown as functions of coolant to primary inlet total-pressure ratio p'_c/p'_0. The coolant flow for the tip endwall is about twice that for the hub endwall because of the larger number of coolant holes on the tip endwall. The in-line coolant injection configuration has a 10 to 15 percent higher coolant flow than the 15° to in-line coolant injection configuration. Since the number of coolant holes were the same in each configuration, this flow difference is caused by hole size differences (due to fabrication tolerances) and possibly to different coolant flow discharge coefficients. At a pressure ratio p'_c/p'_0 of 1.0 (which is representative of first-stage engine conditions), the total endwall coolant flow fractions y_c are 1.0 and 0.9 for the in-line and the 15° to in-line coolant injection configurations, respectively.

Total-Pressure Contours and Secondary Flows

Contours of vane exit to inlet total-pressure ratio p'_3/p'_0 are shown in figures 12 and 13 for the two cooled-endwall configurations at selected coolant to primary total-pressure ratios p'_c/p'_0. The survey probe total-pressure data were used to generate these computer contour plots. Also shown again, for ease of comparison, are the results obtained for the solid (uncooled) version of each endwall set. The higher loss regions in figures 12 and 13 (i.e., $p'_3/p'_0 \leq 0.93$) have again been crosshatched for comparison purposes.

At a total-pressure ratio p'_c/p'_0 of 1.0, both configurations show larger vortex core losses (more area) than do the corresponding solid (uncooled) endwalls. This indicates, as might be expected, that the low-momentum endwall coolant has migrated to the passage vortex regions. The in-line coolant injection configuration has somewhat larger losses than the 15° to in-line coolant injection configuration. This is shown by the appearance of higher loss contours (N and M) in the hub and tip regions of the in-line coolant injection configuration where none existed in the solid configuration. In addition, comparing loss contours J indicates that more tip endwall coolant has migrated radially down the trailing-edge region for the in-line coolant injection configuration. From these results it is concluded that the coolant injected at an angle of 15° to the in-line direction has, to some extent, been successful in impeding the secondary flows that occur in cooled-endwall stators. Further improvements may also be possible if the coolant is injected at angles greater than 15° to the in-line direction.

At total-pressure ratios p'_c/p'_0 greater than 1.0, the total-pressure losses decrease for both cooled-endwall configurations. Again the improvements are larger for the 15° to in-line coolant injection configuration. At a total-pressure ratio p'_c/p'_0 of 1.8, comparing the total-pressure contours with the trailing-edge projection shows that the underturning of the flow that occurs at lower total-pressure ratios p'_c/p'_0 and for the solid endwall has to a large extent been eliminated. This is due to the increased momentum of the endwall coolant. It is particularly striking in the tip region and is probably enhanced by the row of coolant holes downstream of the vane trailing edge (fig. 5). The improvement in the flow conditions to the rotor blades would be expected to increase the turbine performance by decreasing the primary airflow blockage and rotor incidence losses.

laboratory combustion air system. The desired coolant flow rate was obtained by setting the pressure upstream of the venturi with a pressure regulator and controlling the venturi pressure ratio with a throttle valve located downstream of the venturi run.

The two endwall cooling configurations were tested at an exit static- to inlet total-pressure ratio that corresponded to the design, mean-radius, ideal, aftermixed, critical velocity ratio of 0.778. Nominal coolant to primary inlet total-pressure ratios p'_c/p'_0 of 1.0, 1.2, 1.4, 1.6, 1.8, and 2.0 were set by varying the coolant flow rates from 0.9 to 3.1 percent of the primary flow. For any given test, this pressure ratio was maintained the same for the hub and tip endwall coolants, as this would correspond to usual engine operation.

At a given flow condition, probe survey data were obtained at a number of different radii (typically 23) from hub to tip. At any fixed radius, the probe moved circumferentially in a continuous manner behind the middle three vanes of the five-vane test section, with survey data being recorded at 0.08-degree increments (fig. 7). The vane spacing θ of 10° results in about 125 measurement points per vane. The output signals of the thermocouples and pressure transducers were digitized for all the data and recorded on magnetic tape for permanent record.

Data Reduction

The cooled aerodynamic performance presented herein was calculated from the measurement of the survey probe total pressure, the wall static pressures at the survey plane (station 3), and the probe position. Data from the middle test vane (of the three vanes that were surveyed) were used in these calculations. Since only the vane exit total pressure was measured for these tests, the following assumptions were made for data reduction purposes:

(1) The static pressure at the survey plane (station 3) is constant circumferentially and varies linearly with radius. The hub and tip wall static pressures at station 3 were used for this interpolation.

(2) The flow angle at the survey plane is constant circumferentially and radially. The design value of 67° was used for the performance data presented herein.

(3) The total temperature at the survey plane is constant and equal to the total temperature at the bellmouth inlet (station 0).

The calculated vane performance was compared in reference 3 with data obtained from a total-pressure probe (similar to the one used in this paper) by using the previous assumptions and from a combination probe (measuring total pressure, static pressure, and flow angle). Excellent agreement was found in the results obtained for the two probe types. The main advantage of the probe type used herein is that measurements close to both walls can be made without changing probes.

The calculation of vane performance is based on the determination of a hypothetical state where it is assumed that the flow has mixed to a circumferentially uniform condition. The application of the conservation equations to an annular-sector control volume to obtain this aftermixed state, at each radius, has been described fully in reference 8 and is summarized in the appendix. The aftermixed vane efficiency, based on kinetic energy, is used herein because it is theoretically independent of the location of the survey measurement plane. In addition, the aftermixed state represents the "average" conditions seen by the rotor. Note that the aftermixed efficiency contains not only the solid boundary friction losses but also the mixing losses.

RESULTS AND DISCUSSION

Presented in this section are the experimentally determined, survey plane, total-pressure contours, the variation of aftermixed total pressure with radius, and the overall vane aerodynamic performance. Comparisons are made between the two cooled-endwall configurations and the solid endwall. The solid-endwall performance, which serves as a basis of comparison for the cooled endwalls, is discussed first.

Solid (Uncooled) Endwalls

For test program flexibility, two physically distinct sets of hollow vane rings (endwalls) and vanes were used for the endwall cooling investigation reported herein. With this arrangement, one configuration could be tested while the other configuration was being fabricated. Having two distinct endwall sets did, however, lead to some difficulties as it was observed that there were some small geometric differences in the two sets. Because of this the performance of the solid (uncooled) version of each endwall set had to be experimentally determined. These results then formed the basis of comparison for the corresponding cooled version of each vane and endwall set.

The survey plane total-pressure p'_3 characteristics for the solid (uncooled) endwall sets are compared in figure 9. The higher loss regions in figure 9 (i.e., $p'_3/p'_0 \leq 0.93$) have been crosshatched for easier comparison of the two configurations. Two cores of high loss, centered at approximately 10 and 80 percent of vane height, are located on

the suction side of the trailing-edge projection, for each endwall set. As discussed in reference 3, these loss regions are associated with the movement of secondary flows within the endwall boundary layers from the pressure surface to the suction surface in the vane passage. This flow is then turned away from the endwalls and rolls up to form passage vortices in the corners formed by the endwalls and the vane suction surface. Close inspection of figure 9 shows that the losses are somewhat higher and extend further into the mean section (fig. 9) for the endwall set that was subsequently used for the in-line coolant ejection tests. This can be more easily seen in the next figure.

Another comparison of the two solid endwall sets is shown in figure 10, where the aftermixed to inlet total-pressure ratio $\bar{p}'_{3M}/p'_0$ is presented as a function of vane height. The wall static to inlet total-pressure ratios (at the survey plane) were 0.65 and 0.73 for the hub and tip walls, respectively. The solid endwall set used for the in-line coolant injection tests again shows higher losses, particularly, in the vortex core regions. The overall aftermixed efficiency $\bar{\eta}_{3M_{t,s}}$ for this endwall set was 96.17 percent, while that for the solid endwall set used for the coolant injected at 15° to the in-line direction was 96.53 percent.

Also shown in figure 10 is the vane inlet to bellmouth inlet total-pressure ratio p'_1/p'_0 as a function of vane height, which was determined for the in-line configuration only. The inlet boundary layer probe was removed prior to obtaining the vane exit survey data to prevent any interference effects. The calculated displacement and momentum thickness per percentage of vane height were 1.51 and 0.56, respectively. Because of the small difference between p'_0 and p'_1 and the negligible effect on the results, the bellmouth total pressure p'_0 has been used as a basis of comparison in all figures and calculations.

Endwall Coolant Flow Characteristics

The coolant flow characteristics for the two endwall configurations are shown in figure 11. The hub, tip, and total endwall coolant flows as percentages of primary flow are shown as functions of coolant to primary inlet total-pressure ratio p'_c/p'_0. The coolant flow for the tip endwall is about twice that for the hub endwall because of the larger number of coolant holes on the tip endwall. The in-line coolant injection configuration has a 10 to 15 percent higher coolant flow than the 15° to in-line coolant injection configuration. Since the number of coolant holes were the same in each configuration, this flow difference is caused by hole size differences (due to fabrication tolerances) and possibly to different coolant flow discharge coefficients. At a pressure ratio p'_c/p'_0 of 1.0 (which is representative of first-stage engine conditions), the total endwall coolant flow fractions y_c are 1.0 and 0.9 for the in-line and the 15° to in-line coolant injection configurations, respectively.

Total-Pressure Contours and Secondary Flows

Contours of vane exit to inlet total-pressure ratio p'_3/p'_0 are shown in figures 12 and 13 for the two cooled-endwall configurations at selected coolant to primary total-pressure ratios p'_c/p'_0. The survey probe total-pressure data were used to generate these computer contour plots. Also shown again, for ease of comparison, are the results obtained for the solid (uncooled) version of each endwall set. The higher loss regions in figures 12 and 13 (i.e., $p'_3/p'_0 \leq 0.93$) have again been crosshatched for comparison purposes.

At a total-pressure ratio p'_c/p'_0 of 1.0, both configurations show larger vortex core losses (more area) than do the corresponding solid (uncooled) endwalls. This indicates, as might be expected, that the low-momentum endwall coolant has migrated to the passage vortex regions. The in-line coolant injection configuration has somewhat larger losses than the 15° to in-line coolant injection configuration. This is shown by the appearance of higher loss contours (N and M) in the hub and tip regions of the in-line coolant injection configuration where none existed in the solid configuration. In addition, comparing loss contours J indicates that more tip endwall coolant has migrated radially down the trailing-edge region for the in-line coolant injection configuration. From these results it is concluded that the coolant injected at an angle of 15° to the in-line direction has, to some extent, been successful in impeding the secondary flows that occur in cooled-endwall stators. Further improvements may also be possible if the coolant is injected at angles greater than 15° to the in-line direction.

At total-pressure ratios p'_c/p'_0 greater than 1.0, the total-pressure losses decrease for both cooled-endwall configurations. Again the improvements are larger for the 15° to in-line coolant injection configuration. At a total-pressure ratio p'_c/p'_0 of 1.8, comparing the total-pressure contours with the trailing-edge projection shows that the underturning of the flow that occurs at lower total-pressure ratios p'_c/p'_0 and for the solid endwall has to a large extent been eliminated. This is due to the increased momentum of the endwall coolant. It is particularly striking in the tip region and is probably enhanced by the row of coolant holes downstream of the vane trailing edge (fig. 5). The improvement in the flow conditions to the rotor blades would be expected to increase the turbine performance by decreasing the primary airflow blockage and rotor incidence losses.

Aftermixed Total-Pressure Characteristics

The variation of aftermixed to inlet total-pressure ratio $\bar{p}'_{3M}/p'_0$ with vane height is shown in figures 14 and 15 for the two cooled-endwall configurations at selected coolant to primary total-pressure ratios p'_c/p'_0. The corresponding solid-endwall cases are also shown in the figures for comparison with the cooled-endwall results. At a total-pressure ratio p'_c/p'_0 of 1.0, there is an increase in the total-pressure loss as compared with the solid endwalls, particularly in the vortex core regions, for both cooled-endwall configurations. These losses are somewhat higher for the in-line coolant injection configuration and persist into the vane mean section. This is consistent, as it should be, with the results shown previously for the total-pressure contours of figures 12 and 13. At the higher total-pressure ratios p'_c/p'_0 the total-pressure losses decrease, with the 15° to in-line coolant injection configuration being slightly better. The vortex core regions at a total-pressure ratio p'_c/p'_0 of 1.8 are significantly modified, particularly in the tip region. The higher momentum of the coolant apparently impedes, to a large extent, the formation of the large passage vortex and the radial migration down the vane trailing-edge region.

Overall Aerodynamic Performance

Aftermixed efficiencies. - The overall aftermixed thermodynamic efficiency, $\bar{\eta}_{3M,T}$ (eq. (11), appendix) as a function of coolant to primary total-pressure ratio p'_c/p'_0 is shown in figure 16 for the two cooled-endwall configurations. The efficiencies are shown as percentages of change (from the solid endwalls) per percentage of coolant. This was done because of the small differences between the two solid-endwall sets (figs. 9 and 10) and the slightly different endwall coolant flow characteristics (fig. 11). Both endwall configurations show similar trends, with the thermodynamic efficiency decreasing with increasing total-pressure ratio p'_c/p'_0. The data for both configurations have been least-squares fit to straight lines in figure 16. Over the range of coolant flow tests, the 15° to in-line coolant injection configuration has a higher efficiency (lower losses) than the in-line configuration. The differences, however, appear to be small even though the two configurations were seen to have larger differences in the endwall regions (figs. 12 to 15). This results from the fact that the overall aftermixed efficiencies represent an "average" for the whole vane and as such tend to mask the differences in the endwall regions. Also, the larger change in efficiency for the in-line coolant injection configuration is offset by larger coolant fractions (fig. 11). At a total-pressure ratio of 1.0, the changes in thermodynamic efficiency per percentage of coolant are -0.760 and -0.737 for the in-line and 15° to in-line coolant injection configurations, respectively.

Effect of total-temperature ratio. - As discussed previously, the performance of the cooled endwalls was determined at a primary to coolant total-temperature ratio T'_0/T'_c of 1.0. Although a valid comparison can probably be made at this temperature ratio, it is also of interest to estimate the performance at actual engine conditions. A method for doing this has been described in reference 6. The basic model assumed that the aerodynamic losses (total-pressure losses due to boundary layer growth and mixing) were constant if the coolant to primary momentum ratios (or coolant to primary total-pressure ratios p'_c/p'_0 for constant cooling hole areas) were maintained the same for tests at different total-temperature ratios T'_0/T'_c. It was shown (ref. 6) that at a coolant to primary inlet total-pressure ratio p'_c/p'_0 of 1, which is representative of actual engine first-stage stator operating conditions, the thermodynamic efficiency is independent of the total-temperature ratio T'_0/T'_c. The coolant fraction y_c was also shown to vary as the square root of the total-temperature ratio T'_0/T'_c (for constant cooling hole area). Therefore, at the design total-temperature ratio T'_0/T'_c of 2.7 for this stator, the percentages of change in thermodynamic efficiency per percentage of coolant are estimated to be -0.463 (i.e., $-0.760/\sqrt{2.7}$) and -0.449 for the in-line and the 15° to in-line coolant injection configurations, respectively. These values are somewhat lower than found (ref. 9) for full-film-cooled vanes tested in two-dimensional cascades. If desired, the effect of total-temperature ratio on the performance at other measured total-pressure ratios p'_c/p'_0 can also be estimated by the method described in reference 6.

CONCLUDING REMARKS

At a coolant to primary inlet total-pressure ratio of 1, which is representative of first-stage engine operating conditions, the low-momentum endwall coolants migrated to the passage vortex regions and increased the losses as compared with the solid (uncooled) endwalls. However, comparing the two cooled-endwall configurations did indicate that the coolant injected at 15° to the inviscid streamline direction was more successful in impeding the secondary flows that can occur in this type of stator. This was seen from the smaller total-pressure losses in the passage vortex regions and by less radial migration of the tip endwall coolant down the trailing-edge region. Further aerodynamic improvements are thought to be possible if the coolant is injected at angles greater than 15° (i.e., 30° or possibly 45°) to the inviscid streamline direction.

More important than aerodynamic gains are the probable implications of the results to the heat transfer characteristics of cooled endwalls in low-aspect-ratio blading. For if the endwall coolant separates and migrates away from the endwalls, the effectiveness of the film cooling will be considerably decreased. Fortunately, recent flow visualization studies (on flat plates) have shown that coolant injected at 45° to the streamwise flow direction tends to prevent the cooling film from separating from the surface even at

high blowing rates. In an attempt to use this effect, further aerodynamic tests are currently planned to study the behavior of endwall coolant injected at 30° and 45° to the inviscid streamline direction. Corresponding heat transfer tests are also needed. In addition, it is hoped that the effect of other design parameters (such as hole location, hole size, and blowing rate) on the secondary flows in cooled stators will also be determined. To complement the experimental investigation, theoretical calculation procedures (i.e., endwall boundary layer and three-dimensional viscous computer programs) are currently being developed. These methods should find wide use in the experimental program.

SUMMARY OF RESULTS

The performances of two similar endwall cooling configurations were experimentally determined in a cold-air, full-annular cascade, where three-dimensional effects could be obtained. In the first configuration, three rows of cooling holes were oriented so that the endwall coolant was injected in line with the inviscid streamline direction. In the second configuration, the coolant was injected at an angle of 15° to the inviscid streamline direction and oriented toward the vane pressure surface. In both configurations, the coolant was injected at an angle of 15° to the endwall surface. The stator vanes were solid and uncooled so that the effect of endwall cooling could be obtained directly. The investigation was conducted at the vane design, mean-radius, ideal, aftermixed, critical velocity ratio of 0.778. The coolant to primary inlet total-pressure ratios were varied from 1.0 to 2.0, which corresponds to endwall coolant flows from 0.9 to 3.1 percent of primary flow. All tests were conducted at ambient conditions with a primary to coolant inlet total-temperature ratio of 1. Total-pressure contours downstream of the vanes were obtained from survey probe data and were used to determine the effect of endwall cooling on the secondary flows in the stator. The probe data were also used to calculate the overall vane aerodynamic performance. Both cooled-endwall configurations were compared with each other and with the results obtained for the solid (uncooled) endwalls. The results of the investigation were summarized as follows:

1. At a coolant to primary inlet total-pressure ratio of 1, the endwall coolant migrated to the passage vortex regions, increasing the losses as compared with the solid endwalls. The percent changes in the overall thermodynamic efficiency (as compared with the solid endwalls) per percent coolant were -0.760 and -0.737 for the in-line and 15° to in-line coolant injection configurations, respectively.

2. For coolant to primary inlet total-pressure ratios greater than 1, the increased momentum of the endwall coolant improved the secondary flow characteristics (decreased total-pressure losses and underturning in the passage vortex regions) of the whole vane.

3. The 15° to in-line coolant injection configuration was more successful in impeding the vane secondary flows and, therefore, had somewhat better aerodynamic performance than did the in-line coolant injection configuration over the range of coolant flows investigated.

REFERENCES

1. Szanca, Edward M., Schum, Harold J., and Hotz, Glen M., "Research Turbine for High-Temperature Core Engine Application. I - Cold-Air Overall Performance of Solid Scaled Turbine," NASA TN D-7557, February 1974.

2. Stabe, Roy G., and Kline, John F., "Aerodynamic Performance of a Core-Engine Turbine Stator Vane Tested in a Two-Dimensional Cascade of 10 Vanes and in a Single-Vane Tunnel," NASA TM X-2766, March 1973.

3. Goldman, Louis J., and McLallin, Kerry L., "Cold-Air Annular-Cascade Investigation of Aerodynamic Performance of Core-Engine-Cooled Turbine Vanes. I - Solid-Vane Performance and Facility Description," NASA TM X-3224, April 1975.

4. McDonel, J. D., et al., "Core Turbine Aerodynamic Evaluation - Test Data From Initial Turbine," NASA CR-2596, February 1976.

5. Colladay, Raymond S., and Russell, Louis M., "Streakline Flow Visualization of Discrete Hole Film Cooling for Gas Turbine Applications," Journal of Heat Transfer, Vol. 98, No. 2, May 1976, pp. 245-250.

6. Goldman, Louis J., "Cooled-Turbine Aerodynamic Performance Prediction from Reduced Primary to Coolant Total-Temperature-Ratio Results," NASA TN D-8312, October 1976.

7. Krause, Lloyd N., and Gettelman, Clarence C., "Considerations Entering into the Selection of Probes for Pressure Measurements in Jet Engines," Instrument Society of America Proceedings. Vol. 7, 1952, pp. 134-137.

8. Goldman, Louis J., and McLallin, Kerry L., "Cold-Air Annular-Cascade Investigation of Aerodynamic Performance of Cooled Turbine Vanes. I - Facility Description and Base (Solid) Vane Performance," NASA TM X-3006, March 1974.

9. Moffitt, Thomas P., Stepka, Francis S., and Rohlik, Harold E., "Summary of NASA Aerodynamic and Heat Transfer Studies in Turbine Vanes and Blades," SAE Paper 760917, 1976.

APPENDIX - CALCULATION OF AFTERMIXED CONDITIONS AND VANE EFFICIENCY FROM SURVEY MEASUREMENTS

The aftermixed conditions (station 3M) are obtained from the survey measurements by applying the conservation equations to an annular-sector control volume of infinitesimal radial thickness as shown in figure 17. The stream surfaces downstream of the vanes are assumed to be cylindrical because of the axial character of the annular cascade. In application of the conservation equations, it is also assumed that the viscous terms are negligible and that the pressure terms on the side faces of the control volume cancel due to symmetry.

The conservation of mass requires that

$$\int_0^\Theta \rho_3(r,\theta)V_{3,z}(r,\theta)d\theta = \rho_{3M}(r)V_{3M,z}(r)\Theta \equiv \bar{m}(r) \tag{1}$$

The conservation of momentum gives

$$\int_0^\Theta \left[\rho_3(r,\theta)V_{3,z}^2(r,\theta) + gp_3(r)\right]d\theta = \left[\rho_{3M}(r)V_{3M,z}^2(r) + gp_{3M}(r)\right]\Theta \equiv J_z(r)\bar{m}(r) \tag{2}$$

$$\int_0^\Theta \left[\rho_3(r,\theta)V_{3,z}(r,\theta)V_{3,\theta}(r,\theta)\right]d\theta = \left[\rho_{3M}(r)V_{3M,z}(r)V_{3M,\theta}(r)\right]\Theta \equiv J_\theta(r)\bar{m}(r) \tag{3}$$

The energy equation for the special case of equal coolant and primary total temperatures is

$$C_pT_3(r,\theta) + \frac{V_3^2(r,\theta)}{2gJ} = C_pT_{3M}(r) + \frac{V_{3M}^2(r)}{2gJ} = C_pT'_{3M} = C_pT'_0 \equiv E = \text{Constant} \tag{4}$$

The perfect-gas relation completes the system of equations

$$\rho_{3M}(r) = \frac{p_{3M}(r)}{RT_{3M}(r)} \tag{5}$$

Solving for the axial velocity $V_{3M,z}(r)$ gives (ref. 8)

$$V_{3M,z}(r) = \frac{\gamma}{\gamma+1}J_z(r) - \sqrt{\left[\frac{\gamma}{\gamma+1}J_z(r)\right]^2 - \frac{\gamma-1}{\gamma+1}\left[2gJE - J_\theta^2(r)\right]} \tag{6}$$

The tangential velocity $V_{3M,\theta}(r)$ is obtained from equation (3)

$$V_{3M,\theta}(r) = J_\theta(r) \tag{7}$$

and the velocity $V_{3M}(r)$ from

$$V_{3M}(r) = \sqrt{V_{3M,z}^2(r) + V_{3M,\theta}^2(r)} \tag{8}$$

The aftermixed conditions of density $\rho_{3M}(r)$, static temperature $T_{3M}(r)$, and static pressure $p_{3M}(r)$ are found from equations (1), (4), and (5), respectively. The aftermixed total pressure $p'_{3M}(r)$ is then obtained from

$$\frac{p'_{3M}(r)}{p_{3M}(r)} = \left[1 + \frac{\gamma-1}{2}M_{3M}^2(r)\right]^{\gamma/(\gamma-1)} \tag{9}$$

where

$$M_{3M}(r) = \frac{V_{3M}(r)}{\sqrt{\gamma gRT_{3M}(r)}} \tag{10}$$

The aftermixed conditions have been determined in terms of the parameters $\bar{m}(r)$, $J_z(r)$, $J_\theta(r)$, and E, which are calculated from the survey measurements.

The aftermixed thermodynamic efficiency is defined as the ratio of the actual aftermixed kinetic energy to the sum of the ideal aftermixed kinetic energies of both the primary and coolant flows. The thermodynamic efficiency for the total vane passage

is

$$\bar{\eta}_{3M,T} = \frac{\int_{r_i}^{r_o} \left[\rho_{3M}(r) V_{3M,z}(r) V_{3M}^2(r)\right] r \, dr}{\int_{r_i}^{r_o} \rho_{3M}(r) V_{3M,z}(r) \left\{ y_p(r) \left[V_{3M,id}^2(r)\right]_p + y_{c,h}(r) \left[V_{3M,id}^2(r)\right]_{c,h} + y_{c,t}(r) \left[V_{3M,id}^2(r)\right]_{c,t} \right\} r \, dr} \tag{11}$$

where the ideal velocities are given by

$$\left[V_{3M,id}(r)\right]_p = \sqrt{\left(\frac{2\gamma}{\gamma - 1}\right) g R T_0' \left\{ 1 - \left[\frac{p_{3M}(r)}{p_0'}\right]^{(\gamma-1)/\gamma} \right\}} \tag{12}$$

$$\left[V_{3M,id}(r)\right]_{c,h} = \sqrt{\left(\frac{2\gamma}{\gamma - 1}\right) g R T_{c,h}' \left\{ 1 - \left[\frac{p_{3M}(r)}{p_{c,h}'}\right]^{(\gamma-1)/\gamma} \right\}} \tag{13}$$

$$\left[V_{3M,id}(r)\right]_{c,t} = \sqrt{\left(\frac{2\gamma}{\gamma - 1}\right) g R T_{c,t}' \left\{ 1 - \left[\frac{p_{3M}(r)}{p_{c,t}'}\right]^{(\gamma-1)/\gamma} \right\}} \tag{14}$$

The total pressure at the bellmouth inlet p_0' was used (instead of p_1') to calculate the ideal velocity of the primary flow (eq. (12)). This was done because the vane inlet total pressure $p_1'(r)$ was measured only for the solid endwall tests of the in-line coolant injection vane rings and because of its negligible effect on the results. The fraction of coolant flow to total flow was assumed to be independent of radius and equal to

$$y_{c,h}(r) = \frac{\bar{\bar{m}}_{c,h}}{\bar{\bar{m}}} = \text{Constant} \tag{15}$$

$$y_{c,t}(r) = \frac{\bar{\bar{m}}_{c,t}}{\bar{\bar{m}}} = \text{Constant} \tag{16}$$

$$y_p(r) = 1 - \left[y_{c,h}(r) + y_{c,t}(r)\right] = \text{Constant} \tag{17}$$

where $\bar{\bar{m}}_{c,h}$ and $\bar{\bar{m}}_{c,t}$ are the measured total coolant flow rates per passage for the hub and tip endwall coolants, respectively. And $\bar{\bar{m}}$ is the total flow rate per passage and is given by

$$\bar{\bar{m}} = \int_{r_h}^{r_t} \int_0^{\theta} \rho_3(r,\theta) V_{3,z}(r,\theta) r \, d\theta \, dr = \int_{r_h}^{r_t} \bar{m}(r) r \, dr \tag{18}$$

TABLE I. - ENDWALL COOLING HOLE COORDINATES

(a) Hub wall

Cooling hole	X (fig. 5)		Y (fig. 5)		A (fig. 5), deg	
	cm	in.	cm	in.	Configuration 1[a]	Configuration 2[b]
1	2.433	0.958	2.350	0.925	56.67	71.67
2	2.586	1.018	2.088	.822	58.42	73.42
[c]3	2.738	1.078	1.829	.720	59.08	74.08
[c]4	2.891	1.138	1.560	.614	60.75	75.75
[c]5	3.043	1.198	1.300	.512	66.25	81.25
[c]6	3.195	1.258	1.036	.408	72.67	87.67
[d]7	3.348	1.318	.777	.306	90.00	-----
8	1.331	.524	1.179	.464	39.42	54.42
9	1.519	.598	1.031	.406	39.42	54.42
10	1.717	.676	.869	.342	41.08	56.08
11	1.915	.754	.711	.280	45.92	60.92
12	2.113	.832	.554	.218	52.58	67.58
13	.345	.136	-.041	-.016	33.17	48.17
14	.523	.206	-.147	-.058	33.17	48.17
15	.701	.276	-.254	-.100	33.17	48.17
16	.879	.346	-.361	-.142	33.17	48.17
17	1.057	.416	-.467	-.184	33.17	48.17
18	.325	.128	-.269	-.106	33.17	48.17
19	.503	.198	-.376	-.148	33.17	48.17
20	.681	.268	-.483	-.190	33.17	48.17
21	.859	.338	-.589	-.232	33.17	48.17
[c]22	1.036	.408	-.696	-.274	33.17	48.17
23	2.840	1.118	-0.193	-0.076	-75.00	-90.00
24	2.764	1.088	-.320	-.126	-70.58	-85.58
25	2.680	1.055	-.457	-.180	-70.58	-85.58
26	2.601	1.024	-.584	-.230	-65.42	-80.42
27	2.520	.992	-.721	-.284	-63.25	-78.25
28	2.438	.960	-.848	-.334	-59.83	-74.83
29	2.357	.928	-.980	-.386	-58.17	-73.17
30	2.276	.896	-1.113	-.438	-56.25	-71.25
31	2.200	.866	-1.234	-.486	-52.92	-67.92
32	2.118	.834	-1.367	-.538	-48.50	-63.50
33	2.037	.802	-1.494	-.588	-48.50	-63.50
34	1.966	.774	-1.621	-.638	-48.50	-63.50
35	1.875	.738	-1.765	-.695	-46.92	-61.92
36	1.463	.576	.671	.264	-36.00	-51.00
37	1.341	.528	.579	.228	-36.00	-51.00
38	1.219	.480	.483	.190	-36.00	-51.00
39	1.097	.432	.396	.156	-36.00	-51.00
40	.975	.384	.300	.118	-36.00	-51.00
41	.853	.336	.213	.084	-36.00	-51.00
42	.737	.290	.122	.048	-36.00	-51.00
43	.610	.240	.030	.012	-36.00	-51.00
44	.493	.194	-.066	-.026	-36.00	-51.00

(b) Tip wall

Cooling hole	X (fig. 5)		Y (fig. 5)		A (fig. 5), deg	
	cm	in.	cm	in.	Configuration 1[a]	Configuration 2[b]
45	-0.419	-0.165	4.293	1.690	-34.00	-34.00
46	-.419	-.165	4.031	1.587	-34.00	-34.00
47	-.419	-.165	3.769	1.484	-34.00	-34.00
48	-.419	-.165	3.510	1.382	-34.00	-34.00
49	-.419	-.165	3.249	1.279	-34.00	-34.00
50	-.419	-.165	2.987	1.176	-34.00	-34.00
51	-.419	-.165	2.728	1.074	-34.00	-34.00
52	-.419	-.165	2.466	.971	-34.00	-34.00
53	-.419	-.165	2.205	.868	-34.00	-34.00
54	-.419	-.165	1.946	.766	-34.00	-34.00
55	-.419	-.165	1.684	.663	-34.00	-34.00
56	-.419	-.165	1.422	.560	-34.00	-34.00
57	-.419	-.165	1.163	.458	-34.00	-34.00
58	-.419	-.165	.902	.355	-34.00	-34.00

[a]Cooling holes in line with inviscid streamlines.
[b]Cooling holes at 15° to inviscid streamlines and directed toward vane pressure surface.
[c]Cooling holes could not be machined in configuration 2. Holes filled with epoxy in configuration 1.
[d]Cooling holes could not be machined in configurations 1 and 2.

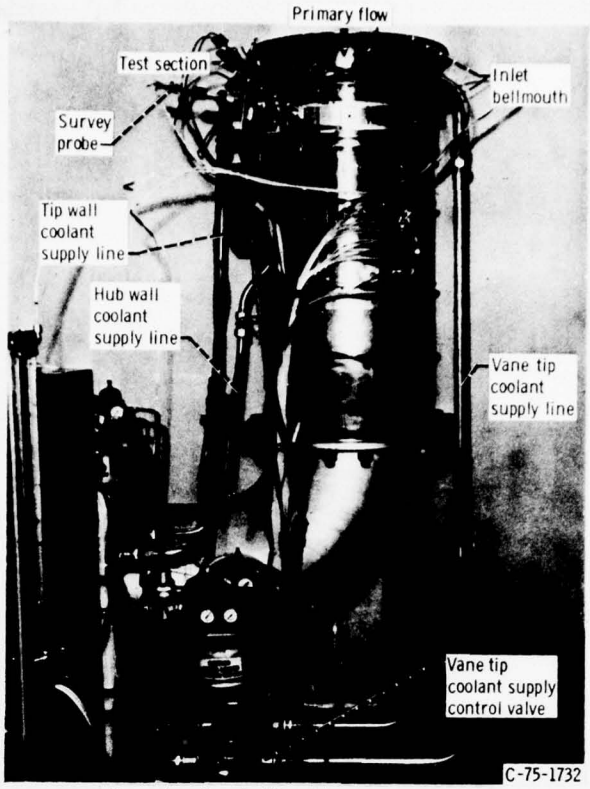


Figure 1. - Core-turbine stator annular cascade.

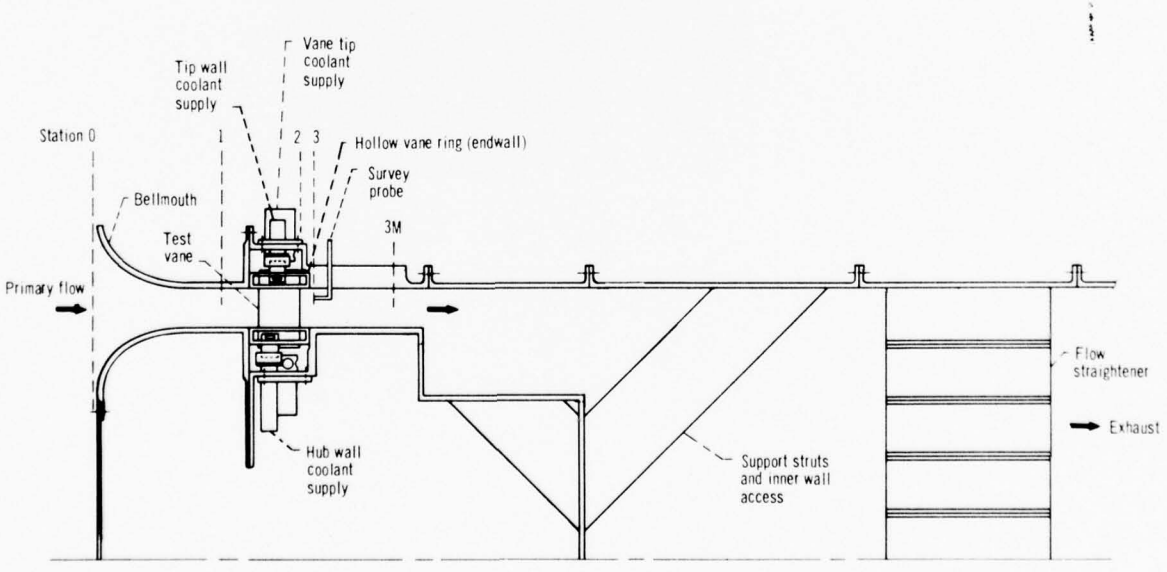


Figure 2. - Schematic cross-sectional view of core-turbine stator cascade.

X		Y_L		Y_U	
cm	in.	cm	in.	cm	in.
0	0	0.508	0.200	0.508	0.200
0.127	0.050	-----	-----	.851	.335
.254	.100	-----	-----	1.003	.395
.381	.150	-----	-----	1.120	.441
.508	.200	-----	-----	1.212	.477
.635	.250	-----	-----	1.285	.506
.762	.300	.061	.024	1.341	.528
.889	.350	.117	.046	1.389	.547
1.016	.400	.163	.064	1.425	.561
1.143	.450	.201	.079	1.448	.570
1.270	.500	.236	.093	1.463	.576
1.397	.550	.267	.105	1.471	.579
1.524	.600	.292	.115	1.476	.581
1.778	.700	.328	.129	1.461	.575
2.032	.800	.358	.141	1.427	.562
2.286	.900	.376	.148	1.377	.542
2.540	1.000	.384	.151	1.321	.520
2.794	1.100	.381	.150	1.255	.494
3.048	1.200	.368	.145	1.191	.469
3.302	1.300	.353	.139	1.110	.437
3.556	1.400	.328	.129	1.026	.404
3.810	1.500	.297	.117	.942	.371
4.064	1.600	.262	.103	.848	.334
4.318	1.700	.221	.087	.747	.294
4.572	1.800	.178	.070	.635	.250
4.826	1.900	.130	.051	.521	.205
5.080	2.000	.084	.033	.399	.157
5.334	2.100	.025	.010	.267	.105
5.552	2.186	.089	.035	.089	.035

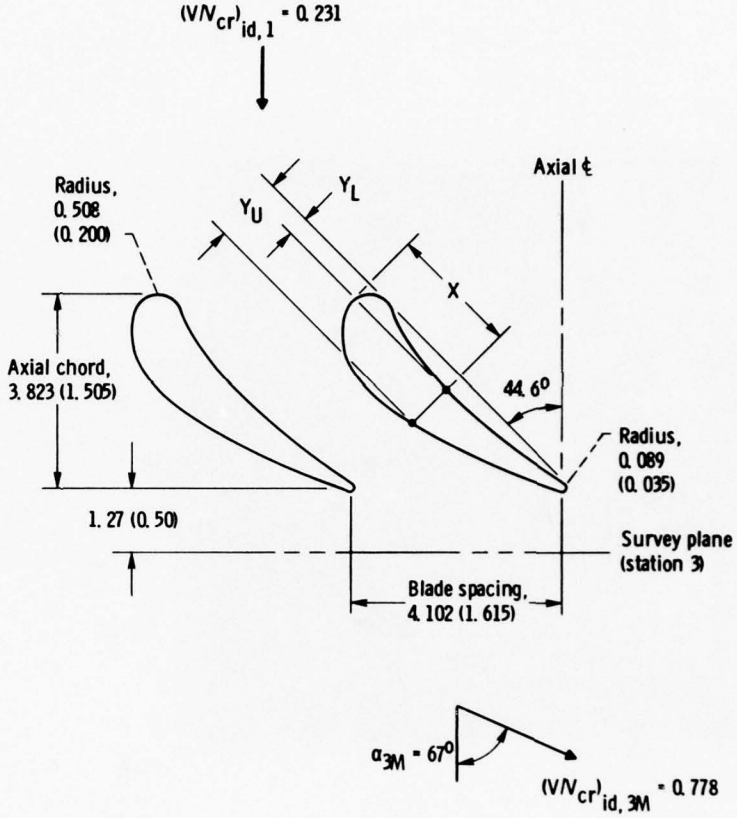
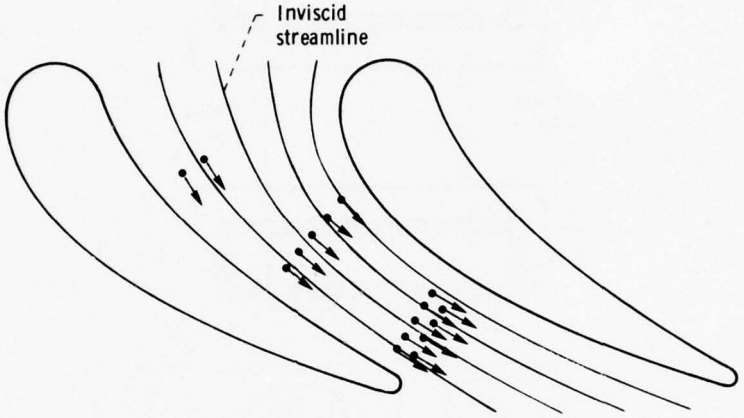
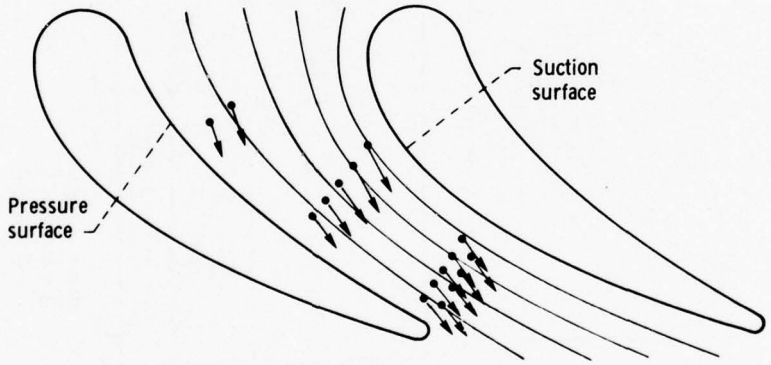


Figure 3. - Core-turbine stator vane geometry at mean section. (All dimensions in cm (in.) except as noted.)



(a) Coolant injected in line with inviscid streamlines.



(b) Coolant injected at 15^{0} to inviscid streamlines and directed toward pressure surface.

Figure 4. - Schematic of two cooled-endwall configurations (showing hub wall only).

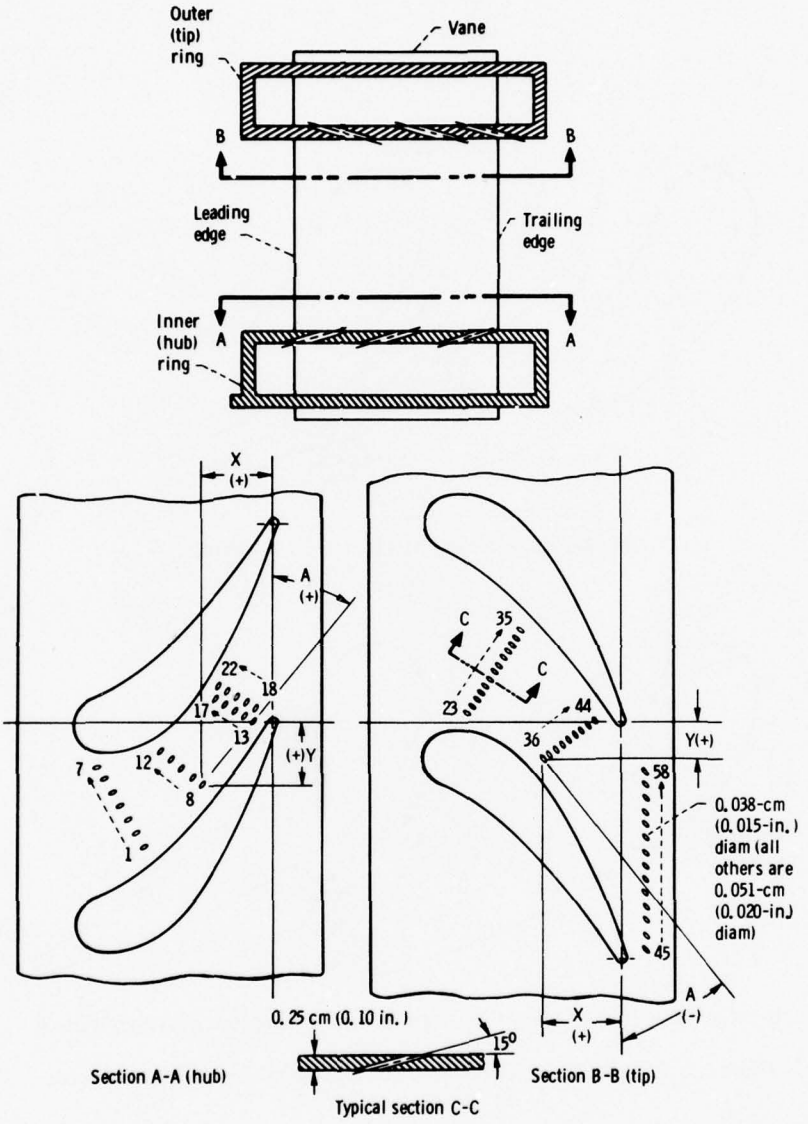
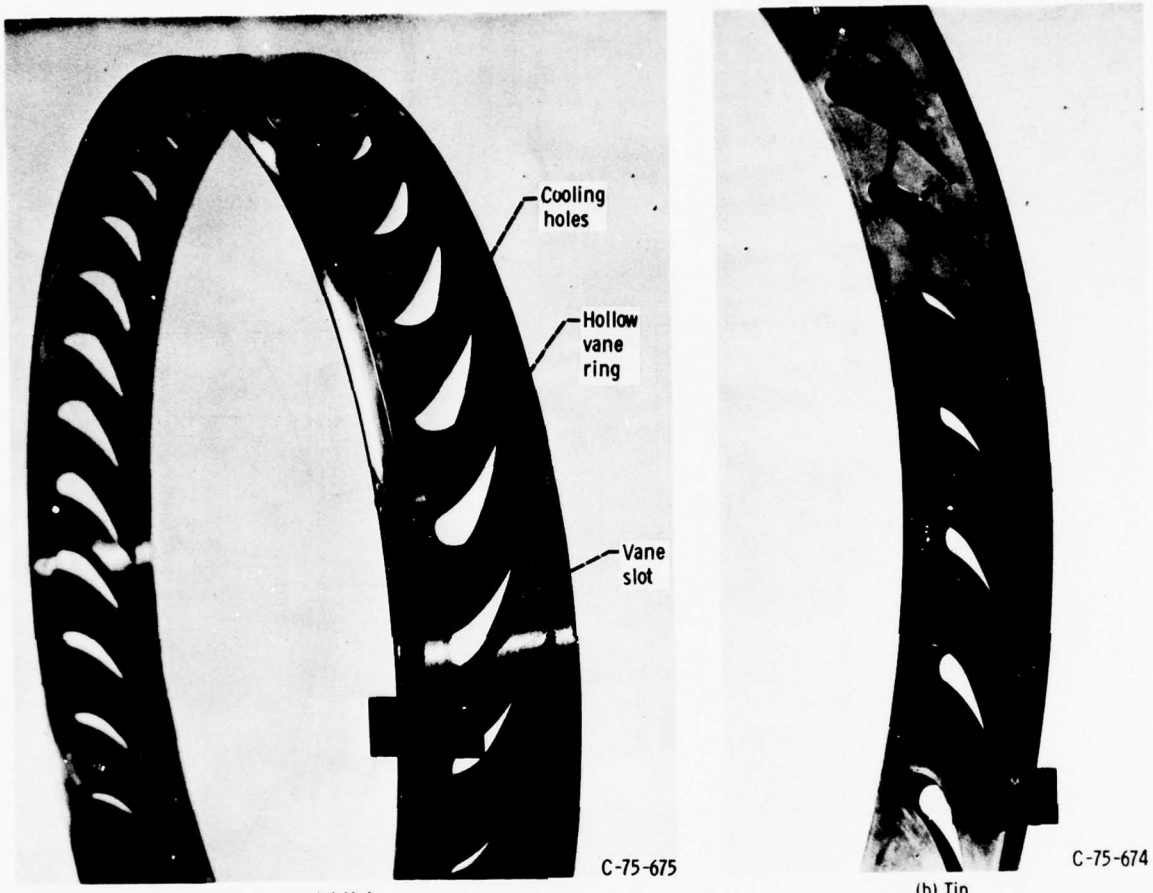


Figure 5. - Schematic of endwall cooling geometry.



(a) Hub. (b) Tip.

Figure 6. - Hollow vane rings showing endwall cooling pattern.

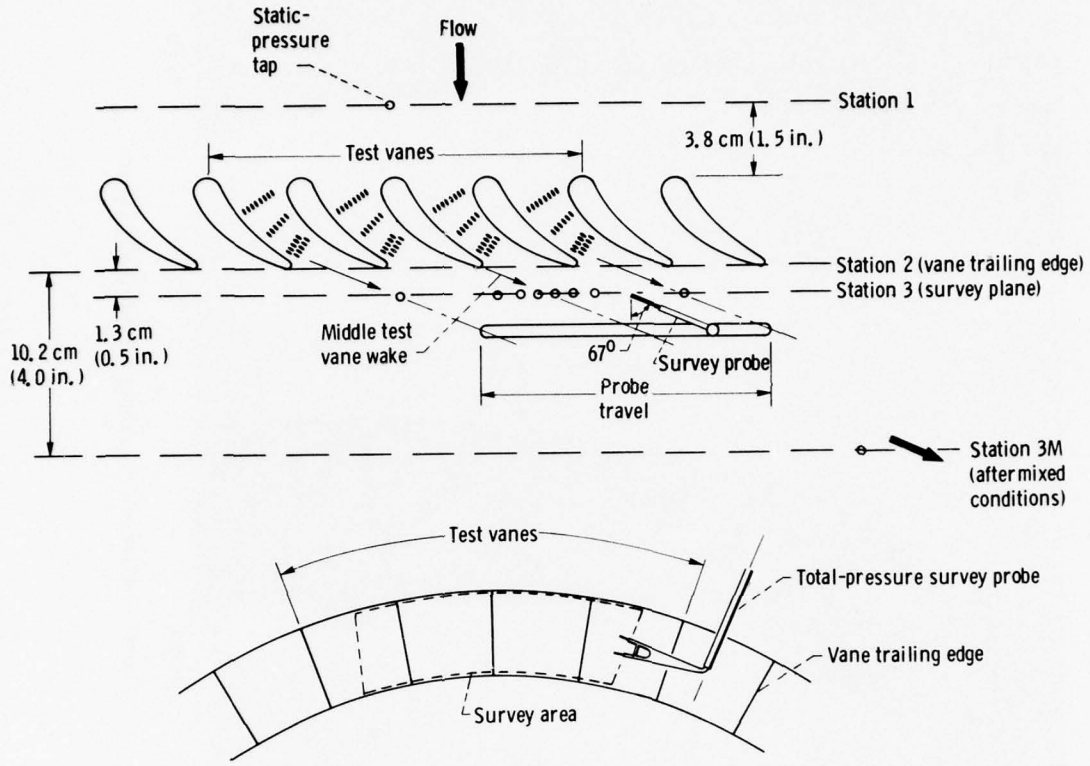


Figure 7. - Schematic of instrumentation for survey data.

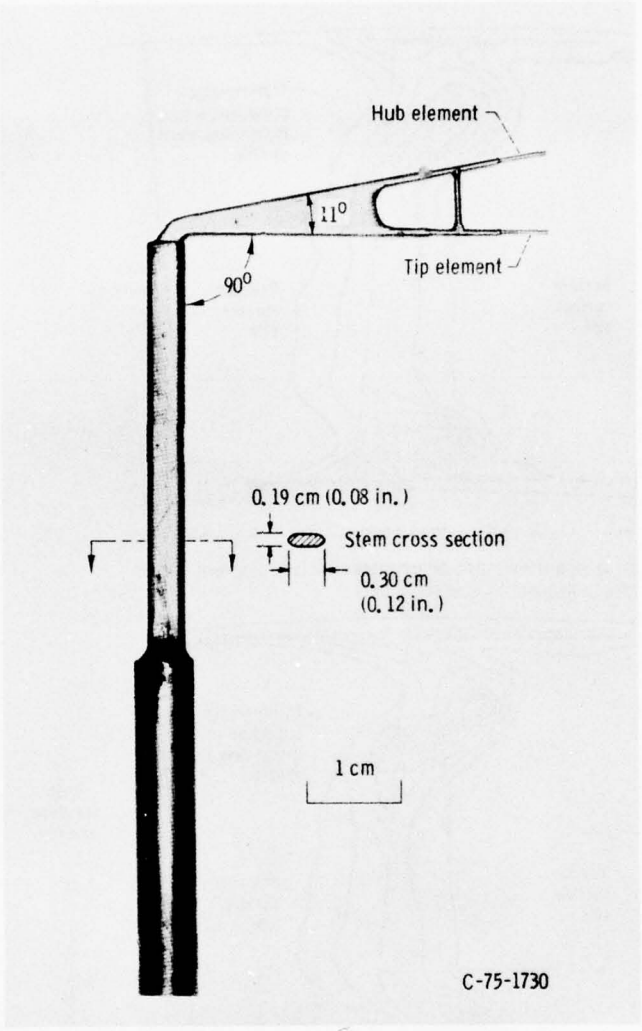
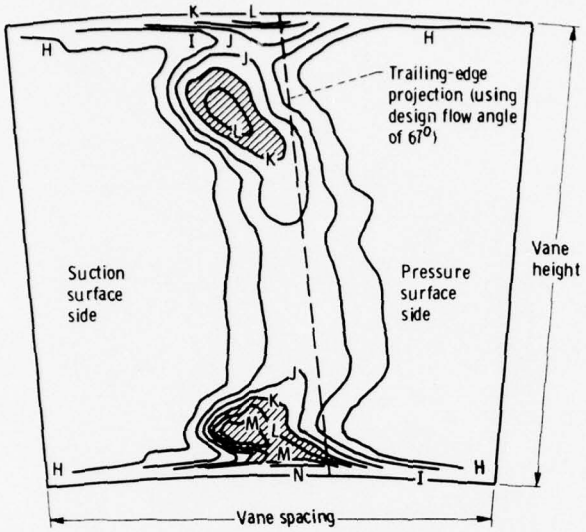
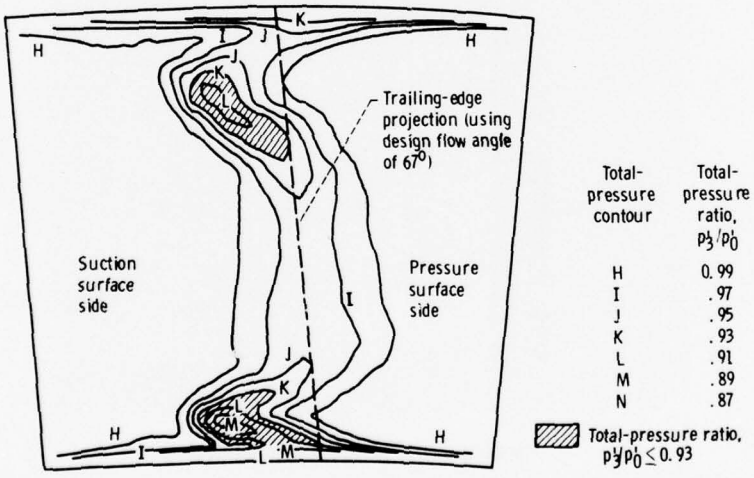


Figure 8. - Total-pressure survey probe.



(a) Solid vanes and endwalls used for subsequent tests of endwall coolant injected in line with inviscid streamlines.



(b) Solid vanes and endwalls used for subsequent tests of endwall coolant injected at 15° to inviscid streamlines.

Figure 9. - Comparison of survey plane total-pressure contour plots of two sets of solid (uncooled) vanes and endwalls used for subsequent cooled-endwall tests.

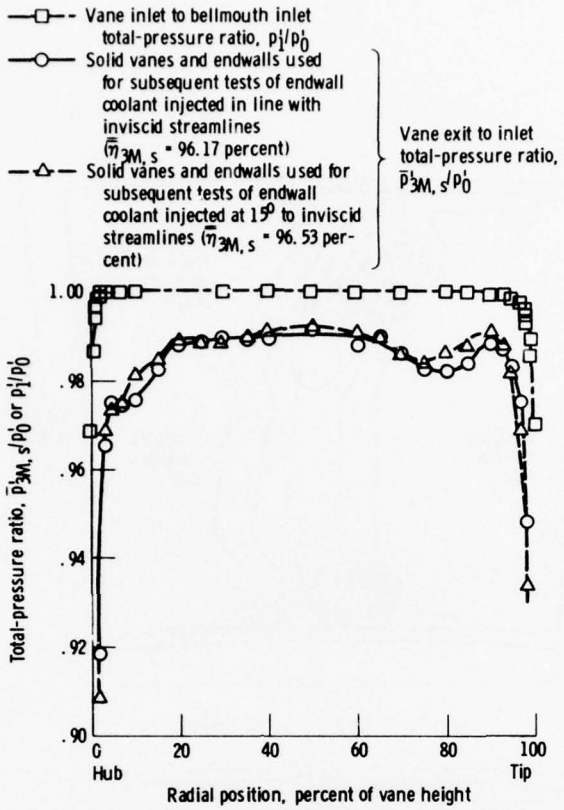


Figure 10. - Comparison of vane exit aftermixed total-pressure characteristics for two sets of solid (uncooled) vanes and endwalls used for subsequent cooled-endwall tests.

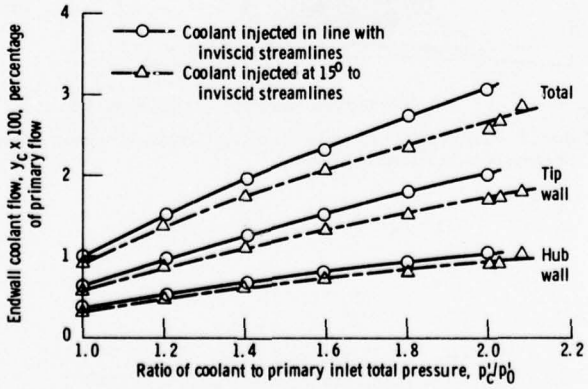
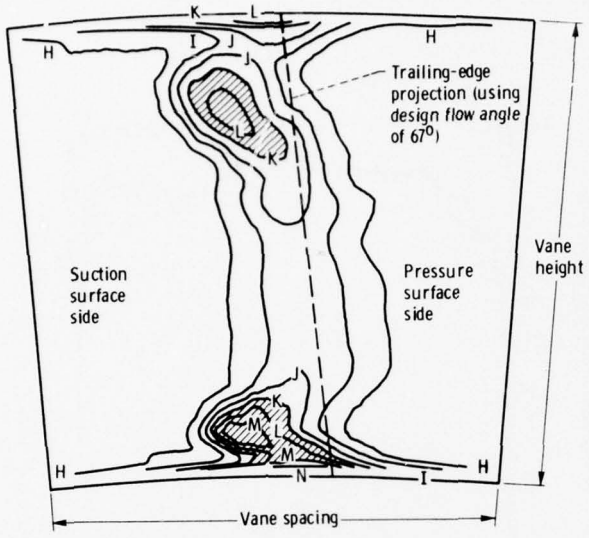
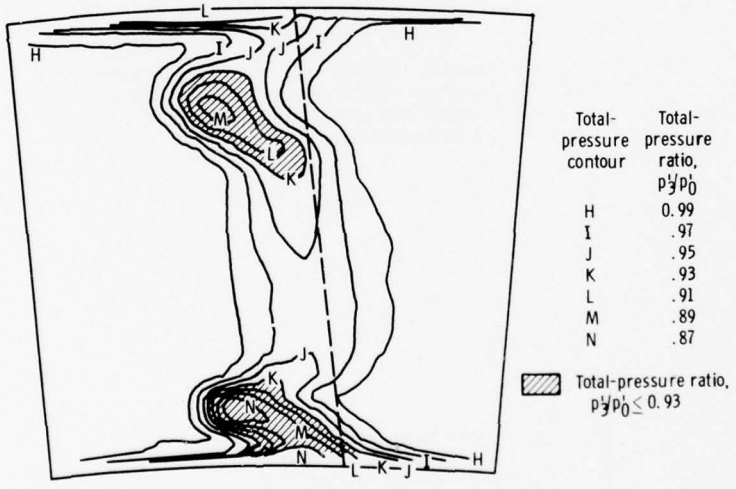


Figure 11. - Coolant flow as function of coolant to primary inlet total-pressure ratio for two cooled-endwall configurations.

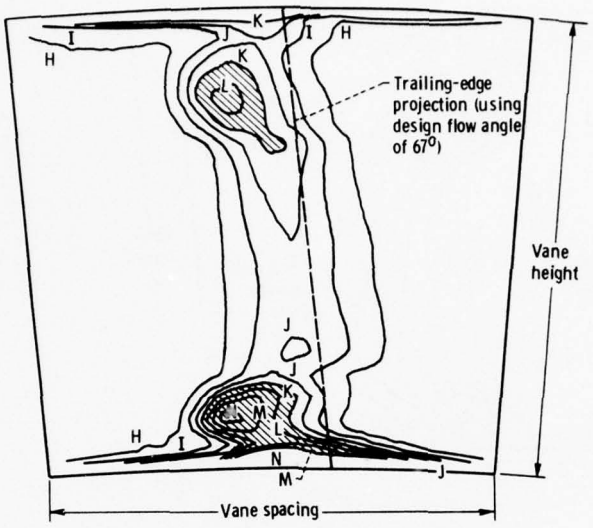


(a) Solid (uncooled) vanes and endwalls.

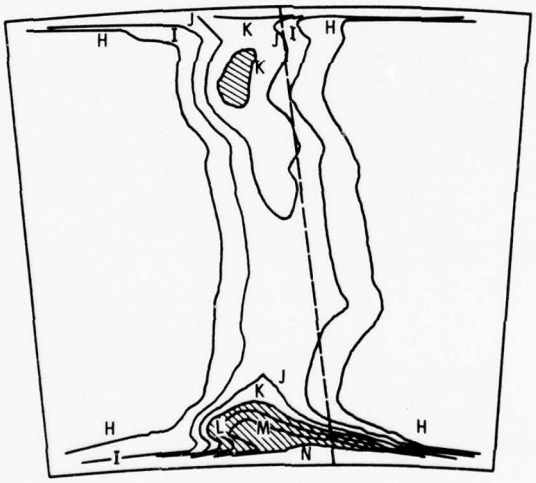


(b) Coolant to inlet total-pressure ratio, p'_c/p'_0, 1.0.

Figure 12. - Survey plane total-pressure ratio contour plots for endwall coolant injected in line with inviscid streamline direction.



(c) Coolant to inlet total-pressure ratio, p'_c/p'_0, 1.4.

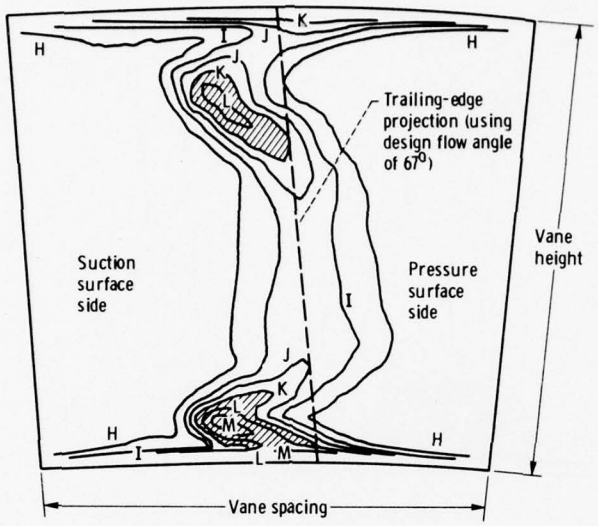


Total-pressure contour	Total-pressure ratio, p'_3/p'_0
H	0.99
I	.97
J	.95
K	.93
L	.91
M	.89
N	.87

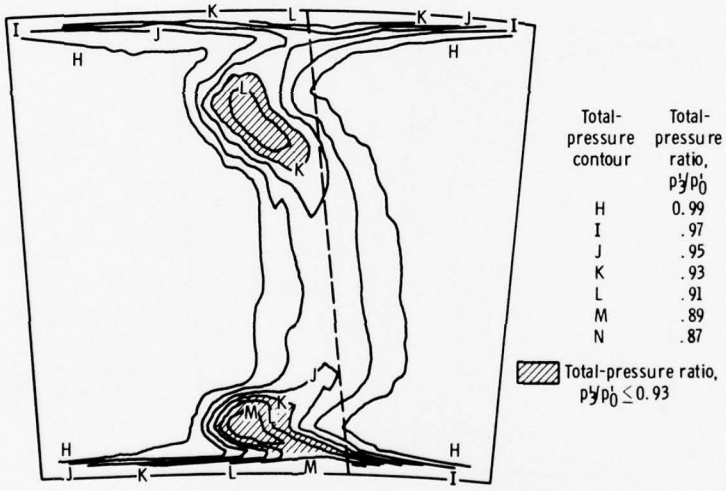
Total-pressure ratio, $p'_3/p'_0 \leq 0.93$

(d) Coolant to inlet total-pressure ratio, p'_c/p'_0, 1.8.

Figure 12. - Concluded.

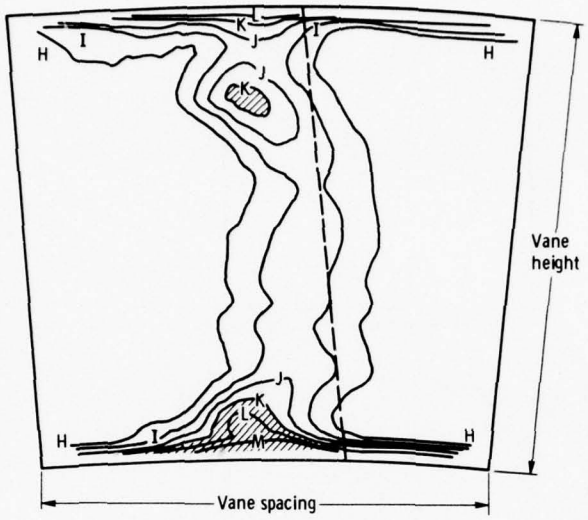


(a) Solid (uncooled) vanes and endwalls.

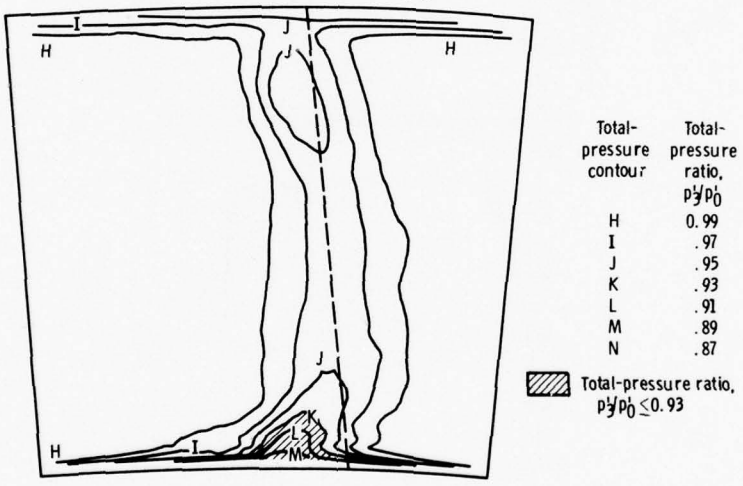


(b) Coolant to inlet total-pressure ratio, p_c'/p_0', 1.0.

Figure 13. - Survey plane total-pressure ratio contour plots for endwall coolant injected at 15° to inviscid streamline direction and oriented toward pressure surface.

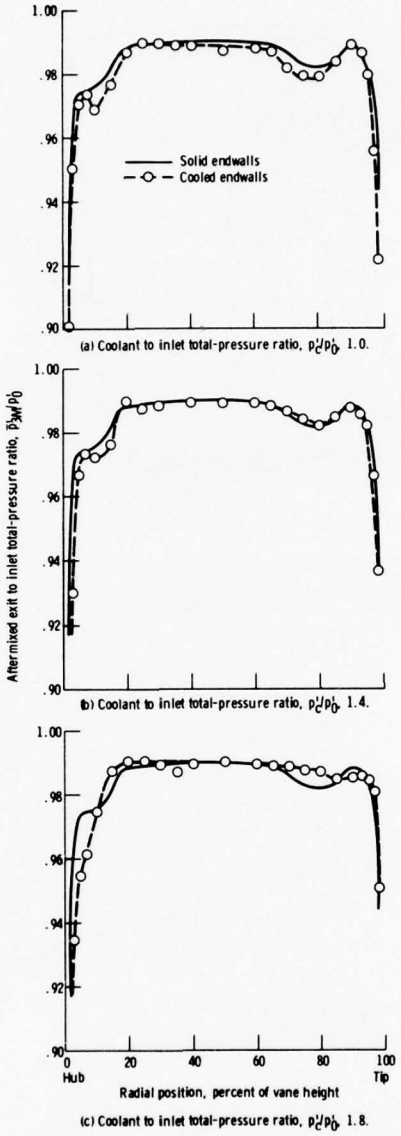


(c) Coolant to inlet total-pressure ratio, p_c'/p_0', 1.4.



(d) Coolant to inlet total-pressure ratio, p_c'/p_0', 1.8.

Figure 13. - Concluded.

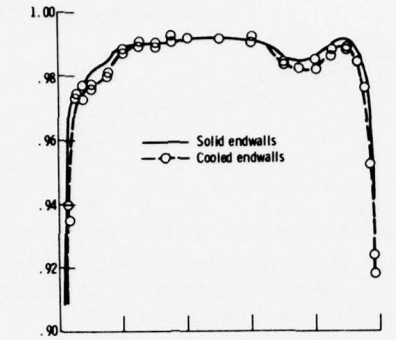


(a) Coolant to inlet total-pressure ratio, p'_c/p'_0, 1.0.

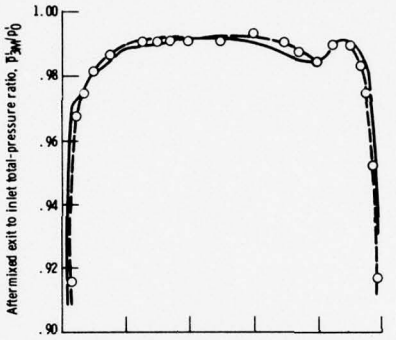
(b) Coolant to inlet total-pressure ratio, p'_c/p'_0, 1.4.

(c) Coolant to inlet total-pressure ratio, p'_c/p'_0, 1.8.

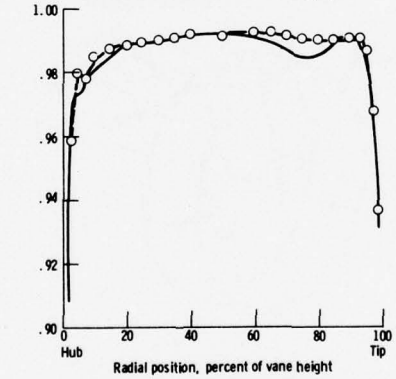
Figure 14. - Vane exit aftermixed total pressure as function of radial position for endwall coolant injected in line with inviscid streamlines.



(a) Coolant to inlet total-pressure ratio, p'_c/p'_0, 1.0.



(b) Coolant to inlet total-pressure ratio, p'_c/p'_0, 1.4.



(c) Coolant to inlet total-pressure ratio, p'_c/p'_0, 1.8.

Figure 15. - Vane exit aftermixed total pressure as function of radial position for endwall coolant injected at 15° to inviscid streamlines and oriented toward pressure surface.

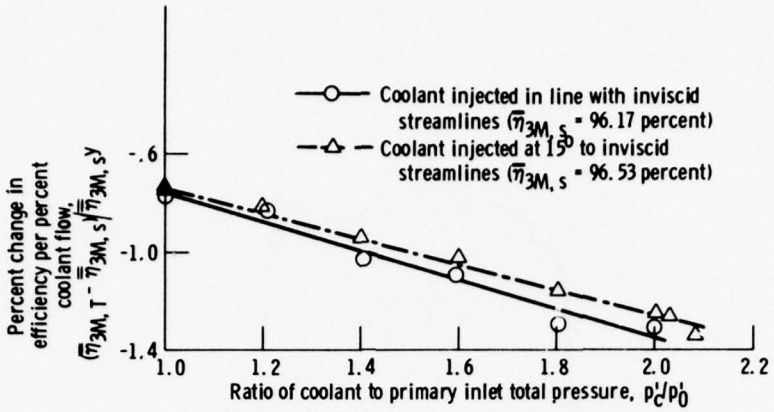


Figure 16. - Overall vane aftermixed efficiency characteristics as function of coolant to primary inlet total-pressure ratio for two cooled-endwall configurations.

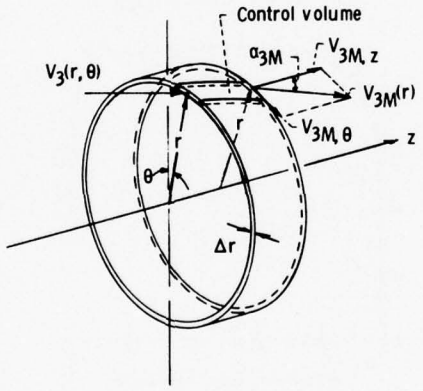


Figure 17. - Control volume for determination of aftermixed conditions (station 3M).

DISCUSSION

A.Spurr

I wonder if you have found any flow reversal at the hub of station 3M of your configuration?

Author's Reply

Station 3M is a theoretical station. It is not the measuring station.

A.Spurr

I see, because, whenever we tried to impose a constant static pressure downstream of an annular cascade we found that we got cross flow reversal at the hub which would come right upstream and interfere with the flow at the trailing edge. I wonder if you have come across this problem at all.

Author's reply

No, we haven't.

B.Barry

Your experiment appears to have been run at a $T_c/T_g = 10$. Have you done experiments at a more representative temperature ratio ($T_c/T_g < 10$)?

Were the effects significant?

If you have not done this, do you expect the effects to be significant?

Author's reply

The answer to the first question is: No, I have not run other temperature ratios more realistic to engine design conditions. Some annular cooling tests were done under the same contract by G.E. that have been discussed previously. However, their tests were with vane cooling also, so that the effects cannot be separated.

W.Kümmel

Can you give data of the percentage of cooling airflow as referred to the main airflow by rating the pressure ratio?

Author's Reply

It is in the report on Figure 11. It shows the fraction of cooling to primary flow as a function of cooling to inlet total pressure.

S.L.Dixon

Are the positions of the cooling holes chosen to optimize the cooling effects or to reduce the secondary flow (cross-wise flow) effect?

Author's Reply

The design of the endwall cooling configuration having the coolant injected in-line with the inviscid streamline direction was done (as indicated in the paper) under contract to NASA. It is my understanding that heat transfer effects were the main design consideration. For the modified endwall configuration having the coolant injected 15° to the inviscid streamline direction, which is designed, the main consideration was reducing the secondary flow effects. The results that we obtained suggest that by decreasing the secondary flows the heat transfer characteristics should also be improved (by preventing the endwall coolant from migrating away from the walls). Therefore, minimizing the secondary flow effects is felt to be intimately related to optimizing the cooling performance.

A NUMERICAL TIME-DEPENDENT APPROACH FOR DESCRIBING COMPRESSIBLE INVISCID NON-ISENTROPIC ROTATIONAL FLOWS IN CURVED DUCTS

G.Bussi and M.Pandolfi
Istituto di Macchine e Motori per Aeromobili
Politecnico di Torino
Torino 10129, Italy

According to the development in the investigation of secondary flows as indicated by Horlock in his opening lecture, one of the tools for understanding the nature of such flows is represented by the detailed analysis of inviscid 3D duct flows.

This short presentation deals with the numerical analysis of compressible inviscid non-isentropic rotational 3D flows in curved ducts, based on a time-dependent technique (TDT).

TDT computations are widely used for achieving the steady state flow as the asymptotic configuration in time of a transient. The transient starts from initial conditions which may be guessed (e.g. the typical blunt body computations) or it may represent the unsteady flow which occurs in a physical experiment.

Let us show how the actual 3D flow we are interested in may be obtained experimentally. Imagine a curved duct (Fig.1) connected at the inlet to a high-pressure reservoir and at the exit to a low-pressure capacity.

A grid is set at the inlet, with a porosity variable in the z direction in order to generate gradients of entropy in the incoming flow. Initially a diaphragm is placed at the end of the duct so that the gas inside the duct is at rest at the same pressure as in the feeding reservoir. The diaphragm is then removed and expansion waves are generated there; these waves travel upstream, reach the inlet grid and are reflected downstream. After some travels of pressure waves up and down in the duct, a steady state flow will be reached.

The TDT we have used describes this kind of transient and the steady flow pattern.

The complete Euler equations for 3D unsteady flow (hyperbolic partial differential equations) are integrated in time according to a two-level scheme of integration (MacCormack scheme). A crucial point in these problems is represented by the computation at the boundaries. The philosophy has been the one indicated by G.Moretti and consists in matching local quasi-steady conditions representing the boundary (e.g., for solid walls, the flow tangency condition) and compatibility equations along characteristic lines. More details on the algorithms at solid walls, and at the inlet and the outlet of the duct are given in References 1 and 2.

Results are here presented about a duct with a square cross section; the side walls are circular cylinders ($b = 3$ and $c = 4$); the deflection amounts to 90°. While at the inlet the flow velocities are directed in the only ϑ direction, a cross flow pattern is developed along the channel; Figure 2 shows the swirling in the cross section at $\vartheta = 75°$ as due to the deflection and to the vorticity generated at the inlet. Figures 3 and 4 show the displacement of stream surfaces from the inlet ($\vartheta = 0$) at the $\vartheta = 75°$ station. The vortex shown in Figure 2 induces the rotation of the stream surfaces which are here plotted as constant entropy surfaces generated at the inlet.

Even with the very rough mesh used (4 x 4 intervals in the cross section and 12 intervals along the duct), the results seem to describe correctly the inviscid development of the secondary flow.

REFERENCES

1. Moretti, G. — *A Circumspect Exploration of a Difficult Feature of Multidimensional Imbedded Shocks.* AIAA 2nd Computational Fluid Dynamics Conference, Hartford, Conn., June 1975.

2. Pandolfi, M. Zanetti, L. — *Some Tests on Finite Difference Algorithms for Computing Boundaries in Hyperbolic Flows.* Workshop on Boundary Algorithms for Multidimensional Inviscid Hyperbolic Flows, University of Stuttgart, February 1977.

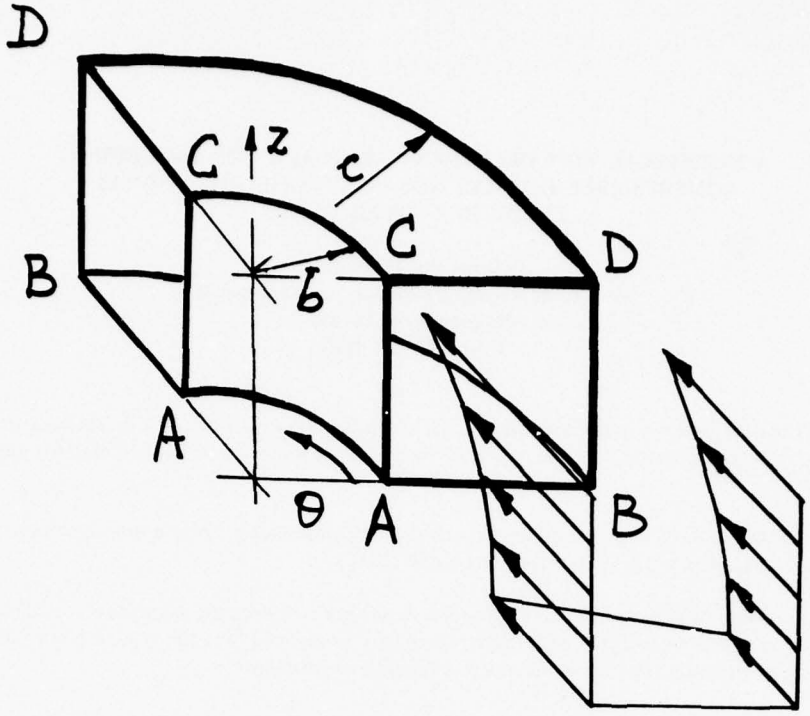


Figure 1

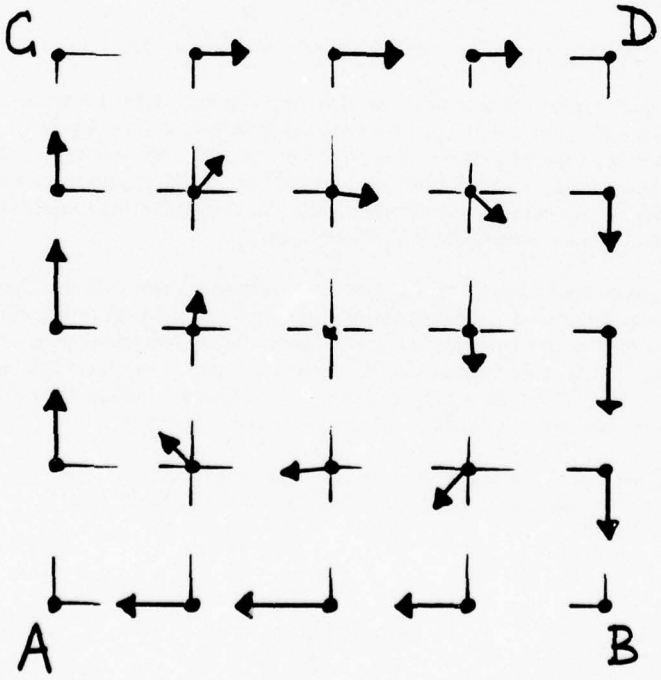


Figure 2

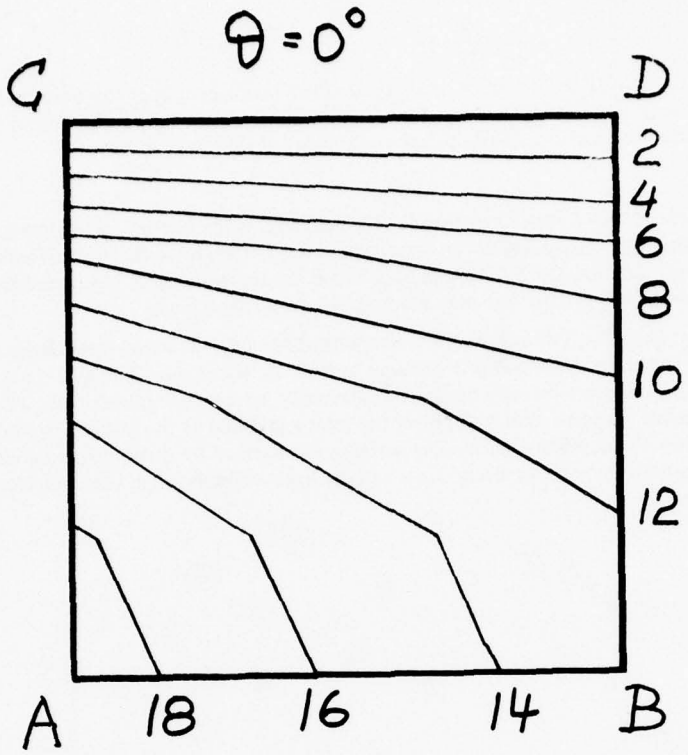


Figure 3

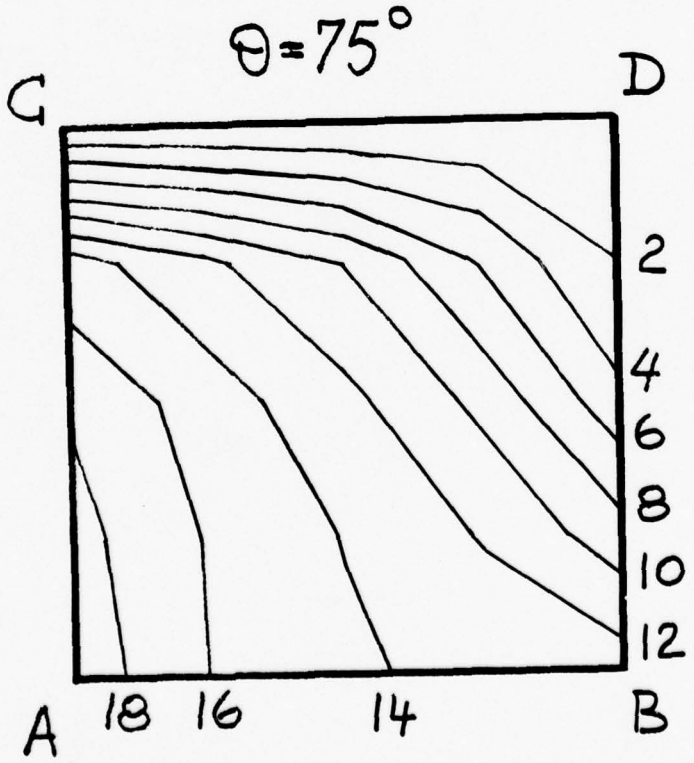


Figure 4

DISCUSSION

Ch.Hirsch

I have a question about the difference method you use, more precisely, about the time integration. Is it an explicit system or is it an implicit system and if it is an explicit system what are the limitations? And a second question: what are the boundary conditions that you impose at inlet and at outlet?

Author's Reply

The integration system, which I didn't mention for lack of time, is the explicit system which was suggested by McCormack a few years ago. It is a predictor-corrector method. Of course the explicit integration limits you to the time step which is related to the F.C.L. rule. So, this is the reason why in 3-D computations we want to find accurate and good algorithms so that one may work with a very rough mesh.

As regards the second question, I didn't mention anything about inlet or outlet boundaries also for lack of time, even if this is one of the most important problems, in hyperbolic equations. The way we treat the inlet and outlet boundary conditions are a bit long to explain. Basically we simulate numerically what may really occur in a physical experiment. Suppose that you put at the inlet a grid and at the outlet a permeable wall with straighteners. The flow through these permeable surfaces is described by quasi-steady equations. These are matched with compatibility equations along characteristic lines which bring in the computation the information about the unsteadiness.

SECONDARY FLOW STUDIES IN HIGH-SPEED CENTRIFUGAL COMPRESSOR IMPELLERS

by

D. Eckardt and H. Krain

DFVLR-Institut für Luftstrahlantriebe
Linder Höhe, 5000 Köln 90, W. Germany

SUMMARY

The flow fields within radial discharge and backward leaning impellers, running at tip speeds up to 400 m/s, have been investigated by means of a new laser technique, developed at DFVLR, Cologne. Some results, concerning the through-flow pattern of a radial bladed impeller, are presented. Detailed information about the superimposed secondary flow pattern have been derived from flow angle measurements. On the basis of these studies an impression of the complex secondary vortex distribution in radial compressor impellers is gained. Finally a comparison between measured and calculated streamwise vorticity near the exit of a radial discharge impeller is presented.

NOMENCLATURE

b/b_i	=	streamtube thickness referred to inlet thickness
b/t	=	blade height to blade spacing ratio
$\vec{c}$	=	absolute velocity vector
$d\bar{s}$	=	dimensionless streamline element
$h_{t,rel}$	=	relative total enthalpy $h_{t,rel} = h + w^2/2 - u^2/2$
I/ρ	=	relative total enthalpy for incompressible flow $I/\rho = p/\rho + w^2/2 - u^2/2$
H/B	=	aspect ratio of a bend
$\dot{m}$	=	mass flow rate
n	=	shaft speed
PS	=	pressure side
$p_{t,rel}/p_{t0,N}$	=	relative total pressure, referred to standard inlet total pressure $p_{t,rel}/p_{t0,N} = e^{-(s-s_0)/R}$
q	=	absolute fluctuation intensity $q = (c_{max} - c_{min})/(2u_2)$
R	=	gas constant
R/R_2	=	radius ratio in the vaneless diffuser
$\bar{r}_k$	=	dimensionless radius of curvature in the osculating plane
SS	=	suction side
t, t'	=	blade spacing
u	=	impeller speed
$\bar{w}$	=	relative velocity referred to impeller tip speed u_2
x/s_m	=	relative meridional shroud length ($x/s_m = 0$, inducer inlet tip)
y/t	=	relative blade spacing
z/b	=	relative meridional channel width
α	=	absolute flow angle
β	=	relative flow angle
$\Delta\beta$	=	cross-flow angle $\Delta\beta = \beta_{b,op} - \beta$ (Fig.2)
γ	=	angle between principal normal and the vector $\nabla h_{t,rel} \times \vec{w}$
δ	=	angle between angular velocity $\vec{\omega}$ and $\nabla h_{t,rel}$
δ	=	pressure correction factor for standard conditions $\delta = p_{t0}/1.0133$ bar
μ	=	slip factor $\mu = c_{u2}/u_2$
$\bar{\xi}_c$	=	dimensionless absolute vorticity
$\bar{\xi}_w$	=	dimensionless relative vorticity
Θ	=	temperature correction factor for standard conditions $\Theta = T_{t0}/288.1$ K
∇	=	gradient

SUBSCRIPTS

0	=	compressor inlet
2	=	impeller tip
m	=	meridional
max	=	maximum
min	=	minimum
N	=	standard condition
red	=	corrected to standard conditions
u	=	component in tangential direction y

INTRODUCTION

In general secondary flows are defined by the deviation of the real flow path from the potential flow pattern. According to this definition all cross-flows occuring in turbomachine rotors and stators belong to secondary flows. In fluid dynamics [1] it is well known that there appear considerable cross-flows in the side wall boundary layers of bends, even if they have high aspect ratios ($H/B \approx 3.5$). In these regions the flow is deflected from the outer to the inner wall, due to the imposed pressure gradient. In the mid-channel the flow traverses in the opposite direction, thus two oppositely oriented vortices are established. If the height/width ratio is reduced ($H/B \approx 0.5$), both regions merge together and the whole primary flow field is influenced.

Similar effects are observed in radial compressor impellers. In comparison to bends, radial impellers have extremely small height/width ratios. Especially near rotor exit this ratio becomes small ($b/t \approx 0.4$). So considerable secondary losses are to be expected in this region. Furthermore Coriolis and centrifugal forces are acting on the fluid particles, leading to instabilities in the unsteady relative flow. These effects lead to an accumulation of weak fluid particles at the suction side and the shroud, whereas high-energetic particles are shifted to the pressure side and to the hub. Additionally streamline curvature effects and system rotation either stabilize or destabilize the flow field, as has been pointed out in [2, 3].

Nowadays, advanced laser velocimetry [4, 5] is available to resolve the flow field, even in high-speed centrifugal impellers. Measurements yield the absolute velocity pattern, the flow angle distribution and the turbulence intensity, so that also detailed investigations of the relative flow pattern are possible under realistic operation conditions [6, 7].

EXPERIMENTAL SET-UP AND INSTRUMENTATION

Fig.1 shows the DFVLR centrifugal compressor test rig with the laser-2 focus-velocimeter (L2F) in front. The compressor is driven by a d-c motor with a maximum power input of 1 500 kW [5, 6, 7]. The measurement principle is illustrated in Fig.2 [4, 8]. The absolute velocity $\vec{c}$ and flow direction α as well as the fluctuation intensity $q = (c_{max} - c_{min})/(2u_2)$ are determined by this two-dimensional technique in the laser focal plane. The measurements have been carried out at several selected measuring planes, designated by 5 - 14 (Figs. 8 and 9) along the impeller flow path . In these planes secondary flows are defined by $\Delta\beta = \beta_{b,op} - \beta$, the difference between the blade angle $\beta_{b,op}$ in the focal plane and the relative flow angle β.

DEVELOPMENT OF IMPELLER THROUGH-FLOW

Figs.3 to 7 show perspective distributions of the meridional velocity c_m, referred to the rotor tip speed u_2, illustrating a flow development typical for high-speed radial-discharge impellers from inducer inlet to rotor exit. The measuring position is indicated by the dimensionless meridional shroud contour length x/s_m. The presented investigations were performed at $n = 14\,000\ min^{-1}$, $\dot{m} = 5{,}31$ kg/s.

Fig.3 displays the meridional velocity pattern within the rotor, about 11 mm aft of the inducer leading edge. The pressure side, denoted DS, is situated on the left, the suction side SS on the right, hub and shroud in the rear and in front respectively. The measurements reveal a nearly potential theoretical flow character with a positive velocity gradient from pressure to suction side and from hub to shroud. Similarly Fig.4 represents a very regular velocity pattern at $x/s_m = 0.43$, although with increased blade loading. Maximum loading is reached at $x/s_m = 0.593$ (Fig.5), where the flow channel turns to the radial direction. First velocity distortions occur in the shroud wall region at $y/t \approx 0.7$. Downstream, Figs.6 and 7, these distortions enlarge rapidly, so that the wake covers about 35 per cent of the rotor discharge area; simultaneously a decreasing blade-to-blade loading is to be observed in the jet core (Figs.5 - 7).

SECONDARY FLOW PATTERN WITHIN IMPELLER AND VANELESS DIFFUSER

Figs.8 and 9 illustrate the continuous development of the secondary flow pattern, represented by the $\Delta\beta$-distribution, for a 60 deg backswept impeller. Positive $\Delta\beta$ indicates a flow deflection towards the pressure side. The measurements have been carried out close

to the design point. Plane ⑤, Fig.8, displays the incidence distribution about 5 mm in front of the inducer leading edge. The incidence variation is between 7 and 15 deg. from shroud to hub. At plane ⑦, 11 mm aft of the inducer leading edge, the flow is nearly blade-congruent. Plane ⑩ shows the corresponding distribution at the end of the inducer. In this region the flow has a tendency towards the suction side, but still no distinct secondary vortex is established. Fig.9 represents the secondary flow pattern within the impeller. Corresponding to the introductory considerations, an increased cross-flow intensity is observed in this part. A marked cross-flow component towards the suction side occurs near the shroud, where a comparison of Figs.5 to 7 reveals the thickening boundary layer. Strongest secondary flows appear obviously in plane ⑬ with a subsequent distinct damping in the impeller exit/diffuser entry region. Corresponding to the general slip effect, the main flow is leaning towards the pressure side, whereas at the shroud and - to a weaker extent - at the hub an overturning towards the suction side is appearing. Another representation of these data is given in Fig.10. The plot of relative velocity vectors follows the same trend as in Fig.9.

The secondary flow development in the vaneless diffuser entry region is pointed out in Fig.11. Relative velocity distributions w/u_2 are presented for 4 radius ratios R/R_2. At $R/R_2 = 1.017$ a considerably skewed pattern is observed. In the shroud/suction side region the wake is still visible and has not yet mixed with the jet. The development of circumferential and meridional velocity components leads to a decreasing inclination of the relative flow streamlines.

FLOW PHENOMENA DUE TO SECONDARY FLOWS

A basic secondary flow pattern in the radial part of a centrifugal compressor impeller has been reconstructed based on the preceding considerations (Fig.12). The main cross-flow closes to a dominating primary vortex ①. A weaker vortex ② appears near the suction side; additionally tip clearance flow from the adjacent channel ③ feds low-energetic particles into the wake area.

The following secondary flow effects can be anticipated from this vortex distribution:

1. Due to the impingement of different secondary vortices in the shroud/suction side area, the fluctuation intensity q will raise in this region.

2. The primary vortex will influence the local energy transfer and correspondingly the slip distribution in the radial impeller.

3. Secondary flow transport will also lead to a loss accumulation in the wake region.

An experimental proof of these assumptions is given in Figs.13, 14 and 15, presenting an impression of fluctuation, energy and loss distributions at the exit of a radial bladed impeller. Fig.13 illustrates that maximum fluctuation intensities $q = (c_{max} - c_{min})/(2u_2) < 0.3$ exist in the wake region, exceeding nearly two times the values in the jet core. The interpolated pattern is based on 35 measuring points; the jet/wake borderline is constructed by the velocity contour line $c_m/u_2 = 0.3$ (Fig.7). The corresponding total enthalpy distribution, represented by the slip factor $\mu = c_u/u_2$ (Fig.14), reveals the effect of secondary flows on energy transfer. Slip factors $\mu \geq 1$ are observed near the shroud, as could have been anticipated from the cross-flow pattern. Finally Fig.15 displays the loss distribution, represented by the relative total pressure distribution $p_{t,rel}/p_{t0,N}$. The expected loss accumulation appears in the wake region, whereas the jet core is characterized by nearly isentropic flow.

PREDICTION OF STREAMWISE VORTICITY BASED ON INVISCID THEORY

According to the preceding considerations, it may be anticipated, that inviscid secondary flow theories will predict realistic results only in the nearly isentropic jet flow, whereas in the loss-affected wake region larger deviations should occur. In order to compare measured and theoretical secondary flow patterns, an inviscid theory has been applied to calculate the distributed secondary vorticity. References [9 - 16] represent the necessary theoretical background. The actual approach is based on [9, 10, 13, 14] where the fundamental relations for induced vorticity growth within a centrifugal impeller are derived in detail. The effect of developed distributed vorticity on impeller efficiency and diffuser flow has been pointed out by Ellis [13] and Howard [15]. Streamwise vorticity may be generated by total enthalpy gradients, turbulence and tip clearance effects. Simplifying, an inviscid steady and incompressible flow was assumed for the calculations. Although total enthalpy gradients, resulting partially from viscous effects, have been taken into account, additional viscous effects were neglected. The governing equation for these assumptions is given in[10, eq. 21], [15, eq. 11]:

$$\frac{\bar{\xi}_c - \bar{\xi}_{c1}(\bar{w}/\bar{w}_1)}{|\overline{\nabla(1/\rho)_i}|} = 2\bar{w}\int_1^{\bar{s}} \frac{\cos\gamma}{\bar{w}^2\,\bar{r}_k\,(b/b_i)}\,d\bar{s} + 2\bar{w}\int_1^{\bar{s}} \frac{\cos\delta}{\bar{w}^3\,(b/b_i)}\,d\bar{s}$$

γ is the angle between the principal normal and the vector $\nabla h_{t,rel} \times \vec{w}$, δ is the angle between the angular velocity $\vec{\omega}$ and $\nabla h_{t,rel}$.

A solution of this equation necessitates some information on the streamlines, represented by ds and r_k, the local relative velocity w and a reasonable assumption concerning the surfaces $h_{t,rel}$ = const. Streamline co-ordinates have been derived from a quasi-threedimensional calculation [16]. The measured relative velocity was assumed to be tangential to the calculated streamlines. Furthermore, surfaces of constant relative total enthalpy were taken as surfaces of revolution - an assumption, which is especially doubtful in the wake region. The calculations have been performed along 30 selected streamlines with corresponding vorticities ξ_{cl}, deduced from the measured inlet velocity profile. The experimental secondary vorticity has been derived from the measured circumferential relative velocity component for a plane near impeller discharge (x/s_m = 0.866), Fig.16. Fig.17 shows a comparison between calculated and "measured" dimensionless relative secondary vorticity $\bar{\xi}_w / |\overline{\nabla(I/\rho)_s}|$. Obviously, good coincidence is obtained in the jet region, whereas, as expected, pronounced deviations occur close to the shroud and in the wake area.

REFERENCES

[1] Truckenbrodt, E.: "Strömungsmechanik", Springer-Verlag Berlin, Heidelberg, New York 1968.

[2] Johnston, J.P., Eide, S.A.: "Turbulent Boundary Layers on Centrifugal Compressor Blades: Production of the Effects of Surface Curvature and Rotation", Journal of Fluids Engineering, TRANS.ASME, Sept.1976, pp.374-381.

[3] Rothe, P.H., Johnston, J.P.: "Effects of System Rotation on the Performance of Two-Dimensional Diffusers", Journal of Fluids Engineering, TRANS.ASME, Sept.1976, pp.422-436.

[4] Schodl, R.: "A Dual-Focus-Velocimeter for Turbomachine Applications", von Karman-Institute, Lecture Series 78, Advanced Testing Techniques in Turbomachines, April 1975, p.39.

[5] Eckardt, D.: "Detailed Flow Investigations Within a High-Speed Centrifugal Compressor Impeller", Journal of Fluids Engineering, TRANS.ASME, Sept.1976, pp.390-402.

[6] Eckardt, D.: "Instantaneous Measurements in the Jet-Wake Discharge Flow of a Centrifugal Compressor Impeller", Journal of Engineering For Power, TRANS.ASME, Series A, Vol.97, No.3, July 1975, pp.337-346.

[7] Eckardt, D.: "Applications of Dynamic Measurement Technique for Unsteady Flow Investigations in Centrifugal Compressors", von Karman-Institute, Lecture Series 66, Advanced Radial Compressors, March 1974, p.101.

[8] Schodl, R.: "Laser Dual-Beam Method for Flow Measurements in Turbomachines", ASME-Paper No.74-GT-157.

[9] Kramer, J.J., Stanitz, J.D.: "A Note on Secondary Flow in Rotating Radial Channels", NACA Report 1179, 1954, p.12.

[10] Smith, A.G.: "On the Generation of the Streamwise Component of Vorticity for Flows in Rotating Passages", The Aeronautical Quarterly, Vol.8, Nov.1957, pp.369-383.

[11] Hawthorne, W.R.: "Rotational Flow through Cascades", Quarterly Journal of Mechanics and Applied Mathematics, Vol.VIII, Sept.1955, pp.266-279.

[12] Marris, A.W.: "Secondary Flows in an Incompressible Fluid of Varying Density in a Rotating Reference Frame", Journal of Basic Engineering, TRANS.ASME,June 1966, pp.533-538.

[13] Ellis, G.O.: "A Study of Induced Vorticity in Centrifugal Compressors", Journal of Engineering for Power, TRANS.ASME, Jan.1964, pp.63-76.

[14] Horlock, J.H.: "Vorticity Transfer and Production in Steady Inviscid Flow", Journal of Basic Engineering, March 1968, pp.65-70.

[15] Howard, J.H.G.: "Analytical Theory of Secondary Flow in a Centrifugal Impeller", Trans.of the Engg. Inst.of Canada, Vol.9, 1966, pp.1-10.

[16] Hawthorne, W.R.: "Secondary Circulation in Fluid Flow", Proc.Roy.Soc.A, 206, 1951, pp.374-387.

[17] Krain, H.: "Beitrag zur Berechnung der quasi-dreidimensionalen Strömung in Radialverdichter-Laufrädern", Thesis, Univ.Aachen, June 1976, p.185.

[18] Sturge, D.P., Cumpsty, N.A.: "Two-Dimensional Method for Calculating Separated Flow in a Centrifugal Impeller", ASME-Paper 75-FE-6, 1975, p.9

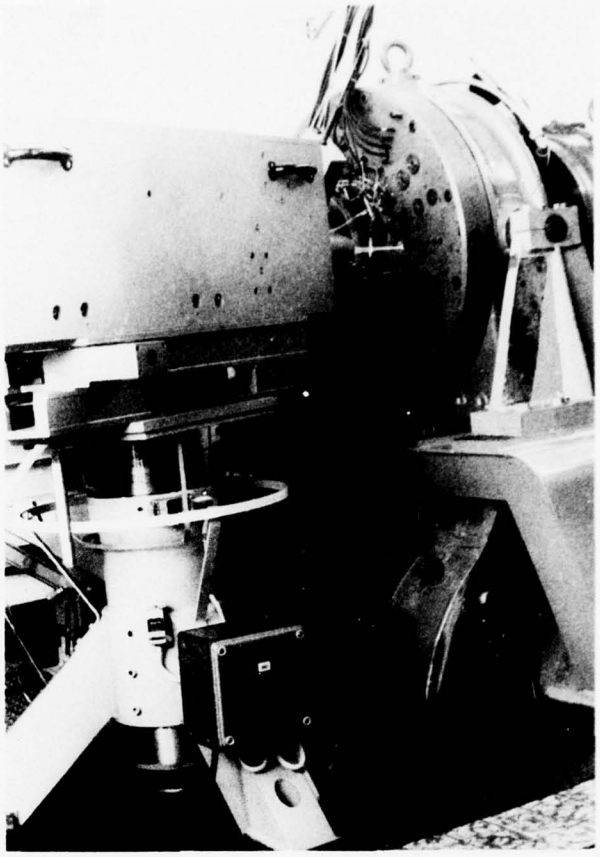
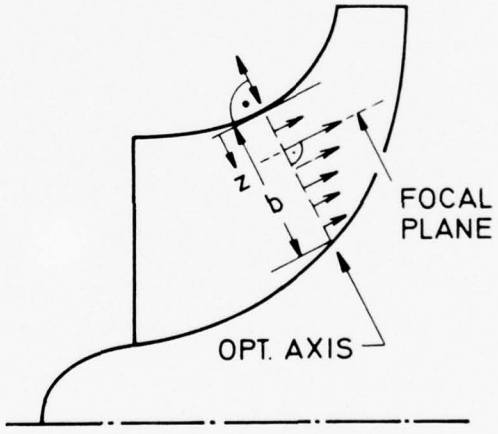


Fig.1 L2F velocimeter at centrifugal compressor test rig



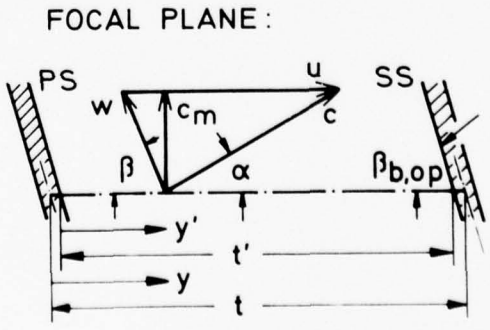


Fig.2 Definition of the L2F measuring location (y,z) and of the flow angles α and β

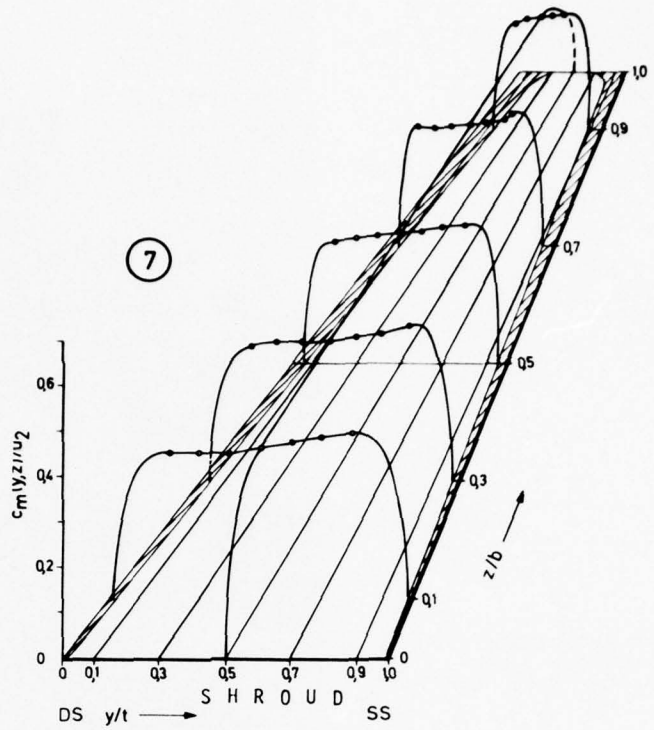


Fig.3 Meridional velocity distribution c_m/u_2 at $x/s_m = 0.08$, $n = 14000\ min^{-1}$, $\dot{m} = 5.31$ Kg/s

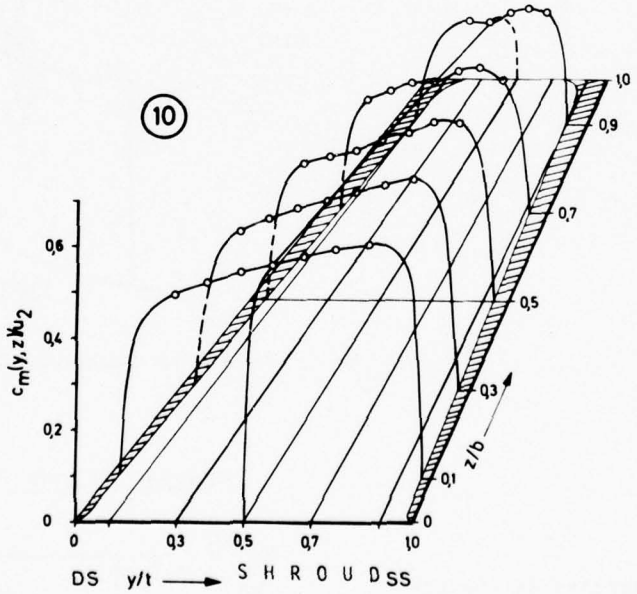


Fig.4 Meridional velocity distribution c_m/u_2 at $x/s_m = 0.431$, $n = 14000\ min^{-1}$, $\dot{m} = 5.31$ Kg/s

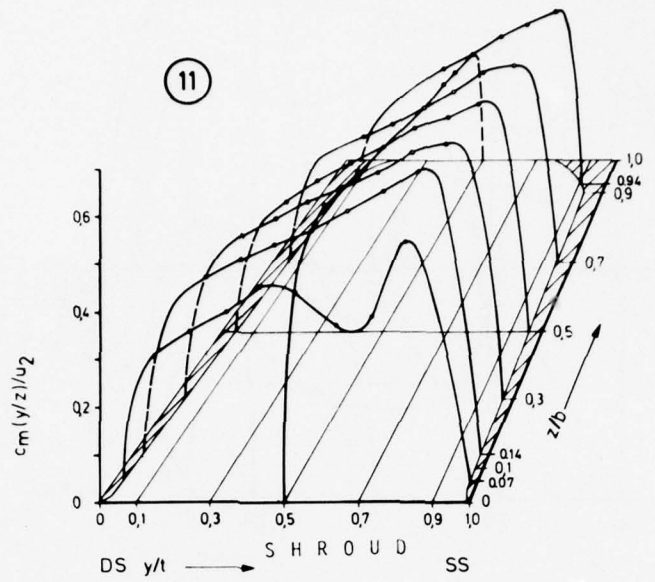


Fig.5 Meridional velocity distribution c_m/u_2 at $x/s_m = 0.593$, $n = 14000\ min^{-1}$, $\dot{m} = 5.31\ Kg/s$

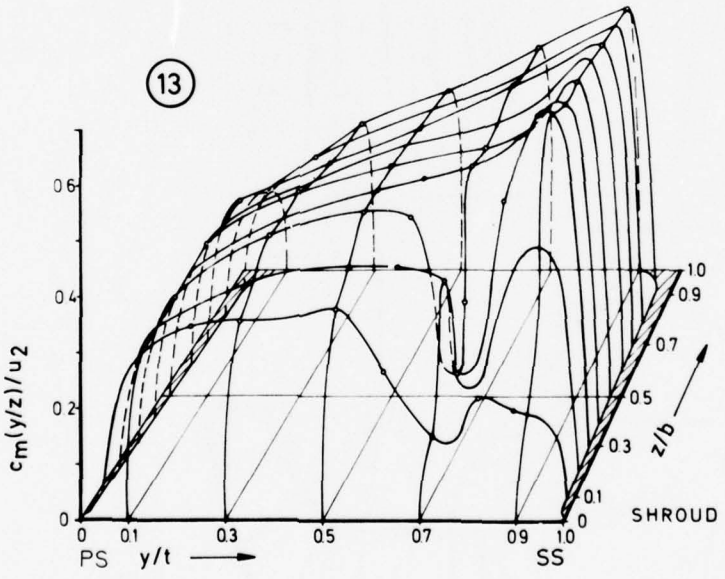


Fig.6 Meridional velocity distribution c_m/u_2 at $x/s_m = 0.866$, $n = 14000\ min^{-1}$, $\dot{m} = 5.31\ Kg/s$

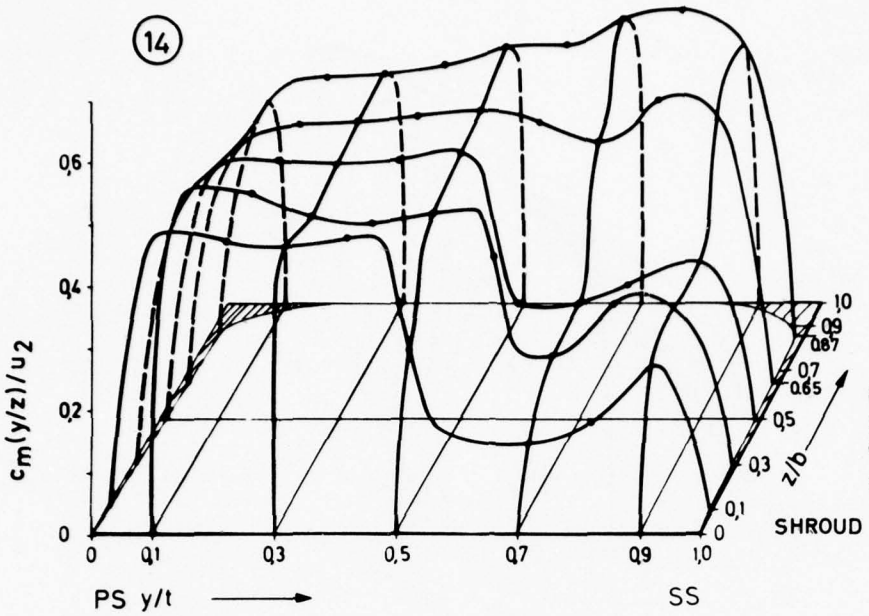


Fig.7
Meridional velocity distribution c_m/u_2 at $x/s_m=1.01$, $n=14000\ min^{-1}$, $\dot{m}=5.31$ kg/s

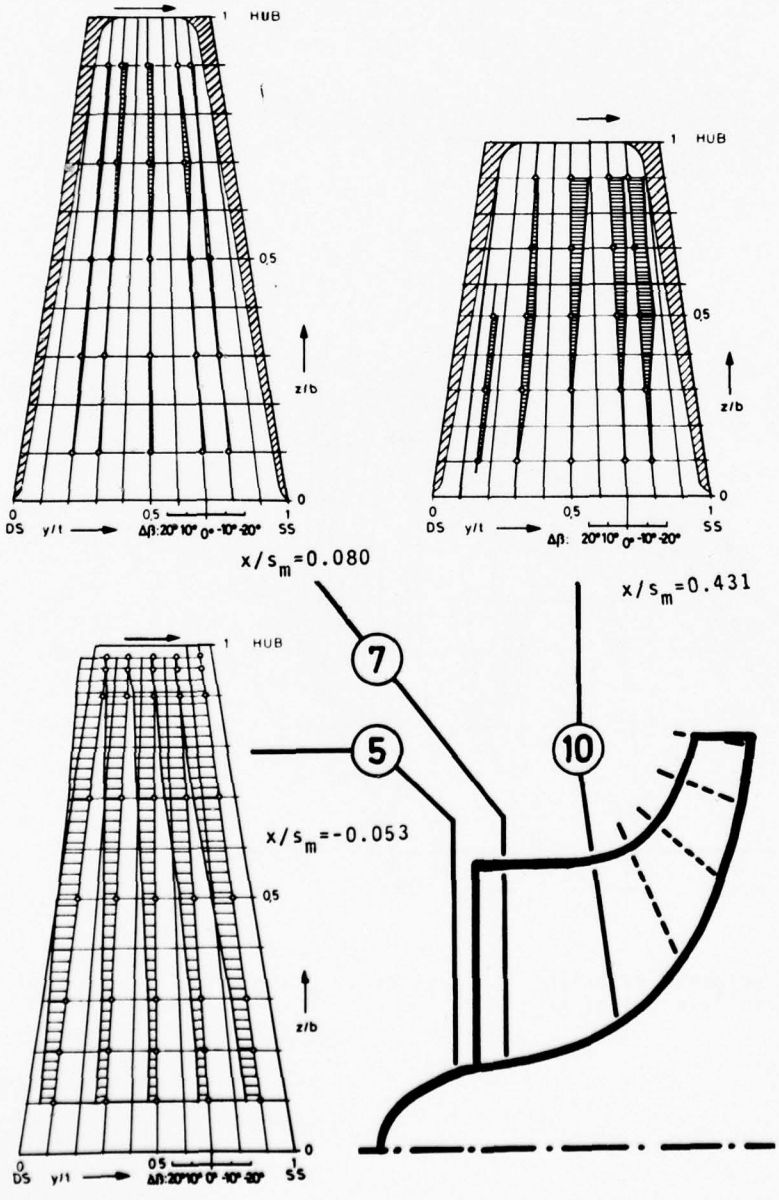


Fig.8
Δβ-distribution in front of and within the inducer, $n=14000\ min^{-1}$, $\dot{m}=4.54$ kg/s

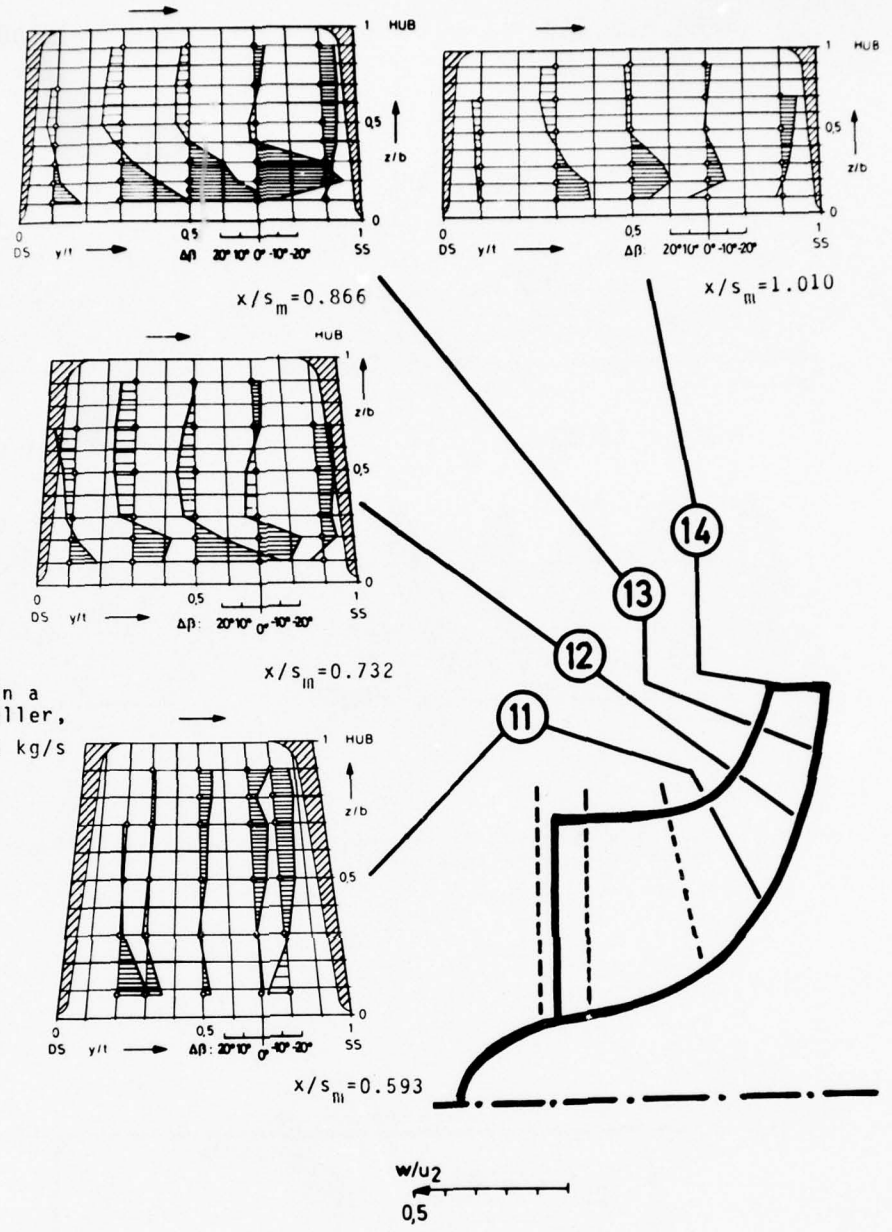


Fig.9
Δβ-distribution within a backward leaning impeller, n=14000 min^{-1}, $\dot{m}$=4.54 kg/s

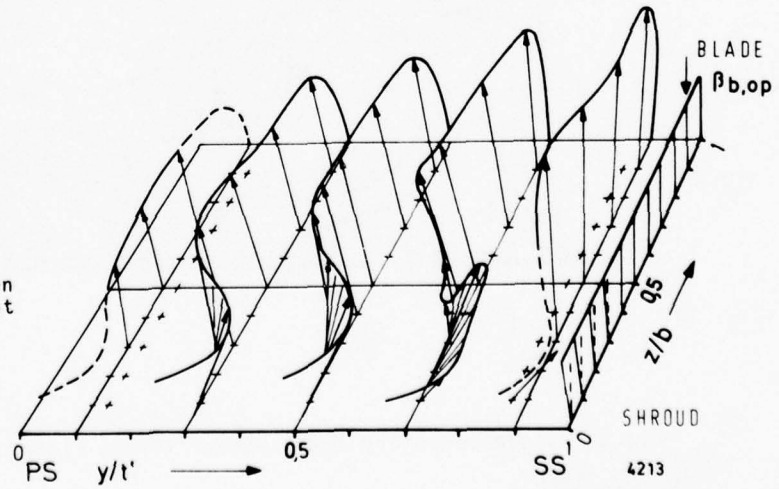


Fig.10
Relative velocity distribution in a radial bladed impeller at x/s_m=0.866, n=14000 min^{-1}, $\dot{m}$=5.31 kg/s

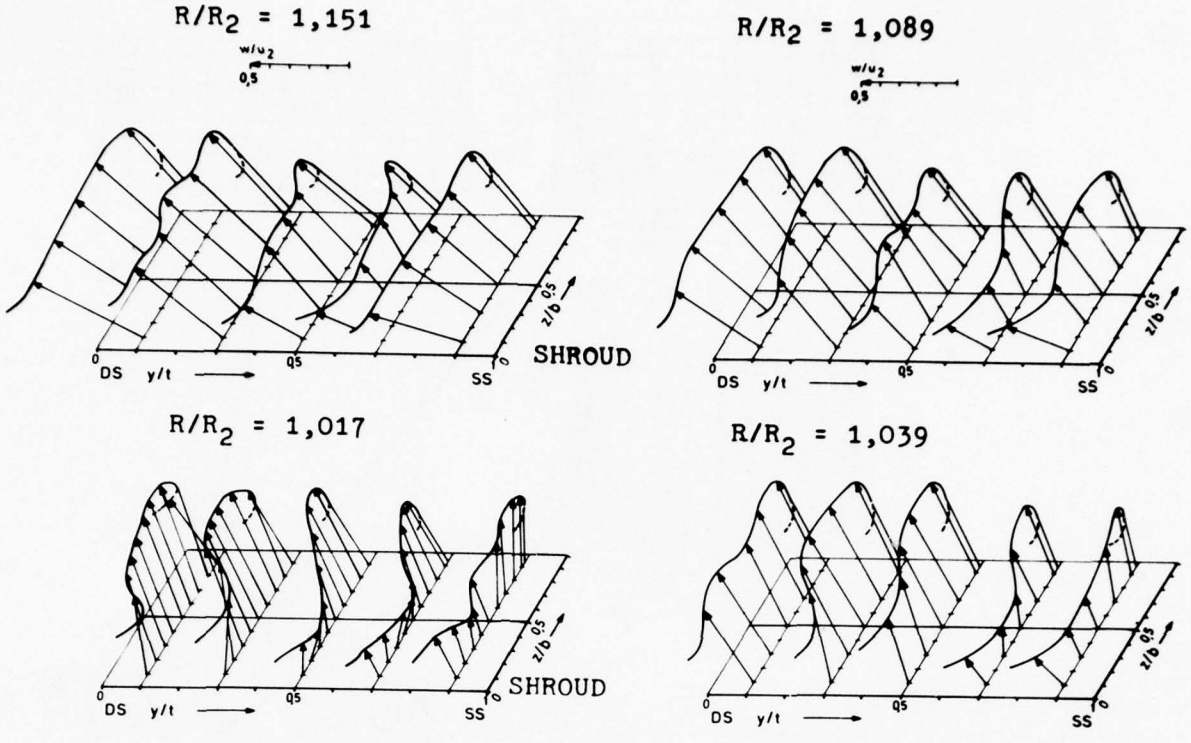


Fig.11 Relative velocity development in the vaneless diffuser aft of radial discharge impeller

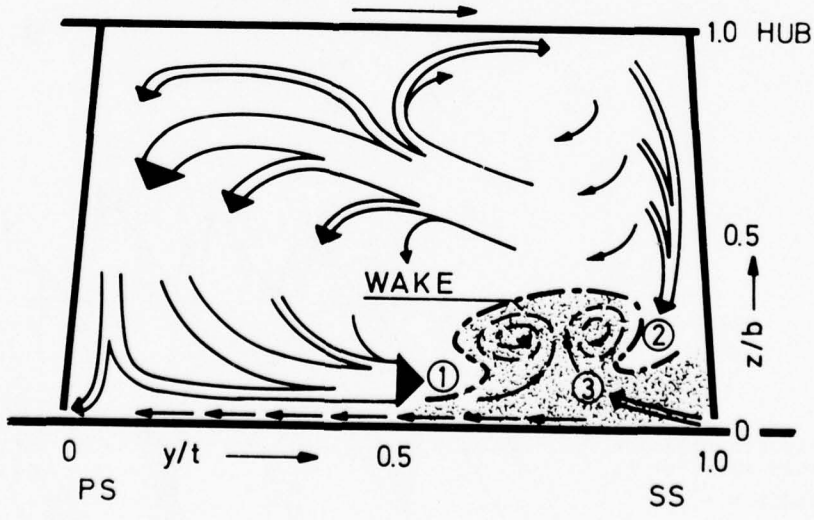


Fig.12 Basic secondary flow pattern in the radial part of the impeller

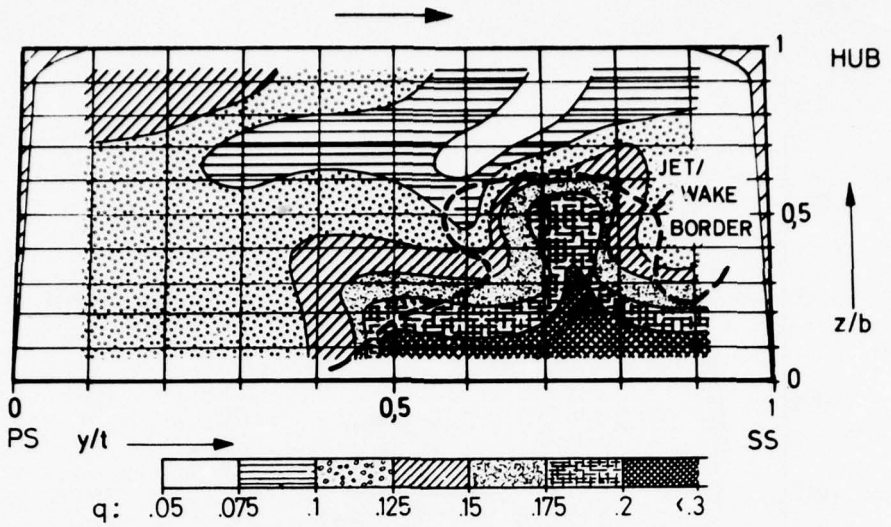


Fig.13 Distribution of fluctuation intensity q at impeller discharge, x/s_m=1.01, n=14000 min^{-1}, $\dot{m}$=5.31 Kg/s

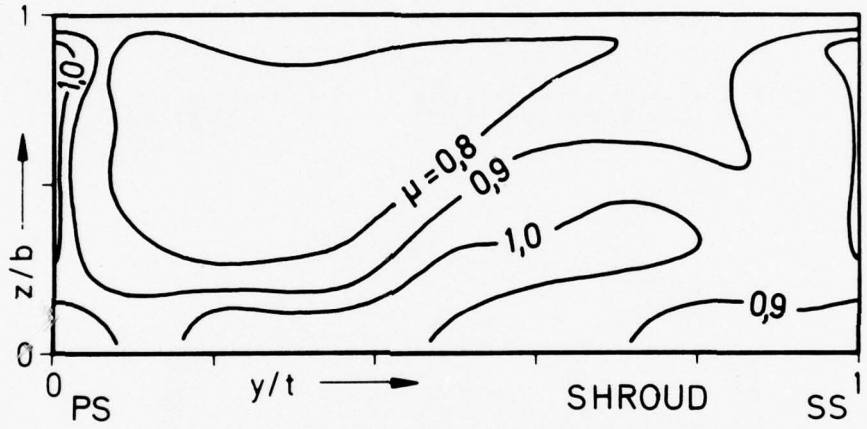


Fig.14 Distribution of slip factor $\mu=c_{u2}/u_2$, n=14000 min^{-1}, $\dot{m}$=5.31 Kg/s

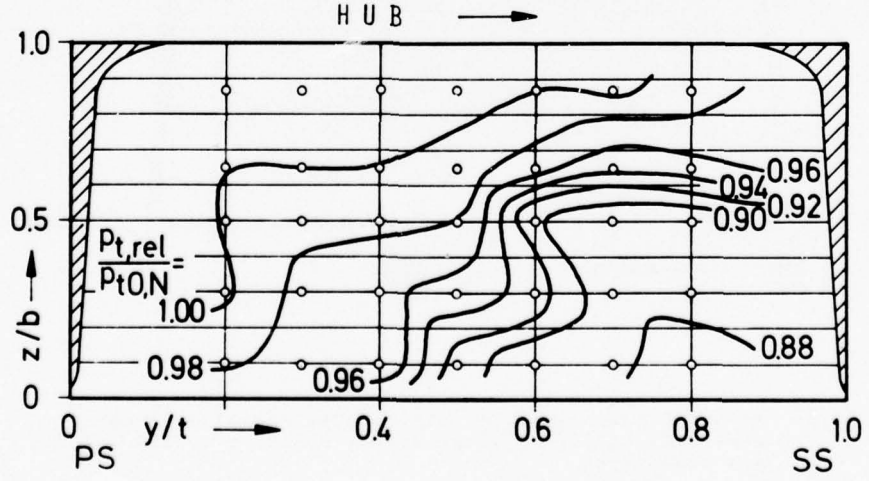


Fig.15 Distribution of relative total pressure $p_{t,rel}/p_{t0,N}$ at impeller discharge, x/s_m = 1.01, n = 14 000 min^{-1}, $\dot{m}$ = 5.31 kg/s

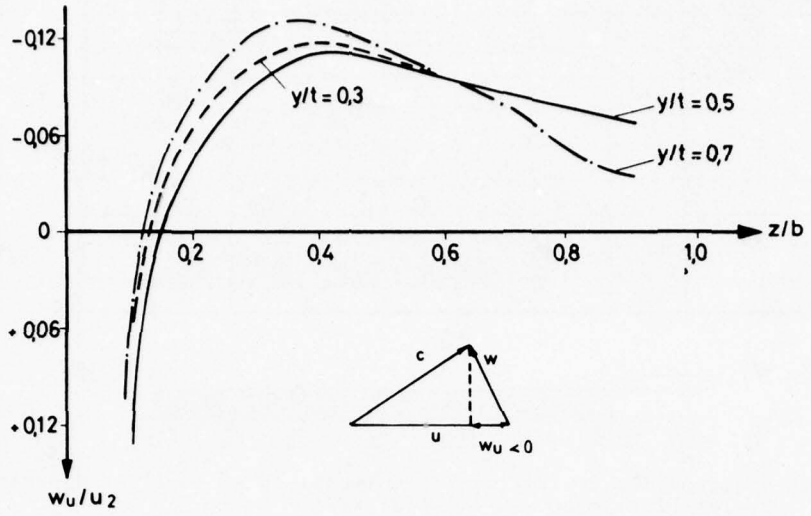


Fig.16 Circumferential relative velocity component w_u/u_2 at $x/s_m = 0.866$, $n = 14000\ min^{-1}$, $\dot{m} = 5.31\ Kg/s$

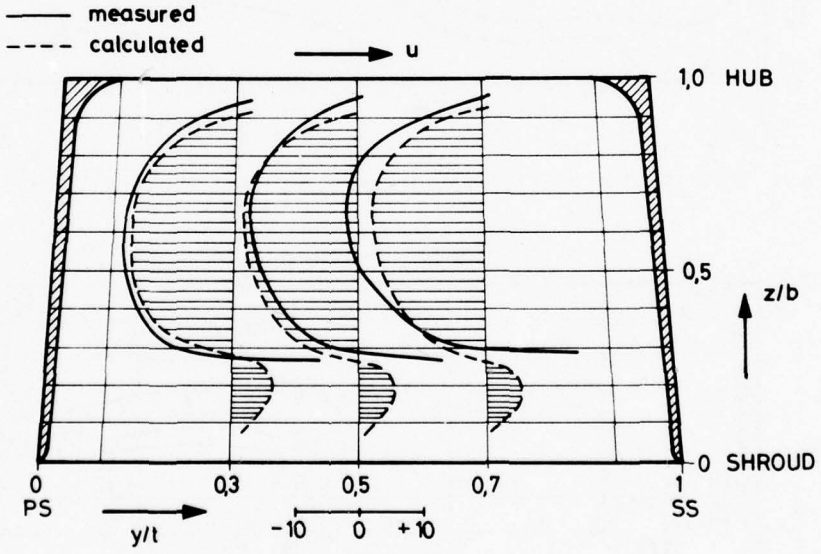


Fig.17 Measured and calculated distributed relative secondary vorticity $\xi_w/|\overline{\nabla(1/\rho)i}|$ at $x/s_m = 0.866$, $n = 14000\ min^{-1}$, $\dot{m} = 5.31\ Kg/s$

DISCUSSION

P.Runstadler

Mr. Eckardt and his co-workers at DFVLR should be congratulated for the kind of measurements that they have displayed here today, tackling a rather complex flow situation and using an extremely difficult measurement technique to get the measurements that we have seen. There is one point that you did not bring out today. If we look at one of the common parameters used by the centrifugal compressor designer – the slip factor at the exit of the wheel – some rather simple correlation rules are commonly used. Your measurements shed some light on it; what types of correlations are valid for centrifugal compressors? Can you tell us, whether the slip factor, that you have been able to measure at the tip of the wheel, follows for example the recent work by Sturge and Cumpsty (18), who were trying to find a predictive method and some rational explanation for the behavior of slip factor for this type of machine.

Author's Reply

I have not compared all the slip factor correlations well known in the literature in too much detail. We found a general tendency of slip factor variation with mass flow for a radial-bladed impeller, which coincides with common empirical slip relations, but we also found certain discrepancies concerning the backward-leaning impeller. In principle, good coincidence with the theoretical predictions by Sturge and Cumpsty (18) has been obtained. They showed, to my knowledge for the first time, a quite different distribution of slip factor with mass flow for S-shaped blades. They were able to predict theoretically, that due to the wake flow, there can be an increase of slip factor with mass flow and that due to the wake flow, there can be an increase of slip factor with mass flow and they could prove, based on usual definition, that there can be slip factors $\mu > 1$. Besides the latter result, we were able to verify the general trend surprisingly well. I think, that the influence of the flow separation on the slip factor depends on the overall impeller geometry and *not only* on blade exit angle (as assumed in most correlations). E.g. in our case, with a S-shaped impeller, the flow is forced into the backward turning (to 60 deg from neg. tang. direction) relatively close to impeller exit. So it appears, that the quoted slip factor distribution with mass flow is typical for this special backward leaning impeller configuration.

SOME OBSERVATIONS FROM LOW-SPEED CASCADE TESTS CONCERNING SIDE WALL BOUNDARY LAYER SUCTION

by B.A.Gustafson,
Department of Turbomachinery, Chalmers University of Technology, Gothenburg, Sweden

Introduction

At a two-dimensional cascade test in the windtunnel, boundary layers are built up on the side walls, giving cause to a reduction of the effective flow area behind the cascade (figure 1). Usually this effect is described by the axial-velocity-density ratio

$$\Omega = \frac{\rho_2 \cdot c_{2ax}}{\rho_1 \cdot c_{1ax}}$$

and presented together with other test data. Different values of the axial-velocity-density ratio are realized by means of side wall boundary layer suction.

In general the side wall boundary layers are removed through porous walls of constant porosity. Because of the static pressure distribution around the blades a distributed suction effect is obtained over the side wall. At the blade pressure surface a larger mass flow per unit area will pass through the side wall than at the suction surface.

Visualizations of the flow indicate that in particular the boundary layer in the corner between the blade suction surface and the side wall is important for the development of secondary flow.

In these corners, however, the pressure difference over the side wall and thereby also the local suction flow are comparatively small.

From this example we learn that side walls of constant porosity can give low local suction rates at zones with thick boundary layers and high suction rates at zones with thin boundary layers.

Considerations like these form the background to an investigation of the influence of distributed porosity on cascade test results.

Test set up

Geometrical data of the test cascade are presented in figure 2. Measurements were taken at an inlet velocity of about 50 m/s corresponding to

a Reynold's number of $2.5 \cdot 10^5$. The aspect ratio of the cascade is 1.75.

Three different side wall configurations were included in the investigation (figure 3). The first one represents the constant porosity case and will later on be referred to as the 24-holes side wall.

In the second configuration (12 holes) the perforation is located to the corners formed by the suction surfaces and the side walls.

In the third configuration (6 holes) the complete suction effect is concentrated to the downstream part of the suction surface.

The upper illustration to the right in figure 3 shows Ω-values measured at mid-span, at which the local flow through the side wall reverses due to suction. At Ω-values greater than 1.04 air is blowing into the cascade at low-pressure points.

Results

Flow on blade surfaces

The flow pattern on the blade surfaces was visualized in the following way. The blade was covered with a thin piece of paper. Droplets of ink were placed close to the blade leading edge and the wind tunnel was started. Ink traces from tests like these are reproduced in figure 4. Strong deviations from the parallel flow can be observed on the suction surface at high Ω-values. At lower values of Ω the streamlines on the blade suction surface are straightened out. On the pressure surface the flow has a velocity component towards the wall. This is partly an effect of the side wall through-flow and partly a secondary flow effect due to boundary layer cross flow. The latter effect will occur even at solid walls.

Parallel flow on the suction surface can be observed at $\Omega \simeq 1$ for the 24-holes side wall and at $\Omega \simeq 1.04$ for the 12-holes wall.

Similar results were obtained by observing the behaviour of tufts applied on the blades.

As far as the flow on the blade surfaces is concerned differences can easily be recognized between the two side wall configurations.

Blade pressure distributions

Blade pressure distributions for different values of the axial-velocity-density ratio are illustrated in figure 5. Decreasing Ω-values (increasing suction) give increasing pressures (decreasing velocities) except for the upstream part of the suction surface. Decreasing Ω-values also mean increasing deceleration and increasing static pressure rise.

In figure 6 the blade pressure distributions for two different side wall configurations are compared at the same Ω-value. The 12-holes case shows higher pressures (lower velocities) on both pressure- and suction surfaces than the constant porosity case. Anyhow the differences between the two cases are big enough to be recognized on the blade mid-span pressure distributions.

Deviation angle and static pressure rise

The deviation angle increases as increasing suction (decreasing Ω-values) is applied (figure 6). This is a wellknown trend, which has been reported by many investigators. The change of deviation angle with Ω in figure 6 is somewhat larger than the usually recommended formula $\delta = \delta_{\Omega=1} - 10\ (\Omega-1)$.

Differences with respect to the three side wall configurations are small.

The static pressure rise over the cascade increases as the axial-velocity-density ratio decreases (figure 8). As for the deviation angle a significant influence of the side wall perforation cannot be observed.

Incidence angle

It was felt that larger differences of flow parameters due to side wall perforation could possibly occur at higher blade loading. This was checked by means of increasing the incidence angle.

The earlier described trends could again be observed. As expected all effects at $i = 6^{o}$ were stronger than at $i = 0^{o}$. This is also true for the scatter of the data points.

As illustrated in figure 9 both static pressure rise and deviation angle, of course, increase with increasing incidence angle. At $i = 6^{o}$ the data points for static pressure rise show somewhat lower values for the 12-holes perforation. In spite of the data scatter this seems to be a clear trend.

Looking to the total pressure loss coefficient $\bar{\omega}$ a much stronger Ω-influence appears as a consequence of higher blade loading (figure 10). As the total pressure loss is sensitive to the blade surface pressure distribution (in particular on the suction surface), an influence of the side wall configuration is expected. When suction is concentrated to the suction surface corner, higher losses are observed for a certain Ω-value.

Conclusions

The influence of side wall boundary layer suction on the results of cascade tests has been investigated.

Three different side wall configurations (distributed perforation) were used.

At low blade loading ($i = 0^{o}$) influence of the side wall configurations could be recognized on the blade surface pressure distribution but was not measurable for overall performance parameters.

At higher blade loading ($i = 6^{o}$) all effects were stronger. In this case a limited influence could be recognized even for the static pressure rise and for the total pressure loss coefficient.

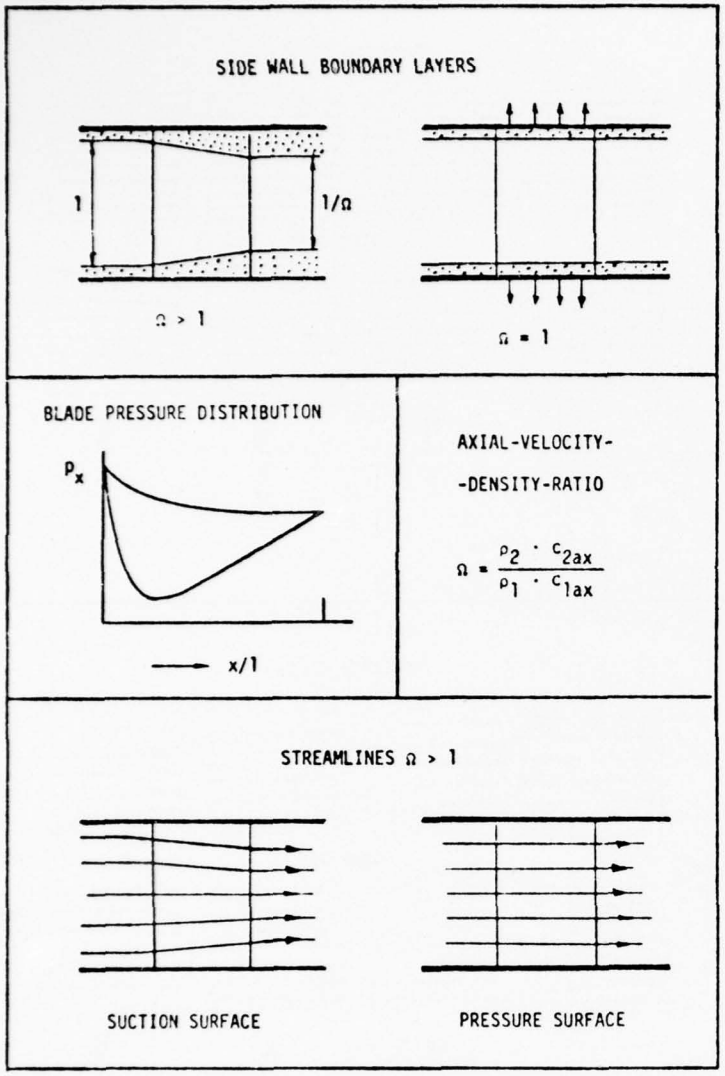


Fig 1. Illustrations of side wall boundary layer behaviour.

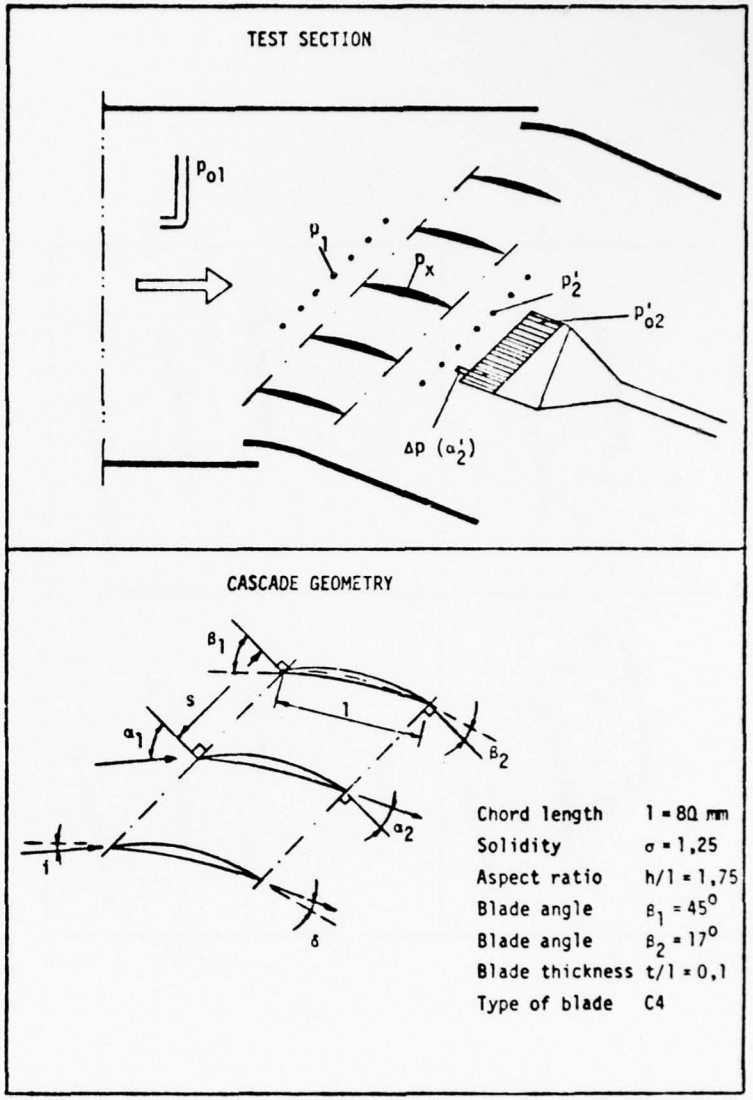


Fig 2. Cascade set up.

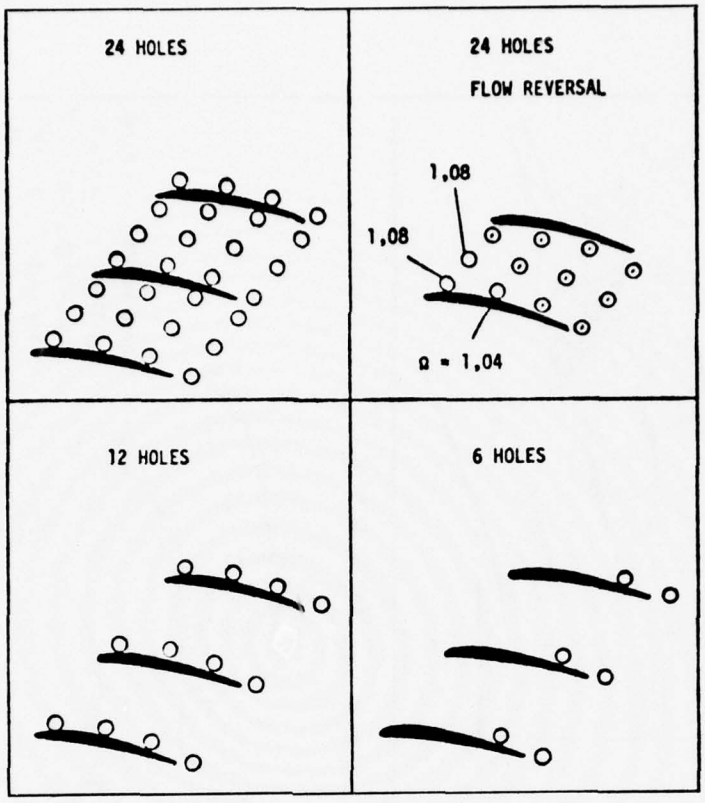


Fig 3. Side wall configurations.

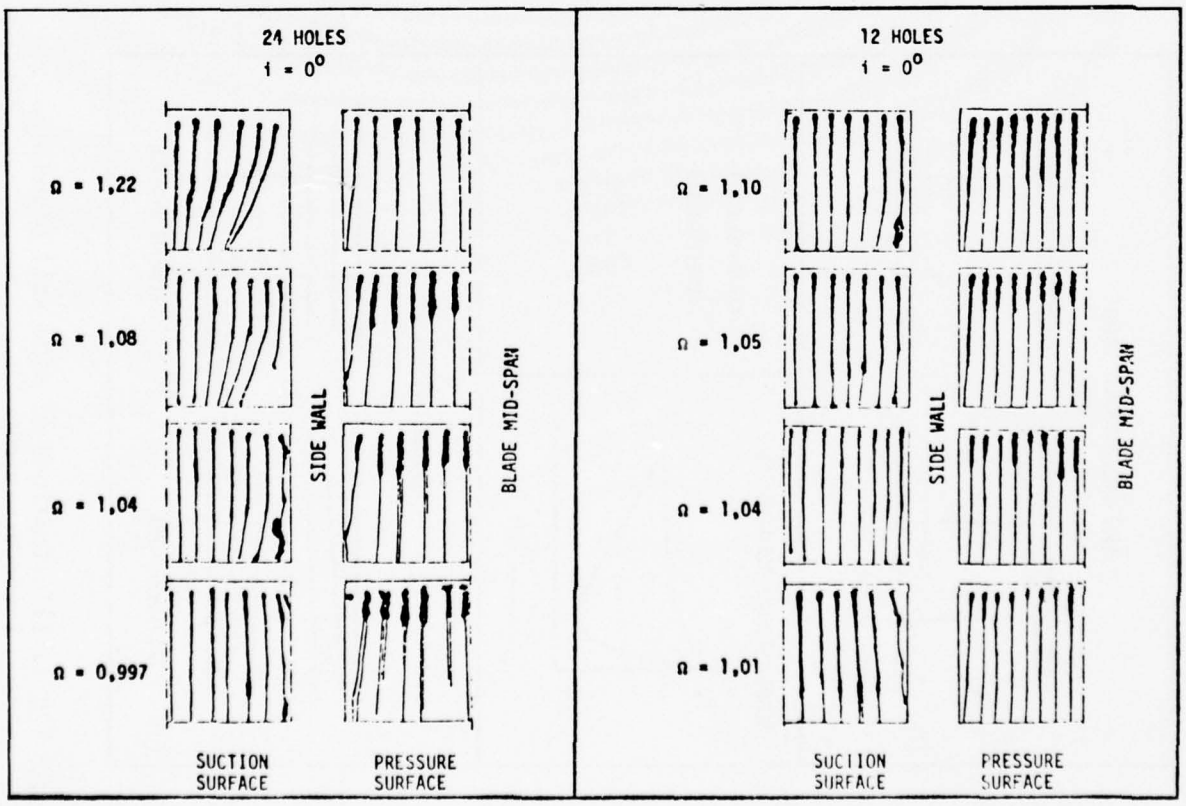


Fig 4. Flow on blade surfaces.

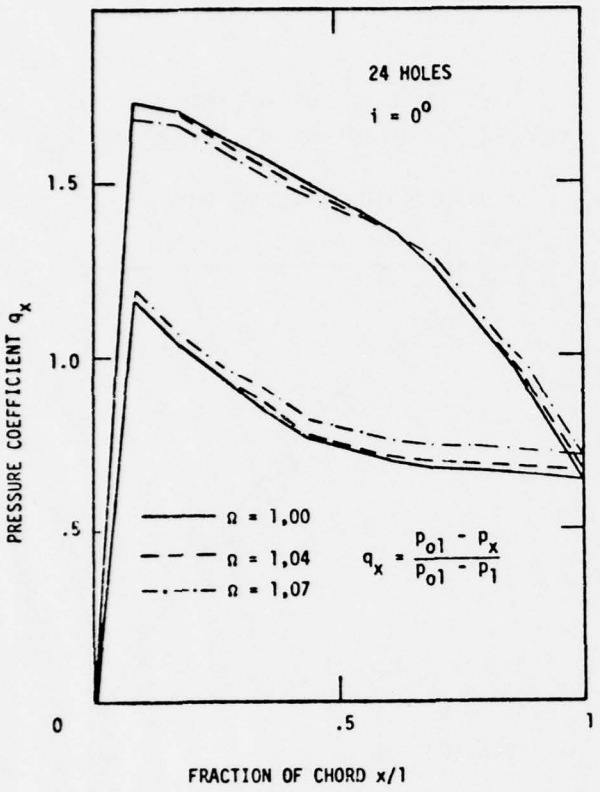


Fig 5. Blade pressure distribution for different values of axial-velocity-density ratio.

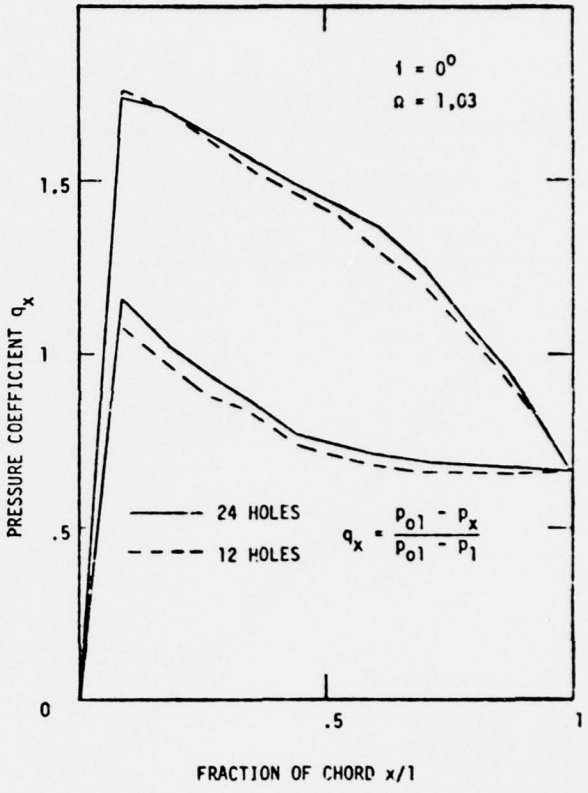


Fig 6. Comparison of blade pressure distribution for two different side wall configurations.

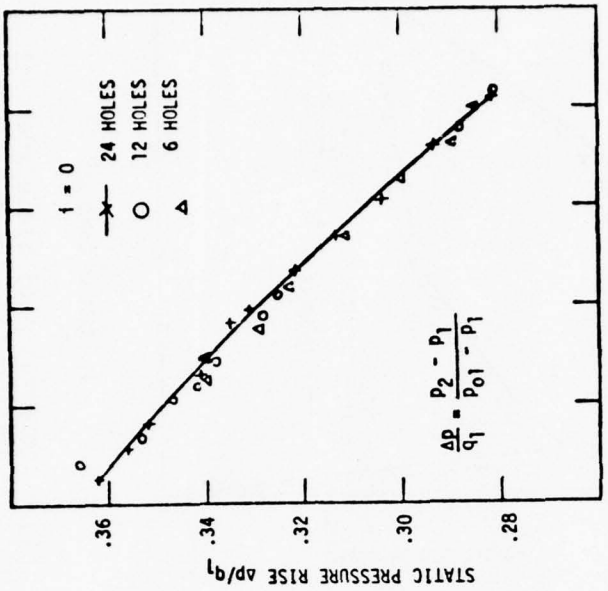


Fig 8. Static pressure rise versus axial-velocity-density ratio.

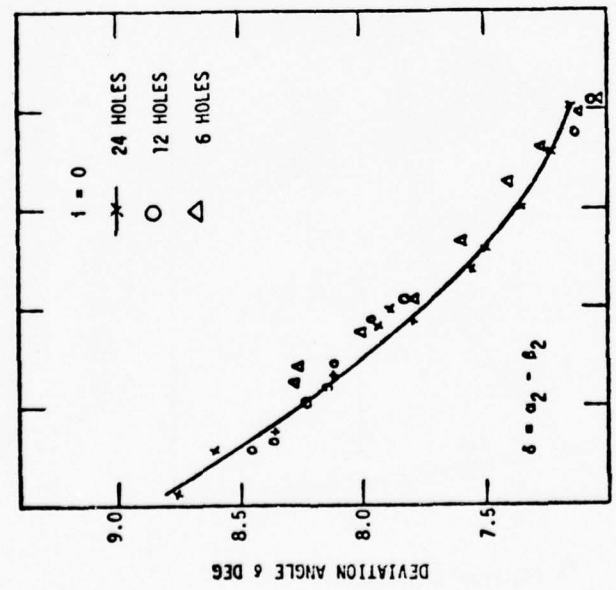


Fig 7. Deviation angle versus axial-velocity-density ratio.

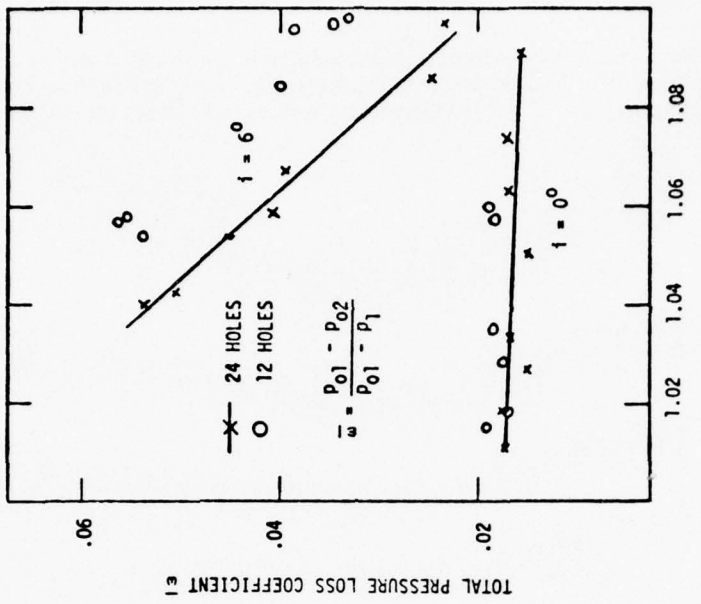


Fig 10. Total pressure loss coefficient versus axial-velocity-density ratio.

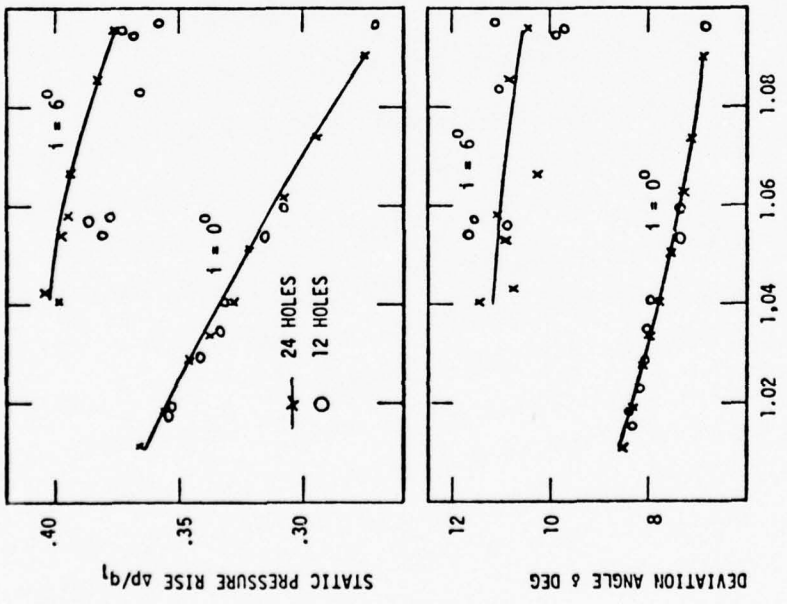


Fig 9. Deviation angle and static pressure rise at two different incidence angles.

DISCUSSION

G.Serovy

The trends that are shown by your data seem to be similar to those found by Mašek and Norbury at Liverpool University and reported in the Proc. IME* a few years ago. Have you compared the two sets of data?

Author's Reply

The influence of the axial-velocity-ratio and the distribution of porosity on the deviation angle is best illustrated in Figures 7 and 9. The change of δ with Ω is somewhat larger than the usually recommended formula $\delta = \delta_{\Omega=1} - 10(\Omega - 1)$. Comparisons of data from in particular Norbury and Mašek have not been carried out.

---

* Mašek, Z. and Norbury, J.F.: *Low Speed Performance of Compressor Cascade Designed for Prescribed Velocity Distribution and Tested with Variable Axial Velocity Ratio.* IME Conf. Publ. 3 (*Heat and Fluid Flow in Steam and Gas Turbine Plant*), 1973.

THREE-DIMENSIONAL FLOW IN HIGHLY LOADED ANNULAR CASCADES WITH ZERO SECONDARY VORTICITY

Hans-Heiner Fruehauf
Institut für Raumfahrtantriebe
Universität Stuttgart
Pfaffenwaldring 31
D-7000 Stuttgart 80

SUMMARY

Significant three-dimensional effects can occur in inviscid high Mach number irrotational stator flows and absolute rotor flows. The magnitude of these effects is determined quantitatively. Limitations of simplified flow models in predicting these flows are discussed.

1. INTRODUCTION

High Mach number flows in annular cascades are usually flows with a large amount of rotation and differing stagnation properties. When stagnation pressure gradients exist, secondary flows with a non-vanishing streamwise vorticity can be defined [1]. These secondary flows are usually associated with viscous flows where the streamwise vorticity is generated primarily in the annular wall boundary layers. Since stagnation pressure gradients usually exist also in inviscid flows through annular cascades, secondary flows can occur in these flows too [2]. Secondary flow effects appear to have been the most easily identified of the three-dimensional phenomena that have been observed in blade row flows. Significant three-dimensional effects other than secondary effects can occur, however, even in high Mach number irrotational stator flows and absolute rotor flows. Vavra [3] derived qualitatively, that these flows are non-axisymmetric and have twisted stream surfaces. The author confirmed quantitatively the three-dimensional nature of supersonic irrotational stator flows and absolute rotor flows by non-linear fully three-dimensional numerical calculations. He determined the influence of geometrical and gasdynamical parameters on three-dimensional effects in supersonic flows through axial blade rows with radial blades. In this paper the essential results are summarized and compared to the latest results obtained for irrotational absolute flows in supersonic rotors with non-radial blades. The basic intention is to demonstrate the magnitude of the three-dimensional effects in high Mach number turbomachinery flows. Details of the flow model and the flow field structure are not discussed within this short contribution.

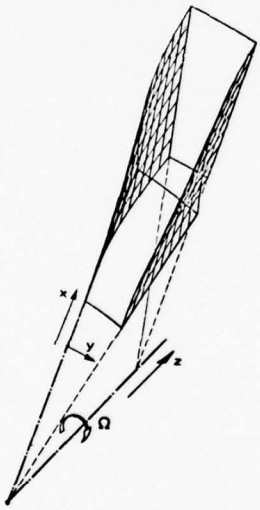


Fig.1: Rotor with radial blades

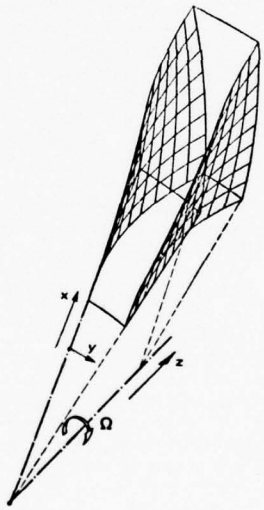


Fig. 2: Rotor with non-radial blades

2. NUMERICAL COMPUTATION OF ANNULAR CASCADE FLOW

To ensure a clear understanding of the three-dimensional effects, supersonic flows through annular cascades with simple geometries and uniform inflows are investigated. More complex flows through supersonic impulse rotors are discussed in [4].

2.1 ASSUMPTIONS

The steady irrotational absolute annular cascade flows of a thermically and calorically ideal gas are homentropic and homoenergetic. The heat conductivity of the flow medium is neglected. The oncoming supersonic absolute flow is meridional, uniform and irrotational. Strictly speaking only flow fields without shocks can be computed due to the homentropic flow assumptions. Recently performed 3-D computations exemplified however, that oblique shocks of moderate strength can be predicted with sufficient accuracy even for high Mach number cascade flows using the homentropic shock approximation. The rotating and stationary

annular cascades with cylindrical hub and casing consist of infinitely thin twisted blades. The non-disappearing principal curvature of the blades dimishes towards the leading and trailing edges. In the entrance region of rotors and stators the blades are identical with the flow surfaces of the undisturbed oncoming (hypothetical) relative flow and absolute flow, respectively. The selected aspect ratio of the blades is typical for supersonic axial annular cascades. Figs. 1 and 2 show a flow channel of a supersonic rotor with radial and non-radial blades respectively.

2.2 METHOD OF SOLUTION

Fully three-dimensional and simplified two-dimensional flow models have been developed for supersonic annular cascade flows. The basic equations of the spatial supersonic blade row flows are integrated with the help of a method of characteristics in three independent spatial variables [5]. The fundamental equations are transformed to body-orientated curvilinear coordinates and subsequently reduced to a characteristic form. In the entrance plane of a blade row the values for the flow quantities have to be specified. Additionally boundary conditions have to be introduced along the channel walls. Difference equations are derived from the characteristic differential equations and then integrated in the streamwise direction by employing a characteristic network of the inverse type. Before the three-dimensional numerical method was applied to blade row flows, the accuracy of its solutions was tested very carefully against analytical solutions for 2-D potential vortex flow, 2-D RINGLEB flow and 3-D source flow. These studies clearly reveal, that sufficient accuracy can be obtained for supersonic flows in 3-D channels of arbitrary geometry using nearly orthogonal body-orientated coordinates. Using the same method of solution, methods of characteristics in two independent spatial variables for the axisymmetric flow (2-D-AS model) and the blade-to-blade flow on cylindrical surfaces of revolution (2-D model) have been established.

3. APPLICABILITY OF SIMPLIFIED FLOW MODELS

The applicability of simplified flow models for the prediction of three-dimensional supersonic flows through blade rows can be judged on the magnitude of 3-D corrections to solutions given by these approximative flow models.

3.1 3-D CORRECTIONS FOR RADIAL BLADES

These corrections are determined quantitatively in [4], [6], [7] for rotors and stators with radial blades and cylindrical annular walls as functions of blade number, hub ratio, aspect ratio, blade turning angle, inlet Mach number and angular velocity. The calculated dependence of the 3-D corrections on these parameters can be explained qualitatively for irrotational stator flows and absolute rotor flows in annular cascades of simple geometry. The magnitude of the 3-D corrections to the solutions given by the blade-to-blade flow model on cylindrical surfaces of revolution is generally great, indicating heavily twisted stream surfaces even in supersonic absolute potential flows. It is exemplified on the other hand that the magnitude of the 3-D corrections to the solutions given by the axisymmetric flow model is small in comarison with the above mentioned one. This is due to the "integral nature" of the axisymmetric flow model as is demonstrated theoretically and quantitatively in [6].

Typical size of the magnitude of 3-D effects in the rotor with radial blades, fig. 1, are given in Section 3.2 together with the corresponding size of 3-D effects in the rotor with non-radial blades, fig. 2.

3.2 3-D CORRECTIONS FOR NON-RADIAL BLADES

So far the 3-D corrections have been summarized for annular cascades consisting of radial blades with a spanwise non-uniform circulation distribution. The objection might arise, that the great 3-D corrections which were found are necessarily associated with the non-uniform spanwise circulation distribution. The scalar equations of motion (specialized to the condition of zero absolute vorticity) show indeed that spanwise velocities are induced when radial gradients of the circulation exist in the flow. Below, calculations will be discussed, which were performed in order to find out, whether the 3-D corrections can be reduced by an appropriate selection of the spanwise circulation. The flow in a rotor with a non-radial blading of approximately free-vortex-type, shown in fig. 2, is investigated. The non-radial blades are derived from the radial blades shown in fig. 1, in a simple mathematical manner. So they are not optimal as regards their aerodynamical and structural performance. Both the radial blades and the non-radial blades possess identical leading edges and tip sections. The free-vortex rotor has 40 blades. This cascade rotates with an angular velocity $\Omega = 1$ in a cylindrical annular space with a hub ratio $\nu = 0.6$. The geometrical deflection of the infinitely thin blades is $\Delta\beta = 20$ deg at the casing. The axial width of the blade row is $z_1 = 0.5$. The relative Mach number of the oncoming flow at the tip is $M = 2$. The identical data are valid for the flow through the rotor with radial blades, fig. 1. Fig. 3 shows in the meridional plane the contours of constant absolute angular momentum, both for the rotor with non-radial blades (solid lines) and the rotor with radial blades (dashed lines), calculated with the axisymmetric flow model. The non-radial blading generates a flow with an approximately spanwise uniform distribution of the angular momentum.

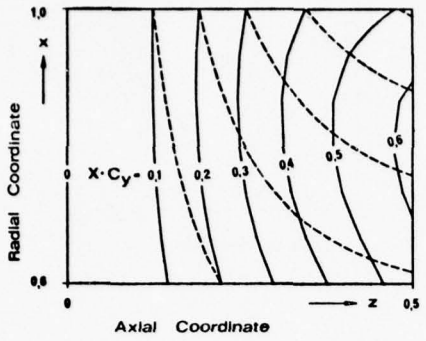


Fig. 3: Angular momentum contours
— Nonradial blade
-- Radial blade

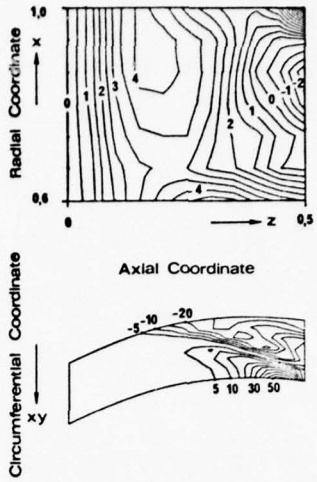


Fig. 4: 3-D corrections to simplified flow models

In the upper part of fig. 4 contours of constant 3-D corrections to the axisymmetric solution for the static pressure $[\langle p_{3D}\rangle - p_{2D\text{-}AS}] \cdot 10^2$ are plotted in the meridional plane. These corrections are calculated with circumferentially averaged values $\langle p_{3D}\rangle$ of the three-dimensional pressure distribution, see [6]. Contours of constant 3-D corrections to a blade-to-blade solution for the static pressure $[p_{3D} - p_{2D}] \cdot 10^2$ on a cylindrical surface of revolution lying equidistant between hub and casing are plotted in the lower part of fig. 4. The numbers on the contours give immediately the magnitude of these corrections as a percentage of the entry static pressure. The greatest value $[\langle p_{3D}\rangle - p_{2D\text{-}AS}] \cdot 10^2$ is about 4% (4%) while the greatest value $[p_{3D} - p_{2D}] \cdot 10^2$ is about 50% (30%). The numbers in the brackets ( ) give the corresponding values of the 3-D corrections for the rotor with radial blades, fig. 1. Thus the 3-D correction $[p_{3D} - p_{2D}] \cdot 10^2$ could not be reduced, by selecting approximately a free-vortex blading. On the contrary, the $[p_{3D} - p_{2D}] \cdot 10^2$ corrections become significantly greater. The greatest value of the $[\langle p_{3D}\rangle - p_{2D\text{-}AS}] \cdot 10^2$ corrections, however, remained unchanged, neglecting the correction on trailing edge at the rotor tip, which is probably due to a shock. One reason for the increase of the 3-D corrections $[p_{3D} - p_{2D}] \cdot 10^2$ is, that the radial displacement of the meridional streamlines (calculated with the 2-D-AS model) is greater for the non-radial than for the radial blades. The displacement of the midspan meridional streamline at the rotor exit is about 3% (1,3%) of the blade height. More general axisymmetric calculations showed indeed, that the smallest radial shift of the meridional streamlines is not necessarily obtained for free-vortex bladings, as often assumed in the literature.

The 3-D corrections indicate, that circumferentially integrated (3-D) flow quantities are usually predicted sufficiently accurately, while the computation of local (3-D) flow quantities can be associated with significant errors using simplified flow models. This may lead for instance to significant errors in predicting the blade pressure distributions. Fig. 5 shows the 3-D static pressure distribution for the pressure and suction side of the non-radial blade. For the radial blade the corresponding 3-D and 2-D static pressure distributions are given in fig. 6. Note that the 3-D and 2-D isobars are qualitatively similar. Thus 3-D effects are not easily identified unless fully 3-D computations or measurements are performed.

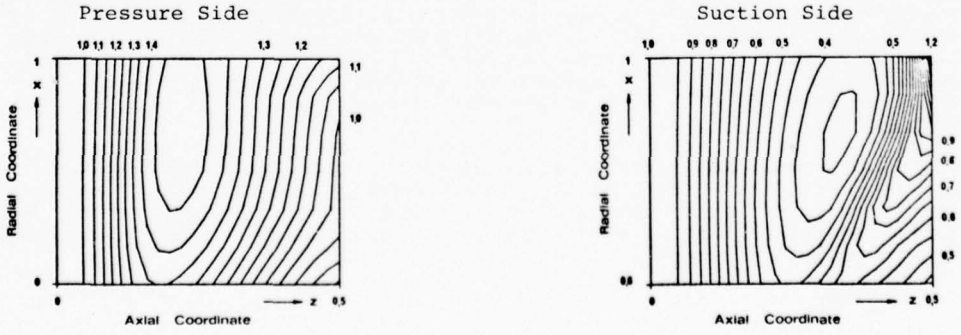


Fig. 5: 3-D Isobars along the non-radial blade surfaces

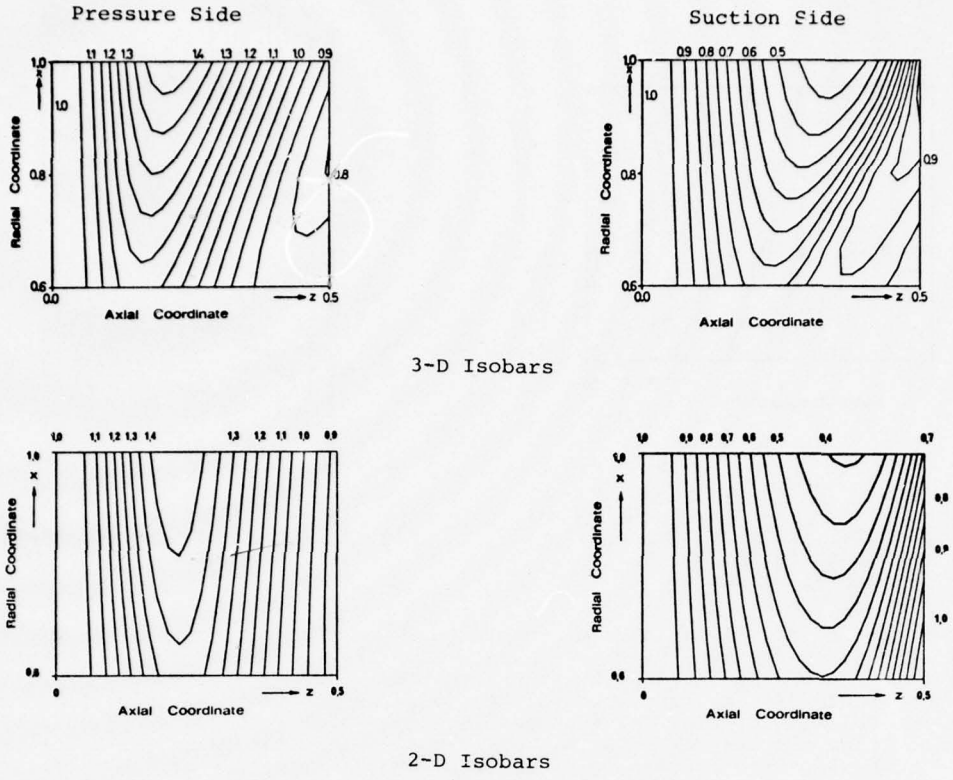


Fig. 6: 3-D and 2-D Isobars along the radial blade surfaces

4. 3-D FLOW PHENOMENA

In Section 3 differences between the 3-D solutions and the solutions of the simplified flow models have been investigated formally. It is quite evident, that the calculated 3-D corrections are a result of 3-D flow effects. These 3-D flow effects will be discussed below very shortly.

4.1 STREAM SURFACE TWIST

The flow through stationary or rotating annular cascades cannot be axisymmetric if the flow must exert a moment on the blades. It is for this reason, that an arbitrary flow through an annular cascade does not have stream surfaces, which are surfaces of revolution [3]. It is clearly evident and can be shown formally, that the twisting of the stream surfaces results in part from secondary flows. The 3-D corrections to the blade-to-blade solutions determined in Section 3 indicate, that a significant twist of stream surfaces can occur in high Mach number rotor and stator flows even in the absence of absolute secondary vorticity. In general a stream surface will be skewed upward along one surface of a blade and downward along the other surface. Spanwise flows are associated with the twisted stream surfaces. The downstream development of the spanwise velocities in the rear part of the free-vortex-rotor ($z \geq 0.3$) can be seen in fig. 7 where the projections of the 3-D relative velocity vectors in equidistant planes normal to the rotor axis are shown. The radial velocity components are generally positive in this part of the rotor. The change of the sign of the circumferential velocity component in the radial direction can be easily deduced from the rotor geometry shown in fig. 2. The value of the greatest radial velocity component refered to the local speed of sound is 12,2 % (10%) of the relative oncoming tip Mach number. The twist of the stream surface can be seen also from the change in sign of the 3-D correction $[p_{3D} - p_{2D}] \cdot 10^{-2}$ across the (non-plotted) zero 3-D correction line in the lower part of fig. 4.

Recently a similar significant stream surface twist was numerically predicted for the irrotational transonic flow through an isolated compressor rotor with a comparable hub ratio but an essentially greater aspect ratio [8]. The 3-D effects in transonic blade rows are expected to be greater than in supersonic blade rows, due to the strong coupling between different areas of the flow field.

4.2 OVERTURNING

In fig. 8 are plotted 3-D corrections $[\beta_{3D} - \beta_{2D}]$ to blade-to-blade solutions for the relative exit flow angle $\beta = \text{arctg}\,(w_y/w_z)$. Note that nearly in the whole exit plane the 3-D correction is negative, i.e., in the two-dimensional approximation the flow undergoes an overturning with respect to the spatial flow almost across the whole blade height. The value of the greatest 3-D correction $[\beta_{3D} - \beta_{2D}]$ is about -12^{o} (-6^{o}). Similarly a 3-D

correction [$\langle \beta_{3D} \rangle - \beta_{2D-AS}$] could be regarded as the correction to the axisymmetric relative outlet angle required to allow for 3-D flow effects within a blade passage of finite width.

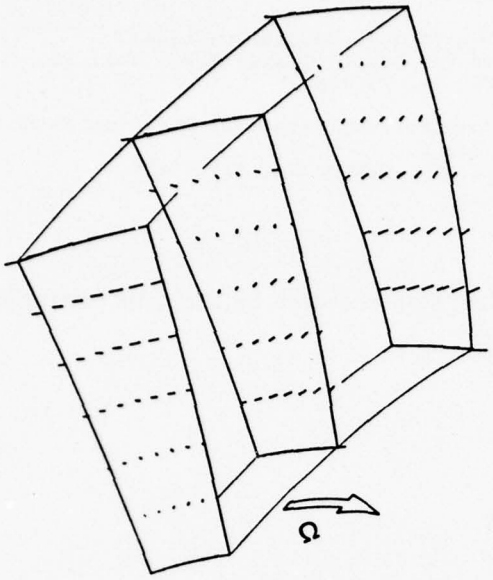


Fig. 7: Downstream development of spanwise flow



Fig. 8: 3-D correction to the exit flow angle

5. CONCLUSIONS

The magnitude of three-dimensional flow effects (stream surface twist, cross flows, overturning) was determined by fully three-dimensional computations for irrotational supersonic flows through axial annular cascades.

- The maximum size of three-dimensional corrections to solutions given by a blade-to-blade flow model on cylindrical surfaces of revolution is found to be generally great, typically for instance 30 % for the static pressure.
- Contrarily the maximum size of three-dimensional corrections to solutions given by the axisymmetric flow model is usually small, typically not exceeding 4% for the static pressure.
- A brief study on flows in rotating blade rows with different spanwise circulation distributions seems to indicate, that minimal three-dimensional flow effects are not necessarily obtained with free-vortex bladings.

Greater three-dimensional effects are expected in rotational high Mach number flows through rotating and stationary blade rows, especially in transonic cascade flows.

6. REFERENCES

[1] Lakshminarayana, B. Horlock, J.H.: Generalized Expressions For Secondary Vorticity Using Intrinsic Coordinates. J. Fluid Mech., Vol. 59(1), 1973, p. 97

[2] Squire, H.B., Winter, K.G.: The Secondary Flow In A Cascade In A Nonuniform Stream. J. Aero. Sci. Vol. 18, 1951, p. 271

[3] Vavra, M.H.: Aero-Thermodynamics And Flow In Turbomachines. Huntington, New York, R.E. Krieger Publishing Company, 1974.

[4] Fruehauf, H.H.: Mehrdimensionale Lösungen für Überschall-Strömungsfelder in Turbomaschinen. Köln, Deutsche Gesellschaft für Luft- und Raumfahrt, DGLR-Jahrbuch, 1976, p. 165-1-9.

[5] Fruehauf, H.H.: Ein Charakteristikenverfahren für die dreidimensionale stationäre Überschallströmung in rotierenden und feststehenden Ringgittern. Deutsche Luft- und Raumfahrt, Forschungsbericht DLR-FB 73-12, 1973.

[6] Fruehauf, H.H.: Applicability Of Axisymmetric Analysis In Predicting Supersonic Flow Through Annular Cascades.
Journal of Engineering for Power, Trans. ASME, Vol. 99, Series A, No. 1., 1977, pp. 115-120

[7] Fruehauf, H.H.: Spatial Supersonic Flow Through Annular Cascades.
Journal of Engineering for Power, Trans. ASME, Vol. 98, Series A, No. 2., 1976, pp. 274-280

[8] Thompkins, W.T., Jr.: An Experimental And Computational Study Of The Flow In A Transonic Compressor Rotor.
MIT Gas Turbine Laboratory, Report No. 129, 1976.

ACKNOWLEDGEMENTS

The author would like to acknowledge the support of this research by DEUTSCHE FORSCHUNGSGEMEINSCHAFT.

DISCUSSION

C.Bosman

I wonder if in your finite-difference 3D calculation you checked the relative circulation around the boundaries running up the blade and then across the shroud, down the blade and across the hub because we know precisely what this is and it gives a good check on the accuracy of these schemes which tend, in fact, not to be accurate. I wonder if you have done that check and, if you have, what the results are? Check the relative circulation, which is known in this case.

Author's Reply

For the supersonic flows through annular cascades we didn't check the relative circulation. We tested the accuracy of the 3-D method of characteristics very carefully before calculating annular cascade flows by comparing the solutions of this method to analytical 2-D and 3-D solutions, for instance to the plane potential vortex flow or to the 3-D source flow.

A.Spurr

I would like to ask you two quick questions. Firstly what method of calculation did you use to calculate the axisymmetric flow and secondly, on the blade to blade calculation did you take into account the influence of stream tube divergence?

Author's Reply

To answer the first question: the axisymmetric method of characteristics was developed a long time ago by myself (you can find it in the literature). It was modified for the calculations in this way, that its numerical scheme can be derived from the numerical scheme of the 3-D method of characteristics. For the second question: in the case of annular cascades discussed, with a cylindrical hub and a cylindrical casing, I compared the 3-D flow solution with 2-D blade-to-blade solutions on cylindrical flow surfaces. If you do axisymmetric calculations you will find small radial shifts of the meridional streamlines. In the case of the rotor with non-radial blades, the radial shift of the midspan meridional streamline at the rotor exit is about 3% of the blade heights. So looking at the great differences between 2-D blade-to-blade solutions and the 3-D solution which are essentially due to the twist of the actual blade-to-blade stream surfaces, the influence of the streamtube divergence on the errors seems to be comparatively small.

CORNER BOUNDARY LAYER AND SECONDARY FLOW WITHIN A STRAIGHT COMPRESSOR CASCADE

Jürgen H. Renken

DFVLR-Institut für Luftstrahlantriebe
Linder Höhe, 5 Köln 90, W.-Germany

SUMMARY

Measuremants at Mach numbers $M < 0.3$ and Reynolds numbers $Re > 3.0 \cdot 10^5$ in a straight compressor cascade with 48 degrees cambered double circular arc profiles and contractable sidewalls are presented and compared with two- and three-dimensional calculations. From the differences between measurement and calculation and from the evaluation of numerous corner layer publications some conclusions have been drawn towards secondary flow effects.

LIST OF SYMBOLS

β_1	inlet flow angle, Fig. 2
β_2	outlet flow angle, Fig. 2
β_s	stagger angle, Fig. 2
c	blade chord, Fig. 2
d	max. blade thickness, Fig. 2
h_1	channel width upstream of the cascade, Fig. 2
h_2	channel width downstream of the cascade, Fig. 2
Ω_G	$= h_1/h_2$ channel contraction ratio
p	static pressure
p_1	static pressure on sidewall upstream of the cascade
p_{t1}	total pressure of inlet flow
$\vec{r}$	radiusvector of the curvature of a particle path
ρ	density
S'	$= (p_{t1} - p)/(p_{t1} - p_1)$ pressure coefficient
t	cascade pitch, Fig. 2
θ	blade camber angle, Fig. 2
$\vec{v}$	resultant velocity vector of a fluid particle
x,y,z	cartesian coordinates, Fig. 1c

INTRODUCTION

The original aim of the investigations from which a part is presented in this paper was to provide experimental data of straight compressor cascade flow appropriate for comparison with three-dimensional incompressible potential flow calculations [1]. For this reason emphasis has been paid to produce a cascade flow at low Mach numbers ($M < 0.3$), high Reynolds numbers ($Re < 3.0 \cdot 10^5$) and thin, turbulent wall boundary layers with a correspondingly small displacement thickness.

In spite of all these efforts a pressure gradient in the spanwise direction occured on the suction side of blade surfaces even in the case of parallel cascade sidewalls. Since the experimental pressure distribution in the cascade mean section agreed very well with calculations, a more detailed investigation of the flow along the corners formed by sidewall and blade surfaces seemed to be necessary.

TEST SETUP

The measurements have been performed in the transonic windtunnel at the DFVLR in Porz-Wahn. Fig. 1 shows different views of the test section; the high turning DCA-profiles are mounted between plexiglas sidewalls. In order to produce three-dimensional flow within the blade passage, additional internal flaps could be turned into the passage as shown in the photo of Fig. 1b and in the sketch of Fig. 1c.

The geometry of the cascade is shown in Fig. 2. According to scale, the test section and adjacent parts of the windtunnel are shown in Fig. 3. Further details of the complete test facility and test procedure are discribed in [2].

Concerning the presented test-results, attention should be paid to the pressuretap distribution on sidewall, pressure side and suction side of two adjacent blades in Fig. 3 and the appertaining pressure distribution upon these surfaces.

TEST RESULTS

Two characteristic test examples are presented in the following in order to enlighten the phenomena of non-zero pressure gradient in spanwise direction on the suction side in the case of parallel sidewalls.

A cartesian coordinate system as shown in Fig. 1c is defined with y-axis in the spanwise direction, z-axis in the circumferential direction and x-axis in the axial direction. The x, z-plane is the plane of symmetry of the cascade.

Using the measured pressures, a pressure coefficient

$$S' = \frac{p_{t1} - p}{p_{t1} - p_1}$$

is defined with

p_{t1} total pressure upstream of the cascade

p_1 static pressure upstream of the cascade

p static pressure on the surfaces of sidewall and blades within the measured passage

The distribution of S' is plotted in Fig. 4a ($\beta_1 = 38^0$, $\beta_2 = 2^0$, $\Omega_G = 1.0$) and Fig. 5a ($\beta_1 = 38^0$, $\beta_2 = 1^0$, $\Omega_G = 1.2$) for the symmetrical half of one passage. The visual point corresponds to the one shown in Fig. 1c. The surfaces of pressure side, sidewall and suction side are plotted separately in the x,y,z-coordinate system. As demonstrated by the arrows, the values of S' are plotted as equivalent lengths at the location of a pressure tap on

these surfaces in the negative y-direction (sidewall) and z-direction (pressure and suction side) respectively. The numbers 1 to 14 denote pressure tap lines in the streamwise direction; number 1 indicates the midspan location on the pressure side, number 14 on the suction side. In Fig. 4b and Fig. 5b the values of S' are plotted in conventional manner against the axial direction x, following the same numbering. In Fig. 6 and Fig. 7 the two examples are compared with two and three-dimensional calculations [1].

DISCUSSION OF RESULTS

Because of the low velocities in the experiments the cascade performance i.e. the pressure rise is very low. With that, the growth of boundary layers within the cascade is reduced to a minimum. A flow visualization using smoke from heated oil did not indicate detached flow within the passage with exception of the vicinity of the blades trailing edges. The traces of condensed smoke indicated only the well known transport of low energetic boundary layer material on the sidewall surface from the pressure side to the suction side [3], [4], [5]. In the boundary layer on the surfaces of suction side and pressure side the oil traces did not indicate significant deviation from the undistorted flow direction.

Thus the conditions for the development of cascade flow having the character of potential flow throughout the whole passage should be very good.

In spite of these facts, a pressure rise in the spanwise direction from the midspan towards the sidewall occured on the blade suction side even in the case of parallel side walls; in Fig. 4b the S' -distribution on the suction surface near the sidewall (dashed line 10) is different from the one at midspan location (line 14).

A comparison of experimental data with potential flow calculation shows a good agreement at midspan location, Fig. 6 (Θ_G = 1.0, parallel sidewalls, 2-dim.) and Fig. 7 (Θ_G = 1.2, contracted sidewalls, 3-dim.), whereas there is a disagreement on the suction side near the sidewall as demonstrated by the shaded areas. Attention should be paid to the fact, that this difference between potential flow and real flow is very similar at two- as well as at three-dimensional conditions.
Obviously these differences cannot be caused by extensively growing corner layers, because these would form a convergent channel in the streamwise direction due to the displacement thicknesses, and with that accelerate the flow in connection with a drop in static pressure outside the boundary layer. In addition, this effect should be similar on suction side and pressure side. Instead of this, a rise in pressure towards the sidewall occured only on the suction side.

Fig. 8a shows a plane x=const within the passage at two dimensional conditions. The dotted intersection line along pressure side, sidewall and suction side is plotted as a straight line in Fig. 8b. The corresponding static pressures from the experiment and from potential flow calculation [1] are plotted against this line in order to demonstrate the problem under consideration. In the following, an attempt is done towards an explanation of this phenomenon.

The turbulent boundary layer in a streamwise corner has been investigated experimentally by MOJOLA and YOUNG [6]. The distribution of the static pressure and the velocity within the corner is shown in Fig. 9a and Fig. 9b. The field of isobars and iso-velocity lines indicates a pressure rise and a drop in velocity towards the corner.

Within a straight duct having a rectangular cross section with aspect ratio 1:1, Fig. 10a, and 2:1, Fig. 10b, secondary flow profiles have been measured by GESSNER and JONES, [7]. Secondary streamlines at aspect ratio 1:1 are plotted in Fig. 10c.

In addition to the references [6] and [7] the references [8] to [20] have been evaluated in order to enlighten the problem of corner layers.

From the investigations concerning corner layers and from cascade measurements associated with the potential flow calculation, there result the following statements:

1. The behaviour of a boundary layer within the corner of a straight duct having a rectangular cross section is significantly three-dimensional. Within the boundary layer there exist large pressure and velocity gradients perpendicular to the direction of the undistorted flow, i.e. there exists a secondary flow that should not be neglected. Secondary flow is defined here to represent all deviations from potential flow.

2. Concerning the cascade flow, a secondary flow pattern can thus be deduced from the qualitative superposition of the secondary flow in a straight duct, Fig. 11a, and the flow due to the pressure gradient in a cascade from pressure to suction side. The resulting cascade secondary flow pattern is shown in Fig. 11b and 11c. This pattern is well known and has been stated by many authors, for instance [3],[5]. According to this pattern, low energetic boundary layer material is transported towards the suction side corner along the sidewall (arrow I) as well as from flow regions close to the corner (arrow II). Passing the corner, this material enters the suction side surface undergoing a very rapid change in flow direction. This causes a local pressure rise according to the following equation:

$$\frac{\partial p}{\partial \vec{r}} = - \rho \cdot \frac{\vec{v}^2}{\vec{r}}$$

with

$p(\vec{r})$	static pressure
$\vec{r}$	radius of curvature of particle path
ρ	density
$\vec{v}(\vec{r})$	velocity of particle

As known from experiments [3], [4], [5] the flow particles are leaving the pressure side corner in tangential direction, Fig. 11c and no pressure rise is to be expected here.

3. In an additional experiment using a thin wall (0.3 mm) in the cascade mean section as shown in Fig.12, a very similar pressure rise could also be produced on the suction side at midspan.

   If the distance between this wall and mean section 14, Fig. 4a, was equal to the distance of section 10, Fig. 4a, from the sidewall, the distribution of S' in the mean section 14 became nearly equal to the distribution of S' in section 10 (dashed line, Fig. 4a). Attention should be paid to the fact, that the thin wall did not influence the S'-distribution on the pressure side.

4. Since the differences between measurements and potential flow calculation at two dimensional conditions as well as at 3-dim. conditions are limited essentially to the suction side corner region (shading in Fig. 6 and Fig. 7), the overal boundary layers and corner layers must be very thin. This has also been confirmed by some additional pitot measurements. Thus, the pressure rise towards the sidewall must be completed within the very thin corner layers.

From statements 1 to 4 follows that the corner layer has a completely different behaviour than for instance the boundary layer in the cascade mean section, so that the assumption of constant static pressure normal to the boundary layer obviously is not allowed within the corner layer. Thus, near the corner the secondary flow itself produces a flow field heaving significant static pressure gradients in the direct vicinity of sidewall and

suction surface.

From this fact, there result severe limitations to calculation methods using for instance an iterative combination of potential flow and separate first order boundary layer calculations.

Furthermore the considerable contribution of the corner layer to the cascade secondary flow is due to the sharp corners. Thus a very simple rounding of this corners should reduce also the secondary flow.

SUMMARY AND CONCLUSIONS

Two examples of straight compressor cascade measurements [2] at two and three-dimensional conditions have been presented. Emphasis has been paid on obtaining a cascade flow at low Mach numbers ($M < 0.3$) and high Reynolds numbers ($Re > 3.0 \cdot 10^5$) having thin, turbulent boundary layers and otherwise the character of potential flow.

Comparing the surface pressure distribution of measurements with the results of 2-dim respectively 3-dim. potential flow calculation, [1] deviations have been stated in the corner of sidewall and suction side, whereas good agreement could be obtained throughout the entire passage.

Concerning the pressure differences, an attempt has been done towards an explanation. From the evaluation of numerous corner layer investigations [6] to [20], the interpretation of additional test results using a thin wall in the cascade midspan, and a potential flow calculation, some basic facts about the development of secondary flow effects could be found.

Three essential results are:

1. Within the corner layer between sidewall and suction side and adjacent regions in the direct vicinity of the surfaces, the secondary flow itself produces a flow field having significant gradients in static pressure.
2. Calculation methods using for instance an iterative combination of potential flow and separate first order boundary layer calculations should not be applied to flow fields within the entire passage.
3. Furthermore the considerable contribution of the corner layer to the cascade secondary flow is due to the sharp corners. Thus a very simple rounding of this corners should reduce also the secondary flow.

REFERENCES

[1] RENKEN,J.H., Calculation of Three-Dimensional Cascade Flow by Means of a First Order Panel Method.
DLR-FB 76-64, Institut für Luftstrahlantriebe,DFVLR Köln

[2] RENKEN,J.H. Messungen der dreidimensionalen Unterschallströmung in einem geraden Verdichtergitter mit kontrahierbaren Seitenwänden.
Interner Bericht, IB 352 77/2, Institut für Luftstrahlantriebe, DFVLR Köln.

[3] PROMPER,H., Verbesserung des Wirkungsgrades axialer Turbinenstufen durch Reduzierung der Sekundärverluste.
Fakultät für Maschinenwesen der RWTH Aachen, Dissertation 1975.

[4] GRIEPENTROG,H., Prédiction des performance des grilles d'ambes transsoniques à haute défelction et faible allongement.
Institut von Karman de dynamique des fluides, VKI TN 59 Rhode-Saint-Genese, Belgique 1969.

[5] LANGSTON,L.S., NICE,M.L., HOOPER,R.M., Three-Dimensional Flow Within a Turbine Cascade Passage.
ASME Paper No. 76-GT-50, December 11, 1975

[6] MOJOLA,O.O., YOUNG,A.D., An Experimental Investigation of the Turbulent Boundary Layer Along a Streamwise Corner.
AGARD Conference Proceedings No. 93 on Turbulent Shear Flows, London 10 - 13 Sept. 1971.

[7] GESSNER,F.B., JONES,J.B., On some Aspects of Fully-Developed Turbulent Flow in Rectangular Channels.
J.Fluid Mech.(1965) Vol.23, part 4, pp.689 - 713.

[8] LIGGETT,J.A., CHAO-LIN CHIU, LING S. MIAO Secondary Currents in a Corner.
Journal of the Hydraulics Division, Proc. ASCE, Vol.91, No. HY6, 1965.

[9] LEUTHEUSSER,H.J., Turbulent Flow in a Rectangular Duct.
Journal of the Hydraulics Division Proc. ASCE, Vol. 89, No.HY 3, 1963.

[10] EICHELBRENNER,E.A., On the Role of Secondary Flow in Turbulent Layers in Corners (and Salients).
Journal de Mécanique Vol. 10, March 71, pp. 91 - 112

[11] ZAMIR,M., YOUNG,A.D., Experimental Investigations of the Boundary Layer in a Streamwise Corner.
The Aeronautical Quarterly, Nov. 1970 pp. 313 - 339.

[12] GESSNER,F.B., EMERY,A.F., A Reynolds Stress Model for Turbulent Corner Flows.
- Part I : Development of the Model.
ASME Paper No. 76 - FE - C, June 1976 pp. 261 - 268.

[13] GESSNER,F.B., PO,J.K., A Reynolds Stress Model for Turbulent Corner Flows.
- Part II : Comparison Between Theory and Experiment.
ASME Paper No. 76 - FE - D, June 1976, pp. 269 - 277.

[14] ZAMIR,M., Boundary Layer Theory and the Flow in a Streamwise Corner.
The Aeronautical Journal of the Royal Aeronautical Society, Vol.74, April 1970, pp. 330 - 332.

[15] GHIA,K.N., Incompressible Streamwise Flow Along an Unbounded Corner.
AIAA-Journal, July 1975, pp. 902 - 907.

[16] GHIA,K.N., Corner Layer Flow; Optimisation of Numerical Method of Solution.
Computers and Fluids, Vol.2, Pergamonn Press 1924, pp. 17 - 24.

[17] RUBIN,S.G., Viscous Flow Along a Corner: Numerical Solution of the Corner Layer Equations.
Quarterly of Applied Mathematics. Vol.XXIX, No.2, July 1971, pp. 169 - 186.

[18] BRAGG,G.M., The Turbulent Boundary Layer in a Corner.
J. Fluid Mech. (1969), Vol.36, pp. 485 - 503.

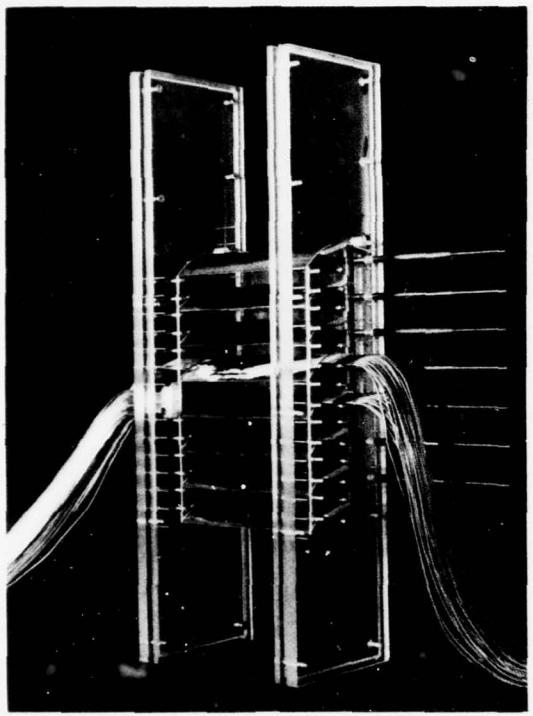
[19] OMAN,R.A., The Three-Dimensional Laminar Boundary Layer along a Corner.
Massachusetts Institute of Technology, Dissertation 1959.

[20] HOAGLAND,L.C., Fully Developed Turbulent Flow in Straight Rectangular Ducts - Secondary Flow, Its Cause and Effect on the Primary Flow.
Massachusetts Institute of Technology,Dissertation 1960.

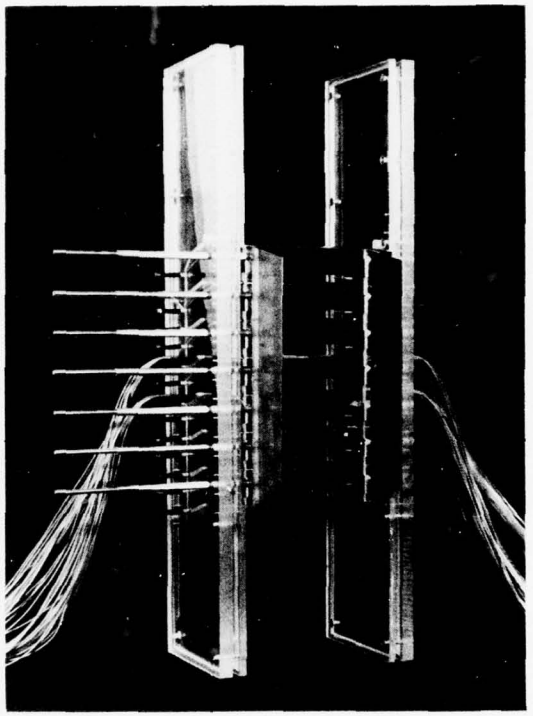
DISCUSSION

B.Barry

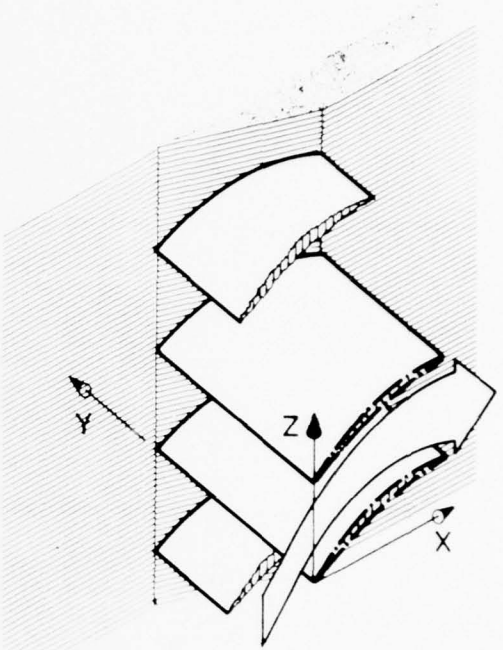
I would like to comment that Dr. Waldhead at Rolls-Royce tested a cascade some years ago with a fillet placed in the suction corner, and what happened was that he got a large concentrated core of secondary vorticity in the main stream. It seemed rather odd that all that vorticity was concentrated in the main stream rather than in the wake.



(a) View in the streamwise direction

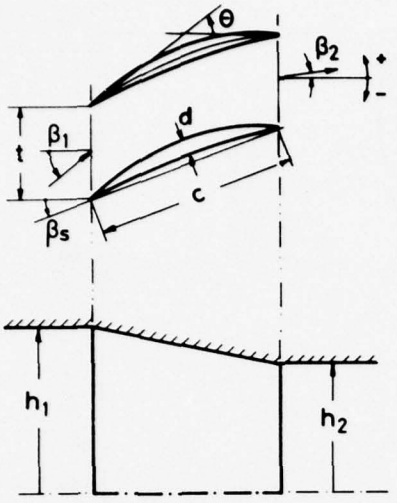


(b) View against the streamwise direction



(c) View in the streamwise direction (as a.)
(symmetrical half of passage)

Fig.1 Several views of the test section and definition of coordinate system



Double circular arc profil DCA-R *

camber	:	θ	= 48°
stagger	:	β_s	= 16°
chord lenght	:	c	= 90 mm
pitch/chord	:	t/c	= 0,45
blade hight/chord	:	h_1/c	= 1,867
max. thickness/chord	:	d/c	= 0,085
leading edge and trailing edge radius	:	6 % of	t/c
inlet flow angle for incidence i = 0°	:	β_1	= 40°
outlet flow angle for deviation e = 0°	:	β_2	= -8°
ratio of channel width	:	Ω_G	= h_1/h_2

Fig.2 Cascade Geometry

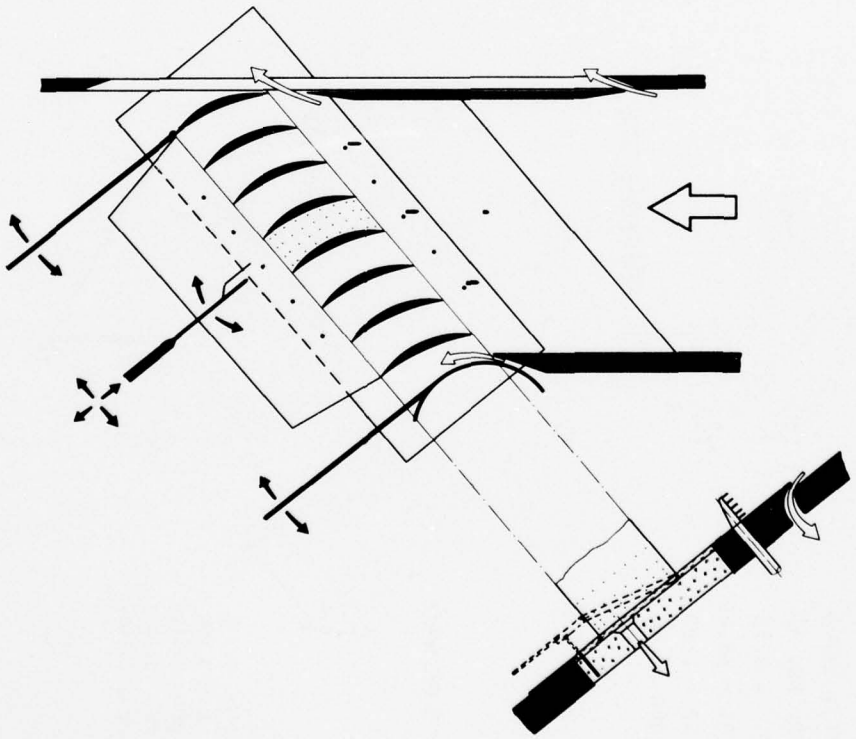
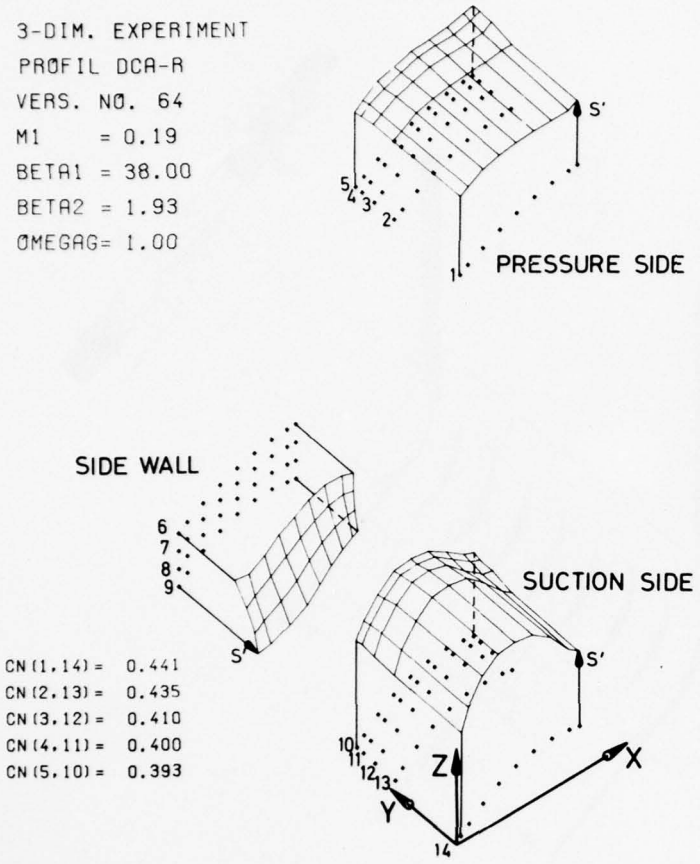


Fig.3 Cross sectional and plan view of cascade test section



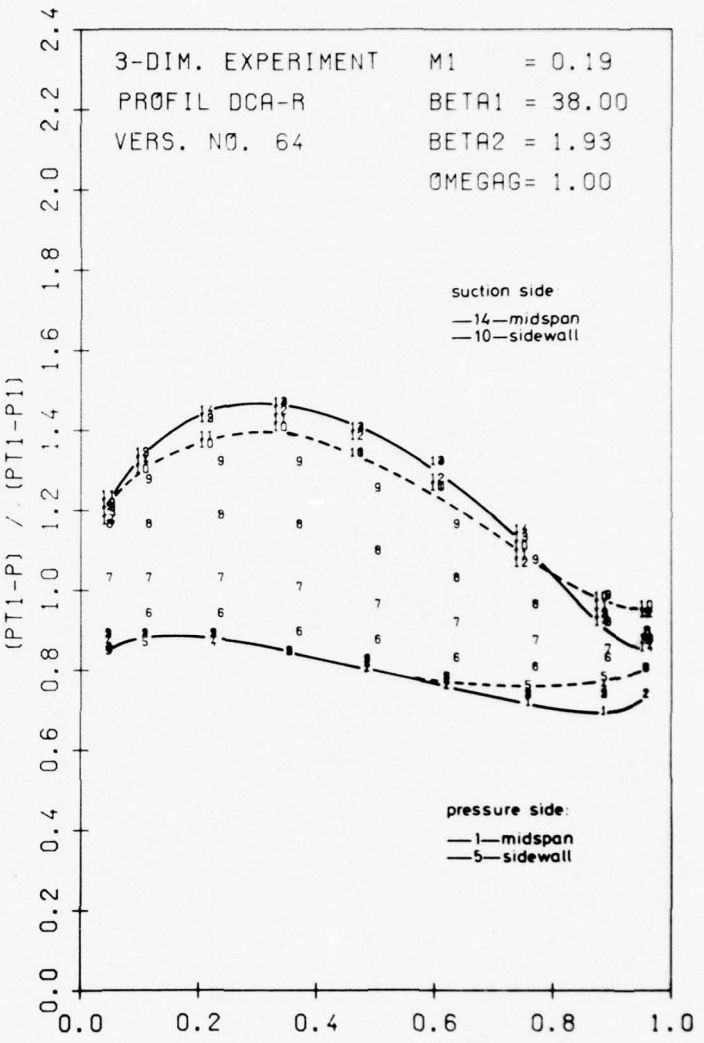


Fig.4a,b Distribution of pressure-coefficient S' on the surfaces of the symmetrical half of one passage

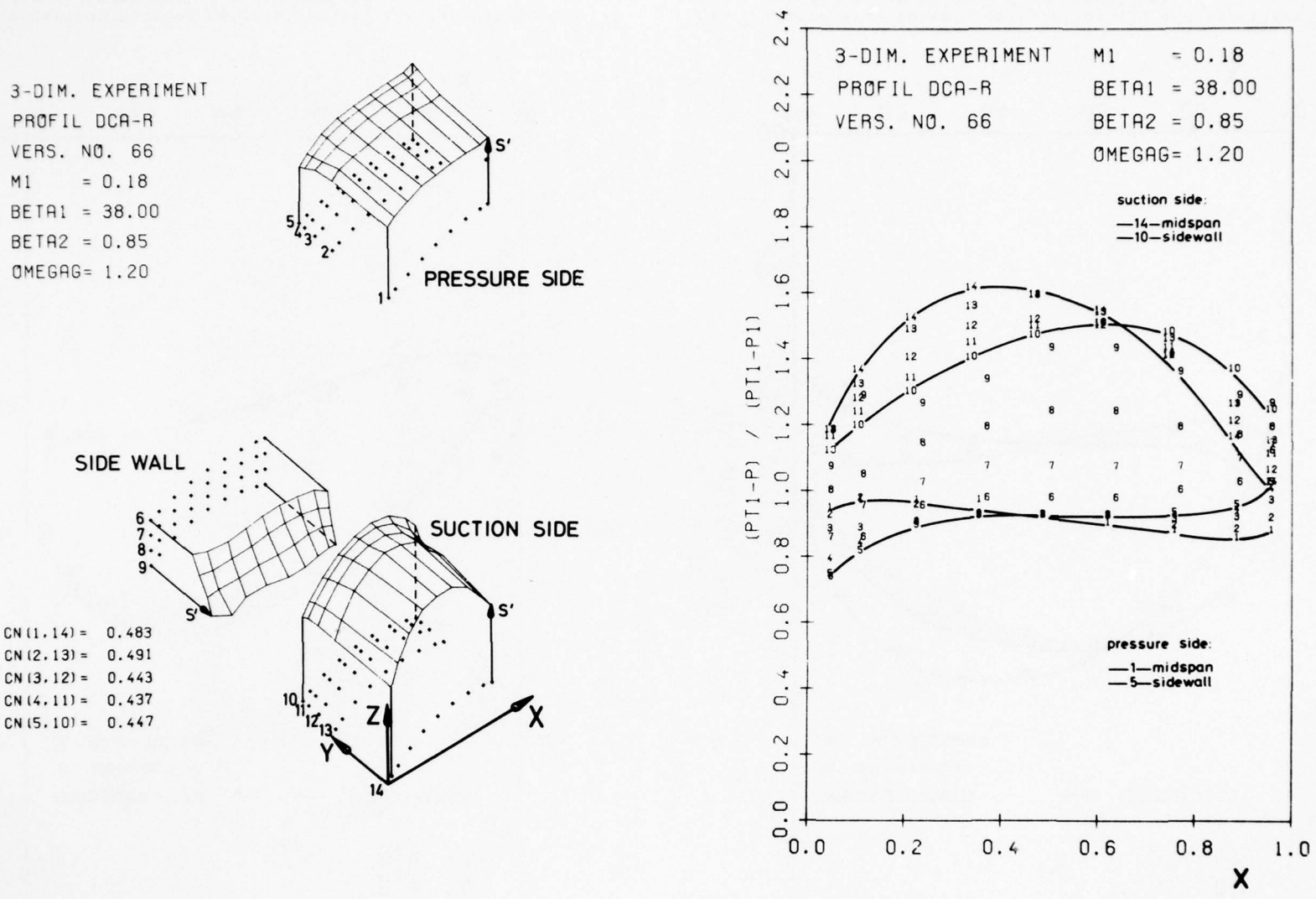


Fig.5a,b Distribution of pressure-coefficient S' on the surfaces of the symmetrical half of one passage

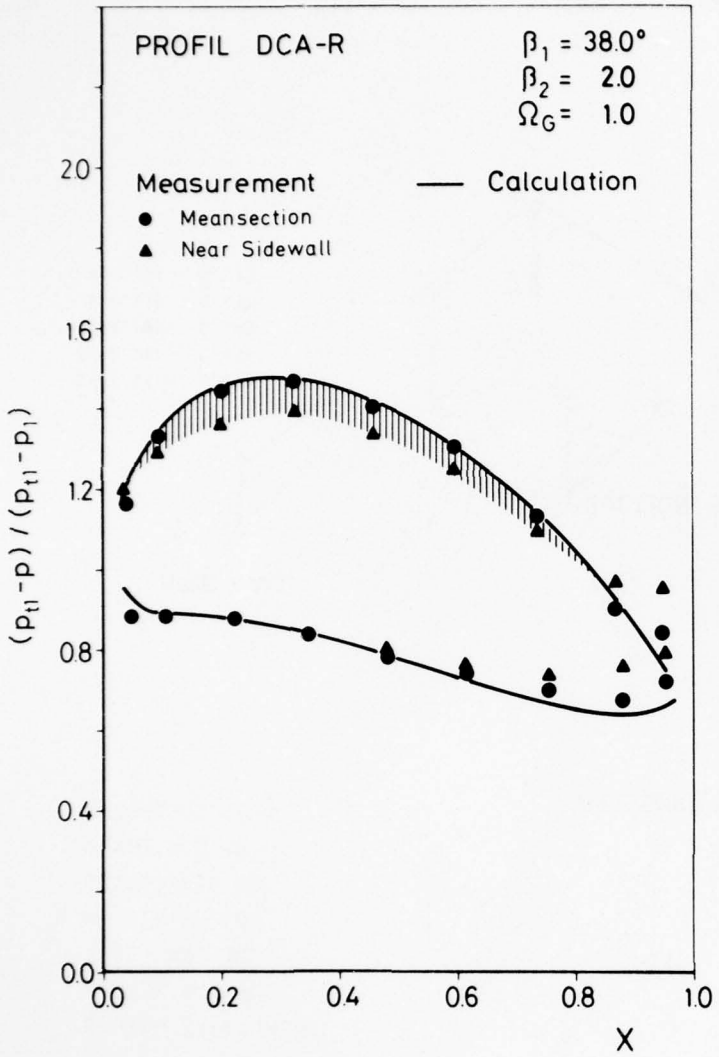


Fig.6 Comparison between calculation [1] and experiment [2] at two-dimensional flow conditions

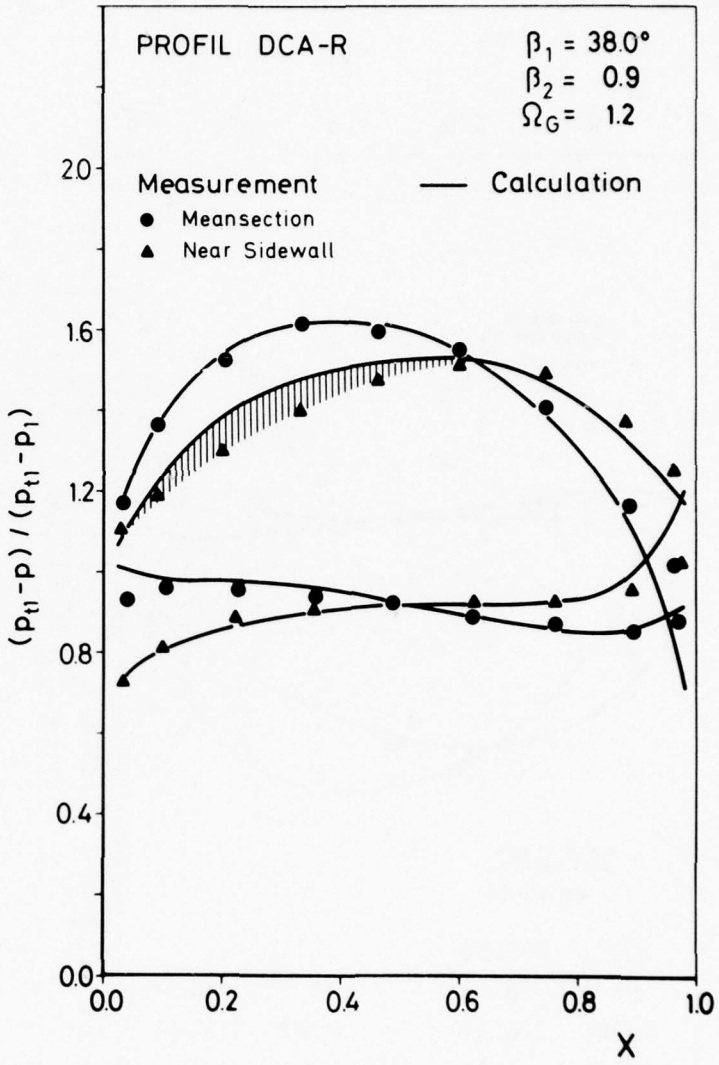


Fig.7 Comparison between calculation [1] and experiment [2] at three-dimensional flow conditions

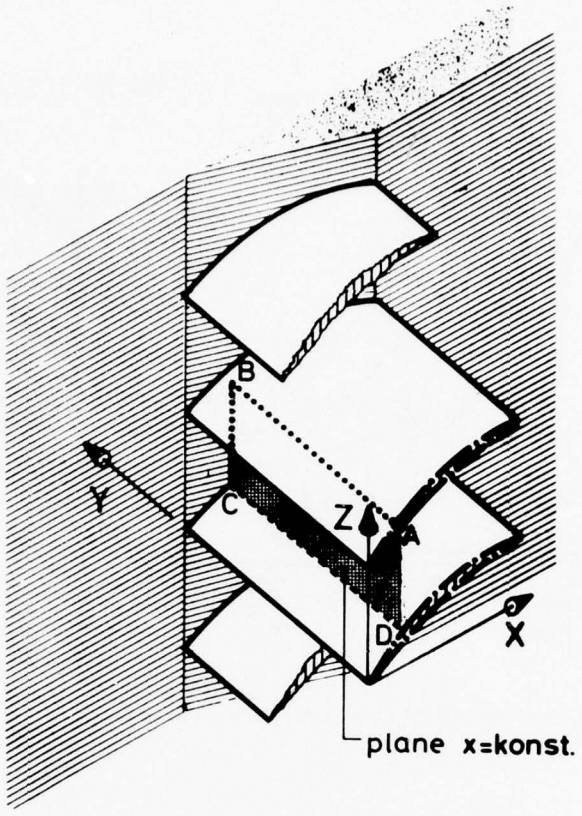


Fig.8a Arbitrary plane x = const
within the passage

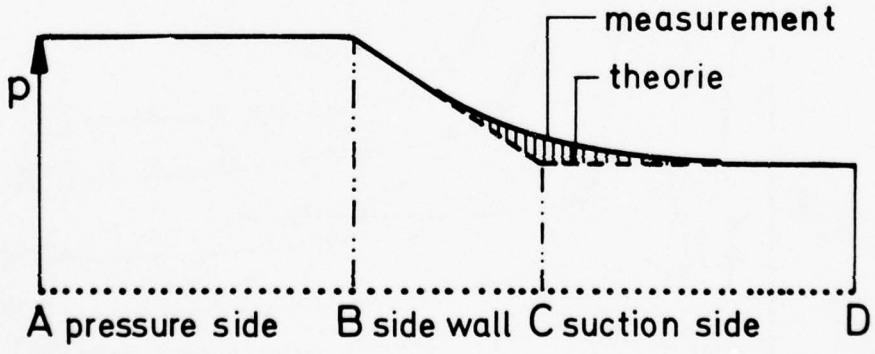


Fig.8b Intersection line along passage surfaces
and associated distribution of static pressure
at two-dimensional conditions (Ω_G = 1.0)

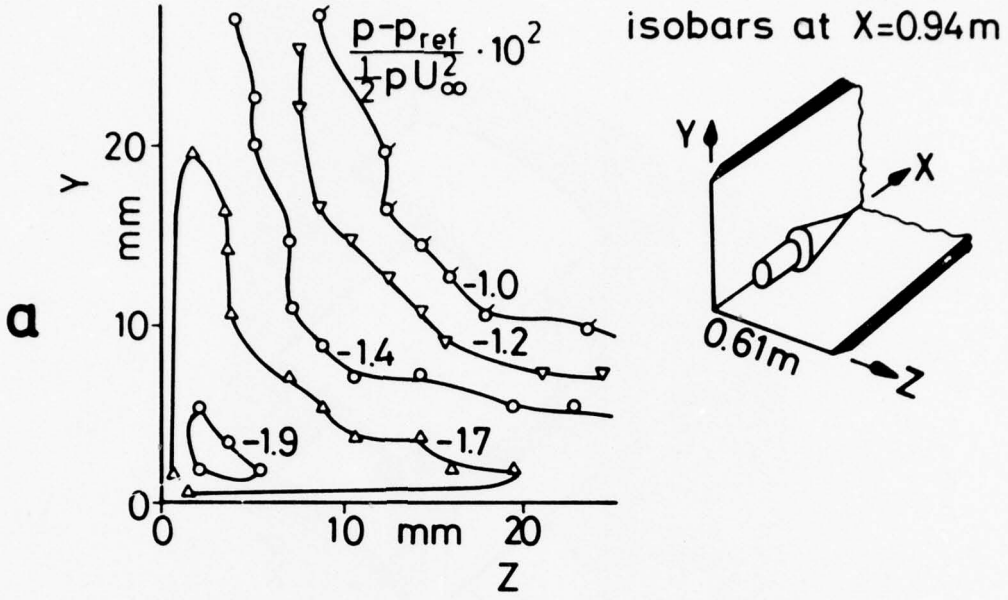


Fig.9a Distribution of static pressure within a streamwise corner layer [6]

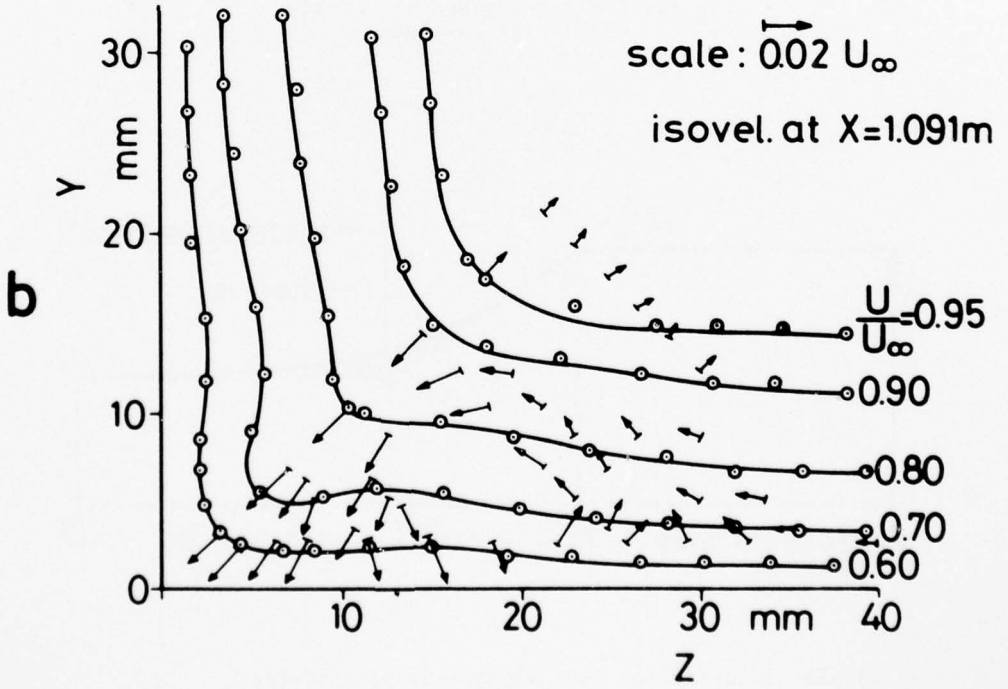
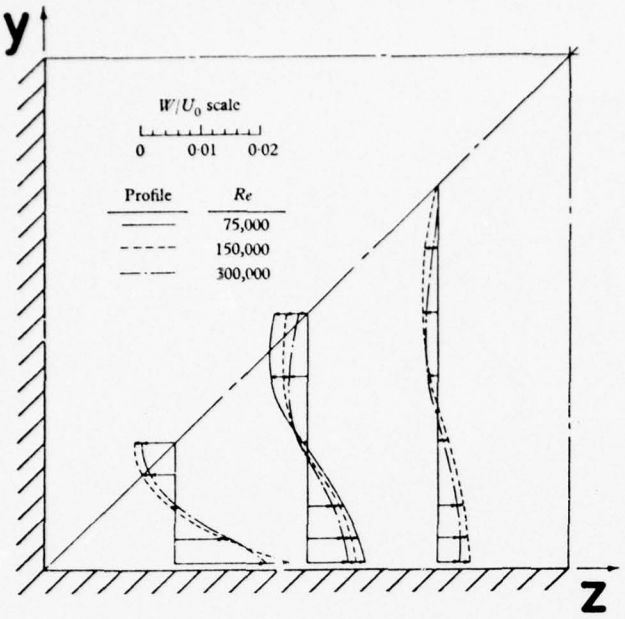
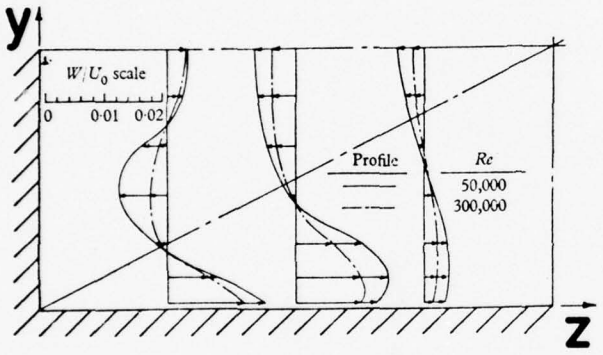


Fig.9b Distribution of velocity within a streamwise corner layer [6]



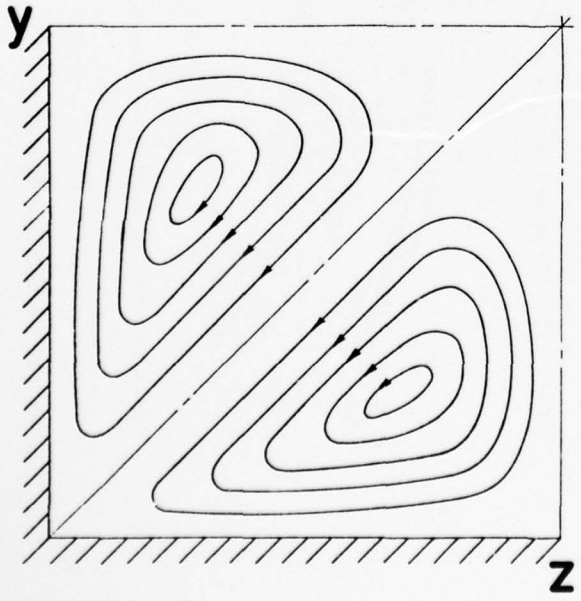
a Secondary flow profiles (z-component of resultant velocity vector) at different Reynolds numbers

aspect ratio 1:1



b Secondary flow profiles (z-component of resultant velocity vector) at different Reynolds numbers

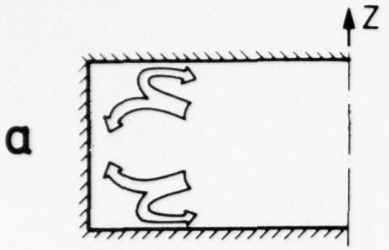
aspect ratio 2:1



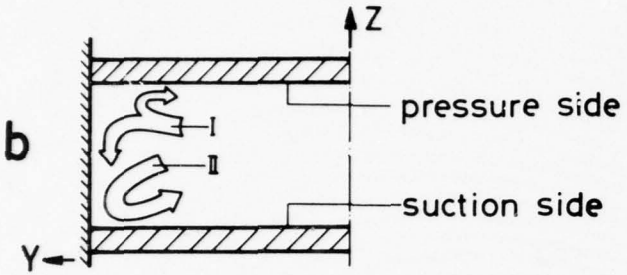
c Secondary streamline pattern (y and z-component of resultant velocity vector)

aspect ratio 1:1

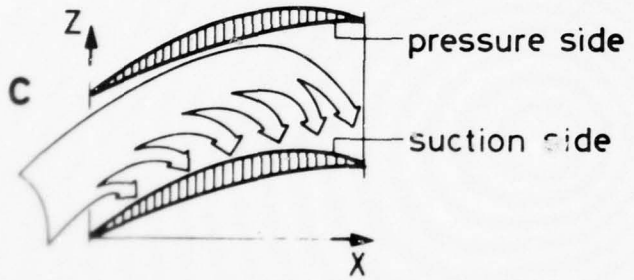
Fig.10 Secondary flow within a straight duct having rectangular cross-section [7]



Straight duct, rectangular cross section



Cross section of a straight cascade



Cross section of a straight cascade

Fig.11 Secondary flow models

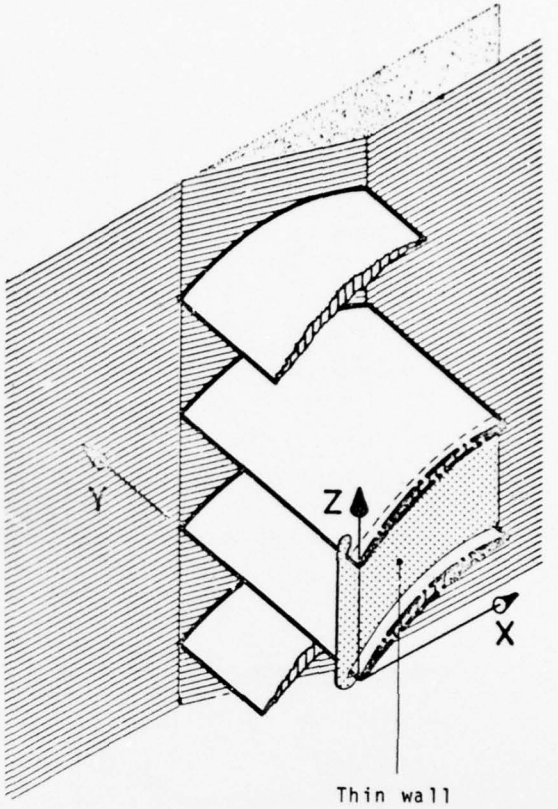


Fig.12 Thin wall near cascade mean section

NOTE ON RELATIVE VORTICITY

J.W.Railly
Department of Mechanical Engineering
University of Birmingham
P.O.Box 363, Birmingham B15 2TT

The question has arisen as to the presence of secondary flows in rotor passages in the flow relative to a rotor which has zero absolute vorticity at entry. Considering axial-flow machines for simplicity it is accepted that we may regard the blades as being replaced by filaments of bound vorticity which lie along surfaces having the shape of the blade camber surfaces (see Figure 1(a)). Further, if we consider surfaces of revolution swept out by meridional lines (such as AA) then providing that such surfaces do not intersect any of these bound vortex filaments then over these surfaces there is constant angular momentum. On the other hand, Figure 1(b), surfaces which do cut the vortex lines have a change in angular momentum across them. Assuming for convenience that the surface swept out by AA is an axial plane then the traces of the blades where they are cut, together with a portion of hub and shroud, will form a more-or-less sectorial shape. We shall assume here that these "cuts" form an exact sector (see Figure 2). The blades will be assumed to be large in number and in the case of Figure 1(a) there is constant angular momentum over AA. Introducing mean absolute and relative whirl velocities at any radius, v_u, w_u, then, from the relation $v_u = w_u + \Omega r$, we have:

$$\Delta\theta(r_2 w_{u2} - r_1 w_{u1}) = \{(r_2 v_{u2} - r_1 v_{u1}) - \Omega(r_2^2 - r_1^2)\}\Delta\theta \tag{1}$$

where $\Delta\theta$ is the sectorial angle, Ω is rotor angular velocity and r_1, r_2 are hub and tip radii. For Figure 1(a), the first term on the right is zero and the second term may also be obtained by integration of -2Ω over the area of the sector, while the left-hand side may be obtained from a line integral around the sector provided there is no contribution from the sides AB and CD. We see here that the presence of relative vorticity, -2Ω, is exactly satisfied by the mean relative velocity, w_u, but on the other hand w_u appears to violate the geometry along the lines AB and CD as there appears to be a "flow" across these boundaries. In fact this is possible because the inclination angle, β, between the blade surface and an intersecting cylinder is exactly given by the relation:

$$\tan\beta = -v_z/w_u . \tag{2}$$

There is thus zero circulatory flow. A particularly simple example of this is when the absolute flow consists of a uniform axial component and the blades are exact helices. The above geometrical condition was pointed out to the Author by Smith (1972).

Considering now the case when the angular momentum is not constant (having a change, K, between hub and tip) then we may write

$$K = \Delta\theta\{(r_2 w'_{u2} - r_1 w_{u1}) + \Omega(r_2^2 - r_1^2)\} \tag{3}$$

where the prime denotes a different value of w_u at the tip. Clearly the first term on the right cannot give the total circulation by line integration; instead we assume that it corresponds to a changed value of Ω, Ω' say, a mean value giving rise to the integrated quantity $-\Omega'(r_2^2 - r_1^2)$. Now the velocity w'_u across the boundaries AB and CD is just sufficient as to satisfy the blade tangency condition there (Equation (2)) but fails, as we have seen, to give the correct integrated vorticity. This has been pointed out by Fairbairn (1976); he introduced a third relative vorticity component defined by

$$\Omega'' = -\Omega' + \Omega \tag{4}$$

which, if added to Ω', produces the correct value, but must now satisfy a geometric condition along AB, CD corresponding to zero tangential whirl velocity. The solution to this (now circulating) flow may be found by the use, in some circumstances, of a stream function in the sector plane which satisfies the equation.

$$\nabla^2\psi = -2\Omega'' \tag{5}$$

with the condition ψ = constant over ABCD. It is important to realise that a circulatory flow will only be produced when K is non-zero. With an absolutely irrotational flow at entry this situation will prevail when the bound vortex lines behave as in Figure 1(b). Considering an axial plane exactly at the row trailing edge, the resulting velocity components along AB, CD will give the strength of the trailing vortex sheet.

It would be sufficient in order to carry out an analysis, to determine the mean angular momentum distribution throughout a (single) rotor by means of an S2 solution and by the solution of Equation (5) at a series of axial planes to obtain the secondary flows. Equation (5) would need modification to cope with the case when the axial velocity was changing in the downstream direction.

REFERENCES

1. Smith, A.G. Personal communication, 1972.

2. Fairbairn, G.W. *Three-Dimensional Flows Through the Rotor Passages of Mixed-Flow Fans.* Ph.D thesis, University of Newcastle-Upon-Tyne, 1976.

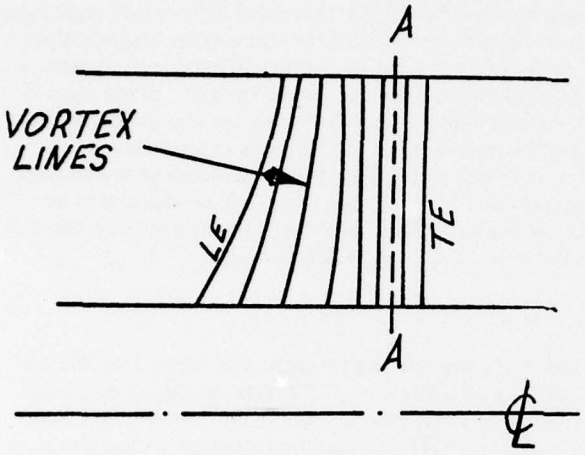


Figure 1a

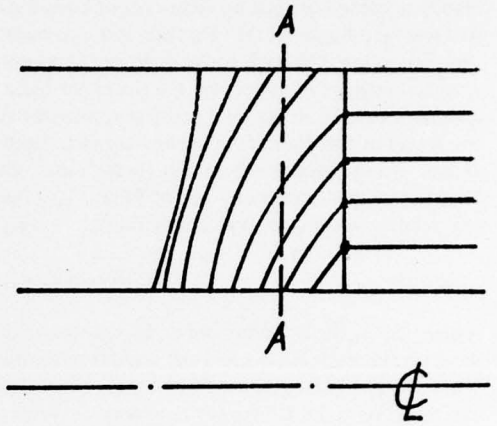


Figure 1 b

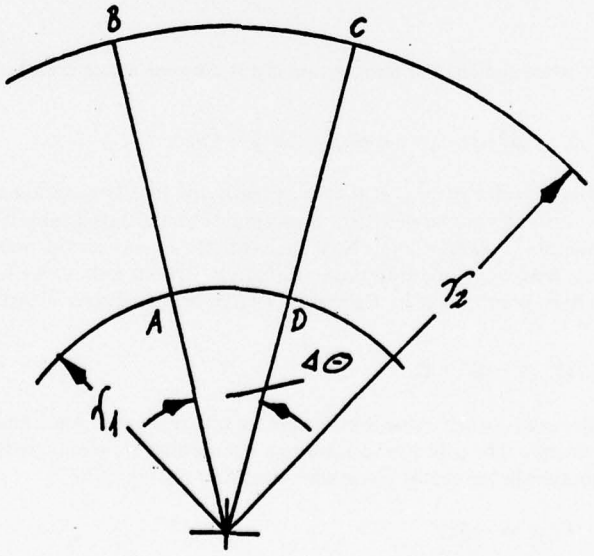


Fig.2 Section on AA

ROUND TABLE DISCUSSION

Speakers:

J.H.HORLOCK, University of Salford, UK (Moderator)
R.BOUILLET, SNECMA, France
J.CHAUVIN, Von Kármán Institute, Belgium
D.ECKARDT, DFVLR, Germany
P.W.RUNSTADLER Jr, Creare Incorporated, Hanover, NH, USA

ROUND TABLE DISCUSSION

J.H.Horlock: We have four contributions which are listed and the way I propose to organize this session is as follows. I shall ask Mr. Bouillet to start giving the view point of the engine manufacturers. We might have some discussion about that aspect after he's spoken. Then I'll ask the other three contributors to follow: Mr. Chauvin to talk to us about theoretical research, Mr. Eckardt to talk about experimental research and Mr. Runstadler to talk about also experimental research emphasizing flow visualization. We shall have a further discussion after those three people have spoken. I should be asking the three of them to concentrate on two things. First of all, how they see the current state of the art in the particular subjects they are talking about and secondly, how they see the way ahead in these three areas. Then following these discussions I shall try to summarize the results of this meeting.

* * * * * * *

R.Bouillet: Une bonne connaissance de tout ce qui concerne les écoulements secondaires est absolument nécessaire pour l'ingénieur qui a la charge de concevoir et de mettre au point une turbomachine. Historiquement, on peut d'ailleurs rappeler, que l'un des plus anciens critères utilisés par les ingénieurs s'occupant des compresseurs est le critère de De Haller qui n'est autre chose qu'un critère de limitation des pertes aux parois de la veine. Je parlerai surtout des écoulements secondaires en tant que besoin de connaissance qu'a l'ingénieur de ce problème.

Il y a trois principaux aspects qui interessent l'ingénieur.

(a) Les pertes secondaires elles-mêmes auxquelles est directement lié le rendement qu'on peut espérer d'une machine.
(b) L'influence des écoulements secondaires sur l'écoulement principal à laquelle est directement liée la géométrie des aubes.
(c) La réduction des écoulements secondaires dans la procédure du dessin d'une machine.

Au sujet du premier aspect, celui des pertes, je crois qu'il faudrait modifier cette appellation d'écoulements secondaires. On peut considèrer par exemple que dans une turbine du type haute pression ou dans un étage moyen de compresseur les pertes secondaires sont souvent du même ordre que les pertes de profil, donc contribuent pour moitié à la chute de rendement vis-à-vis de l'unité. Il est, donc, absolument nécessaire que l'ingénieur puisse disposer de méthodes de prédiction des pertes secondaires. Ces méthodes doivent avoir plusieurs caractères:

(a) elles doivent absolument inclure les effects des jeux radiaux
(b) elles doivent avoir un caractère suffisament général pour pourvoir être utilisées par l'ingénieur depuis le stade du project de la machine.

Un ingénieur spécialement en aéronautique, est toujours confronté à des compromis. On a, par exemple, à choisir un compromis entre les performances d'une part et des considérations de poids ou de prix de la machine d'autre part. Une méthode suffisament générale de prédiction des pertes secondaires peut déjà guider l'ingénieur à ce stade du projet. Je prendrai un seul exemple: l'ingénieur dispose d'un volume donné pour faire un compresseur multiétage et recherche le meilleur choix du nombre d'étages pour la longueur donnée. Il est évident qu'un compresseur à sept étages par exemple sera meilleur marché qu'un autre à huit étages, mais que payera-t-on en performances? J'insiste beaucoup pour que ces méthodes soient disponibles au début du projet, donc aient caractère assez général pour qu'elles puissent être appliquées avec ce que l'on connait à ce stade du projet, c.a.d. essentiellement sous l'aspect aérodynamique

(a) des charges d'étage
(b) des triangles de vitesse

et sous l'aspect technologique

(a) des jeux radiaux
(b) des allongements moyens.

Ceci n'empêche pas qu'à la fin du projet on puisse utiliser les mêmes méthodes ou d'autres plus sophistiquées pour un calcul plus précis. J'insiste également sur un autre aspect: il est nécessaire de tenir compte de ce qui se passe d'étage à étage dans un compresseur multiétage ou plus généralement dans une machine multiétage, puisque hier nous avons vu que dans une turbine les mêmes phénomènes existent, phénomènes qui sont très importants.

Le seond aspect des écoulements secondaires est la repercussion de ces écoulements sur l'écoulement principal. Cette repercussion est bien connue. Elle peut prendre différents degrés de complexité pour sa représentation. Le plus simple est le concept bien connu du coefficient de blocage dans les compresseurs axiaux, le plus compliqué étant une description complète de l'écoulement sur toute la hauteur de l'aube aussi bien en vitesses qu'en angles, y compris dans la zone des écoulements secondaires. Il est donc nécessaire de développer des méthodes couplées entre l'écoulement principal et les écoulements secondaires. Il est clair par exemple que, en turbine on ne peut pas adopter le concept du coefficient de blocage et que, même en compresseur, dans les étages arrière, on ne peut pas non plus se contenter de ce concept simplifié.

Sur ces deux aspects d'estimation des pertes et de calcul de l'écoulement principal, il faut aussi bien insister sur le fait que les calculs doivent être faits au point d'adaptation de la machine, mais également en dehors de ce point d'adaptation. En particulier, si on veut prédire la limite de pompage d'un compresseur multiétage, il est impossible de concevoir cette prédiction sans une méthode assez précise d'estimation des écoulements secondaires correspondants.

Je voudrais maintenant passer au troisième aspect, très important pour l'ingénieur qui est celui de la réduction des pertes secondaires. Un premier moyen dérive directement des méthodes d'estimation des pertes. Si ces méthodes sont suffisament précises, elles doivent permettre au niveau du projet de choisir le meilleur compromis. Le second est de chercher à réduire tout ce qui est fuite marginale, donc de réduire les jeux radiaux.

L'ingénieur aérodynamicien est alors en conflit avec l'ingénieur mécanicien, qui veillant à la sécurité de sa machine demande certaines valeurs minimales de jeux radiaux. Là, on voit l'interêt des études de matériaux abradables.

Une troisième voie pour réduire les écoulements secondaires est ce que je pourrais appeler des moyens externes, tels que l'utilisation de "fences" ou de fentes ou d'aspiration des couches limites aux parois. Là aussi, plusieurs problèmes se présentent à l'ingénieur. Le premier c'est qu'évidement ces dispositifs compliquent le moteur; on doit donc, également chercher des compromis en considérant le poids et le prix. Le second porte sur la fiabilité de ces dispositifs. C'est donc, une question de durée de vie du moteur. Le troisième point concerne plus specialement les aspirations des couches limites aux parois. Il faut faire attention à ce que le bilan thermodynamique se traduise en un gain pour le moteur. Il se peut très bien que le rendement d'un composant soit amélioré mais que l'air qui est ainsi prélevé soit perdu ou mal utilisé pour le cycle et que finalement il n'y ait aucun gain de performances globales du moteur.

Dans l'ensemble, les moyens d'amélioration externes, ne sont pas très commodes. C'est pourquoi je pense personnellement beaucoup plus à des moyens de réduction des pertes secondaires à la source. Par exemple en choisissant des distributions de vitesses adéquates sur les profils ou une distribution radiale de travail appropriée ou également des formes particulières de parois ou encore une inclination des aubes. Il est sûr que l'ingénieur préfèrera toujours des moyens qui ne changent pas l'architecture générale du moteur.

Je pense vous avoir résumé suffisament le point de vue d'un ingénieur utilisateur et je pense également qu'il y a beaucoup de réponses à ces questions dans ce qui a été dit pendant ces deux derniers jours. Maintenant, il faut sans doute voir comment ces études fondamentales ou expérimentales peuvent être appliquées par l'ingénieur et surtout être transformées en des méthodes suffisament générales et d'une application pratique.

DISCUSSION

J.H.Horlock

Could we now have a general discussion on the viewpoint from the engine manufacturers. We have had three particular divisions here of this subject:

(a) – The question of secondary losses
(b) – The question of interaction between secondary and primary flow
(c) – The question of the reduction of losses

If I could be a little provocative I would say that if I were designing a compressor or turbine to-morrow, which I should not be doing, I think that the results of this meeting probably would not have much effect upon the way that I designed that machine. I don't think there would be anything in this meeting that would cause me to change the estimates of secondary losses, which I have used for the last ten or fifteen years, the Howell and the Vavra loss correlations. I think I would be tempted, perhaps, to calculate the blockage in an axial compressor from the boundary layer theories or from Smith's experimental correlations. I think I would not allow for any blockage in a turbine, because it seems from all the experimental results that the boundary layer is swept off the wall and it doesn't block the flow at the end walls at all. The area where I would be completely uncertain, I think, is the work distribution through the boundary layer region. We have talked a lot about the secondary losses. We have seen many examples of flow angle changes through the boundary layers and, if you do simple estimates of the work transfers associated with these angle changes, those variations are much larger than the losses that we talk about. And we don't allow for those angle changes in the design.

So that would be my own attitude, I would use very little of what has been shown, I think, in the actual design. Another area, where I would be very uncertain, is the interaction between the secondary flow and the surge limits in a compressor. Surely it is very clear, from all the work on wall treatment, that secondary flow has an important effect on the stalling of a blade row. If it were not so none of the effects of wall treatment would be very large, but they can be very large. I think the only other way, that I would alter a design to take account of this interaction would be to try to reduce the blade loading anywhere that I have a tip clearance. That would be the only attempt to modify the design.

But that would be a personal view. There are many people in this room that design compressors or turbines every day of the week. What have they got to say?

R.Hetherington

I agree with Prof. Horlock's remarks:

Turbomachinery designers cannot use the "state-of-the-art" secondary flow methods as revealed at the meeting.

We are still in the analysis stage of the individual components of secondary flow. When this is satisfactorily completed it will be necessary to put the science together again for the design engineer. Meanwhile the designer must revert to his simple correlations.

J.Dunham

I agree with what has been said and wish to draw attention to the particular problems of a turbine. Considering a single nozzle row, the theory tells us that the peak underturning occurs at a distance from the wall equal to one upstream-wall-boundary-thickness. The N.G.T.E. data quoted by Marsh agree but the Marchal and Sieverding data apparently disagree. Please, could this point be discussed?

The major unresolved problems occur when more than one blade row is present. Should the large local incidence change on the rotor be applied to deduce locally high profile losses on the rotor? What values of streamwise and normal vorticity should be assumed at rotor inlet?

I suggest that more experiments involving more than one blade row (such as Barry's) are needed.

H.Marsh

Dr. Dunham has suggested that the peak underturning occurs at a distance δ from the wall. The early work of Hawthorne shows that the position of peak underturning occures at a distance which is determined by the ratio

$$\delta/(S \cos \alpha_2) .$$

For low values of this ratio, the peak underturning occures at δ , but for higher values, the maximum underturning occurs much closer to the wall.

J.H.Horlock

I would like to add one point to that. I would never dream of using the Hawthorne type solution for deflections greater than about 30°, because surely the rotation of the flow that we saw in Carrick's work must make that analysis, in which it is assumed that the Bernouilli planes do not rotate, invalid. So it would be all right for a guide vane row but I would be very hesitant about using it for a turbine row.

J.Chauvin: I would like to discuss some of the questions raised during this discussion. Maybe I will be slightly optimistic. Let's see, where we are from the theoretical point of view. I think my task is very light because the state of the art was certainly extremely well summarized by John Horlock in his introductory lecture. As Roy Hetherington pointed out we are really in a second phase of the study of the secondary flows. We have lived for a long time with some theoretical approaches, which were not used at all in the design and with empirical correlations which have been shown by using them in advanced contemporary design to be, to say the least, not of a general nature but appropriate to particular types of design. This is true for compressors as well as for turbines. We are thus in a phase which is, I think, quite typified by this meeting. We are trying to revise our position on the understanding of secondary flows, which, in fact, in practice, especially when considering the design requirement, cover a very wide variety of effects. Those have first to be identified. We have to try to understand the mechanism of the flow in a situation as realistic as possible, ideally for high loading, multistage machines at design and off-design. The difficult problem lies in the latter case: prediction of surge margin, clearance effect with varying loading, etc. The aim that we must have, as finally we want to build better machines, is for a clear understanding of the physics of the phenomenon to derive the kind of tool that the industry needs. It should not be an order of magnitude more complicated than the present empirical rules. We must identify the important parameters and express their effects with as simple rules as possible.

This can be done in two ways; by using theoretical and numerical methods and also, as it will be discussed by other people, by extremely detailed measurements. I will go back to the theory per se. As Professor Horlock pointed out we have three different approaches at the moment: the non-viscous one which deals with the transport and deformation of vorticity, essentially through cascades (that is the oldest one in existence) the one which follows a pseudo-boundary layer approach with pitch averaging value both for cascades and for machines and finally the 3D approach which can be considering either the Euler type of flow, that is non-viscous flows, but can use distributions of entropy change imposed from the outside or the one which takes totally or partly account of viscosity.

I think that from the oldest approach we have learned quite a lot. It is certainly being continuously improved and Harry Marsh has shed some new insight on what was happening and this made him able to connect the calculation results with the old experimental rule of de Haller. However, one can say that the local values of the predicted velocities, for instance in cascades, do not agree very well with the measurements but that the results integrated on a pitch are in semi-quantitative agreement with the experiments. They give a proper evolution of the angle with some difference on the position of maximum turning and amplitude of the turning. When they are integrated on the whole blade height they give a change of turning which agree with the experimental data practically within the measuring accuracy. This is true for secondary flow without clearance. With clearance the same kind of conclusion can be drawn but the state of the art is certainly not as good.

There are two main conclusions that can be derived from the non-viscous cascade approach. First, that the angle variation is essentially due to a non-viscous effect. Second, that this approach can by no means represent the mechanism of the generation of losses.

This is important as most of the existing correlations for secondary flows and tip clearance have been based on an estimation of the kinetic energy loss in the non-viscous secondary flows (in that case the losses are proportional to the lift coefficient to the 3/2 power) or of the induced drag which then is proportional to the square of the lift coefficient.

Of course with that approach some correlation with experimental data has been obtained, but I frankly believe that it is because in the lift coefficient is included implicitly the driving forces for the mechanism, that is difference in pressure, in axial and tangential direction.

It is possible to extend the inviscid methods to skewed inlet flow and probably to twisted blading, but maybe then one is coming close to the complexity of a 3D flow calculation.

The second approach for secondary flow prediction is based on the boundary layer of pseudo-boundary layer concept, which is backed by a lot of thorough measurement in cascades, and in rotating machinery. I think that it is quite a promising one for compressors. For compressor cascades one has been able to show, by using for instance Horlock's approach and by detailed measurements that the essential source of loss, for blades of conventional type is the friction contribution of the main stream component of the end wall boundary layer, when there is zero clearance, and that the 3D corner separation is not generating very much losses. An exception occurs for peculiar velocity distributions of the blade velocity with very great loading near the leading edge, which the type of blading that can be obtained by an inverse method based on 2D boundary layer optimization for instance. We know that if we take some of the compressor cascade correlations derived from those results and incorporate them in the machine design system, the results are quite good. John Horlock explained that this is due in part to the favorable effect of the relative motion, it can be explained also by the boundary layer calculation.

For turbines this procedure is certainly not valid. If one compares the correlations made from cascades data and those which have been made using experimental machines data one finds an order of magnitude of difference in the predicted losses.

One typical example for instance is the method of correlation of Lakshminarayana for clearance, which gives quite good results as compared to machine data. It introduces losses due to secondary motion in the boundary layer. To fit the data measured in machines, one has to introduce a boundary layer displacement thickness which is ten times the pitch. This proves that we don't know too much about what is really happening.

Now, for the compressors, I think that the pseudo-boundary layer approach as introduced by many people who are here, like Professor Railly, Dr Marsh, Professor Horlock, Mellor and Smith, is quite interesting: it can provide an

evaluation of blockage. It can provide the losses and, additionally Mellor introduced a very clever idea which can be used by the designer, and in fact is equivalent, with a better justification to the old work done factor. Mellor considers that some or all the material in the endwall boundary layer is attacking the blade at such an angle that the energy which is communicated to it by the blade motion is lost.

This pseudo boundary layer method seems to give some indication on proximity of stall, when the surge and stall originate at the wall, which corresponds to a fairly large category of compressors. It can also predict that in compressors the boundary layer can reach an asymptotic state. At the moment its state is relatively crude. The closure equations for the system of calculation are rather arbitrary. The effect of variation of blade twist on the boundary layer thickness, which can be as large as half the blade height is not taken into account and limited use has been made of the possibility of calculating the change in angle and in loss inside the boundary layer. The work of John Horlock on bounded boundary layers and some work which is in progress both in Lyon and at the University of Brussels by Professor Hirsh, shows that improvement can be made and a better matching between the external flow and the pseudo-boundary layer can be obtained.

This approach does not work for the turbines tending to provide negative losses. There we must do something different and really we don't understand the mechanism. We have some hints in that the relative motion encourages secondary flow motion and probably that the kinetic energy, which is given to the boundary layer plus what happens in the so called leading edge vortex is causing a loss under the form of a kinetic energy loss. Most probably, we will only understand what happens, when we calcualte three-dimensionally.

This is the third way of attacking the problem. There exist a number of methods which are not prohibitive in time; they can be divided into two approaches: the old Wu approach of coupling the S_1 and S_2 surfaces but this of course precludes the treatment of rolling up of vortices, and the true 3D approach. In both, inviscid or viscous flows can be considered. I think both are useful. The inviscid one will tell you if additional secondary effects than those identified by the cascade approach exist and will allow to introduce the relative motion effect on the change in turning. Such an approach can be coupled with a pseudo-boundary layer calculation or like in the through flow method an experimental distribution of entropy can be introduced along the chord for instance.

The viscous one of course will give a more complete picture, and to start with one can try to give a predominant viscosity in one direction with respect to the others.

At the moment in the public domain one can find the non-viscous methods of Thompkins, of Denton, for us, at VKI, of McDonald and de Michele which are time marching methods, Smolderen is producing one for transonic flow with vorticity, then you have the finite difference method and finite elements methods which are available at several other places.

Those 3D methods, as was concluded at the meeting last year in Porz-Wahn, will not become part of the design systems in the near future. They are, as are the laser experiment, an experiment, but of a numerical nature which can provide a better understanding of the phenomena. For instance some of the questions raised by Mr Bouillet can be answered. Can you optimise by changing the work distribution, the loading, the dihedral inclination of the blade, the wall shape? An answer can be provided by numerical methods probably much easier and at less cost than by experimental measurements that additionally take a long time. The use of the numerical approach will probably be one of the things which will bring an important contribution. Without a better understanding of what happens in the real environment, we just cannot improve the machine. After this phase of understanding which probably will last a number of years we will have to derive intelligent design rules which have to be incorporated from the beginning in the compromise that was discussed by Mr Bouillet and Dr Hetherington.

DISCUSSION

W.Schlachter

In relation to turbine cascades do we expect that the simple model of splitting the flow into a core flow and two side-wall regions, as in compressor cascades, can be adopted for a turbine, or, do we have to face the fact that the full 3-D viscous procedure is the only adequate tool for treating the secondary flow in turbine cascades even if the end-wall regions do not merge together?

J.H.Horlock

Maybe Professor Chauvin has answered that partly already.

Author's Reply

Yes. Maybe I can qualify my answer. We have to do something in the mean time. I think that, from the limited amount of experiments that we have, maybe we could divide the turbine blade in two regions. I am speaking now of a multistage environment. In the first part near the leading edge, because of the horse shoe vortex, and of the relative motion, an extremely quick mixture probably occurs and there one could try and correlate some bulk losses in total pressure. As John Dunham pointed out boundary layer is completely swept and from some of the experimental evidence that I've seen, you can suppose that a new boundary layer is restarting from the throat, or about it, with a secondary flow mechanism similar to that of compressors. In that region maybe you could take again a treatment with an averaged boundary layer. This is a pure guess at this stage.

J.W.Railly

The point made in discussion regarding the inapplicability of annulus wall boundary layer methods to turbines brings to mind a calculation I did in about 1949* which used an admittedly crude and inaccurate model for secondary flow (that of A.D.S.Carter of the N.G.T.E.). This calculation assumed a cascade with a 6 per cent blockage (at the end walls, 3 per cent per wall) and assumed a trailing vortex system at the 3 per cent positions. The result was that for a compressor cascade, blockage and induced angle effects worked together, so that a stage using this model had a work done factor of about 0.75 to 0.8. On the other hand, in a turbine stage, the effects cancelled out giving a work done factor of 1.003. In recalling this calculation in the context of much more sound calculation methods, the point is made that unless accurate blockage (annulus wall) and outlet angle are achieved simultaneously then single corrections are likely to be less accurate than none at all. The fact that Marsh has achieved reasonable agreement with outlet angle computation in a turbine cascade with a deflection of 62 degrees, requires, in my view, the need to calculate blockage also, for otherwise the inclusion of the outlet angle change alone will lead to greater error.

Author's Reply

I think that you are right. One thing what we should do immediately is to start calculating, because in reality we have not checked on too many cases the validity of the available computation methods. I think we are in the period where we can use systematically some of the tools available. It will be one of the objectives of a working group we are planning to set up in this panel.

J.Fabri

Si les durées des calculs theoriques tri-dimensionnels sont très longues et qu'il faut faire des approximations sévères pour pouvoir effectuer ces calculs, peut-on espérer aboutir par ces méthodes à des optimisations de turbomachines?

Author's Reply

First, I would say that even if it took 24 hours with Thompkins calculation, it is still less expensive than to build and test a compressor. The fact is that Thompkins' program is far from optimised and I think, as Professor Hirsch confirms it, that we have gained an order of magnitude in the time needed and that a reasonable time to calculate a single row is now 2 or 3 hours on a large computer. I did not imply that we should not make experiments anymore. On the contrary, we need much more sophisticated tests and instrumentation to understand what is happening and to cross-check with our models.

F.Rekos

I get the feeling, based on your comments, plus those of MM Horlock and Hetherington that the secondary flow theories being developed and discussed during this symposium are a long way from being used by the engine compressor and turbine designer, who has developed a sophisticated "rule-of-thumb" based on the conventional brute force "trial-and-error", or "make-break-fix" experimental factors used in developing engines.

My question is: what is needed from the secondary flow experts before the engine designers will pay attention to them? Are the theories based on single rotating stages and cascades useful?

J.H.Horlock

I think that's a very good question. I think it's a paradox, really, but the person here who has developed the most sophisticated numerical analysis, Mr Hetherington, doesn't use it in his designs at Rolls-Royce.

P.W.Runstadler

I would like to make a comment, which in fact is more in terms of a question to the analyst, to the experimentalists, and also to the people who are doing engine design: listening to the papers that have been presented at this symposium, I think most of the results of experimental work and analysis have been done on cascade or on the first stages of machines. It seems to me that one of the puzzling questions that must face engine designers is how to analyse the flow through the downstream stages of engines. Our results are certainly valid for the kind of geometry in the first stage but, as the secondary flow shed from the first stage passes through the latter stages of multistage machines, we are forced to deal with a flow that is not only complicated by the secondary flow mechanisms but is also unsteady in both the stationary and rotating frames. It seems to me that while this is a very difficult problem it ought to be one of the focuses of research and design analysis being done to understand how to better treat secondary flows in actual engines. That is, from where we are to-day how can we understand the important and fundamental mechanisms that must be taking place in this more complicated flow situation downstream? I would like to hear some comments on that point?

J.H.Horlock

That is a very interesting point. You are really saying that, perhaps, the major impact of theoretical methods may be restricted to the design of the early stages. I don't know if there is anybody here from G.E., but one gets the impression that Smith has used calculation methods in the early stages of the machine a great deal. You only have to look in the front stages of the engines of the DC-10 to see the influence that he has had on the design of that blading.

---

* Railly, J.W. (1949): *A Note on Work Done Factor*. C.A.Parsons Ltd., Newcastle upon Type, England. Internal Memorandum.

H.Marsh

I would like to comment on the role of theory in turbomachinery flow calculations. The complexity of the flow has been demonstrated in several of the papers at this meeting. The theories focus attention on the interpretation of the observed flow and they help in our understanding of a complex flow situation. It may be unrealistic to expect a very high level of agreement and it may be necessary to accept a fair level of agreement together with a better understanding of the flow process. We may be reaching for the moon if we expect accuracies of 1 per cent or better and I don't foresee this level of accuracy within the next five to ten years. I think that we must be realistic about the role of theory.

Author's Reply

I fully agree with you. What we are expecting from theories and from refined experiments are, what are the factors of the order of magnitude one, which are influencing the phenomenon?

H.Marsh

Dr Dunham has suggested that the peak underturning occurs at a distance δ from the wall. The early work of Hawthorne shows that the position of peak underturning occurs at a distance which is determined by the ratio $(\delta/s \cos \alpha_2)$. For low values of this ratio, the peak underturning occurs at δ, but for higher values, the maximum underturning occurs much closer to the wall.

G.Serovy

At this meeting Mr Tall described a program in which the performance of a turbine stage was substantially improved by controlling secondary flows in the design phase. The design system was one in which the "secondary flow" influences were estimated as an integral part of the flow model, not as arbitrary add-on-features. The design of some compressor stages, for example the CF-6 fan designed by General Electric (L.H.Smith, Jr), has also incorporated the secondary flow influence directly.

Therefore it seems likely that secondary flow analyses should not be independent from the mainstream of the design process, but should be included in the normal flow field calculation system. Correction factors are obsolete.

J.Dunham

I believe manufacturers will pay attention to secondary flow theory – or any theory – when they have found it explains a problem otherwise unexplained, or makes a new successful prediction, or leads directly to an efficiency improvement. But who should do this work of initially proving the value of a new theory? The manufacturers? The researchers? Professor Chauvin has suggested that a Working Group organised by the Panel could do useful work in assessing theories against data. For this the cooperation of manufacturers is necessary and I hope it will be forthcoming.

R.Hetherington

In my opinion, and I would like this audience's views, we are always going to design in a two dimensional way. This will be the way we look at overall parameters and lay out the overall dimensions of our machines. It is difficult to think in 3D and it is necessary to think in 2-D at this stage, though at some stage in the design procedure we will be performing a 3D calculation. This is what has been happening in R-R. We have been using the sophisticated 3D method to analyse one or two selected cases to teach ourselves what is happening. We have not been particularly successful and the work has been restricted because of manpower.

N.A.Cumpsty

The models for secondary flow do not allow prediction of losses, moreover we have no model at present for the way in which losses are generated. The present work therefore can give no indication of the direction for reducing losses. The flow angles in regions of small velocity defect are the usual result – what is really needed is the loss and the flow distribution in regions close to the walls. Whilst some calculation methods do allow prediction of loss for compressors, it is only by including large amounts of empirical information.

For these reasons the manufacturers cannot be expected to show very much interest in the present theoretical work or results – the problems of real interest are not being addressed.

Author's Reply

I might slightly disagree with Dr Cumpsty. It's certain that we must first get a proper idea of the physics and I think that this is what we are beginning to do with the kind of information, which has been reported for axial machines by Papailiou, by Weyer and by Cumpsty and other people in the centrifugal field, but I think that one can get guide lines from a theoretical approach once the physics are identified and the way to introduce the approximation are set to take account of all the first order parameters.

Mr. D. ECKARDT (DFVLR, Germany)

Taking into account some aspects of the experimental research in secondary flows, which emerged during this meeting, I am grateful that Prof. Chauvin covered already the experimental work in cascades in the context of his theoretical review, so that I may concentrate my comments on the rotating machine.

I think, we can state that by far the majority of the presented papers which dealt explicitly with experimental research, concentrated on the testing of secondary flow effects in cascades and among those were also the finest examples of coincidence between theoretical predictions and measurements. But I think, it also showed up during this meeting that there is an urgent need for additional information:

- the cascade work is certainly still worthwile to be done, especially if it is extended in a way (which e.g. Mr. Carrick demonstrated with this moving belt experiments) to investigate separately the influence of typical rotor flow phenomena in the simpler cascade test set-up,

- on the other hand,we need more detailed information on the realistic rotor flow pattern itself. This is also related to the increasing capability of the newly emerging 3-D flow calculation methods.

There should be a strong interrelation between the developing theory and experiments. The improved experimental insight into complex flow situations should yield the sound basis for a possibly simplified, but physically still relevant theoretical flow modelling. With respect to radial machinery, the significant influence of Coriolis forces requires anyhow the detailed experimental analysis of the rotating impeller flow.

So summarizing the demands on experimental research in secondary flows, as they were outlined during this meeting, I think, we need more information on 3-D through-flow in general, on the local energy transfer within the rotor, on the development of streamwise vorticity and, what is closely related with secondary flows, the problems of the 3-D boundary layer development, e.g. the annulus wall boundary layer. We need reliable data and detailed information with respect to the boundary layer profiles, the exit angle distributions - and we need the information not only in a basic model rotor flow but also in real stages, high-speed applications, multistage axial compressors as well as turbines and in high-speed, high-pressure-ratio centrifugal compressors. This is mainly due to the fact that the interrelation between 3-D boundary layers and secondary flows is especially predominant in critical regions of the flow field, where wall stall occurs, where secondary flows (superimposed by tip clearance effects) and the effects of non-conservative body forces on the boundary layer structure exert not easily surveyable influences on the onset of corner stall.

Considering the presented experimental techniques, suited for a detailed analysis of rotor flows, I think the paper by Hirsch, de Ruyck and Kool presented an excellent example of what can be done,resolving complex 3-D turbomachinery flows. The skilled application of the hot-wire anemometry (with slanted hot-wires) enabled a detailed insight into the 3-D flow development; we also saw the informative development of the boundary layers in the through-flow and cross-flow directions. But, I think, the authors will agree that the practical application of hot-wire techniques for quantitative measurements in turbomachines is limited to the low-speed range. The application in high-speed, high-pressure-ratio machines would result in a nearly insurmountable calibration effort, which would not be justified in view of the short operation periods (wire breaking).

Recognizing these preconditions, it is understandable that the non-intrusive laser velocimetry has become a very powerful tool also for secondary flow studies, since the short time of its extension to high-speed turbomachinery flows some 2-3 years ago. Typical applications for high-speed axial as well as centrifugal compressors have been demonstrated during this meeting in the contributions of Dr. Weyer and myself. You have seen that the laser velocimetry is capable to yield detailed information even in very complex flow situations. Internal transonic flows with pronounced shocks in an axial compressor or the heavily distorted jet/wake flow pattern in a centrifugal compressor have been analysed at realistic tip speeds in the order of 400 m/s. The influence of the secondary flows on the development of the overall flow pattern and on the jet/wake distribution has been also illustrated.

Besides the present uniqueness of laser velocimetry, there has been always one essential draw-back, which is of certain relevance to the fundamental research on secondary flows and especially 3-D boundary layers:

It was impossible to measure in the immediate vicinity of the flow channel surfaces - consequently it was impossible to get an overall flow pattern in very shallow flow channels as well as a deepened insight into the wall layer structure, especially into the incipient flow separation.

In technical terms - the signal-to-noise ratio, between the (signal) light intensity,backscattered from the seeding particles,and the background radiation reflected from the walls, is normally too low.

With respect to the latter point, the continuous further development of the laser-2 focus-velocimeter (L2F) by Schodl, DFVLR, resulted in a decisive improvement during the last months. The basic L2F measuring principle is preserved:

Two focussed laser beams create some kind of a "light gate", the backscattered light from the seeding particles, which traverse this "gate", is detected and correlated, so that the mean flow velocity and direction as well as the turbulence intensity in a measuring plane normal to the beam axis are determinable. In the case of the modified L2F-fluorescence-technique (L2F-F), some fluorescent material is added to the seeding particles, so that the backscattered particle radiation has a different wave-length with respect to the background radiation and an extra filter unit in front of the photodetector(s) makes a distinct differentiation between signal and noise information possible, thus increasing the S/N ratio.

Fig.1 shows the new modular design of the L2F velocimeter, with which all sub-systems (2-4) around the central unit 1 are exchangeable and adaptable to special measurement demands. Due to the compact set-up, only a small observation window has to be inserted into the turbomachine casing.

A comparison of original and modified techniques is presented in Fig.2. The flow pattern was determined in the radial part of a centrifugal compressor impeller - in the region of beginning flow separation. Fig.2a shows the meridional velocity profile c_m/u_2 between hub and shroud, at a mean pitch position (y/t = 0.5). The original L2F technique allowed measurements close to the walls down to about 10 per cent of the local channel height b = 36.6 mm. Typically the L2F-F modification extended the measurement range down to about 1 mm off the channel surfaces, as demonstrated in the hatched shroud region. The corresponding Fig. 2b illustrates the relative velocity profile in a perspective view across the blade height; most striking is the strong skewing of the shroud wall boundary layer towards the blade suction side (SS).

The general meaning of this advancement is obvious - it holds out the prospect of an overall flow analysis in high-speed, high-pressure-ratio turbomachinery, even with extremely small blade heights, as well as an improved insight into the complex structure of 3-D boundary layer flows under realistic operation conditions.

Summarizing, I think, one can be optimistic that the strengthened use of advanced experimental techniques for internal flow studies will improve our understanding of complex turbomachinery flows decisively, will accelerate the further development of physically relevant, but mathematically still tractable theoretical prediction methods, so that, finally, the possibility of more accurate design techniques becomes apparent.

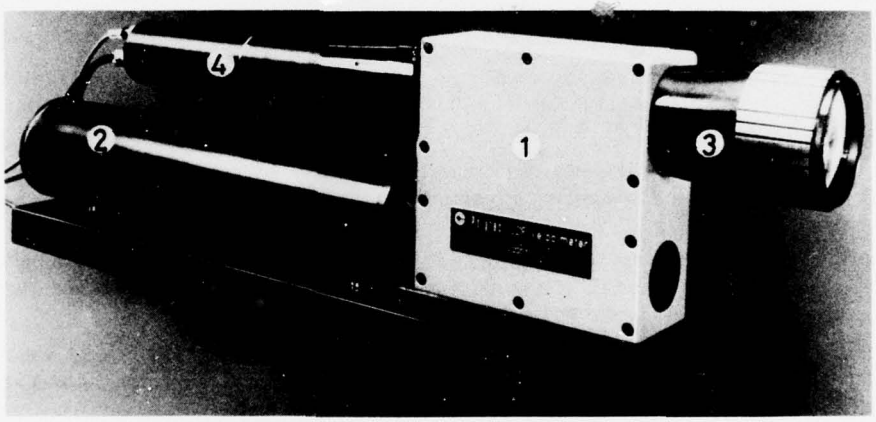


Fig.1 L2F velocimeter (licence DFVLR):
1 - central unit, 2 - laser, 3 - image and observation objective,
4 - photodetector(s) (1 or 2, L2F-F filter unit optional).

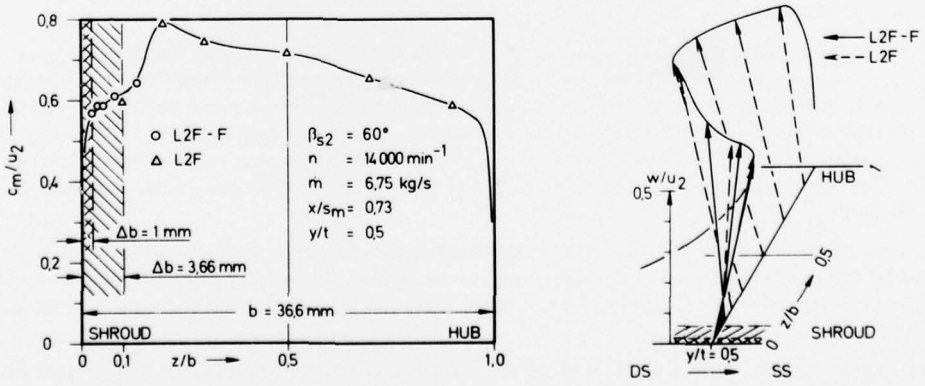


Fig.2 Application of the L2F-fluorescence-velocimeter in a high-speed centrifugal compressor impeller. Nomenclature - see paper by Eckardt/Krain.

P.W.Runstadler, Jr: In summary, I will be covering the following points relative to flow visualization in secondary flows:

(i) What is the purpose of using visualization techniques in secondary flow research?

(ii) Time only permits a discussion of some of the techniques that can be used. I will do this in relation to the general principles underlying the use of these methods.

(iii) I want to mention some problem areas that confront the experimentalist using some of these visualization approaches. I also want to discuss what may be desirable in using visualization techniques to answer some major unresolved questions of secondary flows and the consequent losses they incur in actual machines.

First, then, what are the purposes of using flow visualization? While flow visualization often produces beautiful, and esthetically pleasing pictures, more than artistic merit is usually necessary to justify flow visualization work. Visualization is used to give an overall, qualitative understanding of the flow field. Properly used, visualization of the flow permits an identification of the basic and controlling phenomena. Obviously the purpose of this type of research study is to identify what is happening in the flow so that the analyst can appreciate the assumptions that must be made to simplify the flow. This hopefully permits the construction of an adequate mathematical representation of the observed phenomena. Qualitative information such as can be obtained by visualization can be of invaluable assistance in this regard.

I would like to cite one example where visualization, properly used, produced a significant impact, in fact almost revolutionized thinking, in a problem area that had been studied for years. For a long time researchers have been working on the fundamental mechanisms of turbulent production and turbulent mixing. A few years ago some very simple flow visualization techniques showed that large scale, rather coherent structures were an important part of these flows – a fact which detailed point by point measurements had missed for years.

In my opinion, flow visualization, properly used, provides a zeroth order understanding that can produce enormous payoff in more directly leading the analyst to the proper appreciation of how to model the flow. Some researchers, I am afraid, shy away from the proper use of visualization just because the zeroth order or qualitative aspect of these techniques, and their results, do not appear to be sufficiently precise and quantitative.

In addition to the above zeroth order understanding, some visualization methods can indeed be quantitative. Perhaps the best example, familiar to us all, is the use of interferometry techniques to visualize the flow. The interferometer technique can produce detailed, quantitative measurements of the variations in density throughout the flow. I will return to discuss interferometer and related techniques in a moment.

All the various flow visualization methods fall into one of several categories.

The first of these categories are the surface or wall coating techniques. These methods reveal the limiting wall streamlines of the flow. A good example of the use of wall trace methods was seen in the paper and live film by Heinemann which was delivered yesterday.

For highly skewed cases, these methods may sometimes mislead the experimenter since only the limiting streamlines at the wall are revealed. Caution must be exercised in extrapolating the wall traces to imply flow away from the wall in such highly skewed flows.

Other flow visualization methods are useful to visualize the flow away from surfaces. A commonly used method which works well in liquids and low-speed flows is streamline tracing. This method can only be used where turbulent diffustion of the tracer particles is not severe.

The first slide taken from the classic work of Hanson, Herzig, and Costello of the NACA (1953) shows the use of this type of technique in a reasonably low speed cascade study. For high speed transonic flows, which have been the main interest of this meeting, these techniques are difficult if not impossible to apply.

A more appropriate method for the type of flows that have been discussed at this meeting is the so-called "sheet-of-light" technique. This method visually displays local concentration gradients of particles introduced into the flow – usually uniformly upstream. An excellent example of the method was given in the paper by Marchal and Sieverding yesterday. This method depends upon large gradients in the density of particles being developed in the flow – such as produced by local separations of the flow.

A second variation of this method is the use of light-induced fluorescence. This method has been pioneered by Kerrobrock and his co-workers at the Massachusetts Institute of Technology. As developed to date, this method is much more sensitive than the more commonly used light plane technique – in fact it can be used to quantitatively measure the instantaneous variations in the density of the flow. In liquids, an ideal method to visualize the flow is the hydrogen bubble technique. Even in the middle of a flow, a uniform distribution of tracer particles can be created along a line and then followed downstream. So far, the direct analogy to the hydrogen bubble method has not been developed in gas flows.

Finally, there are the shadowgraph and Schlieren methods, which are rather simple ways to visualize flows with significant density variations such as occur through shock waves. The shadowgraph method is sensitive to focusing caused by the second derivative of the refractive index field. Only regions where the index varies rapidly are revealed by this method.

Schlieren methods use the prismatic effect of the flow field to measure the first spatial derivative of the index of refraction.

Finally there is interferometry, the most sensitive of these techniques, which measures the refractive index field, and hence the density field, directly. Unlike shadowgraphs and Schlieren work, which can be performed with incoherent, pulsed white light, interferometry techniques require a highly monochromatic source of light for which purpose lasers are ideally suited.

Unfortunately, all of the latter techniques, the shadowgraph, Schlieren, and interferometer approaches, are optical path dependent. That is, they do not measure variations just at a point in the flow but are the integrated effect over the length of the optical path of the light passing through the flow. As a result, they reveal nicely the details of fundamentally two-dimensional flows but become confusing to interpret for highly three-dimensional flows. Basically secondary flows are highly three-dimensional and therefore these methods will require special techniques if they are to be applied for secondary flow research.

What are the problems of using visualization techniques in secondary flow work?

First there are difficulties of getting adequate access to the flow. This is bad enough in cascade rigs where ingenious use of windows, mirrors, and special lenses have produced good and workable approaches. In rotating hardware, the problems become much harder. Even when these geometry problems are surmounted, the problems of vibrations of optical surfaces, the difficulty of introducing visualization trace materials and the harsh environment of operating stages often discourages the experimenter from using or trying new or old methods.

What are some of the methods that look more promising for use in secondary flow research?

The use of wall trace and light plane techniques are simple and can produce interesting and valuable information of the sort displayed in several of yesterday's presentations.

A most promising method is the sheet-of-light fluorescence technique. It is relatively simple to use and implement (outside of the use of light intensifier tubes) and can instantaneously capture an entire plane of the flow field and can produce quantitative measurements.

Perhaps a promising technique is the use of holographic methods adapted for three-dimensional flow fields. The second slide is an example of a turbine cascade interferogram made using holographic techniques. This interferogram is taken from the work of Brandt, Rozelle and Patel at Westinghous Electric Corporation. While this result is for an essentially two-dimensional flow, the use of similar techniques using zeroth order holograms, where it is possible to develop such interferograms but taken from a number of different angles, may be able to resolve some of the three-dimensional, secondary flow effects. These methods are also relatively easy to adapt to Schlieren and shadowgraph work if properly designed. However, their use in real rotating hardware will certainly require ingenious experimental techniques to obtain the same definition of the flow field that has been obtained in cascade work.

Finally a word of caution may be necessary for flows which contain unsteady behavior. Some visualization methods are susceptible to misinterpretation under unsteady behavior; wall trace and fluid streamline tracing methods fall into this class. For example, one has to be aware of the difference between streamline, streak lines, and path lines in basically unsteady flows.

This leads me to a concluding remark about secondary flow research which is quite apart from flow visualization. As I remarked earlier this morning, most of the work reported at this meeting has concerned the basic secondary flows developed either in cascades or the first stage of a compressor or turbine. However the engine designer is also interested in the secondary flow losses induced in the latter stages of the machine. It is the latter stages which are forced to swallow the secondary flow patterns produced upstream. Furthermore, the secondary flow patterns interact with the downstream blade row by mechanisms which are basically unsteady, or non-stationary, in both the relative and absolute frames of reference. It seems to me that this is a problem which is extremely important in understanding secondary flow losses in actual machines, is one which has been little investigated, and could produce secondary flow losses by mechanisms which are quite different from those which have been intensively studied to date. It appears that work needs to be done in this area using experimental techniques including flow visualization.

DISCUSSION ON PAPERS BY D.ECKARDT AND P.W.RUNSTADLER, JR

J.H.Horlock

That is the position of our two contributors on the experimental side, are there any comments on the experimental work?

E.E.Covert

In using flow visualization techniques in unsteady flow one must keep in mind that streamlines, streaklines and pathlines are different in this case. It is sometimes useful when one starts out on a flow visualization program in unsteady flow, to try some simple cases first where one can compare what one sees with what one can calculate and so knows what is happening.

P.W.Runstadler, Jr

In trying to understand this basic phenomenon, there is a good film produced by Steve Kline of Stanford University some years ago by N.C.F.M.F. group on flow visualization. This film nicely displays the difference between pathlines, streaklines and streamlines.

J.H.Horlock

The ideal exercise, I think, is to try and draw the three – pathlines, streamlines and meanlines for rotating stall.

R.Flot

I think that speaking about flow visualization techniques at the wall we have to be very careful, because we have discovered big differences between measurements and visualization of limitive streamlines at the wall, concerning the angle. Everybody knows the importance of the knowing of the limiting streamlines for the analysis. We have to be very careful when we try to estimate the angle at the wall.

J.W.Railly

In regard to the use of fluorescent dust in connection with the laser velocimeter used, is 1 mm the closest distance that one can approach a surface?

D.Eckardt

I think, it is the limit for the moment. As I mentioned, it is a very new development and we were quite happy to reduce the limiting wall distance from 3–4 mm down to 1 mm. You have not to forget that the 1 mm-distance is an average value. The measuring volume itself has a certain extension in the order of 0.5–1.0 mm^3. So a slight reduction may be possible, but I see no chance for further decisive improvements in the near future. You have also to observe that in the backscattering operation mode, which is generally applied for turbomachinery testing, the optical axis orientated normally to the hub and shroud walls. In the literature some boundary layer measurements have been demonstrated with a better spatial resolution. In these cases the laser beams were in parallel to the investigated wall shear layers; possibly P.Runstadler may add some comments on this subject.

P.W.Runstadler, Jr

I think that 1 mm is certainly valid for the back reflected or back scattered mode, which is the method that Eckardt is using now with the two beams approach. We are using another method that can be used on the hub of a compressor, centrifugal or axial, or on a blade surface, or on the wall surface of a diffuser by putting a mirrored surface in the wall. When this is done you have to change your optics, so that you actually aperture your system on the mirror image. Then you can take advantage of the forward scattered radiation which is one and sometimes two orders of magnitude higher in signal strength than the back scattered radiation. Using this technique we have to be able to make measurements down to fractions of a millimeter from the wall. The problem is of course that this gets you out of the back scattered mode. The back-scatter mode is very nice, because in the back scattered mode you are not sensitive to wall vibrations and movement of the compressor both of which can produce misalignement of the optics. Mr Eckardt made another comment concerning measurements parallel to the surface. With proper optics (divergence and convergence angle of the laser beams) you can get extremely close to the wall in terms of the type of boundary layer measurements we were talking about.

G.Serovy

Commenting about the measurements one millimeter away from the wall, I would like to say that most of the phenomena that have been demonstrated in this meeting to cause large losses seem to be taking place more than 1 mm away from the wall. It seems to me that the kind of data you have produced and Dr Weyer has produced and others in your Institute have shown us, is of immediate value even if it is not extended in the region very close to the passage boundaries. The problem here is to decide how we can use this information in a design system. The design systems in use now do not permit us to use this detailed set of velocity distributions very well. We don't know how to use them to control the geometry and that is what I think we need to do with the data that you are getting now.

D.Eckardt

In principle I agree with Prof. Serovy. The deepened insight into complex flow situations *alone* is of little help for an improved stage design. For a long time we will have to play the game of "trial and error" between design and measurements. But now – for the first time – we can check in detail the impact of a modified design on the flow pattern itself – and not *only* on the basis of a performance map. It is well-known design practice to replace complicated flow situations by simplified, but physically relevant (or at least credible) flow models. Accurate measurements should yield the sound basis for theoretical flow models. In the field of centrifugal compressors this school of thinking has been promoted by R.C.Dean for years. It is only recently that an increasing number of centrifugal compressor design procedures appear, which take into account the distorted jet/wake flow pattern, typical for highly-loaded centrifugals, e.g. Sturge and Cumpsty (1975), Osborne and Howard (1976).

The extended spatial resolution power of advanced laser velocimetry opens the prospect for a further design model sophistication with respect to flow separation, 3D boundary layer development, tip clearance flow etc. within the wall regions or – in the case of small blade heights with merging boundary layers – should enable even only first checks of theoretical assumptions on the overall flow field.

P.W.Runstadler, Jr

When I look at the centrifugal type of compressor that I have been doing work upon, the component which is the most important to understand, for high pressure ratio machines, is the vaned diffuser component. This component is so to speak the second row downstream of the wheel. It is this type of phenomena, the unsteady, highly

distorted secondary flows, emerging from the rotor upstream that one must deal with. As I said before, some of this unsteady phenomena must be important for axial machines also. I think the development of the optical anemometer techniques as well as the fluorescent technique developed by M.I.T. offers a way now in getting at those flows in a nondisturbing fashion. They require a lot of work to do them and a lot of ingenuity and a lot of money to back up the research that's required, but without that type of information you cannot do the type of flow modelling that George Serovy is talking about. That's where the important breakthrough is going to come. We have to understand quantitatively as well as qualitatively what these flows are doing and change our assumptions accordingly in order to produce new design methods.

J.H.Horlock

We have had one written contribution that goes back to the numerical calculations we were talking about.

M.Pandolfi

A comment on the state of the art about the use of numerical methods for predicting flows in turbomachines.

It seems to me that a lot of experience has been gained in working in numerical methods in classical Aero-Gas-Dynamics, namely flows about vehicles in flight. It seems that such effort has not yet been turned to turbomachinery problems and we are at a very early stage in using numerical methods of calculation of flow fields.

J.Chauvin

This is not right. I will refer you to earlier lecture series or Lectures. In fact the numerical method advancements are proceeding in parallel for external and internal aerodynamics, which has its own problems especially with boundary conditions. In fact in recent cases, which I know from first hand, for instance in the unsteady methods, the advances have been faster in internal and duct flow than they have been for external flows. There has been a large effort devoted, and well documented, that is not the subject of this meeting. For the particular point that you raise for Mr Thompkins method, it has been presented in the last March Meeting of AGARD. As Mr Thompkins himself pointed out his program is by no means optimized. As I have just mentioned in the discussion that since an order of magnitued in time has been gained, I don't think it's fair to say that we are late in the turbomachinery field in that. All the techniques that I know for external flow aerodynamics have been applied, to internal flow with stronger requirements (you can be non-conservative on external flow aerodynamics, you cannot do it in internal flow aerodynamics), so I think that the state is at about the same level. The recent methods that are about to be published have been developed to treat rotational flow inside turbomachinery passages and those are in advance in respect to what exists in external aerodynamics.

CONCLUDING REMARKS

J.H.Horlock: I was asked to try and summarize the situation resulting from this meeting. I think that that is an almost impossible task but I shall attempt to say a few things by way of summary. I think to begin with, it must be accepted that my own definition of secondary flow, which I started with on Monday morning, has not been accepted by the meeting. It has not been accepted at this conference that the academic definition of secondary flow (that associated with secondary vorticity) is sufficient. I think a better definition would have been "anything that stops the flow from following the blades". I shall be looking at the analytical and the experimental work separately.

As far as the analytical work is concerned, I should like to concentrate on two things; what this meeting may have done for us and what the future holds.

On the analytical work I would have thought we have had some further contribution towards understanding secondary flows. Professor Marsh's contribution certainly helped me in understanding how you calculate the components of secondary vorticity. I think Professor Hirsch's work has confirmed in my own mind that the idea of tracing absolute vorticity and relative vorticity through two or more rows of a machine at least is a valid one; he has provided some experimental confirmation for those ideas. At the same time I think that his work perhaps concealed the unsteadiness of the whole flow phenomenon, which was referred to earlier on this morning. As the flow moves from a steady flow in one row of blades to the next rotating row of blades the relative flow becomes highly unsteady, as that blade row meets all the separate components of vorticity. (I think that Professor Railly and I probably do agree that you should not substract the 2Ω twice over, when you are calculating the flow in a rotor. You should only substract it once.)

As far as 3-D boundary layer work is concerned, I think that Papailiou's work with his colleagues showed that there is some progress in this area, but I think he would admit, as all of us would admit, that there are many empirical factors that have to be used in these calculations, if you have to get the right answer for boundary layer growth.

You must guess the wall shear stress, you must guess the way the blade force deficit varies through the boundary layer, you must guess the effect of the tip clearance on that. There are many empirical things that you have to put in. I myself felt that Carrick's work was useful in that it showed that the pitch averaging of the boundary layer flow in a turbine cascade simply cannot be used very far through the blades – 30% of the chord, perhaps, no further. He didn't

do very much better with boundary layer calculations, but I thought that his development of the Stuart and Hetherington numerical calculations was surprisingly good, encouragingly good. It gives us some kind of description of the real flow that takes place.

I was a little disappointed that we didn't spend some further time on the numerical methods that may be used to calculate these 3-D flows. We have not heard very much of the Stuart and Hetherington method; we have heard nothing from the Spalding group on the development of their own methods. We have heard a little bit about time marching from Dr Bussi; we have heard Dr Fruehauf's contribution on calculations with 3-D characteristics and with S_1 and S_2 surfaces. I am worried about all these methods when they get to the trailing edge of the flow. I don't know how they are going to deal with the trailing edge. Professor Spalding would say: "Just let the computer take care of it and all will come well." But you've got to deal with this by a finite-difference method, so that it must become a finite vortex sheet rather than a discontinuity.

On the experimental work, my own major impression has been that of the striking effect of all the new methods of measuring flows that we have seen. Surely we do now have very much better descriptions of the experimental flows that have been observed. If I am critical, I would be critical of the experiments themselves in that I am not sure that they were always very well planned. It seems to me that they were very often just simply descriptions of what was happening in a particular machine, rather than an experiment which was planned to give an understanding or a comparison with a theoretical description of the flow. I counted up 23 different experiments which have been described to us and I would only be able to summarize them by saying that they are "secondary flows that I have known".

I find it impossible to summarize all the results from those experiments. There was only one from industry and that was, perhaps, the most complex. It was reported to us by Mr Barry. I think, perhaps, there was one major point that I got from the experimental results – from the experiments described by Professor Gallus. These confirmed that what I said on the first morning was correct – that blade row by blade row through a *compressor* the secondary flow is substantially reduced. Professor Gallus showed that very clearly in his measurements in the stator downstream of the rotor. On the other hand Mr Barry showed to us that as far as the turbine was concerned, things got worse and worse through the blade rows of the machine.

As for our round table discussion of this morning, we have to begin with the designer's point of view. I think the conclusion was that what we have heard in this conference is not of immediate use to us as designers. We were told that the designer's objectives were to find expressions for the secondary loss, to understand how we should add together the primary and the secondary flows, and then to think about how we should reduce the loss.

I would say that even if I knew how to add the primary and secondary flows together, I'm not sure whether as a designer, I would design on the basis of the primary flow or the primary plus the secondary flow. If you think about the angle changes that we've seen (those that Marsh predicted, for instance) would you really design a rotor blade downstream of that nozzle row to run at zero incidence? Highly twisted blades would result and nobody would really expect to design a rotor blade that way. One might go back and modify the primary flow slightly but I don't think any designer would ever add the two together and base his design completely on primary plus secondary flow.

On the theoretical work I think we did conclude we had some better understanding. Professor Marsh made a good point – you can never expect to get the completely right answer from these theoretical calculation methods. They give us a better understanding rather than a precise description of exactly what happens.

On the experimental side our contributors emphasized the wide range of experimental techniques that we have now available to us. Mr Eckardt made the point that we must now start measuring on real machines, not just single rows, cascades, and rotors; we should be measuring in high speed multistage machines. He pointed out that 3-D measurements were now possible (with considerable accuracy) and that we should take advantage of this. Mr Runstadler made one very important point to start with: the purpose of flow visualization must be obtaining physical understanding so that we can have a starting point for simplified analysis subsequently. In describing the many techniques that were available, he gave a very important warning about placing too much emphasis on wall coatings and visualizations of the flow from wall coatings. I remember that Dr Head made an estimate a few years ago of the angle change in a 3-D boundary layer through that last millimeter near the wall. I think he calculated the angle change to be some 25°, so don't rely too much on what you see with wall coatings.

So that's an attempt at a summary of the situation from this morning's discussion and from this meeting. As far as the future is concerned I am going to make one appeal, and that is in the future planning of experiments. I don't think they are going to help, unless they have specific objectives. One objective should be that of improving our correlations, correlations of losses, blockage, angle change; and in those correlations, we have to put everything in, entry skewing, flow unsteadiness. Another objective of the experiments should be that which Mr Runstadler described, the objective of improvement of understanding, to give us some starting points for the analytical work explaining to us how the blade force does vary through the boundary layer, explaining to us what the effect of the clearance is on the force variation. So, I make a plea for some planning of experiments to further these two objectives, rather than collecting in a mass of more experimental data, which might add further to our confusion.

One final comment. Could we not ask AGARD to review this field to make recommendations for work on the gaps that have to be filled on the theoretical and the experimental side and to ask people to come back in three or four years and report whether they have filled those gaps? Could AGARD not, for instance, bring together all these experiments we have seen today and correlate secondary losses as Dr Dunham did some years ago; could we ask the international body to coordinate this work in the future? Well, I think, that concludes our discussion of this morning, gentlemen.

REPORT DOCUMENTATION PAGE

1. Recipient's Reference	2. Originator's Reference	3. Further Reference	4. Security Classification of Document
	AGARD-CP-214	ISBN 92-835-0199-3	UNCLASSIFIED

5. Originator Advisory Group for Aerospace Research and Development
North Atlantic Treaty Organization
7 rue Ancelle, 92200 Neuilly sur Seine, France

6. Title

SECONDARY FLOWS IN TURBOMACHINES

7. Presented at the 49th Meeting of the AGARD Propulsion and Energetics Panel held at the Koninklijk Instituut van Ingenieurs, Prinsessegracht, 23, The Hague, The Netherlands, from 28 to 30 March 1977.

8. Author(s)	9. Date
Various	September 1977
10. Author's Address	**11. Pages**
Various	312

12. Distribution Statement This document is distributed in accordance with AGARD policies and regulations, which are outlined on the Outside Back Covers of all AGARD publications.

13. Keywords/Descriptors

Axial flow compressors	Boundary layer flow
Centrifugal compressors	Rotor blades (turbomachinery)
Turbines	Stator blades

14. Abstract

Improvement of the theoretical calculation of the inviscid core of the high performance turbomachines are more and more demanding the better understanding of the secondary flows, i.e. the part of the flow field that is close to the inner or the outer walls and is therefore subjected to high viscous stresses as well as to the effect of the vortices induced by the blade-casing junction. The meeting was divided into four sessions – a total of fifteen invited papers and seven short presentations – followed by a round table discussion.

Representatives from industry made clear: – why up to now they were not able to use the theoretical approaches available in the literature; – the need for a theoretical estimation of the blockage factor to help them to calculate more correctly the low-loss core of the flow; – the need for correct loss estimation formulas.

The response from research workers suggested: – simplified secondary vorticity considerations and pseudo-boundary layer approaches seem to be promising for multistage compressor analysis if backed by experimental results; – this analysis seems to be inadequate for turbines and fully three-dimensional calculation methods must be used. These are still time consuming but are certainly less expensive than experiments; – new experimental techniques must be used, in spite of cost and effort, to provide the necessary flow models. However, experiments must be carefully planned; – lack of understanding and experimental information exists in the areas of multistage environment, tip clearance effects and radial machines.

AGARD Conference Proceedings No. 214
Advisory Group for Aerospace Research and Development, NATO
SECONDARY FLOWS IN TURBOMACHINES
Published September 1977
312 pages

Improvement of the theoretical calculation of the inviscid core of the high performance turbomachines are more and more demanding the better understanding of the secondary flows, i.e. the part of the flow field that is close to the inner or the outer walls and is therefore subjected to high viscous stresses as well as to the effect of the vortices induced by the blade-casing junction. The meeting was divided into four sessions – a total of fifteen invited papers and seven short presentations – followed by a round table discussion.

P.T.O.

AGARD-CP-214

Axial flow compressors
Centrifugal compressors
Turbines
Boundary layer flow
Rotor blades (turbomachinery)
Stator blades

AGARD Conference Proceedings No. 214
Advisory Group for Aerospace Research and Development, NATO
SECONDARY FLOWS IN TURBOMACHINES
Published September 1977
312 pages

Improvement of the theoretical calculation of the inviscid core of the high performance turbomachines are more and more demanding the better understanding of the secondary flows, i.e. the part of the flow field that is close to the inner or the outer walls and is therefore subjected to high viscous stresses as well as to the effect of the vortices induced by the blade-casing junction. The meeting was divided into four sessions – a total of fifteen invited papers and seven short presentations – followed by a round table discussion.

P.T.O.

AGARD-CP-214

Axial flow compressors
Centrifugal compressors
Turbines
Boundary layer flow
Rotor blades (turbomachinery)
Stator blades

AGARD Conference Proceedings No. 214
Advisory Group for Aerospace Research and Development, NATO
SECONDARY FLOWS IN TURBOMACHINES
Published September 1977
312 pages

Improvement of the theoretical calculation of the inviscid core of the high performance turbomachines are more and more demanding the better understanding of the secondary flows, i.e. the part of the flow field that is close to the inner or the outer walls and is therefore subjected to high viscous stresses as well as to the effect of the vortices induced by the blade-casing junction. The meeting was divided into four sessions – a total of fifteen invited papers and seven short presentations – followed by a round table discussion.

P.T.O.

AGARD-CP-214

Axial flow compressors
Centrifugal compressors
Turbines
Boundary layer flow
Rotor blades (turbomachinery)
Stator blades

Representatives from industry made clear: – why up to now they were not able to use the theoretical approaches available in the literature; – the need for a theoretical estimation of the blockage factor to help them to calculate more correctly the low-loss core of the flow; – the need for correct loss estimation formulas.

The response from research workers suggested: – simplified secondary vorticity considerations and pseudo-boundary layer approaches seem to be promising for multistage compressor analysis if backed by experimental results; – this analysis seems to be inadequate for turbines and fully three-dimensional calculation methods must be used. These are still time consuming but are certainly less expensive than experiments; – new experimental techniques must be used, in spite of cost and effort, to provide the necessary flow models. However, experiments must be carefully planned; – lack of understanding and experimental information exists in the areas of multistage environment, tip clearance effects and radial machines.

Papers presented at the 49th Meeting of the AGARD Propulsion and Energetics Panel held at the Koninklijk Instituut van Ingenieurs, Prinsessegracht, 23, The Hague, The Netherlands, from 28 to 30 March 1977.

ISBN 92-835-0199-3

Representatives from industry made clear: – why up to now they were not able to use the theoretical approaches available in the literature; – the need for a theoretical estimation of the blockage factor to help them to calculate more correctly the low-loss core of the flow; – the need for correct loss estimation formulas.

The response from research workers suggested: – simplified secondary vorticity considerations and pseudo-boundary layer approaches seem to be promising for multistage compressor analysis if backed by experimental results; – this analysis seems to be inadequate for turbines and fully three-dimensional calculation methods must be used. These are still time consuming but are certainly less expensive than experiments; – new experimental techniques must be used, in spite of cost and effort, to provide the necessary flow models. However, experiments must be carefully planned; – lack of understanding and experimental information exists in the areas of multistage environment, tip clearance effects and radial machines.

Papers presented at the 49th Meeting of the AGARD Propulsion and Energetics Panel held at the Koninklijk Instituut van Ingenieurs, Prinsessegracht, 23, The Hague, The Netherlands, from 28 to 30 March 1977.

ISBN 92-835-0199-3

Representatives from industry made clear: – why up to now they were not able to use the theoretical approaches available in the literature; – the need for a theoretical estimation of the blockage factor to help them to calculate more correctly the low-loss core of the flow; – the need for correct loss estimation formulas.

The response from research workers suggested: – simplified secondary vorticity considerations and pseudo-boundary layer approaches seem to be promising for multistage compressor analysis if backed by experimental results; – this analysis seems to be inadequate for turbines and fully three-dimensional calculation methods must be used. These are still time consuming but are certainly less expensive than experiments; – new experimental techniques must be used, in spite of cost and effort, to provide the necessary flow models. However, experiments must be carefully planned; – lack of understanding and experimental information exists in the areas of multistage environment, tip clearance effects and radial machines.

Papers presented at the 49th Meeting of the AGARD Propulsion and Energetics Panel held at the Koninklijk Instituut van Ingenieurs, Prinsessegracht, 23, The Hague, The Netherlands, from 28 to 30 March 1977.

ISBN 92-835-0199-3

Representatives from industry made clear: – why up to now they were not able to use the theoretical approaches available in the literature; – the need for a theoretical estimation of the blockage factor to help them to calculate more correctly the low-loss core of the flow; – the need for correct loss estimation formulas.

The response from research workers suggested: – simplified secondary vorticity considerations and pseudo-boundary layer approaches seem to be promising for multistage compressor analysis if backed by experimental results; – this analysis seems to be inadequate for turbines and fully three-dimensional calculation methods must be used. These are still time consuming but are certainly less expensive than experiments; – new experimental techniques must be used, in spite of cost and effort, to provide the necessary flow models. However, experiments must be carefully planned; – lack of understanding and experimental information exists in the areas of multistage environment, tip clearance effects and radial machines.

Papers presented at the 49th Meeting of the AGARD Propulsion and Energetics Panel held at the Koninklijk Instituut van Ingenieurs, Prinsessegracht, 23, The Hague, The Netherlands, from 28 to 30 March 1977.

ISBN 92-835-0199-3

AGARD
NATO OTAN
7 RUE ANCELLE · 92200 NEUILLY-SUR-SEINE
FRANCE
Telephone 745.08.10 · Telex 610176

DISTRIBUTION OF UNCLASSIFIED AGARD PUBLICATIONS

AGARD does NOT hold stocks of AGARD publications at the above address for general distribution. Initial distribution of AGARD publications is made to AGARD Member Nations through the following National Distribution Centres. Further copies are sometimes available from these Centres, but if not may be purchased in Microfiche or Photocopy form from the Purchase Agencies listed below.

NATIONAL DISTRIBUTION CENTRES

BELGIUM
Coordonnateur AGARD – VSL
Etat-Major de la Force Aérienne
Caserne Prince Baudouin
Place Dailly, 1030 Bruxelles

CANADA
Defence Scientific Information Service
Department of National Defence
Ottawa, Ontario K1A OZ2

DENMARK
Danish Defence Research Board
Østerbrogades Kaserne
Copenhagen Ø

FRANCE
O.N.E.R.A. (Direction)
29 Avenue de la Division Leclerc
92 Châtillon sous Bagneux

GERMANY
Zentralstelle für Luft- und Raumfahrt-
dokumentation und -information
Postfach 860880
D-8 München 86

GREECE
Hellenic Armed Forces Command
D Branch, Athens

ICELAND
Director of Aviation
c/o Flugrad
Reykjavik

ITALY
Aeronautica Militare
Ufficio del Delegato Nazionale all'AGARD
3, Piazzale Adenauer
Roma/EUR

LUXEMBOURG
See Belgium

NETHERLANDS
Netherlands Delegation to AGARD
National Aerospace Laboratory, NLR
P.O. Box 126
Delft

NORWAY
Norwegian Defence Research Establishment
Main Library
P.O. Box 25
N-2007 Kjeller

PORTUGAL
Direccao do Servico de Material
da Forca Aerea
Rua de Escola Politecnica 42
Lisboa
Attn: AGARD National Delegate

TURKEY
Department of Research and Development (ARGE)
Ministry of National Defence, Ankara

UNITED KINGDOM
Defence Research Information Centre
Station Square House
St. Mary Cray
Orpington, Kent BR5 3RE

UNITED STATES
National Aeronautics and Space Administration (NASA),
Langley Field, Virginia 23365
Attn: Report Distribution and Storage Unit

THE UNITED STATES NATIONAL DISTRIBUTION CENTRE (NASA) DOES NOT HOLD STOCKS OF AGARD PUBLICATIONS, AND APPLICATIONS FOR COPIES SHOULD BE MADE DIRECT TO THE NATIONAL TECHNICAL INFORMATION SERVICE (NTIS) AT THE ADDRESS BELOW.

PURCHASE AGENCIES

Microfiche or Photocopy
National Technical
Information Service (NTIS)
5285 Port Royal Road
Springfield
Virginia 22151, USA

Microfiche
Space Documentation Service
European Space Agency
10, rue Mario Nikis
75015 Paris, France

Microfiche
Technology Reports
Centre (DTI)
Station Square House
St. Mary Cray
Orpington, Kent BR5 3RF
England

Requests for microfiche or photocopies of AGARD documents should include the AGARD serial number, title, author or editor, and publication date. Requests to NTIS should include the NASA accession report number. Full bibliographical references and abstracts of AGARD publications are given in the following journals:

Scientific and Technical Aerospace Reports (STAR),
published by NASA Scientific and Technical
Information Facility
Post Office Box 8757
Baltimore/Washington International Airport
Maryland 21240, USA

Government Reports Announcements (GRA),
published by the National Technical
Information Services, Springfield
Virginia 22151, USA

Printed by Technical Editing and Reproduction Ltd
Harford House, 7–9 Charlotte St, London W1P 1HD

ISBN 92-835-0199-3